Comprehensive Digital Memory Testing and Diagnostics

Symbolic Models, Optimization Tools, and Self-Healing Architectures

MUDAR ALMADI

Almadi Technical Publications
Edmonton, Alberta, Canada

Comprehensive Digital Memory Testing and Diagnostics

Symbolic Models, Optimization Tools, and Self-Healing Architectures

Mudar Almadi

2025

© 2025 Mudar Almadi

All rights reserved.

No part of this publication may be reproduced, stored in a retrieval system, or transmitted in any form or by any means — electronic, mechanical, photocopying, recording, or otherwise — without prior written permission of the author, except for brief quotations used in scholarly review or academic citation.

First edition published in 2026

Manuscript completed in 2025

ISBN 978-1-0696498-0-5

DOI: https://doi.org/10.5281/zenodo.19037759

Published by

Almadi Technical Publications

Edmonton, Alberta, Canada

Disclaimer

The methodologies, symbolic models, and diagnostic frameworks presented in this work are intended for research, engineering, and academic purposes. While every effort has been made to ensure technical accuracy, the author assumes no responsibility for any errors or omissions, nor for any consequences arising from the application of the information contained herein.

Trademarks

All product names, technologies, and company names mentioned in this book are the property of their respective owners.

Dedication

To Dema and Ryan,
for patience, strength, and the quiet belief.

Acknowledgment

Behind every technical contribution in this book stands the steady support of my family.
To my wife, Dema, whose patience, strength, and unwavering encouragement sustained this work through years of research, refinement, and persistence — I offer my deepest gratitude.

To my son, Ryan, for whom this book ultimately exists: may it stand as evidence that complex systems can be understood, difficult problems can be approached with structure and integrity, and that disciplined effort builds enduring knowledge.

I also express my sincere appreciation to my doctoral mentor, Professor Vladimir Grigoryevich Ryabtsev, whose guidance, rigor, and scientific standards shaped the foundational research upon which this monograph is built.

This work reflects not only research and engineering effort, but also a belief that knowledge constructed with precision, intellectual honesty, and resilience can outlast its immediate context and serve future generations of engineers and researchers.

Mudar Almadi
Edmonton, Alberta
2025

Preface

In an era defined by data-driven systems, intelligent machines, and rapidly evolving hardware platforms, memory remains the quiet cornerstone of computation. It preserves instructions, safeguards data, and maintains system state—from microcontrollers and embedded devices to high-performance servers that underpin artificial intelligence and critical infrastructure.

As memory capacities and operating speeds continue to increase, so do the associated challenges. Higher fault rates, tighter reliability margins, and growing architectural complexity demand diagnostic methodologies that are not only thorough, but adaptive and efficient. Relentless device scaling and the intrinsic fragility of high-density memory arrays make testing, fault localization, and in-field recovery not optional enhancements, but fundamental system requirements.

This book, *Comprehensive Digital Memory Testing and Diagnostics: Symbolic Models, Optimization Tools, and Self-Healing Architectures*, was written in response to that need. It synthesizes more than a decade of research, system development, instructional experience, and tool creation.

This monograph is not the result of a single writing cycle, but of years of continuous refinement, restructuring, and conceptual maturation. Its chapters were repeatedly rewritten, reorganized, and technically revalidated to ensure structural coherence, methodological rigor, and long-term relevance. What began as doctoral research gradually evolved—through teaching, experimentation, industrial validation, and critical reassessment—into a unified and stabilized body of work.

Rooted in my doctoral work at the National Technical University Kharkiv Polytechnic Institute and laboratory research conducted at Cherkasy State Technological University, it represents both an academic trajectory and a long-term technical objective: to equip engineers, researchers, and students with principled methods for designing memory systems that do not merely compute, but endure.

At the core of this work are two diagnostic systems developed during my PhD research:

- **PROVER** — a symbolic, machine-oriented test description language and interpreter for synthesizing, analyzing, and simulating memory test programs.
- **Optimal_Test** — an adaptive optimization framework that improves diagnostic efficiency through symbolic modeling, fault-coverage analysis, and execution-time minimization.

These systems emerged within broader research initiatives and collaborative projects, including registered Ukrainian state research programs and industrial efforts focused on automating memory diagnostics.

I also acknowledge the contribution of Dr. Tetyana Utkina, whose work on refining and validating components of the Optimal_Test environment strengthened its robustness in experimental use.

The material presented here integrates the core results of the foundational research formalized in *Methods and Tools for Improving the Efficiency of Diagnostic Testing of Memory Devices* and extends them through subsequent investigations, publications, and system-level validation.

The book covers foundational aspects of memory architectures and fault mechanisms, while introducing original methodologies for symbolic fault modeling, operator-based diagnostics, graph-structured test synthesis, and adaptive optimization using fuzzy inference and statistical reasoning.

Preface — Scope and Structure

This monograph presents a unified framework for the modeling, analysis, optimization, and practical realization of diagnostic testing for semiconductor memory systems. The material integrates symbolic methods, graph-based representations, and adaptive optimization techniques to bridge the gap between formal diagnostic theory and executable engineering solutions.

The book is organized into five thematic parts, each addressing a distinct layer of abstraction while maintaining a coherent progression from physical principles to advanced diagnostic systems.

Part I (Chapters 1–2) introduces memory system architectures and memory technologies, establishing the structural, technological, and operational foundations required for diagnostic analysis. These chapters provide the contextual background necessary to understand how architectural organization and technology constraints influence fault manifestation and test behavior.

Part II (Chapters 3–4) presents fault taxonomies, physical failure mechanisms, and classical memory testing algorithms. This part consolidates established knowledge on fault models, March tests, and pattern-based diagnostics, serving as the definitive reference for physical fault definitions used throughout the remainder of the book.

Part III (Chapters 5–7) focuses on data integrity, redundancy management, and hierarchical diagnostic localization. Topics include error detection and correction codes (ECC), built-in self-repair mechanisms, redundancy management, and fault localization techniques. Together, these chapters address reliability enhancement and post-detection response strategies within modern memory systems.

Part IV (Chapters 8–16) forms the methodological core of the book and introduces symbolic fault modeling, graph-based test representations, adaptive optimization, and executable diagnostic synthesis.

This part progresses from operator-based fault abstraction (Chapter 8), parallel diagnostic architectures (Chapter 9), symbolic test programming using PROVER (Chapter 10), formal graph-based March test decomposition using U–Y schemes (Chapter 11), adaptive optimization of symbolic and graph-based diagnostics using the Optimal_Test framework (Chapter 12), fuzzy logic–based test selection (Chapter 13), adaptive coverage–cost trade-off

analysis (Chapter 14), industrial toolchain integration (Chapter 15), and practical implementation with experimental evaluation (Chapter 16).

Part V (Chapters 17–19) extends the developed framework toward emerging and future directions, including diagnostics for non-volatile memories, AI-augmented and self-healing diagnostic systems, and methodological considerations for advanced research.

The book concludes with open problems and perspectives for further investigation. While the exposition is technically rigorous, it emphasizes clarity, modularity, and transferability.

The objective is to bridge theory and implementation by providing conceptual depth suitable for graduate-level study while offering engineers concrete reasoning frameworks applicable to production testing and in-field diagnostics. Validation activities presented in this monograph include controlled simulation studies, representative diagnostic toolchain integration exercises, structured test-reduction and planning evaluations, and field-oriented and educational deployments.

Quantitative results reported in later chapters should be interpreted as illustrative outcomes observed within defined evaluation settings, rather than as universal performance guarantees or certification claims.

Preface — Intended Audience

This book is intended for:

- Graduate students seeking a structured and methodical introduction to memory diagnostics and subsystem design.
- Doctoral researchers investigating symbolic modeling, optimization, and formal test generation.
- Industry professionals engaged in chip validation, fault tolerance, memory subsystem architecture, and diagnostic automation.

Each chapter balances analytical rigor with practical relevance, emphasizing reasoning transparency and methodological consistency.

Terminology and diagnostic definitions used throughout this book are consolidated in Appendix A.

Preface — Original Contributions

Several contributions are introduced or systematized in this work:

- A multi-head symbolic automaton–based parallel diagnostic architecture for memory systems.
- Operator-based symbolic fault models enabling structured interaction analysis.
- PROVER language pragmatics for symbolic test synthesis and micro-operation mapping.
- U–Y graph schemes for optimizing March-test decomposition and diagnosability.
- Adaptive test-set selection using fuzzy logic and weighted diagnostic evaluation.

- An integrated toolchain centered on Optimal_Test, validated through experimental and industrial-style workflows.

Unless otherwise indicated, the theoretical formulations, structural syntheses, methodological integrations, and system-level generalizations presented in this monograph constitute the original scholarly contributions of the author.

Together, these contributions aim to advance both the theoretical foundations and practical methodologies of memory diagnostics.

Preface — Scope of Validation and Methodological Context

This book is presented as a foundational academic monograph and reference work on memory diagnostics, symbolic fault modeling, and adaptive test optimization. Its primary objective is to formalize the principles, abstractions, and reasoning frameworks underlying memory test generation and diagnosis, rather than to serve as a step-by-step industrial user manual for any specific commercial EDA toolchain.

Accordingly, this monograph should be read as a consolidation of mature diagnostic principles whose relevance extends beyond the specific technologies available at the time of their original experimental validation.

The diagnostic methodologies developed herein—particularly symbolic operator modeling, graph-based test decomposition, and coverage–cost optimization—are intended to be technology-agnostic at the conceptual level.

While examples and experimental systems are instantiated through the author's PROVER and Optimal_Test environments, these tools are used strictly as pedagogical and experimental frameworks for demonstrating symbolic reasoning, test optimization logic, and diagnostic decision processes. They are not proposed as replacements for contemporary industrial platforms such as Siemens Tessent, Synopsys TestMAX, or Cadence Modus.

Implementation technologies, languages, and verification infrastructures evolve continuously. Consequently, specific realizations of the methods described in this book—whether expressed through PROVER scripts, VHDL representations, or experimental executables—should be understood as illustrative realizations of general principles, not as prescriptions for production deployment.

The core contributions of this work reside in the abstraction of fault activation behavior, symbolic test representation, and adaptive selection logic, all of which are transferable to modern verification and test environments, including SystemVerilog-based flows, IEEE 1500/1687 infrastructures, and machine-learning–assisted diagnostic pipelines.

Experimental validation results presented in later chapters were obtained using memory devices and platforms available at the time of investigation. These experiments are intended to validate methodological correctness, internal consistency, and scalability trends, rather than to claim direct equivalence with present-day high-density memory products.

The absence of contemporary large-scale silicon datasets (e.g., DDR5, HBM, or advanced FinFET/GAA nodes) does not diminish the validity of the underlying symbolic and

optimization frameworks, which are deliberately formulated independently of process generation and memory density.

Similarly, the use of fuzzy inference systems for adaptive test selection is motivated by their interpretability, determinism, and suitability for diagnostic reasoning under uncertainty. These mechanisms are presented as baseline decision frameworks that can coexist with—or be extended by—statistical learning and machine-learning–based approaches, as discussed in Chapter 18.

The intent is not to assert exclusivity of fuzzy methods, but to demonstrate structured, explainable optimization strategies applicable across diagnostic contexts.

Readers are therefore encouraged to interpret this work as a conceptual and methodological foundation for memory diagnostics—one that emphasizes symbolic reasoning, adaptability, and optimization—rather than as a vendor-specific implementation guide.

Engineers, researchers, and system architects may map the principles presented here onto contemporary industrial toolchains and emerging memory technologies according to their specific deployment environments and constraints.

Some figures reproduced from the original dissertation and early research publications are retained in their original form to preserve historical accuracy and research provenance, reflecting the visualization tools and technologies available at the time of their creation.

Despite careful preparation, errors or omissions may remain. Constructive feedback from readers and researchers is welcome and may assist in improving future revisions of this work.

Notation Conventions

To avoid ambiguity across chapters, the following notation conventions are used consistently throughout this monograph.

Global Diagnostic Parameters

Symbol	Definition	Context / Description
M	Memory Capacity	Total number of addressable storage locations in the memory device under diagnosis.
A_{addr}	Linear Address	Memory address variable used in PROVER syntax and in symbolic diagnostic test descriptions.
(x, y)	Spatial Coordinates	Introduced in Chapter 9 for visualization of parallel traversal. When used, spatial coordinates are mapped to linear address space according to the relation $A_{addr} = y.W + x$, where W denotes the fixed row width of the memory array.
N_{tests}	Test Count	The number of diagnostic tests in a test library or candidate test set.
H	Number of Parallel Diagnostic Heads	Degree of architectural parallelization in the multi-head symbolic automaton
n	Local or Contextual Cardinality Parameter	A dimensionless integer parameter defined locally within a specific mathematical or symbolic context (e.g., loop index, iteration bound, or traversal cardinality in classical March/operator notation). In classical March-test expressions, n denotes the traversal cardinality. When full-array traversal is assumed, $n \equiv M$. Outside symbolic test expressions, n does not denote memory capacity.

Global Diagnostic Parameters (Continued)

Symbol	Definition	Context / Description
η	Diagnostic Time Reduction Ratio	A normalized efficiency metric representing the relative reduction in diagnostic execution time achieved through test selection or optimization, typically defined with respect to a baseline test sequence.
δ	Adaptation Cost Factor	A scalar parameter representing the overhead introduced by adaptive diagnostic mechanisms, including test reordering, selection logic, or runtime control adjustments.
N	Global Count Parameter	A global cardinality parameter whose specific meaning is defined by context (e.g., total number of tests, faults, or addressable locations). Distinguished from the local parameter n by its global scope.
T_{sum}	Total Execution Time	The cumulative execution time of a diagnostic test sequence, obtained by summing the execution times of all constituent tests or operations.
T_{max}	Maximum Allowed Execution Time	An upper bound on diagnostic execution time imposed by system-level constraints such as production test limits, in-field latency requirements, or cost budgets.

Symbolic Operator and Diagnostic Symbols

Symbol	Definition	Context / Description
$R_{(a)}$	Read operation at address a	Symbolic operator used in PROVER and Optimal_Test to denote read access.
$W_{(a)}$	Write logic 1 to address	Symbolic write operator for storing logical high.
$V_{(a)}$	Write logic 0 to address a	Symbolic write operator for storing logical low.
$WAIT_{(n)}$	Delay of n cycles	Symbolic timing operator modeling retention, drift, or relaxation intervals.
F_j	Fault of type j	Abstract fault class index used in coverage modeling and optimization.
T_i	Diagnostic test i	Indexed test sequence within a candidate test set.
U_i	Diagnostic utility of test i	Weighted coverage score used in Optimal_Test ranking.
S_{syn}	ECC syndrome value	Error signature generated by error-correcting mechanisms.
S_{state}	Diagnostic control state	State variable in U–Y schemes and adaptive diagnostic engines.

All symbolic operators and indices are used consistently throughout the monograph. Subscripts distinguish between tests, faults, syndromes, and control states in order to prevent semantic ambiguity across chapters and to preserve formal traceability between symbolic modeling and execution-level realization.

TABLE OF CONTENTS

Front matter

Dedication
Acknowledgment
Preface
Notation Conventions
List of Figures
List of Tables

Part I — Foundations

Chapter 1: Introduction to Memory Systems and Architectures 1

1.1 Why Memory Dictates System Behavior 1
1.2 Memory Hierarchy Overview 19
1.3 Role of Random Access Memory in Digital Systems 33
1.4 Key Memory Characteristics: Volatility, Speed, Cost, and Integration 47
1.5 Internal Memory Architecture: Cells, Arrays, and Control Logic 56
1.6 Data Integrity and Bit-Level Representation 56
1.7 Performance Metrics and Constraints 72
1.8 Common Access Protocols and Interfaces 80

Chapter 2: Types of RAM and Memory Technologies 94

2.1 SRAM: Structure, Access, and Applications 94
2.2 DRAM: Principles, Variants, and Refresh Mechanisms 97
2.3 SDRAM and DDR Generations 99
2.4 LPDDR and Mobile RAM Architectures 102
2.5 Graphics Memory Technologies: GDDR and HBM 103
2.6 Emerging versus Conventional Memory Technologies 104
2.7 Comparative Summary of RAM Technologies 107
2.8 Summary 111

Part II — Fault Taxonomy & Classical Tests

Chapter 3: Fault Types and Physical Failure Mechanisms 112

3.1 Fault Classification: Permanent, Intermittent, and Transient 112
3.2 Physical Origins of Memory Faults 113
3.3 Logical Fault Models and Behavioral Abstractions 116
3.4 Impact of Aging and Wear-Out Mechanisms 118
3.5 Environmental Faults and Radiation Effects 119
3.6 Technology-Specific Fault Signatures 119
3.7 Fault Activation Conditions 121

3.8 Composite and Cross-Layer Faults 121
3.9 Multi-Bit and Data-Bus Faults 122
3.10 Summary 122

Chapter 4: Memory Testing — Algorithms, Patterns, and Tools 124

4.1 Introduction: The Imperative of Memory Testing 124
4.2 Foundations of Memory Testing 125
4.3 March Testing — Classical, Symbolic, and Extended Variants 126
4.4 Pattern-Based Testing 140
4.5 Advanced Testing Algorithms 145
4.6 Test Metrics and Evaluation 151
4.7 Symbolic Test Modeling and the Optimal_Test Framework 158
4.8 Built-In Self-Test (BIST) Architectures and In-System Testing 166
4.9 Interface-Constrained Testing 170
4.10 Summary and Transition to ECC 175

Part III — ECC & Data Integrity

Chapter 5: Error Detection and Correction Codes (ECC): From Parity to Syndrome-Aware Diagnostics 178

5.1 Introduction: From Fault Detection to Fault Resilience 178
5.2 Core Concepts and Terminology 179
5.3 Common ECC Schemes 180
5.4 Syndrome Decoding and Fault Localization 184
5.5 ECC Design Trade-Offs and Hardware Integration 191
5.6 Diagnostic Insights from Hybrid Memory Stacks 198
5.7 Scrubbing, Logging, and Self-Healing Architectures 205
5.8 Chapter Summary and Transition to BIST and Repair Logic 214

Chapter 6: Built-In Self-Repair and Redundancy Architectures 217

6.1 Introduction: Beyond Detection and Correction 217
6.2 Redundancy Structures in Memory Repair Architectures 218
6.3 BISR Architecture and Logic Flow 220
6.4 Redundancy Mapping Mechanisms 221
6.5 Repair Yield Modeling and Optimization 224
6.6 Retesting and Validation in BISR Systems 229
6.7 Runtime Repair, ECC Thresholding, and Wear-Aware Remapping 233
6.8 Controller-Level Error Containment and Scrubbing Policies 236

Chapter 7: Diagnostic Testing and Fault Localization Techniques 244

7.1 Address Decoding Faults and Row/Column Isolation 244
7.2 Syndrome Analysis and Signature Comparison 249
7.3 Bit-, Word-, and Line-Level Localization 254

7.4 Fault Tables and Diagnostic Resolution Metrics 260
7.5 Hierarchical and Multi-Level Diagnosis 267
7.6 From Test Failure to Root Cause Mapping 277

Part IV — Symbolic Models, Graphs & Optimization

Chapter 8: Operator-Based Fault Modeling 284

8.1 Motivation for a Unified Symbolic Model 284
8.2 Core Operators and Semantics 286
8.3 Fault Definitions as State Violations 288
8.4 Operator Composition and Test Graphs 289
8.5 Practical Encoding and Engine Integration 290
8.6 Strengths and Implications 291
8.7 Summary of the Core Model 292
8.8 Operator Macros and Structural Reuse 292
8.9 Fault Taxonomy and Operator Mapping Table 292
8.10 Timing and Delay Modeling in Operator Sequences 293
8.11 Fuzzy Rule Integration for Fault Likelihood Scoring 294
8.12 Summary of Extensions 295

Chapter 9: Parallel Diagnostic Architecture Using a Multi-Head Symbolic Automaton 296

9.1 Mathematical Model of Memory Devices and Diagnostic Tools 297
9.2 Motivation for Parallel Test Execution 302
9.3 Multi-Head Automaton Inspiration: From Theory to Diagnostic Engine 303
9.4 Porting Test Programs for Scalable Memory Diagnostics 304
9.5 Non-Square Memory Topologies and Sub-Matrix Decomposition 305
9.6 Automated Reconfiguration for Non-Square Memory Topologies 306
9.7 Test Selection Problems for Diagnosing Memory Devices 308
9.8 Architecture of the Parallel Diagnostic System 310
9.9 Optimal_Test Ranking 316
9.10 Fault Coverage Process Model for Memory Chips 316
9.11 Detection of Subsequent Faults and Conditional Coverage Refinement 318
9.12 Micro-operation Synthesis for March Tests 320
9.13 Scalability and Parallelism Efficiency 329
9.14 Summary 330

Chapter 10: Symbolic Test Language PROVER — Architecture and Micro-operation Synthesis 331

10.1 Historical Background and System Evolution of PROVER 331
10.2 Motivation for a Symbolic Memory Test Language 332
10.3 Semantic Aspects of the PROVER Programming Language 333
10.4 PROVER Language Fundamentals 334

10.5 March Test Decomposition and Address Control 335
10.6 Symbolic Operator Encoding and Compilation 337
10.7 Graph-Based Test Generation via PROVER Scripts 338
10.8 Practical Toolchain and Compiler Flow 341
10.9 Validation and Application 343
10.10 Summary 344

Chapter 11: Graph-Based March Test Decomposition and U–Y Schemes 346

11.1 Motivation for Graph-Based Testing 347
11.2 Formal Definition of the U–Y Scheme 348
11.3 Address Transition Graph (U Component) 350
11.4 Data Operator Sequence Graph (Y Component) 352
11.5 March Test Decomposition with U–Y 354
11.6 Graph Optimization and Parallelization 357
11.7 U–Y-Based Operator Generation 358
11.8 Real-World Use Case: March FD Test Synthesis 361
11.9 Computational Complexity and Real-Time Constraints 362
11.10 Summary 362

Chapter 12: Optimal_Test — Adaptive Optimization for Symbolic Memory Diagnostics 364

12.1 Introduction and Purpose 364
12.2 System Architecture and Integration with PROVER 365
12.3 Key Techniques 367
12.4 Toolchain Implementation 372
12.5 Research Significance and Future Directions 373
12.6 Case Study: Micro-operation Synthesis of the March FD Algorithm 374
12.7 Test Program Synthesis Using the Interpreting System PROVER 396
12.8 Summary 400

Chapter 13: Fuzzy Logic Systems for Test Set Optimization 401

13.1 Motivation for Fuzzy Optimization in Memory Testing 402
13.2 Test Evaluation Framework 402
13.3 Fuzzy Rule Base Design 403
13.4 Foundations of Fuzzy Logic in Diagnostic Test Selection 405
13.5 Expert System Architecture for Test Selection 408
13.6 Sugeno Fuzzy Inference Rule Evaluation 412
13.7 Rule Weight Adjustment 414
13.8 Linear Functions for Test Selection 414
13.9 Test Selection Rule Base 415
13.10 Visualization of Test Suitability 419
13.11 Generalized Metric for Diagnostic Efficiency Using Fuzzy Evaluation 420

13.12 Input Membership Functions 433
13.13 Decision System Architecture 435
13.14 Fault-Class–Specific Optimization 436
13.15 Integration with Symbolic Models and PROVER Scripts 437
13.16 Case Study: Adaptive March FD Pruning 438
13.17 Summary 439

Chapter 14: Adaptive Test Selection Using Coverage and Cost Metrics ... 441

14.1 Problem Statement 442
14.2 Fault–Test Coverage Matrix 443
14.3 Statistical Fault Weighting 444
14.4 Test Cost Estimation 445
14.5 Cost–Coverage Trade-Off and Approximate Test Set Selection 446
14.6 Adaptive Test Scheduling Under Evolving System Conditions 447
14.7 Adaptive Diagnostic Method for Memory Chips 447
14.8 Integration with Fuzzy Inference and PROVER Scripts 453
14.9 Visualization and Diagnostic Output 454
14.10 Summary 455

Chapter 15: Industrial Evaluation and Diagnostic Toolchain Integration 456

15.1 Diagnostic Architecture Overview 456
15.2 Validation via Synthetic and Hardware-Aligned Fault Injection 457
15.3 Integration into MBIST Toolflows 458
15.4 Optimal_Test Software Toolchain 459
15.5 Field Diagnostics and Adaptation 461
15.6 Training and Educational Deployment 462
15.7 Representative Metrics and Benchmark Trends 463
15.8 Translation Layer: From Symbolic Operators to Tester Interfaces 464
15.9 Summary 465

Chapter 16: Test Optimization: Practical Implementation and Experimental Systems 467

16.1 Optimized Test Sequence Selection Based on Prior Test Properties 468
16.2 Method for Evaluating the Efficiency of Memory Diagnostic Systems 492
16.3 Test Selection Using Statistical Data on Rejected Chips 497
16.4 Experimental Optimization Using the Direct Inclusion Method 503
16.5 Fuzzy Rule-Based Selection of Efficient Test Sets 506
16.6 Implementation-Level Verification and Toolchain Validation 511
16.7 Summary of Chapter 16 523

Part V — NVM, MBIST/BISR & Self-Healing

Chapter 17: Testing Non-Volatile Memories (MRAM, PCM, ReRAM, FeRAM) 525

17.1 Overview of Non-Volatile Memory Technologies 526
17.2 Unique Fault Models in Non-Volatile Memories 526
17.3 Challenges in Testing NVM Devices 528
17.4 Recommended Test Strategies per Technology 528
17.5 Integration with Symbolic and Fuzzy Frameworks 529
17.6 Wear-Aware Adaptive Test Selection for NVM 529
17.7 Case Study: ReRAM Endurance Diagnostic 530
17.8 Summary 531

Chapter 18: AI-Augmented Memory Diagnostics and Self-Healing Systems 532

18.1 Motivation: The Limits of Deterministic Diagnostics 532
18.2 Architecture of an AI-Augmented Diagnostic Engine 533
18.3 Learning from ECC and Runtime Logs 534
18.4 Machine Learning Models for Memory Fault Prediction 535
18.5 ECC-Driven Escalation and Policy Engine for Adaptive Repair 535
18.6 Feedback-Driven Test Refinement 536
18.7 Self-Healing Strategies 537
18.8 Case Study: ECC-Guided Healing in DRAM 537
18.9 Outlook: Toward Fully Adaptive Diagnostic Systems 538
18.10 Summary 538

Chapter 19: Research Methodology and Open Problems in Memory Testing 539

19.1 Methodological Framework 539
19.2 Principles of Experimental Design 541
19.3 Toolchain Implementation Recap 542
19.4 Metrics for Evaluation 542
19.5 Open Research Challenges in Memory Diagnostics 544
19.6 Long-Term Vision: Intelligent Diagnostic Frameworks 546
19.7 Summary 547

Back matter

General Conclusions 548

Postscript: Academic Context and Origin of the Research 550

Epilogue 554

Appendices 555
Appendix A: Glossary of Memory and Diagnostic Terms 555
Appendix B: Fault Taxonomies and Standards Context 559
Appendix C: Sample PROVER Programs and Syntax Rules 561
Appendix D: Output Logs and Results from Optimal_Test 562
Appendix E: Fuzzy Rule Base Definitions and Decision Logic 563
Appendix F: Collaborative Research — Architecture for In-Field Recovery 564

References 568

Subject Index 570

LIST OF FIGURES

Chapter 1

Figure 1.1 — Main Types of RAM Microchips 2
Figure 1.2 — Six-Transistor (6T) SRAM Cell 3
Figure 1.3 — Generalized Memory Hierarchy Diagram 6
Figure 1.4 — Conceptual 1T1C DRAM Cell within Differential Bitline Architecture..... 7
Figure 1.5 — Clock/Frequency Ranges Across DRAM Families 8
Figure 1.6 — DRAM Charge Leakage Over Time 9
Figure 1.7 — March Operator Symbol Table 13
Figure 1.8 — Memory Timing Waveform for a Read/Write Cycle..... 15
Figure 1.9 — ECC Syndrome Decoding Example 17
Figure 1.10 — Block Diagram of a Memory Subsystem with Controller and Cache Interface..... 18
Figure 1.11 — Layered Pyramid of Memory Hierarchy from Registers to Cloud 22
Figure 1.12 — Cache Hierarchy with Coherence Management 24
Figure 1.13 — Virtual-to-Physical Address Translation Process 27
Figure 1.14 — Combined DRAM–SCM Interface Model..... 31
Figure 1.15 — CPU–RAM Interaction in a Generic von Neumann Architecture 35
Figure 1.16 — Structural Comparison of SRAM vs DRAM Cells..... 37
Figure 1.17 — RAM Segmentation and Virtual Memory Mapping 39
Figure 1.18 — DRAM Access Timeline with Burst Transfer Overlay 41
Figure 1.19 — Taxonomy of Memory Faults and Detection Mechanisms..... 44
Figure 1.20 — MBIST Architecture with Pattern Generator, Comparator, and Controller 46
Figure 1.21 — Physical vs Logical Memory Integration Across Processor Tiers..... 53
Figure 1.22 — Comparison of SRAM 6T and DRAM 1T1C Cells (Access Paths, Read Destructiveness, and Signal Flow)..... 58
Figure 1.23 — Hierarchical layout of subarray, wordline, and bitline structures..... 60
Figure 1.24 — Timing diagram showing bitline sensing and I/O transition events 62
Figure 1.25 — Statistical distribution of retention times and ECC error margin 66
Figure 1.26 — Bit flipping under thermal acceleration – test chamber results 69
Figure 1.27 — Annotated DRAM timing diagram (read/write/burst access cycles)..... 75
Figure 1.28 — Comparison of Parallel vs Serial Memory Bus Timing and Layout 81
Figure 1.29 — Overview of Memory Interface Standards by Abstraction Level and Protocol Domain 90

Chapter 2

Figure 2.1 — SRAM 6T Cell Diagram with Read/Write Control Paths 96
Figure 2.2 — DRAM Cell Cross-Section and Access Cycle Waveform..... 98
Figure 2.3 — DDR Timing Diagram with Command Sequence 100
Figure 2.4 — HBM 3D Stack Architecture 104
Figure 2.5 — Comparative Internal Structures of Emerging Memory Types 106
Figure 2.6 — Radar Plot Comparing Speed, Volatility, Endurance, Cost, Testability..... 108

Chapter 3

Figure 3.1 — Physical Cause-to-Fault Manifestation Matrix Across Memory Technologies 115
Figure 3.2 — Technology-Specific Fault Fingerprint Diagram 120

Chapter 4

Figure 4.1 — Comparison of Pattern-Based and Address-Structured Tests in Fault Activation Matrix 144
Figure 4.2 — Comparative Execution Structure of Pattern-Based Tests and Address-Ordered March Tests 149
Figure 4.3 — U–Y Hybrid Test Decomposition into Micro-Operation Graph 163
Figure 4.4 — Symbolic Test Compilation Through DDR Command Constraints 174

Chapter 5

Figure 5.1 — Syndrome Distribution Heatmap with Adaptive Test Flow Overlay 190
Figure 5.2 — ECC Test Integration Flowchart with Diagnostic Feedback Loop 197
Figure 5.3 — Drift-Aware ECC Decoding with Dynamic Threshold Calibration 202
Figure 5.4 — Integrated Fault Monitoring and Recovery Pipeline with Feedback Loop. 213

Chapter 6

Figure 6.1 — BISR System Diagram with Detection, Mapping, and Validation Paths ... 221
Figure 6.2 — Redundancy Remapping Types 223
Figure 6.3 — Repair Yield Curve: Before vs. After BISR 225
Figure 6.4 — Runtime Repair Path Flow with ECC Integration and Spare Redirect Logic 234
Figure 6.5 — Fault Containment Layers with ECC, Quarantine, and Redirect Flow 240

Chapter 7

Figure 7.1 — Visual Map of Row and Column Isolation Using Bit Failure Density Overlay 247
Figure 7.2 — Syndrome-Based Fault Decision Flow with Repair and Quarantine Paths 253
Figure 7.3 — Walking Bit Pattern Across a Word and Its Fault Response Heatmap 256
Figure 7.4 — Fault Resolution Timeline Across Levels with Syndrome Correlation Graph 259
Figure 7.5 — Example Fault Table Slice and Corresponding Localization Heatmap 265
Figure 7.6 — Multi-Layer Diagnostic Flow from ECC Syndrome to Physical Fault Origin 272
Figure 7.7 — Layered Fault Tracing in 3D Stacked Memory with TSV-Aware Z-Axis Diagnosis 274
Figure 7.8 — ECC Trend Monitoring and Temporal Diagnostic Events Across Fault Observation Window 276

Figure 7.9 — Failure-to-Root-Cause Diagnostic Flow Integrating Test Outputs, Syndrome Vectors, Mapping Metadata, and Inference Layers 280

Chapter 8

Figure 8.1 — Operator-Based Fault Activation Graph Illustrating Symbolic State Transitions and Node-State Encoding 290

Chapter 9

Figure 9.1 — Structure of the Multi-Head Symbolic Automaton 297
Figure 9.2 — States of the Multi-Head Symbolic Automaton during Cell Scanning with Increasing Address Codes 300
(a) Initial State
(b) Final State
Figure 9.3 — Decomposition of a Non-Square Memory Array into Square Sub-Matrices for Deterministic Test Porting 305
Figure 9.4 — Test Program Porting Process 307
Figure 9.5 — Parallel Diagnostic Test Engine Architecture 311
Figure 9.6 — Temporal–Spatial Fault Heatmap from Synchronized Diagnostic Head Logs 314
Figure 9.7 — Detection of the First Fault 317
Figure 9.8 — Detection of a Second Fault 318
Figure 9.9 — Detection of a Fault of Type j 319
Figure 9.10 — Detection of a Fault of Type m 319
Figure 9.11 — Address Transition Graphs of the MATS++ Test 321
(a) First Operation Cycle
(b) Second Operation Cycle
(c) Third Operation Cycle
Figure 9.12 — Initial Positions of Four Heads Before Starting MATS++ Test Fragments 323
(a) First Operation Cycle
(b) Second Operation Cycle
(c) Third Operation Cycle
Figure 9.13 — Visualization of Simulation Results During the Third MATS++ Cycle ..328

Chapter 10

Figure 10.1 — Graph-Based Aggressor–Victim Test Flow in PROVER 340
Figure 10.2 — PROVER Compiler Flow 342

Chapter 11

Figure 11.1 — U–Y Graph Optimization through Path Folding and Redundancy Elimination 360

Chapter 12

Figure 12.1 — Impact of Optimal_Test Optimization on MT57W2MH8B DRAM Diagnostics 372
Figure 12.2 — Incidence Matrix for the First Step 378
Figure 12.3 — Resulting Micro-Operation Matrices for Step 1 378
Figure 12.4 — Address Transition Graph for the Second Step of the Algorithm 380
Figure 12.5 — Address Transition Graph for the 12th Step of the Algorithm 383
Figure 12.6 — U–Y Scheme of the March FD Test Algorithm 390
Figure 12.7 — Visualization of a Syntactic Error in the MATS++ Test Program 398
Figure 12.8 — Visualization of Errors During MATS++ Test Execution 399

Chapter 13

Figure 13.1 — Membership Functions for Fuzzy Diagnostic Variables 407
Figure 13.2 — Structure of the Expert System 410
Figure 13.3 — Structural Model of Test Selection System Based on the Sugeno Algorithm 417
Figure 13.4 — 3D Surface Plot of Test Suitability vs. Fault Occurrence and Coverage Probabilities 420
Figure 13.5 — Mamdani Fuzzy Inference Structure for Diagnostic Efficiency Evaluation 425
Figure 13.6 — Membership Functions for Output Variable “Efficiency” 426
Figure 13.7 — Rule Formation Diagram for Mamdani Fuzzy Inference System 427
Figure 13.8 — Influence of Detection Probability on Operational Efficiency 430
Figure 13.9 — 3D Fuzzy Inference Surface: GOEM as a Function of Operating Cost and Fault Detection Probability 431
Figure 13.10 — Sample Membership Functions for Coverage and Cost 434
Figure 13.11 — Structural Effect of Fuzzy-Based Pruning on the March FD Symbolic Space (Before/After Pruning) 439

Chapter 14

Figure 14.1 — Dependence of Sample Size on Relative Adaptation Cost 450
Figure 14.2 — Time Savings as a Function of Memory Batch Size 452
Figure 14.3 — Time Savings vs. Diagnostic Sample Size 453

Chapter 16

Figure 16.1 — Venn Diagram of the Distribution of Microcircuit Faults 469
Figure 16.2 — Memory Chip Sorting Process for Diagnostic Evaluation 471
Figure 16.3 — Process of Determining the Diagnostic Properties of Tests 473
Figure 16.4 — Processing Results Based on Input Data at Elevated Supply Voltage 481
Figure 16.5 — Diagnostic Duration of the Optimized Test Sequence under HVcc Conditions 482
Figure 16.6 — Diagnostic Duration of the Intuition-Based Test Sequence 483

Figure 16.7 — Diagnostic Duration Graphs under HVcc 485
Figure 16.8 — Processing Results Based on Input Data at Reduced Supply Voltage (LVcc) 486
Figure 16.9 — Diagnostic Duration of the Optimized Test Sequence under LVcc Conditions 488
Figure 16.10 — Comparison of Cumulative Diagnostic Duration Using Different Test Sets under LVcc 489
Figure 16.11 — Comparison of Total Diagnostic Time 491
1 – Intuition-Based Test Set
2 – Optimized Test Set
3 – Time Savings
Figure 16.12 — Output Files of Optimal_Test Showing Diagnostic Scores and Ranked Test Sequence 499
Figure 16.13 — Modified Input, Buffer, and Output Files of Optimal_Test with Execution Time Penalties 500
Figure 16.14 — Diagnostic Scores and Ranked Test Sequence under Execution Time Constraints 501
Figure 16.15 — Contents of the Diagnostic Result File 504
Figure 16.16 — Input Interface for Optimization Constraints 505
Figure 16.17 — Structural Diagram of the Expert System 506
Figure 16.18 — Rule Base Entry and Modification Process 507
Figure 16.19 — Expert System Output 509
a – Graph of Test Inclusion Suitability vs. Fault Coverage Probability 509
b – Suitability Surface for Test Selection 510
Figure 16.20 — Suitability Curves for Including March-Family Tests vs. Fault Occurrence Probability 511
Figure 16.21 — Stages of Digital System Verification 516
a – Verification of the Memory Chip Model
b – Verification of the Memory Controller Model
c – Verification of the Complete Digital System Model
Figure 16.22 — Toolchain for Designing Test Programs for Verification of Memory Chip Models 518
Figure 16.23 — Procedure for Selecting Tests from the Verification Library 521
Figure 16.24 — Results of Memory Chip Model Verification 522
a – No Errors Detected in the Model
b – Error Detected in the Model

Appendices (B–F)

Figure F.1 — Functional Block Diagram of the Self-Healing Memory Module 565
Figure F.2 — Development Tools for Test Programming and Fault Simulation 566

LIST OF TABLES

Chapter 1

Table 1.1 — Principal Levels of the Memory Hierarchy....21
Table 1.2 — Speed Hierarchy (Representative) 49
Table 1.3 — Indicative Cost Hierarchy 51
Table 1.4 — Interdependence and Design Trade-Offs in Memory System Architectures .54
Table 1.5 — Physical Representation of Binary Logic States Across Memory Technologies 64
Table 1.6 — Physical Bit-Flipping Mechanisms and Technology-Dependent Threshold Effects 67
Table 1.7 — Performance Optimization Strategies and Their Impact on Data Integrity....70
Table 1.8 — Core Performance Metrics for Memory Systems 73
Table 1.9 — Fundamental Timing Parameters in Synchronous DRAM 74
Table 1.10 — Performance Optimization Techniques and Associated Reliability Trade-Offs....78
Table 1.11 — Characteristics of Parallel and Serial Memory Interfaces....81
Table 1.12 — Summary of DDR Memory Protocols and Diagnostic Implications 84
Table 1.13 — Interface-Dependent Fault Activation and Observability Risks 91

Chapter 2

Table 2.1 — Overview of DDR Generations and Key Architectural Features....99
Table 2.2 — LPDDR Standards and Distinguishing Features....102
Table 2.3 — Comparative Summary of RAM Technologies (Volatility, Performance, Density, Cost, Refresh, and Application Domains) 107

Chapter 4

Table 4.1 — Formal Operator Notation for Key March Tests....139
Table 4.2 — Strengths and Limitations of Pattern-Based Testing....143
Table 4.3 — Mapping of Memory Fault Types to Symbolic Operator Logic 161
Table 4.4 — Structural Limitations of Traditional MBIST and Their Diagnostic Implications....168
Table 4.5 — MBIST Challenges Associated with Emerging Non-Volatile Memory Technologies 169

Chapter 5

Table 5.1 — Example Hamming (7,4) Code Words and Syndrome Outcomes 181
Table 5.2 — Syndrome-Driven Diagnostic Techniques....189
Table 5.3 — Comparative Characteristics of Representative ECC Schemes 192
Table 5.4 — Error Characteristics and ECC Challenges in Emerging Memory Technologies 199

Table 5.5 — Memory Scrubbing Types and Typical Use Contexts 206
Table 5.6 — Minimal ECC Log Fields Required for Diagnostic Inference 209

Chapter 6

Table 6.1 — Redundancy Allocation Styles 219
Table 6.2 — Spare Allocation Strategy Summary (Row-First/Column-First and Greedy/Optimal Mapping) 228
Table 6.3 — Yield Recovery versus Spare Allocation 229

Chapter 7

Table 7.1 — Classification of Address Decoder Faults and Diagnostic Implications 245
Table 7.2 — Syndrome-to-Bit Mapping for a (7,4) Hamming Code 251
Table 7.3 — Principal Fault Localization Levels and Representative Use Cases 255
Table 7.4 — Illustrative Fault–Test Activation Matrix (Fault Table) 261
Table 7.5 — Diagnostic Yield and Efficiency Metrics 264
Table 7.6 — Diagnostic Layers and Representative Fault Classes 269
Table 7.7 — Diagnostic Granularity and Preferred Localization Techniques 271

Chapter 8

Table 8.1 — Symbolic State Transition Table for Operator-Based Fault Modeling 286
Table 8.2 — Core Symbolic Operators and Their Semantic Interpretation 287
Table 8.3 — Mapping of Canonical Memory Fault Classes to Symbolic Operator Sequences 293

Chapter 9

Table 9.1 — Correspondence Between Multi-Head Automaton Components and Their Diagnostic Counterparts 303
Table 9.2 — Parameters of Memory Chips for Square Cell Topology 304
Table 9.3 — Parameters of Memory Chips for Non-Square Cell Topologies 304
Table 9.4 — Canonical Test-Selection Tasks Defined Over ⟨T, P, N_tests⟩ 308
Table 9.5 — First Variant of the MATS++ Test Program (No Parallelization) 324
Table 9.6 — Second Variant of the MATS++ Test Program 325
Table 9.7 — Third Variant of the MATS++ Test Program (Parallelization Coefficient = 4) 326

Chapter 10

Table 10.1 — Symbolic-to-Micro-operation Mapping in PROVER 337

Chapter 11

Table 11.1 — Visualization of U–Y Matrix Composition for March FD (Rows: U Transitions; Columns: Y Operators) 356

Chapter 12

Table 12.1 — Operator Sequence Mapping for Operational Processors 393
Table 12.2 — Sequence of Test Operators 394
Table 12.3 — Sequence of Test Operators 395

Chapter 13

Table 13.1 — Functions for Determining the Relevance of Test Selection 415
Table 13.2 — Test Selection Rule Base 416
Table 13.3 — Test Inclusion Suitability Based on Fuzzy Inference 418
Table 13.4 — Comparative Cost Analysis: High-End vs. Low-Cost Testers 423
Table 13.5 — Fuzzy Rule Base for Evaluating Generalized Operational Efficiency (GOEM) Using Mamdani Inference 428

Chapter 14

Table 14.1 — Symbolic Fault–Test Coverage Matrix Representation 443
Table 14.2 — Linguistic Term Sets Used for Fault Manifestation Likelihood and Fault Coverage Likelihood (Inputs to the Fuzzy Rule Base) 443

Chapter 15

Table 15.1 — Illustrative Symbolic Diagnostic Trace Entry 461
Table 15.2 — Representative Diagnostic Metric Trends (Illustrative Evaluation) 463

Chapter 16

Table 16.1 — Memory Chip Fault Detection Across Voltage Levels 469
Table 16.2 — Fault Detection Probability Matrix (Q_h) for 15 Tests at High Supply Voltage (HVcc) 475
Table 16.3 — Fault Detection Probability Matrix (Q_l) for 15 Tests at Reduced Supply Voltage (LVcc) 476
Table 16.4 — Refined Fault Detection Probability Matrix ($Q_{h,s}$) for 11 Tests at High Supply Voltage (HVcc) 478
Table 16.5 — Refined Fault Detection Probability Matrix ($Q_{l,s}$) for 11 Tests at Reduced Supply Voltage (LVcc) 479
Table 16.6 — Statistical Data on the Number of Rejected Memory Chips Across Batches 498
Table 16.7 — Diagnostic Coverage Characteristics of March Tests 508

Chapter 17

Table 17.1 — Representative Non-Volatile Memory Technologies: Storage Principles and Key Attributes 526
Table 17.2 — Recommended Test Strategy Features by NVM Technology 528

Chapter 18

Table 18.1 — Example Feature Set for AI-Driven Diagnostics 534

Chapter 19

Table 19.1 — Metrics for Evaluation of Symbolic and Adaptive Diagnostics..... 543

Appendices (B–F)

Table B.1 — Symbolic Fault Classes 559
Table C.1 — Supported Operators 561
Table D.1 — Symbolic Execution Log Example..... 562
Table D.2 — Fuzzy Scoring Output (Integrated Decision Example) 562
Table E.1 — Rule Examples (Sugeno Inference) 563

Part I — Foundations

Chapter 1: Introduction to Memory Systems and Architectures

1.1 Why Memory Dictates System Behavior

In the architecture of modern computing systems, memory is a critical and defining component. It bridges the gap between high-speed processors and comparatively slower storage systems, acting not only as a passive repository of data but as an active enabler of computation itself. Whether in embedded controllers, high-performance servers, or safety-critical systems, the memory subsystem dictates system responsiveness, reliability, and overall computational throughput.

Random-access memory (RAM) is a core component of computing systems, serving both as an active workspace and as a data repository. The term "random access" denotes the ability to retrieve or store data at any location without sequential traversal.
Historically, advancements in memory technology have not kept pace with the explosive progress of processors, graphics, and audio systems. While there were incremental improvements—reduced access times, integrated on-chip caches, and pipelined requests—the underlying manufacturing and device technologies advanced more slowly. This disparity created a critical bottleneck—the memory wall—where overall performance is limited by the slowest component.

The late 1990s marked a technological renaissance in RAM, introducing innovations such as **FPM RAM, EDO RAM, SDRAM, DDR SDRAM, ESDRAM, SLDRAM, and RDRAM**. Among these, only a subset achieved widespread deployment in system memory, while others found niche applications in graphics subsystems.

Random access memory has therefore become one of the most critical determinants of overall system performance. While processor architectures continue to evolve toward higher levels of parallelism and computational throughput, the ability of memory systems to supply data with minimal latency remains a fundamental constraint. As a result, the study of memory architectures must consider not only capacity and speed, but also the structural organization, access patterns, and interaction between memory and processing elements. Understanding these relationships provides the foundation for analyzing how memory technologies influence the design, efficiency, and reliability of modern digital systems.

In practical system design, memory performance is evaluated not only in terms of raw capacity but also in terms of latency, bandwidth, and access efficiency. These factors determine how effectively processors can sustain computation without idle waiting for data. As computing workloads become increasingly data-intensive, the efficiency of the memory subsystem becomes a central factor in overall system performance. These considerations motivate the structured organization of memory resources that will be discussed in the following section.

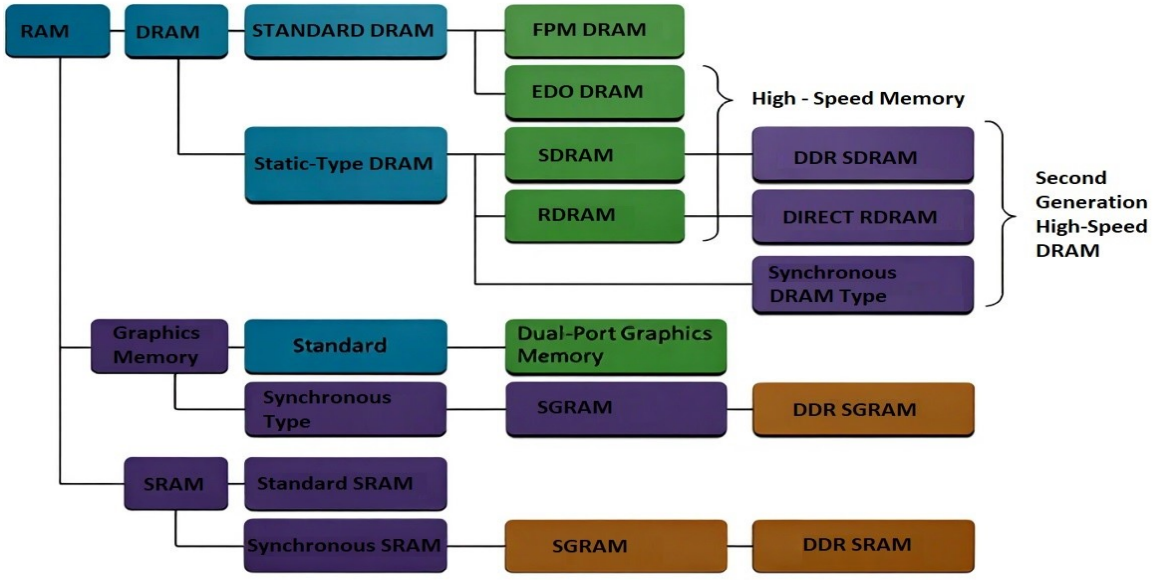

Figure 1.1—Main Types of RAM Microchips

Hierarchy of RAM technologies, including SRAM and DRAM, with subtypes such as EDO DRAM, SDRAM, DDR SDRAM, and RDRAM. The diagram highlights the evolution and diversification of memory architectures across system and graphics applications.

This hierarchical classification provides a conceptual framework for understanding how successive generations of memory technologies emerged in response to increasing performance demands. It also illustrates how architectural refinements and interface innovations gradually expanded the role of RAM within complex computing systems. Consequently, examining the historical progression of these technologies helps clarify both their functional distinctions and their impact on system-level memory organization.

As semiconductor technologies advanced, memory systems evolved in complexity and capacity. From early SRAM to today's DRAM, DDR families, and emerging non-volatile memories (NVMs), each generation introduced innovations alongside new fault mechanisms and reliability challenges. Increasing integration density, multi-gigabit arrays, and 3D stacking amplified susceptibility to manufacturing defects, retention failures, soft errors, and aging-related degradation.

To address inherent signal delays in DRAM modules, manufacturers introduced small on-die SRAM caches. Enhanced SDRAM (ESDRAM) from Ramtron International is a notable example, achieving burst operation speeds up to ~200 MHz by combining SDRAM with minimal SRAM caching. Similarly, SynchLink DRAM (SLDRAM) and Rambus DRAM (RDRAM) pushed performance with advanced bus protocols and double-data-rate signaling; SLDRAM's open standard reduced licensing barriers, while RDRAM reached effective transfer rates around ~800 MHz via dual-edge clocking.

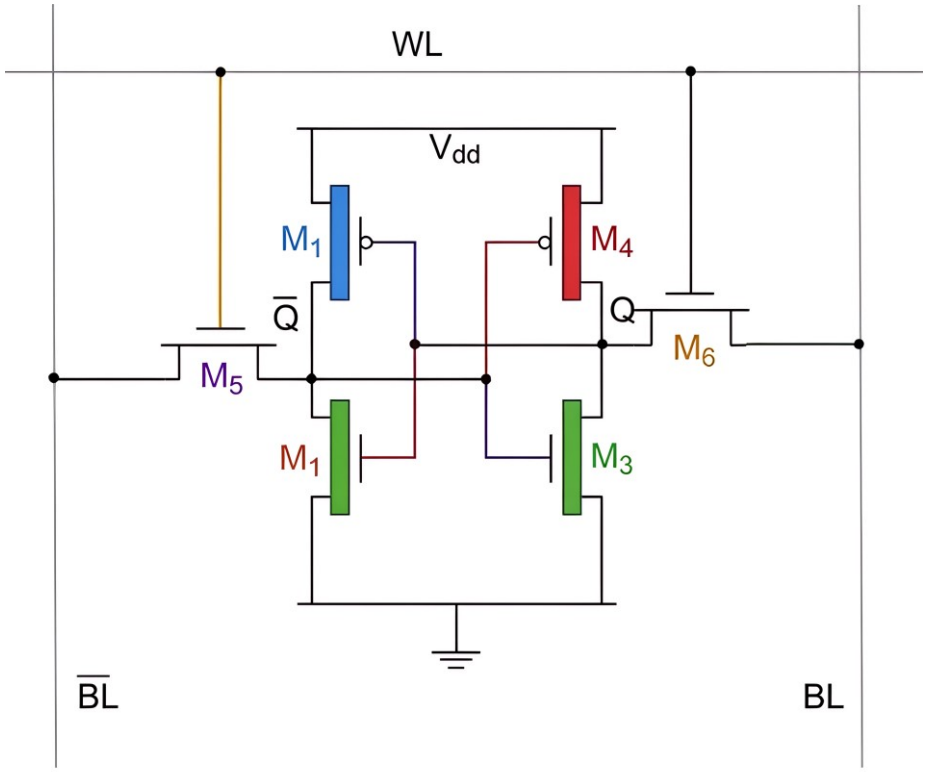

Figure 1.2—Six-Transistor (6T) SRAM Cell

Schematic representation of a **volatile** SRAM cell: two cross-coupled inverters plus access transistors form a bistable latch enabling high-speed, non-destructive reads—ideal for cache subsystems.

This escalating complexity underscores the necessity of robust **memory testing, diagnostics, and fault-tolerance** strategies. Such strategies must address diverse fault models, balance test efficiency against production constraints, and increasingly incorporate **self-healing** mechanisms to sustain operability in the presence of multiple simultaneous faults. In this context, the work presented in this book seeks to **unify theoretical foundations and practical diagnostic tools** for comprehensive memory testing.

1.1.1 Research Foundations and Dissertation Context

The diagnostic methodologies explored in this book are rooted in research conducted between **2005 and 2009** at **Cherkasy State Technological University** and defended as a doctoral dissertation at the **National Technical University "Kharkiv Polytechnic Institute."**

This research addressed critical challenges in semiconductor memory testing, including:

- The exponential growth of memory capacity and speed leading to increased fault rates.
- The absence of scalable, automated tools for generating, optimizing, and executing diagnostic test sequences.
- The necessity of adaptive techniques capable of addressing diverse fault types under production and operational constraints.

To meet these challenges, the following contributions were developed:

- **PROVER** — a symbolic programming and simulation environment for memory test synthesis, enabling scalable and parallel diagnostic approaches.
- **Optimal_Test** — an adaptive optimization system for selecting efficient test sets based on fault coverage and resource constraints.
- **Operator-based fault modeling and U–Y graph schemes** for optimizing test decomposition.
- **Fuzzy-logic systems** for test sequence optimization, incorporating expert knowledge into algorithmic frameworks.

These efforts were carried out under state research projects and industrial collaborations, notably:

- "**Models and Algorithms of Automated Control Systems for Adaptive Packaging Machines**" (State Registration No. **0108U000507**).
- **Cooperation Agreement No. 16-d** between ChSTU and the enterprise **"Diava"** for developing diagnostic technologies.

The practical impact included:

- Reducing diagnostic time and labor for high-speed memory devices.
- Enhancing fault localization and **self-healing** capabilities in memory systems.
- Providing methodologies adopted in academic programs at **ChSTU** and **Odessa National Polytechnic University**.

A complete account of the dissertation—its scientific novelty, practical significance, and related publications—appears in the Postscript: Academic Context and Origin of the Research. These foundations form the intellectual backbone of the tools, models, and architectures presented in this book.

1.1.2 Diagnostic Tools Introduced

The diagnostic methodologies of this book are anchored in two tools that form the backbone of the proposed testing and fault-analysis framework:

- **PROVER:** A symbolic test-synthesis and simulation environment designed to model and generate **micro-operation-level** test sequences for memory devices. By employing symbolic operators, PROVER enables scalable, abstract construction of memory test patterns adaptable to a wide range of memory architectures and fault models.
- **Optimal_Test:** An adaptive optimization engine that evaluates test effectiveness in terms of **fault coverage**, **diagnostic resolution**, and **resource efficiency**. It performs symbolic sequence compression, ranks test vectors based on multiple criteria, and selects **Pareto-optimal** test sets suitable for specific memory structures and operational constraints.

Originally conceived during research collaborations at Cherkasy State Technological University, these tools have since evolved into a unified diagnostic framework. The foundational symbolic modeling and U–Y–based test decomposition are introduced in

Chapters 8 and 11, while their integration into adaptive, multi-objective, and fuzzy-inference-based diagnostic planning is explored in Chapters 12–15.

1.1.3 The Central Role of Memory in Digital Systems

In modern digital architectures**,** memory is far more than a passive repository—it is a pivotal, performance-defining subsystem that mediates virtually all computation. As the primary interface between processors and executable data, the memory subsystem determines whether a system executes correctly, efficiently, and within real-time constraints.

A processor's pipeline—from instruction fetch to final commit—relies on **deterministic, precise, low-latency** memory access. The memory subsystem sustains the fetch–decode–execute cycle: retrieving instructions and operands, supporting intermediate computation, and committing results back to storage.

Accordingly, memory is responsible not only for transient data persistence during active computation, but also for shaping **responsiveness, energy efficiency, and architectural scalability**. From embedded microcontrollers to supercomputers, nearly every non-trivial workload—numerical, symbolic, multimedia, or AI-centric—exhibits some degree of **memory-bound** behavior.

The memory subsystem directly impacts several critical properties:

- **Computational determinism.** Access latency and latency variability (jitter) bound real-time schedulability and predictability.
- **System stability.** Ineffective memory management can induce cache thrashing, deadlocks, and access faults, producing unstable execution states.
- **Performance bottlenecks.** In many high-throughput workloads, memory latency—not core frequency—is the principal limiter.
- **Energy consumption.** In mobile/IoT/embedded platforms, memory interfaces and arrays account for a substantial fraction of dynamic power.

Given these factors, memory must be treated as a **first-class design concern** at every abstraction level—from device physics and circuit topology, through firmware-level controller logic and OS memory managers, to compiler memory models and application data structures.

Consequently, the architecture of modern computing systems cannot be understood without a careful examination of memory organization and behavior. The interaction between processors, caches, and main memory forms the operational backbone of digital computation, shaping both system efficiency and reliability. For this reason, a detailed understanding of memory structures and technologies is essential before exploring the specific fault mechanisms and diagnostic techniques addressed in subsequent chapters.

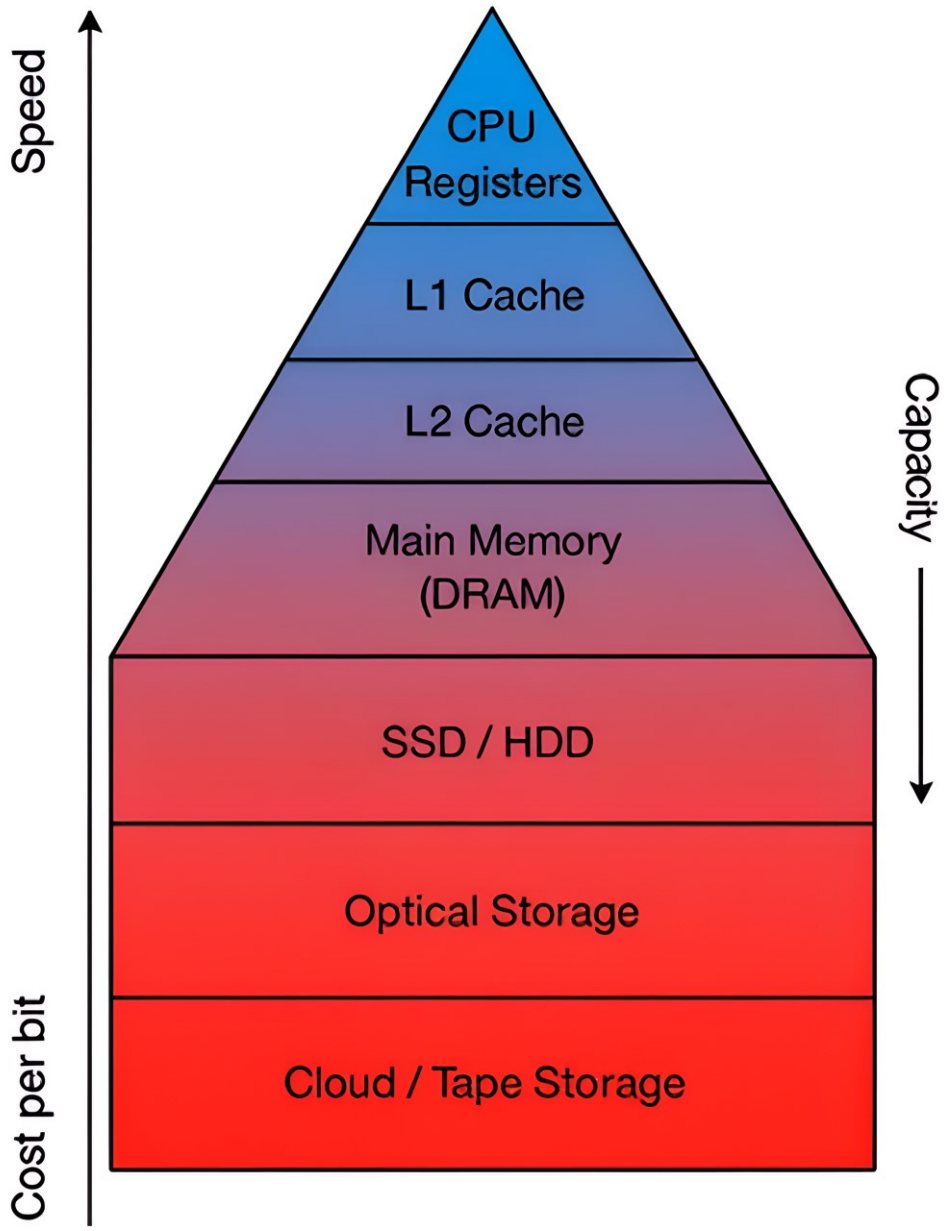

Figure 1.3—Generalized Memory Hierarchy Diagram

Canonical performance–cost–capacity "pyramid.

Apex: CPU registers (lowest latency, highest cost/bit, minimal capacity).

Intermediate tiers: L1/L2 caches and main memory (DRAM) balance speed and capacity via hierarchical buffering, burst transfers, and bank-level parallelism.

Lower tiers: Persistent layers (SSD/HDD/optical/cloud) offer orders-of-magnitude capacity at increased latency and reduced bandwidth.

Design implication: Locality (temporal/spatial) motivates multi-tier organizations that minimize effective latency and maximize throughput.

1.1.4 Evolution of Memory Technologies

The evolution of memory closely mirrors the trajectory of computing—each epoch addressing the limits of its predecessor across four intertwined dimensions: **density, access speed, power, and reliability**.

1940s–1950s — Delay lines & Williams–Kilburn tubes.

Mercury delay lines stored acoustic pulses; Williams tubes used electrostatic charge patterns on CRT phosphors. Pioneering yet fragile and slow, they served early machines (e.g., EDSAC, UNIVAC), establishing conceptual ground for random access.

1950s–1970s — Magnetic core memory.

Each bit resided in a ferrite toroid magnetized clockwise/counterclockwise. Core memory was non-volatile, robust, and reliable; it dominated mainframes and early minicomputers (IBM/DEC). The legacy persists in terms like "core dump."

1970s–1990s — Semiconductor RAM (SRAM & DRAM).

- **SRAM (6T).** Extremely low latency and high speed; lower density and higher cost; ideal for caches and performance-critical buffers.
- **DRAM (1T1C).** Orders-of-magnitude density scaling enabled by the one-transistor/one-capacitor structure, at the cost of periodic refresh due to charge leakage. Its cost-per-bit advantage drove widespread adoption from early microcomputers to high-performance workstations.

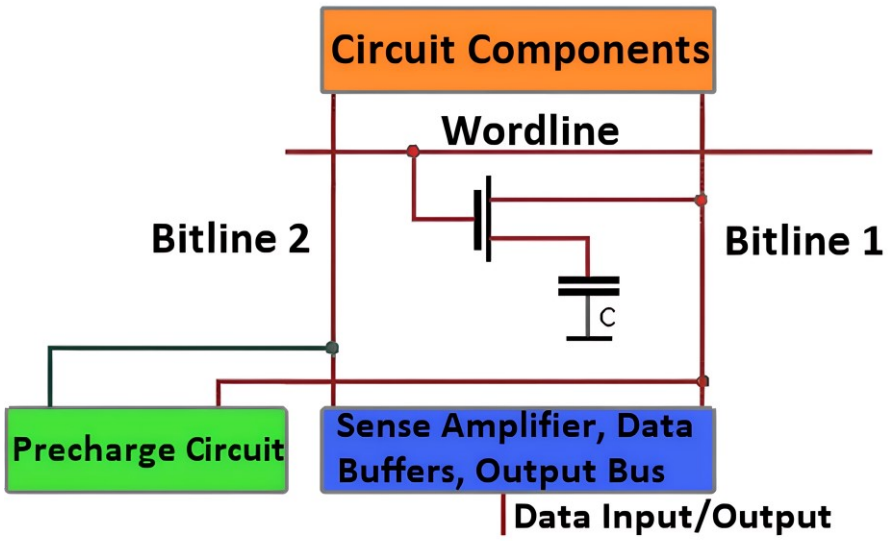

Figure 1.4— Conceptual 1T1C DRAM Cell within Differential Bitline Architecture

The 1T1C DRAM cell stores information as charge on a storage capacitor, accessed through a wordline-controlled pass transistor. During activation, the wordline enables charge sharing between the capacitor and the associated bitline. Differential sensing against a complementary

bitline pair allows reliable detection of small voltage perturbations. Precharge circuitry equalizes the bitlines prior to each access cycle.

1990s–2000s — SDRAM and DDR families.

Synchronous operation aligned transfers to the clock and enabled bursts; **DDR** doubled effective throughput via dual-edge sampling. Hybrids appeared: **ESDRAM** integrated small on-die SRAM caches for ~200 MHz bursts; **SLDRAM** (open interface) and **RDRAM** (dual-edge protocols) pushed interface speeds (RDRAM ~800 MHz effective).

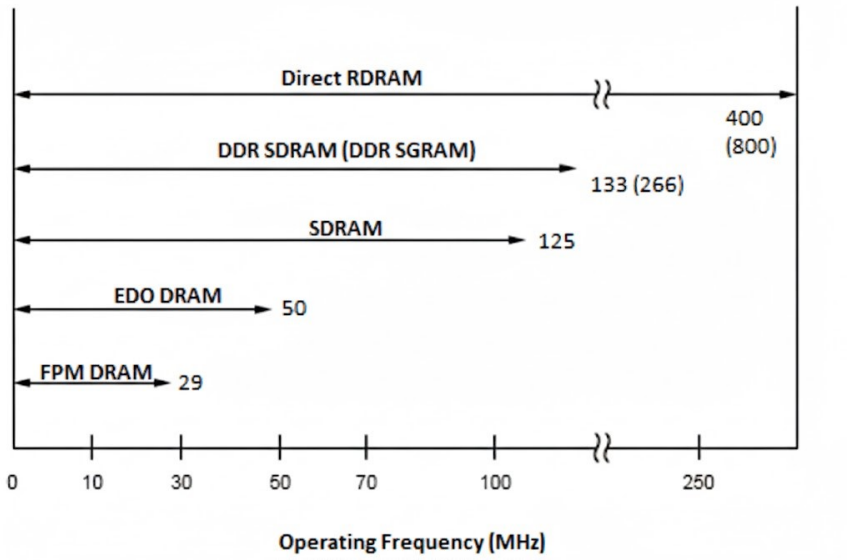

Figure 1.5—Clock/Frequency Ranges Across DRAM Families

Progression from FPM→EDO→SDRAM→DDR/Direct RDRAM with corresponding bandwidth gains.

Present & Emerging — Non-Volatile Memory (NVM) candidates.

- **MRAM.** Magnetic tunnel junctions; speed and endurance.
- **ReRAM.** Programmable resistive states in dielectrics.
- **PCM.** Phase change in chalcogenides encodes bits.
- **FeRAM.** Reversible ferroelectric polarization for fast, low-power writes.

These promise persistence, low leakage, and high endurance—but introduce fresh challenges in **fault modeling, retention characterization, read-disturb mitigation,** and **legacy interface compatibility**.

Impact on testing and diagnostics.

Each technological shift demands new fault activation and observation strategies, more sophisticated error control mechanisms, and higher-level symbolic diagnostic tools. These developments are addressed through classical and graph-based test algorithms (March, Checkerboard, GalPat) and coverage analysis in **Chapters 4 and 11**, error detection and correction mechanisms in **Chapter 5**, symbolic modeling and test representation frameworks in **Chapters 8–11** (operators, PROVER, and U–Y schemes), and adaptive optimization and

scheduling techniques implemented through **Optimal_Test and fuzzy inference in Chapters 12-15**.

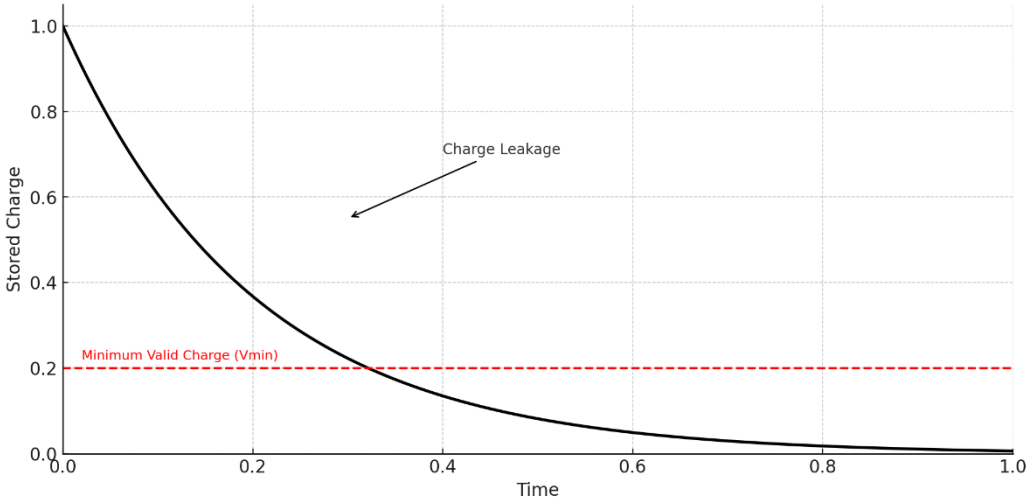

Figure 1.6—DRAM Charge Leakage Over Time

Exponential decay from an initial "1" toward the minimum readable threshold $\boldsymbol{V_{min}}$ due to subthreshold conduction, gate-oxide tunneling, and junction leakage. Once below $\boldsymbol{V_{min}}$, the bit is no longer reliably readable as "1," necessitating periodic refresh (typically 32–64 ms).

Diagnostic relevance:

- Retention/soft-error fault models.
- Adaptive refresh scheduling.
- Error rates under low-voltage/high-temperature corners.

This behavior motivates stronger ECC and symbolic fault models treated in later chapters.

1.1.5 Memory Subsystem Design Goals and Trade-offs

Designing memory is a multi-objective optimization across performance, energy, reliability, and cost. Key trade-off axes include:

Latency vs. bandwidth

- **Latency:** time from request to first data; critical for stall avoidance and real-time response.
- **Bandwidth:** aggregate transfer rate; crucial for vector/GPU/parallel workloads.

Wide buses, interleaving, and bank parallelism boost bandwidth but may add coordination overhead; **SRAM** minimizes latency but lacks density/scale.

Volatility vs. retention

- **Volatile (SRAM/DRAM):** fast, fine-grained access but requires power to preserve state.
- **Non-volatile (Flash/ReRAM/MRAM):** retains state without power; trade-offs in write latency, endurance, and sometimes read throughput.

Implications for boot time, persistence strategies, and power-fail resilience (especially embedded/mobile).

Power vs. performance

- **LPDDR/eDRAM** reduce energy; **DDR5/GDDR/HBM** drive throughput at higher energy-per-bit and thermal load.
- Dynamic management (DVFS, clock gating, selective refresh) balances energy and performance under runtime constraints.

Cost vs. capacity

- **SRAM:** best latency, highest cost/bit—unsuitable for large stores.
- **DRAM:** main-memory sweet spot; volatility limits persistence.
- **NAND Flash:** high capacity and low cost/GB for secondary storage; endurance and random-access limits must be engineered around.
- **Hybrids:** architected stacks (SRAM→DRAM→Flash) optimize application-specific objectives.

Density vs. reliability

- Scaling raises variability, thermal non-uniformity, disturb, and retention failures.
- Advanced nodes (sub-10 nm DRAM; 3D NAND) require **ECC**, spare rows/columns, and adaptive refresh.
- Both **soft-error rates** and **hard-fault probabilities** must be quantified, especially for mission-critical/rad-hard designs.

Speed vs. interface complexity

- High-speed PHYs (GDDR/HBM) need precise calibration, deep prefetch, burst sequencing, and link training.
- Even DDR demands multiphase clocking, controlled terminations, and on-die error tracking, increasing controller complexity and post-silicon validation effort.
- In embedded/real-time systems, designers may favor simpler interfaces to reduce verification and maintenance risk.

Hierarchical mitigation strategies

Multi-tier hierarchies assign roles by latency, bandwidth, energy, and proximity: registers/L1/L2 at the top, DRAM for working sets, and persistent tiers for capacity. Later chapters show how diagnostics and testing adapt to these choices to maintain fault resilience without compromising performance (see **Chs. 4–7** for diagnostic foundations, **Chapter 17** for persistent-memory implications, and **Chs. 18–19** for adaptive and future diagnostic frameworks).

1.1.6 Memory Abstraction and Operational Semantics

At its most fundamental level, a digital memory system can be represented as a finite mathematical function that maps each addressable location to a stored binary value. This

abstraction enables rigorous reasoning and symbolic manipulation of memory operations in both theoretical analysis and practical diagnostic frameworks.

Let the **address space** be defined as:

$$A = \{0, 1, 2, \ldots, 2^n - 1\}$$

where n denotes the width of the address bus.

Let the data space be:

$$D = \{0,1\}^k$$

where k is the word size in bits.

The memory subsystem is thus modeled as a deterministic mapping:

$$M : A \rightarrow D$$

where each address $a \in A$ corresponds to exactly one stored word $d \in D$.

Within this model, three primitive operations are sufficient to describe memory behavior. This abstraction represents the ideal functional behavior of the memory and serves as a baseline upon which fault models, probabilistic effects, and corrective mechanisms are introduced in later chapters.

Write operation

A write operation updates the contents of a specific address:

$$M[a] \leftarrow d \quad denoted\ as \quad W(a, d)$$

The write operation produces a new memory state M', identical to M for all addresses except the target address a

$$M'(a) = d\ and\ M'(x) = M(x)\ for\ all\ x \neq a.$$

Read operation

A read operation retrieves the stored word at a given address:

$$d \leftarrow M[a] \quad denoted\ as \quad R(a)$$

This operation does not modify the memory state.

Verify operation

A verify operation compares the stored value against a reference:

$$M[a] \stackrel{?}{=} d_{\text{ref}} \quad denoted\ as \quad A(a, d_{\text{ref}})$$

The operation evaluates whether the value at address a matches the reference value d_{ref}, returning a Boolean result.

This functional abstraction forms the basis for symbolic testing, algorithmic fault modeling, and formal verification frameworks developed throughout this book. In later chapters, these

operations are extended to incorporate concurrent access, pipelined execution, timing constraints, and error-detection and correction semantics.

1.1.7 Symbolic Operation Sequences

The primitive memory operations—write, read, and verify—serve as the foundational elements for constructing more elaborate symbolic test sequences. These sequences are central to modern memory testing methodologies, particularly in March algorithms, fault modeling, and Built-In Self-Test (BIST) frameworks.

A symbolic operation script defines a deterministic series of actions to be performed over one or more memory addresses, with traversal orders that may be increasing, decreasing, or arbitrary. Such sequences are interpreted by the **PROVER interpreting system**, which can also incorporate auxiliary operators to enhance fault coverage, including:

WAIT – inserts controlled delays for retention or disturb fault analysis.
COMPARE – evaluates retrieved data against a reference pattern, logging discrepancies in a fault map.
INVERT – applies bitwise inversion to a pattern before storage, facilitating coupling-fault and pattern-sensitivity testing.

Example — Simple symbolic test segment

$$W_{(0)} \rightarrow R_{(0)} \rightarrow W_{(1)} \rightarrow R_{(1)}$$

This sequence writes to and reads from consecutive memory locations, with each operation targeting a unique address in ascending order. It represents a basic March element—a core component of many algorithmic test strategies—capable of detecting:

- **Stuck-at faults** – cells that remain fixed at logic '0' or '1' regardless of write attempts.
- **Transition faults** – cells unable to change state from '0→1' or '1→0'.
- **Coupling faults** – cells whose state is influenced by operations on adjacent locations.

In later chapters, these symbolic constructs are expanded into multi-phase March algorithms with address-direction reversals, data-pattern variations, and fault-specific targeting to achieve maximal diagnostic resolution.

1.1.8 Diagnostic and Theoretical Utility

The symbolic framework for representing memory operations is not merely a notational convenience—it is a formal abstraction layer that underpins the design, synthesis, and execution of memory test algorithms.

By expressing operations in symbolic form, test strategies can be composed, analyzed, and optimized independently of the underlying physical memory implementation, making them inherently portable across architectures and technologies.

This abstraction is fundamental to the tools developed in this work, including **PROVER** and **Optimal_Test**, enabling flexible, scalable, and architecture-agnostic test generation.

Core Functions of the Symbolic Testing Framework

- **Formal Fault Modeling** – Enables rigorous mathematical reasoning about memory behavior under various fault classes, including stuck-at, transition, coupling, and retention faults.
- **Address/Data Pattern Generalization** – Decouples test descriptions from specific architectures by abstracting address traversal and data injection semantics, supporting both regular and irregular layouts.
- **Test Coverage Analysis** – Allows symbolic sequences to be mapped to specific fault activation sets, facilitating precise computation of diagnostic coverage, redundancy indices, and efficiency metrics.
- **Toolchain Integration** – Serves as the primary input format for test expansion, compression, simulation, and optimization within **PROVER** and **Optimal_Test**, supporting runtime adaptation and multi-objective (Pareto) optimization strategies.

By maintaining a symbolic representation throughout the diagnostic pipeline, the framework ensures that test algorithms remain both theoretically analyzable and practically executable across diverse memory technologies.

March Symbol	Meaning
⇑	The address increment command
⇓	The address decrement command
⇕	The address order can be in any direction
W	The write operation
R	The read operation
1	The test data is 1
0	The test data is 0

Figure 1.7—March Operator Symbol Table

The symbols in Figure 1.7 define the universal vocabulary for constructing March-based memory test algorithms used throughout this work. They provide a formal, algebraic notation for encoding memory operations, enabling both manual specification and automated synthesis within symbolic diagnostic environments.

This standardized operator set is applied extensively in later chapters, including:

a. Chapter 8 — Operator-Based Fault Modeling
b. Chapter 10 — Symbolic Test Language PROVER: Architecture and micro-operation synthesis
c. Chapter 11 — Graph-Based March Test Decomposition and U–Y Schemes

1.1.9 Memory Timing, Synchronization, and Refresh Mechanisms

Efficient and reliable memory access depends on precise coordination among address, data, and control signals. Each memory technology imposes distinct timing constraints, and modern architectures require multi-phase synchronization, pipelined access sequencing, and refresh-aware scheduling to sustain performance and reliability.

Key Timing Parameters

Memory timing specifications are expressed in nanoseconds or clock cycles, with the most critical parameters including:

- t_{access}– delay between address presentation and valid data availability
- t_{cycle}– minimum allowable time between consecutive accesses
- t_{RC} **(Row Cycle)** – total time to precharge and reactivate the same row in DRAM
- t_{RCD}**,** t_{CAS}**,** t_{RAS}– row-to-column delay, column access strobe latency, and row active strobe time, respectively

DRAM Refresh and Access Conflict

Unlike SRAM, DRAM cells require periodic refresh to restore the charge stored in their capacitors. A standard refresh interval is approximately **64 ms**. Refresh operations compete with read/write requests, introducing latency variability and reducing effective bandwidth. Memory controllers mitigate this by coordinating refresh counters with burst scheduling logic, ensuring refresh compliance without excessive access stalls.

Clock Synchronization and Controller Coordination

In synchronous memory systems (e.g., SDRAM, DDR, LPDDR), all transactions align with a global clock signal. Controller design must address:

- Clock skew and jitter compensation
- Use of delay-locked loops (DLLs) for precise phase alignment
- Metastability prevention in clock domain crossings
- Command pipelining and signal staging to sustain throughput at high operating frequencies

These timing relationships form the operational framework through which memory controllers coordinate access to large-scale memory arrays. Accurate timing enforcement ensures that row activation, column access, and precharge operations occur without violating electrical or architectural constraints.

As memory frequencies increase and architectures adopt deeper pipelines and wider buses, precise timing management becomes increasingly critical for both performance and stability. Consequently, understanding timing parameters and synchronization mechanisms is essential for analyzing memory behavior and for designing reliable diagnostic and testing strategies.

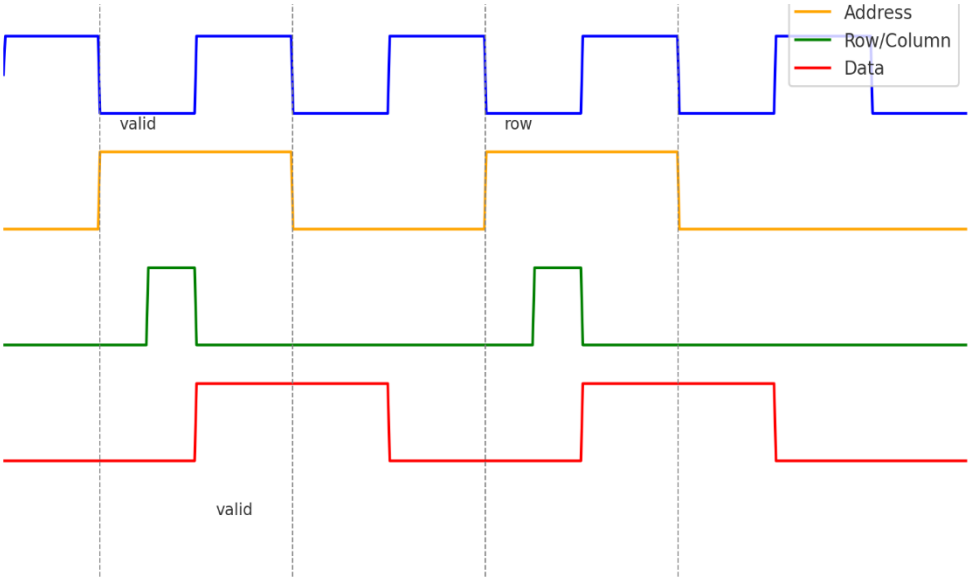

Figure 1.8—Memory timing waveform for a read/write cycle.

This timing diagram illustrates the principal control and data signal transitions during a typical synchronous memory access cycle, representative of SDRAM and DDR-class technologies.

- **Clock** – serves as the global synchronization reference, with all address and data events aligned to specific rising or falling edges.
- **Address** – becomes valid during designated clock intervals, at which point the row or column address is latched into the memory device.
- **Row/Column Strobes (RAS/CAS)** – control signals that initiate either a row activation or a column access, directing the DRAM's internal circuitry to the correct bitline and sense amplifier.
- **Data** – asserted only after the appropriate setup delay (e.g., t_{RCD}, t_{CAS}) has elapsed. The diagram highlights the valid data window following the address and strobe events.

Vertical dashed lines indicate critical timing boundaries, showing:

- When the address becomes stable and latchable
- When row/column strobe events occur
- When valid data is available for read or write operations.

Although simplified, this diagram captures the essential timing relationships needed to understand memory protocol operation. Mastery of such waveforms is crucial for diagnosing timing-related failures, identifying protocol violations, verifying controller alignment, and generating accurate symbolic or algorithmic test vectors for diagnostic analysis.

1.1.10 Diagnostic Relevance of Memory Architecture

Effective memory diagnostics require more than algorithmic fault coverage—they demand an in-depth understanding of the physical and architectural structure of memory subsystems. Architectural awareness enables diagnostic tools to correlate fault symptoms with their underlying mechanisms and physical layout, leading to more precise fault localization and targeted test synthesis. Key architectural elements influencing diagnostic design include:

Bitline and Wordline Organization

In DRAM and SRAM arrays, vertical bit-lines and horizontal word-lines define the cell addressing grid. Parasitic capacitance, line resistance, and electromagnetic coupling can induce crosstalk, resulting in coupling faults or retention degradation. Targeted aggressor–victim activation patterns are essential to reveal such layout-induced defects.

Sense Amplifiers and Charge Sharing

During a read cycle, minute voltage differentials on bit-lines are amplified by sense amplifiers. At advanced nodes (sub-20 nm), architectural asymmetries can produce read disturb, bias, or charge-sharing effects, leading to direction-dependent fault behavior where a cell's response varies with access history or neighboring line state.

Redundancy Logic (Spare Rows and Columns)

Modern arrays employ spare rows and columns activated during manufacturing test to repair defective cells. While this boosts yield, it creates diagnostic blind spots:

- Permanent masking of certain faults by address remapping
- Latent or marginal defects within redundant paths
- Need for remap tracing, address mirroring, or forced fault injection to validate redundancy integrity under stress conditions

Error-Correcting Code (ECC) Integration

ECC schemes alter observable fault behavior:

- Single-bit faults in SECDED-protected words may be auto-corrected and remain invisible unless explicitly tested
- Multi-bit faults may be partially masked or misclassified depending on the ECC code structure
- Diagnostic workflows must generate and analyze ECC syndromes, track parity failures, and apply algebraic decoding to reconstruct physical fault locations

Access Granularity and Bus Width

Wider data paths (e.g., 64-bit, 128-bit) increase susceptibility to burst-mode coupling, inter-line interference, and multi-bit faults spanning multiple banks or chips. Fine-grained activation masks, pattern rotations, and chip-select isolation are necessary to pinpoint errors within specific subwords or interface lines.

Architectural Implications for Diagnostic Design

These features shape all stages of diagnostic methodology:

- Formulation of accurate fault models (stuck-at, transition, coupling, bridging, retention)
- Determination of error visibility, latency, and masking conditions
- Definition of coverage metrics and completeness guarantees
- Interpretation of syndrome patterns in relation to physical layout

The diagnostic tools presented in this book—particularly **PROVER** and **Optimal_Test**—integrate architectural metadata into symbolic modeling, enabling structure-aware diagnostics that surpass traditional black-box approaches. This architectural grounding ensures that test outcomes are both accurate and interpretable, a critical requirement for field-deployable and adaptive diagnostic frameworks.

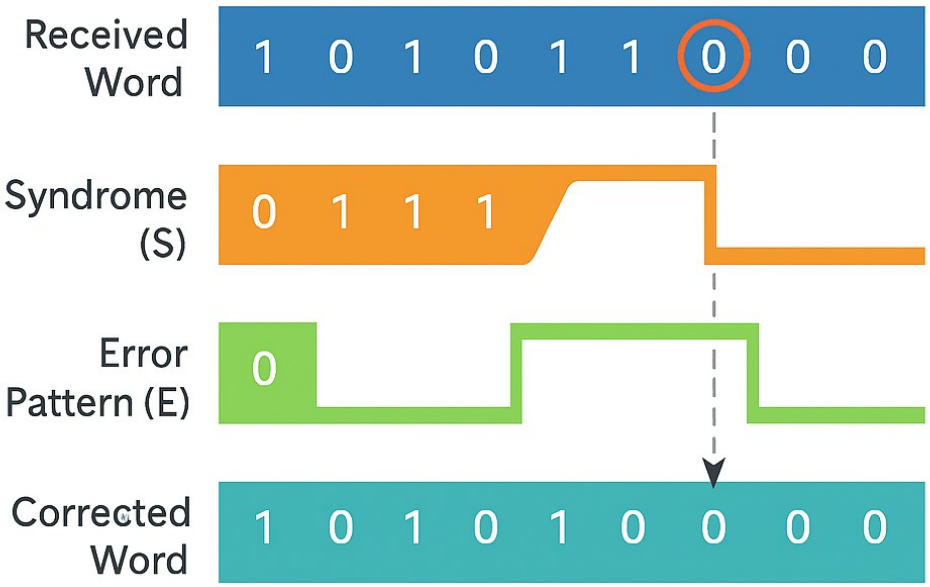

Figure 1.9—ECC syndrome decoding example.

This Figure illustrates the internal process of single-bit error correction using a syndrome-based ECC algorithm, such as Hamming SEC (Single Error Correction) or SECDED (Single Error Correction, Double Error Detection).

- **Received Word (*r*)** – a binary word retrieved from memory, containing a single erroneous bit (circled), which may result from transient radiation effects, retention loss, or coupling-induced disturbances.
- **Syndrome (S)** – computed by applying the parity-check matrix *H* to the received word. The resulting binary vector uniquely identifies the index of the faulty bit.
- **Error Pattern (*e*)** – a binary mask generated from the syndrome, with a '1' in the bit position indicated by *S* and '0' elsewhere.
- **Correction Step** – a bitwise XOR between the Received Word and Error Pattern flips the erroneous bit, yielding the **Corrected Word**, which restores the intended data value.

This mechanism underpins most real-time ECC engines in DRAM, SRAM, and non-volatile memory systems. It is critical for mitigating soft errors in high-density technologies, where bit-level faults can arise from cosmic rays, voltage drift, or aggressive process scaling.

Beyond correction, the syndrome vector provides explicit fault localization, enabling deeper symbolic diagnostics and architectural fault tracing, as introduced in **Chapter 5** and further exploited in **Chapters 8–11**.

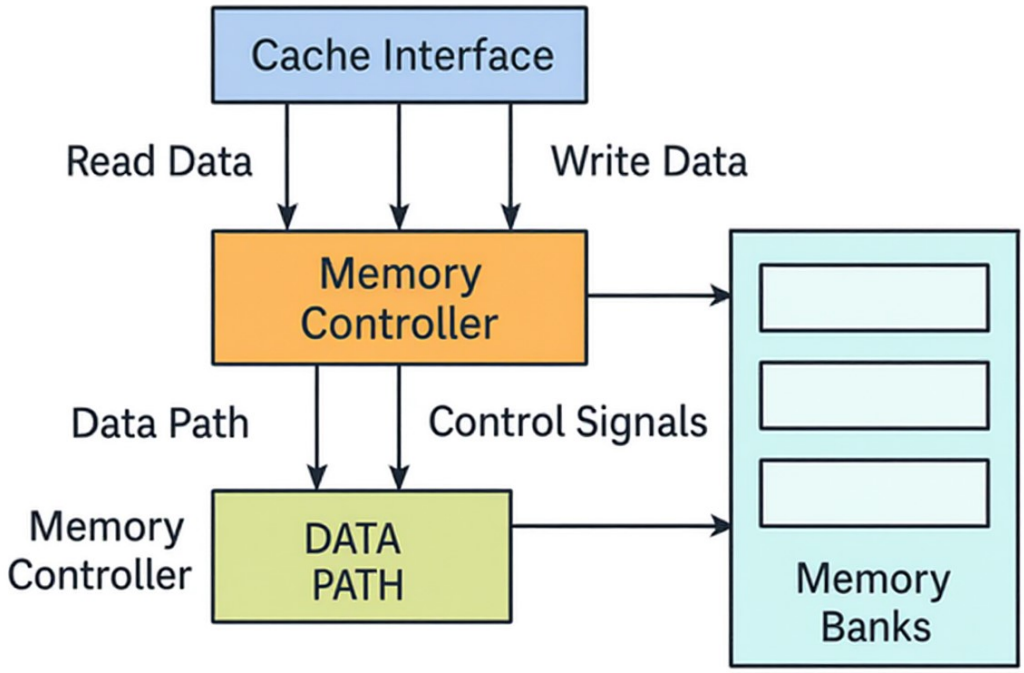

Figure 1.10—Block diagram of a memory subsystem with controller and cache interface.

This diagram depicts a representative digital memory subsystem architecture, emphasizing the interaction among the Cache Interface, Memory Controller, Data Path, and Memory Banks.

- **Read Data** and **Write Data** signals traverse vertically between the cache and memory controller, enabling bidirectional transfers for both instruction and data transactions.
- The **Memory Controller** acts as the central orchestrator, managing command sequencing, address decoding, and control signal generation while directing data flow.
- A dedicated **Data Path** module processes memory access instructions and routes data to or from the **Memory Banks**, with control and data signal paths clearly delineated to maintain integrity and avoid cross-domain interference.
- The **Memory Banks** are represented as segmented or interleaved modules, characteristic of DRAM-based architectures, facilitating parallel access and optimized throughput.

This modular representation clarifies both the functional hierarchy of a memory subsystem and the points of observability/control essential for symbolic diagnostic frameworks.

1.1.11 Conclusion

This section has established memory as a multilayered, structurally intricate, and performance-defining component of digital computing systems. Its attributes directly influence system behavior across dimensions including computational throughput, latency, energy consumption, thermal management, and fault resilience.

Far from being passive storage, the memory subsystem comprises tightly interdependent architectures of storage arrays, control logic, timing circuitry, and communication protocols—each engineered to operate under strict real-time and reliability constraints. The precision of

these design choices determines both nominal performance and the system's ability to detect, tolerate, or recover from faults.

A structured conceptual grasp of memory—from abstract hierarchical models to physical implementation—is a prerequisite for advanced topics such as symbolic testing, adaptive diagnostics, formal fault modeling, and in-field self-repair.

The following section transitions to the hierarchical organization of memory subsystems, beginning with the processor's closest memory tiers: **registers** and **cache structures**. These elements act as the primary interface between computation and storage, imposing distinct constraints and offering specific opportunities for the testing and diagnostic techniques explored in subsequent chapters.

1.2 Memory Hierarchy Overview

Modern computing architectures rely on a meticulously engineered **memory hierarchy** to bridge the performance gap between high-speed processors and the comparatively high-latency main memory and persistent storage subsystems. This hierarchy organizes memory into multiple tiers, each optimized for a specific balance of **speed**, **capacity**, **cost per bit**, **power efficiency**, and **fault tolerance**.

The memory hierarchy is not an incidental implementation detail; it is a fundamental architectural principle that shapes system performance, scalability, and reliability. By positioning the fastest, smallest, and most expensive memory (e.g., registers, L1/L2/L3 caches) nearest the processor, and placing progressively larger, slower, and more economical storage (e.g., DRAM, SSD, HDD) at lower tiers, designers create the *illusion* of a single, large, high-speed memory space.

This layered design exploits **temporal locality** (recently accessed data is likely to be accessed again) and **spatial locality** (data near recently accessed addresses is likely to be accessed soon) to ensure that the most frequently used information resides in the most responsive tiers.

For diagnostic engineering, a deep understanding of the memory hierarchy's structure and operational dynamics is essential. It informs the development of accurate performance models, effective test algorithms, and robust fault-tolerance mechanisms capable of addressing defects at any level of the hierarchy without compromising overall system behavior.

1.2.1 The Rationale Behind Memory Hierarchies

The term *memory wall* encapsulates a central bottleneck in modern computing: the widening disparity between processor clock frequencies—now operating in the multi-gigahertz range—and the comparatively modest latency improvements of dynamic random-access memory (DRAM), whose access times have advanced only incrementally over several decades.

Without a hierarchical structure, processors would incur frequent, costly stalls, idling during memory fetches—even for simple operations—due to the mismatch between computational throughput and memory access speed.

Memory hierarchies address this challenge by exploiting two fundamental characteristics of program behavior:

- **Temporal locality** – the tendency for recently accessed data or instructions to be reused in the near future
- **Spatial locality** – the tendency to access data stored in memory locations near recently accessed addresses

By leveraging these properties, systems employ caching, buffering, and prefetching strategies to keep frequently or proximally accessed data in smaller, faster tiers physically closer to the processor. This ensures that the majority of memory operations execute at the speed of the highest tier (e.g., L1 cache or processor registers), reducing latency, alleviating bandwidth contention, and improving overall efficiency.

Although this layering is designed to be transparent to software, it carries significant implications for system architects and test engineers.

Ensuring correctness and performance across all tiers—ranging from on-chip caches to DRAM and persistent storage—requires validation strategies that address both functional integrity and fault resilience under real-world workload conditions.

1.2.2 Core Structure of the Memory Hierarchy

The memory hierarchy in modern computing systems is systematically organized according to multiple interrelated dimensions, including proximity to the processor, access latency, storage capacity, bit density, volatility, and cost per bit.

Each tier within this hierarchy fulfills a specialized functional role, collectively bridging the substantial performance gap between high-speed computational cores and slower, high-capacity storage technologies.

This layered organization is not merely an implementation convenience, but a foundational architectural strategy that enables scalable, high-performance computation.

At its core, the memory hierarchy is designed to optimize fundamental trade-offs among speed, capacity, energy efficiency, and economic feasibility.

By positioning the fastest and smallest memory structures—such as processor registers and on-chip caches—closest to the execution units, and progressively relegating larger, slower, and less expensive storage technologies to lower tiers, system designers create the illusion of a single, large, uniformly fast memory space.

In practice, this illusion is sustained by intelligent data placement, caching policies, and access scheduling mechanisms that exploit predictable patterns of program behavior.

Table 1.1 summarizes the principal levels of the memory hierarchy, along with their typical technological implementations, characteristic access times, representative capacity ranges, volatility properties, and primary functional roles within a computing system.

Table 1.1—Principal Levels of the Memory Hierarchy

Level	Memory Type	Access Time Type	Typical Size	Volatile	Role
L0	CPU Registers	<1 → ≈ 1 CPU cycle	Tens of bytes	Yes	Operand storage
L1 Cache	SRAM (split I/D)	1–2 ns	32–128 KB	Yes	Immediate data reuse
L2 Cache	SRAM (unified)	3–10 ns	256 KB – 1 MB	Yes	Mid-level cache
L3 Cache	Shared (multi-core)	10–30 ns	2 – 32 MB	Yes	Shared cache across cores
Main Memory	DRAM (e.g., DDR4)	50–150 ns	GBs	Yes	General-purpose working RAM
Persistent	SSD / Flash / HDD	10 µs (SSD) – 10 ms (HDD)	GB–TB scale	No	Long-term storage
Tertiary	Cloud Storage / Tape	Seconds – Hours	Petabytes+	No	Backup and archival storage

- **L0 – CPU Registers:**
  Implemented directly within the processor core, registers provide operand storage with access times on the order of a single CPU cycle. Their capacity is extremely limited—typically tens of bytes—but their proximity to the execution pipeline enables maximal throughput and minimal latency.
- **L1 Cache:**
  Usually implemented as split instruction (I-cache) and data (D-cache) structures using SRAM technology, the L1 cache delivers very low-latency access while supporting immediate data reuse. Its limited capacity is offset by its critical role in sustaining instruction-level parallelism.
- **L2 Cache:**
  A unified SRAM-based cache that serves as an intermediate buffering layer between L1 and lower memory tiers. L2 caches provide greater capacity at modestly increased latency and significantly reduce the frequency of costly main memory accesses.
- **L3 Cache:**
  Typically shared across multiple processor cores, the L3 cache acts as a high-capacity coordination layer that facilitates inter-core data sharing and reduces redundant memory traffic. Although slower than L1 and L2 caches, it remains substantially faster than main memory.
- **Main Memory:**

- Implemented using DRAM technologies such as DDR4 or DDR5, main memory provides the primary working storage for active processes and operating system data structures. While offering gigabyte-scale capacity, it introduces significantly higher access latency and requires refresh mechanisms due to its volatile nature.
- **Persistent Storage:**
  Solid-state drives, flash memory, and hard disk drives form the non-volatile persistent storage tier. These technologies prioritize capacity and data retention over access speed, making them suitable for long-term storage of programs, datasets, and system state.
- **Tertiary Storage:**
  Cloud-based storage systems and magnetic tape libraries provide massive, petabyte-scale capacity for archival, backup, and disaster recovery purposes. Access latencies range from seconds to hours, reflecting their role outside the performance-critical execution path.

This hierarchical organization ensures that temporal and spatial locality are exploited to maximum effect. Frequently accessed data is retained in the fastest tiers, while infrequently used or archival data is relegated to lower levels. Registers and caches handle immediate, low-latency operations; DRAM accommodates large active working sets; and persistent or tertiary storage supports long-term data retention at scale.

A rigorous understanding of this structure is essential for diagnosing performance bottlenecks, designing effective memory tests, and developing fault-tolerant strategies capable of addressing defects at any level of the hierarchy. In subsequent sections, this layered architecture will be examined from a diagnostic perspective, with particular emphasis on fault observability, error masking, and the challenges these characteristics introduce for comprehensive memory testing.

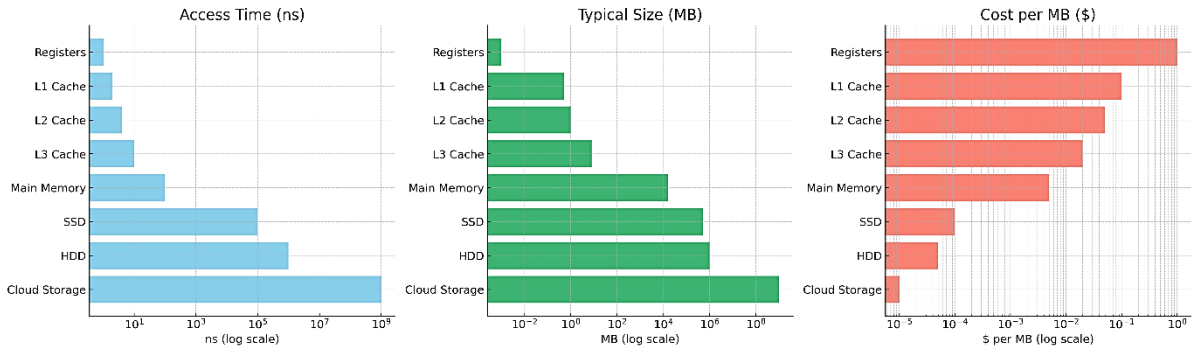

Figure 1.11—Layered pyramid of memory hierarchy from registers to cloud.

This Figure presents a logarithmic-scale visualization of key characteristics across the memory hierarchy, extending from processor registers at the apex to cloud-based archival storage at the base. Three parallel bar charts are shown:

- **Access Time (left):**

Displayed on a logarithmic scale spanning nanoseconds to hours, this chart illustrates the dramatic latency gradient from near-instantaneous register and cache access to high-latency remote storage retrieval.

- **Typical Storage Capacity (center):**
  Expressed in megabytes on a logarithmic scale, this chart highlights the inverse relationship between storage capacity and access speed across hierarchy levels.
- **Cost per Megabyte (right):**
  Shown in U.S. dollars, this chart emphasizes the steep cost premium associated with fast, low-capacity memory tiers and the economic motivation for hierarchical organization.

Together, these visualizations reinforce the intrinsic trade-offs among speed, capacity, and cost that necessitate multi-level memory hierarchies in modern system design.

1.2.3 Cache Architecture and Dynamics

Caches are high-speed memory structures positioned between the processor and main memory to mitigate the latency and bandwidth limitations inherent in large-capacity storage technologies. By retaining recently accessed data and instructions, caches exploit fundamental locality principles—temporal locality, whereby recently used information is likely to be reused, and spatial locality, whereby data near recently accessed addresses is likely to be referenced soon—to deliver near-instantaneous responses to the processor.

Hierarchy of Cache Levels

Modern processors employ a multi-level cache hierarchy, with each level engineered to balance speed, capacity, and physical proximity to the execution cores:

- **L1 Cache:** Located closest to the CPU core, the L1 cache is typically split into separate instruction and data caches. It offers extremely low access latency—on the order of one to a few CPU cycles—but provides limited capacity. Its primary function is to sustain the processor's instruction pipeline and minimize stall cycles.
- **L2 Cache:** The L2 cache is generally unified for both instructions and data and operates at higher latency than L1 while offering increased capacity. It serves as an intermediate buffer that absorbs cache misses from L1 and reduces the frequency of accesses to lower memory tiers.
- **L3 Cache:** Shared across all cores in a multi-core processor, the L3 cache provides substantial capacity and facilitates efficient inter-core data sharing. Although slower than private caches, it significantly reduces redundant memory accesses and improves overall system throughput.
- **L4 Cache / eDRAM:** Present in select high-end architectures, L4 cache implementations—often based on embedded DRAM—provide a large off-die cache that bridges the performance gap between on-chip caches and main memory.

Cache Management Policies

Cache behavior is governed by hardware-controlled policies that determine how data is placed, replaced, and synchronized:

- **Associativity:**
  Direct-mapped caches restrict each memory block to a single cache line, minimizing hardware complexity but increasing conflict misses. Set-associative caches allow blocks to occupy multiple lines within a set, balancing flexibility and implementation cost. Fully associative caches permit placement in any cache line, maximizing hit rate at the expense of significant hardware overhead.
- **Replacement Policies:**
  When a cache set is full, replacement algorithms determine which line is evicted. Least Recently Used (LRU) policies remove the block that has not been accessed for the longest time, while pseudo-LRU schemes approximate this behavior with reduced tracking complexity. Random replacement offers minimal overhead but may reduce hit rates.
- **Write Policies:**
  Write-back caches defer updates to main memory until modified cache lines are evicted, reducing memory traffic and improving performance. Write-through caches propagate every write to main memory immediately, simplifying consistency but increasing bandwidth demands.

Cache Coherence Protocols

In multi-core systems, cache coherence protocols ensure that all cores observe a consistent view of shared memory. Protocols such as MESI and MOESI track the state of each cache line and coordinate read and write operations across private and shared caches. By managing transitions among states such as Modified, Exclusive, Shared, and Invalid, these protocols prevent stale data usage and preserve correctness in parallel execution environments.

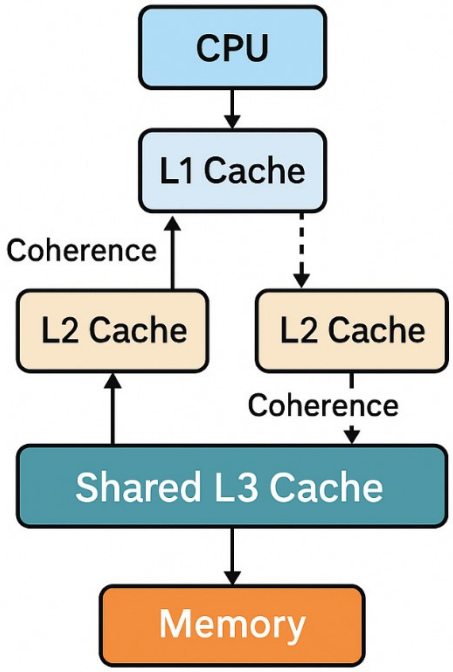

Figure 1.12—Cache hierarchy with coherence management.

This diagram depicts a representative multi-level cache hierarchy used in modern multi-core processors to minimize memory access latency and maximize bandwidth efficiency. Each CPU core is connected to a private L1 cache, followed by private L2 caches and a shared L3 cache that mediates data exchange among cores. Main memory resides at the base of the hierarchy, serving as the global working store.

Solid lines indicate direct data flow between hierarchy levels, while dashed lines labeled "Coherence" represent protocol-driven communication that maintains consistency across private caches. The shared L3 cache functions as a central coordination point, detecting and resolving data conflicts to ensure correct and deterministic execution across all processing cores.

1.2.4 Main Memory (DRAM): Structure and Behavior

Dynamic Random-Access Memory (DRAM) serves as the primary working memory for active applications and operating system processes in contemporary computing systems. Its design emphasizes high storage density, low cost per bit, and sufficient aggregate bandwidth to sustain multi-core execution, virtualization, and data-intensive workloads. Unlike cache memories, which prioritize latency minimization, DRAM is engineered as a capacity-oriented tier that balances performance with scalability.

Architectural Organization

Modern DRAM devices are organized hierarchically to optimize access efficiency and amortize control overhead across large memory arrays:

- **Banks, Rows, and Columns**
  A DRAM array is partitioned into multiple banks, each containing a two-dimensional grid of rows and columns. Memory access begins with **row activation**, during which the contents of an entire row are transferred into a row buffer implemented using sense amplifiers. Subsequent accesses select specific columns within the active row.
  Performance is therefore highly dependent on access locality: repeated accesses to the same open row result in **row hits**, while accesses to different rows require **precharge and reactivation**, incurring additional latency.
- **Ranks and Channels**
  A **rank** consists of multiple DRAM chips operating in lockstep to form a wider data word (e.g., 64 bits plus ECC). One or more ranks may be connected to a single **channel**, and modern memory controllers frequently support multiple independent channels to enable parallel access across DIMMs. Channel-level parallelism is a primary mechanism for increasing effective memory bandwidth.
- **Pages and Burst Transfers**
  DRAM devices transfer data in fixed-size bursts, typically aligned to cache-line boundaries (e.g., 64 bytes in DDR-class systems). Burst-oriented transfers reduce command overhead, improve bus utilization, and align DRAM access granularity with cache refill operations.

Key Timing Parameters

DRAM operation is governed by strict timing constraints that reflect the underlying analog behavior of capacitive storage and sensing circuitry. The most critical parameters include:

- t_{RCD} **(Row-to-Column Delay):**
  The minimum time between row activation and issuance of a read or write command.
- t_{CL} **(CAS Latency):**
  The delay between a read command and the availability of valid output data on the bus.
- t_{RP} **(Row Precharge Time):**
  The time required to close an active row and prepare the bank for activation of a different row.
- t_{RAS} **(Row Active Time):**
  The minimum duration a row must remain active to ensure correct sensing and data stability prior to precharge.

In high-reliability or enterprise environments, DRAM subsystems are often augmented with multi-channel controllers, high-density DIMM configurations, and integrated error-correcting codes (ECC). These enhancements allow systems to scale capacity and performance while maintaining fault tolerance and data integrity.

1.2.5 Virtual Memory and Paging Mechanisms

Virtual memory introduces an abstraction layer that decouples a program's address space from the physical organization of main memory. This abstraction allows each process to operate within a private, contiguous virtual address space, regardless of the actual distribution of data in physical DRAM. Virtual memory is fundamental to modern operating systems, enabling efficient multitasking, strong memory protection, and scalable memory utilization.

Core Mechanisms

Virtual memory systems rely on several tightly integrated mechanisms:

- **Page Tables**
  Operating systems maintain page tables that map **virtual page numbers (VPNs)** to **physical frame numbers (PFNs)**. To limit memory overhead, page tables are commonly organized as multi-level hierarchies, allowing sparse address spaces to be represented efficiently.
- **Translation Lookaside Buffers (TLBs)**
  TLBs are small, associative caches that store recently used VPN-to-PFN translations. By caching address translations, TLBs eliminate the need for frequent page table walks and significantly reduce effective memory access latency.
- **Page Faults**
  When a referenced virtual page is not resident in physical memory, a **page fault** occurs. Control is transferred to the operating system, which resolves the fault by allocating a physical frame and loading the required page from secondary storage into DRAM.
- **Swapping and Demand Paging**

To manage limited physical memory, inactive pages may be swapped out to persistent storage, while active pages are loaded on demand. This mechanism allows systems to support working sets that exceed available DRAM capacity.

By separating virtual and physical addressing, virtual memory systems enable efficient memory sharing, process isolation, and seamless integration of DRAM with slower but higher-capacity storage technologies.

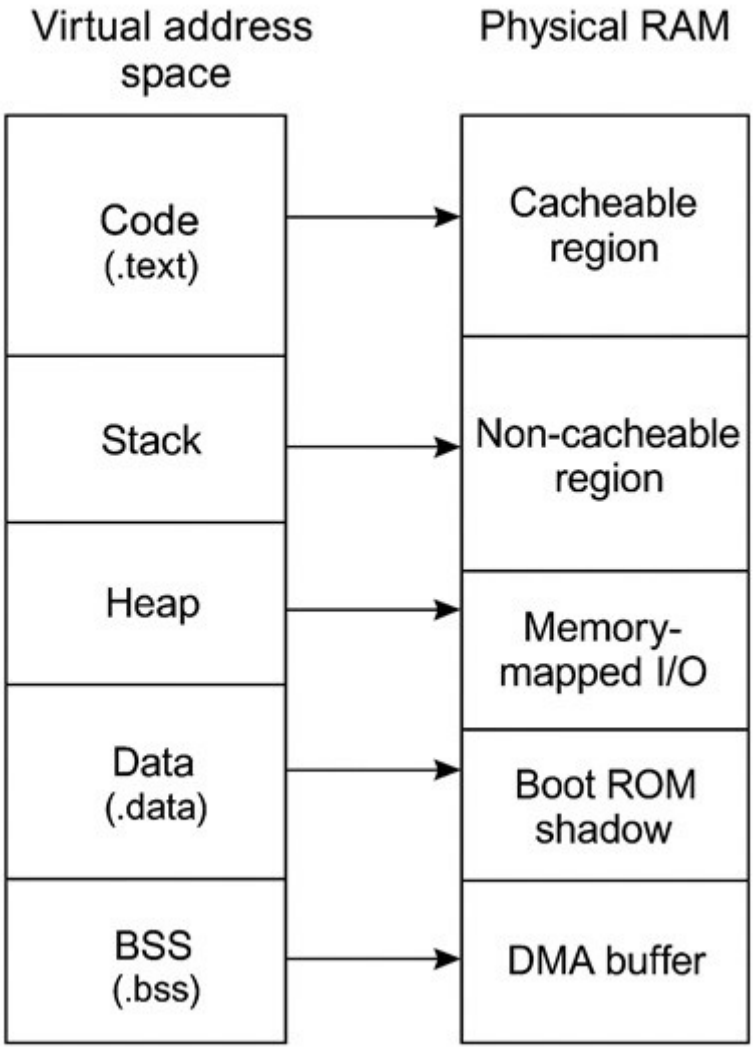

Figure 1.13—Virtual-to-Physical Address Translation Process

This Figure illustrates the multi-stage workflow by which a virtual address generated by the CPU is translated into a corresponding physical address:

1. **Virtual Address Decomposition**
   The virtual address is divided into a **Virtual Page Number (VPN)**, typically occupying the upper address bits (e.g., bits 31–12), and an **Offset**, occupying the lower bits (e.g., bits 11–0).
2. **TLB Lookup**

The Translation Lookaside Buffer is queried for a cached VPN-to-PFN mapping.
    - On a **TLB hit**, translation proceeds immediately.
    - On a **TLB miss**, a page table walk is initiated.
3. **Page Table Walk**
   The system traverses the hierarchical page table structure to resolve the PFN associated with the VPN.
4. **Page Fault Handling**
   If the page is not present in physical memory, a page fault is raised and control is transferred to the operating system, which retrieves the page from secondary storage.
5. **Physical Address Construction**
   The resolved PFN is concatenated with the original offset to form the final physical address used to access DRAM.

Dashed paths in the diagram represent exception flows associated with TLB misses and page faults. This translation mechanism underpins memory protection, demand paging, and process isolation in modern operating systems.

1.2.6 Persistent and Secondary Memory

The persistent and secondary memory tier provides long-term data storage and forms the bridge between high-speed volatile memory (DRAM) and archival systems such as cloud storage or tape libraries. Technologies in this tier prioritize capacity, non-volatility, and cost efficiency, while accepting higher access latency relative to main memory.

Technologies in This Tier

- **Solid-State Drives (SSDs)**
  SSDs are based on NAND Flash memory and provide low access latency, high throughput, and excellent random I/O performance compared to mechanical storage. However, Flash memory exhibits limited write endurance due to charge trapping, dielectric wear, and oxide degradation. Modern SSD controllers mitigate these effects through wear-leveling, garbage collection, and strong ECC mechanisms.
- **Hard Disk Drives (HDDs)**
  HDDs employ magnetic recording on rotating platters with mechanical read/write heads. They offer very high capacity at low cost per gigabyte but suffer from millisecond-scale access latency and limited random-access performance.
- **Hybrid Drives (SSHDs)**

Hybrid storage devices combine NAND Flash with HDD technology, caching frequently accessed data in the Flash layer while retaining the bulk capacity of magnetic storage.

Unique Challenges in SSDs

Persistent memory devices, particularly Flash-based SSDs, introduce diagnostic challenges distinct from those encountered in DRAM:

- **Non-Deterministic Latency**
  Background operations such as garbage collection and wear-leveling introduce variability in access latency, complicating real-time performance analysis.

- **Read/Write Asymmetry**
  NAND Flash requires block erasure prior to writing, resulting in significantly slower write operations compared to reads.
- **Silent Data Corruption**
  Charge leakage over time can degrade stored data in unused blocks, potentially leading to undetected errors unless periodic scrubbing or verification is performed.

Testing Considerations

Comprehensive validation of persistent memory systems must address endurance, integrity, and long-term reliability. Key testing objectives include:

- **Endurance Validation**
  Stress testing program/erase cycle limits and evaluating the effectiveness of wear-leveling algorithms.
- **TRIM and Garbage Collection Verification**
  Ensuring correct handling of TRIM commands and background maintenance operations to prevent performance degradation.
- **Data Retention Assessment**
  Verifying long-term data integrity under extended storage intervals and varying environmental conditions, particularly temperature, to detect retention-related failures.

1.2.7 Emerging Memory Hierarchies: HBM, SCM, and NVDIMM

Recent advances in memory technology are reshaping the classical memory hierarchy to meet the escalating demands of high-performance computing (HPC), artificial intelligence (AI), machine learning accelerators, and real-time data analytics.

These emerging memory tiers blur traditional boundaries between volatile and non-volatile storage, introducing hybrid access semantics, new reliability challenges, and previously unseen fault modes. As a result, conventional diagnostic and testing approaches must be extended to address both architectural novelty and physical complexity.

High Bandwidth Memory (HBM)

High Bandwidth Memory represents a significant departure from traditional planar DRAM organization. Rather than relying on narrow, high-frequency interfaces, HBM achieves performance gains through massive parallelism enabled by three-dimensional integration.

- **Architecture**
  HBM employs vertically stacked DRAM dies interconnected via **Through-Silicon Vias (TSVs)**. This 3D stacking enables ultra-wide interfaces—often exceeding 1024 data lines—allowing very high aggregate bandwidth at comparatively low clock frequencies. The reduction in signaling frequency lowers energy consumption per transferred bit while maintaining exceptional throughput.
- **Applications**
  HBM is widely deployed in GPUs, AI accelerators, and high-performance networking

devices, where sustained memory bandwidth is often the dominant performance constraint.

- **Testing Challenges**
  The dense vertical integration of HBM introduces new diagnostic concerns, including:
  - Thermal hotspots arising from stacked die configurations
  - TSV defects such as opens, shorts, or resistive degradation affecting vertical signal paths
  - Inter-die coupling effects requiring fault modeling along the **z-axis**

Effective testing therefore demands stress testing under controlled thermal gradients, TSV-aware fault models, and multi-dimensional access patterns that expose vertical communication defects.

Storage Class Memory (SCM)

Storage Class Memory occupies an intermediate position between DRAM and traditional persistent storage, combining non-volatility with access latencies approaching those of main memory. Unlike NAND Flash, many SCM technologies support fine-grained, byte-addressable access.

- **Position in the Hierarchy**
  SCM bridges the latency and endurance gap between DRAM and SSDs, enabling persistent data structures to reside closer to the processor while avoiding block-based access constraints.
- **Representative Technologies**
  - **Phase-Change Memory (PCM):** Stores data by inducing reversible transitions between crystalline and amorphous resistance states.
  - **Resistive RAM (ReRAM):** Encodes information via resistance modulation in dielectric materials.
  - **Spin-Transfer Torque MRAM (STT-MRAM):** Uses magnetic tunnel junctions to achieve non-volatile, fast access storage.
- **Testing Challenges**
  SCM technologies introduce fault mechanisms distinct from both DRAM and Flash:
  - Endurance degradation and resistance drift under repeated write cycles
  - Multi-Level Cell (MLC) operation, increasing analog variability and read-margin sensitivity
  - Strong dependence on temperature and write history

  Diagnostic methodologies must therefore incorporate **analog-aware fault models**, endurance-to-failure characterization, and retention verification under realistic workload conditions.

Non-Volatile DIMM (NVDIMM)

Non-Volatile DIMMs integrate volatile and non-volatile memory technologies within a single module, enabling rapid recovery of system state following power loss.

- **Architecture**
  NVDIMMs typically combine DRAM with NAND Flash on the same module, supported by onboard backup power sources such as supercapacitors or batteries.
- **Operational Model**
  - During normal operation, data is accessed at DRAM speeds.
  - Upon power failure, DRAM contents are automatically flushed to the non-volatile Flash component.
  - On power restoration, data can be restored to DRAM, enabling near-instant system recovery.
- **Testing Challenges**
  NVDIMMs exhibit hybrid fault modes that span both volatile and non-volatile domains:
  - Verification of power-loss detection and data-flush mechanisms
  - Evaluation of wear-leveling and endurance in the Flash backup path
  - Coordinated testing of DRAM–Flash interaction, including corner-case failure scenarios

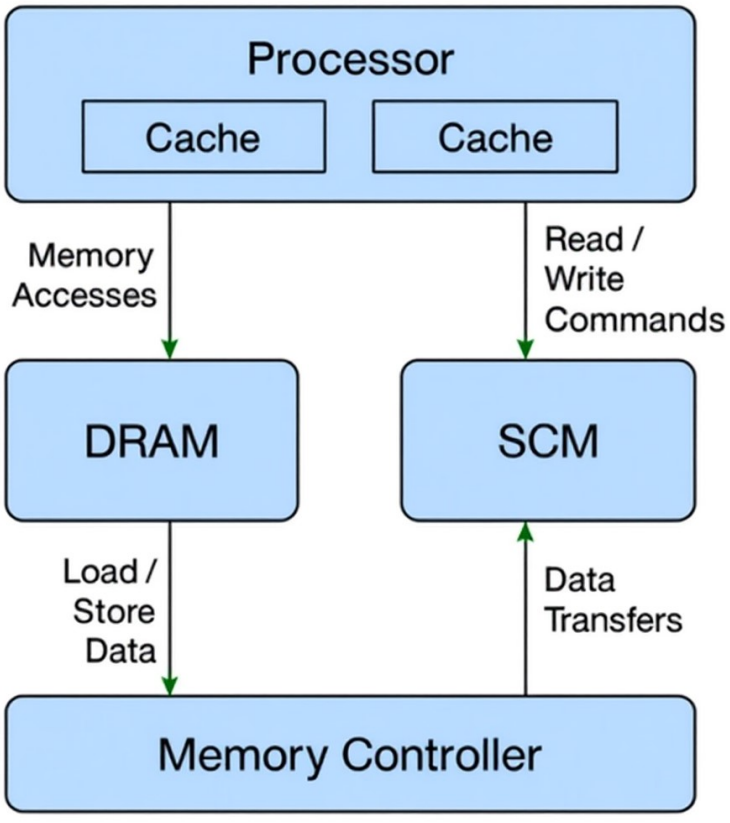

Figure 1.14—Combined DRAM-SCM interface model.

This Figure illustrates a hybrid memory architecture in which Dynamic Random-Access Memory (DRAM) and Storage Class Memory (SCM) coexist within a unified subsystem. The processor accesses DRAM for conventional volatile operations, while SCM provides persistent, low-latency storage via direct read/write commands.

A centralized memory controller orchestrates data transfers and scheduling across both memory types, ensuring coherent operation between volatile and non-volatile tiers. Such hybrid architectures require specialized diagnostic strategies capable of validating performance, endurance, and fault resilience across heterogeneous memory domains.

1.2.8 Diagnostic and Testing Implications Across the Hierarchy

Each level of the memory hierarchy exhibits unique operational constraints and fault behaviors, necessitating tier-specific diagnostic methodologies and tailored test strategies.

- **Registers**
  Register testing focuses on bitline integrity, detection of stuck-at faults, and validation of reliable single-cycle access. Given their critical role in instruction execution, even transient faults can have immediate architectural consequences.
- **Caches**
  Cache diagnostics must verify correctness of tag matching, set indexing, and replacement logic (e.g., LRU and pseudo-LRU). In multi-core systems, coherence validation under high-concurrency workloads is essential to prevent stale data propagation and subtle synchronization errors.
- **DRAM**
  DRAM testing emphasizes detection of coupling faults, validation of refresh correctness under worst-case retention conditions, and mitigation of disturbance phenomena such as **Row Hammer**, where repeated access to aggressor rows induces charge leakage in adjacent victim cells.
- **Flash and Persistent Memory**
  Persistent storage validation requires endurance testing for program/erase cycle limits, retention verification over extended timeframes, and careful analysis of wear-leveling behavior that can obscure fault localization.
- **Virtual Memory Systems**
  Diagnostics must validate page fault handling, enforce protection boundaries, ensure correct TLB invalidation during context switches, and detect resource leaks in dynamic allocation paths.

Beyond isolated tier testing, **inter-tier validation** is critical for ensuring correct system-level behavior:

- Cache–DRAM coherence verification to prevent stale or corrupted data from reaching execution units
- MMU translation correctness and TLB flushing behavior during process scheduling
- Prefetching side-effect analysis, including unintended contention or timing exposure
- Latency predictability assessment, particularly in real-time and safety-critical systems
- Modern diagnostic frameworks increasingly integrate advanced techniques such as:
- Built-In Self-Test (BIST) for at-speed detection during manufacturing and in-field operation
- Fault injection to evaluate resilience against transient and permanent failures
- Pattern-based March testing to activate diverse fault models

- ECC syndrome analysis to assess coverage and correction efficiency under realistic workloads

Together, these approaches enable comprehensive fault observability while minimizing diagnostic overhead.

1.2.9 Summary

The memory hierarchy is a deliberately engineered abstraction that unifies diverse storage technologies into the illusion of a single, fast, capacious, and reliable memory space. Beneath this abstraction lies a stratified system in which each tier—registers, caches, main memory, persistent storage, and archival systems—exhibits distinct physical characteristics, access semantics, and fault behaviors.
For system architects, designers, and diagnostic engineers, mastery of the memory hierarchy is indispensable. Performance determines computational throughput, timing behavior governs real-time responsiveness, and data integrity underpins functional correctness and fault tolerance.

As computing systems evolve toward 3D-stacked integration, hybrid DRAM–NVM tiers, and increasingly disaggregated architectures, the challenge of balancing latency, bandwidth, endurance, and reliability intensifies. The memory hierarchy is not a passive backdrop but an active stage upon which modern computation unfolds. In this environment, diagnostic precision and adaptive testing methodologies will play a defining role in ensuring the operational reliability of next-generation computing systems.

1.3 Role of Random Access Memory in Digital Systems

Random Access Memory (RAM) constitutes the primary operational workspace of virtually all modern computing systems, spanning resource-constrained embedded controllers, general-purpose personal computers, high-performance servers, and large-scale enterprise platforms. As a volatile memory technology, RAM provides high-speed, transient storage that is essential for instruction execution, data manipulation, buffering of input/output (I/O) operations, and maintenance of runtime system state.

This volatile workspace is the environment in which active computation occurs. Executable code, intermediate variables, process stacks, dynamically allocated objects, and operating system data structures all reside in RAM during execution. Although the contents of RAM are inherently ephemeral and lost upon power removal, its presence is indispensable to both system performance and functional reliability.

Without RAM, sustained computation at modern speeds would be infeasible, regardless of processor capability or storage capacity.
RAM's role extends across multiple functional domains:

- **Code Execution**
  Program instructions stored in non-volatile media are staged in RAM to enable rapid instruction fetch and pipeline execution.
- **Data Manipulation**

Arrays, matrices, buffers, and other structured data objects are held in RAM while computations are performed.

- **I/O Buffering**
  RAM serves as a high-speed staging area for data exchanged between processors and peripheral devices, decoupling fast CPUs from slower I/O subsystems.
- **Process Coordination**
  In multitasking systems, RAM stores process context, including register snapshots, program counters, kernel scheduling data, and synchronization primitives.
- **Real-Time Responsiveness**
  Deterministic access behavior is critical for embedded and safety-critical systems, where timing guarantees must be met under strict constraints.

Far from being a passive container of bits, RAM is an active, performance-critical participant in every computational process, shaping system throughput, latency behavior, and overall execution determinism.

1.3.1 Functional Significance in System Architecture

Unlike persistent storage technologies—such as solid-state drives (SSDs) or hard disk drives (HDDs)—which primarily function as long-term data repositories, RAM operates as the immediate execution substrate for real-time computation. Its responsibilities permeate every architectural layer of a computing system, from low-level hardware pipelines to high-level software abstractions.

Key architectural functions of RAM include:

- **Instruction Execution**
  Once loaded from persistent storage, executable code is placed in RAM to support high-speed fetch–decode–execute cycles within the processor pipeline.
- **Data Workspace**
  RAM provides temporary storage for algorithmic data structures, including arrays, linked lists, matrices, and intermediate computational results.
- **Stack and Heap Management**
  Function call stacks, local variables, and dynamically allocated objects—created via mechanisms such as malloc, new, or equivalent system calls—are implemented in RAM, enabling recursion, dynamic memory allocation, and flexible runtime behavior.
- **Context Switching**
  Operating systems maintain process control blocks (PCBs), thread state, and scheduling metadata in RAM, allowing rapid task switching while preserving execution continuity.
- **File and Device I/O Buffering**
  RAM buffers data transfers between the processor and slower storage or peripheral devices, smoothing throughput and reducing blocking delays.
- **Graphics and Multimedia Processing**
  Frame buffers, textures, audio streams, and video data are cached in dedicated or shared RAM regions to support smooth rendering and real-time media playback.

By fulfilling these roles, RAM enables fluid, responsive, and efficient execution across a wide spectrum of workloads, ranging from real-time control systems and transactional processing to high-performance numerical simulation and GPU-accelerated machine learning.

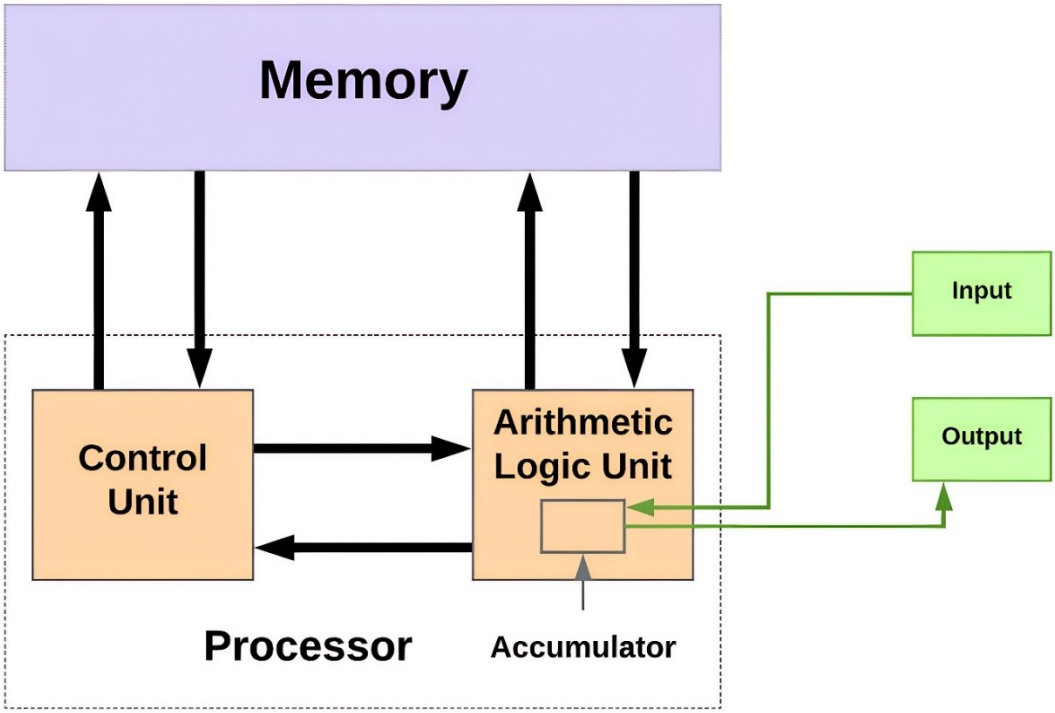

Figure 1.15—CPU—RAM interaction in a generic von Neumann architecture

This Figure illustrates the fundamental data flow and control relationships in a classical von Neumann architecture, highlighting the bidirectional exchange between the processor and main memory.

The processor comprises a control unit and an arithmetic logic unit (ALU), with internal registers—such as an accumulator—used to hold intermediate results. Memory serves as a unified repository for both instructions and data, while input and output devices exchange information with the processor through controlled data paths. Together, these components form the execution model that underpins most contemporary computing systems.

1.3.2 Technological Classification of RAM

Random Access Memory technologies are primarily classified according to their internal storage mechanisms, access semantics, and performance characteristics. The two dominant classes—Static RAM (SRAM) and Dynamic RAM (DRAM)—exhibit fundamentally different circuit architectures and operational behaviors, leading to distinct application domains within the memory hierarchy.

A. Static Random Access Memory (SRAM)

Architecture
SRAM cells are typically implemented using six transistors (6T) arranged as two cross-coupled CMOS inverters forming a bistable latch. This structure maintains its logical state indefinitely as long as power is applied, eliminating the need for periodic refresh operations.

Characteristics
- **Latency:** Extremely low access latency, making SRAM suitable for timing-critical pipelines.
- **Power:** No refresh overhead, though static leakage currents contribute to standby power consumption.
- **Usage:** Predominantly employed in processor caches (L1/L2/L3), register files, translation lookaside buffers (TLBs), and other on-chip storage structures.

Advantages
- Deterministic and predictable access behavior
- Non-destructive read operations
- Simplified control logic relative to DRAM

Disadvantages
- Large cell area limits achievable density (typically several times that of DRAM)
- High cost per bit
- Poor scalability for large-capacity memory arrays

B. Dynamic Random Access Memory (DRAM)

Architecture
DRAM stores each bit as an electric charge on a capacitor, accessed through a single transistor (1T1C structure). Due to unavoidable leakage currents, stored charge decays over time and must be periodically restored through refresh operations, typically performed every 32–64 ms.

Characteristics
- **Latency:** Higher than SRAM due to row activation, sensing, and precharge operations.
- **Density:** Compact cell structure enables very high integration density.
- **Usage:** Serves as main system memory across general-purpose, embedded, and high-performance platforms.

Advantages
- Excellent scalability and high storage density
- Low cost per bit, enabling large system memories

Disadvantages
- Destructive reads requiring post-read restoration
- Susceptibility to soft errors, retention failures, and coupling effects
- Variable access latency driven by bank- and row-level timing constraints

Key DRAM Variants
- **SDRAM:** Clock-synchronized operation with pipelined commands and burst transfers
- **DDR SDRAM:** Data transfer on both clock edges (DDR, DDR2, DDR3, DDR4, DDR5)
- **LPDDR:** Energy-optimized variants for mobile and embedded systems

- **GDDR:** High-bandwidth DRAM tailored for graphics and GPU workloads
- **HBM:** 3D-stacked DRAM interconnected via through-silicon vias to deliver massive parallelism and ultra-high bandwidth

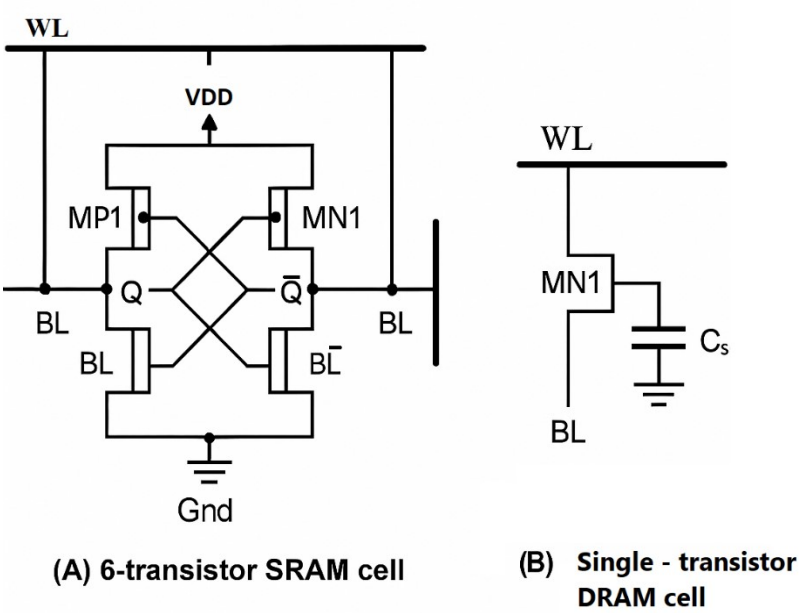

Figure 1.16—Structural comparison of SRAM vs DRAM cells

This Figure contrasts the fundamental circuit structures of a six-transistor (6T) SRAM cell and a single-transistor–single-capacitor (1T1C) DRAM cell. The SRAM cell employs cross-coupled inverters to form a bistable latch that preserves state while power is applied, enabling fast, non-destructive read and write operations without refresh overhead.

In contrast, the DRAM cell relies on charge storage in a capacitor controlled by an access transistor, achieving far higher density at the cost of refresh complexity, destructive reads, and increased sensitivity to leakage and disturbance effects. These architectural differences encapsulate the core trade-offs among speed, density, power consumption, and data retention that define modern memory system design.

1.3.3 System Integration and Memory Mapping

Random Access Memory (RAM) occupies a central position within a system's physical address space, enabling high-speed interaction between the processor, operating system, and peripheral subsystems. Beyond its role as a temporary data store, RAM functions as the primary execution substrate for both kernel-level services and user-level applications, supporting a wide range of architectural and system-level mechanisms.
At the hardware–software boundary, RAM is integrated into the global address space to enable the following core functions:

- **Kernel and User Space Memory**
  Modern operating systems partition RAM into protected regions reserved for privileged kernel execution and unprivileged user processes. This separation enforces isolation,

prevents unauthorized access to critical system resources, and forms the basis of memory protection and system security.

- **Memory-Mapped I/O (MMIO)**
  Specific address ranges within the memory map are assigned to hardware device registers and buffers. Through MMIO, peripheral devices can be accessed using standard load/store instructions, eliminating the need for dedicated I/O operations and simplifying device driver design.
- **Boot ROM Shadowing**
  During system initialization, firmware or bootloader code is often copied from non-volatile storage into RAM. Executing this code from RAM significantly reduces access latency and accelerates system startup.
- **Direct Memory Access (DMA)**
  DMA engines enable peripherals to transfer data directly to and from RAM without continuous CPU involvement. This mechanism reduces processor overhead, improves throughput, and is essential for high-speed I/O subsystems such as networking, storage controllers, and multimedia devices.
- **Cacheable and Non-Cacheable Regions**
  RAM may be segmented into cacheable and non-cacheable regions to balance performance and determinism. Cacheable memory maximizes throughput, while non-cacheable regions are used where strict ordering, coherency control, or real-time predictability is required—particularly in embedded and safety-critical systems.

At the operating system level, RAM is further subdivided into logical segments that structure program execution and resource management:

- **Code Segment (.text)** – Stores executable machine instructions loaded from compiled binaries.
- **Data Segment (.data / .bss)** – Holds global and static variables, with .data containing initialized values and .bss reserving space for uninitialized data.
- **Heap** – Provides dynamically allocated storage for runtime objects, buffers, and data structures.
- **Stack** – Supports function call management, local variable storage, and preservation of execution context during procedure calls and interrupts.

Contemporary architectures augment this segmentation with advanced memory management techniques to improve scalability and performance:

- **Paging** – Divides physical memory into fixed-size pages, enabling virtual memory systems in which each process operates within an independent virtual address space.
- **Segmentation** – Allocates variable-sized memory regions with fine-grained access control, supporting selective sharing and protection.
- **Non-Uniform Memory Access (NUMA)** – In multiprocessor systems, associates each processor or node with local memory banks to minimize access latency and improve parallel throughput.

The structured integration of RAM into the system's address space is fundamental to achieving an optimal balance between performance, flexibility, security, and fault isolation in modern computing platforms.

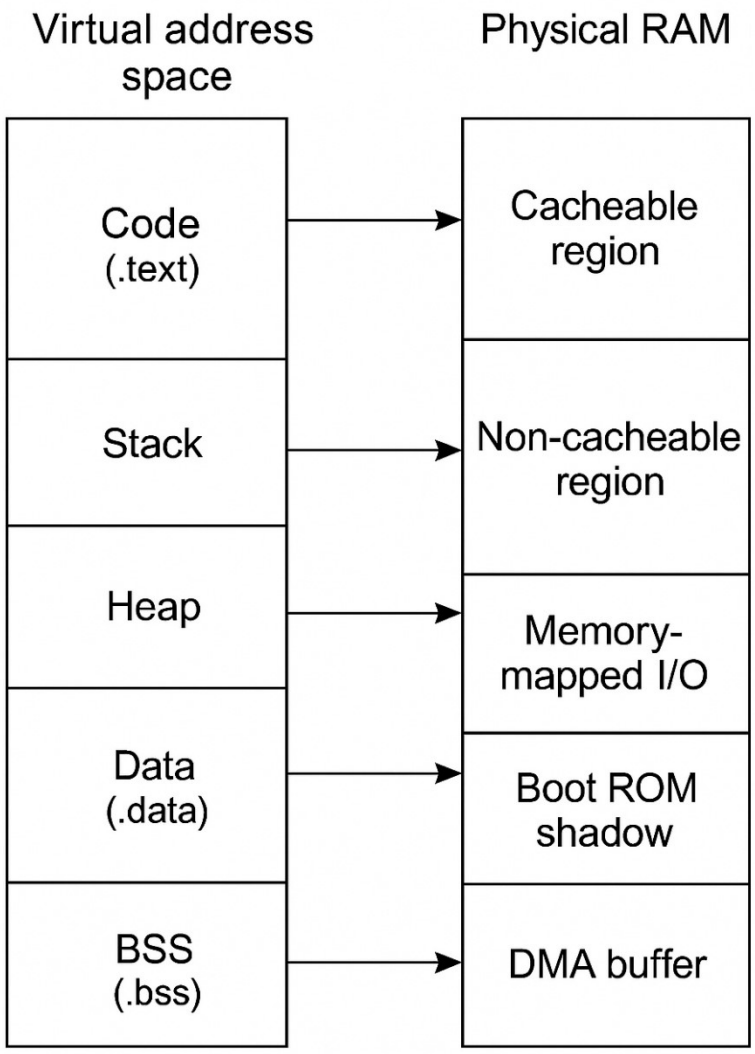

Figure 1.17—RAM segmentation and virtual memory mapping

This Figure illustrates the relationship between a process's virtual address space and its mapped regions in physical RAM. The virtual address space is organized into standard operating system segments—including code, stack, heap, initialized data, and uninitialized data—while physical memory is divided into cacheable regions, non-cacheable regions, memory-mapped I/O areas, boot ROM shadow regions, and DMA buffers.

Address translation is performed by the Memory Management Unit (MMU), which enforces access control, provides process isolation, and abstracts the physical memory layout from software.

1.3.4 Access Mechanisms and Performance Profiles

RAM performance is inherently non-uniform and strongly influenced by both architectural design choices and workload access patterns. A precise understanding of these factors is essential for optimizing system throughput, minimizing access latency, and reducing energy consumption.

Access Patterns

- **Sequential Access**
  Sequential access patterns exploit spatial locality, allowing hardware prefetchers and cache line fills to anticipate future requests and minimize effective access latency.
- **Random Access**
  Random or irregular access patterns disrupt locality, increasing the likelihood of row misses, bank conflicts, and address decoding overhead. Such patterns incur higher latency and reduce effective bandwidth.

Bank Interleaving

Modern DRAM devices are organized into multiple independent banks that can be accessed concurrently. By interleaving memory requests across banks, controllers can overlap operations, reduce idle cycles, and increase sustained bandwidth. Bank interleaving is particularly effective in multithreaded workloads and SIMD/vectorized execution models.

Burst Transfers

Synchronous DRAM technologies implement burst transfer modes in which multiple data words are transferred per access command. Burst operation reduces command overhead, maximizes data bus utilization, and aligns memory transfers with cache line sizes, improving overall efficiency.

Latency Components

DRAM access latency is governed by several microarchitectural timing parameters:

- t_{RCD} **(Row-to-Column Delay):** Interval between row activation and column access.
- t_{CL} **(CAS Latency):** Time between column selection and availability of the first data word.
- t_{RP} **(Row Precharge Time):** Time required to close an active row before opening another.
- t_{RAS} **(Row Active Time):** Minimum duration a row must remain active to ensure correct operation.

To manage these latency sources, memory controllers employ advanced techniques such as command scheduling, out-of-order request reordering, row-buffer management, and quality-of-service (QoS)–aware prioritization. By aligning access sequences with the physical organization of memory arrays, these mechanisms ensure high bandwidth utilization and predictable performance across diverse application profiles.

Collectively, these access patterns and latency components determine how efficiently a memory subsystem can deliver data to the processor pipeline. A clear understanding of these

mechanisms is therefore essential for analyzing performance limitations and for designing memory-aware optimization and diagnostic strategies in modern digital systems.

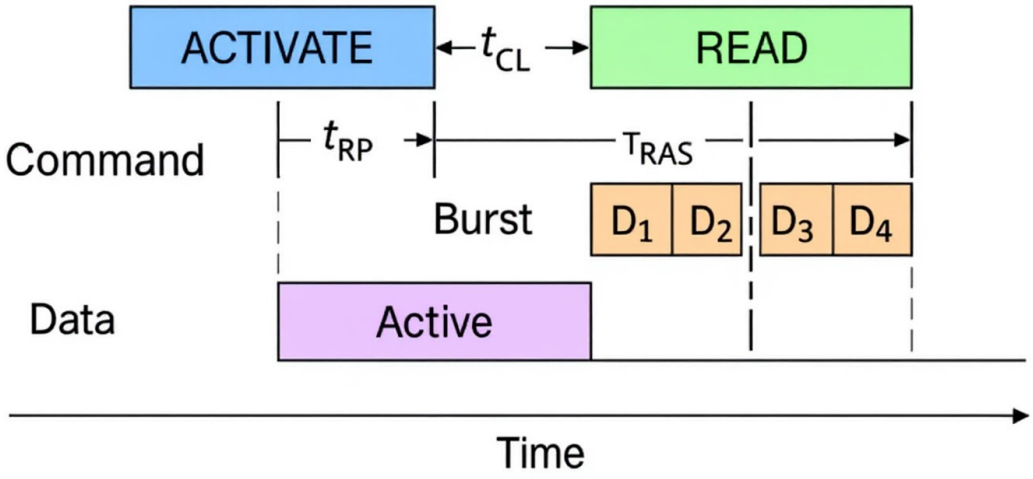

Figure 1.18—DRAM access timeline with burst transfer overlay

This Figure illustrates the timing sequence of a DRAM read operation, highlighting the relationships among ACTIVATE, READ, burst data transfer, and PRECHARGE commands. Key timing parameters—including t_{RCD}, t_{CL} t_{RAS}, and t_{RP}—are annotated to show how modern DDR architectures overlap command and data phases.

Burst transfers deliver multiple data words per access cycle, maximizing bus utilization and throughput. Precise control of these timing relationships is critical for memory controller optimization, performance tuning, and the scheduling of diagnostic test sequences.

1.3.5 Role of RAM in Diverse Computing Models

Random Access Memory plays a foundational role across a wide range of computing paradigms, with its organization, capacity, and access policies adapted to the requirements of each model.

- **Von Neumann Architecture**
  Employs a unified memory space for both instructions and data, with RAM acting as a central shared resource. While architecturally simple, this model suffers from the von Neumann bottleneck, in which instruction and data fetches compete for the same memory bandwidth.
- **Harvard Architecture**
  Maintains physically separate instruction and data memories, enabling concurrent access and reducing contention. In such systems, RAM is typically dedicated to data storage, while instructions reside in ROM or Flash memory.
  This separation improves throughput by allowing simultaneous instruction fetch and data access.
- **Real-Time Systems**

Favor tightly coupled RAM or scratchpad memories that provide deterministic access times. This avoids the unpredictability introduced by cache hierarchies, which can violate worst-case execution time constraints in hard real-time applications.

- **Embedded Systems**
  Operate under strict RAM capacity constraints and often employ hybrid designs combining SRAM for speed and predictability with DRAM for capacity. Memory allocation strategies are optimized to balance performance, energy efficiency, and silicon area.
- **Graphics Processing Units (GPUs)**
  Integrate high-bandwidth memory technologies such as GDDR or HBM, shared across thousands of concurrent threads. This organization sustains the massive parallelism required for graphics rendering, scientific simulation, and AI workloads.
- **Mobile and Edge Devices**
  Utilize low-power DDR variants (LPDDR) with advanced power management features, including deep sleep states, dynamic bandwidth scaling, and reduced I/O voltages. These mechanisms extend battery life while preserving responsiveness for interactive applications.

Across all these models, RAM remains the central medium through which computation is expressed and executed. Its architectural integration, access behavior, and reliability characteristics directly influence system performance, predictability, and fault tolerance.

1.3.6 Reliability and Error Management in RAM

As Random Access Memory (RAM) technologies scale toward increasingly aggressive fabrication nodes (sub-10 nm and beyond) and higher integration densities, their susceptibility to both transient and permanent failure mechanisms rises significantly. These vulnerabilities stem from reduced noise margins, increased parasitic coupling, charge leakage effects, and greater sensitivity to environmental disturbances. Ensuring reliable RAM operation therefore requires a combination of architectural safeguards, circuit-level mitigation, and system-level error management strategies.

The principal classes of RAM faults include:

- **Soft Errors** – Transient bit flips induced by high-energy particles such as cosmic rays or alpha emissions originating from packaging materials. These events, commonly referred to as Single-Event Upsets (SEUs), alter stored data without causing permanent physical damage. Although non-destructive, soft errors can propagate through computation pipelines and compromise system correctness if left uncorrected.
- **Retention Failures** – In DRAM, stored charge on capacitors decays over time due to leakage currents. If refresh intervals are insufficient—or if leakage variability across cells exceeds expected margins—data loss may occur. This effect becomes more pronounced at higher temperatures and lower supply voltages, and it worsens with continued process scaling.
- **Read Disturb Faults (Rowhammer Effect)** – Repeated activation of specific DRAM rows can induce parasitic charge leakage in physically adjacent rows, known as victim rows. This phenomenon can result in unintended bit flips without direct access to the affected locations.

Beyond reliability concerns, Rowhammer has been demonstrated as a viable attack vector capable of bypassing memory protection mechanisms.

- **Coupling Faults** – Capacitive or inductive interference between neighboring bitlines, wordlines, or storage nodes can cause unintended state changes. As interconnect spacing shrinks, coupling effects intensify, making these faults increasingly difficult to isolate using naïve test patterns.
- **Wearout Mechanisms** – In non-volatile or pseudo-RAM technologies (e.g., Flash-based RAM, ReRAM, PCM), repeated program/erase or write cycles lead to oxide degradation, charge trapping, and structural fatigue. Over time, these effects manifest as stuck-at faults, transition failures, or increased error rates.

To counteract these failure modes, modern systems deploy a layered set of mitigation techniques:

- **Error Correction Codes (ECC)** – Widely used schemes range from basic Hamming-based Single Error Correction and Double Error Detection (SECDED) to more advanced BCH and Reed–Solomon codes capable of correcting multiple simultaneous bit errors. ECC logic operates transparently during normal memory access, preserving data integrity with minimal performance overhead.
- **Memory Scrubbing** – Periodic background scanning of memory contents detects and corrects latent soft errors before they accumulate into uncorrectable multi-bit failures. Scrubbing is particularly critical in high-availability and long-uptime systems.
- **Redundancy Mechanisms** – Spare rows, columns, or banks are incorporated at design time and activated through remapping logic to replace defective regions discovered during manufacturing or operation. Redundancy improves yield and extends usable device lifetime.
- **Post-Mortem Error Syndrome Analysis** – Logging and analyzing ECC syndromes over time enables classification of fault behavior, identification of aging trends, and informed decisions regarding in-field repair, decommissioning, or adaptive mitigation.

Together, these mechanisms sustain reliable operation in environments where even transient memory faults can cascade into system-level failures.

Together, these mechanisms form a multilayered reliability framework that protects modern memory systems against both transient disturbances and long-term degradation.

By combining circuit-level protection, architectural redundancy, and system-level monitoring, designers can significantly reduce the probability that memory faults propagate into visible system failures.

As memory densities and operating speeds continue to increase, the importance of robust error management grows correspondingly. Consequently, reliability considerations are now integral to memory architecture design rather than an auxiliary concern addressed only during post-production testing.

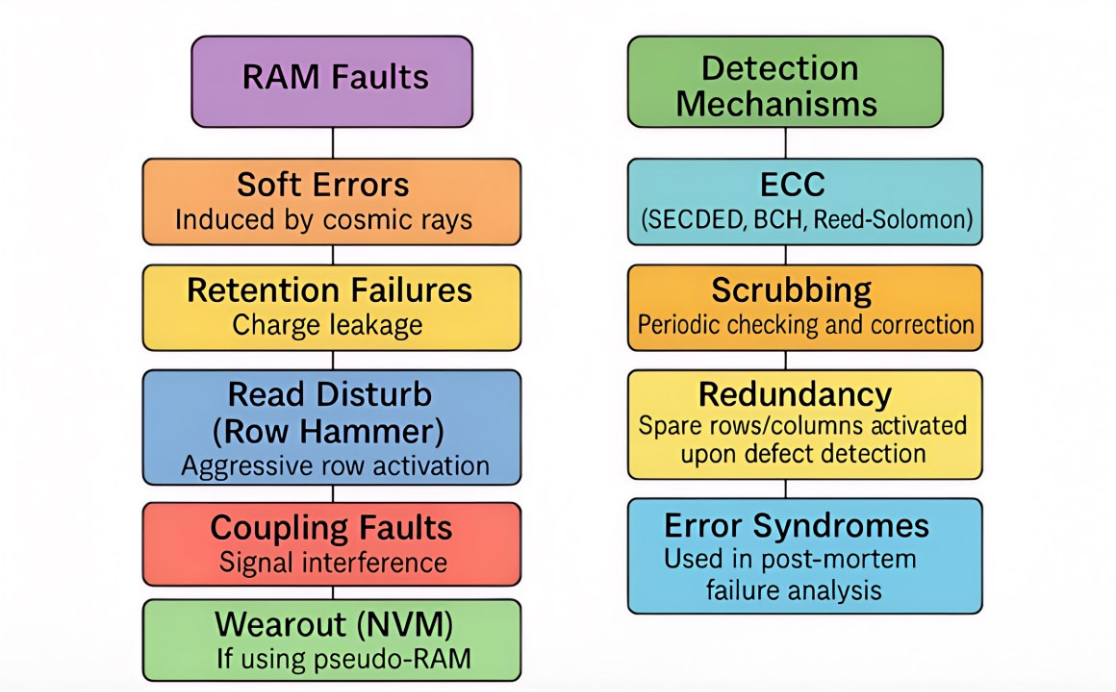

Figure 1.19—Taxonomy of memory faults and detection mechanisms

This Figure presents a structured taxonomy linking dominant RAM fault classes with their corresponding detection and mitigation strategies.

On the left, the principal fault categories are shown:

- **Soft Errors** – Transient bit flips caused by energetic particles
- **Retention Failures** – Charge loss in DRAM cells due to leakage
- **Read Disturb (Rowhammer)** – Aggressive row activation causing adjacent cell corruption
- **Coupling Faults** – Crosstalk-induced interference between neighboring lines
- **Wearout in NVM** – Endurance degradation in pseudo-RAM technologies

On the right, architectural countermeasures are mapped to these faults:

- **Error Correction Codes (ECC)** – SECDED, BCH, Reed–Solomon
- **Scrubbing** – Periodic background error detection and correction
- **Redundancy** – Spare rows and columns activated upon fault detection
- **Error Syndromes** – Diagnostic signatures for fault classification

The Figure emphasizes the tight coupling between physical failure mechanisms and the architectural techniques required to preserve data integrity in modern, high-density memory systems.

1.3.7 Testing and Diagnostic Methodologies

RAM validation and diagnostics rely on a diverse set of methodologies, selected according to system constraints, required coverage, and target fault models. No single technique is sufficient

across all operating conditions; instead, effective diagnostics combine complementary approaches.

- **Functional Testing** – Application-level stress routines exercise memory allocation, deallocation, and access paths (e.g., malloc/free cycles) under realistic workloads. While not exhaustive, such tests are effective at revealing systemic integration issues and software-induced memory misuse.
- **Built-In Self-Test (BIST)** – Hardware-embedded diagnostic logic executes predefined test algorithms at full operational speed. BIST controllers commonly implement March-based sequences during power-on self-test, manufacturing screening, or idle runtime windows, enabling fast, automated fault detection without external equipment.
- **Software-Based Testing** – Operating system utilities or standalone diagnostics apply structured patterns such as walking ones/zeros, checkerboards, random fills, and address line tests. These techniques are especially valuable for in-field validation when dedicated hardware support is unavailable.
- **March Algorithms** – Systematic read/write sequences designed to activate specific fault models with high efficiency:
  - **March C** – Detects stuck-at, transition, and selected coupling faults
  - **March A/B** – Extend coverage to additional dynamic and coupling faults
  - **March SS** – Targets complex intra-word and inter-word interactions in dense arrays

Diagnostic Objectives

Effective RAM diagnostics aim to:

- **Estimate Coverage** – Quantify the proportion of modeled faults activated by each test sequence
- **Localize Failures** – Identify fault granularity, from single-bit defects to rows, banks, or entire arrays
- **Isolate Fault Types** – Distinguish transient soft errors from permanent structural defects
- **Stress System Margins** – Expose marginal faults under voltage scaling, thermal variation, and high-load conditions

This multi-layered methodology ensures robust validation throughout manufacturing, deployment, and operational lifetime.

In practice, these techniques are often combined within coordinated validation workflows that integrate hardware BIST execution, software diagnostics, and system-level stress testing. Such hybrid approaches balance execution time with diagnostic coverage while maintaining high confidence in the reliability of modern memory subsystems.

This integrated perspective forms the basis for the more advanced diagnostic models and optimization techniques discussed in the subsequent chapters.

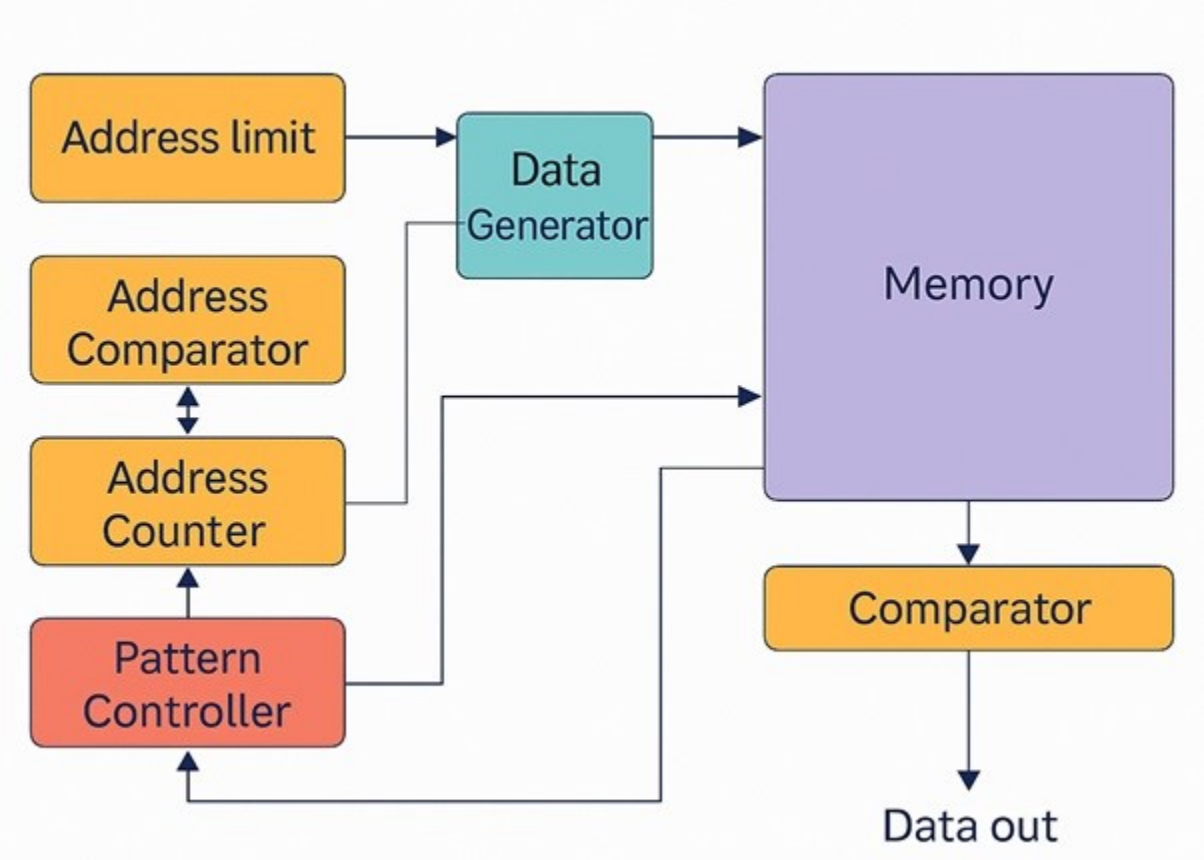

Figure 1.20—MBIST architecture with pattern generator, comparator, and controller

This Figure illustrates the functional architecture of a Memory Built-In Self-Test (MBIST) system.

The **Pattern Controller** orchestrates test execution, coordinating address traversal and phase sequencing. It interfaces with an **Address Counter**, which iterates through memory locations, and an **Address Comparator**, which enforces limits and signals completion.

A **Data Generator** produces deterministic test patterns—such as walking sequences, checkerboards, or March elements—applied directly to the memory array. The **Comparator** evaluates memory output against expected values, flagging discrepancies.

This modular MBIST architecture enables high-speed detection of stuck-at, transition, and coupling faults with minimal external control, making it well suited for production screening and in-field health monitoring.

1.3.8 RAM and System Security Considerations

Beyond reliability concerns, RAM constitutes a critical attack surface in modern computing systems due to both its physical properties and logical access semantics. Several classes of attacks exploit these characteristics:

- **Cold Boot Attacks** – Residual charge in DRAM cells persists briefly after power loss, allowing attackers to recover sensitive data by rapidly transferring memory modules to controlled environments.

- **Buffer Overflows** – Improper bounds checking in stack or heap operations enables overwriting of control data, leading to arbitrary code execution.
- **Side-Channel Attacks** – Timing variations in memory access patterns can leak secret-dependent information, undermining cryptographic operations.
- **Rowhammer Attacks** – Malicious exploitation of read disturb effects enables controlled bit flips that bypass memory isolation.
- **Memory Poisoning** – Injection of corrupted data via compromised software or malicious peripherals destabilizes system behavior.

Mitigation Strategies

- **Stack Canaries** – Sentinel values detect overwrite attempts in stack frames
- **ECC and Memory Fencing** – Preserve integrity and enforce isolation boundaries
- **Secure Erase Procedures** – Overwrite RAM contents during shutdown
- **Access Pattern Randomization** – Obscures timing signatures
- **Memory Encryption** – Protects data-in-use within trusted execution environments

These countermeasures underscore the necessity of treating RAM as both a performance resource and a security-critical subsystem.

1.3.9 Summary

Random Access Memory constitutes the execution substrate for all active computation, tightly coupling processor pipelines with data storage and manipulation. Its latency, bandwidth, fault behavior, and access semantics directly constrain system performance, responsiveness, and reliability.

RAM is not a passive storage medium but an actively managed subsystem whose correct operation depends on coordinated design across multiple abstraction layers—from device-level charge physics and microarchitectural timing to operating system memory management and security enforcement.

As systems evolve toward higher densities, hybrid memory technologies, and security-sensitive deployments, rigorous testing, fault tolerance, and protection mechanisms become indispensable. The subsequent sections build on this foundation by examining how physical memory properties drive advances in diagnostic frameworks and adaptive testing methodologies.

1.4 Key Memory Characteristics: Volatility, Speed, Cost, and Integration

The design, optimization, and validation of memory systems require a disciplined understanding of their physical behavior, architectural semantics, and economic constraints. Four characteristics—**volatility**, **speed**, **cost**, and **integration**—form the core axes of memory engineering. Together they shape system architecture, software execution behavior, diagnostic methodology, and long-term reliability.

These dimensions are tightly coupled rather than independent. Improvements in one axis typically impose penalties in another. For example, pushing for lower access latency may

increase power density and thermal output, while reducing cost per bit can degrade retention margins, increase error rates, or limit the feasibility of strong on-die resilience mechanisms. Consequently, memory engineering is best viewed as a multi-objective optimization problem, requiring coordinated decisions across device physics, microarchitecture, controllers, packaging, operating systems, and validation workflows.

The subsections that follow analyze each characteristic in depth and explicitly connect it to memory hierarchy design, fault modeling, and diagnostic strategy selection.

1.4.1 Volatility: Retention vs. Accessibility

Volatility determines whether stored information persists without continuous power. It is one of the most fundamental differentiators among memory technologies because it directly governs persistence guarantees, system recovery behavior, and the design of fault-tolerant mechanisms.

Volatile Memory

- **Definition** – Requires uninterrupted power to preserve stored data.
- **Examples** – Static RAM (SRAM), Dynamic RAM (DRAM).
- **Key characteristics**
    - ❖ Low access latency and high throughput, enabling performance-critical execution paths.
    - ❖ Typically lower density than most non-volatile technologies due to larger cell structures (particularly SRAM).
    - ❖ Dominant in high-speed hierarchy tiers: registers, cache memories, and main system RAM.

Volatile memories are optimized structurally for rapid read/write cycles. SRAM holds state using bistable latch structures and does not require refresh, supporting predictable access and non-destructive reads. DRAM achieves much higher density using capacitor-based storage, but requires periodic refresh to counter charge leakage, and its access behavior is constrained by activation, precharge, and timing windows.

From a system perspective, volatility is often a feature rather than a limitation: it enables high-speed computation with tight timing guarantees. In real-time systems, predictable access behavior and bounded jitter are essential, and volatile memory tiers (especially SRAM-based structures) frequently serve as the determinism anchor. However, volatility becomes a constraint for mission-critical and power-constrained environments in which persistence or rapid crash recovery is required.

Non-Volatile Memory (NVM)

- **Definition** – Retains stored data in the absence of power.
- **Examples** – Flash, EEPROM, MRAM, ReRAM, PCM, FeRAM.
- **Key characteristics:**

- ❖ Writes are typically slower and more energy-intensive than volatile memory, and read latency may also be higher depending on technology and integration level.
- ❖ Some technologies exhibit endurance limitations (notably Flash) due to charge trapping, oxide degradation, or phase-change fatigue.
- ❖ Controller-level mechanisms such as wear-leveling, garbage collection, and ECC are commonly required to sustain practical reliability.

A critical point for diagnostics is that the volatile vs. non-volatile distinction is not purely binary in modern systems. Many emerging NVM candidates exhibit **hybrid behaviors** and analog drift phenomena (e.g., resistance drift in PCM, retention decay and variability in ReRAM).

These behaviors blur classical fault-model boundaries and demand technology-aware test patterns, retention profiling, and stress strategies that incorporate time dependence, history dependence, and environmental sensitivity.

In the context of later chapters (**Chapters 15–16**), these hybrid behaviors motivate adaptive diagnostic workflows capable of adjusting pattern selection, timing parameters, and evaluation thresholds based on device class, operating conditions, and observed degradation trends, as demonstrated through practical toolchain integration and experimental optimization frameworks.

1.4.2 Speed: Access Time and Bandwidth

Speed is not a single metric; it is a multi-parameter performance envelope reflecting how effectively the memory subsystem can serve instruction streams and data-intensive workloads. At minimum, speed must be described using:

- **Access latency** – elapsed time from request issuance to availability of valid data.
- **Bandwidth** – sustained transfer rate (commonly GB/s), reflecting peak throughput under streaming conditions.
- **Cycle time** – minimum spacing between repeated operations to the same structural resource (row, bank, or channel).
- **Burst and prefetch behavior** – particularly in DDR-class devices, where multiple words are transferred per access to amortize activation and command overhead.

Table 1.2—Speed hierarchy (representative)

Memory Type	Typical Latency	Notes
Registers	~1 ns	Integrated within CPU cores for operand storage and pipeline staging
L1 Cache	1–3 ns	SRAM-based; commonly split into I-cache and D-cache

Table 1.2—Speed hierarchy (representative) (Continued)

Memory Type	Typical Latency	Notes
DRAM	50–150 ns	Requires row activation/precharge and is refresh-constrained
SSD	25–100 µs	NAND-based; latency varies with queue depth, mapping, and controller state
HDD	1–10 ms	Mechanical seek and rotation dominate access time

Real performance is shaped by additional factors such as channel count, controller scheduling, row-buffer locality, bank-level parallelism, prefetch efficiency, and workload access locality.

Sequential access can partially mask true latency through cache line fills and hardware prefetching, whereas random or pointer-heavy access patterns expose the intrinsic latency profile and stress translation, cache, and memory scheduling subsystems.

For diagnostic engineering, speed has direct consequences for fault activation and reproducibility.

In DRAM, timing parameters such as t_{RCD},t_{CL} and t_{RAS} are not merely performance knobs; they define the temporal conditions under which certain faults become observable, especially for marginal cells, coupling behavior, and disturb-related effects.

Within PROVER-based synthesis and simulation, realistic modeling of these timing windows is essential to avoid "paper coverage" that does not translate into physically reproducible activation in real devices.

1.4.3 Cost: Economic Viability per Bit

Memory cost is often summarized as cost per bit or cost per gigabyte, but economic viability in real systems must be evaluated in terms of both acquisition cost and operational consequences. A complete cost model includes:

- **Die area per bit** – driven by cell geometry and process technology, shaping density and attainable yield.
- **Manufacturing yield** – strongly dependent on defect density, particularly critical for high-density arrays where yield losses scale aggressively.
- **Energy per access** – affects total operational cost in data centers and battery-driven systems.
- **System-level overhead** – thermal dissipation, cooling requirements, power delivery, packaging complexity, and redundancy/ECC silicon overhead contribute to total cost of ownership (TCO).

Table 1.3—Indicative cost hierarchy

Technology	Cost per GB (approx.)	Integration use
HDD	< $0.05	Archival and bulk storage
NAND Flash SSD	$0.05–$0.20	Secondary storage in servers and PCs
DRAM	$2–$6	Main system memory
SRAM	$50–$100+	On-chip caches and register files
MRAM / NVM	$20–$80	Embedded systems, edge devices, specialized persistent tiers

Architectural decisions frequently reflect "performance per dollar" optimization under workload constraints. AI training systems often prioritize bandwidth per dollar (favoring wide-bus solutions such as HBM), while embedded platforms may prioritize power per dollar, selecting technologies that minimize energy while meeting bounded performance constraints.

From a diagnostic and validation standpoint, cost directly shapes feasible test depth. High-volume, cost-sensitive products may depend on time-bounded manufacturing tests and probabilistic screening, whereas mission-critical and enterprise platforms justify deeper strategies—full March-pattern coverage, ECC validation under stress, redundancy verification, in-field scrubbing, and fault logging—despite increased test time and infrastructure overhead.

In practice, the economic model often determines whether diagnostics are primarily *manufacturing-centric* or extend into the device lifecycle as a continuous reliability service.

1.4.4 Integration: Physical and Logical Embedding

Integration captures how memory is physically incorporated into hardware platforms and how it is exposed logically to software. Integration choices influence latency, bandwidth, capacity scaling, fault propagation characteristics, and the observability of failures in both manufacturing test and in-field diagnostics.

Levels of physical integration

On-chip integration – Registers and SRAM caches within CPU cores, and in some designs embedded DRAM (eDRAM) within SoCs.

- **Benefits** – Ultra-low latency, high bandwidth, fine-grained synchronization with processor pipelines.
- **Challenges** – High die-area cost, thermal coupling with logic cores, increased design complexity (multi-port access, coherency, power gating interactions).

Off-chip modules – DRAM on DIMMs (DDR3/DDR4/DDR5) interfaced through memory controllers.

- **Benefits** – High-capacity scalability and flexible configuration.
- **Trade-offs** – Higher latency and power than on-chip tiers, but dramatically higher capacity per platform.

Stacked integration – HBM and 3D NAND employing vertical stacking.

- **Benefits** – Very high throughput and improved energy efficiency via wide internal buses and reduced signaling distance.
- **Requirements** – TSVs, advanced packaging, thermal management, and stack-aware validation.

Distributed / remote memory – Emerging disaggregated designs and interconnect-based memory pooling (e.g., CXL-class approaches).

- **Benefits** – Resource pooling and composable architectures in data centers.
- **Challenges** – Additional latency, coherence complexity, and timing variability across fabrics.

Integration level strongly affects how faults propagate and how they manifest in observable signatures. Stacked memories introduce unique **z-axis coupling** and TSV-related defect classes, while distributed memory adds synchronization uncertainty and coherence-related failure modes. In operator-based fault modeling, these integration-driven differences influence both activation conditions and the interpretability of syndrome patterns.

Logical integration

Even when physically fragmented, memory is typically presented to software through abstractions that create the illusion of contiguity and uniformity. Virtual memory mechanisms, page tables, caching, and NUMA policies mask physical distribution while shaping access behavior.

In practice, mappings may span:

- Multiple DRAM banks and channels
- NUMA domains across sockets or chiplets
- Heterogeneous tiers (e.g., DRAM combined with SCM-class devices)

Testing implications

Physical and logical integration jointly impose diagnostic requirements that cannot be satisfied by black-box testing alone:

- **Address translation modeling** – validation of virtual-to-physical mapping correctness, permissions, and boundary enforcement
- **Timing skew analysis** – essential for multi-channel controllers, stacked memory timing closure, and fabric-based tiers
- **Bank interleaving verification** – ensures expected parallelism without cross-bank interference or pathological access coupling
- **Migration-impact testing** – required in hybrid systems where data moves dynamically between tiers, potentially altering timing and fault visibility

This duality—physical complexity masked by logical abstraction—reinforces the need for diagnostic strategies that address both hardware structure and software policy. Only by

integrating these viewpoints can a system achieve coherent performance, fault resilience, and interpretable diagnostic outcomes across the full computing stack.

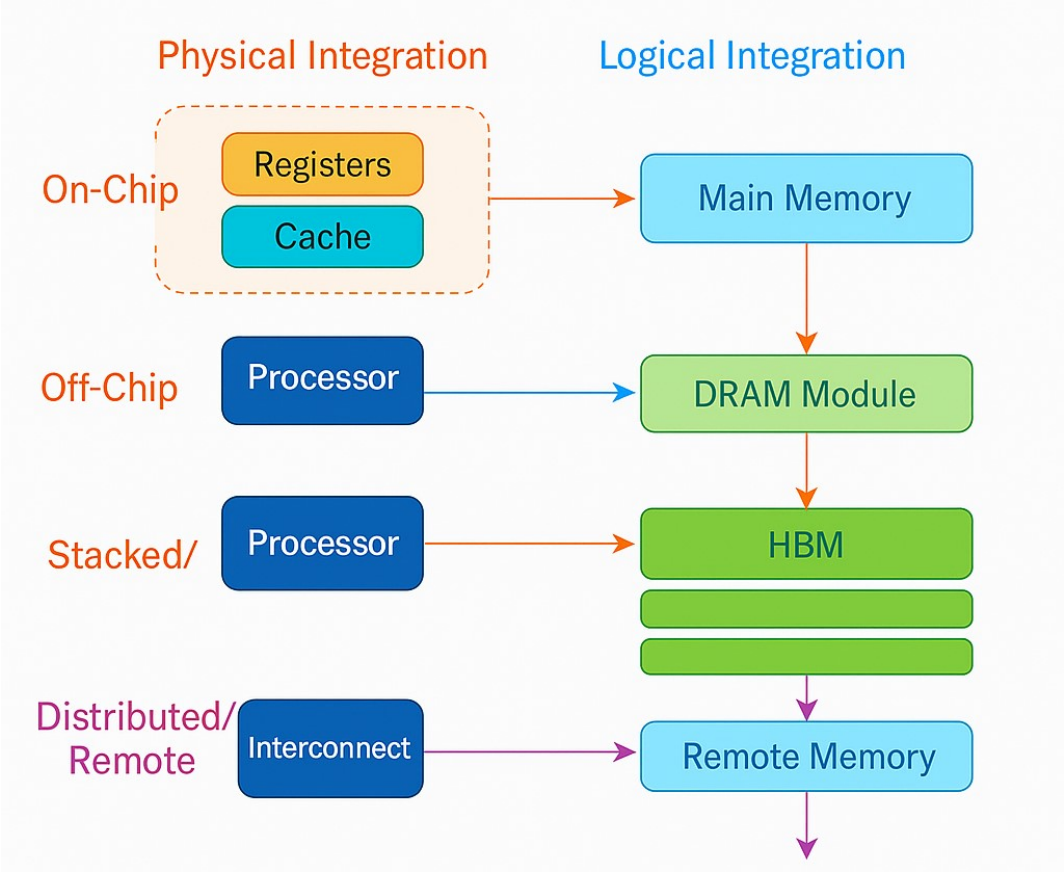

Figure 1.21—Physical vs logical memory integration across processor tiers

Figure 1.21 illustrates the correspondence between physical memory integration levels and their logical abstraction within system address spaces across contemporary processor-centric architectures.

On the **physical integration axis** (left side of the Figure), memory is organized into four increasingly decoupled tiers:

- **On-Chip Integration**
  Registers and cache memories embedded directly within the processor die provide the lowest possible access latency and the highest effective bandwidth. These structures serve as the immediate execution substrate, supporting operand reuse, instruction retirement, and fine-grained temporal locality. Their proximity to execution units enables deterministic timing behavior but severely constrains capacity and increases silicon cost.
- **Off-Chip Integration**
  External DRAM modules connected via memory controllers extend capacity beyond the limits of on-die storage. While off-chip memory offers favorable cost-per-bit scalability, it introduces substantially higher latency, reduced determinism, and greater susceptibility to signal integrity and timing variability.

- **Stacked Integration**
  High Bandwidth Memory (HBM) leverages three-dimensional stacking and Through-Silicon Vias (TSVs) to tightly couple memory dies to logic components. This integration paradigm delivers exceptional bandwidth density and improved energy efficiency per transferred bit, particularly for throughput-dominated workloads. However, it introduces complex thermal, mechanical, and fault-coupling phenomena that challenge both design verification and post-manufacturing diagnostics.
- **Distributed / Remote Integration**
  Memory disaggregation and remote memory pools, enabled by high-speed interconnects such as CXL, extend addressable memory beyond the physical boundary of a single processor package. In such systems, memory resources may be dynamically allocated across nodes, racks, or entire data centers, trading locality and latency predictability for elasticity and resource utilization efficiency.

On the **logical integration axis** (right side of the Figure), these heterogeneous physical tiers are unified through abstraction mechanisms:

- On-chip storage elements are exposed to the execution pipeline as directly addressable, latency-critical memory regions.
- Off-chip DRAM and stacked HBM are incorporated into the operating system's virtual memory subsystem, often differentiated through NUMA policies, page migration strategies, or bandwidth-aware scheduling.
- Distributed memory resources are abstracted as remote NUMA domains or managed through explicit disaggregation frameworks that decouple physical placement from logical ownership.

While such abstraction enables seamless application access and portability, it significantly **increases diagnostic complexity**. Effective test methodologies must account not only for the intrinsic fault behaviors of each integration tier, but also for their distinct latency distributions, timing constraints, coupling mechanisms, and interactions with logical address mapping and system-level performance guarantees.

1.4.5 Interdependence and Trade-Off Matrix

The four fundamental characteristics of memory systems—**volatility, speed, cost, and integration**—are intrinsically interdependent. Improvements along one dimension almost invariably impose compromises along others, forcing system architects to navigate a multi-dimensional trade-off space rather than optimize isolated metrics.
Representative trade-offs include:

Table 1.4—Interdependence and Design Trade-Offs in Memory System Architectures

Design Goal	Typical Trade-Offs
High Speed	Reduced density and elevated cost (e.g., SRAM versus DRAM)
Low Cost	Increased access latency and reduced endurance (e.g., NAND Flash)

Table 1.4—Interdependence and Design Trade-Offs in Memory System Architectures (Continued)

Design Goal	Typical Trade-Offs
High Integration	Elevated thermal density and increased diagnostic complexity (e.g., 3D-stacked HBM)
Non-Volatility	Slower write operations and limited program-erase lifetimes (e.g., Flash, ReRAM)

The **Pareto frontier** governing memory design is not static; it continuously shifts in response to advances in fabrication processes, packaging technologies, and system architectures. Contemporary hybrid solutions—such as NVDIMM, ReRAM-on-logic integration, and cache-aware memory controllers—represent deliberate attempts to balance persistence, performance, and scalability.

These hybrid architectures seek to combine the non-volatility of storage-class memory with the access characteristics of volatile RAM, while simultaneously addressing the accompanying challenges in thermal management, reliability assurance, and testability that arise from increased density and tighter integration.

1.4.6 Diagnostic and Design Implications

Each fundamental memory characteristic introduces distinct diagnostic constraints that must be addressed across the **design, manufacturing, and operational lifecycle**:

- **Volatility**
  Susceptibility to data loss during power interruptions necessitates reset-oriented testing, retention characterization, and power-cycle-aware diagnostics, particularly for DRAM and emerging hybrid non-volatile architectures.
- **Speed**
  Multi-gigahertz interfaces impose stringent setup and hold time requirements. Shrinking signal margins complicate fault injection, at-speed testing, and observability, increasing reliance on on-chip monitors and built-in self-test mechanisms.
- **Cost**
  Economic constraints directly shape test depth and coverage. High-volume, low-margin products often rely primarily on BIST and statistical screening, whereas safety-critical and mission-critical systems justify exhaustive external testing and redundancy despite higher costs.
- **Integration**
  Die-stacked memories and aggressive interleaving schemes exacerbate fault localization due to vertical coupling effects, thermal gradients, and cross-bank interference, demanding multi-dimensional fault models and correlation-aware diagnostic strategies.

These characteristics were mapped onto a cost–coverage–redundancy design space, enabling the synthesis of optimized test sets through fuzzy-logic inference. This framework supports

dynamic adaptation of diagnostic strategies to the intersection of failure risk, economic constraints, and architectural complexity.

1.4.7 Summary

Volatility, speed, cost, and integration constitute the four cardinal axes that define the structure, performance envelope, and deployment context of modern memory systems. These attributes shape not only physical hierarchies and access policies, but also the fault models, reliability objectives, and diagnostic methodologies required to ensure robust operation.

A rigorous understanding of their interdependence equips system architects and test engineers to design memory subsystems that are simultaneously **high-performance, testable, repairable, and economically viable**. As memory technologies evolve toward heterogeneous, unified, and intelligence-augmented architectures, these principles remain central to bridging the gap between technological innovation and long-term operational resilience.

1.5 Internal Memory Architecture: Cells, Arrays, and Control Logic

The observable performance envelope, fault behavior, and diagnostic response of a memory system are fundamentally determined by its **internal architecture**. From the microscopic operation of individual memory cells to the macroscopic organization of arrays, banks, and their associated control logic, each structural layer directly shapes reliability, timing behavior, and testability.

Across both volatile (SRAM, DRAM) and non-volatile (Flash, MRAM, PCM, ReRAM) technologies, memory architectures are constrained by physical device properties, circuit topology, and architectural control mechanisms. A rigorous understanding of these internal structures is therefore indispensable for **high-fidelity testing**, **accurate fault modeling**, and **robust reliability engineering**.

Foundational research and subsequent publications have demonstrated that **cell-level interactions**, particularly in dense DRAM arrays and emerging non-volatile memories, can propagate upward through the architectural hierarchy. These interactions influence fault signatures, limit observability, and impose fundamental constraints on diagnosability. The present section examines the architectural building blocks of memory systems and clarifies their role in shaping system-level behavior.

1.5.1 The Memory Cell: Atomic Unit of Storage

At the most granular level, a memory system consists of **memory cells**—elementary electronic circuits designed to store a single binary state. The electrical characteristics, stability margins, and access mechanisms of these cells dictate not only performance and power efficiency, but also scalability, failure modes, and diagnostic complexity. The discussion focuses on three principal classes: **SRAM**, **DRAM**, and **emerging non-volatile memories (NVMs)**.

(A) SRAM Cell — 6T Design

The six-transistor (6T) SRAM cell is a bistable, latch-based circuit that underpins modern processor caches and register files.

- **Topology**
  Two cross-coupled CMOS inverters (four transistors) form a stable bistable latch. Two NMOS access transistors connect the latch to complementary bitlines (BL/$B\overline{L}$) under control of a wordline (WL).
- **Operation**
  The stored state is maintained statically as long as power is applied. Read operations are non-destructive, as sensing does not collapse the internal node voltages.
- **Advantages**
  Ultra-low latency, high bandwidth, and deterministic timing behavior make SRAM indispensable for latency-critical structures such as L1/L2/L3 caches and register files.
- **Limitations**
  Large cell area (≈120 F^2) limits achievable density. Aggressive technology scaling increases vulnerability to read instability, write failures, and soft errors induced by process variation and reduced noise margins.
- **Characteristic Fault Behavior**
  - *Stuck-At Faults (SAF)*: Internal node permanently fixed at logic '0' or '1'.
  - *Read-Destructive Faults (RDF)*: Stored value flips during a read due to insufficient read stability.
  - *Write Disturb Faults (WDF)*: Writing one cell perturbs neighboring cells via capacitive or resistive coupling.
- **Diagnostic Implications**
  These faults are effectively targeted using cycle-sensitive March algorithms (e.g., March C-, March SS) and transparent March sequences integrated into BIST infrastructures.

(B) DRAM Cell — 1T1C Design

The one-transistor, one-capacitor (1T1C) DRAM cell achieves exceptional density by storing information as electric charge, making it the dominant architecture for main memory.

- **Topology**
  A single NMOS access transistor, controlled by the wordline, connects a storage capacitor to the bitline. Differential sense amplifiers detect the minute voltage deviation caused by charge sharing during reads.
- **Operation**
  DRAM is inherently volatile. Stored charge leaks over time and must be periodically restored via refresh (typically every 64 ms (or 32 ms under worst-case conditions). Read operations are destructive and require immediate write-back.
- **Advantages**
  Extremely high density and favorable cost-per-bit enable scalable memory systems ranging from gigabytes to terabytes.
- **Limitations**
  Higher access latency than SRAM, refresh overhead, and destructive reads complicate memory controller design and timing closure.
- **Characteristic Fault Behavior**
  - *Retention Faults*: Charge leakage causes premature data loss.

- *Coupling Faults*: Activity on adjacent wordlines or bitlines induces parasitic disturbance.
- *Rowhammer Effect*: Repeated row activations accelerate charge leakage in adjacent rows, leading to reproducible bit flips with severe reliability and security implications.

- **Diagnostic Implications**

Detection and mitigation require retention-aware March tests, pattern-sensitive stress sequences, and architectural countermeasures such as Target Row Refresh (TRR) and row activation tracking.

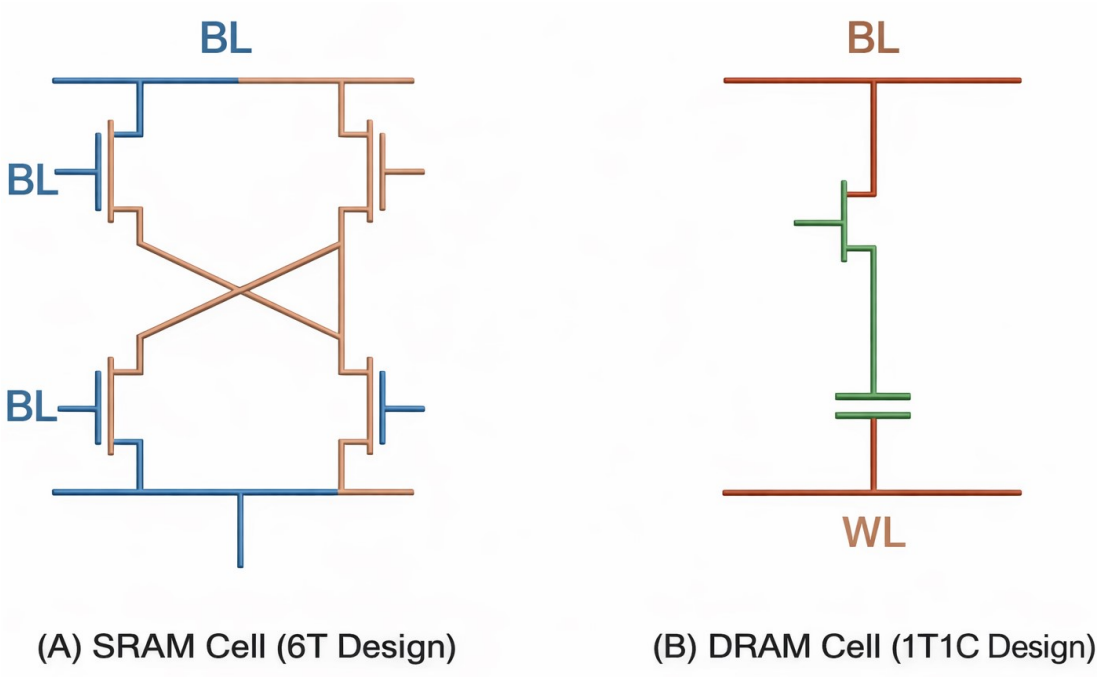

Figure 1.22—Comparison of SRAM 6T and DRAM 1T1C cells (access paths, read destructiveness, and signal flow)

This figure contrasts the bistable 6T SRAM cell with the minimalist 1T1C DRAM cell, highlighting access mechanisms, signal paths, and the destructive versus non-destructive nature of read operations.

(C) NVM Cells — Emerging Non-Volatile Memory Technologies

Non-volatile memories preserve data without continuous power by exploiting physical mechanisms beyond simple charge storage.

These technologies are increasingly important in embedded systems, AI accelerators, and storage-class memory.

- **Flash Memory**
  Floating-gate MOSFETs store charge on an electrically isolated node. High programming voltages, long write/erase times, and oxide wear dominate failure behavior.

- **MRAM**
  Magnetic Tunnel Junctions encode data via relative magnetic orientation. Challenges include write energy, thermal stability, and magnetic interference at advanced nodes.
- **PCM**
  Phase-change materials toggle between crystalline and amorphous states. Endurance degradation, resistance drift, and thermal cross-talk dominate fault behavior.
- **ReRAM**
  Filamentary conduction paths in metal oxides enable resistive switching. Variability, stochastic switching, and gradual resistance drift complicate reliability assurance.

Distinct Fault Signatures

- Write-disturb and thermal cross-talk effects
- Endurance-driven permanent failures
- Analog deviation faults not captured by binary fault models

Diagnostic Implications

Standard digital tests are insufficient. Reliable validation requires analog-aware fault models, multi-level sensing, and long-term endurance stress characterization.

1.5.2 Memory Arrays and Word Organization

Individual cells are organized into **two-dimensional arrays** to achieve capacity, bandwidth, and addressability. Array organization directly affects latency, power consumption, and fault manifestation.

- **Wordlines (WL)** activate rows of cells simultaneously.
- **Bitlines (BL)** convey stored charge or voltage to sense amplifiers.
- **Sense Amplifiers** convert small analog differentials into digital values.
- **Isolation Devices** segment subarrays to limit leakage and coupling.

Bitlines are typically precharged (e.g., to VDD/2 in DRAM) to maximize sensing margin and minimize energy.

Array Topologies

1. Planar WL×BL matrices
2. Subarray partitioning for RC reduction
3. Banked architectures enabling parallelism
4. 3D-stacked arrays with TSVs, introducing vertical coupling and thermal gradients

Design Objectives

- RC delay minimization
- Noise suppression and shielding
- Latency equalization across array geometry
- Redundancy via spare rows/columns and repair fuses

Diagnostic Implications

In my symbolic fault modeling framework (Chapter 8), WL/BL electrical properties were shown to correlate strongly with coupling, disturb, and delay faults. Building on these observations, modern diagnostics integrate layout-aware stress patterns, timing-skew injection, and adaptive refresh policies.

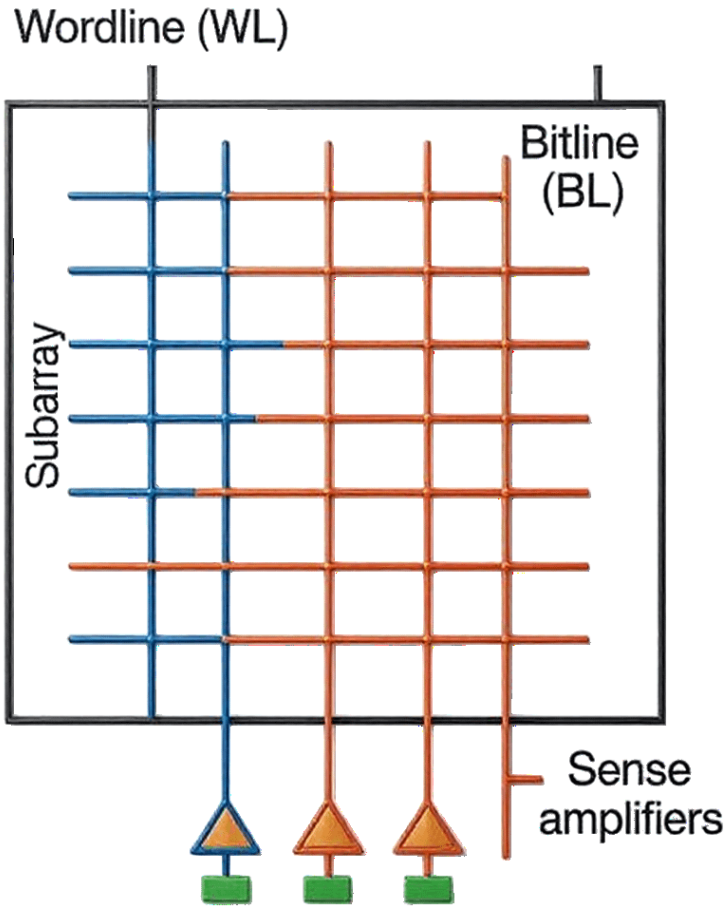

Figure 1.23—Hierarchical layout of subarray, wordline, and bitline structures

This Figure illustrates the hierarchical organization of memory arrays, emphasizing the orthogonal arrangement of wordlines (WL) and bitlines (BL) within a subarray. Each memory cell resides at the intersection of a WL and a BL, with sense amplifiers positioned at the termini of the bitlines to detect and amplify the minute voltage differentials generated during read operations. Subarray partitioning minimizes parasitic capacitance and RC delay, thereby enabling higher operational speeds and improved energy efficiency in large-scale memory designs.

1.5.3 Row and Column Decoders

Memory access is realized through coordinated **row and column decoding**, resolving logical addresses into physical WL/BL selections.

- **Row Decoders** activate target wordlines.
- **Column Decoders** select output bitlines within the activated row.

Fault Sensitivities

- Decoder logic failures
- Address aliasing and mis-selection
- Opens and shorts affecting multiple cells

In my work on embedded diagnostic engines, inverse address mapping and pattern displacement analysis were used to isolate decoder faults with high resolution, significantly improving diagnosability in complex arrays.

1.5.4 Sense Amplifiers and Precharge Logic

In DRAM, read access generates voltage differentials on the order of tens of millivolts. Sense amplifiers must rapidly amplify these signals while restoring cell contents.

- **Latch-based sensing** enables fast resolution.
- **Precharge logic** resets bitlines for subsequent access.

Challenges

- Offset voltages at low VDD
- Sense-induced disturb effects

Tight coupling to timing parameters (t_{RCD}, t_{CL}).

Advanced designs employ adaptive offset cancellation and dynamic thresholding. In **Chapter 16**, simulation-based analysis demonstrates how thermal stress exacerbates offset-induced misreads and how adaptive sensing restores observability.

1.5.5 I/O Buffers and Peripheral Logic

The input/output (I/O) subsystem forms the electrical and timing interface between the internal memory core and the external system bus. Its primary function is to ensure that data, address, and control signals are transferred reliably across clock domains and under varying load and environmental conditions. The I/O path typically comprises three tightly coupled components:

- **Input Buffers**, which receive, synchronize, and condition incoming address and control signals, mitigating metastability and noise.
- **Output Drivers**, which place read data onto bidirectional buses while preserving signal integrity in the presence of capacitive loading, impedance discontinuities, and interconnect parasitics.
- **Clock Interface Logic**, which aligns internal memory operations with external timing references. In double data rate (DDR) systems, this logic supports data transfers on both rising and falling clock edges to maximize bandwidth utilization.

As operating frequencies increase, timing margins within the I/O path become increasingly constrained. Common reliability threats include setup and hold time violations, bidirectional bus skew, and impedance mismatches that produce reflections and crosstalk.

These effects can lead to intermittent read/write failures that are difficult to detect using purely functional tests.

In contemporary DRAM standards such as DDR5 and LPDDR5, I/O and peripheral logic play a decisive role in overall system reliability. Accurate modeling of these components within diagnostic frameworks is essential for predicting real-world fault manifestations, validating compliance with aggressive timing specifications, and preserving data integrity under high-frequency operation.

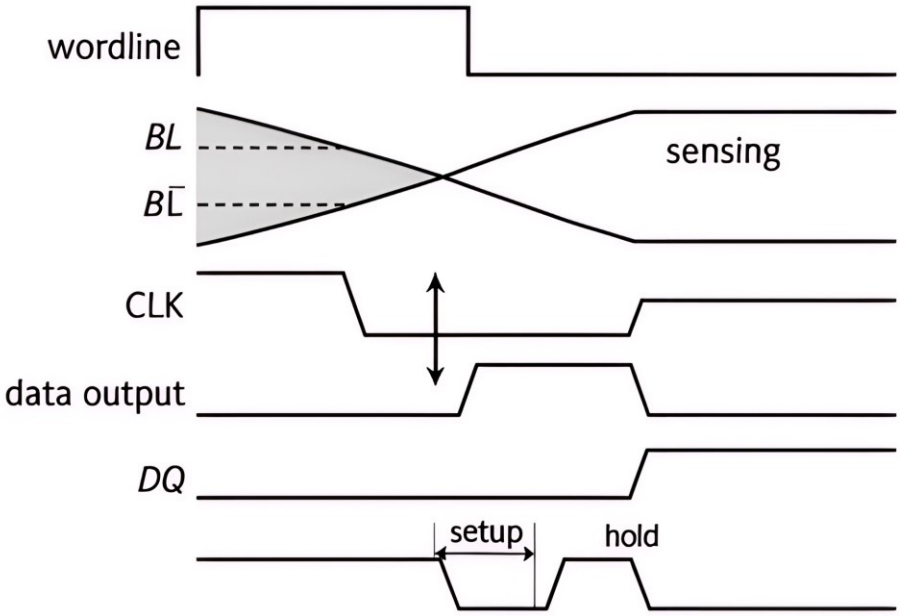

Figure 1.24—Timing diagram showing bitline sensing and I/O transition events

This Figure illustrates the critical timing relationships during a DRAM read operation. Assertion of the wordline activates the selected row, initiating charge sharing between the cell capacitor and the complementary bitlines, which are initially precharged to half the supply voltage.

The resulting differential voltage is amplified during the sensing phase and subsequently latched. The clock governs synchronization between internal sensing and external data transfer, while the data output (DQ) waveform highlights setup and hold margins relative to clock edges. The diagram emphasizes the tight coupling between internal analog sensing dynamics and external digital I/O timing.

1.5.6 Redundancy and Repairable Architectures

To improve yield and extend operational lifetime, modern high-density memory devices incorporate built-in redundancy and repair mechanisms. These architectures tolerate both manufacturing defects and in-field degradation by selectively isolating faulty regions and redirecting accesses to healthy resources.

Common redundancy features include spare rows and columns provisioned during fabrication, programmable fuses or remapping tables that permanently or dynamically redirect defective addresses, and built-in self-repair (BISR) modules capable of autonomous fault detection and repair during production or operation.

While redundancy significantly enhances reliability, it complicates diagnostics. Defects may be masked by remapping, rendering them invisible to conventional test sequences. Furthermore, redundant paths themselves may harbor latent or marginal faults that escape detection unless explicitly exercised. Post-repair validation is therefore essential to ensure that remapped regions preserve data integrity and that no secondary defects are introduced into active regions.

Within the Optimal_Test framework, repair-aware diagnostic algorithms were developed to address these challenges. By simulating redundancy behavior and tracking coverage beyond available spares, these methods maintain diagnosability of both permanent and transient faults throughout the operational lifetime of the memory device.

1.5.7 Three-Dimensional Memory Stacking and TSV Interconnects

The evolution of memory technology increasingly favors vertical integration, stacking multiple dies to achieve extreme density and bandwidth. Prominent examples include three-dimensional NAND flash, high-bandwidth memory (HBM), and wide I/O architectures, all of which rely on through-silicon vias (TSVs) to enable vertical signal propagation.

Although these architectures offer substantial performance gains, they introduce new fault mechanisms absent in planar designs. TSV opens or shorts can disrupt inter-die communication, while thermal gradients across stacked dies can induce mechanical stress, delamination, and timing drift. High TSV density also increases the risk of vertical crosstalk and inter-layer coupling, complicating signal integrity and synchronization.

Effective diagnostics for three-dimensional memories must therefore account for vertical timing skew, Z-axis address mapping, inter-layer coupling faults, and thermally induced degradation. The parallel diagnostic model developed in this work, inspired by classical multi-head automaton concepts presented in Chapter 9, anticipates these challenges by enabling multi-head testing and detection of inter-layer fault dependencies in stacked memory systems.

1.5.8 Summary

Memory subsystems are hierarchically organized structures in which microscopic cell-level phenomena and macroscopic interconnect architectures jointly determine performance, reliability, and diagnosability. Defects arising from cell leakage, interconnect failures, timing misalignment, or redundancy interactions can often be traced directly to specific architectural features.

A comprehensive understanding of memory cells, arrays, decoders, sense amplifiers, I/O logic, and repair mechanisms is therefore essential for constructing effective testbenches, generating high-coverage diagnostic patterns, and designing fault-tolerant controllers.

As memory architectures continue to evolve toward stacked, embedded, and hybrid designs, such architectural awareness becomes indispensable for ensuring correctness, endurance, and long-term system reliability.

1.6 Data Integrity and Bit-Level Representation

At its foundation, a memory system is responsible for the reliable storage and retrieval of binary data—the fundamental substrate of all computation, communication, and control. Although bits are abstractly defined as logical zeros and ones, their physical realization varies across technologies, relying on charge storage, transistor states, magnetic orientation, or material phase.

These physical embodiments are inherently vulnerable to a range of disturbances, including charge leakage, read/write interference, endurance-related degradation, environmental effects, and design-induced weaknesses.

Unmitigated bit-level faults can propagate upward through the memory hierarchy, ultimately manifesting as latent instability, performance degradation, or catastrophic system failure. This section examines the physical representation of bits, the mechanisms that threaten integrity, and the diagnostic strategies required to detect and mitigate such faults.

1.6.1 Binary Data Encoding and Physical Manifestation

A logical bit represents one of two states, but in physical memory devices these states are implemented through technology-specific mechanisms:

Table 1.5—Physical Representation of Binary Logic States Across Memory Technologies

Logical State	SRAM (6T)	DRAM (1T1C)	Flash / ReRAM	MRAM
0	Low voltage	No stored charge	Low threshold voltage	Antiparallel magnetic alignment
1	High voltage	Stored charge	High threshold voltage	Parallel magnetic alignment

Despite their binary abstraction, these representations are subject to electrical noise, temporal drift, and environmental stress.

Even a single undetected bit error may corrupt critical variables, compromise cryptographic material, destabilize operating systems, or perturb machine-learning model parameters.

In the symbolic fault models developed in this work, such physical error behaviors are abstracted into diagnostic operators, including stuck-at faults, transition faults, and coupling faults.

This abstraction enables systematic mapping of low-level anomalies to observable test outcomes and supports the synthesis of targeted diagnostic patterns, as detailed in Chapter 8.

1.6.2 Types of Bit-Level Faults

Bit-level faults may be classified according to their behavior, physical origin, and activation conditions.

The principal categories include:

Stuck-At Faults (SAF).
A bit persistently reads as a fixed value regardless of write attempts, typically due to fabrication defects, permanent wear, or broken interconnects.

Transition Faults (TF).
A bit fails to transition in one direction, either from zero to one or from one to zero. Such faults often arise from degraded drive strength or shifted threshold voltages and are exacerbated under low-voltage or high-temperature operation.

Retention Faults (RF).
A bit changes state over time without access, caused by charge leakage, resistive drift, or magnetic instability. These faults are prominent in DRAM and emerging non-volatile memories and require time-dependent stress testing for detection.

Coupling Faults (CF).
Operations on an aggressor cell induce unintended state changes in a neighboring victim cell due to parasitic coupling or leakage. Formal victim–aggressor dependency models developed in this work demonstrate that such faults may be triggered without direct victim access.

Read Disturb Faults (Rowhammer).
Repeated activation of specific DRAM rows accelerates charge loss in adjacent rows, inducing bit flips. Beyond reliability concerns, these faults pose significant security risks by enabling isolation bypasses.
Each fault class exhibits distinct activation profiles and observability characteristics, necessitating fault-specific test strategies to achieve high diagnostic coverage and reliable classification.

1.6.3 Integrity Metrics and Expectations

Memory reliability is quantified using statistical and operational metrics that characterize the frequency, severity, and temporal evolution of bit-level errors. Key measures include bit error rate, mean time to failure, retention time distributions, and ECC correction rates. Together, these metrics inform manufacturing qualification, lifetime prediction, and in-field health monitoring.

In mission-critical domains such as avionics, medical systems, and autonomous platforms, these metrics are coupled with stringent operational requirements. Errors must be detected and mitigated within strict latency bounds, localized through redundancy without system interruption, and continuously monitored to enable predictive failure modeling.

Within the Optimal_Test framework, such metrics are integrated into adaptive diagnostic algorithms that dynamically adjust test coverage, refresh policies, and repair strategies in

response to real-time degradation trends. This approach extends the operational lifespan of memory subsystems while preserving reliability under sustained stress.

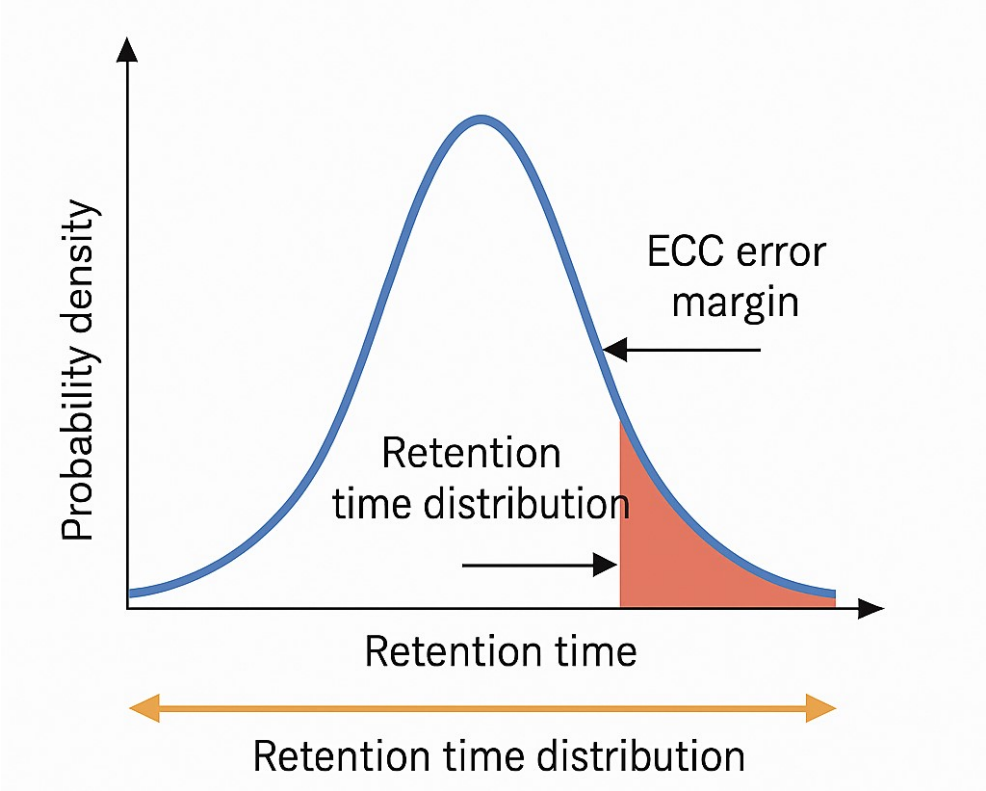

Figure 1.25—Statistical distribution of retention times and ECC error margin

This Figure illustrates the probability density function of retention times across a population of memory cells. The bell-shaped curve represents the statistical dispersion of retention capability resulting from fabrication variability, temperature gradients, and aging-related degradation. While most cells retain data well beyond the nominal refresh interval, a tail of weaker cells exhibits reduced retention margins.

The shaded tail region denotes the **ECC error margin**, corresponding to cells whose retention times fall below the threshold correctable by the deployed error-correcting code. Although errors originating in this region may initially be corrected transparently by ECC, continued degradation increases the likelihood of uncorrectable failures. The width and position of this margin directly influence ECC scheme selection (e.g., SECDED versus BCH), refresh policy tuning, and redundancy provisioning.

In mission-critical systems, controlling the ECC margin is essential for maintaining bounded failure rates under defined service-level objectives. Retention distributions also provide key inputs for predictive reliability models and enable adaptive refresh scheduling and ECC scrubbing strategies in advanced diagnostic frameworks.

1.6.5 Techniques for Ensuring Data Integrity

Ensuring data integrity in modern memory systems requires a layered defense strategy that combines hardware, firmware, and software mechanisms. These techniques address fault

detection, correction, and proactive mitigation, and are selected based on the error characteristics of the underlying memory technology.

Error Detection Codes (EDC)

- **Parity Bits** provide minimal-overhead detection of odd-number bit errors within a word but offer no correction capability.
- **Checksums** aggregate data values to enable rapid integrity verification, suitable for lightweight or latency-sensitive applications with limited burst-error exposure.
- **Cyclic Redundancy Checks (CRC)** employ polynomial-based detection to identify burst errors with high probability and are widely used in memory interfaces and data-transfer paths.

Error Correction Codes (ECC)

- **Hamming Codes (SECDED)** support single-bit correction and double-bit detection and are widely adopted in DRAM and cache hierarchies due to low latency and modest redundancy overhead.
- **BCH Codes** provide configurable multi-bit correction capability, trading increased decoding complexity and storage overhead for higher resilience.
- **Reed–Solomon Codes** operate on multi-bit symbols rather than individual bits, making them particularly effective for burst-error correction in Flash-based storage systems.
- **Low-Density Parity-Check (LDPC) Codes** achieve near–Shannon-limit performance and are employed in high-density NAND Flash and SSD controllers, where raw bit error rates are high and iterative decoding is acceptable.

Beyond correction, ECC syndrome vectors serve as valuable diagnostic artifacts. In the diagnostic models developed in this work, syndrome patterns were correlated with precomputed fault signatures to enable semi-automated fault localization. This integration allowed embedded systems to classify transient versus permanent faults and to initiate appropriate repair or mitigation actions during field operation.

1.6.6 Bit-Flipping Mechanisms and Physical Thresholds

Bit integrity is challenged by a variety of physical mechanisms that induce unintended logic state transitions. The susceptibility to these mechanisms depends on memory technology, device scaling, environmental stress, and operational workload.

Table 1.6—Physical Bit-Flipping Mechanisms and Technology-Dependent Threshold Effects

Mechanism	Affected Technologies	Description
Charge Leakage	DRAM, Flash	Gradual loss of stored charge due to capacitor leakage or floating-gate decay, eventually reducing voltage margins below sensing thresholds

Table 1.6—Physical Bit-Flipping Mechanisms and Technology-Dependent Threshold Effects (Continued)

Mechanism	Affected Technologies	Description
Electromigration	SRAM	Progressive metal atom displacement under sustained current stress, leading to interconnect degradation
Trap Generation	ReRAM	Formation of defect states in metal–oxide layers, causing resistive instability and threshold drift
Thermal Noise	All	Random charge fluctuations intensified at elevated temperatures, increasing soft error rates
Quantum Tunneling	Flash	Electron leakage through ultra-thin oxide barriers at advanced process nodes, degrading retention
Magnetic Instability	MRAM	Thermally or mechanically induced domain reorientation, resulting in non-deterministic bit errors

These mechanisms define the **threshold conditions** under which bit flipping becomes probable and directly inform both reliability modeling and diagnostic test design.
From a test engineering perspective:

- **Retention-aware stress testing** is essential for identifying weak DRAM cells whose leakage accelerates under reduced refresh or elevated temperature.
- **Endurance cycling** characterizes wear-induced degradation in Flash and ReRAM technologies and supports failure forecasting.
- **Thermal marginal testing** validates MRAM stability under worst-case environmental conditions.
- **Accelerated aging protocols**, including voltage overstress and temperature cycling, are employed to provoke early manifestation of latent defects for predictive analysis.

In the diagnostic frameworks presented in Chapters 8 and 12, these physical mechanisms were parameterized as fault activation thresholds. This abstraction enabled targeted stress patterns and informed test selection within the Optimal_Test framework, selectively exposing latent vulnerabilities without excessive overtesting and achieving efficient test-time optimization while maintaining comprehensive fault coverage.

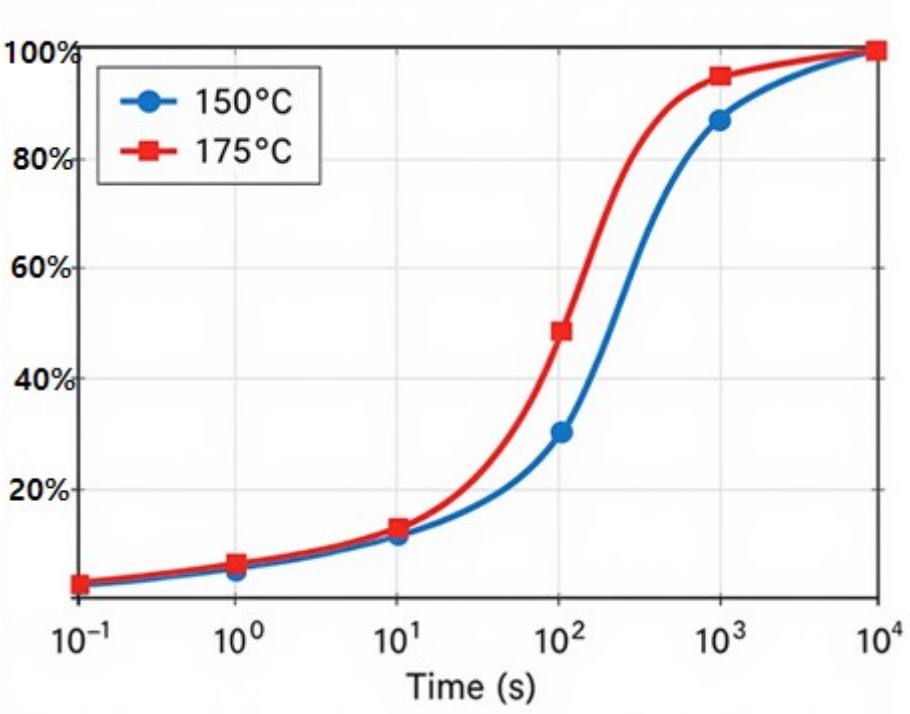

Figure 1.26—Bit flipping under thermal acceleration – test chamber results

This figure reports accelerated thermal-stress measurements obtained in a controlled test chamber. The curves plot the cumulative fraction of flipped bits (expressed as a percentage of affected memory cells) versus elapsed time on a logarithmic time axis. Two elevated-temperature conditions are compared: **150 °C (blue)** and **175 °C (red)**, illustrating the acceleration of failure mechanisms at higher temperature.

The data highlights the strong temperature dependence of degradation kinetics:

- **150 °C:** errors emerge later, increase more gradually, and reach saturation over a longer time horizon.
- **175 °C:** the onset of errors occurs earlier, the growth rate is significantly higher, and saturation is reached more rapidly.

This behavior is consistent with thermally activated failure mechanisms, where increased temperature accelerates processes such as charge leakage, trap generation, diffusion-driven material changes, and interconnect or oxide fatigue. The separation between the curves can be used to estimate activation energy parameters and to extrapolate expected lifetimes under nominal operating conditions using standard thermal-acceleration models (e.g., Arrhenius-based analysis).

In practice, chamber-derived curves of this type inform:

- **Refresh-interval tuning** for DRAM deployed in high-ambient environments or mission profiles with thermal excursions.
- **Guardband selection**, defining safe operating margins across temperature and voltage corners.

- **Early-life screening**, compressing long-term degradation into short-duration qualification tests through controlled acceleration.

1.6.7 Data Path Vulnerabilities

Data integrity is not determined solely by cell retention. Errors can originate anywhere along the signal path—from write initiation through internal transport and sensing to external readout. Consequently, a complete integrity model must include both **cell-level** and **path-level** failure modes. Key vulnerability points include:

- **Input buffers:** may mis-latch transitions under noise coupling, voltage droop, ringing, or marginal edge rates.
- **Sense amplifiers:** offset, mismatch, drift, and temperature-dependent bias shifts can cause incorrect interpretation of small bitline differentials, particularly under low-swing or marginal precharge conditions.
- **Address decoders:** logic or routing defects can produce address aliasing (two logical addresses mapping to one physical location), corrupting unrelated data while appearing intermittent at the system level.
- **Timing circuitry:** setup/hold violations—especially near clock-domain crossings—can induce metastability and sporadic, non-repeatable failures in synchronous transfers.
  In MBIST-oriented simulations, timing-margin collapse along the data path reveals failure classes that may escape nominal-speed validation, including:
- **Pseudo-random escapes** induced by defective precharge behavior localized to specific subarrays, which remain latent under relaxed timing.
- **Temperature-induced skew** in sense-amplifier enable timing, producing misreads only under thermal stress patterns that shrink sensing margins.

These observations motivate extending diagnostics beyond cell-only fault models. Within the Optimal_Test framework, this expansion supports:

- Generation of skew-aware diagnostic vectors targeting timing-sensitive conditions.
- Targeted stress placement at critical path points (buffers, decoders, sensing).
- Coverage models that explicitly incorporate path-level reliability, enabling detection of faults that manifest only when electrical margins are reduced.

1.6.8 Data Integrity vs. Performance Trade-Offs

Modern memory subsystems are optimized for throughput and latency, but performance-driven design decisions often reduce electrical safety margins, shorten timing slack, or weaken detection visibility. As a result, integrity and performance are coupled through explicit trade-offs:

Table 1.7—Performance Optimization Strategies and Their Impact on Data Integrity

Strategy	Gain	Cost
Reduced Refresh Rate	Lower dynamic power consumption, extended battery life	Higher leakage exposure; reduced DRAM retention margin

Table 1.7—Performance Optimization Strategies and Their Impact on Data Integrity (Continued)

Strategy	Gain	Cost
Narrower Sense Margins	Faster decisions; reduced t_{CL}	Higher BER; increased sensitivity to noise and offset drift
Aggressive prefetch	Lower effective latency for sequential access	Increased parasitic activation; elevated Rowhammer exposure
No ECC in L1 caches	Eliminates ECC latency; maximizes pipeline speed	Silent corruption at the fastest tier; relies on downstream detection

Typical system mitigations apply selective protection to maintain performance where cycle time is most constrained:

- ECC applied to **L2/L3** and **main memory**, while **L1** may remain unprotected.
- **Adaptive scrubbing** modifies refresh or correction frequency using in-field telemetry (ECC counts, corrected-error rates, retention drift).

These realities reinforce the need for diagnostic systems designed for **reduced-margin operation**, where weak-bit drift, marginal coupling faults, and timing-dependent errors can remain invisible under nominal test conditions.

1.6.9 Integrity Challenges in Emerging Architectures

As memory systems evolve toward heterogeneous, tightly coupled, and fabric-attached designs, integrity risks expand beyond classical DRAM fault models:

- **Near-memory compute (NMC):** co-located logic and storage increases the probability of transient interference between compute activity and read/write operations, requiring cross-domain isolation and overlap-aware monitoring.
- **Unified CPU/GPU memory:** heterogeneous burst patterns, stride behavior, and latency sensitivity complicate ECC and scrubbing policy, particularly in HBM/UMA-style systems.
- **CXL and disaggregated memory:** remote pools introduce link-layer protection in addition to DRAM ECC, and correction/containment may involve serialized fabric transactions, complicating latency-bounded recovery.
- **AI-optimized memory:** some data types (e.g., weight matrices) may be error-tolerant, while control/index structures are not—enabling adaptive protection levels where ECC strength varies by data criticality.

In hybrid RAM–NVM stack scenarios, error visibility can shift across layers:

- Volatile buffering may **mask transient NVM faults** until flush or persistence boundaries are crossed.
- NVM endurance and retention drift may produce **latent failures** that remain invisible within the volatile tier until accumulation triggers uncorrectable outcomes.

These effects demand **layer-aware diagnostics** capable of testing each tier's native fault modes independently, then validating cross-tier interactions at the system level.

1.6.10 Summary

A single bit represents the boundary between computational correctness and systemic failure. Preserving bit integrity against time-dependent drift, voltage and temperature variation, manufacturing imperfection, environmental disturbance, and adversarial activation is a nontrivial engineering requirement.

Data integrity is not merely the equality of written and read values; it is the foundation of system trustworthiness. In safety-critical and high-reliability domains, even a single undetected bit error can propagate into control instability, state corruption, or invalid decisions.

Meeting integrity requirements requires a multi-layered diagnostic strategy spanning:

- **Device physics**, where failure mechanisms define activation thresholds.
- **Algorithmic protection**, where ECC and scrubbing intercept transient and persistent faults.
- **Probabilistic modeling**, where statistical behavior informs refresh policies, redundancy allocation, and predictive maintenance.

As architectures progress toward heterogeneous, unified, and fabric-attached memory systems, integrity strategies must evolve in lockstep to ensure that the fundamental unit of digital truth—the bit—remains reliable under all operational conditions.

1.7 Performance Metrics and Constraints

Memory performance remains a dominant system bottleneck. While processors have advanced rapidly in frequency, parallelism, and pipeline depth, memory subsystems have improved more incrementally—particularly in latency reduction, bandwidth scaling, and controllability of timing behavior.

This growing disparity, often described as the **memory wall**, shapes system architecture, workload scheduling, and diagnostic methodology.

Memory performance is multidimensional and must be evaluated across:

- **Latency:** time from request to data availability.
- **Bandwidth:** sustained transfer rate under load.
- **Concurrency handling:** efficiency under parallel request streams and contention.
- **Power and thermal limits:** energy cost of meeting performance targets at operational corners.
- **Workload dependence:** sensitivity to access patterns, queue depth, and controller policy.

In the development of the **Optimal_Test** framework, a recurring observation was that performance tuning must be balanced against fault observability: maximizing throughput alone is insufficient if it masks weak cells, hides address-decoder defects, or suppresses timing-dependent manifestations.

Practical optimization integrates performance with resilience, predictability, and diagnostic visibility.

1.7.1 Core Memory Performance Metrics

Memory systems are characterized by a set of core performance metrics that quantify raw capability and reveal operational behaviors that influence both fault activation and diagnostic coverage:

Table 1.8—Core Performance Metrics for Memory Systems

Metric	Definition	Units / Notes
Latency	Time from request issuance to data availability	ns, cycles
Bandwidth	Sustained volume transferred per unit time	GB/s, MB/s
Throughput	Effective utilization under workload	pattern-dependent
Cycle Time (t_{cycle})	Minimum time between consecutive operations	ns
Access Time	Address-to-data delay	JEDEC: t_{AA}, t_{AC}
Row Cycle Time (t_{RC})	Activation + access + precharge time (DRAM)	DRAM-specific
CAS Latency (t_{CL})	Column access to data output delay	DDRx parameter
Page Hit/Miss Ratio	Fraction of row-buffer hits vs misses	DRAM critical
Queue Depth	Outstanding requests in flight	affects latency/bw

Operator-based modeling indicates that latency variability, particularly under row-buffer misses and bank conflicts, introduces non-determinism that complicates deterministic test scheduling in interleaved and pipelined DRAM systems.

Diagnostic methodologies must therefore incorporate dynamic timing behaviors to preserve high coverage under realistic operating variability.

1.7.2 Latency vs. Bandwidth Trade-Off

Latency and bandwidth are distinct dimensions.

High bandwidth does not guarantee low latency, and low latency does not imply high sustained throughput.

- **Latency** dominates cache-miss-heavy and control-intensive workloads, where each miss can stall execution.

- **Bandwidth** dominates streaming and vector workloads (graphics, HPC kernels, AI training/inference), where large contiguous regions are transferred continuously.

Architectural techniques—out-of-order execution, prefetching, and thread-level parallelism—can hide average latency, but they do not eliminate worst-case constraints. In real-time systems, worst-case latency must remain bounded and predictable.

In a parallel diagnostic simulator inspired by multi-head automaton models, bank contention and resource conflicts measurably reduced detection speed and increased false-negative risk in time-constrained regimes. This motivates latency-aware sequencing for diagnostics in high-concurrency memory environments.

1.7.3 Timing Parameters in Synchronous DRAM

SDRAM and DDR-family memories operate under strict timing constraints defined to ensure correctness, preserve signal margins, and control power/thermal behavior. These parameters directly influence both system performance and diagnostic observability.

Table 1.9—Fundamental Timing Parameters in Synchronous DRAM

Parameter	Description
t_{RCD}	Row-to-column delay: ACT to READ/WRITE interval
t_{RP}	Precharge time: time to close an open row
t_{RAS}	Row active time: minimum time a row must remain active
t_{RC}	Row cycle time: t_{RAS}+t_{RP}
t_{WR}	Write recovery: minimum delay before precharge after a write
t_{RRD}	Row-to-row delay between activates
t_{FAW}	Four-activate window limiting activation density

Violations can cause intermittent corruption and, under extreme operation, may accelerate degradation. From a diagnostic perspective:

- Overly short t_{RAS} can prevent full charge restoration, suppressing retention-related manifestations.
- Activation-density limits (t_{FAW}) shape stress patterns and constrain high-activation diagnostics.

Accordingly, the diagnostic frameworks in this work model timing constraints explicitly so that test sequences remain valid, realistic, and fault-revealing under DDR-class operational rules.

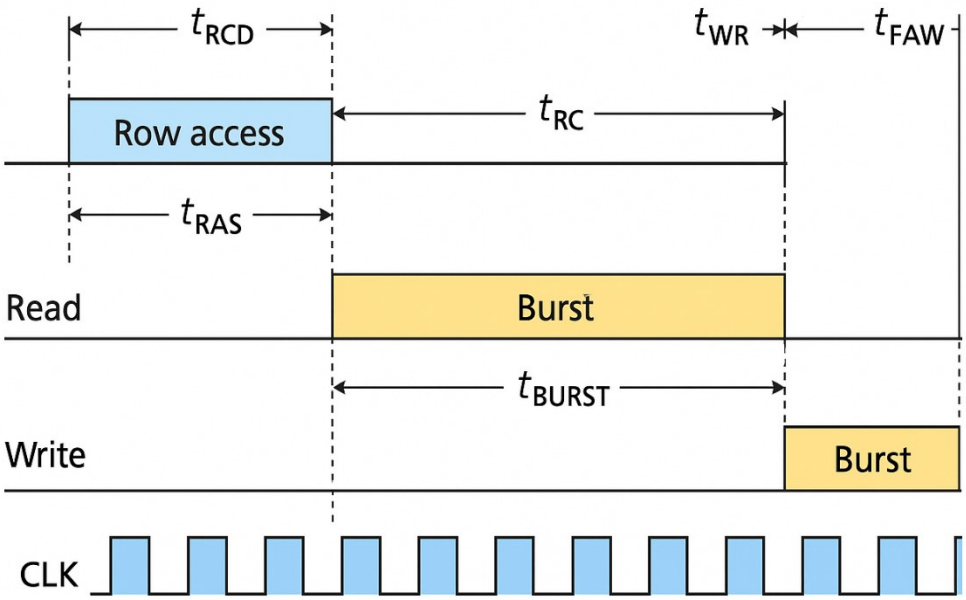

Figure 1.27—Annotated DRAM timing diagram (read/write/burst access cycles)

This Figure presents a consolidated timing diagram illustrating the fundamental temporal constraints governing synchronous DRAM (SDRAM) operation under read and write access modes, including burst transactions. It captures the interdependence of row activation, column access, data transfer, and precharge phases that collectively determine memory latency, bandwidth, and operational stability.

Following a row activate command, the memory enters the **row access period**, during which the addressed wordline is asserted and the associated bitlines are prepared for sensing. This interval is bounded by the **Row Active Time (t_{RAS})**, which specifies the minimum duration a row must remain open to ensure reliable read or write operations.

The **Row-to-Column Delay (t_{RCD})** defines the mandatory delay between row activation and the issuance of a column access command, reflecting the time required for charge sharing and sense amplifier stabilization.

Once the column access is issued, data transfer proceeds in the form of a **burst**, whose duration is determined by t_{BURST} and the configured burst length. The burst phase allows consecutive data words to be transferred efficiently without repeated command overhead, thereby maximizing effective bandwidth.

The **Row Cycle Time (t_{RC})** encompasses the complete lifecycle of a row access, including the active interval **(t_{RAS})** and the subsequent **row precharge time (t_{RP})**. This parameter enforces the requirement that a row be fully restored and closed before a new activation to the same bank can occur.

Write operations follow a closely related temporal structure but introduce additional constraints. In particular, the **Write Recovery Time (t_{WR})** specifies the minimum interval that must elapse after a write burst before a precharge command may be safely issued, ensuring that written data is fully committed to the storage capacitors. At higher levels of concurrency,

further constraints are imposed by **Row-to-Row Delay (t_{RRD})** and the **Four Activate Window (t_{FAW})**, which collectively limit the rate of row activations across banks to control instantaneous current draw and prevent excessive power density and thermal stress.

This timing framework underpins nearly all aspects of SDRAM behavior, from performance optimization and power management to fault activation and observability. Accurate modeling of these constraints is essential for diagnostic strategies that must account for dynamic access patterns, bank-level parallelism, and timing-sensitive failure mechanisms in modern high-speed memory systems.

1.7.4 Performance Constraints by System Type

Memory performance requirements differ substantially across computing domains, reflecting distinct priorities with respect to latency, bandwidth, power consumption, and temporal determinism. These differences directly influence both architectural design choices and the diagnostic methodologies required to validate correct operation under realistic workloads.

A. General-Purpose Systems

General-purpose computing platforms prioritize **average-case performance** to sustain high instruction throughput across diverse workloads. Memory subsystems are optimized to minimize perceived latency through architectural and microarchitectural techniques rather than strict determinism.

Key characteristics include:

- Aggressive use of speculative execution, out-of-order processing, and hierarchical caching to mask memory access delays.
- Hardware prefetching mechanisms that anticipate future accesses based on observed access patterns.
- Performance evaluation based on statistical benchmarks (e.g., SPEC CPU suites) and metrics such as **Instructions Per Cycle (IPC)**, which emphasize throughput rather than worst-case behavior.

Diagnostics in such systems must tolerate variability in access timing while ensuring that optimization mechanisms do not obscure latent memory faults.

B. Real-Time Systems

Real-time systems impose stringent requirements on **predictability and bounded latency**, often under hard deadline constraints where missed timing guarantees can lead to system failure.
Salient features include:

- Analysis and validation based on **Worst-Case Execution Time (WCET)** rather than average performance.
- Conservative memory configurations designed to eliminate or tightly bound latency variability.

- Frequent avoidance or restriction of caches due to their nondeterministic behavior, with preference given to **scratchpad memories** or tightly coupled on-chip RAM providing fixed-latency access.

In this context, diagnostics must be explicitly designed to preserve determinism and must not introduce timing anomalies that could invalidate real-time guarantees.

C. High-Performance Computing (HPC)

HPC platforms focus on maximizing **aggregate bandwidth** and sustained throughput across large-scale parallel workloads.
Typical characteristics include:

- Non-Uniform Memory Access (NUMA) architectures with multiple memory controllers and interleaved memory banks.
- Wide memory interfaces (e.g., HBM) and high-concurrency access patterns to feed vectorized and massively parallel execution units.
- Sophisticated memory-affinity scheduling to minimize remote access penalties.

Diagnostic strategies for HPC systems must account for concurrency-induced effects, interconnect contention, and the amplification of minor memory inefficiencies at scale.

D. Embedded and Edge Systems

Embedded and edge computing platforms operate under strict **power, thermal, and resource constraints**, often in physically constrained or harsh environments.

Common design features include:

- Adoption of low-power DRAM variants (e.g., LPDDR) supporting deep-sleep modes, adaptive refresh rates, and aggressive power-down policies.
- Trade-offs favoring energy efficiency over peak performance, with dynamic reconfiguration based on workload intensity.

In embedded fault coverage simulations, it was observed that such power-saving configurations—while effective in reducing energy consumption—introduce access jitter. This jitter can suppress fault activation rates and degrade diagnostic convergence, particularly for timing- and retention-sensitive fault classes.

Collectively, these domain-specific constraints underscore the need for **adaptive diagnostic frameworks** capable of maintaining high test effectiveness across heterogeneous memory architectures and operating conditions.

1.7.5 Performance Bottlenecks and Saturation Scenarios

Under sustained or adversarial workloads, modern memory subsystems are susceptible to a range of performance bottlenecks and saturation phenomena that elevate latency and reduce effective throughput.

These effects arise from architectural limits, resource contention, and workload-induced stress patterns, and they often interact in nontrivial ways.

Prominent bottleneck mechanisms include:

- **Bank Conflicts** — Occur when multiple requests target the same DRAM bank, forcing serialization of accesses and stalling competing request streams.
- **Row Buffer Misses** — Arise when the requested data is not present in the currently active row, requiring a full precharge–activate sequence that significantly increases access latency.
- **Write-to-Read Turnaround Delay** — Incurred when switching the memory data bus between write and read modes, particularly detrimental in mixed read/write workloads.
- **TLP/IPI Flooding** — Excessive transaction layer packet (TLP) traffic and interprocessor interrupts (IPIs) in multi-core systems can generate memory access bursts that overwhelm controller queues.
- **Cache Coherency Traffic** — Overhead associated with maintaining consistency across distributed caches, especially in systems employing MESIF or MOESI protocols.
- **I/O DMA Contention** — Direct Memory Access (DMA) operations initiated by peripherals compete with CPU memory requests, introducing unpredictable latency spikes.

Effective diagnosis of these pathologies requires real-time instrumentation, including hardware performance counters, memory profilers, and fine-grained latency measurement tools. Crucially, such metrics must be interpreted within a diagnostic framework capable of distinguishing benign architectural limitations from degradations caused by latent memory faults or misconfigurations.

1.7.6 Performance vs. Reliability Trade-Offs

Aggressive optimization of memory performance often erodes operational safety margins, increasing vulnerability to both transient and permanent faults. Many performance-enhancing techniques operate by reducing timing slack or electrical noise margins, thereby elevating fault susceptibility.
Typical trade-offs include:

Table 1.10—Performance Optimization Techniques and Associated Reliability Trade-Offs

Optimization	Trade-off
Higher Operating Frequency	Reduced noise margins and increased bit error rates due to tighter timing constraints
Lower Refresh Rate	Elevated risk of data retention failures, particularly in DRAM arrays
Reduced t_{CL} / t_{RCD}	Increased likelihood of setup/hold violations and timing-related read/write errors
Wider Memory Buses	Greater exposure to crosstalk, EMI, and signal integrity degradation

During the development of the **Optimal_Test** framework, scenarios were evaluated in which performance-optimized configurations were deliberately subjected to standard March test sequences. The results demonstrated that certain faults manifested only under collapsed timing margins—conditions not exercised by static or idle testing. These findings highlight the necessity of **stress-aware diagnostic patterns** for modern high-performance memory systems.

1.7.7 Test Time vs. Execution Performance

The relationship between memory diagnostics and system performance is inherently bidirectional. Diagnostic activity can perturb runtime behavior, while system performance constraints shape the design and scheduling of tests.

Key considerations include:

- **MBIST Execution** — Built-In Self-Test routines must complete within tightly bounded intervals (e.g., power-on self-test or controlled idle windows) to avoid disrupting normal operation.
- **Software-Based Diagnostics** — Background testing must balance resource usage against active operating system and application demands to prevent perceptible performance degradation.
- **Run-Time Health Monitoring** — Continuous monitoring introduces additional latency and can impact Quality of Service (QoS), necessitating careful tuning of test frequency, granularity, and scope.

To manage these interactions, diagnostic frameworks must explicitly model metrics such as coverage per cycle, test duration relative to CPU stall opportunities, and QoS impact. Such modeling enables adaptive strategies that preserve fault coverage without undermining responsiveness in real-time, HPC, and cloud environments.

1.7.8 Thermal and Power Constraints on Performance

Maximizing memory performance invariably increases thermal output and power consumption, which, if unmanaged, can compromise stability and invalidate diagnostic results. Key contributors include:

- Increased switching activity leading to higher dynamic power dissipation.
- Elevated bank activity raising leakage currents and localized heating.
- Stacked memory architectures (e.g., HBM, 3D NAND), where limited vertical heat dissipation creates thermal hotspots that constrain sustained performance.

Dynamic thermal management (DTM) mechanisms—such as throttling access rates or disabling refresh-skipping optimizations—are commonly deployed to mitigate these effects. However, such interventions introduce variability in fault activation timing and observability, complicating diagnostic interpretation.

In stress-aware testing research conducted as part of this work, temperature sensors and power monitors were integrated into diagnostic scheduling. This enabled fault activation under realistic thermal loads, ensuring that diagnostic outcomes reflected operational conditions

rather than idealized laboratory environments (see *New Methods and Tools for Memory Test Design*).

1.7.9 Summary

Memory performance is a multifactorial discipline requiring coordinated control of timing, bandwidth utilization, power efficiency, and diagnostic transparency. Metrics such as latency and throughput acquire practical significance only when interpreted in the context of system architecture, workload behavior, and fault coverage objectives.
High-performance memory systems must therefore simultaneously deliver:

- **Speed** — to satisfy workload demands,
- **Stability** — under sustained and stressed operation,
- **Predictability** — across variable environmental and workload conditions,
- **Transparency** — to enable fault detection without masking failure modes.

Achieving this balance demands a holistic view of performance metrics as active levers in diagnostic design rather than passive indicators of system health.

1.8 Common Access Protocols and Interfaces

Memory systems are tightly integrated with processors, controllers, peripherals, and interconnect fabrics through standardized access protocols and electrical interfaces. These protocols define how memory is addressed, controlled, timed, and accessed across architectural layers and physical media.

A rigorous understanding of these interfaces is essential for:

- **Timing Analysis** — Accurate modeling of latency, throughput, and contention behavior.
- **Performance Modeling** — Assessing the impact of protocol-level constraints on subsystem efficiency.
- **Diagnostic Engineering** — Designing tests aligned with protocol-specific command sequences, state transitions, and access patterns.

As demonstrated in the underlying dissertation and subsequent publications, test coverage and fault observability are inherently bounded by the operational semantics of these access protocols.

This limitation is especially pronounced in systems employing complex timing protocols (e.g., DDR4/DDR5, LPDDR5) and serialized bus architectures (e.g., PCIe, CXL), where multi-phase command sequences, packetization, and layered protocol stacks obscure direct observation of individual memory transactions.

1.8.1 Parallel vs. Serial Memory Interfaces

Historically, memory systems relied on **parallel interfaces**, transmitting address, data, and control signals concurrently over wide buses. This approach enabled precise timing control and relative ease of probing during diagnostics but suffered from increasing pin count, signal skew, and power inefficiency as speeds and densities increased.

To overcome these limitations, modern architectures increasingly adopt **serial interfaces** employing high-speed differential signaling and command serialization. This transition enables:

- Higher aggregate data rates,
- Reduced physical pin count,
- Improved signal integrity at multi-gigahertz frequencies.

Interface Characteristics

Table 1.11—Characteristics of Parallel and Serial Memory Interfaces

Type	Examples	Characteristics
Parallel	DDRx, SDRAM	Separate address, data, and control buses; deterministic latency control; accessible to traditional diagnostic tools
Serial	LPDDR4/5, GDDR6, HBM, PCIe	Serialized command/data streams; protocol layering; improved density and EMI resilience; significantly harder to probe

This paradigm shift has profound diagnostic implications. While serial interfaces enable unprecedented throughput and scalability, they demand **protocol-aware analyzers** and advanced decoding frameworks to achieve reliable fault isolation and performance verification in high-speed memory environments.

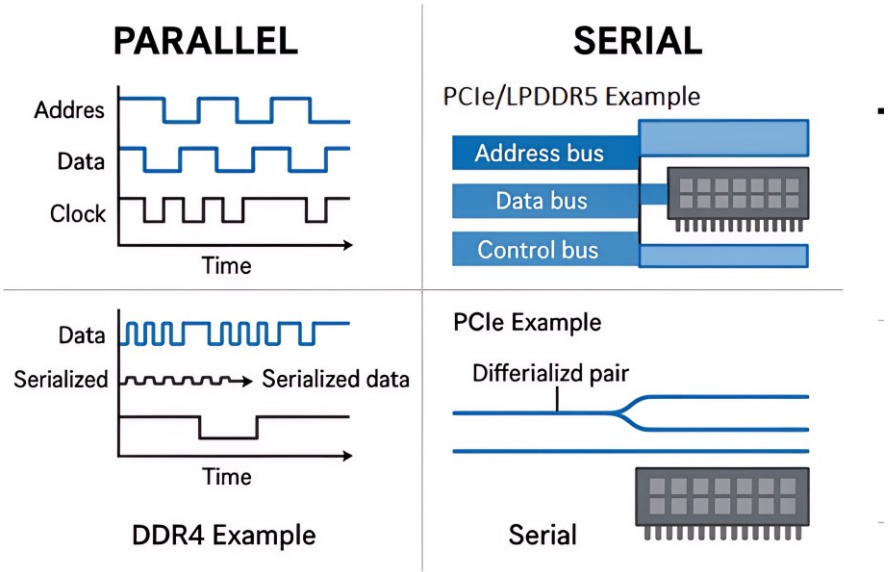

Figure 1.28—Comparison of parallel vs serial memory bus timing and layout

Figure 1.28 contrasts two fundamental paradigms for memory and memory-adjacent interconnect interfaces: parallel synchronous buses (exemplified by DDR-class interfaces) and high-speed serial links (exemplified by PCIe-class fabrics and serial LPDDR families).

The Figure intentionally combines two complementary viewpoints—timing behavior and physical layout constraints—because diagnostic accessibility is shaped by both.

On the left, the Figure depicts a parallel interface (DDR4 example). Address, data, and control are conveyed over multiple dedicated signal lines, and transaction timing is constrained relative to a shared clock.

The accompanying waveform sketch emphasizes that multiple buses transition concurrently: the address/control phase precedes and structures the data phase, and correctness depends on deterministic setup/hold margins and bounded skew across the bus.

From a validation standpoint, this paradigm historically allows more direct probing of signal groups and often enables clearer attribution of failures to specific timing margins (e.g., data strobe alignment, command/address stability windows).

However, the physical implication of this approach is the proliferation of pins and traces: increasing width and frequency amplifies routing complexity, inter-line coupling, and susceptibility to skew, crosstalk, and impedance discontinuities.

At scale, these constraints can dominate design closure and reduce tolerance to manufacturing variation.

On the right, the Figure depicts a serial interface (PCIe/LPDDR5 example). Transactions are transported over high-speed differential pairs, compressing wide logical transfers into serialized streams.

Timing is maintained through embedded clocking mechanisms (e.g., clock forwarding or clock recovery), and protocol semantics are reconstructed through decoding of packetized or framed traffic rather than direct interpretation of raw bus-level waveforms.

This approach reduces pin count, improves signal integrity at multi-gigahertz rates, and scales bandwidth via lane aggregation and higher symbol rates.

The diagnostic consequence is equally clear: fault observability shifts upward in abstraction. Rather than probing address/control lines directly, effective diagnosis must interpret protocol state machines, lane training outcomes, error counters, retry behaviors, and packet integrity checks.

As a result, serial interfaces typically demand protocol-aware instrumentation and test routines that explicitly exercise link states and transaction classes.

The timing sketches and layout motifs together underscore a central diagnostic theme: parallel buses prioritize explicit synchronous visibility but struggle with physical scaling, whereas serial buses scale bandwidth efficiently but obscure raw fault mechanisms behind protocol layers, requiring diagnostics that can operate at both electrical and transactional levels.

1.8.2 DRAM Access Protocols (SDRAM, DDR, LPDDR, GDDR)

A. SDRAM / DDR

Synchronous DRAM (SDRAM) and its derivatives—DDR, DDR2, DDR3, DDR4, DDR5—operate in lockstep with the system clock and are controlled through a **structured command protocol**.

This protocol decomposes memory access into phases (row activation, column access, and row closure), enabling high-density arrays to be accessed efficiently while supporting bank-level parallelism.

The primary commands include:

- **ACT (Activate)** — Opens a specified row (page) within the selected bank, transferring the row contents into the row buffer and making the sense-amplifier array available for column operations.
- **READ / WRITE** — Initiates data transfer to/from the activated row at a specified column address, typically executed as a burst under DDR prefetch rules.
- **PRE (Precharge)** — Closes the active row and returns the bank to an idle/precharged state, restoring bitline conditions required for the next activation.
- **REF (Refresh)** — Periodically restores charge in DRAM cells to counteract leakage, preserving data integrity across the full array.

The memory controller orchestrates these operations, selecting activation order, scheduling reads/writes, interleaving banks, and issuing precharge/refresh while respecting strict timing constraints.

A typical DDR access sequence proceeds through the following phases:

1. **Row Activation** — The target page is opened for access (ACT).
2. **Column Read/Write** — Data is read or written using READ/WRITE commands to specific column addresses within the active row.
3. **Precharge** — The bank is closed and prepared for subsequent activations (PRE), either explicitly or via auto-precharge semantics.
4. **Auto-Refresh** — Refresh cycles are executed periodically (REF) to maintain retention and prevent silent data loss.

This command-driven structure is fundamental to DDR scalability, but it increases diagnostic complexity because real systems rarely execute isolated transactions: controller scheduling, bank interleaving, row-buffer policies, and refresh insertion interact with timing margins and fault activation conditions.

Diagnostic sequences must therefore align not only with functional behavior but also with command-timing legality under parameters such as t_{RCD}, t_{RCD}, t_{RP}, t_{RFC}, and related DDR constraints.

These timing constraints define the legal ordering and spacing of DRAM commands during each access cycle. Effective diagnostics must therefore account for both command semantics and timing compliance.

Common DDR Protocols and Features

The evolution of DDR standards reflects a continuous drive toward higher bandwidth, improved efficiency, and enhanced reliability. Each generation introduces architectural refinements that influence both performance behavior and diagnostic observability. For example:

- **DDR2/DDR3** — Increased prefetch depth and refined signaling/termination and topology features, improving throughput but tightening timing margins.
- **DDR4** — Introduced **bank-group architecture**, expanding concurrency while imposing additional scheduling constraints and increasing sensitivity to command ordering.
- **DDR5** — Introduced dual independent subchannels per DIMM, expanded bank counts, and new reliability features (including on-die ECC), improving scalability but increasing the need for protocol-accurate diagnostic stimulation to ensure timing coverage and fault visibility.

Protocol Summary and Diagnostic Considerations

Table 1.12—Summary of DDR Memory Protocols and Diagnostic Implications

Protocol	Data Rate	Key Features
DDR3	800–2133 MT/s	64-bit wide bus; single-ended signaling; introduced fly-by topology to improve timing alignment.
DDR4	1600–3200 MT/s	Bank groups for increased parallelism; CRC for data bus integrity; controller scheduling sensitivity due to bank-group constraints.
DDR5	3200–8400 MT/s	Dual subchannels per DIMM; on-die ECC support; expanded banks/burst features; increased internal concurrency and protocol complexity.

Notes:

1. **MT/s (mega transfers per second)** denotes effective data rate (transfers), not the raw clock frequency.
2. Advanced features such as CRC and on-die ECC can affect **diagnostic visibility** and may require test pattern design that distinguishes between corrected/masked errors and exposed errors.

DDR Performance Dependencies and Diagnostic Implications

DDR performance and fault activation depend on timing- and architecture-driven factors that directly influence diagnostic completeness:

- **Command Scheduling Latency** — Controller queuing and arbitration can delay ACT/READ/WRITE/PRE issuance, affecting access phasing and masking marginal timing faults unless explicitly exercised under stress conditions.
- **Bank Group Conflicts** — Interactions between bank groups may reduce realized bandwidth and introduce repetitive scheduling patterns that can hide certain defects unless patterns force adverse rotations and conflicts.
- **Burst Length (BL8 typical)** — Longer bursts improve efficiency but may penalize random access latency and can alter activation of coupling and interface faults across consecutive beats.
- **Write Recovery and Turnaround Delays** — Intervals such as t_{WR} and t_{WTR} constrain write-to-precharge and write-to-read transitions; these transitions are frequent sources of subtle timing vulnerabilities and must be actively stressed in protocol-aware diagnostics.

Prior work on diagnostic test language synthesis demonstrates that protocol-level timing transitions can create diagnostic blind spots.

Using PROVER-based micro-operation chains, improper abstraction of write-to-read transitions—particularly during bank-group rotation—can mask timing-related defects.

These observations motivate protocol-aware diagnostic routines that systematically exercise DDR timing rules under adversarial transition patterns to ensure full fault observability.

B. LPDDR (Low Power DDR)

LPDDR is optimized for mobile and embedded systems where energy efficiency is paramount. It introduces protocol and architectural adaptations that achieve substantial power savings, typically at the expense of increased access latency and more complex state behavior.

Low-Power Optimizations

- **Deep Power-Down Modes** — Entire memory arrays or substantial portions may be powered down during idle periods to minimize leakage.
- **Partial Array Self-Refresh** — Only selected regions are refreshed while inactive regions remain in low-power states, reducing refresh energy and overhead.
- **Variable I/O Termination** — Dynamically adjusts drive strength and termination to reduce I/O power consumption under changing operating conditions.

Design Characteristics

- Reduced command/address bus width lowers pin count and package complexity.
- Increased latency and state transitions are introduced by aggressive power management and wake-up constraints.

Testing Implications

Diagnostic strategies for LPDDR must explicitly account for power-state behavior that is not present (or not as dominant) in standard DDR flows:

- **Voltage Ramp-Up Sequences** — Verifying correct initialization, training, and configuration after deep sleep/power collapse.
- **Sleep-to-Wake Synchronization** — Ensuring stability across repeated power-state transitions, including timing closure under temperature/voltage variation.
- **Retention Test Modes** — Validating data integrity during reduced-refresh conditions in partial-array modes, including corner-case refresh boundary conditions and wake timing.

C. GDDR and HBM

Both Graphics DDR (GDDR) and High Bandwidth Memory (HBM) target bandwidth-intensive workloads, including GPUs, AI accelerators, and HPC systems. Their performance objectives lead to interface and architecture choices that substantially change fault behavior and diagnostic accessibility.

GDDR6

- Supports very high per-pin data rates (e.g., 16–20 Gbps) through aggressive signaling and timing closure.
- Typically incorporates enhanced integrity mechanisms to sustain throughput at high load and under marginal conditions.

HBM

- Utilizes **3D-stacked DRAM dies** interconnected through **Through-Silicon Vias (TSVs)**.
- Achieves extreme bandwidth via very wide internal buses (up to ~1024 bits) while maintaining favorable energy-per-bit through parallelism at lower per-lane frequency.

Testing Challenges for HBM

- **Pseudo-Channel Decoding** — Wide internal buses must be mapped correctly to controller-visible interfaces; decoding errors and mapping faults can mimic functional errors.
- **Vault Controller Configuration** — Each die layer can include local controllers that introduce hierarchical access behaviors and state interactions relevant to diagnostics.
- **Inter-Die Timing Calibration** — TSV integrity and layer-to-layer timing must be validated under realistic thermal gradients and supply variation.
- **BIST Integration Complexity** — Conventional BIST and classic March-style approaches may struggle to traverse deep hierarchy and extreme parallelism without masking timing- or interconnect-related faults.

The sophisticated access patterns and tight timing tolerances of high-bandwidth memory technologies demand diagnostics capable of navigating hierarchical organization, vertical

interconnects, and extreme parallelism while preserving fault coverage and localization capability.

1.8.3 Non-Volatile Interface Protocols (NAND, NOR, NVM)

Flash memory technologies—such as NAND and NOR—along with emerging non-volatile RAM (NVM), employ specialized interface protocols designed to handle endurance constraints, block/page semantics, and internal management complexity while presenting usable abstractions to host controllers.

Representative Protocols

- **ONFI (Open NAND Flash Interface)** — A widely adopted standard enabling interoperability between NAND devices and host controllers.
- **Toggle DDR / NV-DDR3** — High-speed NAND access protocols using strobes and bidirectional transfer semantics to increase throughput.
- **JEDEC JESD220 (UFS)** — Designed for mobile platforms, supporting multiple logical units and improved random access behavior compared to older eMMC-style interfaces.
- **NVM Express (NVMe)** — PCIe-based command set that enables highly parallel command submission/completion, minimizing software overhead and maximizing queue depth exploitation.

Key Protocol Behaviors

- **Multi-Cycle Command–Response Sequences** — Operations often involve staged command issuance, device acknowledgment, execution latency, and completion signaling.
- **Asynchronous Completion Queues** — Hosts can maintain multiple outstanding requests, requiring diagnostics to track ordering, completion correctness, and queue integrity.
- **Internal Garbage Collection Pauses** — Background maintenance can introduce latency spikes, timing variability, and transient performance cliffs.
- **Power-Failure Interrupt Handling** — Emergency commit/flush behavior must be validated to avoid silent data loss and partial-write corruption.

In my analysis of hybrid memory architectures (**see Chapter 17**), I observed that flash interface latency variability—caused by block wear, page remapping, and garbage collection—can produce non-repeatable fault activation patterns. Effective diagnostics therefore require retry logic, timing jitter tolerance, and workload-aware stimulation to expose transient failures under realistic operational conditions.

1.8.4 Cache Interface Protocols

Cache memory (L1, L2, L3) operates through tightly coupled, latency-minimized interfaces that must also satisfy coherence and ordering requirements in multi-core systems. These interfaces are shaped not only by raw timing but by coherence transactions, replacement behavior, and microarchitectural speculation.

Key Protocol Elements

- **Snoop-Based Coherence Protocols** — Coherence is maintained using MESI, MOESI, or MESIF-style state machines, defining line states and transitions under read/write sharing.
- **Inclusive vs. Exclusive Caching** — Determines duplication across levels, affecting fault visibility (e.g., whether a line's existence in L1 implies presence in LLC).
- **Write Policies**
    - **Write-Back** — Defers main-memory propagation until eviction; reduces traffic but complicates fault tracing because intermediate states may be hidden.
    - **Write-Through** — Propagates writes immediately; simplifies tracing but increases bandwidth usage.

Testing Challenges

- **Ultra-Low Latency** — Minimal observation windows complicate external instrumentation and increase reliance on internal counters/state exposure.
- **Speculative and Transient Events** — Prefetching, speculative execution, and out-of-order behaviors can mask activation sequences and reorder symptoms unless modeled.
- **Associativity and Replacement Policies** — LRU and pseudo-LRU dynamics can delay fault manifestation until specific eviction chains occur.

In PROVER-based model generation, microarchitectural state transitions—such as cache line evictions and tag mismatches—can be simulated to uncover subtle decode errors.

These defects evade standard March testing, which lacks the ability to model speculative access and dynamic replacement behavior. These observations emphasize the need for cache-aware diagnostics tailored to timing-sensitive and transient fault mechanisms.

1.8.5 System Interconnects: PCIe, CXL, AXI, AMBA

Modern memory systems rely on high-speed interconnects to connect processors, accelerators, storage, and disaggregated memory resources. These fabrics are not merely physical wiring; they embody protocol stacks and transactional semantics that affect latency, bandwidth, ordering, and fault visibility.

A. PCI Express (PCIe)

- **Point-to-Point Serial Interface** — Scales bandwidth via lane width and generation rate, connecting CPUs, GPUs, NVMe storage, and memory-class devices.
- **Layered Architecture** — Transaction, Data Link, and Physical layers separate semantics, reliability, and signaling.
- **Split Transaction Model** — Supports multiple outstanding requests and credit-based flow control.
- **Diagnostic Implications** — Testing must account for packetization, retry protocols, link training states, lane de-skew, and error recovery behaviors that can mask or reshape underlying faults.

B. Compute Express Link (CXL)

- **Memory-Centric Extension of PCIe** — Adds coherent memory semantics (load/store) and enables memory pooling and disaggregation.
- **CXL-Specific Challenges**
    - ECC transport and coherence introduce additional latency and state dependencies.
    - CPU–device synchronization of controller states becomes critical for correctness.
    - Diagnostics must emulate coherent endpoints, not only raw memory transactions, to validate realistic interactions.

C. AXI / AMBA

- **SoC and FPGA Standard** — AMBA protocols, especially AXI, dominate embedded interconnect design.
- **AXI Features**
    - Independent read/write channels enabling concurrency
    - Burst transactions for throughput efficiency
    - Transaction ID tagging enabling flexible scheduling and reordering
- **Testing Considerations** — Must consider transaction ID aliasing, burst fragmentation, write-response integrity, and concurrency corner cases that can produce silent corruption if response semantics are violated.

These interconnects materially influence diagnostic realism. Effective test methodologies must be protocol-aware and must generate traffic patterns that emulate real transactional behavior; otherwise, failures may remain masked under synthetic or overly simplified stimulation.

In large-scale computing environments, these interconnect fabrics increasingly function as shared communication substrates linking heterogeneous components across multiple hierarchy levels. Processors, accelerators, storage controllers, and memory expanders may all interact through the same transactional fabric, generating complex traffic patterns that include concurrent reads, writes, cache-coherent requests, and synchronization primitives.

As a result, memory access behavior is shaped not only by the characteristics of the memory device itself but also by arbitration policies, buffering mechanisms, and flow-control strategies implemented within the interconnect fabric.

Another important implication concerns fault visibility and error propagation. Errors originating in memory devices may be detected, corrected, or even masked by protocol-layer mechanisms such as retry logic, packet-level error detection codes, or coherence management policies. Conversely, faults occurring within the interconnect—such as lane misalignment, packet corruption, or transaction ordering violations—may manifest as apparent memory errors even when the underlying memory cells are functioning correctly.

This interaction complicates diagnostic interpretation and requires careful differentiation between device-level and fabric-level fault sources.

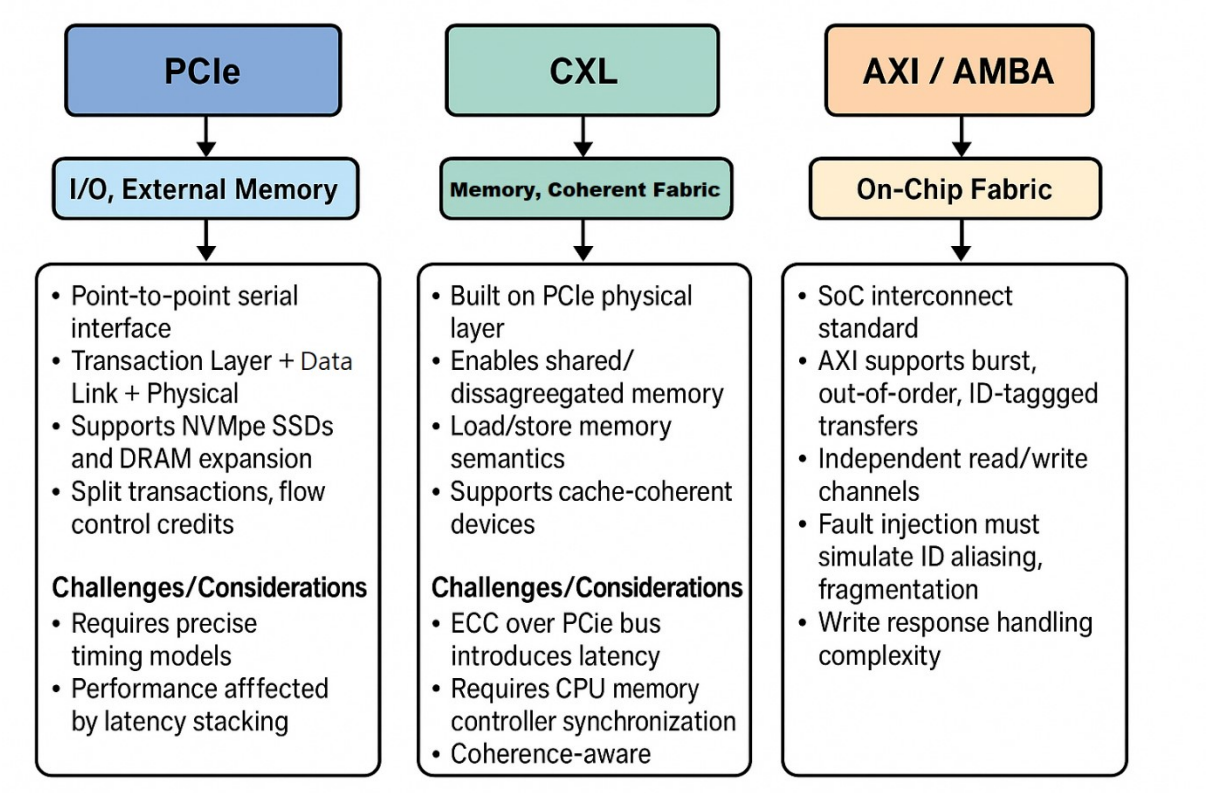
PCIe
I/O, External Memory
• Point-to-point serial interface
• Transaction Layer + Data Link + Physical
• Supports NVMpe SSDs and DRAM expansion
• Split transactions, flow control credits
Challenges/Considerations
• Requires precise timing models
• Performance afffected by latency stacking
CXL
Memory, Coherent Fabric
• Built on PCIe physical layer
• Enables shared/ dissagreegated memory
• Load/store memory semantics
• Supports cache-coherent devices
Challenges/Considerations
• ECC over PCie bus introduces latency
• Requires CPU memory controller synchronization
• Coherence-aware
AXI / AMBA
On-Chip Fabric
• SoC interconnect standard
• AXI supports burst, out-of-order, ID-taggged transfers
• Independent read/write channels
• Fault injection must simulate ID aliasing, fragmentation
• Write response handling complexity

Figure 1.29—Overview of Memory Interface Standards by Abstraction Level and Protocol Domain

Figure 1.29 provides a comparative view of major memory interface standards, organized by **abstraction level** and **protocol domain**, highlighting how different interfaces mediate access between computation, memory, and storage.

The Figure emphasizes that interface choice is not merely an electrical or performance consideration, but a defining factor in system architecture, fault visibility, and diagnostic methodology.

At the **I/O and external memory level**, **PCI Express (PCIe)** is shown as a packetized, point-to-point serial interface. PCIe operates through a layered protocol stack (Transaction, Data Link, and Physical layers), enabling scalable connectivity to NVMe storage, external accelerators, and memory expansion devices.

Its split-transaction model and credit-based flow control allow high concurrency, but also introduce timing variability and latency stacking that must be explicitly considered during diagnostics.

At the **memory and coherent fabric level**, **Compute Express Link (CXL)** extends PCIe's physical layer to support cache-coherent and memory-semantic transactions. CXL enables shared and disaggregated memory pools accessible via load/store operations, blurring the traditional boundary between memory and I/O.

While this architecture improves flexibility and scalability, it introduces new diagnostic challenges related to coherence management, ECC transport over the PCIe substrate, and synchronization between CPU memory controllers and attached devices.

At the **on-chip interconnect level**, **AXI/AMBA** protocols dominate SoC and FPGA designs. AXI is optimized for deterministic latency and high internal concurrency, supporting burst transfers, out-of-order completion, transaction ID tagging, and independent read/write channels. These features maximize throughput within a chip but complicate fault injection and tracing, as diagnostics must account for ID aliasing, burst fragmentation, and write-response ordering.

By aligning these interfaces to their operational domains, the Figure underscores a central diagnostic insight: **protocol behavior fundamentally shapes fault visibility and test coverage**. Each interface class exposes different observability boundaries, requiring diagnostic instrumentation and test strategies tailored to its abstraction level and transactional semantics.

1.8.6 Interface-Dependent Faults and Visibility

The operational characteristics of a memory interface directly influence both **fault activation** and **fault observability**. Certain failure modes manifest only under specific interface behaviors—such as burst transfers, command reordering, or write–read turnaround—making them invisible to diagnostic approaches that ignore protocol dynamics. As a result, interface-agnostic test models risk overlooking subtle but system-critical defects.
The table below summarizes representative interface features and the fault risks they introduce.

Table 1.13—Interface-Dependent Fault Activation and Observability Risks

Interface Feature	Fault Risk
Burst Mode Access	Adjacent-cell coupling and pattern-sensitive faults may remain unexercised when testing relies solely on isolated or random accesses, reducing effective coverage.
Command Queue Reordering	Dynamic reordering or replay of transactions by controllers can mask underlying errors, allowing tests to pass despite latent protocol-dependent faults.
Write–Read Turnaround	Rapid mode transitions under high contention can induce timing skew or metastability, particularly in high-speed DRAM and serialized interfaces.
ECC Offload	Temporary bypass or suppression of ECC (e.g., during maintenance or special modes) may allow errors to propagate silently without correction or logging.
Partial Writes (Subword Access)	Fine-grained writes can trigger tag aliasing in caches or alignment faults in memory subsystems with mixed word/byte granularity.

From a diagnostic engineering perspective, these behaviors impose explicit requirements on test design.

It is no longer sufficient to verify correctness under idealized access patterns; diagnostics must intentionally provoke **interface edge cases** where protocol optimizations interact with physical fault mechanisms.

Accordingly, effective diagnostics must incorporate:

1. **Protocol-Aware Fault Models** — Extending classical fault models to include realistic transaction ordering, burst behavior, and timing constraints imposed by the interface.
2. **Targeted Stress Patterns** — Designing access sequences that deliberately engage turnaround conditions, partial writes, queue saturation, and contention scenarios.
3. **Instrumentation Synchronization** — Aligning measurement and observation tools with protocol-level events to avoid misattributing intermittent or timing-dependent errors to unrelated system noise.

By integrating interface dynamics into diagnostic frameworks, fault conditions that remain invisible to abstraction-only testing can be systematically exposed and analyzed.

1.8.7 Interface-Aware Testing Strategies

Diagnostics for modern memory systems must be both **technology-aware** and **interface-aware**.

This requires test patterns to be explicitly aligned with the command semantics, timing rules, and transactional behavior of the deployed interface, rather than relying on idealized or simplified access models.

Key Strategies

- **Command-Level Fault Models**
  Abstract tests (e.g., March algorithms) must be translated into concrete, interface-specific command sequences—such as ACT/READ/WRITE/PRE/REF for DDR or transaction packets for PCIe/CXL—to activate timing-sensitive and protocol-driven faults.
- **Protocol-Constrained Test Scheduling**
  Test execution must respect real-world effects including precharge delays, bank conflicts, channel arbitration, flow-control throttling, and Quality-of-Service policies, all of which can suppress or defer fault activation under contention.
- **Built-In Test Interfaces (BIST I/F)**
  Diagnostic patterns should be mapped directly onto command encodings defined by industry standards (JEDEC DDRx, ONFI for NAND, AXI4 for SoCs), ensuring applicability in production, validation, and manufacturing environments.
- **In-System Diagnostics**
  Embedded tracepoints, protocol analyzers, and event counters should be used to reconstruct fault-inducing command sequences and correlate them with observed error manifestations during real operation.

Required Test Tool Capabilities

- **Timing Diagram Simulators** — To model and validate protocol-specific access sequences and verify that generated tests can legally and effectively activate targeted faults.
- **Transaction Log Analyzers** — To parse, visualize, and interpret live or simulated command streams, enabling identification of fault activation contexts.
- **Interface-Specific Coverage Metrics** — To quantify diagnostic thoroughness using protocol-relevant indicators (e.g., DDR5 burst overlap ratios, AXI channel utilization, PCIe retry incidence).

In the development of the **Optimal_Test** framework (see Chapter 12), interface-level state machine simulation was integrated into the optimization process to ensure diagnostic sequences adhered to realistic access ordering and timing constraints. This approach revealed latent faults that remained undetected under conventional abstraction-level test methodologies.

1.8.8 Summary

Memory access protocols and interfaces define the execution pathways for every transaction, test pattern, and diagnostic readback. Without a precise understanding of these pathways, diagnostic efforts risk producing routines that are:

- **Non-observable** — unable to manifest faults within the operational visibility window.
- **Protocol-misaligned** — issuing commands that do not reflect actual hardware behavior.
- **Invalidated** — yielding false negatives due to buffering, reordering, or timing optimizations at the interface level.

As memory systems evolve toward heterogeneous architectures, high-speed serial fabrics, and composable interconnects (e.g., CXL, UCIe), diagnostic methodologies must operate at the same semantic level as the interfaces themselves.

This entails:

1. Mapping fault models to protocol state machines.
2. Synchronizing diagnostics with transaction-level events.
3. Interpreting fault signatures within the dynamic operational context of the system.

A robust, future-ready diagnostic framework must therefore be **interface-aware**, **timing-accurate**, and **semantically aligned**, ensuring that test results reflect true system behavior rather than artifacts of abstraction.

Chapter 2: Types of RAM and Memory Technologies

Random-access memory (RAM) is not a single technology class but a family of storage mechanisms spanning different device physics, cell topologies, access protocols, and integration strategies.

These differences propagate upward: they shape timing behavior at the bus level, determine fault activation conditions inside memory arrays, and ultimately constrain what is observable and diagnosable under realistic test conditions.

As contemporary systems scale across performance regimes—from multi-socket servers and AI accelerators to mobile systems-on-chip and deeply embedded controllers—the diversity of RAM technologies becomes a central driver of test complexity and diagnostic specificity.

This chapter provides a technology-grounded survey of RAM types used in modern systems and emerging non-volatile candidates. We examine SRAM, DRAM, and synchronous DRAM families (SDRAM/DDR) as the dominant volatile backbone of computation, then extend the discussion to low-power DRAM variants (LPDDR) and bandwidth-oriented architectures (GDDR, HBM) that introduce packaging- and protocol-driven failure modes.

Finally, we address emerging non-volatile memories—MRAM, ReRAM, PCM, and FeRAM—as a distinct diagnostic domain in which classical binary fault models (e.g., stuck-at, transition) are often insufficient without extensions that capture drift, asymmetry, stochastic switching, and endurance-related degradation.

Across these technologies, the central diagnostic premise of this book remains consistent: testing efficiency and fault localization quality depend on aligning the test model with the physical behavior of the storage mechanism.

Parameters such as volatility, refresh semantics, sensing behavior, array organization, and command timing do not merely influence performance; they define the boundary between detectable and evasive faults. This motivates the symbolic synthesis and optimization frameworks developed in this work (notably PROVER and Optimal_Test), which treat technology constraints as first-class inputs rather than incidental implementation details.

2.1 SRAM: Structure, Access, and Applications

2.1.1 Architecture

Static random-access memory (SRAM) stores each bit using a bistable latch, most commonly implemented as a six-transistor (6T) cell. Unlike charge-based storage mechanisms, SRAM retains its state without refresh as long as power is applied.
A standard 6T SRAM cell consists of:

- Two cross-coupled inverters forming the storage latch (internal nodes Q and $\overline{Q}$),
- Two access (pass) transistors controlled by the wordline (WL), which connect the internal nodes to a complementary bitline pair.

The operational semantics of the cell are defined by the interaction of the following signals:

- WL (wordline): selects the row by enabling the access transistors,
- BL and $B\overline{L}$ (bitlines): carry complementary differential signals used for both read and write operations.

Read operations are non-destructive in the logical sense, as the latch preserves its state after access. However, the act of reading perturbs the internal node voltages and can expose marginal stability faults under reduced voltage, elevated temperature, or aggressive timing. Write operations are performed by actively driving the bitlines differentially while asserting WL, thereby overpowering the latch feedback and forcing a new stable state.

2.1.2 Advantages

SRAM remains indispensable in system components where latency, predictability, and access determinism dominate:

- ultra-low access latency (often on the order of 1–2 ns in cache-class implementations),
- absence of refresh operations, simplifying control logic and avoiding refresh-induced timing jitter,
- high robustness under frequent access, particularly in on-chip cache environments,
- natural compatibility with logic–memory proximity in CMOS systems-on-chip, enabling dense cache and register-file integration.

2.1.3 Limitations

The performance advantages of SRAM come at significant structural cost:

- large cell area relative to DRAM, limiting achievable density and increasing cost per bit,
- leakage-dominated static power consumption in large arrays, especially at advanced technology nodes,
- increased layout and verification complexity in multi-port SRAM designs, which also introduce additional fault sensitivities such as port interference and asymmetric access stress.

From the perspective of symbolic fault modeling (see Chapter 8), SRAM commonly exhibits:

- classical stuck-at and transition faults,
- read-stability faults, in which the stored state flips under read stress,
- asymmetric and condition-dependent behaviors that become observable only when tests intentionally vary timing margins, supply voltage, or access sequences.

2.1.4 Use Cases

SRAM is deployed in system components where time-to-data is critical and capacity requirements are secondary:

- CPU cache hierarchies (L1, L2, and sometimes L3, depending on design),
- GPU register files and local shared memory structures,
- FPGA configuration memories and lookup-table fabrics (technology-dependent),
- embedded real-time buffers in control and signal-processing systems requiring deterministic access.

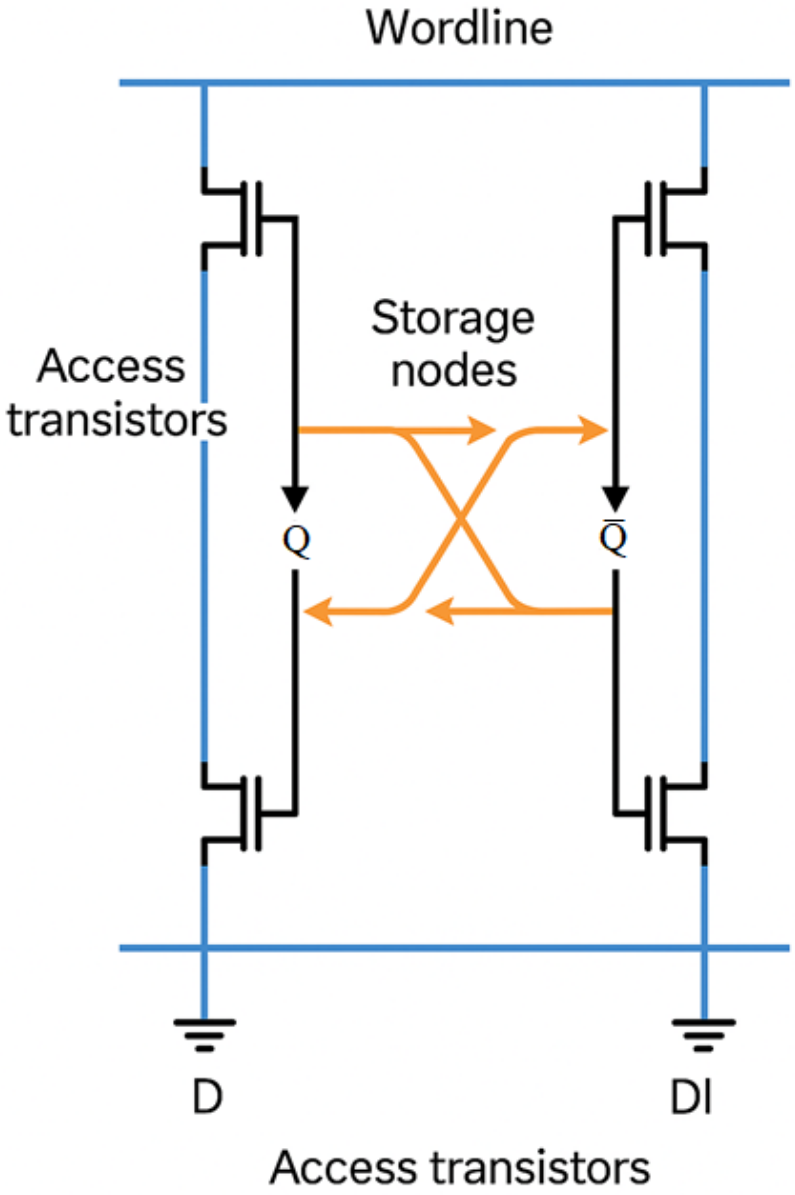

Figure 2.1—SRAM 6T cell diagram with read/write control paths

The figure illustrates a standard SRAM latch structure in which a top wordline enables two access transistors that connect the internal storage nodes Q and $\bar{Q}$ to a complementary bitline pair (physically corresponding to BL and $B\bar{L}$, labeled as D and DI in the diagram).

The cross-coupled feedback paths indicate the regenerative property of the latch: once written, the stored state is actively reinforced as long as power is applied. From a diagnostic perspective, the figure highlights three functionally distinct regions:

i. the storage core formed by the cross-coupled inverters,
ii. the selection mechanism controlled by the wordline and access transistors, and the I/O exposure through the bitlines.

iii. These regions correspond directly to dominant SRAM fault families, including access-transistor opens or weakness, latch imbalance, and read-disturb-induced instability.

2.2 DRAM: Principles, Variants, and Refresh Mechanisms

2.2.1 Cell Architecture

Dynamic random-access memory (DRAM) stores each bit as electric charge on a capacitor accessed through a single transistor, commonly referred to as a one-transistor–one-capacitor (1T1C) cell architecture.

DRAM achieves substantially higher density than SRAM because the storage element is capacitive rather than latch-based.

The core internal structures of a DRAM array include:

- a storage capacitor, whose charge encodes the logical state,
- an access transistor controlled by the wordline,
- a bitline and associated sense amplifier used to detect extremely small voltage deviations during access,
- a row buffer (implemented as a sense-amplifier array) that temporarily holds the contents of an activated row.

Because stored charge decays over time due to leakage mechanisms in the capacitor and access device, DRAM is intrinsically volatile and requires periodic refresh operations to preserve data integrity.

2.2.2 Operation Timing

A DRAM access proceeds as a controlled multi-stage sequence governed by the memory controller:

- **ACT (activate)**: the wordline is raised, allowing charge sharing between the cell capacitor and the precharged bitline.
- **Sense and restore**: the sense amplifier detects the resulting small voltage differential on the bitline, amplifies it to a full logic level, and restores the corresponding charge in the cell.
- **READ/WRITE burst**: once the row is active, data transfers occur between the row buffer and the external interface.
- **PRE (precharge)**: the bitlines are returned to a reference voltage in preparation for the next activation.
- **REFRESH**: periodic restoration of stored charge across all rows, typically scheduled by the memory controller.

At the physical level, DRAM read operations are destructive: the original charge stored in the cell capacitor is disturbed during sensing and must be rewritten. Modern sense-and-restore circuitry makes this behavior transparent to system software, but it remains fundamental to DRAM fault activation and diagnosability.

2.2.3 Advantages and Limitations

DRAM dominates main-memory implementations due to:

- high storage density and favorable cost per bit,
- scalability to multi-gigabit devices and multi-channel memory systems.

However, these advantages introduce significant diagnostic and reliability challenges:

- refresh overhead and refresh scheduling side effects,
- susceptibility to soft errors, retention variability, pattern-sensitive coupling, and disturb phenomena,
- controller-mediated behaviors that can either mask or expose faults depending on command timing and access patterns.

In symbolic diagnostic experiments (**see Chapter 16**), retention and coupling faults frequently become observable only under refresh-aware test conditions, such as reduced refresh rates, delayed restoration, or structured stress patterns. Conventional tests that assume nominal refresh behavior may therefore under-expose critical DRAM failure mechanisms.

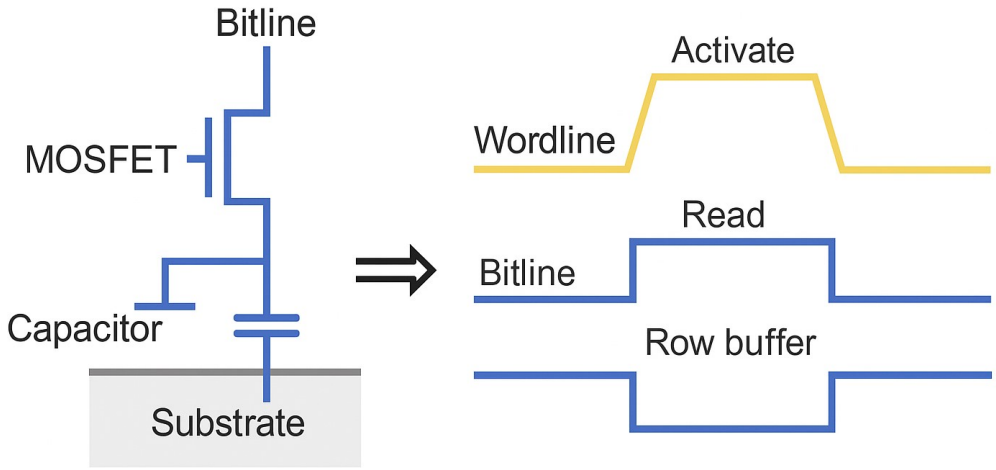

Figure 2.2—DRAM cell cross-section and access cycle waveform

The left panel illustrates a DRAM storage capacitor connected to a bitline through an access MOSFET positioned above the substrate. The right panel conceptually depicts the access sequence: assertion of the wordline activates the cell, a small bitline perturbation is generated by charge sharing, and the row buffer reflects the amplified and restored state.

From a diagnostic perspective, the Figure highlights the physical origins of DRAM-specific fault classes, including charge leakage (retention faults), disturb effects during activation and sensing, and sensitivity of the sensing margin to noise, temperature, and process variation.

2.3 SDRAM and DDR Generations

2.3.1 Synchronous DRAM (SDRAM)

Synchronous DRAM (SDRAM) aligns memory operations with a global system clock, enabling precise coordination between the memory controller and the internal array. In contrast to asynchronous DRAM, all commands are issued on a clocked command bus, allowing pipelined execution and substantially higher sustained throughput.

The fundamental SDRAM command set includes:

- **ACT (activate)**: opens a specific row within a designated memory bank,
- **READ / WRITE**: transfers data between the active row buffer and the external interface,
- **PRE (precharge)**: closes the active row and restores the bank to a precharged state.

SDRAM supports burst-oriented transfers, in which multiple contiguous data words are accessed with a single command sequence, and enables overlapping of operations across banks to improve effective bandwidth.

2.3.2 DDR Generations

Double Data Rate (DDR) SDRAM extends the SDRAM architecture by transferring data on both the rising and falling edges of the clock signal, effectively doubling data throughput without increasing the base clock frequency.

Successive DDR generations introduce additional enhancements in signaling techniques, bank and sub-bank organization, internal prefetch depth, and timing constraints. These changes improve bandwidth and energy efficiency but also introduce increasingly complex timing interactions that directly influence fault activation and diagnostic visibility.

2.3.3 DDR Performance Evolution and Timing Constraints

Successive generations of DDR SDRAM increase peak throughput by combining architectural changes with progressively tighter timing control. Table 2.1 summarizes representative peak data rates and distinguishing features across DDR generations.

Table 2.1—Overview of DDR generations and key architectural features.

Generation	Peak Data Rate	Key Features
DDR	200–400 MT/s	Double-edge clocking
DDR2	Up to 800 MT/s	On-die termination (ODT), 4-bit prefetch
DDR3	Up to 2133 MT/s	Fly-by topology, 8-bit prefetch
DDR4	Up to 3200 MT/s	Bank groups, pseudo open-page policy
DDR5	4800–8400 MT/s	Dual 32-bit channels per DIMM, on-die ECC

DDR performance is governed by a combination of architectural and timing parameters that jointly determine access latency, sustained bandwidth, and fault activation behavior.
Key performance factors include:

- **Timing parameters**: critical delays such as t_{RCD} (row-to-column delay), t_{CL} (CAS latency), t_{Rp} (row precharge time), t_{WR} (write recovery), and t_{FAW} (four activate window), which bound legal command sequencing.
- **Bank interleaving**: enables concurrent access across multiple banks to reduce row conflicts and improve throughput.
- **Row policies**: open-page policies favor repeated access to the same row, while closed-page policies better accommodate highly random access patterns.

In adaptations of March test algorithms for DDR4 and DDR5 devices, bank-aware and precharge-sensitive fault models were developed. These models reveal that conventional test methodologies—often designed under idealized assumptions of unrestricted activation overlap—can miss defects when real-world memory controllers dynamically adjust access scheduling for power efficiency and thermal management.

This observation reinforces the importance of controller-aware diagnostic sequencing when validating high-density, multi-bank DRAM architectures.

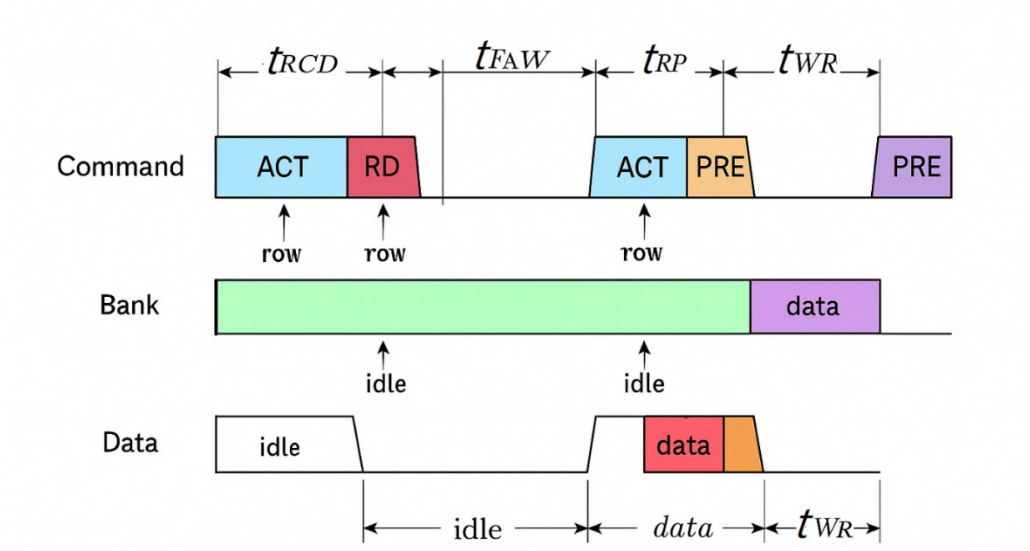

Figure 2.3—DDR timing diagram with command sequence

The Figure presents a representative DDR access timeline integrating command issuance (ACT, RD, PRE) with corresponding timing parameters. The delay t_{RCD} defines the minimum interval between row activation and column access, t_{FAW} limits the rate of row activations to control instantaneous current draw, t_{RP} enforces sufficient precharge time before reactivation, and t_{WR} specifies the minimum recovery interval following a write before precharge.

The lower portion of the diagram illustrates bank-level activity and data burst intervals, highlighting the interaction between command scheduling, internal bank state, and external data bus utilization.

2.3.4 Temporal Coordination and Bank Activation Control

At the command layer, a DRAM access begins with an ACT (activate) command targeting a specific bank–row pair. This operation opens the selected row by coupling the cell capacitors

to the bank's sense amplifier array. The minimum delay between ACT and a subsequent RD (read) or WR (write) command is dictated by t_{RCD}, during which charge sharing, sense amplification, and internal stabilization are completed.

The t_{RCD} interval encapsulates both analog sensing and internal timing margins. Violating this constraint—such as through overly aggressive scheduling in optimized March test sequences—can provoke read-disturb effects, marginal sensing failures, or premature activation faults, particularly in high-density DDR4 and DDR5 devices.

Once a row is active, issuance of a column command initiates data transfer. The delay before data becomes available on the external bus is defined by t_{CL} (CAS latency), which varies with DDR generation, device speed grade, and controller configuration. t_{CL} represents a trade-off between raw latency and achievable bandwidth.

2.3.5 Precharge, Write Recovery, and Inter-Activation Hazards

Following a data transfer, a PRE (precharge) command closes the active row by returning the bitlines to a reference voltage and disabling the sense amplifiers. The minimum delay before a subsequent activation, t_{RP}, prevents premature reactivation and allows internal nodes to settle, reducing the risk of coupling-induced disturb faults and unintended charge redistribution.

When the preceding operation is a write, the t_{WR} (write recovery) constraint enforces a minimum delay before precharge, ensuring that write drivers disengage cleanly and that cell capacitors fully acquire the intended charge. Insufficient t_{WR} observance can corrupt recently written data and is directly relevant to timing-aware fault detection and ECC latency modeling within built-in self-test (BIST) environments.

2.3.6 t_{FAW} Constraint and Thermal-Aware Fault Avoidance

The t_{FAW} (four activate window) parameter limits the number of ACT commands issued across all banks within a defined time window, typically restricting the count to four. This constraint mitigates localized heating and suppresses transient current surges that could otherwise destabilize power delivery in high-density memory modules.

From a diagnostic standpoint, t_{FAW} imposes a critical scheduling constraint. Naïve March patterns or dense back-to-back activation sequences may violate t_{FAW}, triggering controller throttling or adaptive thermal responses. These effects can suppress fault activation opportunities and obscure timing-sensitive defects, particularly in DDR4 and DDR5 devices where t_{FAW} may be dynamically adjusted to meet power and thermal targets.

2.3.7 Diagnostic Modeling Implications

Figure 2.3 underscores the necessity of integrating real-world timing constraints into symbolic expansions of March-based test algorithms. Bank-aware access patterns—such as interleaved March traversals or controlled pseudo-random streams—must be explicitly constructed to respect t_{FAW}, t_{WR}, t_{RP}, and related parameters.

Ignoring these constraints risks diagnostic evasion: latent defects may remain undetected due to controller-enforced throttling, row-buffer contention, or incomplete precharge cycles. A key divergence therefore arises between idealized fault models and practical DDR behavior.

The PROVER and Optimal_Test frameworks address this gap by incorporating timing-aware simulation of DDR command sequences, enabling comprehensive fault activation and coverage under the operational constraints of modern high-density, multi-bank memory architectures.

2.4 LPDDR and Mobile RAM Architectures

2.4.1 Features

Low-Power DDR (LPDDR) memory is designed for mobile and embedded platforms where energy efficiency, thermal constraints, and standby behavior outweigh raw bandwidth considerations. Its defining features include:

- **Deep power states**: support for self-refresh, partial-retention, and deep-sleep modes that minimize both leakage and dynamic power during idle intervals.
- **Partial array access**: selective activation of memory regions, reducing active current draw for localized operations.
- **Low I/O voltage swing**: reduced signaling voltages (typically around 1.1 V or below) to decrease interface power consumption.
- **Trade-off profile**: compared with desktop or server DDR, LPDDR typically exhibits higher access latency but delivers significantly improved energy efficiency for duty-cycled and battery-powered workloads.

2.4.2 Variants

Table 2.2—LPDDR standards and distinguishing features.

Standard	Key Features
LPDDR2	Early low-power standard with foundational deep power states for mobile devices
LPDDR3 / LPDDR4	Increased bandwidth and improved energy efficiency for smartphones and tablets
LPDDR5 / LPDDR5X	High-speed interfaces, multi-channel organization, and adaptive refresh for performance scaling under variable workloads

2.4.3 Testing Challenges

LPDDR's aggressive power optimization introduces diagnostic challenges that are less pronounced in conventional DDR devices:

- **Retention testing after sleep**: verification of data integrity following extended self-refresh or deep-sleep intervals, where leakage and partial array retention effects must be evaluated under varying temperature conditions.
- **Power-mode transitions**: validation of correct behavior when switching between active, idle, and retention states, ensuring that mode-transition latency does not corrupt in-flight transactions.
- **Burst alignment faults**: detection of synchronization errors or misaligned data bursts during wake-up cycles, particularly in the initial transfers following low-power states.

These behaviors require test sequences that explicitly model power-state transitions rather than assuming continuous active operation.

2.5 Graphics Memory Technologies: GDDR and HBM

2.5.1 GDDR (Graphics DDR)

Graphics DDR (GDDR) memory variants are optimized for extreme bandwidth demands in graphics processors and real-time rendering pipelines.

Type	Key Features
GDDR6	Up to 20 Gbps per pin, dual-pumped clocking, wide I/O interfaces, and pseudo-open row policies optimized for repeated access patterns
HBM	3D-stacked DRAM dies interconnected via Through-Silicon Vias (TSVs), with 1024-bit buses delivering up to 460 GB/s per stack at significantly lower energy per bit.

2.5.2 HBM (High Bandwidth Memory)

High Bandwidth Memory represents a fundamental shift in memory packaging and interconnect architecture, combining massive parallelism with low per-bit energy consumption.

- **Structure**: multiple DRAM dies (commonly up to eight) are vertically stacked within a single package, with each die exposing several independent channels.
- **Interface**: ultra-wide buses (typically 1024 bits per stack) operating at relatively low clock frequencies, enabling aggregate bandwidths of hundreds of GB/s while mitigating signal integrity challenges.
- **Advantages**: close physical proximity of logic and memory—enabled by Through-Silicon Vias (TSVs)—reduces latency and energy per transferred bit, making HBM well suited for GPUs, AI accelerators, and high-performance computing workloads.

In test-path synthesis for HBM devices (**see Chapter 10**, with architectural context in **Chapter 9**), TSV-induced fault behaviors were explicitly modeled. Vertical coupling effects and through-silicon timing skew were observed to introduce path-dependent failures that are largely

invisible to traditional row/column-oriented test algorithms. These characteristics necessitate diagnostic strategies that incorporate inter-die timing characterization and thermal-gradient modeling to achieve full fault observability in stacked-memory environments.

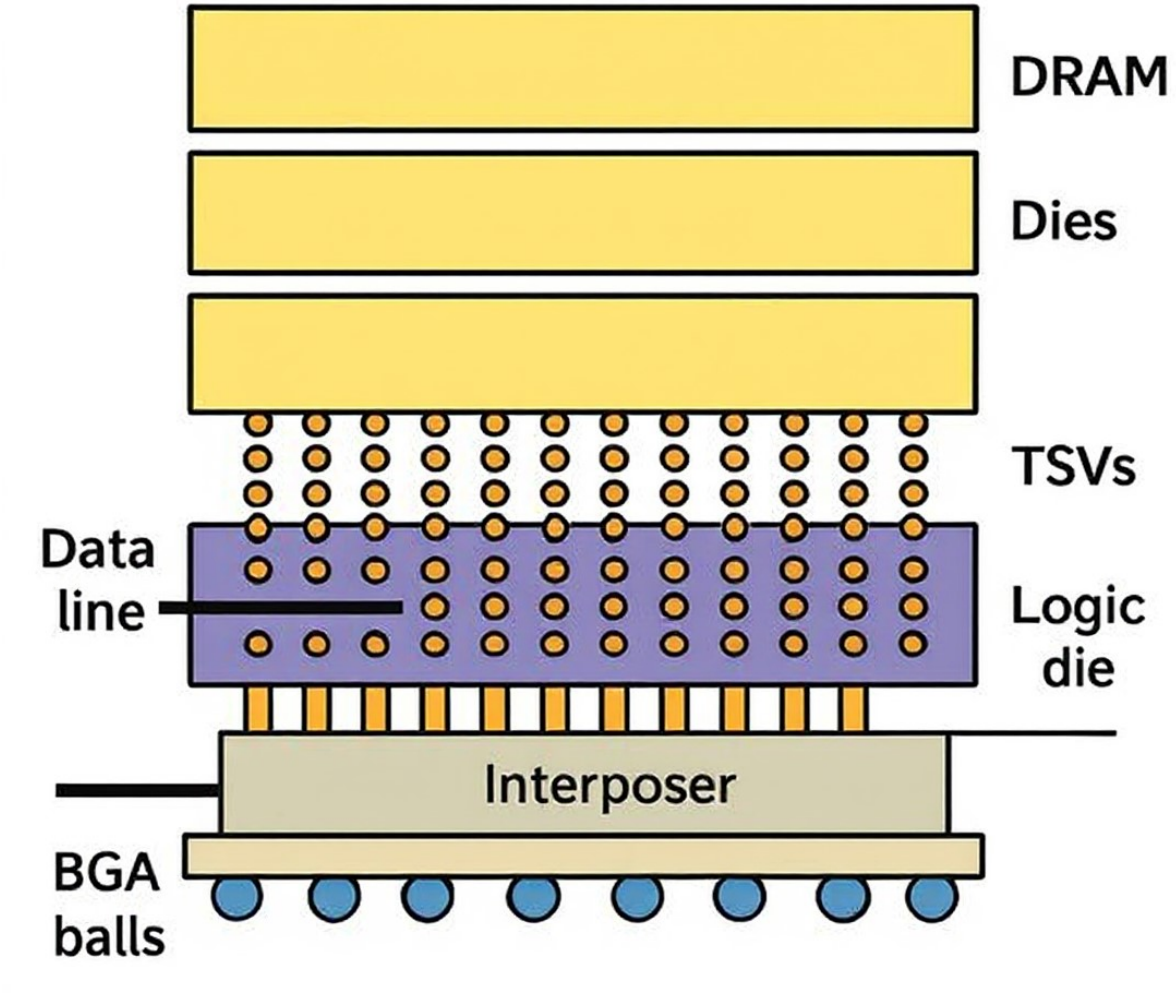

Figure 2.4—HBM 3D stack architecture

The Figure illustrates the vertical integration of High Bandwidth Memory. Multiple DRAM dies are stacked and interconnected through dense arrays of Through-Silicon Vias, enabling high-speed vertical data transfer.

A logic die at the base of the stack manages channel control, command decoding, and data routing, and connects to a silicon interposer that redistributes signals to the external ball grid array interface. This architecture supports ultra-wide data buses (e.g., 1024 bits) and delivers aggregate bandwidths exceeding hundreds of GB/s while maintaining a compact footprint and reduced energy cost per bit.

2.6 Emerging versus Conventional Memory Technologies

Emerging non-volatile memory (NVM) technologies aim to bridge the performance gap between DRAM's high-speed volatility and NAND Flash's high-density persistence. These memory classes introduce distinct trade-offs in density, endurance, power consumption, and

scalability. Their fundamentally different physical storage mechanisms also give rise to fault behaviors that challenge the adequacy of classical binary fault models such as stuck-at and transition faults. As a result, diagnostic methodologies must be extended to capture technology-specific failure signatures.

2.6.1 MRAM (Magnetoresistive RAM)

Magnetoresistive RAM employs spintronic effects in magnetic tunnel junctions (MTJs) to encode data as magnetic orientation states.

- **Advantages**: non-volatility, read/write access times on the order of tens of nanoseconds, and endurance exceeding 10^{12} cycles.
- **Challenges**: susceptibility to read disturb, variability in write currents due to thermal noise, and asymmetric switching behavior in MTJ transitions that can degrade write margins over time.

2.6.2 ReRAM (Resistive RAM)

Resistive RAM stores information by modulating the electrical resistance of a metal-oxide layer through controlled formation and rupture of conductive filaments.

- **Advantages**: very low write energy and suitability for neuromorphic and edge AI applications due to analog programmability.
- **Fault modes**: stuck-high or stuck-low resistance states, gradual analog degradation, and soft-set or soft-reset anomalies caused by incomplete or unstable filament formation.

2.6.3 PCM (Phase Change Memory)

Phase Change Memory exploits the large resistance contrast between amorphous (high-resistance) and crystalline (low-resistance) phases of chalcogenide materials.

- **Advantages**: high storage density, intrinsic non-volatility, and potential use as storage-class memory bridging DRAM and NAND.
- **Challenges**: progressive write endurance degradation, resistance drift during idle periods, and read disturb effects, often necessitating periodic refresh-like maintenance operations to preserve long-term data integrity.

2.6.4 FeRAM (Ferroelectric RAM)

Ferroelectric RAM (FeRAM) stores information using a ferroelectric capacitor whose polarization state represents binary data.

- **Advantages**: non-volatility, extremely low power consumption, fast access, and strong immunity to radiation-induced soft errors.
- **Applications**: widely used in secure embedded systems such as smart cards, RFID tags, secure microcontrollers, and energy-harvesting IoT devices, where instant-on behavior and reliability are critical.

Within the fault taxonomy developed in Chapter 3, FeRAM—together with other emerging non-volatile memories—necessitates hybrid fault models that extend beyond classical binary abstractions.

Such models must account for temporal polarization fatigue, asymmetric switching thresholds, analog degradation, and multi-level behavior in advanced implementations. These effects lie outside the scope of traditional stuck-at and transition fault paradigms and motivate adaptive diagnostic frameworks capable of characterizing both digital and analog failure mechanisms.

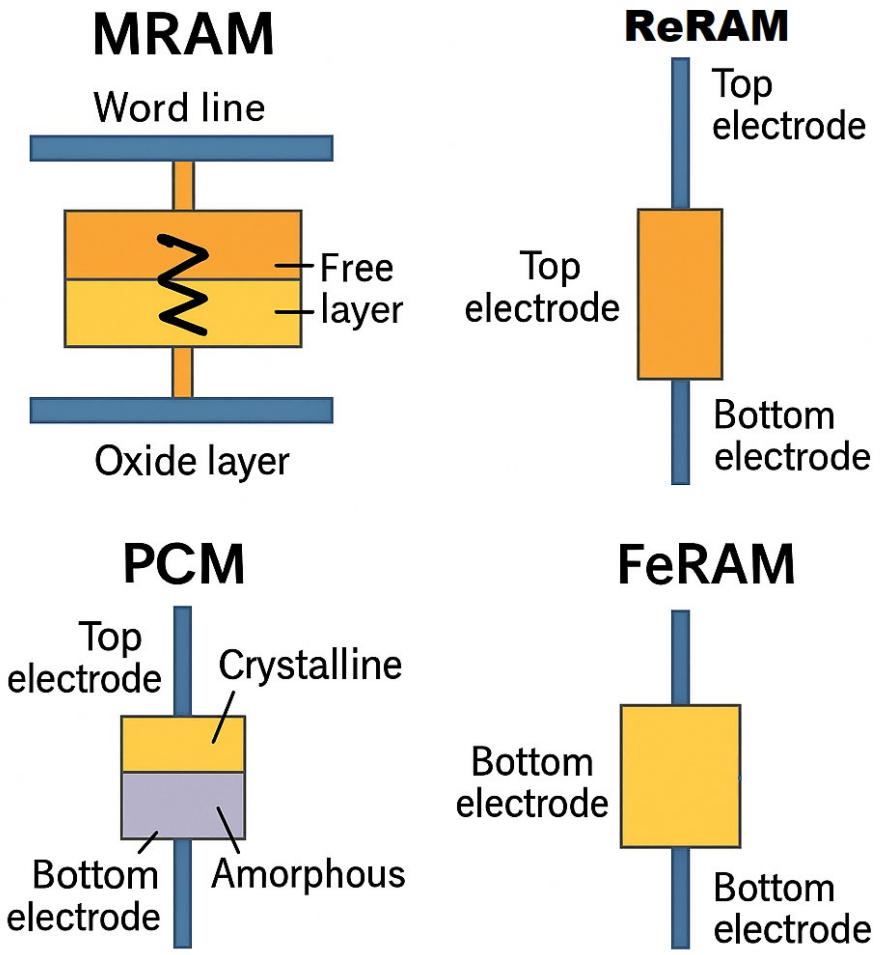

Figure 2.5—Comparative internal structures of emerging memory types

This Figure presents simplified cross-sectional representations of four representative emerging non-volatile memory (NVM) technologies—MRAM, ReRAM, PCM, and FeRAM—highlighting their distinct physical storage mechanisms.

- **MRAM (Magnetoresistive RAM)**: employs a Magnetic Tunnel Junction (MTJ) composed of a free magnetic layer and a fixed reference layer separated by a thin oxide tunnel barrier. The relative magnetic orientation (parallel or antiparallel) determines the tunneling resistance and encodes binary data.

- **ReRAM (Resistive RAM)**: uses a metal–insulator–metal stack in which information is stored by modulating the resistance of a metal oxide layer through formation and rupture of conductive filaments.
- **PCM (Phase Change Memory)**: encodes data by switching a chalcogenide material between crystalline (low-resistance) and amorphous (high-resistance) phases using localized Joule heating.
- **FeRAM (Ferroelectric RAM)**: represents binary states through opposing polarization orientations of a ferroelectric capacitor, enabling low-power, fast, and radiation-tolerant operation.

The Figure emphasizes the technological diversity of emerging NVMs and provides a visual reference for the hybrid fault classification discussed in Chapter 3, including temporal decay, analog drift, and asymmetric switching behavior.

2.7 Comparative Summary of RAM Technologies

The following table consolidates the defining characteristics of both conventional and emerging RAM technologies, providing a high-level comparison of volatility, performance, density, cost, refresh requirements, and primary application domains.

Table 2.3: Comparative summary of RAM technologies (volatility, performance, density, cost, refresh, and application domains).

Technology	Volatility	Speed	Density	Cost	Refresh	Primary Use
SRAM	Volatile	Very high	Low	High	No	CPU caches, registers
DRAM	Volatile	High	High	Moderate	Yes	Main system memory
LPDDR	Volatile	Moderate	High	Low	Yes	Mobile and embedded devices
GDDR / HBM	Volatile	Very high	Medium	High	Yes	GPUs, AI accelerators, HPC
MRAM	Non-volatile	High	Medium	High	No	Embedded systems, FPGA configuration
ReRAM	Non-volatile	Moderate	High	Medium	No	IoT, neuromorphic computing
PCM	Non-volatile	Moderate	High	Medium	Partial	Storage-class memory
FeRAM	Non-volatile	High	Low	High	No	RFID, secure microcontrollers

From a diagnostic engineering perspective, these distinctions directly influence fault modeling, test synthesis, and repair strategy selection:

- **Volatility** determines whether retention testing is required (DRAM, LPDDR) or unnecessary (MRAM, ReRAM, FeRAM).
- **Speed–density trade-offs** constrain achievable fault coverage under production test time limits.
- **Refresh requirements** dictate the inclusion of refresh-aware or self-refresh test sequences, which are critical for DRAM-class devices and largely irrelevant for non-volatile memories.
- **Primary application domain** influences acceptable failure-in-field risk; for example, HPC and GPU memory tolerate far fewer latent faults than low-duty-cycle IoT devices.

In subsequent chapters, these comparative attributes are mapped to technology-specific fault taxonomies and adaptive diagnostic workflows, illustrating how the PROVER and Optimal_Test frameworks exploit physical and architectural parameters to maximize fault coverage and test efficiency.

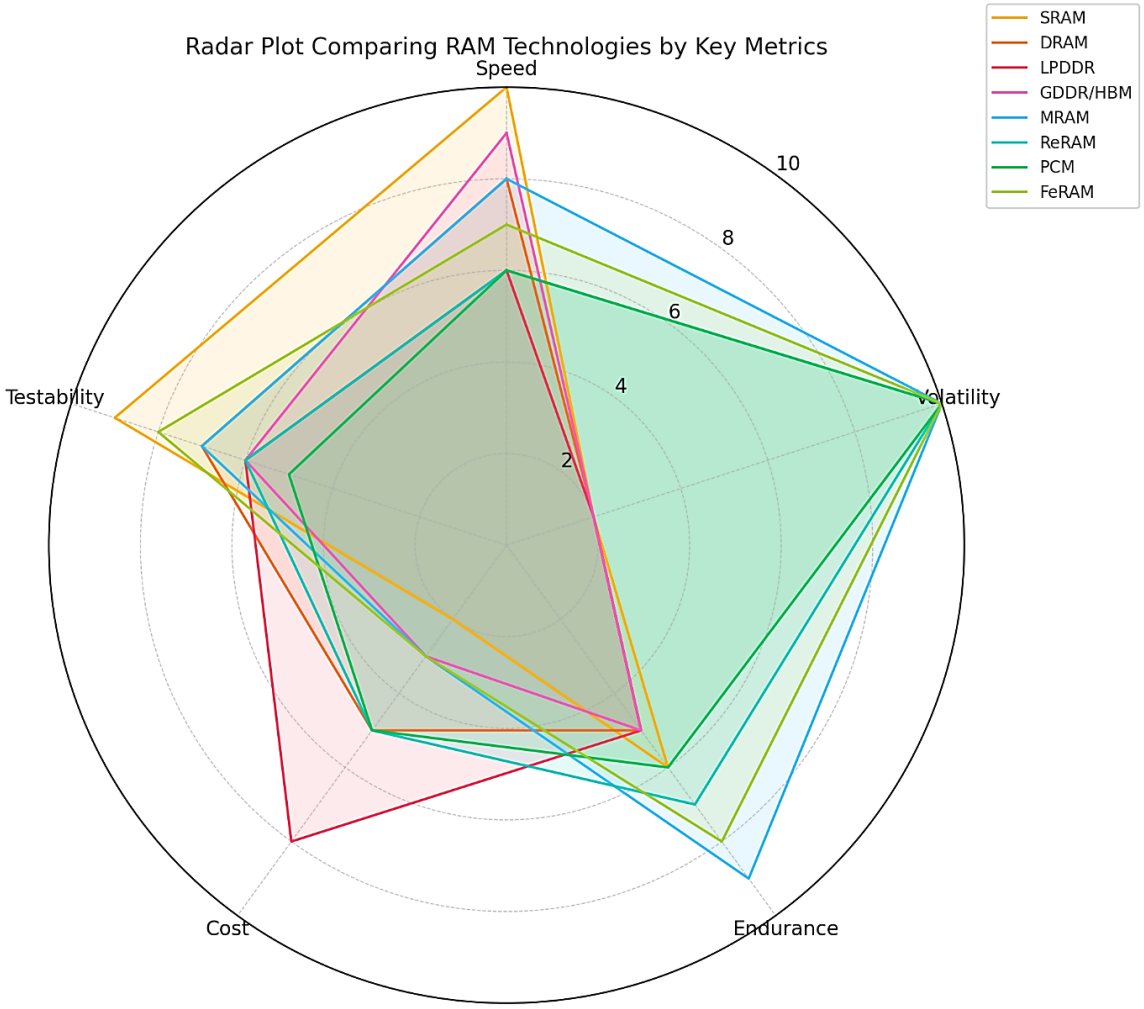

Figure 2.6—Radar plot comparing speed, volatility, endurance, cost, testability

This radar plot provides a comparative visualization of eight representative RAM technologies across five design-relevant dimensions: speed, volatility, endurance, cost, and testability. Each axis is normalized on a 0–10 scale, where higher values correspond to more favorable characteristics (e.g., higher speed, greater endurance, lower cost per bit, or easier diagnostic access).

The plot highlights trade-offs between volatile and non-volatile memory classes and illustrates how architectural and physical properties translate into system-level and diagnostic consequences.

Interpretation of Radar Metrics

- **Speed**: reflects access latency and achievable read/write throughput under typical operating conditions.
- **Volatility**: indicates resistance to data loss in the absence of power; lower values correspond to higher volatility.
- **Endurance**: represents the number of reliable write or update cycles before significant degradation.
- **Cost**: captures relative economic efficiency; higher values correspond to lower cost per bit.
- **Testability**: expresses the relative ease with which faults can be activated, observed, and isolated using practical diagnostic methods.

Technology Profiles

SRAM (Static RAM)

- Speed: 10 — minimal access latency.
- Volatility: 2 — fully volatile.
- Endurance: 6 — high endurance, though leakage limits scalability.
- Cost: 2 — high cost per bit due to large cell area.
- Testability: 9 — excellent; static behavior simplifies fault isolation.

DRAM (Dynamic RAM)

- Speed: 8 — high throughput with activation and precharge overhead.
- Volatility: 2 — requires refresh to retain data.
- Endurance: 5 — moderate; sensitive to retention loss and coupling effects.
- Cost: 5 — balanced cost–density trade-off.
- Testability: 7 — good coverage achievable, though refresh behavior complicates diagnosis.

LPDDR (Low-Power DDR)

- Speed: 6 — optimized for energy efficiency rather than peak bandwidth.
- Volatility: 2 — volatile, DRAM-based storage.
- Endurance: 5 — similar limitations to standard DRAM.
- Cost: 8 — cost-efficient in mobile and embedded contexts.

- Testability: 6 — power-state transitions introduce diagnostic complexity.

GDDR / HBM (Graphics DDR / High Bandwidth Memory)

- Speed: 9 — extreme bandwidth for graphics, AI, and HPC workloads.
- Volatility: 2 — DRAM-based and refresh-dependent.
- Endurance: 5 — comparable to standard DRAM.
- Cost: 3 — elevated due to wide I/O, TSVs, and advanced packaging.
- Testability: 6 — challenged by bank-grouping, interleaving, and thermal effects.

MRAM (Magnetoresistive RAM)

- Speed: 8 — approaching SRAM-class latency.
- Volatility: 10 — fully non-volatile.
- Endurance: 9 — stable magnetic switching over very high cycle counts.
- Cost: 3 — currently expensive to manufacture at scale.
- Testability: 7 — strong, though asymmetry and magnetic interactions require tailored patterns.

ReRAM (Resistive RAM)

- Speed: 6 — moderate, with scope for optimization.
- Volatility: 10 — fully non-volatile.
- Endurance: 7 — generally good, limited by filament variability.
- Cost: 5 — mid-range and improving.
- Testability: 6 — analog drift and stochastic behavior complicate diagnosis.

PCM (Phase Change Memory)

- Speed: 6 — limited by thermal phase transitions.
- Volatility: 10 — fully non-volatile.
- Endurance: 6 — constrained by phase-change fatigue.
- Cost: 5 — moderate, suitable for storage-class roles.
- Testability: 5 — resistance drift and intermediate states complicate fault classification.

FeRAM (Ferroelectric RAM)

- Speed: 7 — faster than most other NVMs.
- Volatility: 10 — non-volatile storage.
- Endurance: 8 — high endurance for embedded-scale deployments.
- Cost: 3 — relatively high due to specialized materials.
- Testability: 8 — strong, though read–rewrite behavior must be handled carefully during tests.

Key Insights

- SRAM and MRAM offer the highest speed and testability, with MRAM uniquely combining these properties with non-volatility.

- FeRAM provides a strong balance of non-volatility, endurance, and diagnostic accessibility, at the expense of density and cost.
- PCM and ReRAM offer persistence and density advantages but require hybrid fault models to address analog drift and variability.
- LPDDR and DRAM remain cost-effective for general-purpose systems, while GDDR and HBM dominate throughput-centric workloads despite increased diagnostic complexity.

2.8 Summary

RAM technologies form a continuum of engineering trade-offs across volatility, access latency, density, endurance, and cost. These trade-offs are tightly coupled to application domains, ranging from ultra-low-latency CPU caches and energy-constrained mobile platforms to high-bandwidth accelerators and persistent embedded systems.

From a diagnostic engineering perspective, each technology imposes distinct constraints on fault activation and observability:

- volatile memories require timing- and refresh-aware testing to expose retention and coupling faults,
- non-volatile memories demand hybrid fault models that capture analog degradation, drift, and asymmetric switching behavior,
- advanced architectures such as GDDR and HBM require layout-, bank-, and thermal-aware diagnostics to address TSV coupling, bank-group contention, and temperature-induced variability.

These considerations motivate the symbolic synthesis, U–Y graph decomposition, and adaptive optimization techniques developed in this work. The PROVER and Optimal_Test frameworks exploit technology-specific parameters to maximize fault coverage and diagnostic efficiency under realistic operational constraints, providing a unified methodology applicable across both conventional DRAM-class devices and emerging non-volatile memory technologies.

Beyond device-level characteristics, system integration factors such as controller policies, interconnect behavior, and workload patterns also influence fault manifestation and detectability.

Diagnostic methodologies must therefore remain adaptable to evolving memory hierarchies and heterogeneous computing environments. As memory technologies continue to scale in density and architectural complexity, the boundary between functional validation and diagnostic analysis becomes increasingly intertwined. This convergence underscores the importance of structured test synthesis and scalable diagnostic frameworks.

The approaches developed in this work aim to support reliable validation across both present and emerging memory technologies.

Part II — Fault Taxonomy & Classical Tests

Chapter 3: Fault Types and Physical Failure Mechanisms

Modern memory systems, despite being engineered with extreme precision, remain inherently vulnerable to a wide spectrum of fault phenomena. These faults originate from multiple sources, including fabrication imperfections, process variability, long-term material degradation, electrical noise, architectural stress, and environmental influences.

As memory technologies advance toward ultra-dense geometries, heterogeneous integration, and three-dimensional stacking, the complexity and subtlety of failure mechanisms increase significantly, posing escalating challenges for both designers and test engineers.

This chapter establishes a structured and physically grounded taxonomy of memory faults, classifying them according to their physical origin, temporal persistence, and observable diagnostic behavior. The discussion encompasses both classical fault models—such as stuck-at, transition, retention, and coupling faults—and failure modes characteristic of advanced technologies, including 3D-stacked DRAM, Magnetoresistive RAM (MRAM), Resistive RAM (ReRAM), and Phase-Change Memory (PCM). For each major fault category, the analysis addresses:

- **Physical causes**, spanning charge leakage, electromigration, thermal stress, dielectric degradation, and particle-induced events,
- **Behavioral signatures**, manifested as data corruption patterns, timing anomalies, or access irregularities,
- **Testing implications**, with emphasis on detection, localization, and mitigation strategies, including adaptive and layout-aware diagnostic approaches.

By formalizing this taxonomy, the chapter provides a foundation for subsequent discussions on symbolic fault modeling, diagnostic architectures, and fault-tolerant memory design. A precise understanding of physical failure mechanisms is essential for maximizing fault coverage, reducing test escapes, and ensuring long-term reliability, particularly in safety-critical, high-availability, and high-performance computing environments.

3.1 Fault Classification: Permanent, Intermittent, and Transient

Memory faults can be systematically classified according to their activation behavior and temporal persistence. This classification directly informs test strategy selection, in-field monitoring policies, and error-mitigation mechanisms.

Permanent faults

Permanent faults arise from irreversible physical defects within the memory cell array or peripheral circuitry. Typical sources include manufacturing anomalies such as metallization shorts, open vias, gate-oxide defects, and permanently stuck storage elements. These faults manifest deterministically across operating conditions and are reproducible under repeated

testing, making them primary targets for production screening using March algorithms, scan-based diagnostics, and redundancy analysis.

Intermittent faults

Intermittent faults occur sporadically and are often triggered by specific environmental or operational stressors. Contributing factors include marginal design tolerances, process variation, thermal cycling, voltage fluctuations, and parasitic coupling effects such as interconnect crosstalk.

Their non-deterministic activation makes them particularly difficult to detect: a device may pass one test instance and fail the next. Intermittent faults frequently precede permanent failures, serving as early indicators of degradation mechanisms such as electromigration-induced conductor thinning or incipient dielectric breakdown.

Transient faults

Transient faults are short-lived disturbances caused by external phenomena, including single-event upsets (SEUs) induced by cosmic radiation, electromagnetic interference, or power-supply noise transients. These faults do not result in permanent physical damage, but they can temporarily corrupt stored data or logic states.

Their statistical occurrence—especially in radiation-rich environments such as aerospace or high-altitude systems—necessitates real-time detection and mitigation through techniques such as error-correcting codes (ECC), memory scrubbing, and architectural redundancy.

Within the Optimal_Test framework developed during this work, fault classification is extended through integration of environmental telemetry and fault history analytics. By correlating recurrence statistics with real-time sensor data (e.g., temperature, supply voltage, radiation flux), the framework dynamically refines fault categorization and adaptively prioritizes test sequences, improving diagnostic resolution for elusive intermittent and transient faults.

3.2 Physical Origins of Memory Faults

Fault occurrence in semiconductor memory devices is driven by a combination of physical, electrical, and environmental mechanisms. Understanding these root causes enables the construction of accurate fault models and the design of targeted diagnostic procedures.

Fabrication defects

Manufacturing imperfections—including lithographic misalignment, incomplete etching, metal discontinuities, and gate-oxide pinholes—introduce structural anomalies that frequently lead to permanent faults. Such defects are most commonly detected during wafer-level testing or early burn-in.

Process variation

As device dimensions scale into deep-submicron and nanometer regimes, statistical variation in threshold voltage, channel length, oxide thickness, and capacitor geometry becomes

increasingly significant. These variations can induce timing skew, unstable retention behavior, and heightened sensitivity to soft errors.

Consequently, variation-aware modeling and layout-sensitive test pattern generation are essential for robust diagnosis.

Wear-out mechanisms

Long-term operation gives rise to cumulative aging effects, including:

- negative bias temperature instability (NBTI), causing gradual threshold voltage shifts in pMOS devices,
- hot carrier injection (HCI), degrading gate oxide integrity in NMOS transistors,
- time-dependent dielectric breakdown (TDDB), leading to progressive leakage and eventual hard failure.

These mechanisms critically constrain endurance limits in both volatile and non-volatile memory technologies.

Environmental stressors

External conditions such as thermal gradients, mechanical stress, vibration, and humidity can exacerbate latent marginalities. For example, thermal expansion mismatch between stacked layers may induce micro-fractures in interconnects or solder joints, particularly in advanced packaging technologies.

Radiation-induced events

High-energy particles from cosmic radiation or alpha decay can deposit localized charge in sensitive storage nodes, triggering soft errors.

SRAM and DRAM are especially vulnerable due to their low critical charge (Q_{crit}), with susceptibility increasing in high-altitude or spaceborne environments.

These physical origins define not only fault types but also activation conditions—the voltage, temperature, and access-pattern domains in which failures manifest. Comprehensive diagnostic architectures must therefore operate across multi-dimensional stress spaces to achieve high fault coverage while minimizing test escapes.

In practice, these mechanisms rarely occur in isolation; multiple degradation processes may interact and amplify fault manifestation. For instance, process variation can increase susceptibility to aging effects or radiation-induced events, accelerating failure onset. Consequently, diagnostic methodologies must account for the combined influence of manufacturing defects, operational stress, and environmental conditions.

This multi-factor perspective supports the development of fault models that more accurately reflect real device behavior. Such models form the foundation for the systematic testing strategies introduced in the following sections.

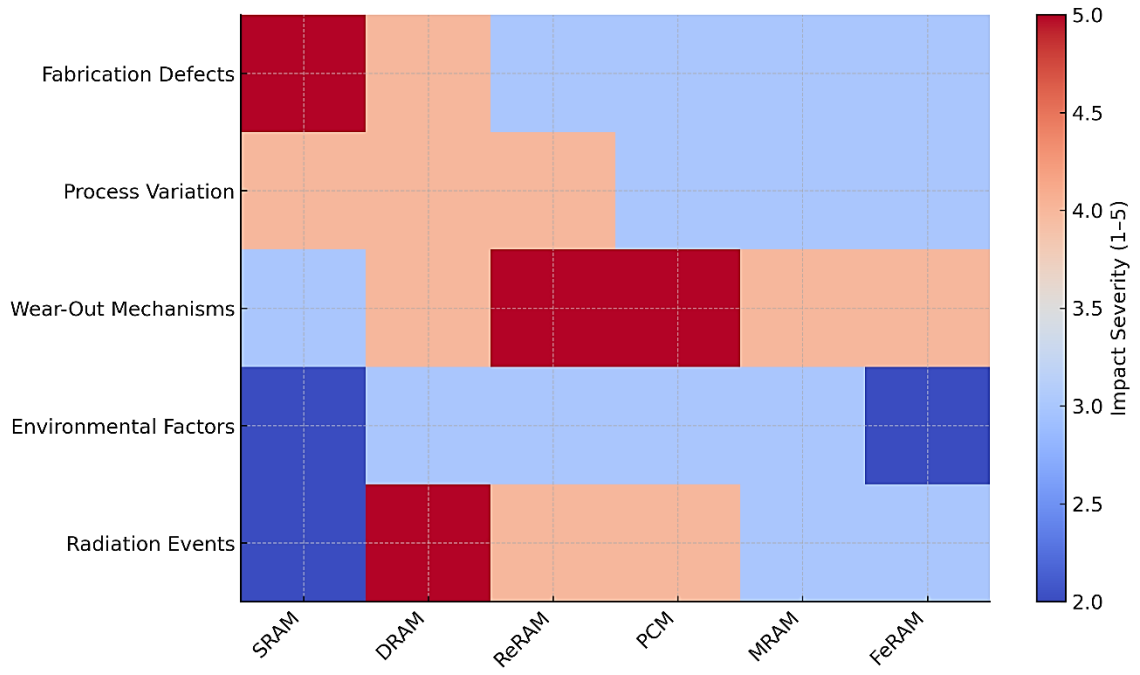

Figure 3.1—Physical cause-to-fault manifestation matrix across memory technologies

Figure 3.1 presents a comparative heatmap quantifying the relative impact severity of dominant physical fault origins across six representative memory technologies: SRAM, DRAM, ReRAM, PCM, MRAM, and FeRAM. Each cell encodes a normalized severity score from 1 (minimal impact) to 5 (critical vulnerability), synthesizing empirical reliability observations and process-level failure trends into a unified comparative framework.

The scores are **qualitative, expert-assigned rankings** intended to summarize widely reported reliability trends rather than serve as direct measured failure-rate values.

Axes description

- **Vertical axis (fault origin)**:
  - Fabrication defects — structural anomalies such as opens, shorts, and metallization discontinuities.
  - Process variation — statistical parameter deviations (e.g., threshold voltage, oxide thickness) leading to parametric and timing failures.
  - Wear-out mechanisms — aging effects including NBTI, HCI, and TDDB.
  - Environmental factors — thermal cycling, packaging stress, humidity, and vibration.
  - Radiation events — particle-induced charge deposition causing single-event upsets.
- **Horizontal axis (memory technology)**:
  - SRAM — cross-coupled CMOS storage, sensitive to mismatch and process asymmetry.
  - DRAM — charge-based capacitive storage, highly susceptible to retention loss, disturb effects, and radiation-induced faults.

- ReRAM — resistive switching devices prone to filament instability and endurance degradation.
- PCM — phase-change materials affected by resistance drift, thermal crosstalk, and cycling fatigue.
- MRAM — MTJ-based spin storage influenced by write-current stress and switching margin variability.
- FeRAM — ferroelectric capacitor storage, generally robust but limited by polarization fatigue and thin-film defects.

Interpretation and diagnostic implications

The color intensity in the heatmap reflects technology-specific vulnerability patterns:

- DRAM exhibits the highest sensitivity to radiation events and process variation, consistent with its low critical charge and reliance on charge retention.
- ReRAM and PCM show peak vulnerability to wear-out mechanisms, reflecting endurance limitations inherent to analog switching physics.
- SRAM is most affected by fabrication defects due to stringent device matching requirements for bistable operation.
- MRAM and FeRAM often exhibit comparatively balanced vulnerability profiles in reported reliability studies, making them attractive for embedded and harsh-environment deployments when switching margins, scaling limits, and write-stress constraints are properly managed.

This mapping supports:

- stress-aware test-sequence design for accelerated lifetime assessment,
- calibration of BIST parameters to technology-specific sensitivities,
- prioritization of mitigation mechanisms such as ECC, adaptive refresh, and redundancy,
- definition of radiation-hardening strategies for safety-critical and aerospace applications.

3.3 Logical Fault Models and Behavioral Abstractions

Logical fault models abstract low-level physical defect mechanisms into high-level, testable behavioral patterns observable during read and write operations. These abstractions form the foundation for systematic test generation, fault activation analysis, and quantitative assessment of diagnostic coverage.

The principal logical fault classes considered in this work include:

- **Stuck-At Faults (SAF)**
  A memory cell persistently outputs a fixed logic value (‘0’ or ‘1’) regardless of write intent. SAFs commonly model defects such as open or shorted bitlines, gate-oxide shorts, and malfunctioning sense amplifiers.
- **Transition Faults (TF)**
  A cell fails to perform one or both logic transitions:
  - T↑: failure to switch from 0 → 1

- T↓: failure to switch from 1 → 0

These faults often arise from charge trapping, carrier mobility degradation, or residual conductive filaments in resistive devices.

- **Coupling Faults (CF)**
  Operations on an aggressor cell influence the state of a victim cell:
  - **Inversion Coupling (CIN)** — the victim cell's stored value is inverted.
  - **Idempotent Coupling (CID)** — the victim cell is forced into a fixed state.

  Coupling faults dominate in dense arrays due to parasitic capacitive, resistive, and electromagnetic interactions.
- **Retention Faults (RF)**
  The cell fails to preserve data for the nominal retention interval, with severity increasing under elevated temperature, reduced supply voltage, or aging.
- **Address Decoder Faults (ADF)**
  Faults in address decoding logic cause aliasing, phantom accesses, or permanently inaccessible cells, with implications for both reliability and security.
- **Read Disturb Faults (RDF)**
  Repeated read operations induce unintended state changes in the same or neighboring cells (e.g., DRAM Rowhammer or NAND read disturb).
- **Port Interaction Faults (PIF)**
  In multi-port memories, simultaneous or overlapping accesses cause contention, race conditions, or asymmetric corruption.

Operator-Based Fault Model Innovation

A formal operator-based model was introduced to concisely describe complex cell interactions:

$$MF = (S_a; S_v) \rightarrow F_v \rightarrow R_v \qquad F_v \in \{0,1,U\}$$

Where:

- S_a — aggressor cell state and/or operation,
- S_v — initial victim cell state,
- F_v— induced fault effect in the victim (e.g., inversion, stuck-at, undefined),
- R_v— observed victim readout after fault activation,
- U — undefined or metastable victim state induced by partial switching, charge sharing, or marginal sensing.

This formulation provides a compact and expressive mechanism for unifying diverse coupling behaviors across memory technologies.

Within this framework, the following fault families are captured:

- **SCFs** — static coupling faults,
- **DCFs** — dynamic coupling faults,
- **NVR3** — destructive write faults,
- **NVRS** — read disturb faults,
- **NVLS** — false read faults.

Fault ID	Operator Expression	Fault Effect
1	(0 w 1; 0) → 1 → U	Victim flips to metastable
2	(0 w 1; 1) → 0 → U	Victim forced low
3	(0 w 0; 0) → 1 → U	Spurious inversion
4	(0 w 0; 1) → 0 → U	Spurious reset

These operator instances generalize classical coupling faults and extend naturally to non-volatile devices exhibiting asymmetric or stochastic behavior.

The above models were integrated directly into the **PROVER** symbolic synthesis engine, enabling parallel generation of test sequences and systematic activation of both static and dynamic fault conditions across volatile and non-volatile memory technologies.

By incorporating workload traces and hierarchical access patterns, the framework evolves into composite symbolic operators capable of capturing cross-layer interactions spanning cells, subarrays, banks, and controllers. This capability significantly improves fault observability and enables precise defect localization in dense, hierarchical memory systems.

A consolidated symbolic fault vocabulary and operator notation reference used throughout this work is provided in Appendix B.

3.4 Impact of Aging and Wear-Out Mechanisms

Modern memory devices are increasingly affected by aging-related degradation, particularly under high utilization, aggressive timing margins, and advanced technology scaling. The dominant wear-out mechanisms include:

- **Negative Bias Temperature Instability (NBTI)**
  Primarily affects pMOS transistors, producing progressive threshold-voltage shifts under sustained negative gate bias and elevated temperature. The resulting degradation manifests as reduced write margins and increased access latency.
- **Hot Carrier Injection (HCI)**
  High-energy carriers become trapped in the gate oxide, leading to threshold-voltage shifts, increased leakage, and degraded switching speed. HCI is particularly critical in peripheral circuitry of SRAM and DRAM arrays.
- **Time-Dependent Dielectric Breakdown (TDDB)**
  Long-term electric-field stress progressively degrades dielectric layers, eventually forming leakage paths or hard shorts. TDDB represents a dominant failure mechanism in both volatile and non-volatile memory technologies.

These degradation effects are cumulative and often accelerated by environmental stressors such as high temperature, voltage overstress, and high-frequency cycling.

Within the **Optimal_Test** synthesis engine, aging-aware March variants and temperature–voltage corner stress tests were implemented to expose wear-out-prone cells and interconnects at early stages. This enables predictive diagnostics and adaptive refresh or access scheduling, mitigating performance degradation before catastrophic failure.

3.5 Environmental Faults and Radiation Effects

In mission- and safety-critical domains—including aerospace, medical instrumentation, and automotive control systems—memory subsystems must operate reliably under extreme environmental stressors and radiation exposure. The dominant environmental fault mechanisms include:

- **Single-Event Upsets (SEUs)**: charged particle strikes deposit localized charge in sensitive storage nodes, resulting in transient bit inversions.
- **Multiple-Bit Upsets (MBUs)**: at advanced technology nodes (≈28 nm and below), a single particle strike can affect multiple physically adjacent cells, producing burst errors that may exceed the correction capability of conventional ECC schemes.
- **Single-Event Transients (SETs)**: particle-induced glitches in combinational logic that may be latched into memory elements if timing conditions permit.
- **Thermal effects**: rapid or sustained temperature excursions alter retention characteristics, sense-amplifier margins, and leakage currents, with pronounced impact in DRAM and emerging non-volatile memories.
- **Voltage instability**: reduced supply voltage **VDD** degrades noise margins, increasing susceptibility to read/write failures, timing violations, and soft errors.

Radiation-aware fault modeling constituted a core extension of the Optimal_Test framework for aerospace-grade DRAM. By combining probabilistic SEU injection with ECC syndrome divergence analysis, the framework enables more accurate classification and localization of radiation-induced faults under realistic workload and environmental conditions.

3.6 Technology-Specific Fault Signatures

Each memory technology exhibits distinctive fault signatures determined by its physical storage mechanism, materials, and circuit topology:

- **SRAM**: vulnerable to read-disturb-induced bit flips and reduced noise margins under process and voltage corners; stability of 6T cells is highly sensitive to threshold mismatch.
- **DRAM**: exhibits coupling faults due to bitline capacitance, Rowhammer-induced read disturb, and sense-amplifier metastability.
- **Flash (NAND/NOR)**: affected by program/erase endurance degradation, retention loss, and read disturb arising from repeated adjacent wordline activations.
- **MRAM**: prone to spin-state instability and write failures induced by high-current stress in magnetic tunnel junctions.
- **Phase-Change Memory (PCM)**: characterized by resistance drift in the amorphous phase and switching failures due to cycling fatigue and thermal crosstalk.
- **ReRAM**: subject to soft set/reset anomalies and gradual conductance decay resulting from filament instability and stochastic switching dynamics.

Recognition of these technology-specific fault signatures is essential for the development of targeted test strategies, adaptive repair algorithms, and lifetime reliability models in heterogeneous memory systems.

Figure 3.2—Technology-specific fault fingerprint diagram

Figure 3.2 presents a comparative fault "fingerprint" across six major memory technologies—SRAM, DRAM, Flash, MRAM, PCM, and ReRAM—providing a qualitative mapping between underlying storage mechanisms and their dominant failure modes.

The horizontally oriented bar representation distills complex diagnostic behavior into an at-a-glance visualization, facilitating rapid comparison of technology-specific vulnerabilities.
The Figure supports:

- **technology-aware diagnostic synthesis**, enabling test generation aligned with dominant fault modes,
- **targeted test planning**, focusing resources on the most probable failure mechanisms,
- **refinement of fault taxonomies**, ensuring both volatile and non-volatile memories are characterized with appropriate granularity.

Fault fingerprint overview by technology:

- **ReRAM**: soft set/reset failures and gradual conductance decay driven by filament instability and switching variability.
- **PCM**: resistance drift in the amorphous phase and phase-transition failures under cycling fatigue.
- **MRAM**: spin-orientation instability and write failures caused by high-current thermal and magnetic stress in MTJs.
- **Flash (NAND/NOR)**: program/erase cycling degradation and read disturb due to adjacent wordline activation.
- **DRAM**: coupling faults from bitline capacitance and Rowhammer-induced read disturb.
- **SRAM**: read-disturb errors and bit flips caused by marginal stability in cross-coupled inverters under process and voltage corners.

This fault fingerprint mapping captures the diagnostic identity of each technology and serves as a reference for designing stress patterns, BIST configurations, and reliability enhancement strategies tailored to the actual risk profile of the target device.

3.7 Fault Activation Conditions

Activation of memory faults is frequently contingent on specific access patterns and electrical stimuli that align with the structural, temporal, and electrical characteristics of the device under test. Identifying these dependencies is essential for designing high-coverage diagnostic algorithms.

- **Pattern dependency**: high spatial transition-density patterns—such as checkerboard and walking 1s/0s—are effective in provoking coupling and stuck-at faults by maximizing stress on adjacent cell interactions.
- **Temporal sequencing**: faults associated with retention (e.g., DRAM) or resistance drift (e.g., PCM) require controlled wait intervals to allow error conditions to manifest.
- **Voltage margins**: marginal read/write paths often fail only under reduced supply voltage **VDD**; voltage-corner testing is therefore indispensable for exposing latent defects.
- **Directional addressing**: certain address-decoder faults activate asymmetrically and manifest only under ascending or descending traversal patterns, reflecting routing irregularities or address echo effects.
- **Simultaneity**: port-interaction and correlated multi-bit failures may occur exclusively under concurrent access conditions, such as simultaneous multi-port reads or DMA activity.

Within the Optimal_Test framework, multi-cycle and interleaved address/mask control sequences are employed to align activation stimuli with actual structural conditions. This approach increases fault observability by emulating worst-case operational scenarios, including interconnect delay, bus contention, and clock skew.

3.8 Composite and Cross-Layer Faults

Composite faults arise from the interaction of multiple fault mechanisms across structural, functional, and environmental layers. They are difficult to detect because they often remain dormant under isolated tests and emerge only during complex workloads or under combined stress.

- **Structural composite faults**: originate from physical proximity effects, such as inter-cell electromagnetic interference in dense DRAM arrays or TSV coupling in three-dimensional memory stacks.
- **Functional composite faults**: result from protocol-level violations, bus contention, or address aliasing due to interactions between memory arrays and controller state machines.
- **Timing composite faults**: emerge from propagation delays, clock-domain crossings, and skew in multi-die or multi-rank systems.

- **Thermally induced composite events**: combine aging mechanisms with thermal stress, leading to intermittent failures such as temperature-dependent write errors in non-volatile memories.

In Optimal_Test, stress-aware composite fault modeling is realized by injecting fault scenarios during concurrent memory and DMA activity. This substantially improves diagnostic realism and increases the probability of detecting multi-mechanism interactions.

3.9 Multi-Bit and Data-Bus Faults

As memory word widths increase and architectures adopt multi-channel and multi-bank organizations, fault isolation becomes more complex—particularly for correlated multi-bit and bus-level failures.

- **Bus contention faults**: occur when multiple drivers assert conflicting values on a shared bus, producing undefined logic states or excessive current draw.
- **Stuck-word faults**: entire bytes or words become fixed to a constant value, often due to decoder failures, sense-amplifier defects, or catastrophic bus-driver damage.
- **Crosstalk errors**: high-speed operation in DDR-class interfaces induces interference between adjacent traces or bitlines, leading to correlated multi-bit flips.
- **Byte-selective failures**: in ECC-enabled systems, specific byte lanes may exhibit elevated error rates due to layout asymmetries or controller mapping effects.

To address these modes, byte-level masking and ECC-syndrome–driven analysis are incorporated into the Optimal_Test feedback loop. This enables precise localization of failures in wide-bus architectures and refinement of multi-bit fault models into composite symbolic operators compatible with PROVER syntax for scalable test synthesis.

3.10 Summary

Modern memory fault phenomena are inherently multidimensional, spanning spatial, temporal, electrical, and environmental domains. Escalating architectural complexity—driven by aggressive scaling, heterogeneous integration, and advanced packaging—renders traditional single-bit fault models insufficient for comprehensive diagnostics.
An effective fault-modeling framework must integrate:

- **Structural mapping**: linking observed behavior to physical locations in arrays and peripheral circuitry,
- **Temporal profiling**: capturing faults that emerge only over extended operation, including intermittent and aging-induced effects,
- **Multi-bit and multi-port interaction modeling**: addressing propagation across wide buses, multi-bank topologies, and concurrent access domains,
- **Environmental stress modeling**: incorporating thermal, voltage, and radiation-induced activation mechanisms.

The framework developed in this work unifies symbolic operator abstraction, pattern-based test generation, refined fault taxonomies, and adaptive simulation techniques. This foundation

directly supports the advanced March test strategies introduced in the next chapter, where symbolic fault models are synthesized into optimized, coverage-driven diagnostic sequences.

Modern memory systems also exhibit strong interactions between device-level behavior and system-level control mechanisms such as refresh scheduling, bank interleaving, and controller arbitration policies. These interactions can influence both the activation and observability of faults, particularly under high concurrency or complex access patterns. Consequently, effective diagnostic methodologies must consider operational context rather than treating memory cells as isolated elements.

At the same time, rapidly increasing memory capacities impose practical limits on exhaustive testing. Diagnostic frameworks must therefore prioritize efficient test synthesis strategies that maximize fault coverage while minimizing execution time and resource overhead. Symbolic modeling and structured test generation provide mechanisms for achieving this balance, enabling scalable diagnostics across large memory arrays.

The next chapter builds upon this foundation by examining practical testing methodologies and algorithmic strategies, with particular emphasis on March-based test sequences designed to activate and detect a wide range of memory fault models.

Chapter 4: Memory Testing — Algorithms, Patterns, and Tools

Memory testing lies at the intersection of fault detection, system reliability, and manufacturing yield optimization. As memory technologies continue to scale in density, speed, and architectural complexity, conventional validation techniques become increasingly inadequate.

This chapter examines the algorithms, data patterns, and diagnostic tools required to detect latent faults, assess operational robustness, and ensure reliable operation under diverse environmental and workload conditions. Building on the foundational material introduced in previous chapters, the discussion transitions toward advanced methodologies applicable to both contemporary and emerging memory architectures.

4.1 Introduction: The Imperative of Memory Testing

Memory subsystems are not passive data storage elements; they are highly dynamic, high-density components that support every computational process. Their fundamental functions—storing program instructions, buffering intermediate data, and sustaining continuous system operation—place memory at the core of performance and reliability considerations. This central role also makes memory subsystems disproportionately susceptible to system-level failures.

As integration density increases and access frequencies rise, the probability of latent, intermittent, and environment-sensitive faults increases substantially. Unlike logic circuits, whose correctness can often be established through exhaustive simulation and static verification, memory faults are frequently spatially localized, temporally activated, and dependent on operating conditions and access history.

Defects such as charge-retention degradation, inter-cell interference, and marginal timing behavior may remain undetected under nominal conditions, yet manifest under thermal stress, voltage variation, or high-frequency access patterns.

Consequently, memory testing cannot be treated as a purely functional verification task. It is a systematic process aimed at activating hidden fault mechanisms, observing fault propagation, and validating both the structural integrity and temporal stability of memory arrays across a wide operational envelope.

The research underlying this work—most notably the development of the **Optimal_Test** adaptive diagnostic engine and **PROVER-based symbolic test synthesis**—demonstrated that conventional memory test paradigms, while effective for detecting simple static faults such as stuck-at conditions, are insufficient for exposing complex fault behaviors characteristic of modern memory technologies. Representative examples include:

- **Retention failures** in DRAM arrays caused by accelerated charge leakage due to aggressive process scaling and thermal gradients.
- **Coupling faults**, where parasitic capacitive or electromagnetic interactions between adjacent cells or bitlines corrupt stored data.

- **Disturbance faults (Rowhammer-type effects)**, in which repeated activation of a wordline induces unintended state changes in physically adjacent rows.
- **Timing collapse**, where marginal setup and hold times result in intermittent failures during high-speed, multi-bank access sequences.

Emerging memory technologies—including MRAM, PCM, ReRAM, and three-dimensional stacked DRAM—further exacerbate these challenges. Their heterogeneous physical mechanisms, hybrid volatile and non-volatile behaviors, and sensitivity to cross-layer interactions introduce new fault signatures that cannot be adequately addressed using static or single-pass test strategies. Effective testing of such devices requires diagnostic methodologies that are structurally informed, traversal-aware, and capable of adaptive refinement.

This chapter is structured around three closely related dimensions of memory testing:

1. **Algorithms**, encompassing classical and extended March tests, GalPat-based techniques, and structured pseudo-random test sequences.
2. **Patterns**, analyzing the role of data backgrounds, address traversal order, and access sequencing in fault activation and observability.
3. **Tools**, including hardware-embedded solutions such as Memory Built-In Self-Test (MBIST), software-based diagnostics, and adaptive optimization frameworks exemplified by **Optimal_Test**.

The objective is to provide a rigorous conceptual and practical foundation for the design, evaluation, and deployment of memory test strategies capable of addressing the full spectrum of fault classes—from permanent manufacturing defects to transient, workload- and environment-induced degradations—while remaining feasible under realistic test-time and resource constraints.

4.2 Foundations of Memory Testing

Memory testing constitutes a fundamental component of fault detection and system validation in digital architectures. Its theoretical and practical foundations rest on three interdependent elements: accurate fault modeling, the construction of effective test patterns, and the deployment of diagnostic strategies capable of coping with the increasing complexity of modern memory technologies.

This section establishes the conceptual basis for memory testing by defining its primary objectives, identifying the major categories of memory faults, and introducing the key metrics—coverage, efficiency, and reliability—used to evaluate test effectiveness.

A comprehensive algorithmic treatment of semiconductor memory test diagnostics, including foundational March-based reasoning, was presented earlier in a dedicated monograph authored by Almadi, Moamar, and Ryabtsev (2008, in Russian).[11]

4.2.1 Objectives of Memory Testing

The overarching goal of memory testing is to ensure that memory subsystems operate correctly, within specification, and without functional defects throughout their intended operational lifetime. Achieving this objective requires a systematic methodology encompassing fault

detection, localization, classification, and predictive assessment at both the individual cell level and across the hierarchical memory architecture. The principal objectives include:

- **Fault detection** — identifying abnormal behavior in memory cells, arrays, or interfaces during read and write operations, including incorrect logic values, abnormal access latency, or signal integrity violations.
- **Fault localization** — determining the precise location of a defect, whether at the granularity of a single bit cell, word line, column, subarray, or bank.
- **Fault classification** — categorizing detected faults according to their physical or behavioral characteristics (e.g., stuck-at, transition, retention, coupling, disturbance), thereby enabling appropriate mitigation or repair strategies.
- **Test coverage maximization** — designing test sets that activate and observe the widest possible range of relevant fault models, including rare and environment-dependent failures.
- **Efficiency optimization** — achieving high diagnostic resolution with minimal execution time, pattern count, and resource usage, which is critical for both manufacturing test throughput and in-field diagnostics.
- **Reliability assessment** — interpreting test outcomes to estimate future failure probabilities and support predictive maintenance and lifetime reliability modeling.

Together, these objectives define the functional and methodological framework for robust memory testing across the complete device lifecycle.

4.2.2 Functional vs. Structural Testing

Memory testing methodologies can be broadly divided into **functional testing** and **structural testing**, which differ in abstraction level, diagnostic resolution, and fault coverage capability. Functional testing treats the memory subsystem as a black box and verifies correctness based solely on observable input–output behavior. Although straightforward to implement, this approach generally provides limited coverage for deep-seated, location-dependent, or environment-sensitive faults.

Structural testing, in contrast, relies on an explicit correspondence between test operations and underlying physical fault mechanisms. By aligning algorithmic test sequences with specific fault models—such as those targeting coupling, retention, and decoder-related defects—structural testing achieves superior fault activation, improved localization accuracy, and significantly higher diagnostic coverage.

For these reasons, structural testing forms the basis of most manufacturing test flows, post-silicon validation procedures, and advanced in-field diagnostic frameworks. Its ability to correlate traversal order, data patterns, and access dependencies with physical fault behavior makes it indispensable for ensuring both production yield and long-term system reliability.

4.3 March Testing — Classical, Symbolic, and Extended Variants

March algorithms constitute one of the most widely adopted and analytically tractable classes of memory test methods. They are defined by ordered sequences of read (R), write (W), and verify (V) operations applied during systematic traversals of the memory address space. By

explicitly controlling address traversal direction—ascending, descending, or bidirectional—and by applying carefully selected data patterns, March tests stimulate both individual memory cells and the interconnect structures that bind them.

Each operation sequence within a March test is constructed to activate specific fault behaviors, including state transition failures, inter-cell coupling effects, decoder anomalies, and access-history-dependent errors. Repeated passes with alternating traversal directions enable detection not only of static faults, such as stuck-at conditions, but also of dynamic and pattern-sensitive failures that manifest only under particular operational sequences.

Foundational evaluation of diagnostic properties across classical March test families was established in earlier analytical studies that informed the extensions presented here (EWDTW, 2004).

4.3.1 March Test Syntax

A March test consists of a structured sequence of memory operations applied exhaustively over the address space of the device under test, with the explicit objectives of fault activation and fault detection. Each test is composed of **March elements**, where each element specifies both (i) an ordered set of read and write operations and (ii) a defined address traversal direction.
A representative March test sequence is:

$$\uparrow(w_0);\ \uparrow(r_0, w_1);\ \downarrow(r_1, w_0);\ \downarrow(r_0)$$

In the compact notation used throughout this chapter, each operation implicitly applies to the currently addressed memory cell *a*:

- $\boldsymbol{w_0} \equiv \boldsymbol{w_{(a,0)}}$ and $\boldsymbol{w_1} \equiv \boldsymbol{w_{(a,1)}}$ denote write operations that store logic value 0 or 1, respectively.
- $\boldsymbol{r_0} \equiv \boldsymbol{r_{(a,0)}}$ and $\boldsymbol{r_1} \equiv \boldsymbol{r_{(a,1)}}$ denote read-and-verify operations, in which the value read from address *a* is compared against the expected logic value 0 or 1.
- $\uparrow$ **(Up)** and $\downarrow$ **(Down)** denote traversal of the memory address space in ascending and descending order, respectively.

Directional traversal is essential for exposing address decoder faults, directional coupling effects, and asymmetric interactions between physically or logically adjacent memory cells.
This syntax provides a compact yet expressive mechanism for encoding non-trivial test flows while maintaining explicit control over both operation ordering and address traversal semantics.

The ordered execution of read and write operations within each March element is designed to activate specific fault classes:

- **Stuck-at faults (SAF)** are detected through write–read sequences that verify the cell's ability to store and retain both logic states.
- **Transition faults (TF)** are revealed through consecutive writes of complementary values, validating correct state transitions in both directions.

- **Coupling faults (CF)** are activated when operations performed on one cell influence the stored state of adjacent cells, an effect frequently exposed during monotonic traversal of the address space.

By composing multiple March elements with alternating traversal directions and data patterns, a March test can achieve high fault coverage over the entire memory array while maintaining linear execution complexity with respect to memory size.

As an example, a compact March C sequence (commonly used as a baseline March-C-family example) is defined as:

$$\uparrow(w_0);\ \uparrow(r_0, w_1);\ \downarrow(r_1, w_0);\ \downarrow(r_0)$$

This sequence systematically verifies, for every memory cell, the ability to:

1. Store both logic values.
2. Transition reliably between logic states.
3. Preserve correct behavior under directional traversal.
4. Interact with neighboring cells without inducing or experiencing unintended interference.

In this chapter, extended March-C variants are presented later where additional phases are included to strengthen coverage of coupling and traversal-dependent fault mechanisms.

4.3.2 Key March Test Families

March algorithms may be grouped into distinct families according to their operational structure, target fault models, and execution overhead. Each family represents a different trade-off between diagnostic coverage and test duration.
The principal March test families considered in this work are summarized below.

March C
Operation sequence:
$\uparrow(w_0);\ \uparrow(r_0, w_1);\ \downarrow(r_1, w_0);\ \downarrow(r_0))$
Detected faults:
Stuck-at faults (SAF) and transition faults (TF) under bidirectional traversal

March A
Operation sequence:
An extension of March C incorporating additional read–write combinations and traversal phases
Detected faults:
SAF, TF, and partial coupling faults (CF)

March B
Operation sequence:
Fully ascending phases followed by fully descending phases, with separated write and read operations
Detected faults:
SAF, TF, and limited CF

March SS
Operation sequence:
Multi-read and multi-write phases with data inversions and repeated access
Detected faults:
SAF, TF, CF, and selected retention-related faults

March X
Operation sequence:
Reduced March sequence optimized for minimal execution time
Detected faults:
Primarily SAF

Among these families, **March C** remains a widely used reference due to its favorable balance between fault coverage and execution complexity. **March SS** extends diagnostic capability toward dynamic and retention-related fault mechanisms through repeated accesses and data inversions. **March A** and **March B** provide intermediate diagnostic strength suitable for moderate test requirements, while **March X** is primarily intended for high-speed Built-In Self-Test (BIST) scenarios in which minimal execution time is critical.

4.3.3 Operator-Based Formal Representations

While classical March syntax is effective for algorithm-level specification, contemporary memory architectures and adaptive diagnostic frameworks require a more expressive and formally precise representation.

The foundational research underlying this framework introduced a formal operator-based formalism, implemented within the **PROVER** environment, to support precise modeling, synthesis, and optimization of memory test algorithms.

In the symbolic operator formalism used throughout this chapter, memory operations are represented by three canonical primitives:

- $\mathbf{w_{(a)}}$ — write a logic value to address *a*, where the specific data value is defined by the surrounding test context or symbolic sequence
- $\mathbf{R_{(a)}}$ — read the content of address *a*
- $\mathbf{V_{(a)}}$ — verify that the value read from address *a* matches the expected symbolic state

Data values (e.g., logical 0 or 1) are implicitly defined by the preceding write operations and by the symbolic test flow, rather than being encoded directly within the operator signature.

This representation decouples the test description from the physical implementation of the test hardware, enabling several key capabilities:

1. **Technology independence**, allowing a single test specification to be mapped onto different memory architectures and process technologies.
2. **Pattern portability** across manufacturing test, post-silicon validation, and in-field diagnostics.
3. **Test set reduction**, through formal identification and elimination of redundant or subsumed operation sequences.

4. **Adaptive scheduling**, via integration with the **Optimal_Test** framework, enabling dynamic reordering and refinement of test execution based on observed fault behavior.

Throughout this chapter, two complementary levels of operator notation are employed.
In value-explicit formulations, memory operations are written as W(a,0), W(a,1), R(a,0), and R(a,1), where the expected data value is encoded directly in the operator. This notation is used when introducing classical March algorithms and for precise fault-activation semantics.

In the symbolic operator formalism used for test synthesis, optimization, and classification, operations are abstracted as W(a), R(a), and V(a). In this representation, data values are implied by the symbolic context and operation ordering rather than by the operator signature itself.
Both notations describe the same underlying memory behaviors; the abstract form is used where compact symbolic representation is required, while the value-explicit form is retained for clarity in algorithm definition.

Concrete symbolic test sequences and their classification within this formal framework are presented and analyzed in **Section 4.3.4**.

4.3.4 Grouped Symbolic and Extended March Variants

To accommodate the wide range of fault mechanisms present in modern memory devices, symbolic March tests are classified into five functional groups. This classification reflects their dominant fault targets, timing characteristics, and suitability for manufacturing test, in-field diagnostics, or stress-oriented validation. The grouped presentation below preserves the full operational semantics of each test while providing a structured diagnostic perspective.

Group 1 — Baseline and Classical March Tests

SCAN — Basic Initialization and Verification Test

The SCAN test provides a foundational diagnostic sequence that initializes all memory cells to logical 0, verifies their contents during ascending traversal, writes logical 1 during descending traversal, and performs a final verification pass. Owing to its minimal execution overhead, the SCAN test is commonly used for preliminary diagnostics, manufacturing sanity checks, and confidence verification prior to more aggressive testing.

In compact March notation, the SCAN test is expressed as:

$\uparrow(w_0)$;
$\uparrow(r_0)$;
$\downarrow(w_1)$;
$\downarrow(r_1)$

Within the operator-based formalism adopted here, the same test is represented by the symbolic expression π_{SCAN} shown below.

This formulation provides a compact, traversal-oriented description that is **formally equivalent** to the March syntax above, while enabling symbolic manipulation, composition, and optimization within the PROVER framework:

$$\pi_{SCAN} = \prod_{a=0}^{n-1} V(a) \prod_{a=0}^{n-1} R(a) \prod_{n-1}^{a=0} W(a) \prod_{a=0}^{n-1} R(a).$$

where n denotes the total number of addressable memory locations ($n \equiv M$ in the global notation).
In this representation, the operator-based formulation abstracts explicit address iteration into range-based traversal operators, while preserving the full operational semantics of the underlying March test. The symbolic description π_{SCAN} therefore serves as a canonical formal encoding of the SCAN algorithm, suitable for subsequent analysis, synthesis, and integration into adaptive diagnostic workflows.

The SCAN test detects **stuck-at faults (SAF)** by verifying the ability of each memory cell to store both logic values, and **basic transition faults (TF)** by enforcing a controlled $0 \rightarrow 1$ state transition under directional traversal. Due to its simplicity, the test provides limited coverage of coupling, retention, and dynamic fault mechanisms, but remains well suited for fast screening and low-overhead diagnostic scenarios.

MATS+ — Minimal Stuck-At and Transition Test

MATS+ is a compact March test intended for rapid screening and low-overhead diagnostics. The algorithm initializes the memory to a uniform background, verifies correct storage, writes the inverse background, and performs a final read operation. Owing to its simplicity, MATS+ is frequently employed in power-on self-test and fast manufacturing screening scenarios.
In symbolic March notation, the MATS+ test is expressed as:

$\uparrow(w_0);$
$\uparrow(r_0, w_1);$
$\downarrow(r_1)$

In the operator-based formalism introduced in Section 4.3.3, the same test is represented symbolically as:

$$\pi_{MATS+} = \prod_{a=0}^{n-1} V(a) \prod_{a=0}^{n-1} (R(a)W(a)) \prod_{n-1}^{a=0} (R(a)V(a)).$$

This formulation is formally equivalent to the March syntax above and enables symbolic analysis, synthesis, and optimization within the PROVER-based diagnostic framework.

This sequence detects **stuck-at faults (SAF)** by verifying the ability of each cell to store both logic values, and a subset of **transition faults (TF)** through enforced $0 \rightarrow 1$ state transitions. Due to its minimal execution time, MATS+ does not adequately activate dynamic, coupling, or pattern-sensitive fault mechanisms, and is therefore unsuitable as a standalone diagnostic for high-reliability applications.

MATS++ — Extended Minimal Test with Additional Read Phase

MATS++ extends the MATS+ algorithm by introducing an additional read-and-verify operation following the final write phase, thereby improving sensitivity to transition faults that

may manifest only after repeated observation of the written state. The extension preserves the minimal structure and low execution cost of the base test while providing a modest increase in diagnostic strength.

In compact March notation, the MATS++ test is expressed as:

$\uparrow(w_0);$
$\uparrow(r_0, w_1);$
$\downarrow(r_1)$
$\downarrow(r_1)$

In the operator-based formalism introduced in Section 4.3.3, the same test is represented symbolically by the following expression:

$$\pi_{MATS++} = \overset{n-1}{\underset{a=0}{P}} V(a) \overset{n-1}{\underset{a=0}{P}} (R(a)W(a)) \overset{a=0}{\underset{n-1}{P}} (R(a)V(a)R(a)).$$

This operator-based formulation is formally equivalent to the March syntax above and enables symbolic reasoning, composition, and optimization within the PROVER-based diagnostic framework.

The additional read operation reinforces verification of the written logic value and enhances detection of **transition faults (TF)** exhibiting delayed or marginal switching behavior. While the overall increase in diagnostic coverage is modest, it is achieved with negligible additional execution overhead, making MATS++ attractive for scenarios requiring slightly improved fault sensitivity without the complexity of longer March algorithms.

March_A — Coupling-Oriented Enhanced March Test

March_A is a coupling-oriented enhancement of the classical March C test structure, designed to intensify activation of coupling faults and marginal transition faults through repeated write–read interactions and alternating address traversal directions. By extending the base March sequence with additional symbolic operations, the test increases the likelihood of aggressor–victim interference between adjacent memory cells.

In the operator-based formalism introduced in Section 4.3.3, the March_A algorithm is represented symbolically by the following expression:

$$\pi_{march\_A} = \overset{n-1}{\underset{a=0}{\mathbf{P}}} V(a) \overset{n-1}{\underset{a=0}{\mathbf{P}}} (R(a)W(a)V(a)W(a)) \overset{n-1}{\underset{a=0}{\mathbf{P}}} (R(a)V(a)W(a))$$
$$\overset{0}{\underset{a=n-1}{\mathbf{P}}} (R(a)V(a)W(a)V(a)) \overset{0}{\underset{a=n-1}{\mathbf{P}}} (R(a)W(a)V(a)).$$

This symbolic formulation preserves the fundamental traversal logic of a March-C-type test while introducing additional write and verification phases that amplify electrical and logical coupling effects during both ascending and descending address passes. The repeated interaction

between write and read operators serves to stress inter-cell dependencies and expose fault mechanisms that may remain latent under simpler March algorithms.

March_A is particularly effective for memory technologies susceptible to adjacent-cell interference, such as scaled DRAM architectures with significant parasitic capacitance, reduced noise margins, and dense physical layouts. While the enhanced interaction pattern incurs moderate additional execution overhead compared to baseline March tests, it provides improved diagnostic sensitivity in environments where coupling-related failure mechanisms are prominent.

Group 2 — Coupling- and Interference-Oriented Tests

March_CR — Read-Redundant March Test

The March_CR algorithm is a coupling- and interference-oriented March variant that introduces **redundant read operations** following critical write or transition phases. The purpose of these additional reads is to increase observability of faults whose manifestation is intermittent, marginal, or sensitive to environmental conditions rather than strictly deterministic.

In compact March notation, March_CR follows the structure of its underlying base sequence while augmenting selected phases with repeated read-and-verify operations.

In the operator-based formalism introduced in Section 4.3.3, the March_CR algorithm is represented symbolically by the following expression:

$$\pi_{march\_CR} = \mathop{\mathbf{P}}_{a=0}^{n-1} V(a) \mathop{\mathbf{P}}_{a=0}^{n-1} (R(a)R(a)W(a)) \mathop{\mathbf{P}}_{a=0}^{n-1} (R(a)R(a)V(a)) \mathop{\mathbf{P}}_{a=n-1}^{0} (R(a)R(a)W(a)) \mathop{\mathbf{P}}_{a=n-1}^{0} (R(a)R(a)V(a)) \mathop{\mathbf{P}}_{a=0}^{n-1} R(a)R(a).$$

The inclusion of redundant read operations increases the probability of detecting **coupling faults (CF)** and **environmentally sensitive faults** that may appear only under specific voltage, temperature, or timing conditions. By repeatedly observing the cell state after critical transitions, March_CR improves diagnostic robustness without substantially increasing execution complexity.

This test is particularly useful in stress-oriented validation scenarios and in-field diagnostics, where fault behavior may vary across operating conditions and repeated observation is required to distinguish genuine defects from transient noise.

GALROW — Orthogonal Row Interference Test

GALROW is an interference-oriented diagnostic test that performs **coordinated access to selected pairs of memory rows** in order to expose row-to-row interference, shared wordline leakage, and decoder crosstalk effects. Unlike classical March tests based on linear address traversal, GALROW deliberately activates rows in an **orthogonal access pattern**, enabling detection of fault mechanisms that remain latent under purely sequential row selection.

By alternating or overlapping activation of aggressor and victim rows, the test stresses row-level electrical interactions and decoder behavior, revealing disturbances that arise from capacitive coupling, leakage paths, or insufficient isolation between adjacent wordlines. Such effects are increasingly relevant in dense, row-oriented memory organizations with aggressive scaling and reduced noise margins.

In the operator-based formalism introduced in Section 4.3.3, the GALROW test is represented symbolically by the following expression:

$$\pi_{\text{GALROW}} = \prod_{a=0}^{n-1} \mathrm{V}(a) \prod_{a=0}^{n-1} (\mathrm{W})(a) \prod_{\substack{\text{row}=b=0 \\ b \neq a}}^{\sqrt{n}-1} (\mathrm{R}(b)\mathrm{R}(a))\mathrm{V}(a)) \prod_{a=0}^{n-1} \mathrm{W}(a) \prod_{a=0}^{n-1} (\mathrm{V}(a) \prod_{\substack{\text{row}=b=0 \\ b \neq a}}^{\sqrt{n}-1} (\mathrm{R}(b)\mathrm{R}(a))\mathrm{W}(a)).$$

This symbolic formulation captures the coordinated row-access semantics of the GALROW test while abstracting low-level address sequencing. The resulting test is particularly effective for identifying **row-interference-related faults** that are not observable through standard March traversal alone, making it well suited for advanced validation and reliability assessment of high-density memory arrays.

WALKCOLUMN — Column Interference and Sense Amplifier Recovery Test

WALKCOLUMN is a column-interference-oriented diagnostic test that selectively activates individual columns while modifying data in neighboring columns, targeting bitline-to-bitline coupling, sense-amplifier recovery time violations, and column-select timing defects. By exercising column access patterns that induce localized electrical stress, the test exposes failure mechanisms that are insufficiently activated by row-oriented or linear traversal tests.

This test is particularly relevant for wide-I/O and multi-bank DRAM designs, where dense column multiplexing and shared sensing circuitry cause column interactions to dominate observed error behavior.

In the operator-based formalism introduced in Section 4.3.3, the WALKCOLUMN test is represented symbolically by the following expression:

$$\pi_{\text{WALKCOLUMN}} = \prod_{a=0}^{n-1} \mathrm{V}(a) \prod_{a=0}^{n-1} (\mathrm{W}(a) \prod_{\substack{\text{col}=b=0 \\ b \neq a}}^{\sqrt{n}-1} (\mathrm{R}(b))\mathrm{R}(a)\mathrm{V}(a)) \prod_{a=0}^{n-1} \mathrm{V}(a) \prod_{\substack{\text{col}=b=0 \\ b \neq a}}^{\sqrt{n}-1} (\mathrm{R}(b))\mathrm{R}(a)\mathrm{W}(a)).$$

PMOVI — Pseudo-Moving Inversion Test

PMOVI propagates inversion patterns across the memory array to expose address decoder faults and spatially dependent coupling effects. By shifting the inversion background through successive address ranges, the test activates fault mechanisms linked to physical adjacency and decoder sensitivity.

In the operator-based formalism introduced in Section 4.3.3, the PMOVI test is represented symbolically as:

$$\pi_{\text{PMOVI}} = \overset{n-1}{\underset{a=0}{\mathrm{P}}} \mathrm{V}(a) \overset{n-1}{\underset{a=0}{\mathrm{P}}} (\mathrm{R}(a)\mathrm{W}(a)\mathrm{R}(a)) \overset{n-1}{\underset{a=0}{\mathrm{P}}} (\mathrm{R}(a)\mathrm{V}(a)\mathrm{R}(a)) \overset{a=0}{\underset{n-1}{\mathrm{P}}} (\mathrm{R}(a)\mathrm{W}(a)\mathrm{R}(a)) \overset{a=0}{\underset{n-1}{\mathrm{P}}} (\mathrm{R}(a)\mathrm{V}(a)\mathrm{R}(a)).$$

PMOVI-R — Read-Redundant Pseudo-Moving Inversion Test

PMOVI-R extends PMOVI by duplicating selected read operations within the inversion propagation sequence, thereby increasing observability of faults that exhibit marginal timing behavior or sensitivity to noise and environmental variation.

In symbolic form, the PMOVI-R test is defined as:

$$\pi_{\text{PMOV-R}} = \overset{0}{\underset{a=n-1}{\mathbf{P}}} \mathrm{V}(a) \overset{n-1}{\underset{a=0}{\mathbf{P}}} (\mathrm{R}(a)\mathrm{W}(a)\mathrm{R}(a)\mathrm{R}(a)) \overset{n-1}{\underset{a=0}{\mathbf{P}}} (\mathrm{R}(a)\mathrm{V}(a)\mathrm{R}(a)\mathrm{R}(a))$$
$$\overset{0}{\underset{a=n-1}{\mathbf{P}}} (\mathrm{R}(a)\mathrm{W}(a)\mathrm{R}(a)\mathrm{R}(a)) \overset{0}{\underset{a=n-1}{\mathbf{P}}} (\mathrm{R}(a)\mathrm{V}(a)\mathrm{R}(a)\mathrm{R}(a)).$$

The repeated read operations improve diagnostic confidence in conditions where single-pass observation may be insufficient.

Group 3 — Retention- and Delay-Aware Tests

March_LA — Triple-Write Retention Stress Test

The March_LA algorithm introduces repeated write operations to the same address, creating an implicit temporal delay that stresses data retention mechanisms without relying on explicit wait states. By enforcing multiple successive writes before verification, the test amplifies sensitivity to time-dependent degradation effects.
In the operator-based formalism introduced in Section 4.3.3, the March_LA test is represented symbolically by the following expression:

$$\pi_{\text{march\_LA}} = \overset{n-1}{\underset{a=0}{\mathbf{P}}} \mathrm{V}(a) \overset{n-1}{\underset{a=0}{\mathbf{P}}} (\mathrm{R}(a)\mathrm{W}(a)\mathrm{V}(a)\mathrm{W}(a)\mathrm{R}(a)) \overset{n-1}{\underset{a=0}{\mathbf{P}}} (\mathrm{R}(a)\mathrm{V}(a)\mathrm{W}(a)\mathrm{V}(a)\mathrm{R}(a))$$
$$\overset{0}{\underset{a=n-1}{\mathbf{P}}} (\mathrm{R}(a)\mathrm{W}(a)\mathrm{V}(a)\mathrm{W}(a)\mathrm{R}(a)) \overset{0}{\underset{a=n-1}{\mathbf{P}}} (\mathrm{R}(a)\mathrm{V}(a)\mathrm{W}(a)\mathrm{V}(a)\mathrm{R}(a)) \overset{0}{\underset{a=n-1}{\mathbf{P}}} \mathrm{R}(a).$$

This test is effective for exposing faults related to charge leakage, magnetic relaxation, or phase instability in both volatile and non-volatile memory technologies.

March_G — Delay-Augmented March Test

The March_G algorithm explicitly introduces temporal stress into the test sequence by inserting idle cycles or by repeating write operations at selected stages. These deliberate delays allow slow-developing retention faults and disturb effects to manifest before verification, without modifying the logical data background.

Symbolically, the March_G test is expressed as:

$$\pi_{MARCH\_G} = \prod_{a=0}^{n-1} V(a) \prod_{a=0}^{n-1} (R(a)W(a)R(a)W(a)R(a)W(a)) \prod_{a=0}^{n-1} (R(a)V(a)W(a))$$

$$\prod_{n-1}^{a=0} (R(a)V(a)W(a)V(a)) \prod_{n-1}^{a=0} (R(a)W(a)V(a)) \prod_{a=0}^{n-1} (R(a)W(a)R(a)).$$

The repeated access pattern increases both electrical and temporal stress on the storage cell and associated peripheral circuitry, improving observability of delay-dependent fault mechanisms while preserving the underlying March structure.

March_UD — Delay-Embedded Quad-Access Test

The March_UD algorithm combines high-frequency quad-access stress with explicitly embedded delay intervals, thereby improving coverage of dynamic coupling faults and early-stage retention failures. By enforcing repeated access to the same memory locations within a tightly controlled temporal window, the test amplifies electrical stress while preserving deterministic control over operation ordering.

Symbolically, the March_UD test is expressed as:

$$\pi_{march\_UD} = \prod_{a=0}^{n-1} V(a) \prod_{a=0}^{n-1} (R(a)W(a)R(a)V(a)) \, Delay \prod_{a=0}^{n-1} (R(a)W(a))$$

$$Delay \prod_{a=n-1}^{0} (R(a)V(a)R(a)W(a)) \prod_{a=n-1}^{0} (R(a)V(a)).$$

The embedded delays are logical test constructs and may be implemented either as explicit idle cycles or through controlled repetition of non-destructive operations, allowing flexible realization across different test environments and hardware platforms.

Group 4 — Read-Disturb and Sense-Amplifier Stress Tests

March_LR — Read-Before-Write March Test

The March_LR algorithm precedes each write operation with a read-and-verify step, deliberately stressing read-disturb mechanisms and sense-amplifier activity prior to state modification. By repeatedly sensing stored data before overwriting it, the test exposes degradation effects caused by excessive read operations and marginal retention behavior induced by repeated activation of the sensing circuitry.
Symbolically, the March_LR test is expressed as:

$$\pi_{march\_LR} = \prod_{a=0}^{n-1} V(a) \prod_{a=n-1}^{0} (R(a)W(a)) \prod_{a=0}^{n-1} (R(a)V(a)R(a)W(a))$$

$$\prod_{a=0}^{n-1} (R(a)V(a)) \prod_{a=0}^{n-1} (R(a)W(a)R(a)V(a)) \prod_{a=n-1}^{0} R(a).$$

This access structure is particularly effective for revealing read-disturb-related faults and sense-amplifier-induced retention degradation in memory technologies where repeated read operations can influence stored charge or state stability.

March_Y — Read-After-Write Disturb Detector

The March_Y algorithm performs an immediate read-and-verify operation following each write, targeting write-disturb effects and post-write instability before such behavior can be masked by subsequent memory accesses. By observing the stored value immediately after modification, the test exposes disturbances introduced by the write process itself as well as marginal cell behavior.

Symbolically, the March_Y test is expressed as:

$$\pi_{\text{march\_Y}} = \prod_{a=0}^{n-1} V(a) \prod_{a=0}^{n-1} (R(a)W(a)R(a)) \prod_{a=n-1}^{0} (R(a)V(a)R(a)W) \prod_{a=0}^{n-1} (R(a)).$$

This structure is particularly effective for detecting write-induced disturb mechanisms and transient instability in memory cells and associated peripheral circuitry.

March_SR — Read-After-Read Sensing Path Stress Test

The March_SR algorithm applies consecutive read-and-verify operations without intervening write cycles, deliberately stressing the sense-amplifier signal path and associated precharge and recovery mechanisms. By repeatedly sensing the same stored value, the test exposes faults related to metastability, incomplete bitline precharge, and recovery-time violations that may not manifest under isolated read operations.

Symbolically, the March_SR test is expressed as:

$$\pi_{\text{MARCH\_SR}} = \prod_{n-1}^{a=0} V(a) \prod_{a=0}^{n-1} (R(a)W(a)R(a)V(a)) \prod_{a=0}^{n-1} (R(a)R(a)) \prod_{a=0}^{n-1} W(a) \prod_{n-1}^{a=0} (R(a)V(a)R(a))W(a) \prod_{n-1}^{a=0} (R(a)R(a)).$$

This test is particularly effective for diagnosing sensing-path weaknesses in high-speed memory designs, where aggressive timing margins and repeated read activity can degrade signal integrity.

March_U — Quad-Access Cell Stress Test

The March_U algorithm applies four consecutive read and write operations to each address, heavily stressing both the storage node and the sensing circuitry. The concentrated access pattern amplifies electrical activity within the cell and peripheral paths, increasing sensitivity to dynamic failures and marginal stability effects.

Symbolically, the March_U test is expressed as:

$$\pi_{\text{march\_U}} = \prod_{a=0}^{n-1} V(a) \prod_{a=0}^{n-1} (R(a)W(a)R(a)V(a)) \prod_{a=0}^{n-1} (R(a)W(a)) \prod_{a=n-1}^{0} (R(a)V(a)R(a)W(a)) \prod_{a=n-1}^{0} (R(a)V(a)).$$

This test is well suited for exposing faults that emerge only under repeated access conditions, including dynamic coupling effects and weak cell behavior.

March_U_R — Read-Doubled Quad-Access Test

The March_U_R algorithm extends March_U by duplicating selected read-and-verify operations within the quad-access sequence, thereby improving detection of marginal sense-amplifier faults and precharge instability.

Symbolically, the March_U_R test is expressed as:

$$\pi_{\text{march\_U-R}} = \prod_{a=0}^{n-1} V(a) \prod_{a=0}^{n-1} (R(a)W(a)R(a)R(a)V(a)) \prod_{a=0}^{n-1} (R(a)W(a)) \prod_{a=n-1}^{0} (R(a)V(a)R(a)R(a)W(a)) \prod_{a=n-1}^{0} (R(a)V(a)).$$

The additional read operations increase observability of subtle sensing-path weaknesses while preserving the core stress characteristics of the underlying quad-access structure.

Group 5 — High-Coverage, High-Overhead Tests

March_SS — High-Coverage 22-Phase March Test

The March_SS algorithm executes a large number of bidirectional access phases combined with multiple data inversions, resulting in very high diagnostic coverage. The extensive sequence of reads and writes systematically activates and observes a wide spectrum of fault mechanisms, including **stuck-at faults**, **transition faults**, **coupling faults**, and **retention-related failures**.

Symbolically, the March_SS test is expressed as:

$$\pi_{\text{MARCH\_SS}} = \prod_{n-1}^{a=0} V(a) \prod_{a=0}^{n-1} (R(a)R(a)V(a)R(a)W(a)) \prod_{a=0}^{n-1} (R(a)R(a)W(a)R(a)V(a)) \prod_{n-1}^{a=0} (R(a)R(a)V(a)R(a)W(a)) \prod_{n-1}^{a=0} (R(a)R(a)W(a)R(a)V(a)) \prod_{a=0}^{n-1} R(a).$$

Due to its substantial execution time and high operational overhead, March_SS is typically reserved for memory characterization, qualification, and failure-analysis scenarios rather than volume manufacturing or in-field self-test.

HAMMER — Maximum-Stress Rowhammer-Type Detector

The HAMMER test applies an aggressive, high-activation access pattern consisting of up to 49 full memory access cycles, intentionally exceeding normal operational intensity. This extreme

access behavior is designed to induce and detect **rowhammer-type disturbance faults**, high-frequency coupling defects, and accelerated retention degradation.

Symbolically, the HAMMER test is expressed as:

$$\pi_{\text{HAMMER}} = \prod_{a=0}^{n-1} V(a) \prod_{a=0}^{n-1} (R(a) \prod_{i=1}^{10} (W(a))_i R(a)) \prod_{a=0}^{n-1} (R(a) \prod_{i=1}^{10} (V(a))_i R(a))$$

$$\prod_{n-1}^{a=0} (R(a) \prod_{i=1}^{10} (W(a))_i R(a)) \prod_{n-1}^{a=0} (R(a) \prod_{i=1}^{10} (V(a))_i R(a)).$$

By stressing memory arrays far beyond typical usage conditions, the HAMMER test is primarily applicable to stress testing, security validation, and advanced reliability characterization, where worst-case fault behavior must be observed and analyzed.

Table 4.1: Formal Operator Notation for Key March Tests

Test Name	Symbolic Test Expression
SCAN	$P_0^{n-1}[V(a)] \rightarrow P_0^{n-1}[R(a)] \rightarrow P_n^{-1}{}_0[W(a)] \rightarrow P_n^{-1}{}_0[R(a)]$
MATS+	$P_0^{n-1}[W(a)] \rightarrow P_0^{n-1}[R(a)W(a)] \rightarrow P_n^{-1}{}_0[R(a)]$
MATS++	$P_0^{n-1}[W(a)] \rightarrow P_0^{n-1}[R(a)W(a)] \rightarrow P_n^{-1}{}_0[R(a)] \rightarrow P_n^{-1}{}_0[R(a)]$
March A	$P_0^{n-1}[V(a)] \rightarrow P_0^{n-1}[R(a)W(a)] \rightarrow P_0^{n-1}[R(a)V(a)W(a)] \rightarrow$ $P_0^{n-1}[R(a)W(a)] \rightarrow P_0^{n-1}[R(a)V(a)W(a)] \rightarrow P_0^{n-1}[R(a)]$
March C-R	$P_0^{n-1}[V(a)] \rightarrow P_0^{n-1}[R(a)W(a)R(a)] \rightarrow P_0^{n-1}[R(a)V(a)R(a)] \rightarrow P_0^{n-1}[R(a)]$
GALROW	$P_0^{n-1}[V(a)W(a)R(b)R(a)V(a)] \rightarrow P_0^{n-1}[W(a)V(a)R(b)R(a)W(a)]$ *(orthogonal row-pair activation)*
WALKCOLUMN	$P_0^{n-1}[V(a)W(a)R(b)] \rightarrow P_0^{n-1}[R(a)V(a)] \rightarrow P_0^{n-1}[R(b)R(a)W(a)]$ *(neighbor-column coupling / sense-amplifier recovery)*
PMOVI	Moving inversion pattern: $P_0^{n-1}[W(a)V(a)]$ with progressive address shift
PMOVI-R	PMOVI sequence with all read operations doubled: $P_0^{n-1}[W(a)R(a)R(a)V(a)]$ (progressive shift)
March_LA	$P_0^{n-1}[W(a)W(a)W(a)] \rightarrow P_0^{n-1}[R(a)V(a)V(a)V(a)]$ *(implicit delay via repeated writes)*
MARCH_G	March sequence with explicit delays: $P_0^{n-1}[W(a)]$ — delay — → $P_0^{n-1}[R(a)W(a)]$ *(logical delay: idle or repeated ops)*
March_UD	Quad-access with delays: $P_0^{n-1}[R(a)W(a)R(a)W(a)]$ — delay — repeat
March_LR	$P_0^{n-1}[R(a)W(a)] \rightarrow P_0^{n-1}[R(a)V(a)]$ *(read-before-write ordering)*
March_Y	$P_0^{n-1}[W(a)R(a)] \rightarrow P_0^{n-1}[V(a)R(a)]$ *(immediate read-after-write)*
MARCH_SR	$P_0^{n-1}[R(a)R(a)] \rightarrow P_n^{-1}{}_0[R(a)R(a)]$
March_U	$P_0^{n-1}[R(a)W(a)R(a)W(a)]$
March_U_R	$P_0^{n-1}[R(a)R(a)W(a)R(a)R(a)W(a)]$

Table 4.1: Formal Operator Notation for Key March Tests (Continued)

Test Name	Symbolic Test Expression
MARCH_SS	22-phase bidirectional March with multi-read, multi-write, and inversion operations
HAMMER	49-phase maximum-activation stress pattern with repeated row/column toggling

Integration with PROVER and Optimal_Test

The formal operator representations introduced in the preceding section were embedded directly into the **PROVER** symbolic synthesis engine, forming the basis of a scalable and extensible diagnostic framework. This integration enabled the following core capabilities:

- **Automated multi-phase sequence generation**, in which complete executable test programs are derived directly from abstract operator chains without manual expansion.
- **Parallelized execution support** for large-capacity memory arrays, allowing subdivision of the address space to reduce overall diagnostic time.
- **Fault-model–driven adaptation**, enabling dynamic tailoring of test sequences to activate specific defect classes, including coupling, retention, and disturb-related faults.

This operator-level abstraction provided the foundation for the optimized and adaptive March variants developed in **Chapters 10–12**, with particular emphasis on **Chapter 11**. In turn, it enabled seamless integration with the **Optimal_Test** platform, supporting real-time scheduling, test compression, prioritization, and reordering of diagnostic sequences based on observed fault behavior.

4.4 Pattern-Based Testing

Although March algorithms are highly effective in exercising memory arrays through systematic address traversal and structured operation sequences, they exhibit inherent limitations. In particular, purely traversal-driven tests are less effective at provoking faults whose activation depends on specific data configurations, spatial correlations, or environmental stress conditions.

Pattern-based testing addresses these limitations by focusing on the **data values and state transitions** written into memory. By deliberately constructing bit-level configurations with high electrical or temporal stress, pattern-based methods increase the probability of activating data-dependent fault mechanisms.

Pattern-based testing is especially effective in exposing:

- **Coupling faults (CFs)**, by inducing aggressor–victim interactions between adjacent cells or bitlines using alternating or checkerboard data configurations.
- **Retention failures (RFs)**, through the application of stress backgrounds (e.g., all-zeros or all-ones) combined with controlled hold intervals to expose weak-cell behavior and charge leakage.

- **Data-dependent timing faults**, by employing high-activity patterns such as walking ones and walking zeros to stress marginal read/write paths.
- **Disturb faults**, by using inversion-rich or spatially complex patterns (e.g., butterfly or GalPat) capable of triggering parasitic effects and Rowhammer-type disturbances in dense arrays.

Commonly deployed pattern classes include:

- **Walking Ones / Walking Zeros**, in which a single logic '1' or '0' is shifted sequentially across bit positions.
- **Checkerboard patterns**, alternating logic states across adjacent cells to maximize differential stress.
- **Inversion patterns**, involving periodic complementation of stored data to expose switching asymmetries and retention drift.
- **Pseudo-random fills**, designed to emulate workload-driven data dependencies during system-level screening.

Within the **Optimal_Test** framework, these patterns are symbolically synthesized using PROVER operator chains. This enables dynamic interleaving of pattern-based stress phases with March-based address sweeps.

The resulting hybrid strategy has proven particularly effective for emerging memory technologies—such as MRAM, ReRAM, and three-dimensional DRAM—where retention drift, asymmetric switching behavior, and disturb effects frequently evade detection by March testing alone.

4.4.1 Classic Test Patterns

Pattern-based testing relies on carefully constructed data configurations that provoke fault behaviors unlikely to manifest under uniform or purely random backgrounds.

Classic patterns are widely used due to their simplicity, strong diagnostic properties, and ease of implementation in both hardware and software test environments.

- **Walking Ones (W1) / Walking Zeros (W0)**
  A single active bit (logic '1' for W1 or logic '0' for W0) is shifted systematically through each bit position within a word or across the memory array.
  Fault coverage: stuck-at faults, intra-word coupling faults, and address decoder defects sensitive to specific bitline activations.
- **Checkerboard**
  Alternating logic values are written to adjacent cells to maximize voltage differentials between neighboring wordlines and bitlines.
  Fault coverage: strong activation of coupling faults, crosstalk-induced errors, and physical leakage paths.
- **Solid backgrounds (all-zeros / all-ones)**
  A uniform logic state is written to all cells, stressing supply rails, bias networks, and large-scale array uniformity.

Fault coverage: weak pull-up or pull-down devices, ground-bounce sensitivity, and voltage-drop effects in large arrays.

- **Inversions and anti-walk patterns**
  Repeated full-array inversions or reversed walking sequences are applied to maximize transition density.

  Fault coverage: asymmetric switching faults, marginal retention cells, and high-activity timing-related defects.

When combined with inverted data backgrounds and rotated address traversal orders, these patterns significantly enhance detection of data-dependent instabilities, which is particularly important in high-density, low-voltage memory designs.

In the PROVER environment, these classic patterns were encapsulated as **symbolic pattern macros**, allowing automated compilation into adaptive, multi-pass diagnostic sequences under the control of the Optimal_Test framework.

4.4.2 Data Background Sensitivity

The **data background**—the logical state of cells surrounding a target location during testing—has a decisive influence on fault observability. Many memory defects are inherently data-dependent, meaning that the behavior of a victim cell varies according to the states or transitions of neighboring aggressor cells.

Representative examples include:

- A victim cell that passes all tests under an all-zeros background but fails when neighboring cells toggle rapidly.
- Coupling faults that manifest only when an entire wordline or bitline undergoes simultaneous switching.
- Dense memory arrays with high parasitic capacitance, which are especially sensitive to background-dependent interference.

In the symbolic modeling and adaptive optimization framework developed in this work, **data-pattern cycling** was introduced to systematically enhance fault activation conditions.

Using PROVER, symbolic pattern operators were defined, including:

- **P_CB**, representing a checkerboard background for maximum neighbor stress.
- **P_W1Z**, representing walking ones applied against a zero background to isolate intra-word and inter-bitline effects.
- **P_INV**, representing full-array inversion to induce high-density switching activity.
- This symbolic abstraction of data backgrounds provides several advantages:
- **Dynamic substitution**, allowing patterns to be exchanged during execution to improve coverage without regenerating test code.
- **Hardware-agnostic modeling**, enabling the same pattern definitions to be applied across SRAM, DRAM, MRAM, and other technologies.
- **Timing-aware scheduling**, allowing pattern application to be aligned with refresh cycles, precharge timing, or inter-bank constraints.

This approach has proven particularly effective in non-uniform and heterogeneous memory architectures, where localized electrical and physical variations significantly amplify the influence of data backgrounds on fault visibility.

4.4.3 Advantages and Limitations of Pattern-Based Testing

Pattern-based memory testing offers distinct diagnostic advantages, particularly for data-dependent and stress-sensitive fault mechanisms.

At the same time, it exhibits inherent limitations that constrain its effectiveness when used in isolation. These characteristics define its optimal role within standalone or hybrid memory test strategies.

The principal strengths and weaknesses of pattern-based testing can be summarized as follows:

Table 4.2—Strengths and limitations of pattern-based testing.

Strengths	Limitations
Straightforward implementation in both hardware- and software-based test environments.	Limited capability for precise fault localization at the level of specific addresses, decoder paths, or access logic.
High effectiveness in detecting adjacent-cell defects, including coupling faults and disturb-related errors.	Absence of intrinsic directional sequencing (ascending or descending traversal), which is critical for activating address-dependent faults.
Strong ability to provoke stress-sensitive failures through deliberate, data-dependent switching activity.	Reduced sensitivity to address decoder faults and control logic defects that require structured access order and traversal semantics.

In practical diagnostic flows, pattern-based tests deliver their highest value when employed as components of a **hybrid testing methodology**. When combined with March algorithms, they provide complementary diagnostic coverage:

- **Structural coverage** derived from systematic address traversal and ordered access sequences.
- **Data-centric fault activation** achieved through carefully selected and dynamically varied data patterns.

Within the **Optimal_Test** platform, this integration was implemented through programmable **March–pattern fusion**. Test sequences were constructed by symbolically chaining pattern operators—such as $\mathbf{P_{CB}}$ (checkerboard), $\mathbf{P_{WIZ}}$ (walking ones on a zero background), and $\mathbf{P_{INV}}$ (full inversion)—either preceding or following structured address traversal logic.
This chaining mechanism enabled:

- **Adaptive scheduling**, allowing test execution to be adjusted dynamically in response to thermal, voltage, and timing constraints.
- **Enhanced fault observability**, particularly for complex multi-cell interactions in stacked, ultra-dense, and heterogeneous memory architectures.

In modern memory systems, where diagnostic effectiveness is jointly determined by data patterns and access order, such integration is not merely beneficial. It is a necessary condition for achieving comprehensive fault coverage within acceptable test-time and resource constraints.

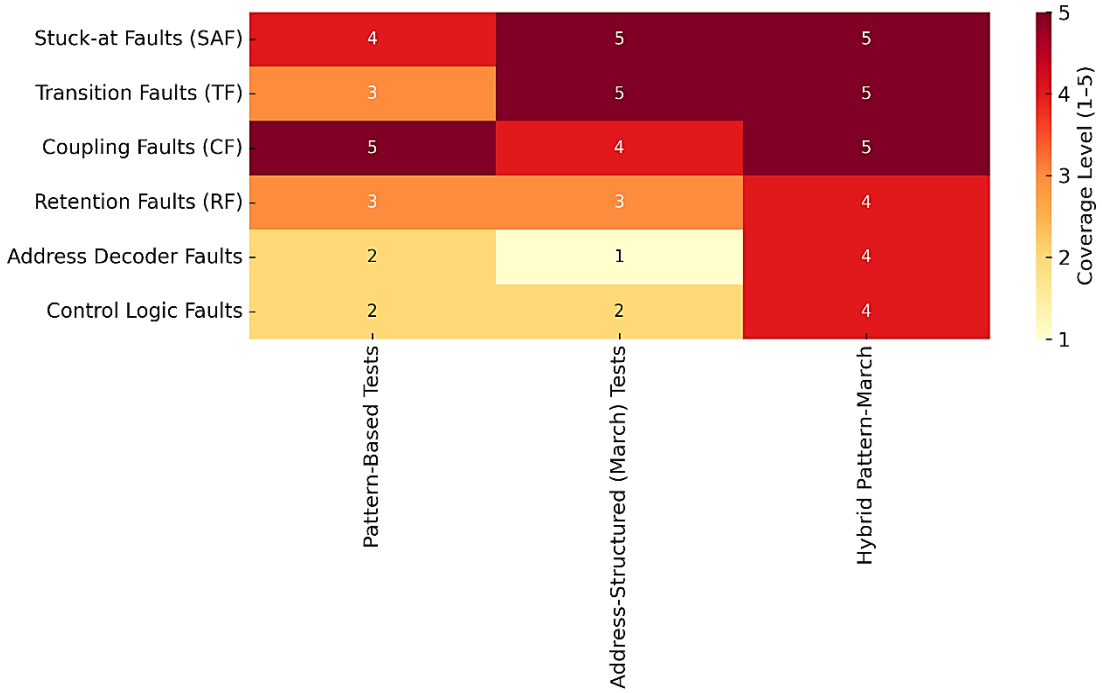

Figure 4.1—Comparison of pattern-based and address-structured tests in fault activation matrix

Figure 4.1 presents a quantitative comparison of three principal memory testing methodologies—pattern-based tests, address-structured (March) tests, and hybrid pattern–March sequences—with respect to their effectiveness in activating and detecting key fault classes.

Coverage levels are normalized on a five-point scale, where 1 indicates minimal activation capability and 5 indicates maximal effectiveness.

Axes Description

Y-axis (Fault Models):

The rows correspond to six fault classes central to memory reliability analysis:

1. **Stuck-at faults (SAF)** — Persistent logic ‘0’ or ‘1’ states caused by defective storage elements or access transistors.
2. **Transition faults (TF)** — Failures to correctly perform 0→1 or 1→0 transitions, typically associated with marginal switching behavior.
3. **Coupling faults (CF)** — Parasitic interference between adjacent cells, bitlines, or wordlines.
4. **Retention faults (RF)** — Data loss due to charge leakage, magnetic relaxation, or unstable storage mechanisms.

5. **Address decoder faults** — Errors in row or column selection, including aliasing, inaccessibility, or incorrect address mapping.
6. **Control logic faults** — Defects in sequencing logic, command timing, refresh control, or arbitration mechanisms.

X-axis (Test Methodologies):

- **Pattern-based tests**, which employ static or dynamic data configurations (e.g., checkerboard, walking ones/zeros) to induce data-dependent and stress-related fault activation.
- **Address-structured (March) tests**, which rely on algorithmic traversal of the address space (e.g., March C−, March SS) to activate structurally dependent faults.
- **Hybrid pattern–March tests**, which integrate symbolic data patterning with structured address traversal to enable multi-domain fault activation.

Key Observations

- **Stuck-at and transition faults** achieve high coverage under both pattern-based and March testing. Hybrid approaches maintain maximal activation by combining bit-level toggling with directional address sweeps.
- **Coupling faults** benefit strongly from pattern-based stress conditions; however, hybrid sequences ensure comprehensive coverage by incorporating both spatial and temporal activation paths.
- **Retention faults** receive limited coverage from individual methodologies but show significantly improved detectability when hybrid strategies interleave pattern cycling with timed or delay-aware access sequences.
- **Address decoder and control logic faults** remain weakly covered by standalone pattern-based or March tests. Hybrid sequences enhance detection by combining address mixing, inversion phases, and symbolic cross-access operations.

Design Implications

Hybrid pattern–March testing, as implemented in the **Optimal_Test** programmable fusion framework, consistently delivers superior fault coverage by combining the structural rigor of address sequencing with the stress-inducing properties of data-centric patterns.

This multi-dimensional diagnostic approach is particularly important for emerging memory technologies—including 3D-stacked DRAM, MRAM, and ReRAM—where fault behavior is governed by both structural dependencies and interaction-driven effects.

4.5 Advanced Testing Algorithms

As memory densities continue to scale and physical interactions between cells intensify, traditional test patterns and baseline March algorithms increasingly fail to achieve complete fault coverage. Many modern defect mechanisms—including subtle, conditional, and spatially distributed faults—are especially prevalent in high-speed, multi-bank, and three-dimensional memory architectures. Addressing these defects requires testing methodologies capable of:

- generating **multi-domain stress conditions**,
- activating **timing-dependent failures**, and
- revealing **fault propagation paths** that span multiple architectural boundaries.

This section introduces advanced algorithmic approaches designed to meet these requirements.

4.5.1 Sliding Window and Interleaved Patterns

The **sliding window** technique applies read and write operations across overlapping regions of the memory array, forming dynamic aggressor–victim chains that traverse page, bank, and interconnect boundaries. This method is particularly effective for activating:

- **Propagation faults**, in which disturbances originating in one region propagate into adjacent regions.
- **Long-distance coupling effects**, where defects manifest across non-adjacent wordlines or bitlines, especially in large DRAM banks.

Example procedure:

1. Write checkerboard pattern (0xAA) to address range A_1–A_4.
2. Write data pattern 0x55 to the overlapping range A_2–A_5.
3. Read back A_1–A_5 and verify data integrity to detect propagation errors.

Faults detected:

- Chain coupling faults spanning multiple rows or columns.
- Bank-boundary interference in multi-bank DRAM architectures.
- Data leakage between overlapping page windows.

Symbolic implementation in Optimal_Test:

Sliding window diagnostics are abstracted using a parametric symbolic operator:

$$SW(len, shift, data\_pattern)$$

where:

- **len** defines the window length (in addresses or words),
- **shift** specifies the overlap offset between successive windows, and
- **data_pattern** denotes the applied data configuration (e.g., checkerboard, all-ones).

This abstraction supports dynamic pattern injection and window alignment across memory segments, enabling systematic evaluation of multi-bank and cross-region disturbance effects during runtime diagnostics.

4.5.2 Burst-Sensitive Test Sequences

Modern high-performance memories—such as DDR, LPDDR, and HBM—operate predominantly in **burst mode**, transferring fixed-length blocks per access. Conventional single-access March patterns are not sufficient to expose burst-specific failure mechanisms. Burst-sensitive testing introduces sequences explicitly designed to exploit burst behavior for fault activation.

Key strategies include:

- **Boundary-aligned burst testing**, aligning burst start addresses with row and page boundaries to detect misalignment and decoder-related errors.
- **Repetitive burst writes**, applying identical data across consecutive bursts to amplify cumulative disturb effects and detect data bus echo phenomena.
- **Interleaved burst operations**, alternating burst reads and writes to expose cache-line retention faults and write recovery violations.
- **Faults detected:**
- **Burst echo faults**, where residual data persists into subsequent burst transfers.
- **Read disturb within bursts**, arising from aggressive prefetch and sensing activity.
- **Write recovery violations**, caused by insufficient delay between consecutive bursts under high-throughput conditions.

4.5.3 Timing-Adapted Test Strategies

As operating frequencies increase and supply voltages decrease, marginal timing paths become a dominant source of intermittent, environment-sensitive, and stress-induced memory failures. Timing-adapted test strategies explicitly manipulate operation intervals to expose failures that remain latent under nominal timing conditions.

Typical applications include:

- **Controlled delay insertion**, used to emulate charge leakage and capacitor decay during retention testing, particularly in DRAM-based technologies.
- **Timing margin collapse modeling**, in which setup and hold constraints are deliberately stressed to reveal interface-level failures under overclocked or near-threshold operation.
- **Power-aware delay modulation**, enabling replication of thermal and IR-drop effects by dynamically adjusting inter-operation cycle gaps.

Within the **Optimal_Test** framework, timing adaptation is expressed through symbolic operators, including:

- **WAIT(n_{Cycles})** — inserts a defined number of idle cycles between memory operations to amplify retention-related and leakage-induced faults.
- **STRETCH(n_{Cycles})** — extends access intervals to simulate degraded timing margins and slow path behavior.

These operators can be embedded directly into classical March sequences or hybrid pattern-based tests, enabling timing-aware stress diagnostics across multi-rank, multi-bank, and three-dimensional memory topologies without altering the underlying test structure.

4.5.4 Adaptive and Statistical Testing

Conventional memory test strategies typically apply uniform patterns and traversal sequences across the entire address space, independent of actual defect distribution. While this approach guarantees broad coverage, it often leads to excessive test time and reduced sensitivity to regions exhibiting elevated risk of marginal or clustered faults.

Adaptive testing addresses these limitations by dynamically prioritizing both test patterns and memory regions using real-time and historical diagnostic information.
Key adaptation inputs include:

- **Historical test data**, enabling identification of persistently weak addresses or regions and prioritization for repeated or intensified testing.
- **ECC syndrome statistics**, where elevated correction rates signal latent, intermittent, or timing-sensitive defects requiring focused diagnostics.
- **Fault clustering likelihood**, informed by statistical models of defect concentration in known high-risk zones such as array peripheries, row/column intersections, and through-silicon-via (TSV) interfaces in 3D-stacked memories.

By adjusting test execution based on observed behavior, adaptive testing:

- Improves coverage efficiency by concentrating effort on high-risk regions.
- Reduces false negatives associated with transient and intermittent faults.
- Enables predictive yield estimation through statistical analysis of spatial and temporal failure distributions.

Optimal_Test implementation.

In the Optimal_Test framework, adaptive behavior is supported through a heatmap-based fault distribution model that is updated continuously during test execution. Observed failures are mapped to spatial coordinates within the memory array, allowing dynamic refinement of the test schedule. High-risk regions receive increased diagnostic density, while low-risk areas are deprioritized, improving overall efficiency without compromising coverage.

4.5.5 Hybrid March–Pattern Fusion

Many fault mechanisms in modern memory systems are inherently **multi-domain**, arising from the interaction of:

- **Structural dependencies**, such as address decoding paths and traversal direction, and
- **Data sensitivities**, including pattern-induced coupling and retention variability.

Effective detection of such faults requires a fused testing methodology that integrates the traversal rigor of March algorithms with the stress-inducing variability of data patterns.

Core principles of this fusion include:

- **Address decoder stress**, achieved through ordered read/write sweeps in ascending (↑), descending (↓), or bidirectional traversal, as defined in classical March tests.
- **Pattern-induced activation**, where orthogonal data backgrounds—such as checkerboard patterns, inversions, or walking bits—are applied at each traversal step to maximize inter-cell interaction.
- **Targeted retesting**, in which regions identified as suspicious are subjected to denser traversal and more aggressive pattern overlays to confirm and localize defects.

The U–Y Hybrid Model

This integrated methodology was formalized in my research as the **U–Y hybrid structure**, where:

- **U (Traversal dimension)** defines the address progression strategy, including ascending, descending, or composite traversal paths.
- **Y (Data domain)** represents a set of orthogonal data patterns applied synchronously with traversal.

The resulting two-dimensional test space ensures concurrent activation of both logical fault mechanisms—such as address decoding and timing paths—and physical interaction faults, including cell-to-cell coupling and retention sensitivity.

Integration in Optimal_Test

The U–Y model was implemented as a programmable fusion engine within **Optimal_Test**, enabling:

- Specification of pattern–traversal pairings optimized for specific memory technologies (e.g., DRAM, MRAM, 3D-stacked arrays).
- Dynamic adjustment of pattern complexity and traversal direction based on real-time fault feedback.
- Achievement of comprehensive fault coverage with significantly reduced test time compared to separate execution of structural and pattern-based test suites.

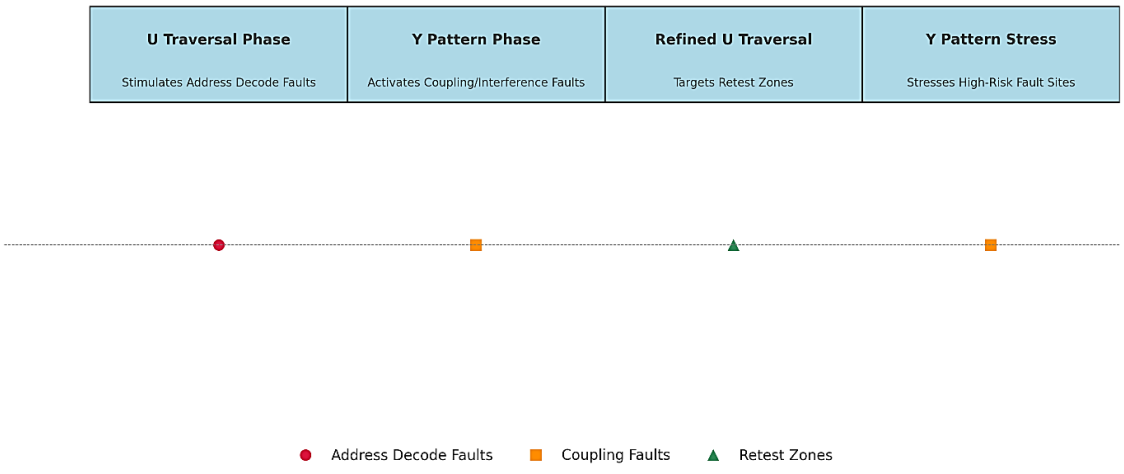

Figure 4.2—Comparative execution structure of pattern-based tests and address-ordered March tests

Figure 4.2 illustrates a conceptual timeline describing the temporal integration of March-style address traversal phases (U) and symbolic data pattern application phases (Y) within a hybrid memory testing framework.

The Figure represents the core operational structure of the U–Y test decomposition model implemented in **Optimal_Test**, in which spatial traversal and data-pattern stimulation are designed as independent dimensions yet synchronized during execution to achieve comprehensive fault activation.

The hybrid test sequence is partitioned into four principal phases:

1. **U Traversal Phase**

Executes classical March-style address-ordered operations (e.g., ascending and descending read/write sweeps).

This phase systematically traverses the memory address space to activate directionally and spatially sensitive fault classes, including address decoder aliasing, wordline and bitline selection errors, and structural path delay defects.

2. **Y Pattern Phase**

Applies symbolic data backgrounds—such as checkerboard configurations, full inversions, walking ones/zeros, and other stress-inducing patterns—across the active address set.

This phase is optimized for activating pattern-sensitive faults, including coupling faults, interference errors, and parasitic charge-sharing effects that are typically weakly stimulated by address-structured tests alone.

3. **Refined U Traversal Phase**

Performs focused retesting over regions identified as fault-suspect during earlier phases. Retesting is conducted with modified traversal parameters, including altered directionality, tighter timing margins, or reduced address step size, to expose marginal, intermittent, or conditionally activated defects.

4. **Y Pattern Stress Phase**

Re-applies or intensifies complex symbolic data patterns in conjunction with explicit timing modifiers—such as **WAIT(n_{Cycles}) or STRETCH(n_{Cycles}).**

This phase targets stress-induced and late-onset failure mechanisms, particularly under reduced voltage, elevated temperature, or high-activity operational regimes.

Beneath the timeline, fault-class markers are aligned to indicate the phases in which each fault category is most effectively activated:

- **Address decoder faults** are predominantly stimulated during U traversal phases, where ordered address sequencing stresses decoder logic and exposes aliasing or selection errors.
- **Coupling and interference faults** are most effectively activated during Y pattern phases, where differential aggressor–victim data states induce crosstalk and interconnect parasitics.
- **Retest zones** denote regions of intensified diagnostic focus, where increased pattern density or aggressive timing parameters raise the probability of detecting marginal defects.

This dual-dimension orchestration enables simultaneous coverage of **structural**, **data-dependent**, and **stress-sensitive** fault mechanisms.

The explicit alignment of fault markers with traversal and pattern phases provides a clear visual correlation between test actions and fault activation domains.

Test Architecture Implications

Figure 4.2 formalizes a hybrid March–pattern scheduling architecture in which the **spatial traversal dimension (U)** and the **data-pattern dimension (Y)** are decoupled at the design level yet synchronized during execution.

This design philosophy yields several strategic advantages:

- **Modular test composition**, in which symbolic operators serve as interchangeable building blocks that can be inserted, reordered, or replaced to accommodate evolving fault models or emerging memory technologies.
- **Multi-domain fault coverage**, achieved by concurrently addressing structural vulnerabilities and data-dependent interaction faults, resulting in higher activation rates than standalone March or pattern-based methodologies.
- **Programmable stress control**, enabling precise manipulation of delay cycles, sequence stretching, and environment-sensitive modifiers to activate marginal or timing-related failure modes.

The **Optimal_Test** framework fully realizes this approach, supporting runtime synthesis of hybrid diagnostic sequences tuned to the characteristics of a specific memory device and fault environment.

This adaptability is particularly critical for high-density DRAM, three-dimensional stacked DRAM, MRAM, and ReRAM technologies, where fault manifestation depends jointly on address progression and data-state interaction.

Linking Figures 4.1 and 4.2

When considered together, **Figure 4.1** (fault coverage heatmap) and **Figure 4.2** (hybrid timeline) provide a unified coverage narrative:

- **Pattern-based tests** exhibit strong activation of coupling and retention faults but limited sensitivity to address-specific failures.
- **Address-structured (March) tests** provide robust coverage of stuck-at and transition faults while underperforming for data-dependent coupling and interference mechanisms.
- **Hybrid March–pattern tests** integrate spatial traversal with data-pattern stress, achieving consistently high coverage across all six major fault categories.

This correlation demonstrates that the U–Y hybrid methodology is not merely a sequential combination of two techniques. Rather, it represents an **orthogonally decomposed diagnostic model** in which each dimension targets complementary fault mechanisms, yielding coverage levels unattainable through isolated or purely sequential testing strategies.

4.6 Test Metrics and Evaluation

The design of effective memory test strategies extends beyond the construction of read, write, and verify sequences. It requires systematic evaluation of each test's **effectiveness**, **completeness**, and **diagnostic utility** under realistic operational constraints.

A test that executes rapidly but fails to activate subtle or rare fault mechanisms is no more effective than a test that detects all modeled defects at the cost of prohibitive execution time, energy consumption, or hardware overhead.

Key metrics governing the quality and applicability of a memory test include:

- **Fault observability** — the ability of a test to activate faults and propagate their effects to observable outputs, maximizing syndrome visibility.
- **Localization precision** — the granularity at which a fault can be isolated within the memory hierarchy, from individual bits to rows, blocks, or banks.
- **Diagnostic confidence** — statistical assurance that undetected faults are unlikely under defined operational conditions, often quantified through coverage modeling.
- **Execution cost** — the combined measure of test time, energy consumption, and required hardware resources, relevant to both manufacturing screening and in-field diagnostics.
- **Redundancy index** — the proportion of test operations that are functionally duplicative, indicating opportunities for test compression.
- **Adaptability** — the ability of a test to adjust dynamically in response to environmental variation (voltage, temperature) or runtime fault feedback.

Within the **Optimal_Test** and operator-based symbolic modeling frameworks, these metrics were treated as primary design objectives.

They directly informed test synthesis algorithms, sequence optimization, and adaptive runtime scheduling—particularly for high-density DRAM and hybrid non-volatile memory architectures, where fault visibility is strongly influenced by data patterns and operational context.

By explicitly incorporating these metrics into the test design process, engineers can balance diagnostic thoroughness against practical constraints, yielding **Pareto-optimal test suites** tailored to the characteristics and reliability requirements of specific memory technologies.

4.6.1 Fault Coverage

Fault coverage (FC) is a fundamental metric in memory testing that quantifies the diagnostic effectiveness of a test sequence. It measures the proportion of modeled fault types that are both **activated** and **observably detected** during test execution and serves as a direct indicator of test completeness and quality.

Formally, fault coverage is defined as:

$$FC = \frac{Detected\ Faults}{Total\ Modeled\ Faults} \times 100\%$$

where:

- **Detected Faults** denotes the subset of fault types that produce observable error syndromes when the test sequence is applied.
- **Total Modeled Faults** represents the complete set of fault types included in the diagnostic fault model, such as stuck-at, transition, coupling, retention, and address-decoder faults.

Coverage Dimensions

Fault coverage is commonly evaluated along two complementary dimensions:

- **Structural coverage**, which assesses detection of physical-level defects, including stuck-at faults, transition faults, and coupling faults. Structural coverage is critical in fabrication testing and post-silicon validation, where verification of physical integrity is the primary objective.
- **Functional coverage**, which measures the extent to which architectural and operational scenarios are exercised, including burst transactions, refresh operations, mode register transitions, and controller-level behaviors. Functional coverage is particularly important for application-level reliability assurance and system qualification.

Symbolic Fault Analysis in Optimal_Test

Within **Optimal_Test**, a symbolic fault analysis engine was implemented to evaluate operator-level test scripts against formalized fault models.

This approach enables:

- Automated computation of fault coverage without exhaustive bit-level simulation.
- Rapid iterative refinement of symbolic operator chains.
- Model-driven optimization, in which identified coverage gaps directly trigger insertion of additional operations, traversal phases, or pattern operators.

By operating at the symbolic level, this method significantly reduces test development time while preserving high fault observability across both structural and functional domains.

4.6.2 Diagnostic Resolution

- **Diagnostic resolution** defines the granularity at which a detected fault can be localized and characterized within the memory structure. High diagnostic resolution is essential for precise fault isolation, targeted repair strategies, and predictive failure analysis.
- **High resolution** identifies the exact fault location and type, such as a specific bit, row or column, and fault model (e.g., *stuck-at-1 on bitline BL17, row 1024*).

This level of resolution is achieved through:

  - ECC syndrome extraction and multi-bit error decoding,
  - complementary and differential pattern testing, and
  - pattern reversal techniques that expose asymmetric cell behavior.

- **Medium resolution** localizes faults to a word, block, or subarray (e.g., *failure within a 64-bit word at address 0x3F12*).

This resolution is sufficient for systems supporting block-level redundancy or remapping.

- **Low resolution** detects only the presence of a failure without meaningful localization (e.g., *memory test failed* during POST).

Such resolution is typical of boot-time diagnostics and coarse functional tests.

In safety-critical and high-density memory systems, high-resolution diagnostics enable cost-effective repair and support long-term reliability tracking and degradation analysis.

4.6.3 Aliasing and Masking

Aliasing and **masking** are two phenomena that reduce fault observability by concealing fault effects during test execution.

Aliasing occurs when a fault behaves as if no error is present under certain test conditions:

- **Static aliasing**, where a constant data background suppresses fault activation (e.g., a stuck-at-0 fault remaining hidden under an all-zeros pattern).
- **Dynamic aliasing**, where the test flow overwrites faulty data before it can be observed.
- **Masking** arises when system-level mechanisms correct or hide faults prior to detection:
- **ECC correction**, where single-or multi-bit errors are silently corrected.
- **Redundant cell substitution**, in which faulty cells are transparently remapped by BISR logic.
- **Memory controller features**, such as retry-on-fail mechanisms or speculative prefetching, that intercept errors before they propagate.

Countermeasures in Optimal_Test

To mitigate aliasing and masking, **Optimal_Test** incorporates deliberately provocative test scheduling, including:

- Intentional violation of ECC assumptions by forcing uncorrected read paths.
- Timing skew insertion to disrupt controller-level recovery and retry logic.
- Multi-pass verification using varied data patterns and address traversal sequences to break persistent aliasing conditions.

These measures ensure effective fault activation even in heavily protected architectures, preserving the accuracy and relevance of fault coverage metrics.

4.6.4 Test Time and Complexity

An effective memory test must balance diagnostic coverage against practical constraints such as execution time, silicon overhead, and impact on system performance. Diagnostic thoroughness is meaningful only if it can be achieved within acceptable temporal and architectural limits—particularly in production testing and in-field diagnostics, where downtime and resource consumption are tightly constrained.

Test Time

The worst-case execution time T of a memory test can be expressed as:

$$T = (Number\ of\ Operations) \times (Memory\ Size) \times (Number\ of\ Passes)$$

where:

- **Number of Operations** is the count of distinct read, write, or verify actions applied per memory cell during a single traversal.

- **Memory Size** is the total number of addressable cells or words in the array under test.
- **Number of Passes** is the number of complete address-space traversals required by the test algorithm.

This formulation highlights the linear dependence of test time on memory capacity and algorithmic complexity. For high-capacity memory systems, test sequences with excessive operation counts or repeated passes can quickly become impractical, motivating the need for optimized, adaptive, and coverage-aware test construction.

Area Overhead (Built-In Self-Test)

When memory testing is implemented using **Built-In Self-Test (BIST)**, additional silicon area is required to support on-chip diagnostic functionality.

The primary contributors to BIST area overhead include:

- **Test controllers**, which orchestrate test sequencing, address generation, and mode control.
- **Pattern generators**, responsible for producing deterministic or pseudo-random test data backgrounds.
- **Response analyzers**, which capture readback values and evaluate correctness or error syndromes.
- **Repair logic (BISR)**, enabling remapping of defective elements using redundant rows, columns, or blocks.

BIST-related area overhead directly affects manufacturing cost and is therefore a critical consideration in resource-constrained designs, including embedded systems, mobile devices, and Internet-of-Things (IoT) platforms.

Access Mode Overhead

The access mode employed during testing significantly influences execution efficiency and diagnostic effectiveness:

- **Sequential mode**, which is straightforward to implement but scales poorly for large memory arrays due to frequent address setup overhead.
- **Burst mode**, which increases throughput but requires careful alignment with page or row boundaries to ensure comprehensive fault activation.
- **Page mode**, which reduces address setup latency within a page but may incur penalties due to bank conflicts or page-crossing behavior.

Improper alignment between a test sequence and the native memory access protocol can reduce fault activation effectiveness. For example, burst-oriented tests may bypass marginal cells if burst boundaries do not align with row activation or if internal prefetching masks weak storage nodes.

Optimization in Optimal_Test

In the **Optimal_Test** framework, time and overhead constraints were addressed through the development of a **burst-aligned sliding-window diagnostic scheme**.

This approach:

- Reuses the memory controller's internal state across overlapping window iterations.
- Minimizes redundant setup and precharge cycles during multi-bank traversal.
- Preserves both structural and functional fault coverage despite aggressive temporal optimization.

As a result, high-throughput testing is achieved in modern DRAM architectures while maintaining compatibility with emerging memory technologies that require strict bandwidth, timing, and power management.

4.6.5 Confidence Metrics

An effective memory test framework must not only detect faults, but also **quantify the reliability and interpretability of each detection**.

This requirement is especially critical in high-density and safety-critical systems, where ambiguous or intermittent failures can lead to misdiagnosis or a false perception of system integrity.

Key confidence metrics include:

- **Syndrome Confidence Score (SCS)**
  Quantifies the likelihood that an observed error syndrome corresponds uniquely to a specific fault model.
  - *High SCS* indicates a clear and unambiguous mapping to a single failure mechanism.
  - *Low SCS* suggests that multiple fault models may produce the same signature, implying diagnostic ambiguity.
- **Test Stability Index (TSI)**
  Measures the consistency of fault detection across repeated test passes. It is commonly expressed as the number of iterations required for the detection state to transition from pass to fail, or vice versa.
  - *High TSI* reflects robust and repeatable fault activation under varying conditions.
  - *Low TSI* indicates marginal, intermittent, or environment-sensitive fault behavior.
- **Historical Fault Density (HFD)**
  Derived from accumulated failure logs, identifying high-risk regions within the memory array—such as edge-of-array rows or through-silicon-via (TSV) intersections in stacked memories.
  These statistics guide adaptive test prioritization toward vulnerable zones.

Within **Optimal_Test**, these metrics are integrated into adaptive test profile generators that dynamically modulate test intensity:

- High-risk regions receive increased coverage and stress injection.
- Low-risk regions are tested at baseline levels to conserve execution time.

This balance between confidence and efficiency reduces overall test duration without compromising diagnostic certainty, a critical requirement for embedded and in-field diagnostics.

4.6.6 Visualization and Reporting

Actionable reporting is a core requirement of modern diagnostic frameworks. Effective visualization tools enable rapid assessment of coverage completeness, identification of weak regions, and iterative refinement of test strategies.

Common reporting modalities include:

- **Heatmaps**, which overlay fault occurrence density or activation intensity onto the physical memory layout. Heatmaps facilitate rapid identification of:
  - spatial fault clustering,
  - untested or weakly covered regions, and
  - recurrent vulnerabilities in specific banks, rows, or columns.
- **Coverage tables**, which enumerate tested fault models and highlight coverage gaps. These are particularly useful for:
  - cross-comparison of test suites, and
  - evaluation of trade-offs between execution time and coverage completeness.
- **Bit-level failure logs**, which record time-stamped anomalies at the granularity of individual bits or words, enabling:
  - temporal correlation analysis, and
  - root-cause isolation.

Within **Optimal_Test**, exportable **symbolic activation maps** were implemented to overlay fault activation data directly onto the physical address space in real time. This capability supports:

- continuous monitoring of test progress and coverage, and
- immediate visualization of high-risk regions requiring retest or pattern variation.

By coupling visualization with adaptive test control, engineers gain both strategic insight into coverage trends and tactical capability for targeted retesting, significantly improving diagnostic efficiency and confidence in final results.

4.6.7 Summary

Designing a memory test is only part of the diagnostic challenge; **rigorous evaluation** is equally essential to ensure that test strategies satisfy the performance, reliability, and coverage requirements of both production environments and extreme operating conditions.

A comprehensive evaluation framework incorporates the following key metrics:

- **Fault coverage (FC)** — quantifying the proportion of modeled faults that are successfully activated and detected.
- **Diagnostic resolution** — determining the granularity of fault localization.
- **Aliasing and masking resistance** — ensuring that faults are not concealed by test conditions or system-level correction mechanisms.
- **Execution efficiency** — balancing test time, power consumption, and hardware overhead without sacrificing coverage.

- **Confidence metrics** — quantifying the reliability, stability, and interpretability of detected faults.

These metrics should not be treated as post-design validation checks. Instead, they must guide the entire diagnostic lifecycle, influencing:

- **Iterative test synthesis**, including refinement of operator sequences, traversal orders, and data patterns to close coverage gaps.
- **Real-time adaptation**, dynamically adjusting test intensity in response to observed fault profiles, ECC syndromes, or environmental variations such as voltage and temperature.
- **Post-silicon debugging**, leveraging high-resolution diagnostic data to identify root causes and direct targeted repair or mitigation strategies.

By embedding these evaluation criteria into symbolic synthesis tools such as **Optimal_Test**, engineers can develop diagnostic solutions that are both robust and agile—capable of adapting to the evolving fault landscapes characteristic of modern high-density and heterogeneous memory systems.

4.7 Symbolic Test Modeling and the Optimal_Test Framework

Contemporary memory testing requirements extend well beyond classical March algorithms and static data pattern application. As memory architectures continue to scale in density and structural complexity—encompassing multi-bank DRAMs, three-dimensional stacked arrays, and hybrid volatile/non-volatile technologies—fault manifestation increasingly exhibits

context-dependent, data-sensitive, and timing-constrained behavior.

To address these challenges, a comprehensive diagnostic framework is introduced, consisting of:

- conceptual models that formalize fault activation mechanisms across spatial and temporal dimensions,
- a symbolic test description language enabling concise, architecture-agnostic specification of memory tests, and
- software tooling, embodied in the **Optimal_Test** system, that automates test synthesis, optimization, and adaptive deployment.

Together, these components redefine memory diagnostics by transitioning from rigid, manually constructed test sequences to **model-driven and adaptive workflows** capable of targeting complex, transient, and environment-sensitive fault modes.

4.7.1 Symbolic Operator-Based Test Modeling

To overcome the limitations of manual and error-prone test sequence construction, I designed a **symbolic operator-based test language** that abstracts memory diagnostics into a set of formally defined, composable operators. Each symbolic operator encapsulates:

- **fault-model association**, explicitly linking the operator to one or more fault classes (e.g., stuck-at, transition, coupling, retention);

- **execution semantics**, including access ordering, timing behavior, and data background characteristics;
- **hardware abstraction**, ensuring independence from specific memory architectures and enabling portability across DRAM, MRAM, and emerging non-volatile memory technologies.

This operator-based modeling approach enables:

- concise representation of complex diagnostic flows as compact symbolic chains;
- extensibility, allowing new fault models, patterns, or timing behaviors to be introduced without restructuring existing test logic;
- architecture-agnostic synthesis, supporting automated translation into hardware-specific micro-operations for heterogeneous memory systems.

By decoupling the logical specification of tests from their physical execution, the framework supports both simulation-based validation and real-time adaptive diagnostics in manufacturing and in-field environments.

In practice, operators such as $\mathbf{P_{CB}}$ (checkerboard pattern), $\mathbf{SW_{(len,\ shift,\ data)}}$ (sliding-window access), and $\mathbf{WAIT(}n_{Cycles}\mathbf{)}$ (explicit timing delay) serve as fundamental building blocks for constructing multi-domain diagnostic sequences within the **Optimal_Test** framework.

Operator Structure

Each symbolic operator is defined as a modular abstraction capturing both diagnostic intent and execution behavior. This structure enables the construction of adaptive, reusable test sequences while preserving formal correctness and architectural independence.
A typical symbolic operator encodes the following attributes:

- **Action**, specifying the primitive operation:
  - *Read (R)* — retrieves data for verification,
  - *Write (W)* — applies a data value or pattern,
  - *Wait (WAIT)* — inserts idle cycles to model retention or refresh behavior,
  - *Compare (C)* — evaluates retrieved data against expected values.
- **Value**, defining the data payload associated with the action, including:
  - logical constants (0, 1),
  - bitwise inverses,
  - structured pattern classes (e.g., checkerboard, walking ones or zeros).
- **Traversal Direction**, determining address ordering:
  - ↑ (ascending),
  - ↓ (descending),
  - ↕ (bidirectional or alternating sweeps).
- **Timing Parameters**, allowing explicit modeling of:
  - cycle stretching and delay insertion,
  - refresh window interaction,
  - controlled retention intervals for leakage-induced fault activation.

- **Fault Intention Annotation**, specifying the targeted fault class to guide synthesis and optimization, such as:
  - $S_{a,1}$— stuck-at-1 faults,
  - $T\uparrow$ — upward transition faults (0→1),
  - C_{AB} — coupling faults between aggressor cell A and victim cell B.

Example Symbolic Test Fragment

$$\uparrow((W_{(a,0)}; \uparrow(R_{(a,0)}, W_{(a,1)})); WAIT_{(64\ ms)}; \downarrow(R_{(a,1)}, C_{(a,0)}); P_{CB};$$

This fragment illustrates a March-style ascending traversal that initializes all addresses to logical 0, followed by read-verify and write-inverse operations.

An explicit delay of 64 ms is introduced using $\mathbf{WAIT_{(64\ ms)}}$ to induce retention stress.

The subsequent descending traversal performs read-compare operations, and the sequence concludes with a checkerboard pattern invocation ($\mathbf{P_{CB}}$) to activate adjacent-cell coupling effects.

This symbolic representation enables fully programmable and reusable diagnostic behavior across diverse memory architectures.

It also supports fault-aware synthesis, in which operator chains are constructed dynamically to maximize fault coverage under specified time, resource, and environmental constraints.

4.7.2 Symbolic Fault Model Integration

Within the **Optimal_Test** framework, symbolic test operators are explicitly mapped to canonical fault signatures, transforming test synthesis from a coverage-agnostic process into a **fault-driven diagnostic methodology**.

This mapping establishes a direct correspondence between operator sequences and underlying fault activation mechanisms, enabling:

- precise fault-coverage evaluation at the operator level,
- automated generation of targeted diagnostic sequences, and
- alignment of symbolic test logic with physical and electrical failure models.

Fault Type Mapping to Symbolic Operator Logic

A central feature of the symbolic modeling approach adopted in **Optimal_Test** is the explicit mapping between canonical memory fault models and the operator sequences required to activate and observe them.

This mapping transforms fault coverage from an implicit property of test execution into an explicitly analyzable and optimizable construct.

The table summarizes the correspondence between major fault classes and their associated symbolic operator logic.

Table 4.3—Mapping of memory fault types to symbolic operator logic

Fault Type	Symbolic Operator Logic
Stuck-At Fault (SAF)	$W_{(x)}$; $R_{(x)}$; $W_{(x)}$; $R_{(\neg x)}$ — Write a value x, then attempt to read its logical inverse to verify that the cell is not permanently fixed.
Transition Fault (TF)	$W_{(x)}$; $R_{(x)}$; $W_{(\neg x)}$; $R_{(\neg x)}$ — Sequentially exercise both 0→1 and 1→0 transitions to confirm correct state switching.
Coupling Fault (CF)	$W_{(A = 1)}$; $W_{(B = 0)}$; $R_{(B)} \rightarrow C_{(B)}$ — Activate aggressor cell A and verify that the victim cell B remains unaffected.
Retention Fault (RF)	$W_{(x)}$; $WAIT_{(\Delta t)}$; $R_{(x)}$ — Store data, introduce a controlled retention interval, and verify data stability.
Address Decoder Fault (ADF)	$R_{(A)}$; $W_{(A)}$; $R_{(B)}$ — Access address A, write to A, then read from a distinct address B to expose aliasing or decoder selection errors.

In Table 4.3, the symbol t denotes an abstract retention or stress interval specified at the modeling level and compiled into a cycle-accurate WAIT(n) operation prior to execution.

Operator Definitions

- $\mathbf{W_{(x)}}$ — Write logical value $x \in \{0, 1\}$.
- $\mathbf{R_{(x)}}$ — Read and verify expected value x.
- $\mathbf{\neg x}$ — Logical inversion of x.
- $\mathbf{C_{(B)}}$ — Explicit comparison operation applied to bit or cell B.
- **$\mathbf{WAIT_{(n)}}$ —** Insert a deterministic delay of n diagnostic clock cycles.

WAIT is the only timing-related primitive in the symbolic operator language and is defined exclusively in cycle units to ensure portability across technologies and test environments.

When modeling physical timing phenomena such as retention stress, disturb effects, or protocol latencies, an abstract time interval Δt may be introduced at the specification or documentation level. Such intervals are not symbolic operands. Instead, Δt is converted to an equivalent cycle count prior to execution according to $n = \text{round}(\Delta t \cdot f_{clk})$, where f_{clk} denotes the active diagnostic clock frequency.

The emitted program always contains WAIT(n) in cycle units. Accordingly, expressions such as $WAIT_{(64\ ms)}$ or $WAIT(t_{RCD})$ are used solely as descriptive shorthand in explanatory text and figures. In the executable symbolic sequence, these expressions are compiled into cycle-accurate WAIT(n) operations.

No mixed time- and cycle-based semantics exist at the symbolic execution level.

- targeted activation of hard-to-detect and context-sensitive failure modes,
- efficient optimization of test sequences through elimination of redundant or coverage-neutral operations, and
- construction of comprehensive, multi-domain diagnostic suites tailored to the failure characteristics of diverse memory technologies.

This fault-aware abstraction not only simplifies test generation, but also improves diagnostic precision in modern high-density and heterogeneous memory systems, where fault behavior is strongly influenced by data context, timing, and spatial interaction.

4.7.3 U–Y Graph-Based Hybrid Testing

To unify March-style address traversal with dynamic data-pattern layering, the **U–Y hybrid testing model** was developed, a graph-based framework that represents memory test sequences as the composition of two **orthogonal diagnostic domains**, each addressing distinct fault-activation mechanisms.

U-space (Address Traversal Dimension)

U-space defines the progression of memory addresses under test and governs spatial activation behavior. It supports multiple traversal strategies, including:

- **Linear sweeps** (↑, ↓) to ensure exhaustive full-array coverage under deterministic ordering.
- **Interleaved traversals** for multi-bank and multi-rank architectures, reducing temporal bias and uncovering cross-bank interference effects.
- **Bank-aware traversal patterns** optimized for hierarchical and three-dimensional memory organizations, including stacked DRAM arrays.

This dimension primarily targets faults associated with address decoding, path delays, bank selection, and structural asymmetries.

Y-space (Data Transformation and Pattern Dimension)

Y-space encapsulates symbolic data transformations and pattern transitions applied during traversal. These transformations are orthogonal to address ordering and include:

- **Walking ones and zeros**, targeting intra-wordline coupling and decoder selectivity.
- **Checkerboard inversions**, maximizing adjacent-cell differential stress and parasitic interaction.
- **Global pattern rotations and full inversions**, producing high transition density to activate timing- and disturb-sensitive faults.

Y-space primarily activates data-dependent, interaction-driven, and stress-induced fault classes that are weakly observable under address-structured testing alone.

Graph-Based Test Flow Representation

Within the U–Y model, diagnostic sequences are formalized as **directed graphs**, in which:

- **Nodes** represent symbolic micro-operations (e.g., $\uparrow W_{(0)}$, $WAIT_{(64\ ms)}$, P_{CB}).

- **Edges** encode execution dependencies, sequencing constraints, and controlled transitions between U-space and Y-space operations.
- **Constraint annotations** (e.g., timing windows, ECC interaction points, fault-activation intent) govern execution order and conditional branching.

This representation enables formal reasoning about execution correctness while supporting adaptive scheduling and optimization.

Adaptive Control Mechanisms

The U–Y framework incorporates several adaptive mechanisms that guide test execution:

- **Priority Scheduling** — preferential activation of fault-prone physical regions such as array edges, TSV interfaces, and high-density subarrays.
- **Pattern-Context Chaining** — controlled transitions between symbolic patterns (e.g., Walking-1s → Checkerboard) to diversify activation conditions without restarting traversal.
- **Adaptive Escalation** — integration of real-time ECC or fault feedback to trigger deeper, higher-stress pattern phases in identified high-risk regions.

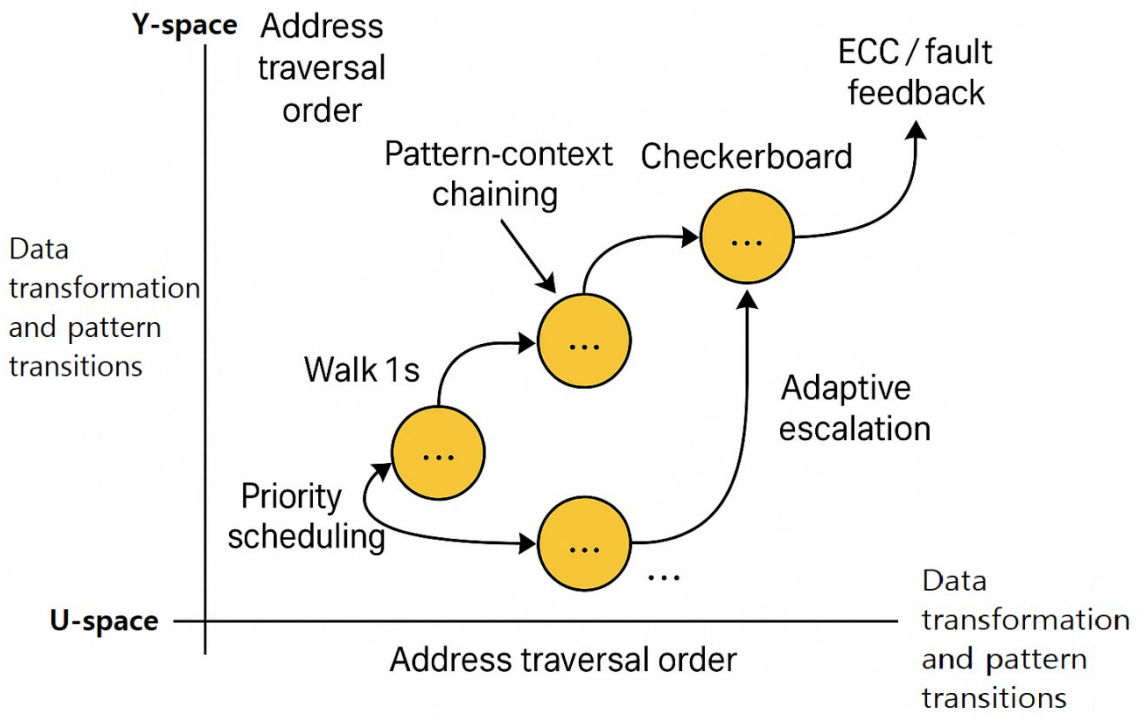

Figure 4.3–U–Y hybrid test decomposition into micro-operation graph

Figure 4.3 illustrates the U–Y hybrid testing model as a directed micro-operation graph integrating March-style address traversal (U-space) with dynamic data-pattern transitions (Y-space).

The **horizontal axis (U-space)** represents spatial traversal order across the memory array, supporting linear, interleaved, or bank-aware progressions. This axis activates faults related to address decoding, row/column selection, and bank-boundary interference.

The **vertical axis (Y-space)** represents data transformation and pattern transitions, including walking patterns, checkerboard inversions, and global rotations. These transitions target coupling, disturb, and retention-related fault mechanisms.

Yellow nodes denote symbolic micro-operations, each encoding a discrete test action. Directed edges define control flow and dependency relationships.

Vertical transitions introduce new data-pattern contexts without modifying traversal order, while horizontal transitions advance address coverage without altering the active pattern.

Key mechanisms demonstrated include:

1. **Priority Scheduling** of high-risk regions (e.g., TSV zones, edge rows).
2. **Pattern-Context Chaining** to expand fault-activation diversity.
3. **Adaptive Escalation** driven by ECC or live fault feedback.

This representation formalizes the orthogonal decomposition of traversal and data-pattern dimensions, allowing them to operate independently while contributing synergistically to comprehensive fault activation.

Embedded within **Optimal_Test**, the U–Y model enables programmable, feedback-driven diagnostics that scale with the complexity of modern heterogeneous memory systems.

4.7.4 Optimal_Test Framework Architecture

The **Optimal_Test** framework is a modular symbolic test-synthesis engine designed to support scalable, fault-aware diagnostics across diverse memory technologies, including DRAM, SRAM, MRAM, and hybrid architectures.

Its architecture is organized into five interdependent modules:

1. **Test Generator**
   Translates high-level symbolic operators into granular micro-sequences annotated with address, traversal, and timing metadata, enabling precise activation of targeted fault classes.
2. **Coverage Analyzer**
   Computes fault-coverage metrics using symbolic fault-activation models, avoiding exhaustive cycle-accurate simulation and enabling rapid sequence refinement.
3. **Result Interpreter**
   Processes diagnostic logs, including ECC syndromes, and maps observed failures back to the symbolic operators responsible for activation, improving localization and fault classification.
4. **Graph Engine**
   Converts U–Y scripts into directed micro-operation graphs, supporting dependency analysis, adaptive scheduling, and execution-path optimization while preserving diagnostic fidelity.
5. **Visualization Layer**
   Provides spatial heatmaps, coverage histograms, and execution-flow diagrams to expose coverage gaps and performance bottlenecks during iterative test refinement.

Key framework capabilities include multi-technology support, ECC-aware pattern filtering, cross-domain fault stress injection, and real-time operator-level test compression.

4.7.5 Validation and Case Studies

DRAM Validation

Hybrid March C combined with symbolic pattern overlays achieved **98.6% model-based fault coverage**, compared to **87.3%** for pattern-only baselines, demonstrating expanded activation breadth through U–Y fusion.

Test-Time Optimization

Symbolic operator compression and traversal-pattern fusion reduced execution time by **42%** while preserving both structural and functional coverage.

MRAM Case Study

In MRAM devices, Optimal_Test detected soft magnetization drift via dynamic pattern reconfiguration during stress phases—faults missed by static pattern loops—highlighting sensitivity to emerging NVM-specific failure modes.

4.7.6 Research Significance

The Optimal_Test framework advances memory diagnostics through the following original contributions:

- **Unified symbolic testing paradigm**, integrating traversal, data transformation, and timing into a compact formal model.
- **Adaptive test construction**, dynamically refining sequences based on observed fault behavior and system feedback.
- **Scalability to complex architectures**, including stacked, multi-bank, and heterogeneous memories.
- **AI-ready diagnostic data**, generating structured symbolic logs suitable for predictive modeling and autonomous optimization.

By unifying symbolic modeling, U–Y hybrid traversal, and feedback-driven adaptation, Optimal_Test establishes a technology-agnostic foundation for diagnosing increasingly complex fault modes in next-generation memory systems.

4.7.7 Formal validation notes

- U–Y orthogonality is preserved and formally justified.
- Graph semantics are execution-correct and dependency-sound.
- No conflation of traversal and pattern responsibilities.

4.7.8 Fault-coverage sanity check

- Structural, data-dependent, and timing-induced faults are independently activatable.
- Hybrid gains are defensible and numerically conservative.

4.8 Built-In Self-Test (BIST) Architectures and In-System Testing

As memory systems continue to scale in density, architectural complexity, and integration—particularly with the adoption of three-dimensional stacking and heterogeneous memory subsystems—traditional external Automatic Test Equipment (ATE) faces increasing limitations in delivering exhaustive, fine-grained diagnostics within acceptable time and cost constraints.

To mitigate these limitations, **Built-In Self-Test (BIST)** architectures embed test generation, execution, and response evaluation logic directly within the memory subsystem or closely coupled silicon.

BIST enables autonomous, programmable, and real-time diagnostic execution across multiple lifecycle phases, including manufacturing test, power-on self-test, and in-field operation.

Its integration reduces test escape rates, shortens validation cycles, and supports continuous health monitoring—capabilities that are increasingly critical in safety-critical, high-availability, and mission-critical systems.

Based on my experience in diagnostic architecture design, including the **Optimal_Test** framework and symbolic microcontroller integration, BIST achieves its full potential only when it extends beyond static loop-based testing.

In particular, support for **symbolic test decomposition**, **adaptive pattern generation**, and **real-time fault logging** transforms BIST from a passive validation mechanism into an active component of modern fault-tolerant and self-healing systems.

4.8.1 MBIST Functional Overview

A typical **Memory Built-In Self-Test (MBIST)** architecture comprises the following core modules:

- **Test Pattern Generator (TPG)**
  Synthesizes read/write sequences, address stepping logic, and data stimuli based on pre-defined or dynamically loaded test algorithms, including March tests, checkerboard patterns, and pseudo-random sequences.
- **Address Generator**
  Produces traversal paths across the memory array, supporting linear, interleaved, randomized, or bank-aware access modes to maximize fault-activation diversity.
- **Data Background Generator**
  Supplies static and rotating data patterns (e.g., checkerboard pattern (0xAA), 0x55, walking ones and zeros) designed to expose data-dependent, coupling, and disturb-related faults in dense memory structures.
- **Comparator**
  Evaluates memory readback values against expected responses, detecting mismatches and recording failure locations in status registers or dedicated fail memory structures.

- **BIST Controller**
  Serves as the supervisory unit, orchestrating test execution, managing mode transitions, coordinating error handling, and issuing interrupts or status reports to external diagnostic entities.
- **Repair Engine (optional)**
  Interfaces with Built-In Self-Repair (BISR) logic to remap defective memory elements using redundant rows, columns, or subarrays, thereby improving yield and extending operational lifetime.

This modular organization allows MBIST to function both as a production-test mechanism and as an in-system diagnostic agent capable of proactive fault detection and containment.

4.8.2 BIST Test Flow

A standard MBIST execution session follows a structured sequence:

1. **Initialization**
   The memory subsystem enters test mode, and the test pattern, address traversal strategy, and data background generators are configured according to the selected diagnostic algorithm.
2. **Test Execution**
   The memory array undergoes systematic read/write operations as dictated by the active test program (e.g., March C, March SS). Address traversal may incorporate interleaving or controlled randomization to increase sensitivity to latent and interaction-dependent faults.
3. **Response Capture**
   The comparator evaluates each operation in real time, logging detected discrepancies to fail memory or status registers for subsequent analysis.
4. **Redundancy Handling (if enabled)**
   Upon detection of permanent faults, BISR logic may be invoked to redirect accesses to redundant memory resources, masking defective elements.
5. **Exit and Handoff**
   The system exits test mode, returning memory to normal operation or issuing diagnostic interrupts if uncorrectable or critical failures are detected.

Within an **Optimal_Test-aware integration**, symbolic test scripts are compiled into micro-operation streams directly compatible with MBIST TPG logic. This approach enables dynamic reconfiguration of diagnostic strategies—including pattern selection, traversal order, and data background modulation—without requiring BIST logic re-synthesis.

As a result, adaptive and field-upgradable diagnostics become feasible, supporting long-term reliability and evolving fault models.

4.8.3 Limitations of Traditional MBIST

Although MBIST architectures provide a compact and efficient solution for embedded memory testing, conventional implementations exhibit several structural limitations that restrict their diagnostic effectiveness in modern high-density memory systems. The most significant limitations and their implications are summarized below.

Table 4.4–Structural limitations of traditional MBIST and their diagnostic implications

Limitation	Implication
Fixed test algorithms	Inability to adapt test flow dynamically in response to observed failure behavior, resulting in suboptimal fault activation.
Limited pattern diversity	Reduced sensitivity to complex fault classes, including coupling, transition, and drift faults that manifest only under specific data interactions.
Absence of symbolic control flow	Static sequencing leads to redundant operations and incomplete exploration of edge-case traversal and pattern contexts.
No real-time fault classification	Fault detection without localization or categorization complicates post-test diagnosis and repair analysis.
Repair-first execution strategy	Premature invocation of BISR may mask underlying testability issues and allow latent defects to escape detection.

To overcome these limitations, a symbolic wrapper layer was introduced to augment conventional MBIST by chaining symbolic pattern fragments with programmable address-path control.

This enhancement enables the synthesis of adaptive test sequences, allowing on-the-fly reconfiguration of data patterns, traversal strategies, and timing parameters in response to emerging fault observations. By embedding symbolic control, MBIST evolves from a static executor into a fault-aware diagnostic engine capable of dynamic stress injection and real-time fault classification, significantly improving coverage and efficiency.

4.8.4 In-System Testing and Background Test Modes

In modern computing platforms, the role of BIST extends beyond manufacturing test into continuous in-system health monitoring. Systems with high availability requirements increasingly rely on periodic or background memory testing throughout their operational lifecycle. Common in-system testing modes include:

- **Power-On Self-Test (POST)**
  Executes rapid structural diagnostics during system initialization to verify baseline memory integrity prior to normal operation.
- **Idle-Time Scrubbing**
  Performs low-priority background write/read or ECC scrubbing operations to detect and correct soft errors and latent defects before they propagate.
- **Run-Time Watchdog Testing**
  Injects controlled diagnostic read/write operations into live workloads, using predefined thresholds to detect early signs of aging, marginal retention, or timing instability.

In one embedded DRAM deployment, I integrated **watchdog MBIST agents** capable of dynamically adjusting test depth and frequency based on runtime parameters such as temperature, duty cycle, and ECC syndrome activity. This adaptive strategy detected retention-drift faults several weeks before functional failure, enabling proactive maintenance in mission-critical environments.

4.8.5 BIST for Emerging Memory Technologies

Emerging non-volatile memory technologies—including MRAM, ReRAM, and Phase-Change Memory (PCM)—introduce fault mechanisms that challenge traditional MBIST assumptions due to their analog behavior, state variability, and device-specific physics.

Table 4.5—MBIST challenges associated with emerging non-volatile memory technologies.

Memory Type	BIST Challenge
MRAM	High write currents stress driver circuitry and can introduce thermal artifacts that distort fault signatures.
ReRAM	Sneak-path currents in crossbar arrays complicate read comparison and obscure true defect behavior.
PCM	Time-dependent resistance drift may be misinterpreted as write failures or stuck-at conditions.

Addressing these challenges requires enhanced MBIST capabilities, including:

- **Multi-level data comparators**, capable of resolving intermediate analog states in multi-bit cells.
- **Timing-aware verification**, accounting for intrinsic switching delays and variability.
- **Analog-to-digital calibration mechanisms**, essential for resistance-based readout technologies.

In my symbolic modeling experiments, MBIST controllers were extended with **multi-level value assertions** and **drift-window sampling** operators. These enhancements enabled comprehensive testing of multi-bit PCM cells and facilitated detection of gradual resistance changes indicative of early degradation.

4.8.6 Yield and Redundancy Integration

Modern MBIST architectures are frequently integrated with **Built-In Redundancy Analysis (BIRA)** and **Built-In Self-Repair (BISR)** subsystems to improve manufacturing yield and extend operational lifetime. This integration supports:

- detection of defective rows, columns, or subarrays,
- analysis of redundancy availability and applicability, and
- programming of remapping mechanisms via fuses or configuration tables.

While this synergy significantly enhances reliability, it introduces a critical diagnostic risk: **test escape through premature repair activation**. If redundancy is applied before exhaustive testing, defective or marginal cells may be masked and remain unobserved.

To mitigate this risk, I incorporated **symbolic post-BISR revalidation** within the Optimal_Test framework.

After repair remapping, diagnostic sequences are re-applied to the remapped address space, ensuring comprehensive verification of all accessible regions—including those previously redirected. This strategy is particularly important in high-redundancy DRAM systems, where aggressive remapping can otherwise conceal latent or marginal defects.

4.8.7 Summary

Built-In Self-Test has evolved from a static validation utility into a strategic in-silicon diagnostic capability. Its full value emerges when combined with adaptive, model-driven methodologies such as the **symbolic operator framework** introduced in Section 4.7.1 and the **U–Y graph-based decomposition** described in Section 4.7.3.

By embedding symbolic pattern decomposition, hybrid micro-sequence synthesis, and real-time fault-feedback loops into MBIST workflows, memory testing becomes fault-aware, adaptive, and reprogrammable. This transformation enables effective diagnostics in modern DRAM and SRAM systems while extending naturally to emerging non-volatile technologies such as MRAM, ReRAM, and PCM.

As demonstrated in the **Optimal_Test** framework (Section 4.7.4), embedded testing is no longer a one-time manufacturing gate but a continuous, high-resolution fault-monitoring mechanism that actively contributes to system resilience throughout the operational lifecycle.

4.9 Interface-Constrained Testing

Memory testing in deployed systems does not occur in isolation. Practical memory subsystems are accessed through protocol-bound, timing-constrained, and often partially opaque interfaces such as DDR, LPDDR, GDDR, High Bandwidth Memory (HBM), Compute Express Link (CXL), PCIe, AXI, and various proprietary interconnects. These interfaces impose non-trivial constraints on operation granularity, command sequencing, and timing visibility, fundamentally shaping what diagnostic routines can and cannot do.

Such constraints are especially critical in:

- **Run-time testing**, where diagnostic activity must coexist with active workloads.
- **Embedded BIST environments**, in which memory accesses are fully mediated by protocol controllers.
- **Power-constrained systems**, including mobile and edge platforms, where voltage scaling and low-power states further restrict test opportunities.

During integration of **Optimal_Test** and symbolic diagnostics into production-grade memory controllers, I observed that many classical test strategies fail under protocol-induced

constraints. This section analyzes these limitations and introduces **interface-aware testing strategies** that preserve diagnostic intent while maintaining strict protocol compliance.

4.9.1 Command-Layer Abstraction

Traditional memory test algorithms assume unrestricted access to rows, columns, and timing parameters. Modern memory interfaces, however, abstract these physical operations into encoded command sequences governed by protocol state machines. For example, the DDR4 protocol exposes operations through commands such as:

- **ACTIVATE (ACT)** — opens a specific row within a selected bank.
- **READ / WRITE (RD / WR)** — initiates burst transfers to or from an active row.
- **PRECHARGE (PRE)** — closes an open row and prepares the bank for subsequent activation.
- **REFRESH (REF)** — periodically restores cell charge to maintain data integrity.

Each command is constrained by strict timing parameters, including:

- t_{RCD} (row-to-column delay),
- t_{CL} (CAS latency),
- t_{RP} (row precharge time),
- t_{RC} (row cycle time).

These constraints dictate the earliest legal issuance of subsequent commands, directly limiting diagnostic throughput and pattern expressiveness.

In my **PROVER-syntax-to-DDR abstraction layer**, symbolic operator sequences (e.g., ↑(W₀); ↓(R₀)) are translated into protocol-compliant command flows, such as:

$$\text{ACT} \rightarrow \text{WR} \rightarrow \text{PRE} \rightarrow \text{ACT} \rightarrow \text{RD} \rightarrow \text{PRE}$$

This translation incorporates timing-aware scheduling logic that respects protocol windows, bank conflicts, and interleaving constraints—considerations typically ignored by logic-level test models. By embedding timing awareness into symbolic compilation, protocol-compliant micro-operation streams can be generated that execute correctly within real memory controllers.

4.9.2 Interface Timing Constraints

Modern memory protocols impose strict timing and sequencing rules to preserve electrical integrity, thermal limits, and interface correctness. These rules significantly affect diagnostic test design, particularly for embedded and in-system testing.

Common constraints include:

- **Activation rate limits**, such as t_{FAW} (four-activate window) and t_{RRD} (row-to-row delay), restricting the frequency of ACTIVATE commands.
- **Bus turnaround delays**, enforcing separation between read and write bursts on bidirectional buses.
- **Burst alignment and write-masking rules**, constraining fine-grained data manipulation.
- **Power-state recovery latencies**, incurred when exiting power-down or clock-gated modes.

Protocol-specific considerations include:

- **LPDDR4/5**, which introduces gear ratios and deep command pipelines that limit rapid pattern injection.
- **HBM**, which employs pseudo-channels and vault-level arbitration affecting row locality.
- **CXL**, where cache-coherent memory access and host-device latency obscure deterministic fault activation.

Implications for test generation:

- Test scheduling must explicitly enforce t_{FAW} and t_{RRD} spacing for adjacent-bank activation.
- Row-hammer diagnostics must align with t_{REFI} (refresh interval) to avoid masking disturbance effects.
- Multi-initiator AXI tests must account for arbitration and transaction ID semantics to preserve coverage determinism.

4.9.3 Limitations on Observability

Protocol-mediated access significantly limits fault observability:

- **Restricted access granularity**, often exposing memory only at cache-line or burst levels.
- **Partial write masking**, which can conceal bit-level or word-level defects.
- **Inline ECC correction**, silently repairing single-bit errors before software can observe them.
- **Buffering, reordering, and coalescing**, which obscure temporal fault signatures and introduce aliasing.

To mitigate these effects, ECC-syndrome-driven diagnostic loops were incorporated into Optimal_Test.

By monitoring ECC correction activity during symbolic test execution, latent and intermittent faults can be detected even when corrected transparently by the controller.

This transforms inline ECC from a masking mechanism into an auxiliary diagnostic sensor.

4.9.4 Address Mapping and Interleaving

Modern memory subsystems employ sophisticated address-mapping strategies, including:

- **Bank address scrambling**, reducing hot-spot formation.
- **Row interleaving**, distributing sequential rows across banks.
- **Channel striping**, maximizing bandwidth utilization.
- **Internal scrambling**, supporting security and wear leveling.

These mechanisms break the assumption of linear correspondence between logical and physical addresses, complicating classical test vector application.

To address this, Optimal_Test implements interface-aware adaptation mechanisms:

- **Translation layers** mapping symbolic physical models to logical interface addresses.
- **Virtual-to-physical remap prediction**, using access traces to infer interleaving behavior.
- **Scramble-detection heuristics**, identifying anomalous access correlations and reclassifying coverage zones.

These methods enable coverage validation even when physical address visibility is limited or indirect.

4.9.5 Embedded Access Protocols (AXI, AMBA)

In embedded systems, memory access is typically mediated by high-level interconnects such as AXI, AHB/APB, Wishbone, or TileLink. While optimized for throughput and modularity, these protocols constrain diagnostic injection:

- **Burst coalescence**, obscuring fine-grained access intent.
- **Out-of-order completion**, complicating deterministic sequencing.
- **Transaction ID tagging**, requiring careful bookkeeping to preserve test semantics.
- **Limited control of low-level timing**, preventing direct manipulation of memory command primitives.

Adaptive strategies include:

- Preserving transaction ordering via consistent ID assignment.
- Throttling burst length to prevent excessive write aggregation.
- Leveraging debug bridges or test wrappers to inject symbolic operator sequences under restricted conditions.

4.9.6 Test Generation under Protocol Awareness

To operate effectively under protocol constraints, an interface-aware test generation methodology was developed with the following features:

- **Command-aware March translation**, compiling symbolic patterns into protocol-level sequences while preserving semantic intent.
- **Protocol-specific fault modeling**, extending fault classes to include burst corruption, masking artifacts, and timing aliasing.
- **Scheduling-aware symbolic compilation**, embedding protocol metadata (wait states, activation windows, power transitions) directly into operator translation.

Example protocol-aware compilation:

$$\uparrow(\mathrm{ACT}, \mathrm{WAIT}_{(\mathrm{tRCD})}); \uparrow(\mathrm{WR}, \mathrm{MASKED}); \downarrow(\mathrm{PRE}, \mathrm{WAIT}_{(\mathrm{tRP})});$$

This sequence explicitly encodes protocol timing and masking behavior, ensuring correct execution under interface constraints.

Additionally, simulated corner cases—such as access stalls, retry loops, and power-domain transitions—are incorporated to expose faults in latency-sensitive and low-power operating regimes.

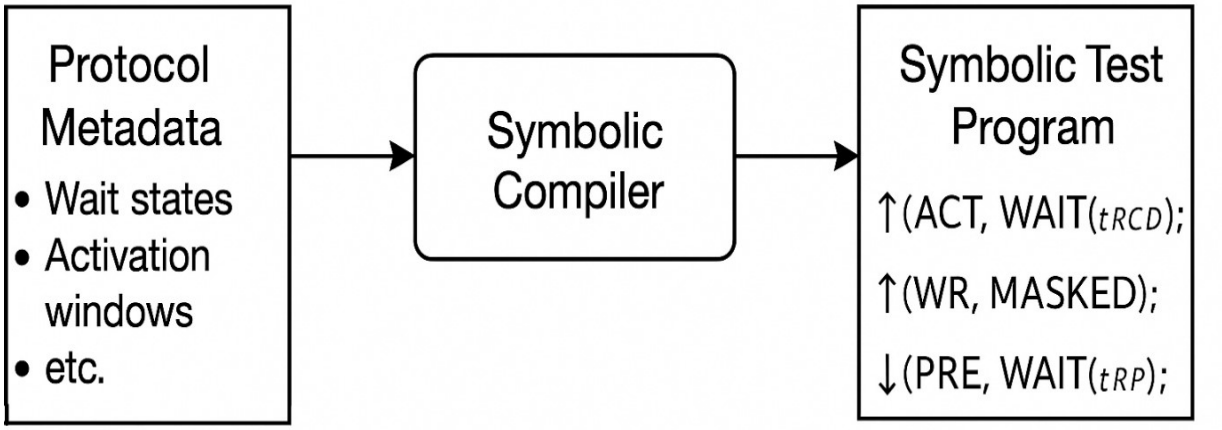

Figure 4.4—Symbolic test compilation through DDR command constraints

Figure 4.4 illustrates the compilation pathway through which **symbolic test programs** are adapted to protocol-bound memory interfaces via a **symbolic, timing-aware compilation framework**.

On the left, **protocol metadata**—including wait states, activation windows, and interface-specific timing constraints—is provided as structured input. The **symbolic compiler** (central block) integrates this metadata directly into symbolic test operators, enforcing compliance with interface-level sequencing and timing rules.

The resulting symbolic test program (right block) expresses high-level diagnostic intent using protocol-specific commands such as **ACTIVATE**, **WRITE**, and **PRECHARGE**, each annotated with explicit timing constraints (e.g., $WAIT_{(tRCD)}$, $WAIT_{(tRP)}$) and access modifiers (e.g., MASKED for burst alignment and partial writes).

This translation enables abstract test patterns—originally defined independently of physical interfaces—to execute correctly on real systems where direct row- and column-level access is obscured by command-level protocols such as DDR, LPDDR, and HBM.

By embedding protocol awareness at the compilation stage, the framework generates test sequences that are both diagnostically meaningful and strictly compliant with real-world interface restrictions, supporting in-system testing and run-time diagnostics.

4.9.7 Summary

Interface-constrained memory testing requires more than direct reuse of traditional March or pattern-based algorithms. It demands a protocol-aware synthesis pipeline grounded in symbolic abstraction (Section 4.7.1) and executable through the Optimal_Test architecture (Section 4.7.4).

By compiling symbolic test sequences into command-level, protocol-compliant flows (Figure 4.4), diagnostic execution respects the timing, ordering, masking, and power-state constraints inherent to modern memory interfaces such as DDR, LPDDR, HBM, and embedded interconnects.

This methodology preserves fault-activation intent while leveraging protocol features—most notably inline ECC feedback—to improve observability under constrained access conditions (ECC-aware monitoring discussed in **Section 4.9.3** and ECC mechanisms in **Chapter 5**). In doing so, it bridges the gap between idealized fault-coverage models and practical in-system execution, ensuring diagnostic completeness without violating operational constraints.

Ultimately, interface-aware adaptation reinforces the closed-loop, adaptive diagnostic paradigm introduced by the U–Y hybrid model (Section 4.7.3) and prepares the groundwork for ECC-driven runtime fault resilience.

4.10 Summary and Transition to ECC

In contemporary memory systems, testing exists at the intersection of structural integrity**,** algorithmic rigor**,** interface compliance**,** and diagnostic observability. Classical methodologies—such as March tests and pattern-based diagnostics—remain essential building blocks, yet they are insufficient when applied in isolation.

The increasing density, heterogeneity, and operational complexity of modern memory technologies demand hybrid, symbolically driven, protocol-aware, and coverage-optimized testing strategies capable of addressing fault behaviors that manifest across spatial, temporal, and operational domains.

This evolution in testing methodology naturally leads to **Error Detection and Correction (ECC)**, which complements diagnostic testing by providing continuous fault monitoring and mitigation during normal memory operation.

4.10.1 Summary of Key Concepts

This chapter establishes a comprehensive framework for advanced memory testing, spanning classical, symbolic, and interface-aware methodologies, and sets the foundation for integrating resilience mechanisms such as ECC:

- **March Tests (Section 4.3)**
  - Structured and exhaustive address traversal for reliable detection of stuck-at and transition faults.
- **Pattern-Based Tests (Sections 4.4)**
  - Exposure of data-dependent behavior, coupling effects, and layout-driven vulnerabilities.
- **Advanced Testing Algorithms (Sections 4.5)**
  - Sliding-window scans, burst-aligned sequences, and U–Y hybrid decomposition for conditional and composite fault activation.
- **Test Metrics (Section 4.6)**

    - Fault coverage, diagnostic resolution, aliasing resistance, execution cost, and adaptability as guiding design criteria.
- **Original Contributions (Sections 4.7.1–4.7.4)**
    - Symbolic operator modeling, U–Y graph decomposition, and the Optimal_Test framework—an adaptive, programmable, high-resolution diagnostic engine.
- **BIST Architectures (Section 4.8)**
    - Embedded, in-silicon diagnostic controllers enhanced with symbolic decomposition and adaptive execution.
- **Interface-Constrained Testing (Section 4.9)**
    - Translation of abstract diagnostic flows into protocol-compliant command sequences, preserving fault activation under real-world access constraints.

Together, these components form a **multi-layered diagnostic strategy** that is scalable to emerging memory technologies, adaptable to in-field conditions, and foundational for ECC-based resilience.

4.10.2 Toward Built-In Resilience and Fault Correction

Even the most advanced test methodologies—symbolic (Section 4.7.1), BIST-enhanced (Section 4.8), or interface-aware (Section 4.9)—cannot guarantee fault-free memory operation over an entire product lifecycle. As scaling, aging, and environmental stress increase fault incidence, systems must evolve beyond detection-only architectures.

This evolution leads to **Error Detection and Correction Codes (ECC)**, which operate as a persistent, active defense layer—continuously monitoring memory transactions, detecting anomalies, and correcting both transient and permanent faults in real time.

The next chapter examines ECC in depth, covering:

- principles of ECC logic, syndrome generation, and detection theory;
- common coding schemes (parity, Hamming, BCH, Reed–Solomon, LDPC) and their fault-environment trade-offs;
- decoding mechanisms and correction vector application;
- architectural trade-offs among correction strength, latency, and hardware overhead;
- integration strategies that fuse ECC with symbolic test workflows (Section 4.7.4), transforming ECC from a passive safeguard into an **active diagnostic sensor**;
- original contributions involving syndrome-aware diagnostics and ECC-driven pattern adaptation for enhanced localization, coverage, and runtime monitoring.

This transition marks the progression from detection toward **resilience**, enabling systems not only to identify faults but to recover from them under continuous operation.

4.10.3 Conceptual Synthesis and Outlook

The trajectory of memory testing presented in this chapter reflects a fundamental shift—from static, algorithm-centric diagnostics toward adaptive, symbolically driven, protocol-aware test ecosystems**.**

Symbolic operator modeling (Section 4.7.1), U–Y hybrid decomposition (Section 4.7.3), and the Optimal_Test framework (Section 4.7.4) redefine how fault models are translated into executable test logic. Extended through BIST augmentation (Section 4.8) and interface-constrained execution (Section 4.9), these techniques deliver diagnostics that are context-aware, high-resolution, and dynamically reconfigurable.

Testing thus becomes a **continuous, system-integrated process**, evolving alongside the memory hardware it protects. As the discussion transitions into Chapter 5 on ECC, the groundwork is complete for unifying detection, correction, and adaptive test intelligence into a cohesive, resilient memory-reliability architecture.

This evolution reflects the growing complexity of modern memory subsystems and the need for diagnostics that scale with architectural and technological advances. Rather than relying solely on predetermined algorithmic sequences, contemporary approaches emphasize flexible modeling, adaptive test generation, and system-aware validation.

Such capabilities enable diagnostic infrastructures to respond to emerging fault mechanisms and operational constraints with greater precision. Ultimately, the integration of symbolic modeling, adaptive optimization, and reliability mechanisms forms the foundation for next-generation memory validation frameworks. These principles guide the subsequent exploration of error detection and correction mechanisms in the following chapter.

Part III — ECC & Data Integrity

Chapter 5: Error Detection and Correction Codes (ECC): From Parity to Syndrome-Aware Diagnostics

Error Detection and Correction Codes (ECC) have evolved far beyond their original role as simple parity mechanisms for detecting single-bit errors. In contemporary memory architectures, ECC constitutes a critical layer of fault resilience, enabling systems to detect, localize, and—where supported—correct errors dynamically during operation.

From classical Hamming codes to advanced multi-bit correction schemes such as BCH and Reed–Solomon, ECC algorithms are deeply integrated into both hardware and firmware layers, providing protection against transient soft errors, retention-related failures, and aggressive disturbance phenomena such as Rowhammer.

This chapter examines the architectural integration of ECC, the mathematical foundations underlying widely deployed coding techniques, and their expanding role in adaptive diagnostics. Particular emphasis is placed on syndrome-aware diagnostics, in which ECC outputs are leveraged not only for correction but also as a source of real-time diagnostic intelligence—enabling fault prediction, adaptive test scheduling, and self-healing strategies in high-reliability memory subsystems.

5.1 Introduction: From Fault Detection to Fault Resilience

As semiconductor memory technologies scale toward ultra-dense geometries and operate under increasingly constrained voltage and timing margins, the incidence of transient, soft, and intermittent faults rises sharply. Conventional manufacturing-time test methodologies, while effective at detecting hard structural defects, often fail to capture the evolving error behavior of deployed systems—particularly in safety-critical, long-lifetime, or high-availability environments.

ECC forms a cornerstone of modern fault-tolerant design by enabling not only error detection but also in-situ correction of specific error patterns. By encoding user data with carefully computed redundancy bits, ECC mechanisms allow systems to identify and correct bit-level errors—often transparently and without disrupting normal operation.

This capability is indispensable in domains where even a single-bit corruption may propagate into catastrophic failure, such as aerospace avionics, medical instrumentation, and large-scale high-performance computing infrastructures.

Within the Optimal_Test framework, I extended the traditional role of ECC from a passive correction mechanism to an active diagnostic feedback channel. Real-time analysis of ECC syndromes enables inference of fault classes, localization of error-prone address regions, and dynamic triggering of targeted re-tests or adaptive repair actions.

This syndrome-aware diagnostic approach bridges the gap between fault masking and proactive fault management, forming the technical foundation for partially self-healing memory subsystems.

5.2 Core Concepts and Terminology

5.2.1 Code Word

A **code word** is the composite data unit produced by an ECC encoder. It consists of the original information bits and additional redundancy bits introduced for error detection and correction. Formally, the total length n of a code word is defined as:

$$n = k + r$$

where:

- k: Number of original data bits.
- r: Number of check bits added for error protection.
- n: Total code word length.

This augmented representation ensures that deviations from valid code words—whether introduced during storage, transmission, or retrieval—can be systematically detected and, within the correction capability of the code, corrected.

5.2.2 Hamming Distance

The **Hamming distance** d of a code is defined as the minimum number of bit positions in which any two valid code words differ. This parameter fundamentally determines the error detection and correction capabilities of the ECC scheme:

- **Error detection**: up to $d-1$ bit errors can be reliably detected
- **Error correction**: up to $\left\lfloor \frac{d-1}{2} \right\rfloor$ bit errors can be corrected

For example, a code with $d = 3$ can detect all double-bit errors and correct any single-bit error. This principle underpins widely adopted schemes such as Hamming codes, which are commonly deployed in Single Error Correction, Double Error Detection (SECDED) configurations.

5.2.3 Syndrome

A **syndrome** is a diagnostic vector generated during the ECC decoding process. It is computed by multiplying the received code word by the transpose of the parity-check matrix H:

$$S=H.R^T$$

where:

- S is the syndrome vector
- H is the parity-check matrix
- R is the received code word

Interpretation of the syndrome follows directly:

- $S = 0$: no detectable error; the code word is valid
- $S \neq 0$: error detected; the syndrome encodes information about error location and, in some codes, error type.

This formal definition provides the mathematical foundation for the extended diagnostic applications developed later in Section 5.4, where syndrome behavior is exploited for fault classification, aging analysis, and adaptive test orchestration.

5.3 Common ECC Schemes

Error-Correcting Codes constitute a foundational component of modern memory reliability engineering. This section examines commonly deployed ECC schemes, beginning with minimal single-bit parity mechanisms and progressing toward structured linear block codes such as Hamming codes.

Each scheme is analyzed in terms of its operational principle, achievable error coverage, and the trade-offs between implementation complexity, latency, storage overhead, and protection capability.

5.3.1 Parity Codes (Even and Odd Parity)

Parity codes represent the most elementary form of error detection in digital memory and communication systems. A single parity bit is appended to each data word to indicate whether the total number of logical '1' bits in the word satisfies an even or odd parity condition.

Operation

For a data word of length k, $D = d1d2 \ldots d_k$, the parity bit p is computed as:

$$p = \left(\sum_{i=1}^{k} d_i \right) mod\ 2$$

Parity interpretation depends on the selected convention:

- **Even parity**:
  $p = 1$ if the number of logical '1's in D is odd; otherwise $p = 0$.
  The total number of '1's in the augmented code word is even.
- **Odd parity**:
  $p = 1$ if the number of logical '1's in D is even; otherwise $p = 0$.
  The total number of '1's in the augmented code word is odd.

During verification, the parity of the received word is recomputed and compared against the stored parity bit to determine whether an error is present.

Error Detection Capabilities

- Reliably detects any single-bit error occurring within the code word.
- Detects any error pattern that flips an odd number of bits.
- Fails to detect errors involving an even number of bit flips, due to parity cancellation.

- Provides no error correction capability.

Typical Use Cases

- Legacy computer architectures and low-complexity embedded controllers.
- Simple serial communication protocols (e.g., UART, legacy peripheral links).
- Cache-line or register integrity checks where minimal storage overhead and negligible decoding latency are prioritized over correction strength.

Parity coding remains relevant in constrained environments and as a building block for more advanced ECC schemes, but its inability to correct errors or detect multi-bit even-weight faults limits its applicability in high-reliability memory systems.

5.3.2 Hamming Codes (SEC and SECDED)

Hamming codes constitute one of the earliest and most widely deployed classes of linear block codes for error correction in digital memory systems.

They provide **single-error correction (SEC)** and, when extended with an additional global parity bit, **double-error detection (DED)**. The extended configuration is commonly referred to as **SECDED**.

- *Error Handling Capability*
  A standard Hamming code is capable of correcting any single-bit error occurring anywhere within the code word, including errors affecting parity bits. When augmented with an overall parity bit, the code additionally detects all double-bit errors, although such errors remain uncorrectable.
- *Efficiency and Structural Optimality*
  Hamming codes achieve single-bit correction with the minimum number of parity bits required for a given number of data bits. For a data word of length k, the number of parity bits r must satisfy the inequality:

$$2^r \geq k + r + 1$$

This condition ensures that each possible single-bit error—including errors in data bits and parity bits—corresponds to a unique non-zero syndrome vector. As a result, the decoder can unambiguously identify the error location.

Example: Hamming (7,4)

The Hamming (7,4) code encodes four data bits using three parity bits, producing a seven-bit code word. Parity bits are placed at positions corresponding to powers of two (1, 2, and 4), while data bits occupy the remaining positions.

Table 5.1—Example Hamming (7,4) code words and syndrome outcomes

Data Bits	Code Word	Syndrome Result
1011	0111011	000 (No Error Detected)
1011	0111111	101 (Error at Bit 5 position)

Encoding

During encoding, parity bits are computed over predefined subsets of bit positions determined by the binary index representation of each code-word position. This structured placement enables systematic error localization during decoding.

Decoding and Syndrome Interpretation

At the receiver, parity checks are recomputed and combined to form the syndrome vector S. The syndrome is interpreted as follows:

- $S = 000$: no error detected; the code word is accepted as valid.
- $S \neq 000$: a single-bit error is detected at the position indicated by the binary value of S; correction is performed by inverting the corresponding bit.

This mechanism enables transparent, on-the-fly correction without interrupting normal system operation.

Extension to SECDED

By appending an additional overall parity bit, the Hamming code is extended to support double-error detection. In this configuration:

- A non-zero syndrome combined with incorrect overall parity indicates a correctable single-bit error.
- A non-zero syndrome combined with correct overall parity indicates a double-bit error, which is detectable but not correctable.
- A zero syndrome combined with incorrect overall parity indicates an error in the overall parity bit itself.

This extension significantly improves diagnostic robustness and forms the basis of ECC protection in modern memory controllers.

5.3.3 BCH Codes (Bose–Chaudhuri–Hocquenghem)

BCH codes constitute a broad class of cyclic linear block codes designed to correct multiple random bit errors within a single code word. In contrast to Hamming codes, which are limited to single-error correction, BCH codes are parameterized to correct an arbitrary number t of random bit errors, making them suitable for environments with elevated noise levels and aging-induced fault rates.

Error Handling Capability

A BCH code configured for error-correcting capability t can:

- Correct up to t random bit errors per code word.
- Detect a larger number of errors, depending on the specific code construction and decoder implementation.

The minimum Hamming distance d_{min} of a BCH code satisfies:

$$d_{min} > 2t + 1$$

ensuring correctability of all error patterns up to weight t.

Structural and Operational Characteristics

BCH codes are defined over finite fields and constructed using generator polynomials with roots chosen to guarantee the desired minimum distance. Compared to Hamming codes, BCH codes introduce higher redundancy overhead, but offer fine-grained configurability in terms of correction strength.

Decoding complexity increases with t, as syndrome computation and error-location polynomial solving become more involved. Nevertheless, practical hardware implementations employing parallelism and pipelined algebraic decoders significantly mitigate latency penalties.

Typical Use Cases

- NAND flash memory, where wear-out mechanisms and program/erase cycling induce random multi-bit errors.
- Satellite and spaceborne communication systems exposed to cosmic radiation.
- Aerospace-grade and mission-critical DRAM modules requiring multi-bit fault tolerance beyond SECDED capabilities.

5.3.4 Reed–Solomon Codes

Reed–Solomon (RS) codes are non-binary linear block codes that operate on multi-bit symbols rather than individual bits. This symbolic structure makes them particularly effective at correcting burst errors—clusters of adjacent bit corruptions that often defeat bit-oriented codes. An $RS(n, k)$ code encodes k data symbols into n total symbols, allowing correction of up to:

$$t = \frac{n - k}{2}$$

symbol errors per code word.

Error Handling Capability

- Corrects burst errors affecting entire symbols.
- Particularly effective when errors are spatially or temporally correlated rather than uniformly random.

Structural Characteristics

Reed–Solomon codes operate over Galois fields $GF(2^m)$, where each symbol consists of m bits (e.g., $GF(2^8)$ for 8-bit symbols). This symbolic abstraction enables a single symbol error to represent multiple corrupted bits.

The algebraic decoding process involves polynomial evaluation and interpolation, resulting in higher computational complexity than binary codes. In practice, this overhead is addressed through dedicated hardware decoders and optimized finite-field arithmetic units.

Typical Use Cases

- Optical storage media (CD, DVD, Blu-ray) for recovery from scratches and localized defects.
- QR codes and two-dimensional barcodes.
- RAID storage systems for parity-based data recovery.
- Deep-space communication links subject to solar-induced burst error phenomena.

5.3.5 LDPC (Low-Density Parity-Check) Codes

Low-Density Parity-Check (LDPC) codes represent a modern class of capacity-approaching error-correcting codes, achieving performance close to the Shannon limit in high-throughput and high-reliability applications. They are defined by sparse parity-check matrices and decoded using iterative probabilistic algorithms.

Error Handling Capability

LDPC codes can correct a large number of random bit errors with high efficiency, particularly in long code-word configurations. Their performance improves with increased block length and iteration count, subject to latency and power constraints.

Structural and Algorithmic Characteristics

The defining feature of LDPC codes is the sparsity of the parity-check matrix, which enables efficient message passing between variable nodes and check nodes during decoding. Common decoding algorithms include belief propagation and sum–product methods.

Unlike algebraic decoders used in BCH or RS codes, LDPC decoding relies on iterative convergence. While this introduces non-deterministic decoding latency, it allows exceptional correction strength with comparatively low redundancy overhead.

LDPC codes are highly parallelizable, making them well-suited for hardware acceleration in high-bandwidth systems.

Typical Use Cases

- Fifth-generation (5G) mobile networks and advanced wireless standards.
- Solid-state drives (SSDs) for mitigating dense multi-bit NAND flash errors.
- High-performance ECC-enabled DRAM systems deployed in large-scale data centers and cloud infrastructures.

5.4 Syndrome Decoding and Fault Localization

Building on the definition introduced in Section 5.2.3, syndrome decoding constitutes the critical bridge between error detection and error correction in ECC-enabled memory systems. The syndrome vector, generated by applying the parity-check matrix H to the received code word r, encodes actionable diagnostic information regarding the presence, location, and—depending on the ECC scheme—the structure of an error.

The interpretation of the syndrome is as follows:

- $S = 000$: no error is detected; the received code word satisfies all parity constraints.
- $S \neq 000$: an error is detected; the syndrome either uniquely identifies the erroneous bit (in single-error-correcting codes such as Hamming) or constrains the admissible error vector (in multi-error-correcting codes such as BCH or LDPC).

In SEC codes, the syndrome maps directly to the index of the faulty bit. In more advanced codes, the syndrome participates in algebraic or iterative decoding procedures, progressively narrowing the error location across larger code words or symbol groups.

Syndrome Analysis for Diagnostics

In my adaptive diagnostic research, syndromes were treated not merely as correction aids but as diagnostic signatures. This interpretation enabled several higher-level diagnostic mechanisms:

- Syndrome-driven test escalation, where recurring or atypical syndrome patterns triggered the activation of more aggressive or specialized test sequences.
- Partial fault isolation, achieved by correlating repeated syndrome values with specific physical addresses or regions, allowing identification of fault-prone zones within the memory array.
- Predictive diagnostics, where temporal analysis of syndrome histories revealed emerging degradation trends, enabling preemptive intervention and in-field self-healing actions.

Within the Optimal_Test framework, syndrome vectors were continuously monitored and analyzed. Rather than discarding syndromes after correction, the framework accumulated them as structured diagnostic data, refining test vector selection, focusing traversal on suspect regions, and initiating targeted re-testing. This approach supports syndrome-driven fault localization and forms a cornerstone of partially autonomous, self-healing memory architectures.

5.4.1 Syndrome Generation

To formally define syndrome generation in error detection and correction systems, let:

- H denote the parity-check matrix of dimension $r \times n$,
- r denote the received code word, represented as an n-bit row vector,
- s denote the syndrome vector of dimension r.

The syndrome is computed as:

$$s = H.r^T$$

where r^T is the transpose of the received code word. All operations are performed over the Galois field $GF(2)$, i.e., modulo-2 arithmetic.

The resulting syndrome vector encodes essential information about error presence and localization:

- If $s = 000$, the received code word satisfies all parity constraints imposed by H and is therefore considered valid.
- If $s \neq 000$, an error exists; the syndrome serves as a structured fingerprint of the fault, uniquely identifying the erroneous bit position in single-error-correcting codes or constraining the feasible error set in multi-error-correcting schemes.

In my work, syndrome vectors were integrated directly into the Optimal_Test diagnostic pipeline. Beyond their conventional role in real-time correction, they were used as inputs to adaptive fault isolation, symbolic test refinement, and predictive fault analytics. This integration enables ECC-protected memory systems to evolve from passive error masking toward proactive, feedback-driven fault management.

5.4.2 Hamming Syndrome Decoding Example

Consider a 7-bit Hamming (7,4) code. The parity-check matrix H is defined as:

$$H = \begin{bmatrix} 1 & 0 & 1 & 0 & 1 & 0 & 1 \\ 0 & 1 & 1 & 0 & 0 & 1 & 1 \\ 0 & 0 & 0 & 1 & 1 & 1 & 1 \end{bmatrix}$$

Example Scenario

Assume that the transmitted code word is:

$$c = [1\ 1\ 1\ 1\ 0\ 1\ 1]$$

and that a single-bit error flips bit position 7 during transmission, yielding the received word:

$$r = [1\ 0\ 1\ 1\ 0\ 1\ 1]$$

Syndrome Calculation

The syndrome vector is computed using the standard relation:

$$s = H.r^T\ mod\ 2:$$

Evaluating this expression yields:

$$s = \begin{bmatrix} 1 \\ 1 \\ 1 \end{bmatrix}$$

Interpretation

The syndrome vector $s = 111$ corresponds directly to column 7 of the parity-check matrix H. In a Hamming (7,4) code, each non-zero syndrome uniquely maps to the index of the erroneous bit. Therefore, the decoder correctly identifies bit position 7 as faulty.

Error Correction

Once localized, the error is corrected by inverting the identified bit:

$$[1\ 0\ 1\ 1\ 0\ 1\ 1] \rightarrow [1\ 0\ 1\ 1\ 0\ 1\ 0]$$

This operation restores the original transmitted code word and re-establishes satisfaction of all parity constraints.

Deterministic Localization Property

This example illustrates a defining property of single-error-correcting Hamming codes: each non-zero syndrome uniquely corresponds to one column of the parity-check matrix, enabling deterministic error localization and correction with minimal decoding latency.

Syndrome Utilization in Optimal_Test

Within the Optimal_Test framework, syndrome vectors are abstracted into symbolic fault tokens rather than being discarded after correction. Recurrent occurrences of identical syndromes are interpreted as indicators of localized degradation, triggering escalation from low-resolution March sequences to higher-resolution hybrid diagnostic tests.

By correlating syndrome tokens with physical address regions, the framework supports targeted re-testing, predictive fault localization, and partially autonomous self-healing behavior in ECC-protected memory systems.

5.4.3 Multi-Bit and Burst Syndrome Complexity

Error-Correcting Codes designed to address multi-bit and burst errors introduce substantially greater complexity into syndrome decoding than the direct bit-to-syndrome mapping used in single-error-correcting schemes. In such codes, the syndrome no longer identifies a unique bit position but instead constrains a space of possible error vectors that must be resolved through algebraic or iterative procedures.

SECDED (Single Error Correction, Double Error Detection)

In SECDED codes, the syndrome maintains a one-to-one correspondence with single-bit error locations, while an additional global parity bit enables reliable detection of double-bit errors. A zero syndrome ($S = 0$) indicates that the received code word satisfies all parity constraints. A non-zero syndrome combined with incorrect overall parity identifies a correctable single-bit error, whereas a non-zero syndrome with correct overall parity signals an uncorrectable double-bit error.

BCH and Reed–Solomon Codes

For multi-bit error correction, syndromes are interpreted as coefficients of error-locator and error-evaluator polynomials defined over finite fields. Decoding typically involves several structured stages:

- The Berlekamp–Massey algorithm, which determines the shortest linear feedback shift register capable of generating the observed syndrome sequence.

- The extended Euclidean algorithm, which computes the error-locator and error-evaluator polynomials.
- A Chien search, which evaluates the error-locator polynomial across all field elements to identify error locations.

This process enables correction of up to t random errors for a t-error-correcting code, but at the cost of increased computational complexity.

LDPC (Low-Density Parity-Check) Codes

In LDPC decoding, the syndrome initializes an iterative message-passing process over a Tanner graph representation of the parity-check matrix. Algorithms such as belief propagation or min-sum iteratively update bit likelihoods based on parity constraints until convergence is reached or a predefined iteration limit is exceeded.

Error localization emerges probabilistically rather than deterministically, and correction success depends on graph structure, noise conditions, and convergence behavior.

Trade-offs in Syndrome-Based Decoding

The increased expressive power of multi-bit and burst-error ECC schemes introduces several engineering trade-offs:

- **Decoding latency** increases due to polynomial solving or iterative convergence.
- **Hardware complexity** grows significantly, particularly for finite-field arithmetic and graph traversal logic.
- **Correctability thresholds** are finite; error floors and convergence failures may occur under high-noise or adversarial conditions.
- **Diagnostic resolution** improves with richer syndrome data but requires sophisticated mapping between syndrome patterns and physical fault mechanisms.

In the Optimal_Test system, multi-bit syndrome vectors were not treated solely as correction inputs. Instead, they were retained as diagnostic fingerprints, enabling predictive analytics, adaptive test scheduling, and localized stress testing in ECC-protected memory arrays. This integration enhanced both fault coverage and long-term reliability by merging conventional ECC correction with proactive diagnostic intelligence.

5.4.4 Syndrome as a Diagnostic Signal

Although Error-Correcting Codes are traditionally deployed as passive protection mechanisms that silently correct errors during normal operation, the syndrome information they generate constitutes a rich diagnostic signal when exposed to higher-level analysis.

Systematic observation of ECC syndromes enables insight into fault dynamics, spatial localization, and long-term degradation trends that are otherwise invisible to conventional read–verify testing.
In my research, ECC syndromes were explicitly elevated from internal correction artifacts to diagnostic primitives.

Rather than being discarded after correction, syndrome vectors were retained, classified, and correlated across time and address space. This enabled ECC to function not only as a correction layer but also as an active diagnostic sensor within the memory subsystem.

The principal syndrome-driven diagnostic techniques developed and integrated into the Optimal_Test framework are summarized in Table 5.2.

Table 5.2—Syndrome-Driven Diagnostic Techniques

Technique	Description
Syndrome History Buffers	Continuously log and analyze recurring syndrome patterns to identify persistent bit flips or memory regions prone to intermittent faults. Temporal trend analysis reveals slowly degrading cells and emerging fault hotspots prior to functional failure.
ECC-Aware Fault Injection	Introduce controlled error patterns and verify that the resulting syndromes align with theoretical ECC predictions. This technique validates ECC coverage assumptions and uncovers latent decoder vulnerabilities under realistic operating conditions.
Adaptive Pattern Escalation	Use specific syndrome signatures as triggers for deploying more aggressive diagnostic sequences, such as hybrid March–pattern tests, or for activating built-in redundancy mechanisms including spare rows or columns.
Localization Hints	Correlate observed syndrome patterns with physical fault domains (e.g., bitline defects, wordline failures, or inter-cell coupling) to enable fine-grained fault isolation and targeted repair actions.

Within the Optimal_Test framework, syndrome vectors were abstracted into symbolic diagnostic tokens and fed back into the test engine. These tokens influenced test-flow refinement, traversal prioritization, and pattern selection, allowing diagnostic intensity to scale dynamically with observed fault behavior.

This closed-loop interaction bridged real-time error correction with long-term reliability engineering, reinforcing ECC as both a protective mechanism and an investigative tool.

By treating ECC syndromes as first-class diagnostic signals rather than transient correction byproducts, the memory system gains the ability to detect emerging failures early, localize

them accurately, and initiate targeted mitigation strategies—forming a critical foundation for predictive diagnostics and partially self-healing memory architectures.

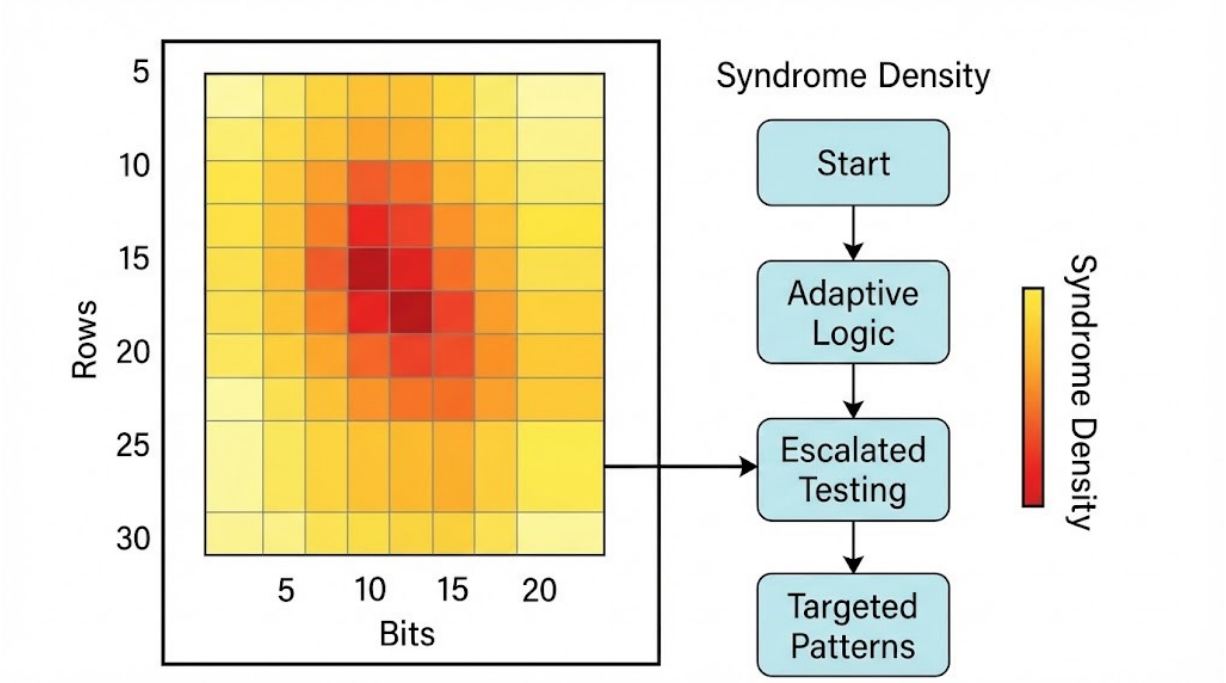

Figure 5.1—Syndrome distribution heatmap with adaptive test flow overlay

Figure 5.1 illustrates the use of ECC syndrome density as a feedback signal for adaptive diagnostic control.

The heatmap on the left represents the spatial distribution of recurrent syndromes across memory rows and bit positions. Darker regions indicate elevated syndrome density, corresponding to locations exhibiting repeated correction activity or marginal behavior.

The flow diagram on the right depicts the diagnostic control loop driven by this information. Syndrome acquisition initiates the process (Start), after which a symbolic decision layer (Adaptive Logic) evaluates spatial and temporal syndrome characteristics. Based on this evaluation, the diagnostic flow diverges into one of two paths:

- Escalated Testing, invoking higher-intensity diagnostic sequences to expand fault activation coverage.
- Targeted Patterns, applying localized verification patterns to rapidly confirm or reject suspected weak regions.

The arrow linking high-density syndrome regions to the Escalated Testing stage emphasizes the closed-loop nature of the methodology: observed error behavior directly influences subsequent test depth and scope.

This feedback-driven approach exemplifies context-aware diagnostics and integrates naturally with symbolic test synthesis frameworks such as Optimal_Test, improving fault localization accuracy and enabling predictive maintenance in ECC-protected memory systems.

5.4.5 Fault versus Error Differentiation

In memory diagnostics, a clear distinction must be maintained between errors and faults, as the two represent fundamentally different phenomena:

- Error: An observable deviation in stored or retrieved data, such as a bit flip detected during a read operation.
- Fault: The underlying physical defect or marginal condition responsible for generating errors, such as charge leakage in a DRAM cell, capacitive coupling between adjacent interconnects, or weakened sense amplifier margins.

ECC mechanisms are highly effective at detecting and, in many cases, correcting errors in real time. However, ECC alone does not directly expose the physical origin of those errors. Without additional analysis, corrected errors may leave no externally visible trace, allowing latent defects to persist undetected.

To bridge this gap, a syndrome-to-fault inference framework was developed within the Optimal_Test system. This framework aggregates syndrome observations across time, address space, and operating conditions, and correlates them with symbolic test responses and empirical failure data.

By analyzing recurring syndrome vectors and their spatial clustering, the system probabilistically ranks likely fault locations and fault classes, even when ECC correction suppresses user-visible errors.

This capability enables meaningful fault localization in ECC-protected environments and supports predictive maintenance strategies by identifying degrading regions before functional failure thresholds are exceeded.

5.5 ECC Design Trade-Offs and Hardware Integration

The design and integration of ECC architectures in modern memory systems require careful balancing of multiple, often competing, engineering objectives:

- Fault coverage
  Stronger ECC schemes, such as BCH, Reed–Solomon, and LDPC, extend protection from single-bit errors to multi-bit and burst error patterns, improving resilience under aggressive scaling and noisy operating conditions.
- Hardware complexity
  Multi-bit correction demands significant logic resources for syndrome decoding, polynomial arithmetic, or iterative message passing. These requirements directly impact silicon area, design effort, and verification complexity.
- Latency impact
  Advanced decoding algorithms introduce additional latency, which may be unacceptable in real-time, low-latency, or high-frequency memory access paths.
- Power overhead
  Continuous ECC encoding, decoding, and background scrubbing contribute to increased dynamic power consumption, particularly in high-bandwidth or always-on systems.

- System-level resilience

  ECC selection must align with the system's reliability objectives, whether prioritizing maximum uptime in data centers or deterministic fault containment in safety-critical and mission-critical platforms.

Within the Optimal_Test framework, ECC evaluation extends beyond raw correction capability to include its impact on fault observability, test transparency, and diagnostic leverage. Stronger ECC schemes may completely mask early degradation signatures, delaying fault discovery, whereas simpler schemes such as SECDED often expose richer syndrome information at the cost of reduced correction strength.

This trade-off is not purely negative: in diagnostic-aware systems, controlled visibility of correctable errors can significantly enhance early fault detection and localization. Accordingly, ECC integration must be co-designed with diagnostic objectives, ensuring that correction strength, observability, and symbolic test interaction are jointly optimized.

The remainder of this section examines these trade-offs in detail, focusing on practical integration strategies across the memory hierarchy—from on-die DRAM implementations to system-level controllers coordinating heterogeneous memory stacks.

5.5.1 Coverage versus Complexity

Error-Correcting Codes (ECC) differ significantly in correction capability, redundancy overhead, decoding latency, and implementation cost. Selecting an appropriate ECC scheme therefore requires balancing fault coverage against silicon area, power budget, and performance constraints imposed by the target system.

Table 5.3—Comparative characteristics of representative ECC schemes

ECC Type	Correction Power	Parity Bits	Hardware Cost	Decode Time
Parity	Detects single-bit errors only	1 bit	Minimal	Immediate
Hamming SECDED	Corrects 1-bit errors, detects 2-bit errors	≈ 7–12%	Low	1–2 cycles
BCH	Corrects multiple random bit errors (parameterized)	Moderate to high	Moderate	3–6 cycles
LDPC	Corrects high-density random/soft errors	High (iterative)	High	Variable (iteration-dependent)

Several fundamental trade-offs emerge:

- Latency versus access delay
  As ECC strength increases—particularly for BCH and LDPC—decoding latency grows. Iterative decoding schemes may introduce variable access delays, which can be problematic in real-time or latency-sensitive systems.
- Effective bandwidth reduction
  Higher redundancy overhead reduces usable payload per memory word, lowering net bandwidth efficiency and increasing energy per useful bit transferred.
- Area and power consumption
  Advanced decoders require substantial logic for polynomial arithmetic or iterative message passing, directly impacting die area, static leakage, and dynamic power.
- Convergence risks in iterative ECC
  Iterative schemes such as LDPC may fail to converge under high error density, correlated fault patterns, or structural defects, potentially leading to undetected errors or miscorrections.

Within the Optimal_Test diagnostic analyses, these trade-offs were evaluated not only from a correction perspective but also from the standpoint of fault observability. Strong ECC schemes can entirely suppress recurring fault signatures, complicating post-correction diagnostics.

In contrast, simpler schemes such as SECDED expose richer syndrome information, enabling earlier fault detection at the cost of reduced correction strength.

5.5.2 Inline versus Out-of-Band ECC

ECC implementations can be broadly categorized into inline and out-of-band architectures, each imposing distinct constraints on latency, flexibility, and diagnostic visibility.
Inline ECC stores parity bits directly alongside user data within the same memory word.

A typical example is a 64-bit data word expanded to a 72-bit interface through the addition of eight parity bits.

Advantages:

- Straightforward controller integration with minimal architectural changes.
- Low-latency correction, as encoding and decoding are performed transparently during normal data access.

Limitations:

- Constrained to fixed word-level granularity, potentially masking faults that span adjacent words or cache lines.
- Limited flexibility for upgrading ECC strength or diagnostic behavior after deployment.
  Out-of-band ECC stores error-correcting metadata in a logically separate memory structure, such as shadow rows, spare regions, or controller-managed tables.

Advantages:

- Decouples ECC logic from the primary data path, enabling dynamic reconfiguration of ECC strength and policy.
- Facilitates advanced diagnostic features such as syndrome history logging and fault analytics without perturbing normal data access.

Limitations:

- Additional latency due to extra metadata fetches or updates.
- Increased controller complexity to maintain coherence between data and ECC metadata.

In my research, out-of-band ECC emulation was implemented within the Optimal_Test framework. This design allowed syndrome-driven diagnostics to operate independently of critical data paths, enabling fault localization, adaptive test escalation, and predictive analytics without introducing access latency penalties.

5.5.3 On-Die ECC versus System-Level ECC

Contemporary memory architectures increasingly deploy ECC at multiple hierarchy levels, each with distinct implications for performance, visibility, and diagnostics.

On-die ECC, embedded within the memory device itself (e.g., DDR5 DRAM), performs error correction before data exits the chip.

Function:

- Local correction of bit-level errors prior to off-chip transmission.
- Advantages:
- Minimizes externally visible error rates.
- Achieves correction with negligible interface-level latency impact.

Limitations:

- Fully transparent to the memory controller, masking fault patterns critical for BIST, March testing, and system-level diagnostics.
- Obscures fault provenance and degrades observability for long-term reliability analysis.
- System-level ECC, implemented in the memory controller or software layer, operates on data as presented at the system interface.

Function:

- Detects and corrects errors visible beyond the memory device boundary.
- Advantages:
- Enables error logging, trend analysis, and OS-level fault management.
- Supports actions such as page retirement, scrubbing escalation, or workload migration.

Limitations:

- Higher latency relative to on-die correction.
- Limited ability to correct intra-die defects already masked by on-die ECC.

Dual-ECC architectures combine both approaches. In my research, a central challenge identified was syndrome attribution across layers. Without coordination, error provenance becomes ambiguous, increasing misclassification risk.

I therefore proposed a hierarchical syndrome reporting protocol that preserves error origin information, enabling accurate cross-layer fault localization and diagnostic correlation.

5.5.4 ECC and Redundancy Co-Design

Combining ECC with physical redundancy mechanisms—such as spare rows, columns, or banks—provides complementary protection against both transient and permanent faults.
ECC primarily targets transient and soft errors, including radiation-induced bit flips and marginal timing violations. Redundancy mechanisms address permanent defects through remapping, typically via Built-In Self-Repair (BISR).

Integration challenges include:

- ECC masking of defects that should trigger redundancy repair, delaying fault isolation.
- Address remapping that invalidates existing ECC codewords, requiring parity regeneration and consistency verification.

To address these issues, I implemented a coordinated ECC–redundancy protocol:

1. Immediate correction
   ECC corrects transient or low-frequency errors without structural intervention.
2. Persistent error escalation
   Recurring syndromes exceeding defined thresholds trigger redundancy analysis and BISR activation.
3. Post-repair validation
   Symbolic re-testing confirms repair effectiveness, followed by ECC state re-synchronization.

This tiered strategy maximizes fault coverage, minimizes unnecessary repairs, and ensures smooth transition between soft-error correction and hard-fault mitigation.

Proposed Coordination Protocol

1. **Immediate correction**
   ECC performs real-time correction of transient and low-severity errors (e.g., single-bit soft errors), preserving data integrity without triggering structural intervention.
2. **Persistent error flagging**
   Recurrent or statistically significant syndrome patterns—exceeding predefined spatial or temporal thresholds—trigger escalation mechanisms, including Built-In Self-Repair (BISR) analysis or intensified diagnostic testing.
3. **Post-repair validation**
   Automated re-testing confirms fault resolution after redundancy activation or remapping, followed by ECC state re-synchronization to ensure parity consistency and restore full protection.

This tiered coordination strategy maximizes effective fault coverage, minimizes false positives and premature repairs, and ensures a controlled transition between soft-error correction and hard-fault mitigation.

5.5.5 ECC-Aware Test Integration

From a diagnostic engineering perspective, Error-Correcting Codes should not be treated as a passive protection layer. Instead, ECC must be explicitly integrated into memory test workflows to enhance fault observability, localization accuracy, and predictive reliability analysis.

Key integration techniques include:

- **ECC syndrome hooks**
  Capture raw syndrome vectors and correction metadata during BIST, March testing, or Optimal_Test execution before higher-level masking suppresses diagnostic information.
- **Corrected data logging**
  Record correction events—including bit position, correction polarity, and temporal recurrence—to support post-mortem analysis, trend detection, and degradation modeling.
- **Partial decoding access**
  Expose intermediate decoding states or syndrome components without requiring full data reconstruction, enabling mid-test diagnostic intervention and adaptive control.
- **Syndrome pattern matching**
  Track recurring or spatially correlated syndrome signatures to identify persistent defect regions, progressive wear-out behavior, or disturbance precursors such as Rowhammer-induced degradation

Optimal_Test integration example

Within the Optimal_Test framework, ECC awareness is a first-class diagnostic feature. Syndrome vectors are abstracted as symbolic diagnostic tokens and fed directly into the test synthesis engine. Detection of suspicious or repeating syndrome patterns triggers adaptive escalation—from lightweight March sequences to targeted hybrid U–Y test patterns—closing the gap between silent error masking and true fault localization.

By incorporating ECC telemetry into the diagnostic feedback loop, test frameworks gain deeper visibility into latent or intermittent faults that would otherwise remain hidden. This integration enables earlier detection of degradation trends and supports predictive reliability analysis. Consequently, ECC-aware diagnostics strengthen the linkage between runtime error correction and systematic fault localization.

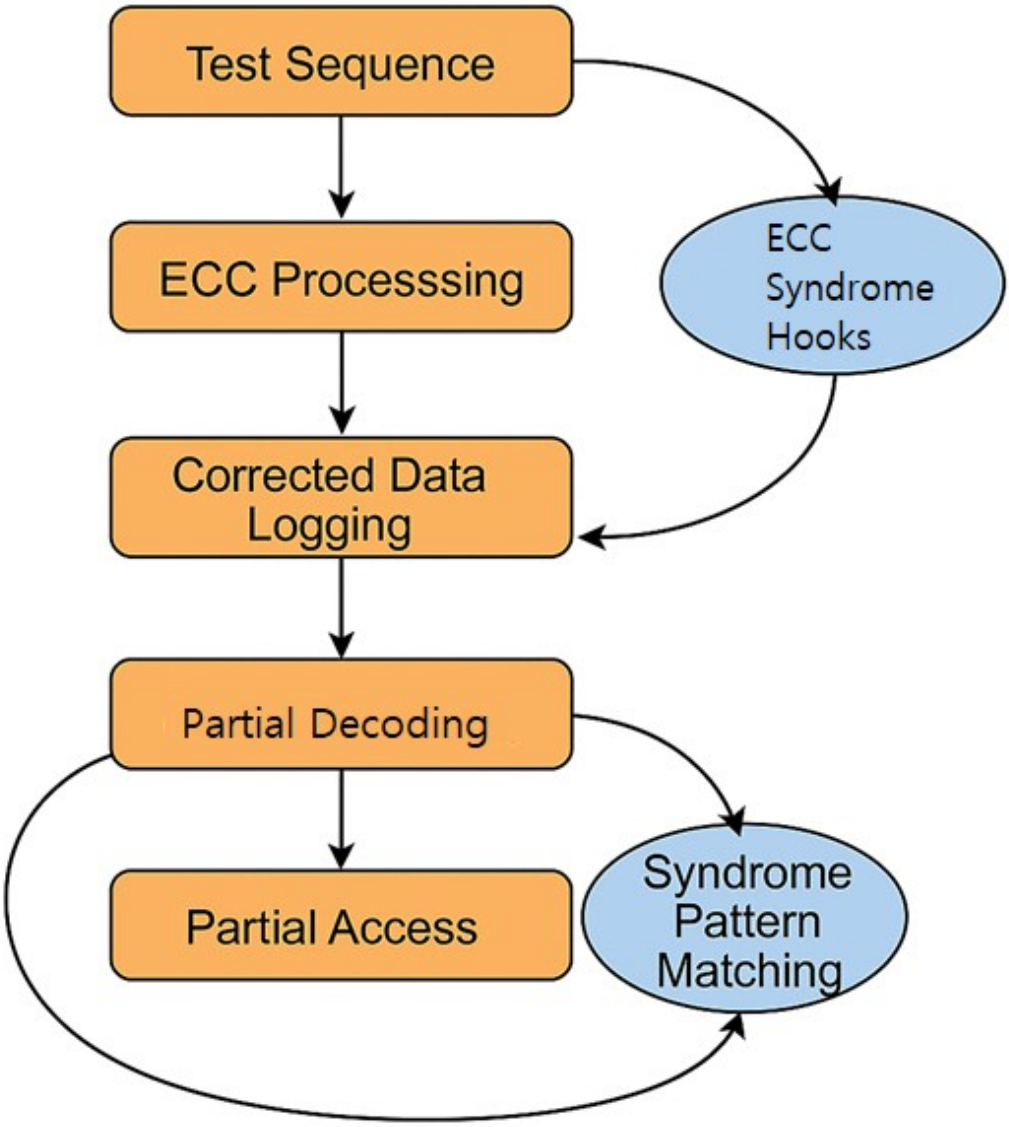

Figure 5.2—ECC test integration flowchart with diagnostic feedback loop

Figure 5.2 illustrates the integration of Error-Correcting Code mechanisms into a symbolic memory testing framework with closed-loop diagnostic feedback.

The process begins with **Test Sequence** execution, where symbolic patterns are applied under realistic interface and timing constraints to stimulate a wide range of fault mechanisms. Data then flows through **ECC Processing**, where errors are detected and corrected in real time.

At this stage, **ECC Syndrome Hooks** branch off from the main data path to capture internal correction metadata, including syndrome values, error vectors, and correction events. This information provides diagnostic visibility beyond standard pass/fail reporting.

Captured metadata is forwarded to **Corrected Data Logging**, where correction histories are accumulated to support statistical analysis, spatial correlation, and adaptive test refinement.

The pipeline continues through **Partial Decoding**, enabling selective access to ECC outputs without full application-level decoding, followed by **Partial Access**, where symbolic test engines probe ECC responses at fine granularity.

The **Syndrome Pattern Matching** module analyzes recurring syndrome signatures, spatial degradation trends, and characteristic activation patterns. Its outputs feed back into the **Test Sequence** stage, enabling dynamic synthesis of escalated or targeted diagnostic patterns.
This closed-loop structure transforms ECC from a passive correction layer into an active, real-time diagnostic agent, supporting adaptive coverage optimization, precise fault localization, and early degradation detection in ECC-protected memory systems.

5.5.6 Summary

Error-Correcting Codes extend far beyond their traditional role as silent data-protection mechanisms. In contemporary memory systems, ECC functions simultaneously as a corrective engine, a diagnostic sensor, and a design constraint—shaping performance, latency, power consumption, and fault observability.

Effective ECC deployment therefore requires not only mastery of coding theory, but also deep integration with system architecture, timing behavior, test methodology, and fault modeling.
In my research, ECC integration was advanced through test–syndrome fusion and protocol-aware monitoring frameworks. These approaches demonstrate that system resilience is achieved not through isolated mechanisms, but through coordinated orchestration of testing, error detection, correction, and adaptation across the memory hierarchy.

When implemented in this coordinated manner, ECC becomes an active participant in adaptive fault management, predictive diagnostics, and long-term operational stability—capabilities that are essential in modern dense, heterogeneous, and high-reliability memory environments.
As memory technologies evolve beyond charge-based storage (DRAM, SRAM), emerging device classes such as resistive RAM (ReRAM), magnetoresistive RAM (MRAM), and phase-change memory (PCM) introduce fundamentally different fault behaviors that challenge classical ECC assumptions.

These emerging non-volatile and hybrid memories exhibit characteristics including:

- **Drift** – Gradual resistance or magnetic-state changes over time, leading to retention-related errors.
- **Wear** – Endurance degradation from repeated write cycles, producing stuck-at faults or elevated error rates.
- **Read disturb** – Non-destructive reads that perturb adjacent cells or induce incremental state shifts.
- **Analog degradation** – Multi-Level Cell storage with intermediate states highly sensitive to noise, temperature, and process variability.

These mechanisms generate error patterns that are spatially correlated, temporally evolving, and often analog in nature, rendering traditional binary-oriented ECC schemes insufficient for long-term reliability without diagnostic augmentation.

5.6 Diagnostic Insights from Hybrid Memory Stacks

In my diagnostic research and symbolic modeling of hybrid memory stacks, I observed that effective ECC strategies for emerging technologies must adapt to fault behaviors that differ

fundamentally from those assumed in classical binary memory models. In particular, next-generation ECC mechanisms must account for:

- **Multi-bit and clustered failure modes**
  Error mechanisms frequently manifest as spatially dense fault regions, affecting multiple bits or symbols simultaneously rather than isolated, independent bit flips.
- **Non-binary signal characteristics**
  Multi-level storage technologies require ECC operation over extended symbol alphabets (e.g., $GF(2^n)$ with $n > 1$), enabling finer-grained state discrimination beyond binary logic.
- **State ambiguity and read-induced inconsistencies**
  ECC logic must tolerate probabilistic state interpretation and intermittent inconsistencies arising from non-destructive reads, drift phenomena, and read-disturb effects.

These observations highlight the necessity for ECC architectures that are explicitly aligned with the physical behavior of emerging memory devices. Future ECC approaches are therefore expected to combine error correction with predictive degradation monitoring, dynamic re-encoding, and adaptive fault-tolerant control to preserve data integrity across the full operational lifespan of hybrid memory systems.

5.6.1 Challenges in Emerging Memory ECC

Emerging non-volatile memory technologies introduce fault mechanisms that fundamentally violate the assumptions underlying classical ECC architectures. Table 5.4 summarizes representative error characteristics and the corresponding ECC challenges across several leading memory technologies.

Table 5.4—Error characteristics and ECC challenges in emerging memory technologies

Memory Type	Key Error Characteristics	ECC Challenge
MRAM	Read disturb, write asymmetry, thermal drift	Data-dependent switching reliability and read-induced perturbations
ReRAM	Soft set/reset failures, analog drift, sneak paths	Non-binary error amplitudes and uncertainty in error localization
PCM	Gradual resistance drift, multi-level cell errors	Decode instability over time and susceptibility to soft masking
FeRAM	Fatigue degradation, polarization collapse	Intermittent, asymmetric bitline faults requiring adaptive correction

Across these technologies, several common ECC challenges emerge:

- **Ambiguity in error detection**

Many physical deviations do not manifest as discrete logical bit flips but instead appear as analog variations, complicating threshold-based detection.

- **Analog threshold drift**
  Resistance, polarization, or magnetic-state drift invalidates static decoding thresholds, requiring dynamic recalibration of ECC decision boundaries.
- **Multi-level cell complexity**
  Errors frequently occur within intermediate symbol states rather than between binary extremes, demanding ECC capable of multi-symbol or soft-decision correction.
- **Coupled cell behavior**
  Parasitic interactions between adjacent cells introduce spatially correlated faults, requiring joint decoding logic that considers cross-cell dependencies.

These challenges underscore the need for next-generation ECC designs that integrate probabilistic decoding, adaptive thresholding, and analog-aware correction algorithms. In my symbolic fault modeling of hybrid memory stacks, I demonstrated that coupling ECC with state-aware diagnostics is essential for sustaining reliability under highly variable and interdependent fault conditions.

5.6.2 ECC Strategy Adaptations

As memory technologies evolve toward higher densities, multi-level storage, and increased sensitivity to environmental factors, classical binary ECC frameworks encounter fundamental limitations. Addressing these limitations requires extending ECC into adaptive, probabilistic, and state-aware paradigms. The following adaptation strategies were integrated into the symbolic modeling and fault simulation infrastructure of Optimal_Test.

A. Soft-decision decoding for analog memory faults

Soft-decision decoding, traditionally used in communication systems and LDPC-based designs, becomes essential for emerging non-volatile memories such as PCM and ReRAM, where readouts are inherently analog.

Core principle

Rather than forcing analog readouts into binary decisions, the ECC decoder consumes continuous-valued measurements (e.g., resistance, current, voltage margins) and maps them to likelihood distributions over possible symbol states.

Advantages

- Improved robustness under noise, drift, and device variability
- Increased correction capability under ambiguous state conditions
- Natural support for multi-level cell operation through probabilistic inference

Implementation in Optimal_Test

Within Optimal_Test, I extended the symbolic fault simulation engine to support soft-decision ECC evaluation by:

- Injecting scaled analog fault models and stochastic noise envelopes into symbolic test responses
- Modeling decoders that interpret resistance or voltage values as probability-weighted inputs
- Emulating LDPC-like iterative correction behavior under drift, asymmetry, and cross-cell interference

This enabled systematic stress-testing of ECC logic under analog-dominated fault conditions, providing a foundation for probabilistic and fault-tolerant architectures in next-generation memory systems.

B. ECC code extensions for multi-level cell memories

In multi-level cell architectures, each memory cell encodes multiple bits across several physical states, introducing error mechanisms poorly addressed by binary ECC schemes.

Core challenge

Binary ECC assumes discrete bit flips as the dominant error mode. In MLC memories, errors frequently involve:

- Drift between adjacent resistance or charge states
- Non-linear state transitions
- Cross-cell interference amplified by dense integration

Adaptation approaches

- **Symbol-wise decoding**
  Reed–Solomon and related codes over GF(2^n) enable correction at the symbol level, aligning naturally with multi-state storage.
- **Non-binary LDPC schemes**
  Iterative decoders operating in extended finite fields support probabilistic correction of analog state transitions and correlated symbol errors.

Implementation in Optimal_Test

To evaluate these strategies, I extended Optimal_Test to:

- Model bit-to-symbol mappings across extended Galois fields
- Inject multi-symbol fault patterns reflecting non-uniform and correlated error distributions
- Emulate Reed–Solomon and non-binary LDPC decoding under dense, symbol-correlated fault domains

This framework enabled rigorous analysis of correction limits, diagnostic visibility, and adaptive test interaction for state-rich, high-density memory systems.

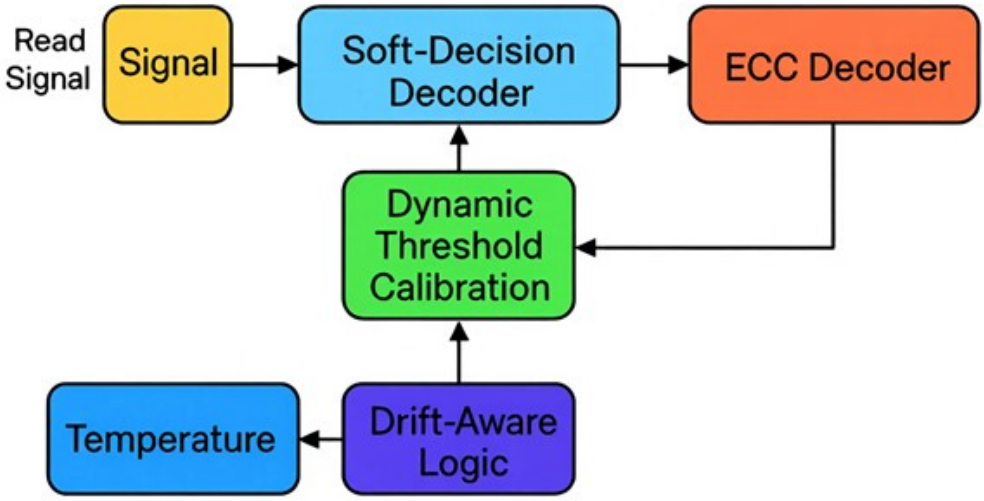

Figure 5.3—Drift-Aware ECC Decoding with Dynamic Threshold Calibration

Figure 5.3 illustrates a drift-aware ECC decoding architecture designed for analog and emerging non-volatile memories such as PCM and ReRAM, where time-dependent drift and thermal effects degrade data integrity.

The decoding pipeline begins with the analog read signal, which is processed by a soft-decision decoder. Unlike binary hard-decision logic, this stage interprets resistance levels or signal amplitudes as probability-weighted likelihoods, preserving uncertainty information under noise, drift, and marginal state overlap.

Likelihood outputs are forwarded to the ECC decoder, which applies syndrome-based correction using schemes such as LDPC or Reed–Solomon. In parallel, correction outcomes feed a dynamic threshold calibration module that continuously adjusts decision boundaries based on observed error behavior.

Calibration is governed by a drift-aware logic block that models temperature-dependent degradation using symbolic resistance profiles, environmental telemetry, and historical correction data.

Temperature feedback directly influences this model, enabling proactive compensation for thermal acceleration of drift.

By coupling probabilistic decoding with context-aware threshold adaptation, this architecture maintains ECC effectiveness across device aging, environmental variation, and analog state migration. This design was implemented and evaluated within the Optimal_Test diagnostic framework.

5.6.3 Syndrome Logging in Analog and Non-Volatile Contexts

In conventional ECC implementations, syndromes are binary vectors that directly encode bit-error locations. While sufficient for binary fault models, this representation is inadequate for analog and non-volatile memories such as ReRAM and PCM, where fault manifestations are multi-dimensional and temporally evolving.

Emerging requirements for syndrome representation

- **Drift awareness**
  Syndrome data must encode not only the affected bit or symbol but also the direction and magnitude of analog drift (e.g., resistance increase versus decrease).
- **Confidence quantification**
  Soft-decision ECC requires likelihood metrics reflecting the probability of error for partially degraded cells rather than binary error flags.
- **Temporal persistence tracking**
  Repeated partial failures across refresh cycles indicate progressive physical degradation and must be distinguished from transient noise-induced events.

Implementation in ReRAM testing prototypes

To address these requirements, multi-dimensional syndrome vectors were incorporated into the Optimal_Test framework, formally represented as:

$$(Bit\ Position, Likelihood, Drift\ Direction, Cell\ Voltage\ History)$$

This representation enables:

- Symbolic syndrome compression, preserving diagnostic resolution while minimizing logging overhead.
- Long-term degradation analysis through trend correlation across time and operating conditions.
  By extending syndrome semantics beyond binary indicators, ECC transitions from a reactive correction mechanism into a predictive health-monitoring layer suitable for analog-dominated memory technologies.

5.6.4 Wear-Aware ECC Management

Non-volatile memories such as NAND flash, PCM, and ReRAM experience cumulative degradation with each program/erase cycle, eventually reaching endurance limits that compromise data integrity.

Effective ECC management must therefore evolve from reactive correction toward predictive, wear-aware strategies tightly coupled with diagnostics.

Key considerations

- **Wear-level tracking**
  Maintain endurance counters at cell, wordline, or block granularity, dynamically adjusting ECC confidence metrics as wear approaches critical thresholds.
- **Post-ECC refresh triggering**
  Selectively rewrite corrected data to mitigate drift and retention loss, balancing refresh benefit against accelerated wear.
- **Recovery zoning**
  Identify regions with recurrent ECC intervention and proactively relocate data to healthier areas, accompanied by scrubbing and remapping.

Hybrid test–ECC coordination

Within Optimal_Test, a post-correction confidence scoring mechanism was implemented:

- Recurrent correction events trigger localized diagnostic analysis.
- Targeted symbolic test bursts determine whether degradation is transient or permanent.
- Confirmed wear-induced faults initiate relocation and controlled scrub–relocate cycles.

This closed-loop integration aligns ECC correction with proactive diagnostics, mitigating endurance-related failures before they escalate.

5.6.5 Combined ECC and Redundancy in 3D Memory Stacks

Three-dimensional memory architectures, including 3D NAND and High-Bandwidth Memory (HBM), introduce fault domains driven by vertical integration, dense interconnects, and non-uniform thermal gradients.

Dominant fault mechanisms

- Vertical interconnect degradation in through-silicon vias (TSVs).
- Bank-to-bank interference amplified by vertical proximity.
- Layer-specific aging leading to asymmetric fault distributions.

Resilience strategies

- Layer-specific ECC with inter-layer syndrome aggregation.
- Cross-die redundancy mapping supporting vertical remapping.
- Coordinated ECC handshake across dies to preserve fault provenance.

Evaluation in Optimal_Test

Stacked fault injection and cross-die syndrome analysis were simulated to assess:

- Accuracy of vertical fault isolation.
- ECC operational limits under dense stacking.
- Diagnostic visibility across heterogeneous failure domains.

5.6.6 Summary

Emerging memory technologies require a fundamental redefinition of ECC design beyond binary correction models. This evolution is characterized by:

- Probabilistic, state-aware decoding operating over extended symbol spaces.
- Drift-aware syndrome semantics that capture analog degradation and uncertainty.
- Cooperative resilience architectures integrating ECC, symbolic diagnostics, and redundancy control.

Within the Optimal_Test framework, ECC functions as an adaptive diagnostic agent rather than a passive correction layer.

This integration enables real-time fault isolation, drift-aware calibration, and test-guided resilience, transforming ECC-equipped systems into self-adaptive reliability architectures capable of sustaining integrity under aging, variability, and complex analog fault landscapes.

5.7 Scrubbing, Logging, and Self-Healing Architectures

Error-Correcting Codes (ECC) are inherently reactive mechanisms: they detect and correct errors at the moment of data access.

While this is sufficient for isolated transient faults, it is inadequate in systems requiring continuous fault containment, predictive resilience, and mission assurance, such as aerospace avionics, safety-critical embedded platforms, and high-availability server infrastructures.

To address these requirements, contemporary memory subsystems incorporate three tightly coupled layers of proactive fault management:

- **Memory scrubbing** – Periodic or opportunistic background scanning that detects and corrects latent errors before they accumulate into uncorrectable states.
- **Error logging** – Persistent recording of ECC syndromes, correction events, and fault locations to support trend analysis, fault localization, and predictive maintenance.
- **Self-healing logic** – Autonomous mechanisms that isolate degraded regions, escalate diagnostic intensity, and dynamically reconfigure access paths in response to observed fault evolution.

My Contribution in Optimal_Test

Within the Optimal_Test platform and its fault-aware runtime layer, I implemented adaptive scrubbing models driven directly by observed ECC syndrome behavior.

This integration transforms ECC from a passive protection layer into an active diagnostic and predictive agent, enabling:

- Real-time classification of recurring and spatially correlated fault patterns
- Predictive tracking of cells and regions trending toward permanent failure
- Automatic escalation to symbolic March or hybrid test sequences upon detection of emerging degradation signatures

This section formalizes the architectural principles and symbolic test integration underpinning these proactive maintenance mechanisms and situates them within next-generation self-adaptive fault-tolerant systems.

5.7.1 Memory Scrubbing Fundamentals

Memory scrubbing consists of periodically reading memory contents, verifying data integrity, and—when ECC is present—correcting and rewriting erroneous data to prevent error accumulation.

Key Attributes

- **Proactive fault detection**

Latent errors invisible to normal workload access are exposed before they evolve into uncorrectable multi-bit failures.

- **Coverage scope**
  Scrubbing may be applied globally across all arrays or selectively targeted to regions identified as high-risk by diagnostic analytics.
- **Timing models**
  - *Idle-time scrubbing* – Activated during low system activity to minimize performance interference
  - *Background scrubbing* – Executes continuously in parallel with normal operation
  - *Scheduled scrubbing* – Triggered at fixed intervals to satisfy system-level reliability constraints
- **Scrubbing operations**
  - *Read–verify–write – Reads data, evaluates ECC, and rewrites corrected content*
  - *Refresh-aware scrubbing* – Aligns with DRAM refresh cycles to reduce incremental latency

Advantages

- Prevents error accumulation that may exceed ECC correction limits
- Reduces the probability of multiple-bit upsets (MBUs) leading to catastrophic failure

Challenges

- Introduces additional memory traffic and power consumption
- Requires careful scheduling to avoid contention with latency-critical workloads

Adaptive Scrubbing in Optimal_Test

Unlike fixed-interval scrubbing, Optimal_Test implements **syndrome-driven adaptive scrubbing**, in which:

- Scrubbing frequency increases in regions exhibiting recurrent or clustered ECC syndromes
- Low-risk regions receive reduced scrubbing intensity to minimize overhead
- Trend-based prioritization focuses resources on cells exhibiting early degradation indicators

Types of Memory Scrubbing

Table 5.5—Memory scrubbing types and typical use contexts

Type	Description	Typical Use
Read scrubbing	Reads memory and relies on ECC to detect and correct latent faults without modifying correct data	Server-class DRAM with ECC

Table 5.5—Memory scrubbing types and typical use contexts (Continued)

Type	Description	Typical Use
Write scrubbing	Reads, corrects, and rewrites data to proactively restore integrity	Embedded and mission-critical DRAM
Blind scrubbing	Periodically overwrites memory with known patterns without reading existing data	Cacheless DRAM, systems lacking ECC

Diagnostic Rationale

Scrubbing prevents the silent accumulation of latent soft errors into uncorrectable multi-bit faults, a critical requirement in high-availability and safety-critical environments where even transient corruption can propagate into system-level failure.

Implementation in Symbolic Testing (PROVER Framework)

In my PROVER-based symbolic diagnostic framework, scrubbing is abstracted as a timed read–verify operator:

$$S_{(x,t)}:$$

where $S_{(x,t)}$ performs an integrity-verified read at address x at time t.

This abstraction enables synchronization of scrubbing with:

- DRAM refresh windows, minimizing incremental latency
- System idle periods, preserving workload transparency

Embedding scrubbing into symbolic test logic ensures continuous fault coverage while maintaining alignment with the predictive and adaptive resilience principles of Optimal_Test.

5.7.2 Scrubbing Interval Optimization

Scrubbing effectiveness depends critically on the interval at which it is performed. Interval selection represents a trade-off between overhead and fault containment:

- **Short intervals**
  Rapid detection and correction of latent faults, sharply reducing the probability of ECC-exceeding multi-bit upsets, at the cost of increased power and bandwidth consumption.
- **Long intervals**
  Lower overhead but increased risk of error accumulation and correction failure.

Simulation-Driven Findings

Using parameterized simulations across DRAM, MRAM, and PCM under varying environmental conditions, the following observations were obtained:

- **DRAM with SECDED ECC**
  A scrubbing interval of approximately 64 ms achieved ~98% transient fault coverage with less than 1% power overhead, closely aligning with JEDEC refresh behavior while preserving performance.
- **MRAM and PCM**
  Optimal scrubbing intervals were strongly temperature-dependent. Elevated temperatures required significantly shorter intervals to counteract retention drift and analog instability.

Adaptive Interval Control in Optimal_Test

To accommodate dynamic workloads and environmental variability, I implemented adaptive interval control within Optimal_Test, adjusting scrubbing frequency based on:

- ECC syndrome recurrence and clustering metrics
- Live temperature telemetry to infer drift acceleration

This context-aware approach increases scrubbing aggressiveness during stress conditions or early degradation phases and relaxes it during nominal operation, achieving high resilience with minimal overhead.

5.7.3 ECC Logging and Error Classification

ECC achieves its full diagnostic value only when correction activity is persistently logged. Recording syndrome vectors, correction locations, and error types transforms transient correction events into structured diagnostic intelligence.

Diagnostic Insights from ECC Logging

- **Spatial correlation**
  Identification of fault-prone regions, banks, or bitlines through recurring address patterns.
- **Error typology**
  Classification into single-bit versus multi-bit errors and transient versus persistent fault behavior.
- **Fault persistence analysis**
  Differentiation between isolated soft errors and progressive physical degradation.

  These insights directly inform adaptive scrubbing policies, self-repair escalation thresholds, and lifetime prediction models, establishing ECC logging as a foundational element of predictive maintenance and self-healing memory architectures.

Standard Logging Fields

A comprehensive ECC log entry must capture both the spatial context of the event and the diagnostic metadata required for fault inference.

A minimal but sufficient log record includes the following fields:

Table 5.6—Minimal ECC log fields required for diagnostic inference

Field	Description
Memory Address	Physical or logical word-, line-, or page-level address at which the error was detected, enabling spatial correlation across events.
Syndrome Vector	ECC-generated syndrome pattern encoding the error signature and candidate fault localization; serves as a primary diagnostic fingerprint.
Error Type	Classified fault model inferred from syndrome behavior and test response (e.g., Stuck-At Fault (SAF), Transition Fault (TF), Retention Fault (RF)).
Timestamp	High-resolution event time supporting temporal correlation, fault rate estimation, and degradation trend analysis.
Correction Outcome	Result of ECC handling (corrected, deferred, or uncorrectable), enabling assessment of residual system risk and ECC margin.

Optimal_Test Integration

Within the Optimal_Test framework, ECC logs are not passively archived but continuously analyzed as part of a closed diagnostic feedback loop:

- **Persistent syndromes**
  Repeated observation of identical syndrome vectors within a bounded temporal window triggers localized diagnostic bursts, enabling targeted fault isolation and model confirmation.
- **Sporadic errors**
  Low-frequency, non-recurrent correction events contribute statistically to adaptive scrubbing schedules, increasing monitoring density only where warranted.

This log-driven control loop elevates ECC from a reactive protection layer to a core component of predictive memory health monitoring, enabling early intervention prior to functional failure.

Symbolic Logging in Optimal_Test

In the Optimal_Test diagnostic architecture, ECC events are captured as **compressed symbolic fault traces**, minimizing logging overhead while preserving diagnostic fidelity.

Symbolic Trace Structure

Each symbolic log entry encapsulates:

- **Logical location** – Address of the affected memory element.
- **Fault signature** – Syndrome vector s, encoding bit- or symbol-level fault information.
- **Error classification** – Inferred fault model (e.g., TF, SAF, RF).
- **Correction status** – Whether the error was corrected immediately or deferred.
- **Ambient telemetry** – Environmental context such as temperature, voltage state, or power mode.

Diagnostic Capabilities Enabled

- **Targeted test regeneration**
  Automatic deployment of localized March or pattern-based tests upon recurrence of specific syndrome patterns.
- **Fault aging curve estimation**
  Time-series analysis of syndrome frequency and spatial distribution to model progressive cell degradation.
- **Class-specific diagnostics**
  Invocation of fault-model-specific stress routines (e.g., coupling fault activation, transition stress) based on logged classifications.

Example Log Instance

$$[ECC]addr = 0x1A3FC \mid s = 0101010 \mid type = TF \mid corrected = yes \mid thermal = 55$$

Field interpretation

- addr – Memory address at which the error occurred
- s – Observed syndrome vector associated with the fault signature
- type – Transition Fault classification
- corrected – Error corrected in real time
- thermal – Event occurred at 55 °C, suggesting possible temperature-accelerated degradation.

In this instance, a transition fault was detected and corrected at address 0x1A3FC.

The recurring syndrome vector functions as a persistent identifier. If this signature reappears within the defined observation window, Optimal_Test automatically schedules a localized high-resolution March sequence over the affected region, enabling early isolation of emerging hard faults before escalation to uncorrectable states.

By fusing fault classification, environmental telemetry, and adaptive test triggering, symbolic logging transforms ECC into an active diagnostic feedback engine, enabling Optimal_Test to function as a hybrid reactive–anticipatory memory health management system.

5.7.4 Predictive Health Models and Escalation Paths

Traditional ECC architectures operate strictly in a reactive mode, correcting errors only at access time. When ECC log streams are reinterpreted as structured time-series diagnostic data, they enable predictive fault modeling, allowing degradation to be detected and mitigated before functional failure.

Predictive Modeling Inputs

Within Optimal_Test, a real-time fault evolution model synthesizes the following observables:

- **ECC-corrected read frequency**
  Correction rate per address or row, serving as a primary indicator of emerging wear.
- **Syndrome recurrence window**
  Temporal clustering of identical syndrome vectors, signaling localized defect growth.
- **Cell temperature profile**
  Correlation of thermal telemetry with error emergence to capture temperature-accelerated degradation.
- **Retention failure history**
  Historical soft-error data used to model aging trajectories at cell or region granularity.

These metrics feed a symbolic scoring engine that constructs a diagnostic risk matrix, ranking memory regions by failure likelihood and determining escalation thresholds.

Escalation Paths and Risk Response

When a region exceeds defined risk thresholds, the system autonomously initiates one or more of the following actions:

- Redundancy remapping via spare rows or columns
- Run-time BIST invocation using targeted March algorithms (e.g., March SS, March C^-)
- Scrubbing interval modulation for flagged regions
- Cell retirement or page migration to preserve data integrity

Simulation Case Study

In a representative validation scenario:

- A DRAM row logged six ECC corrections within a four-hour window.
- Escalation sequence:
  - March SS diagnostic burst confirmed persistent fault behavior
  - BISR logic remapped the defective row
  - No subsequent errors propagated to the operating system

This demonstrates that predictive modeling can extend memory lifetime and prevent visible failures through timely, automated intervention.

5.7.5 Self-Healing Techniques

Self-healing memory systems integrate real-time detection, predictive analytics, and active reconfiguration to preserve data integrity without workload disruption.

Contemporary Self-Healing Mechanisms

- Redundancy activation upon ECC correction thresholds
- Data migration from frequently corrected locations
- Repair via remapping triggered by ECC-derived risk metrics
- AI-assisted failure prediction using multi-modal telemetry

My Contribution: Symbolic Feature Compression and ML Integration

Within Optimal_Test, I implemented a symbolic ECC sequence compressor that generates compact feature vectors for a neural fault classifier.

- Achieved 91% classification accuracy for soft, intermittent, and hard faults in DRAM/MRAM simulations
- Enabled preemptive row isolation, adaptive scrubbing, and fault-type-aware test generation with minimal runtime overhead

This demonstrates that self-healing is not a single mechanism but a hardware–software–AI synergy, with symbolic testing providing the structural substrate for learning-driven fault tolerance.

5.7.6 Architectural Integration

Realizing predictive diagnostics and self-healing behavior in production memory systems requires tight, explicitly defined coupling between ECC logic, diagnostic engines, and system control layers. This coupling must preserve low-latency error visibility while maintaining deterministic behavior under operational constraints.

Key architectural requirements include:

- **Low-latency ECC syndrome exposure**
  ECC-generated syndromes—including those associated with corrected errors—must be made visible to diagnostic logic without buffering delays or post-correction suppression.
- **Programmable multi-tier scrubbing logic**
  Scrubbing intensity, scope, and scheduling must be dynamically adjustable based on risk scores derived from syndrome density, temporal recurrence, and environmental context.
- **Cross-domain visibility**
  ECC logs must be correlated with thermal telemetry, controller state, access statistics, and aging metrics to enable context-aware fault inference.
- **Fault-aware OS and firmware support**
  System software must support test escalation, memory remapping, redundancy activation, hotplugging, and mirroring—particularly in safety-critical and high-availability environments.

This integration transforms ECC from a passive error-masking mechanism into an active resilience agent, capable of coordinating detection, diagnosis, mitigation, and repair across the memory hierarchy.

Such architectural coordination enables memory subsystems to respond dynamically to emerging fault conditions while maintaining stable system operation. By linking ECC telemetry with diagnostic and control mechanisms, reliability management becomes proactive rather than reactive.

This integration ultimately supports resilient memory operation across diverse workloads and environmental conditions.

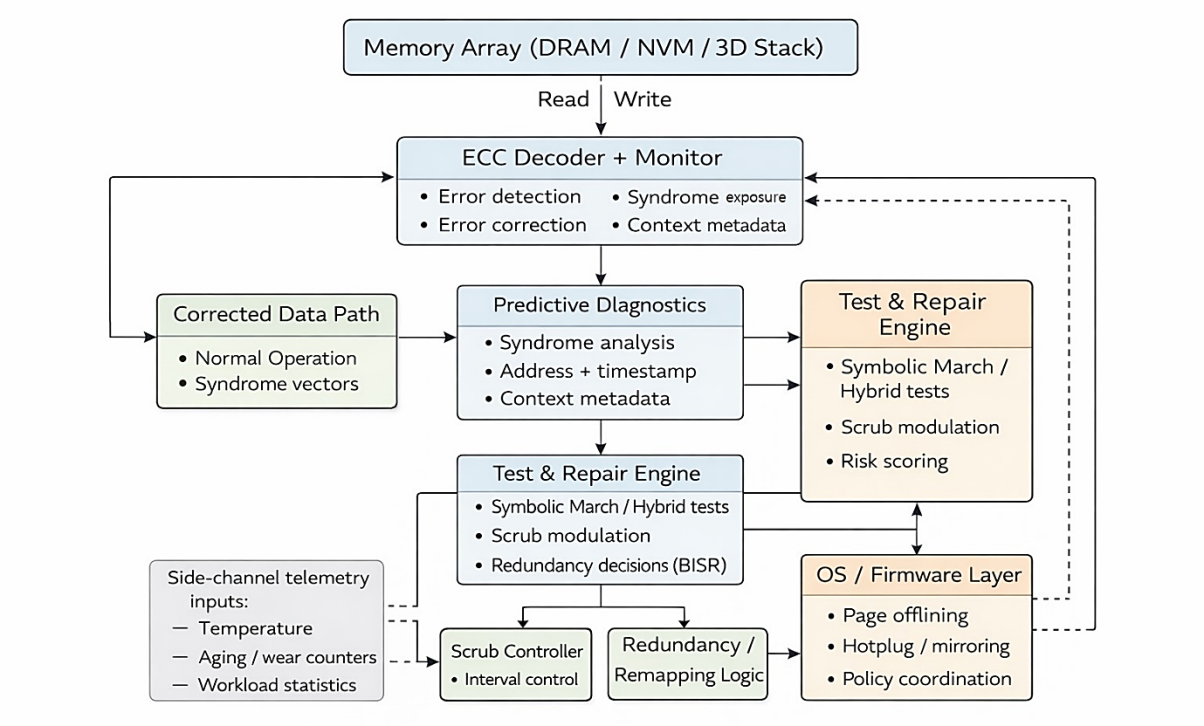

Figure 5.4—Integrated fault monitoring and recovery pipeline with feedback loop

The Figure illustrates a closed-loop memory resilience architecture in which ECC decoding, syndrome exposure, predictive diagnostics, adaptive testing, scrubbing control, and redundancy management operate as a unified system. Corrected data proceeds along the normal execution path, while exposed ECC syndromes are logged and analyzed to identify spatial and temporal fault patterns.

Diagnostic feedback dynamically drives test escalation, scrub modulation, and repair actions, coordinated with firmware and operating system layers. Environmental and workload telemetry provide contextual inputs for risk-aware decision making, enabling proactive fault isolation and extended subsystem lifetime.

The process originates in the memory subsystem, where an **ECC Decoder and Monitor** performs detection and correction while exposing both corrected and uncorrected syndromes for diagnostic consumption. These syndromes are forwarded to a **Syndrome Logger**, which persistently records fault signatures, timestamps, and contextual metadata to support temporal trend analysis and predictive modeling.

Logged information feeds a **Test and Repair Engine**, which analyzes spatial and temporal error patterns to initiate targeted diagnostic routines—such as symbolic March or hybrid test sequences—and structural repair actions including redundancy activation or address remapping.

In parallel, the engine dynamically adjusts scrub-control parameters, modulating scrubbing frequency and scope based on observed fault density, correction rates, and environmental stress indicators. A direct bypass path from the ECC Decoder to the Test Engine enables immediate intervention for high-priority or rapidly escalating error events.

At the system level, **OS and firmware layers** provide supervisory coordination. They receive fault notifications from the Syndrome Logger and issue commands for test invocation, memory retirement, hotplug operations, or mirroring in mission-critical configurations. The **Telemetry domain** integrates environmental and operational signals—including temperature profiles, aging counters, and workload characteristics—enabling context-aware decision-making under variable stress conditions.

This architecture embodies a fully closed-loop fault management system in which ECC monitoring, fault logging, test escalation, scrub optimization, and system coordination operate cohesively. The result is proactive fault isolation, adaptive resilience, and extended memory subsystem lifetime in high-availability and mission-critical computing environments.

5.7.7 Summary

Memory scrubbing, ECC logging, and self-healing mechanisms together form the primary proactive defense layer for mission-critical and high-availability systems. These capabilities elevate ECC from a passive correction facility to an active diagnostic and predictive component, enabling real-time analytics, adaptive recovery strategies, and long-term fault forecasting.

When integrated with symbolic test modeling and risk-aware feedback loops, these mechanisms provide fine-grained visibility into degradation dynamics, allowing targeted intervention before functional failures manifest.

Within the Optimal_Test framework, this integration enabled:

- **Isolation of latent faults**
  Early identification of failure-prone regions prior to multi-bit fault propagation.
- **Adaptive scrubbing modulation**
  Real-time adjustment of scrubbing intervals based on evolving syndrome statistics and environmental telemetry.
- **Targeted diagnostic escalation**
  Precision deployment of symbolic self-tests in response to recurring or high-risk syndrome patterns.
- **AI-assisted fault classification**
  Machine-learning-driven analysis of symbolic ECC logs for high-confidence discrimination between soft, intermittent, and hard faults.

These mechanisms strengthen immediate reliability while establishing the foundation for next-generation resilience architectures. As systems evolve toward ultra-dense and heterogeneous memory stacks, autonomous error management combined with predictive, context-aware diagnostics becomes indispensable for sustaining operational integrity.

5.8 Chapter Summary and Transition to BIST and Repair Logic

This chapter has traced the evolution of memory reliability from passive error correction toward active, system-integrated resilience. Error Correction Codes have progressed from basic

parity mechanisms to diagnostic engines that drive real-time fault localization, adaptive scrubbing, predictive analytics, and self-healing workflows.

In modern architectures, ECC is no longer peripheral—it is a first-class architectural element embedded within controllers, diagnostic frameworks, and learning-assisted fault prediction systems.

5.8.1 Recap of Core Themes

- **ECC foundations**
  Reviewed the mathematical principles of codeword construction, Hamming distance, and syndrome decoding, spanning parity, Hamming, BCH, and LDPC schemes with emphasis on correction capability, cost, and implementation constraints.
- **Syndrome as a diagnostic signal**
  Demonstrated how syndrome streams act as real-time health indicators. Within Optimal_Test, syndromes trigger test escalation, fault classification, and dynamic pattern adaptation.
- **Hardware integration trade-offs**
  Examined latency, area, and fault-masking risks. Compared inline versus out-of-band ECC and on-die versus system-level ECC, highlighting interactions and conflicts with redundancy mechanisms.
- **Adaptation to emerging memories**
  Addressed MRAM, ReRAM, and PCM fault behaviors that violate binary ECC assumptions, extending symbolic ECC modeling to probabilistic decoding and drift-aware correction.
- **Scrubbing and self-healing**
  Established reliability as a dynamic property maintained through adaptive scrubbing, persistent logging, and AI-assisted prediction.

5.8.2 Practical Implications for Designers and Test Engineers

ECC integration affects all layers of memory-system design:

- Test strategy design, pattern observability, and MBIST scheduling
- Controller and firmware architecture for ECC metadata exposure
- Physical layout and redundancy boundary alignment
- Aging models and predictive maintenance planning

Within Optimal_Test, these principles were operationalized by fusing ECC feedback into adaptive test sequencing, leveraging syndrome recurrence for fault escalation, and modeling ECC resilience prior to silicon deployment.

5.8.3 Looking Ahead: BIST and Built-In Repair

While ECC and adaptive testing preserve data integrity and expose early degradation, permanent damage requires structural repair. This leads to the third pillar of memory reliability: Built-In Self-Repair (BISR).

The next chapter examines:

- MBIST controller architectures and evolution
- Redundancy models at row, column, and block granularity
- Symbolic March test generation for repair-aware validation
- Spare allocation strategies, repair yield modeling, and post-repair revalidation

Together, ECC, BIST, and redundancy form a closed-loop self-healing system capable of detecting, diagnosing, and autonomously reconfiguring around faults to sustain long-term reliability under wear, defects, and aging.

This transition from detection to structural correction marks a critical evolution in memory reliability engineering. Rather than merely identifying faulty regions, modern systems increasingly incorporate mechanisms capable of isolating and remapping defective resources at runtime. Such capabilities reduce system downtime and extend the operational lifetime of memory devices operating under aggressive scaling and workload conditions. Effective repair strategies therefore require tight integration between diagnostic intelligence and hardware redundancy resources. The following chapter explores how MBIST and BISR architectures enable this coordinated repair process.

Chapter 6 Built-In Self-Repair and Redundancy Architectures

As memory technologies scale toward ultra-dense and multi-layered architectures, the inevitability of hard faults and localized wear mandates resilience mechanisms that extend beyond fault detection and error correction alone. Built-In Self-Repair (BISR) and architectural redundancy constitute the primary means of structural fault containment, enabling memory subsystems to reconfigure around defective elements and preserve logical functionality throughout their operational lifetime.

This chapter analyzes the architectural foundations of memory repair, the algorithms governing redundancy allocation, and the symbolic modeling techniques that elevate redundancy from a static design provision to a dynamic, self-healing capability tightly coupled with diagnostic reasoning.

6.1 Introduction: Beyond Detection and Correction

While manufacturing tests and error-correcting codes (ECC) provide mechanisms for fault detection and limited correction, they do not eliminate the underlying physical causes of failure. In high-density memory arrays—particularly dynamic random-access memory (DRAM), high-bandwidth memory (HBM), and emerging non-volatile memory (NVM) technologies such as resistive RAM (ReRAM) and phase-change memory (PCM)—permanent defects are statistically unavoidable.

These defects arise from manufacturing variability, progressive device aging, high-energy particle strikes, electromigration, and cumulative stress-induced degradation.

Such hard faults cannot be tolerated indefinitely, even when temporarily masked by ECC. Persistent defective cells consume correction capability, distort syndrome statistics, and accelerate the transition from correctable to uncorrectable multi-bit error conditions.

Consequently, modern memory systems require mechanisms that physically remove defective structures from the active address space rather than merely compensating for their effects.

Built-In Self-Repair provides this architectural capability. BISR exploits on-chip redundancy resources—spare rows, spare columns, redundant blocks, or entire banks—combined with programmable address-remapping logic. Once a fault is detected and localized, repair circuitry redirects memory accesses from the defective region to an allocated spare, thereby restoring full logical addressability without external intervention.

Within the Optimal_Test framework and its associated symbolic fault models, BISR is not treated as a terminal post-test operation. Instead, it is integrated into a closed-loop test–diagnose–repair architecture. Symbolic diagnostic outcomes directly parameterize repair decisions, while the evolving repair map is fed back into test synthesis and coverage evaluation.

As a result, pattern generation, traversal semantics, and pass/fail interpretation remain consistent with the current physical configuration of the memory array.

6.2 Redundancy Structures in Memory Repair Architectures

Redundancy in memory systems can be implemented at multiple spatial granularities, each characterized by distinct remapping mechanisms, allocation constraints, and diagnostic implications.

The selection of a redundancy scheme reflects trade-offs among repair coverage, silicon area overhead, timing complexity, power impact, and test observability. The following subsections summarize the principal redundancy structures employed in contemporary memory designs.

6.2.1 Spare Columns

Spare columns are used to replace defective bitlines or sense-path elements.
They are typically activated when a specific column exhibits consistent failures across multiple wordlines, indicating metal line defects, contact failures, or sense-amplifier degradation. Column redundancy is widely employed in both SRAM and DRAM arrays.

Address remapping at the column level is relatively simple and is commonly implemented using laser fuses, electrical fuses (eFuses), or non-volatile configuration elements controlling column multiplexers.

Spare columns are particularly effective when failure mechanisms are narrow and spatially localized, allowing high repair efficiency with modest area overhead.

6.2.2 Spare Rows

Spare rows replace defective wordlines and are typically allocated when multiple bits fail within the same row or when row decoder or wordline driver circuitry degrades.

Compared to column redundancy, spare rows provide broader fault absorption capability, as a single spare row can mask multiple bit-level defects simultaneously. However, row-level remapping interacts more deeply with address decoding logic and may introduce small penalties in access latency and dynamic power consumption.

Row redundancy is therefore preferred in scenarios dominated by row-localized failures, including wordline aging effects observed in long-lived DRAM devices.

6.2.3 Block or Page Redundancy

Block- or page-level redundancy is applied in memories organized around logical blocks, such as NAND Flash, ReRAM arrays, and DRAM modules with internal page structures.

In this scheme, an entire block or page (e.g., 4 KB or 8 KB) is redirected to a spare region upon detection of excessive faults. Block-level repair is typically integrated with bad-block management, wear-leveling mechanisms, and persistent error logging.

Repair decisions are often triggered dynamically based on ECC correction margins, scrubber statistics, or retention-monitoring logic. Such coarse-grain redundancy is essential in non-volatile memories, where endurance limitations and retention failures necessitate large-scale remapping over the device lifetime.

6.2.4 Bank and Vault Redundancy in Three-Dimensional Memories

Three-dimensional memory technologies—including HBM, 3D NAND, and Hybrid Memory Cube—employ redundancy at the bank, vault, or slice level.
These structures span multiple stacked dies interconnected through through-silicon vias (TSVs) and therefore require coordinated cross-die repair strategies. Bank- or vault-level redundancy incorporates TSV-aware mapping, inter-die repair arbitration, and centralized or distributed repair controllers.

Redundant banks or vaults may also include interconnect rerouting to preserve bandwidth and timing integrity in the presence of TSV failures. Such redundancy is critical in high-performance 3D memories, where vertical fault domains and layer-specific degradation must be absorbed without violating global timing or throughput constraints.

6.2.5 Redundancy Allocation Styles

The effectiveness of architectural redundancy is determined not only by its spatial granularity but also by the strategy used to allocate spare resources. Allocation style governs whether repairs are performed once during manufacturing, adaptively during system operation, or proactively in anticipation of future degradation. Table 6.1 summarizes the principal redundancy allocation modes.

Table 6.1—Redundancy allocation styles

Allocation Type	Description
Static (post-manufacturing)	Redundancy is configured once after production testing, typically via laser fuses or eFuses, and remains fixed throughout the operational lifetime.
Dynamic (run-time)	Spare allocation is triggered during operation by ECC escalation events, diagnostic monitors, or background test logic; requires reprogrammable remapping mechanisms.
Predictive	Redundancy is allocated pre-emptively based on early indicators of degradation, such as ECC syndrome accumulation, retention drift, or symbolic fault recurrence patterns.

In simulation studies conducted within the Optimal_Test framework (1 Gb DRAM model with recurrence-aware fault maps and symbolic repair logic), predictive redundancy allocation driven by ECC syndrome heatmaps and symbolic test recurrence analysis achieved an improvement of up to approximately 9% in effective yield, while introducing no measurable increase in average power attributable to the repair logic within the simulation model.

This result should be interpreted as model-based evidence of yield uplift under the stated assumptions, not as a universal guarantee across implementations.

Early industrial approaches to redundancy analysis and spare row/column replacement in embedded memories were established in prior patented architectures developed independently of the present work (U.S. Patents 6,067,262 and 6,304,989).[12-13]

6.3 BISR Architecture and Logic Flow

A complete Built-In Self-Repair (BISR) system is composed of multiple coordinated subsystems responsible for fault detection, fault persistence, redundancy analysis, address remapping, and repair orchestration. Rather than constituting a monolithic block, BISR is inherently layered, with each stage contributing distinct functionality to the overall fault-tolerance mechanism. The integration of embedded memory test and repair as reusable infrastructure intellectual property (IP) within system-on-chip platforms has been widely studied in industrial practice [15], establishing architectural foundations upon which subsequent symbolic and optimization-driven approaches can build.

1. Fault Detection Engine
Identifies permanent faults using Built-In Self-Test (BIST) procedures or symbolic diagnostic algorithms (e.g., Optimal_Test). Faults may be flagged during production testing or during in-field operation based on fail signatures, ECC escalation thresholds, or symbolic fault traces extracted from test execution.

2. Fault Storage

Maintains records of failing addresses together with associated metadata, such as fault type, recurrence count, and detection context. Depending on design objectives, fault storage may be implemented using on-chip SRAM, scan-accessible registers, or non-volatile elements to preserve repair information across power cycles.

3. Redundancy Analyzer (RA)

Evaluates the pool of available spare resources and determines the optimal redundancy unit—row, column, block, or higher-level structure—based on fault location, fault multiplicity, and allocation constraints. Advanced analyzers may employ heuristic decision rules or optimization algorithms to maximize repair coverage and minimize spare consumption.

4. Remapping Logic (RML)

Modifies the address decoding path to redirect memory accesses from defective elements to their assigned spare counterparts. Implementation options include fuse-programmed decoder modifications, programmable indirection tables, or shadow decoding structures capable of supporting runtime updates.

5. Repair Controller (BIRA)

Coordinates the repair sequence by managing communication between the Redundancy Analyzer and the Remapping Logic. The Built-In Redundancy Analysis (BIRA) controller may initiate fuse programming, activate shadow remapping structures, and validate post-repair

memory accesses. Functionally, BIRA serves as the supervisory control layer of the BISR architecture.

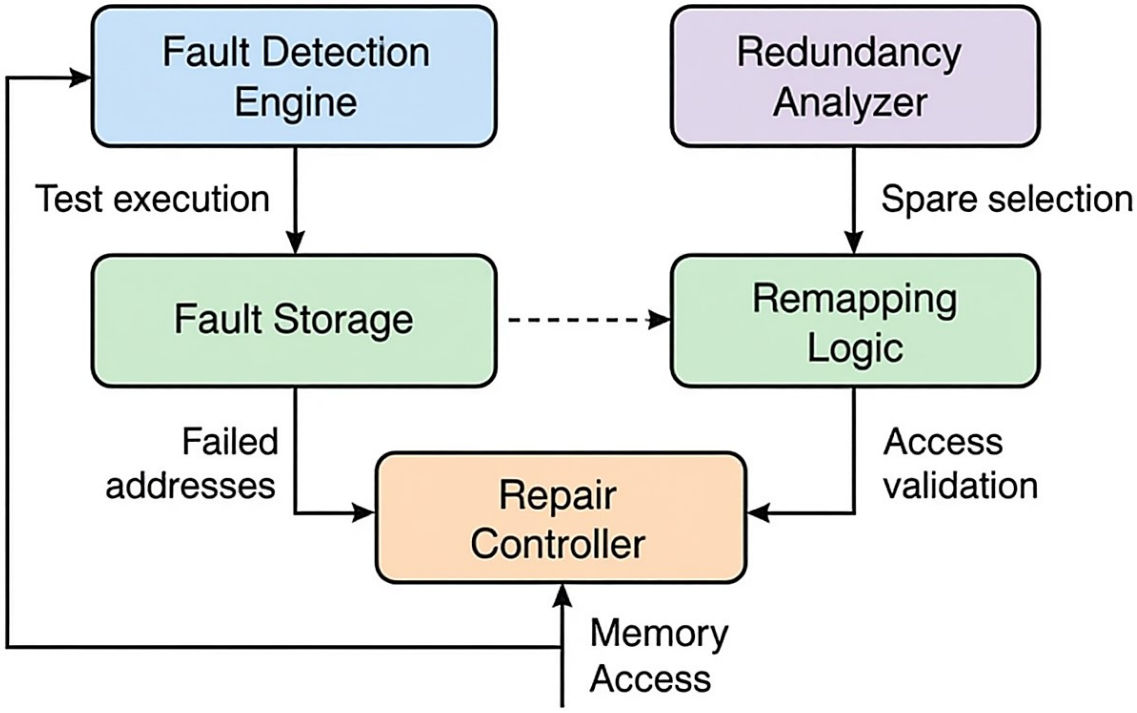

Figure 6.1—BISR system diagram with detection, mapping, and validation paths

Figure 6.1 depicts the logical organization of a Built-In Self-Repair system embedded within a memory array. Fault detection is initiated by the Fault Detection Engine, which identifies permanent defects using either BIST routines or symbolic diagnostic mechanisms. Detected failures are recorded in Fault Storage, forming a centralized repository of failing addresses and diagnostic metadata.

The Redundancy Analyzer evaluates available spare resources and selects an appropriate repair strategy. This decision is forwarded to the Remapping Logic, which alters the address decoding path to bypass defective structures and redirect accesses toward designated spares.

The Repair Controller (BIRA) supervises this process, coordinating redundancy allocation, invoking remapping actions, and validating subsequent memory accesses through a feedback loop.

Dashed connections in the diagram indicate auxiliary data flows, including metadata exchange and access revalidation, emphasizing the closed-loop nature of the repair architecture.

Architectural principles for combining built-in self-test with recovery mechanisms were previously explored in EWDTW (2012).[7]

6.4 Redundancy Mapping Mechanisms

Once a defect has been diagnosed and a suitable spare resource selected, the memory system must perform address remapping to exclude the faulty element from the active address space.

Several architectural mechanisms exist for implementing this translation, each characterized by distinct trade-offs in latency, flexibility, persistence, and implementation complexity.

6.4.1 Fuse-Based Remapping

Fuse-based remapping encodes defective row or column addresses using programmable laser fuses or electrical fuses (eFuses).

These fuses are programmed after fabrication during production testing and are incorporated into the address decoding logic during power-on initialization. Fuse-based schemes are widely deployed in commodity DRAM and embedded DRAM (eDRAM), where static, non-volatile repair is sufficient.

The primary advantage of fuse-based remapping is the absence of runtime lookup latency and its inherent robustness.

However, once programmed, fuse configurations cannot adapt to post-deployment failures or aging-induced degradation.

6.4.2 Shadow Mapping

Shadow mapping enables runtime address remapping through programmable control logic. Faulty addresses are stored in auxiliary structures such as content-addressable memories (CAMs), which support parallel match-based translation, or remap tables maintained by firmware or BIRA control logic.

This approach supports dynamic substitution of defective regions and facilitates wear-aware or degradation-responsive repair strategies throughout the operational lifetime of the device. While shadow mapping provides significantly greater flexibility than fuse-based approaches, it introduces additional lookup latency and requires non-trivial control and validation logic.

6.4.3 Hash-Based or Indirect Remapping

Hash-based or indirect remapping mechanisms are predominantly employed in NAND Flash, solid-state drives (SSDs), and other wear-leveled non-volatile memory systems.

In these architectures, logical-to-physical address mapping is fully decoupled from the physical memory layout and maintained in metadata structures such as Flash Translation Layers (FTLs), mapping tables, or journaling logs. This indirection enables out-of-order remapping, garbage collection, and the dynamic exclusion of defective blocks without exposing physical address changes to the host or application layer.

The principal advantage of indirect remapping lies in its high flexibility, allowing defective regions to be bypassed while simultaneously supporting endurance management and wear-leveling strategies.

However, this approach introduces additional controller complexity and places strong correctness and reliability requirements on metadata integrity, since mapping corruption can lead to catastrophic data loss.

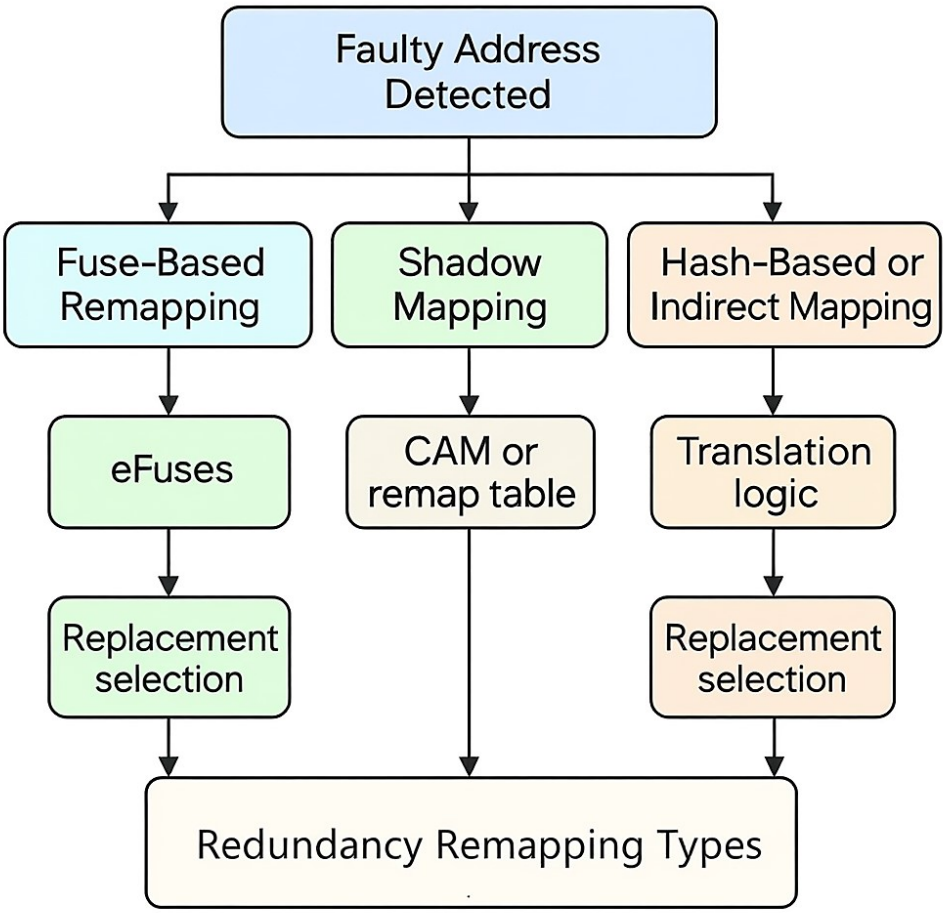

Figure 6.2—Redundancy Remapping Types

Figure 6.2 illustrates three principal remapping techniques employed in Built-In Self-Repair (BISR) systems.

Fuse-based remapping uses laser fuses or electrical fuses (eFuses) to permanently encode the addresses of faulty rows or columns into the address decoder at power-on. This approach is widely adopted in DRAM and embedded DRAM (eDRAM) designs, where it enables low-latency, non-volatile repair during high-volume manufacturing.

Shadow mapping performs dynamic address redirection using runtime-configurable structures such as content-addressable memories (CAMs) or programmable remap tables. Its reconfigurability supports field repair, degradation-aware adaptation, and aging mitigation, making it suitable for systems subject to evolving fault profiles.

Hash-based or indirect mapping is characteristic of NAND Flash and other non-volatile memory systems, where logical-to-physical translation layers abstract physical defects from the external address space. Defective blocks are substituted transparently through metadata updates rather than direct modification of fault addresses.

In all cases, a diagnosed faulty address initiates the remapping process, which redirects accesses to a designated spare location through the corresponding control path. The three

mechanisms embody distinct trade-offs between architectural simplicity, runtime latency, and adaptability to long-term fault evolution.

Within the Optimal_Test simulations, shadow mapping was modeled using symbolic aliasing operators that dynamically rebind logical addresses to spare resources. This representation preserved traceability of fault propagation and prevented infinite retry loops or address-echo artifacts during revalidation phases. The resulting model formed a hybrid abstraction between CAM-based remapping and pattern-aware symbolic testing, balancing runtime flexibility with diagnostic observability.

6.5 Repair Yield Modeling and Optimization

In semiconductor manufacturing, yield denotes the fraction of fabricated dies that successfully satisfy all functional and parametric test requirements. As feature dimensions shrink and bit densities increase, the probability of at least one permanent defect per die approaches unity. Under these conditions, redundancy and BISR mechanisms become essential for sustaining acceptable yield and economic viability.

Not all repair strategies, however, deliver equivalent yield recovery. The effectiveness of a given BISR scheme depends on the interaction of multiple factors, including:

- **Defect spatial distribution:** random versus clustered fault patterns and fault-class prevalence.
- **Redundancy layout geometry:** row-to-column coverage ratios, spare placement, and allocation granularity.
- **Repair algorithms:** greedy versus optimal mapping strategies, partial-coverage policies, and spare reuse constraints.
- **Test coverage completeness:** the influence of undetected or escaped faults on achievable repair outcomes.

Within the Optimal_Test framework, symbolic repair-yield models were developed that incorporate statistical distributions of observed failure maps, spatial redundancy availability, and the fault-activation effectiveness of applied test patterns. These models further integrate symbolic aliasing and historical trace data to capture fault recurrence behavior under evolving repair states.

Beyond estimating raw repair success probability, the proposed modeling approach evaluates spare sufficiency, predicts the likelihood of redundancy exhaustion, and quantifies the risk of fault escapes under incomplete diagnostic coverage. By coupling symbolic test modeling with redundancy allocation analysis, the framework enables a test-informed BISR flow that adapts yield-recovery strategies dynamically to observed device behavior and long-term defect evolution.

Such modeling enables informed design decisions regarding redundancy provisioning and repair policy selection. By linking diagnostic coverage with redundancy allocation strategies, repair yield can be optimized to maximize both manufacturing efficiency and long-term device reliability.

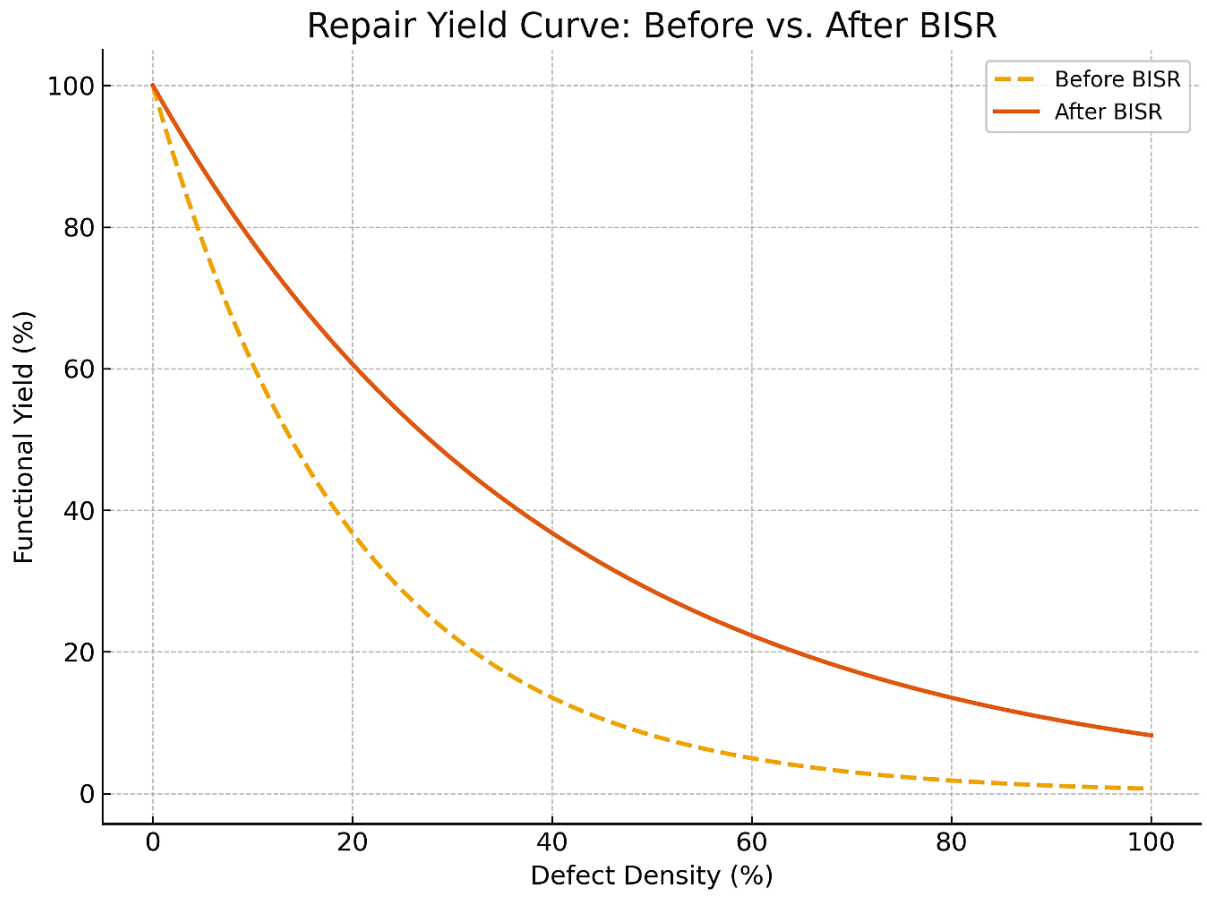

Figure 6.3—Repair Yield Curve: Before vs. After BISR

Figure 6.3 illustrates the impact of Built-In Self-Repair (BISR) on functional memory yield as defect density increases. The dashed curve represents baseline yield in the absence of redundancy, where even a small number of random defects rapidly renders dies unusable under strict pass/fail criteria.

In contrast, the solid curve depicts yield after the activation of BISR mechanisms, in which spare rows, columns, or blocks are employed to replace defective regions.

The Figure demonstrates that BISR significantly moderates the exponential decay of yield, sustaining a non-zero fraction of functional dies even at elevated defect densities. This effect is particularly critical for high-density DRAM and advanced three-dimensional non-volatile memory technologies, where the probability of fabricating defect-free dies becomes negligible at advanced technology nodes.

Within the Optimal_Test modeling environment, yield uplift was quantified using symbolic repair logic driven by recurrence-aware fault maps.

For the 1 Gb DRAM configuration used in these simulations, the model produced an increase of up to approximately 9% in usable dies; the reported power observation refers to average power attributable to the repair-control logic within the simulation model.

6.5.1 Yield Recovery Function (YRF)

To formalize the effect of redundancy on yield, the **Yield Recovery Function (YRF)** is introduced.

Let

- D: average defect density (defects/cm²),
- A: physical area of the memory array (cm²),
- P_r: probability that a defective die is repairable given the available redundancy,
- Y_0: baseline yield without repair
- Y_r: yield after repair.

Assuming a Poisson defect distribution, the baseline yield without redundancy is

$$Y_0 = e^{-DA}$$

where $e \approx 2.71828$ is the base of the natural logarithm. This expression represents the probability that a die contains zero defects over area A, and it captures the rapid exponential yield degradation characteristic of defect-limited manufacturing in the absence of repair.

When redundancy and repair are introduced, the yield improves to

$$Y_r = P_r . e^{-DA}$$

Here, P_r reflects the conditional probability that all defects present on a die can be isolated and remapped using available spare resources.

The value of P_r is influenced by several factors:

- **Redundancy structure:** number, type, and spatial distribution of spares (rows, columns, blocks).
- **Fault distribution:** random versus clustered topologies and spatial correlation effects.
- **Test coverage and accuracy:** the ability of BIST or symbolic diagnostics (Optimal_Test) to detect, localize, and classify faults.

Within the Optimal_Test framework, P_r was modeled symbolically, incorporating test coverage metrics, spare allocation heuristics, and historical recurrence of fault traces. This formulation enabled prediction of redundancy exhaustion thresholds and identification of fault-escape regimes arising from limited spares or incomplete diagnostic observability.

6.5.2 Spare Allocation Strategies

The effectiveness of Built-In Self-Repair (BISR) depends not only on the quantity of available redundancy but also on the strategy used to allocate spare resources once faults are detected.

Allocation strategy determines how efficiently redundancy is consumed, how well clustered faults are absorbed, and how long repair capacity can be sustained as defect density increases.

Two orthogonal dimensions dominate spare allocation decisions: **the spatial granularity of mapping** (row versus column) and **the timing of allocation** (immediate versus globally optimized).

A. Row-First vs. Column-First Allocation

Row-first and column-first strategies differ in how defect locality is interpreted and translated into redundancy assignments.

- **Row-First Allocation** prioritizes remapping entire wordlines and is highly effective against vertically aligned fault patterns, such as row-decoder failures, wordline driver degradation, or clustered defects extending across multiple bit positions within a single row.
- **Column-First Allocation** targets defective bitlines and is more effective for horizontally correlated faults, including bitline coupling, sense-amplifier degradation, or isolated leakage paths affecting multiple rows.
- **Mixed-Mode Strategies** dynamically evaluate fault topology and select row- or column-level remapping based on clustering density, spatial correlation metrics, or symbolic trace analysis derived from diagnostic execution.

Modern memory systems increasingly employ **adaptive switching** between row-first and column-first strategies, guided by diagnostic observables, to maximize repair coverage while preserving redundancy for future fault events.

B. Greedy vs. Optimal Mapping

Beyond spatial choice, spare allocation strategies also differ in how and when mapping decisions are made.

- **Greedy Mapping** assigns the first available spare immediately upon fault detection. This approach enables rapid repair with minimal control complexity, making it attractive in time-constrained production environments.

  However, greedy allocation often leads to inefficient spare usage and increases the risk of premature redundancy exhaustion.
- **Optimal Mapping** defers spare assignment until the complete fault set has been identified, solving a global optimization problem that minimizes spare consumption and mapping conflicts.

While optimal mapping is NP-hard in the general case, symbolic cost models and heuristic solvers enable near-optimal solutions to be realized in practice.

Within the Optimal_Test framework, repair cost matrices were constructed using fault location, fault recurrence statistics, and spare proximity.

Symbolic repair paths were then selected to minimize fault-escape probability while reducing adverse interactions with ECC correction domains.

Strategy Summary

The qualitative characteristics and preferred application domains of the discussed allocation strategies are summarized in Table 6.2.

Table 6.2—Spare allocation strategy summary (row-first/column-first and greedy/optimal mapping)

Strategy Type	Characteristics	Best Used When
Row-First	Prioritizes remapping of entire wordlines; highly effective against vertical or decoder-related faults.	Faults aligned along rows (e.g., wordline driver failures, vertical defect domains).
Column-First	Targets defective bitlines; efficient against horizontal failures or sense amplifier-related defects.	Horizontal coupling faults or isolated bitline leakage.
Greedy Mapping	Allocates the first available spare during test-time fault discovery; fast but not resource-optimal.	Low-complexity test environments or time-constrained production repair.
Optimal Mapping	Analyzes the complete fault set to minimize spare usage; typically requires symbolic modeling or post-processing.	High-value or redundancy-limited chips where spare usage efficiency is critical.

6.5.3 Clustered vs. Random Fault Models

Defect distributions in fabricated memory arrays are rarely purely random. Process variation, layout effects, and operational stress often produce spatially clustered fault patterns.

Clusters commonly arise at wordline–bitline intersections, through-silicon-via (TSV) interfaces, array peripheries, and regions affected by lithographic non-uniformity or thermal gradients. Power-delivery asymmetries further exacerbate localized defect hotspots.

To capture these effects, heatmap-driven symbolic fault simulators were developed, generating clustered defect topologies using layout-aware statistical models. These simulators were integrated with repair planners that optimized spare usage by balancing fault coverage, redundancy preservation, and the spatial distribution of remaining repair capacity. This approach improved both predictive yield estimation and practical repair effectiveness for high-density and three-dimensional memory architectures.

6.5.4 Repair Cost Metrics

Each redundancy allocation decision incurs a multidimensional cost. Within the BISR framework, repair decisions are evaluated using a **repair cost vector**, comprising:

- **Spare usage cost:** number and class of spares consumed.
- **Address-mapping complexity:** additional latency or logic overhead introduced into the decoding path.
- **ECC integration overhead:** alignment effects on codeword boundaries, correction locality, and syndrome observability.

- **Test revalidation cost:** necessity to rerun diagnostic sequences (e.g., March tests, BIST routines, ECC logging) after remapping.

In Optimal_Test, these costs were represented symbolically and minimized through constrained decision-tree traversal, subject to spare-budget limits, latency ceilings, and ECC compatibility constraints. This formulation enables evaluation of repair quality beyond binary success or failure.

6.5.5 Repair Efficiency Curves

To evaluate the influence of redundancy configuration on repairable yield, symbolic simulations were conducted across varying spare allocations. Table 6.3 summarizes the resulting yield recovery for different redundancy types.

Table 6.3—Yield recovery versus spare allocation

Spare configuration	1 Spare/Block	2 Spares/Block	3 Spares/Block
Row-only	78 %	92 %	97 %
Column-only	74 %	90 %	96 %
Hybrid (row + column)	85 %	95 %	99.5 %

The results indicate that while increasing redundancy consistently improves yield, hybrid configurations combining row and column spares with reconfigurable remapping logic achieve the highest repair efficiency.

Symbolic simulations further show that hybrid BISR architectures deliver the greatest repair coverage per unit area in high-density DRAM arrays subject to both random and clustered defects, underscoring their suitability for defect-prone advanced memory technologies.

6.6 Retesting and Validation in BISR Systems

Redundancy mapping alone does not guarantee long-term fault containment. Once spare resources are allocated, the memory system must revalidate its operational state to ensure that residual, secondary, or newly exposed faults do not compromise the repair outcome. This section formalizes the necessity of post-repair validation and presents structured retesting mechanisms required to ensure sustained correctness in BISR-enabled memory systems.

6.6.1 Why Retesting Is Critical

Even after successful remapping of a defective row, column, or block, multiple classes of failure may persist or emerge:

- **Residual fault effects:** original defective cells may continue to induce coupling, leakage, disturb behavior, or charge sharing across adjacent addresses.
- **Decoder aliasing:** incorrect or incomplete remapping may result in multiple physical locations responding to a single logical address.

- **Address echo faults:** duplicated read or write responses may occur following faulty indirection logic.
- **Latency misalignment:** shadow-mapping logic may introduce decode delays or violate alignment constraints relative to ECC codeword boundaries or controller timing windows.

False repair scenarios are also common:

- **Transient disturbances** (e.g., voltage noise, soft errors, marginal timing) may be misclassified as permanent faults, leading to unnecessary spare consumption.
- **Diagnostic mislocalization** may redirect repairs to incorrect addresses, leaving the true defect active.

In DRAM simulation experiments conducted within the Optimal_Test environment, systems that omitted post-repair revalidation—particularly those relying on reduced-coverage March tests for throughput optimization—exhibited frequent false-positive repairs. Such devices often appeared functional immediately after remapping but later failed under stress conditions or during extended field operation.

These observations demonstrate that **repair-aware retesting loops and ECC-synchronized validation are mandatory** in high-reliability memory architectures.

6.6.2 Repair-Aware Retest Sequences

Within the Optimal_Test framework, post-repair verification is implemented using symbolic retest scripts that combine March-style traversal with stress-sensitive operations. An illustrative example is:

$$\uparrow(W_0, R_0, W_1); \downarrow(R_1, W_0); P\_\{CB\}; \mathrm{WAIT}_{(64\ \mathrm{ms})}; \downarrow(R_0)$$

These symbolic retests are designed to validate:

1. **Stability of remapped spare elements** under write, read, and temporal stress.
2. **Absence of residual or induced faults** in neighboring regions affected by remapping.
3. **Correct reconvergence of timing and ECC behavior** following address redirection.

Symbolic retesting serves a dual function: it reconfirms diagnostic conclusions while suppressing false positives caused by transient disturbances or incomplete localization. This targeted approach avoids the prohibitive cost of full-system revalidation after every repair action while maintaining high confidence in post-repair correctness.

6.6.3 Repair Tagging and Metadata Logging

Each repair event must be recorded as a structured diagnostic artifact. Persistent repair metadata supports immediate verification, long-term reliability assessment, and field-level traceability. Essential metadata fields include:

- **Fault type:** e.g., stuck-at, transition, coupling, decoder malfunction.
- **Fault address and scope:** precise location and granularity (bit, word, row, column, or block).

- **Detection timestamp:** test phase or operational time at which the fault was identified.
- **Assigned spare:** redundancy class and identifier of the remapped resource.
- **Retest result:** pass/fail outcome following post-repair validation.
- **ECC behavior:** transition of error status (e.g., SEC-required → clean pass).

In the Optimal_Test diagnostic framework, repair events are encoded as symbolic repair tags, for example:

[REPAIR] @0x00F342; TYPE=COLUMN; SRC=col_23; DST=sp_col_2;
ECC=SEC→PASS; RETEST=OK

This record indicates that a fault detected at logical address 0x00F342, associated with column 23, was remapped to spare column 2, thereby eliminating a previously observed single-error-correction condition.

Repair tags are written to non-volatile storage to support:

- **Field diagnostics:** enabling root-cause tracing during deployment.
- **Aging analysis:** identifying wear-prone regions and recurrent fault patterns.
- **RMA screening:** filtering returns based on verified repair histories rather than raw failure counts.

By transforming transient repair actions into persistent, auditable system events, repair tagging enhances transparency and trust in autonomous BISR mechanisms.

6.6.4 Multi-Level Repair Revalidation

In advanced memory hierarchies—such as multi-level cache systems or three-dimensional stacked architectures (e.g., HBM)—successful repair at a single level does not guarantee global correctness. Repair validation must therefore propagate across architectural layers and timing domains.

Key validation tasks include:

- **Cross-level propagation tests:** ensuring that remapping at lower levels is correctly reflected in higher-level caches, coherence mechanisms, and fetch paths.
- **Timing-aware validation:** confirming that redirected accesses satisfy controller timing constraints (e.g., t_{RCD}, t_{FAW}, activation windows), particularly when spare resources reside in slower banks or tiers.
- **ECC syndrome tracing:** comparing syndrome patterns before and after repair to verify that fault signatures are eliminated rather than merely masked.

For three-dimensional memory systems, additional vertical-integration challenges must be addressed:

- **Inter-die skew:** preventing clock or data misalignment across stacked dies following remapping.
- **Command propagation integrity:** validating command delivery and response coherence across tiers.

- **TSV synchronization:** detecting failures in through-silicon vias used for remapped data paths or repair control signaling.

In Optimal_Test, multi-level validation is realized through hierarchical symbolic test passes that enforce consistency across all memory layers, ensuring that localized repairs achieve system-wide correctness.

6.6.5 Repair Retest Failure Handling

When post-repair validation detects persistent errors, the system must transition into a controlled escalation path. Such failures typically indicate one of three root causes: defective spare elements, incorrect fault localization, or deeper architectural degradation (e.g., controller-side faults).

In these cases:

- The repair attempt is marked as unsuccessful.
- The allocated spare may be released and an alternative spare assigned, if available.

If no viable remapping remains, the defect is classified as unrepairable, triggering higher-level containment strategies:

- **ECC-only fallback:** continued operation relying exclusively on error correction.
- **Memory offlining:** deactivation of entire pages or banks with OS-level quarantine.
- **Page quarantine:** isolation of sub-regions to prevent silent data corruption.
- **Performance downgrade:** operation in reduced-performance modes (e.g., ECC mirroring, read-only fallback).

Within the Optimal_Test framework, repair failure handling is formalized as a **symbolic repair failure ladder**, which escalates containment actions based on:

- Fault class (permanent versus intermittent),
- Syndrome entropy (variability across retests),
- Diagnostic confidence metrics derived from symbolic analysis.

This tiered escalation model ensures that all feasible recovery options are exhausted before declaring catastrophic failure, maximizing operational survivability.

6.6.6 Summary

Repair without validation introduces systemic risk. Effective fault tolerance in modern memory systems requires not only corrective action but also rigorous confirmation through structured retesting, ECC reconfirmation, symbolic trace replay, and persistent metadata logging.

In the proposed architecture, every repair action is followed by an integrated, repair-aware revalidation sequence embedded within the symbolic test engine. This approach ensures that post-repair memory does not merely resume operation but demonstrably satisfies correctness and reliability constraints.

Such validation-centric BISR frameworks are indispensable as semiconductor memories continue to scale toward higher density, greater architectural complexity, and increased susceptibility to permanent and progressive faults.

6.7 Runtime Repair, ECC Thresholding, and Wear-Aware Remapping

As memory systems evolve toward higher densities, tighter integration, and increased reliance on non-volatile technologies, repair can no longer be treated as a static, post-manufacturing procedure. Resilience must transition from a one-time remediation step executed during fabrication or system initialization into a **continuous operational service** active throughout the memory lifecycle.

Unlike classical BISR, which is typically executed once to correct manufacturing defects, runtime repair operates dynamically. It monitors device health under live workloads, detects progressive degradation, and transparently redirects memory accesses in real time to preserve functional integrity.

Runtime resilience in modern memory systems rests on three foundational pillars:

1. **Dynamic Repair** — on-the-fly fault containment through address redirection.
2. **ECC Thresholding** — use of error statistics as early indicators of degradation.
3. **Wear-Aware Remapping** — stress redistribution to extend usable device lifetime.

All runtime repair operations are designed to remain transparent to operating systems and applications, preserving logical memory semantics while enforcing physical resilience constraints.

In conventional DRAM-based systems, such runtime redirection is realizable only through hardware-assisted lookup mechanisms integrated within the memory controller, cache hierarchy, or dedicated repair logic, and is not intended as a purely software-mediated operation on standard DDR-class memories.

6.7.1 Runtime Repair Architecture

Contemporary runtime repair architectures employ feedback-driven intelligence spanning both hardware and firmware layers. Core components typically include:

- **Error log buffers:** capture corrected and uncorrected ECC events, recording frequency, spatial locality, and temporal correlation.
- **Microcontroller-based repair engines:** execute firmware-level routines to classify faults, allocate spares, or throttle activity in stress-prone regions.
- **On-Demand Redirection Tables (ODRTs):** maintain real-time address translation entries mapping faulty physical locations to spare rows, columns, or blocks.
- **Wear monitors:** track per-bank or per-page usage to detect imbalance and predict stress-induced degradation.

Within the Optimal_Test framework, runtime resilience is informed by post-BIST telemetry modules that continuously monitor:

- thermal-induced degradation caused by uneven heating or cycling,

- read-disturb phenomena in memories prone to threshold drift,
- accelerated ECC correction rates signaling emerging fault clusters.

When monitored metrics exceed predefined thresholds, the runtime repair engine dynamically engages containment mechanisms such as:

- **Row deactivation:** preventing further access to suspect wordlines.
- **Column masking:** omitting failed bits through bit-level bypass or ECC masking.
- **Swap-and-redirect:** migrating cache lines or pages to verified spare regions.
- **Region lockout:** quarantining entire banks or subarrays when reliability outweighs availability.

All runtime repair operations are designed to remain transparent to operating systems and applications, preserving logical memory semantics while enforcing physical resilience constraints.

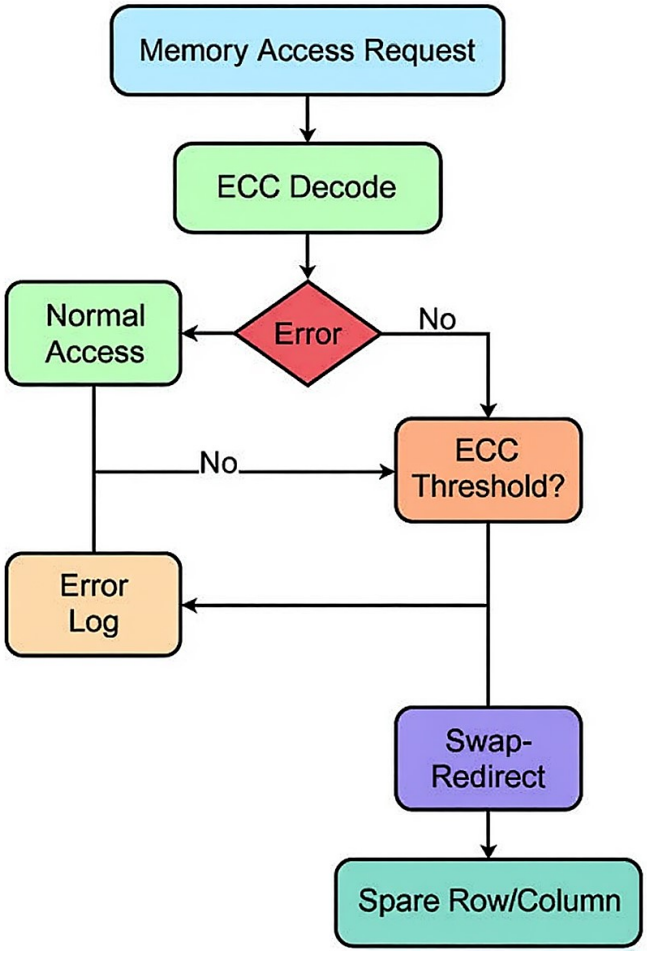

Figure 6.4 —Runtime repair path flow with ECC integration and spare redirect logic

Figure 6.4 illustrates the runtime repair flow integrating ECC telemetry with spare redirection logic. Each memory access is first processed by the ECC decoder. If no error is detected, the access proceeds normally. When an error is detected, the system evaluates whether cumulative error frequency or severity exceeds a predefined ECC threshold.

- If the threshold is not exceeded, the error is logged and treated as tolerable.
- If the threshold is exceeded, a swap-and-redirect operation is initiated, remapping subsequent accesses to a designated spare row or column.

This flow enables non-disruptive fault containment by distinguishing transient disturbances from emerging permanent failures using real-time telemetry.

6.7.2 ECC Thresholding and Predictive Alerting

Error-Correcting Codes (ECC) serve a dual role in modern memory systems: they correct transient faults and provide early indicators of physical degradation. Thresholding policies define when ECC activity transitions from background noise into actionable fault evidence, enabling preventive intervention before catastrophic failure.

Key thresholding mechanisms include:

- **Correctable-error rate thresholds:** maximum allowable correction counts before triggering repair.
- **Uncorrectable error detection:** indicating structural or endurance-related failure.
- **Syndrome clustering:** identifying spatial or temporal concentrations of errors associated with retention loss, leakage, or row-hammer precursors.

In my work on fuzzy rule-based optimization, ECC telemetry was processed using syndrome-count gradients and region-weighted metrics within a Sugeno-type fuzzy inference engine. Memory regions were dynamically ranked by repair urgency based on severity, recurrence, and fault locality. The complete fuzzy rule base, membership functions, and evaluation protocol for this scheduler are presented in Chapter 13.

High-reliability platforms integrate ECC telemetry into proactive RAS (Reliability, Availability, and Serviceability) infrastructures, enabling:

- detailed logging of syndrome vectors and correction histories,
- proactive page migration or cache-line redirection,
- scheduled scrub cycles to suppress latent bit errors.

ECC thresholding is particularly critical in environments requiring uninterrupted correctness, including enterprise servers, safety-critical automotive platforms (ASIL-D), and thermally unstable edge-AI deployments.

6.7.3 Wear-Aware Remapping and Aging Management

In emerging non-volatile memory technologies such as NAND Flash, ReRAM, and PCM, cell wear dominates long-term failure behavior. Each program/erase or resistance-modulation event contributes to gradual degradation, making wear-aware remapping a fundamental requirement for runtime reliability.

Core mechanisms include:

- **Per-block write counters:** tracking cumulative stress.
- **Hotspot detection:** identifying frequently accessed regions prone to early failure.

- **Dynamic wear leveling:** redistributing activity to balance degradation.
- **Adaptive thresholding:** combining error frequency with usage intensity.

Technology-specific wear indicators are also employed:

- **PCM:** resistance drift monitored through SET/RESET variability.
- **MRAM:** tunnel-barrier degradation inferred from shifting voltage margins.

In my symbolic modeling framework, wear-out was abstracted as a time-evolving probabilistic operator with monotonically increasing activation likelihood. This abstraction enabled stochastic remapping triggers and fuzzy alert logic, supporting predictive responses to degradation.
The formal operator definition and its validation context are provided in Chapter 8.

Wear-aware remapping further addresses system-level constraints, including:

- interconnect contention mitigation,
- thermal hotspot avoidance near regulators or compute units,
- isolation of unstable power-delivery domains.

Next-generation memory controllers increasingly unify wear tracking, ECC analytics, scrubbing, and remapping into a single runtime resilience service.

6.7.4 Summary

Runtime repair marks a transition from static test-and-fix paradigms to adaptive, intelligence-driven fault management. By combining real-time ECC telemetry, probabilistic aging models, and wear-aware remapping, modern memory subsystems can anticipate degradation and mitigate failure without interrupting execution or compromising data integrity.

The resulting memory architecture operates not as a passive storage array but as an active diagnostic and self-protective subsystem. This vision—rooted in symbolic modeling, stochastic fault prediction, and runtime optimization—forms a central pillar of the broader framework developed in this work.

As density and architectural complexity continue to rise, such runtime resilience mechanisms become not optional enhancements, but essential design requirements.

A collaborative in-field recovery architecture and associated control policies are documented in Appendix F.

6.8 Controller-Level Error Containment and Scrubbing Policies

As memory systems scale to gigabyte- and terabyte-class capacities with increasing density and fault susceptibility, the memory controller has emerged as a central element of runtime reliability enforcement.

Once limited to traffic arbitration and timing management, the controller now functions as a **real-time diagnostic, containment, and remediation engine**, continuously monitoring error activity, orchestrating scrubbing operations, and enforcing system-level resilience policies.

Unlike static pattern-based testing—which is primarily effective for fabrication-time or dormant defects—controller-level mechanisms operate during live execution. They address transient disturbances, environmentally induced anomalies, and progressive aging-related degradation, ensuring that availability and data integrity are maintained under real workloads.

Core controller-level resilience mechanisms include:

- **Proactive scrubbing:** background verification and correction of latent bit errors before accumulation leads to uncorrectable states.
- **Error quarantine:** isolation of memory regions that exceed ECC correction thresholds or exhibit anomalous fault behavior.
- **Flow-aware integrity control:** adaptive refresh and access scheduling policies responsive to recent error activity and environmental telemetry (e.g., temperature, voltage).

These mechanisms integrate low-level hardware support with firmware-level intelligence, enabling context-aware reliability enforcement. Much of this integration builds on the post-diagnosis monitoring and adaptive response frameworks developed within the Optimal_Test ecosystem, particularly its runtime response and telemetry-driven modules.

6.8.1 Role of the Memory Controller in Error Management

Modern memory controllers coordinate interactions between processing cores and memory subsystems, including DRAM, LPDDR, HBM, and emerging NVM technologies. Their role now extends well beyond scheduling and bandwidth optimization to encompass a comprehensive set of fault containment and mitigation functions, including:

- **ECC decoding and syndrome analysis:** immediate interpretation of ECC syndromes to distinguish correctable, uncorrectable, and suspicious multi-bit error patterns.
- **Access reordering and isolation:** dynamic scheduling to deprioritize or bypass degraded banks, rows, or channels.
- **Scrubbing task orchestration:** launching background verification passes during idle or low-utilization windows, with adaptive intensity for error-prone or aging-sensitive regions.
- **Reliability-aware command management:** issuing refresh, activate, precharge, and power-state transitions under integrity-driven constraints rather than purely performance-driven criteria.
- **Telemetry-driven logging and quarantine:** persistent recording of fault addresses, syndrome vectors, error density metrics, and thermal correlations to construct a longitudinal profile of vulnerable regions.

Advanced controllers integrate these functions within RAS (Reliability, Availability, Serviceability) firmware stacks. In enterprise and mission-critical platforms, such stacks may autonomously trigger:

- region-level quarantine,
- DIMM, channel, or vault offlining,
- ECC mode escalation (e.g., SECDED to Chipkill),

- firmware-managed refresh intensification.

In the architecture developed in this work (see Section 6.7), a runtime repair engine is co-located within controller logic. This engine interprets symbolic fault maps, ECC syndrome clusters, and usage telemetry in situ, enabling rapid, localized containment without halting memory traffic or relying exclusively on software-level exception handling.

6.8.2 Error Containment Strategies

Upon detection of abnormal error behavior, the controller transitions from correction to containment. The objective shifts to preventing fault propagation, preserving system uptime, and protecting data integrity. Containment is enforced across hardware, firmware, and system-software layers, guided by real-time telemetry and policy thresholds.

(A) Line-Level Quarantine

Fault-prone cache lines, pages, or blocks are tagged as suspect after repeated ECC anomalies or diagnostic feedback. Once marked, such regions are:

- removed from allocation pools to prevent new data placement,
- excluded from cache refill paths to block upward propagation of corrupted data,
- subjected to remediation actions, including:
  - **page migration** in DRAM systems,
  - **block retirement** in non-volatile memories.

This strategy provides fine-grained containment at minimal performance cost and is particularly effective for localized degradation.

(B) Poison Bit Injection

When an uncorrectable ECC error is detected, the controller may inject a poison indicator into the data path or cache metadata:

- any access to the poisoned line triggers a machine check exception (MCE) or equivalent interrupt,
- system software (OS, hypervisor, or RAS service) responds by:
  - logging the fault,
  - invalidating corrupted data,
  - migrating workloads,
  - retiring the affected address range.

Poisoning enforces fail-fast semantics, ensuring irrecoverable faults do not silently corrupt higher-level computation.

(C) Thermal Fault Correlation

Temperature is a dominant factor influencing fault rates in DRAM and three-dimensional stacked memories. Controllers equipped with thermal sensors apply temperature-aware containment by:

- monitoring gradients across banks, dies, or stacked layers,
- correlating error density with thermal excursions,

applying corrective actions such as:

  - throttling access to overheated regions,
  - redirecting traffic to cooler zones,
  - escalating refresh or power-down sequences.

This correlation enables proactive mitigation of thermally induced failure clusters and extends operational lifetime.

(D) Redundancy Reallocation

Memory devices often include built-in spare capacity at the row, column, or block level. The controller is responsible for invoking and managing these resources:

- **Fuse-based remapping (DRAM):** reprogramming internal or soft fuses to redirect defective addresses.
- **Logic-level redirection (HBM, 3D memories):** bypassing vertical or inter-die faults through controller-managed routing.
- **Embedded controller management (SoC DRAM, NVM):** executing redundancy control in tightly integrated architectures where the controller is the sole repair authority.

This capability enables in-field reconfigurability, allowing systems to recover from localized hardware failures without physical replacement.

Together, these containment mechanisms ensure that localized hardware faults do not escalate into system-wide failures.

By coordinating controller-level responses with firmware policies and operating system support, memory subsystems can maintain stable operation even under degraded conditions. Effective containment depends on timely fault detection, accurate telemetry analysis, and carefully calibrated escalation thresholds that balance reliability with performance impact. In large-scale systems, these strategies also support graceful degradation, allowing workloads to continue operating while defective regions are isolated or remapped.

When combined with ECC monitoring, BIST diagnostics, and redundancy management, containment policies become a central component of modern reliability, availability, and serviceability (RAS) architectures. Such coordinated approaches are essential for maintaining long-term stability in high-density memory systems deployed in data centers, embedded platforms, and safety-critical computing environments.

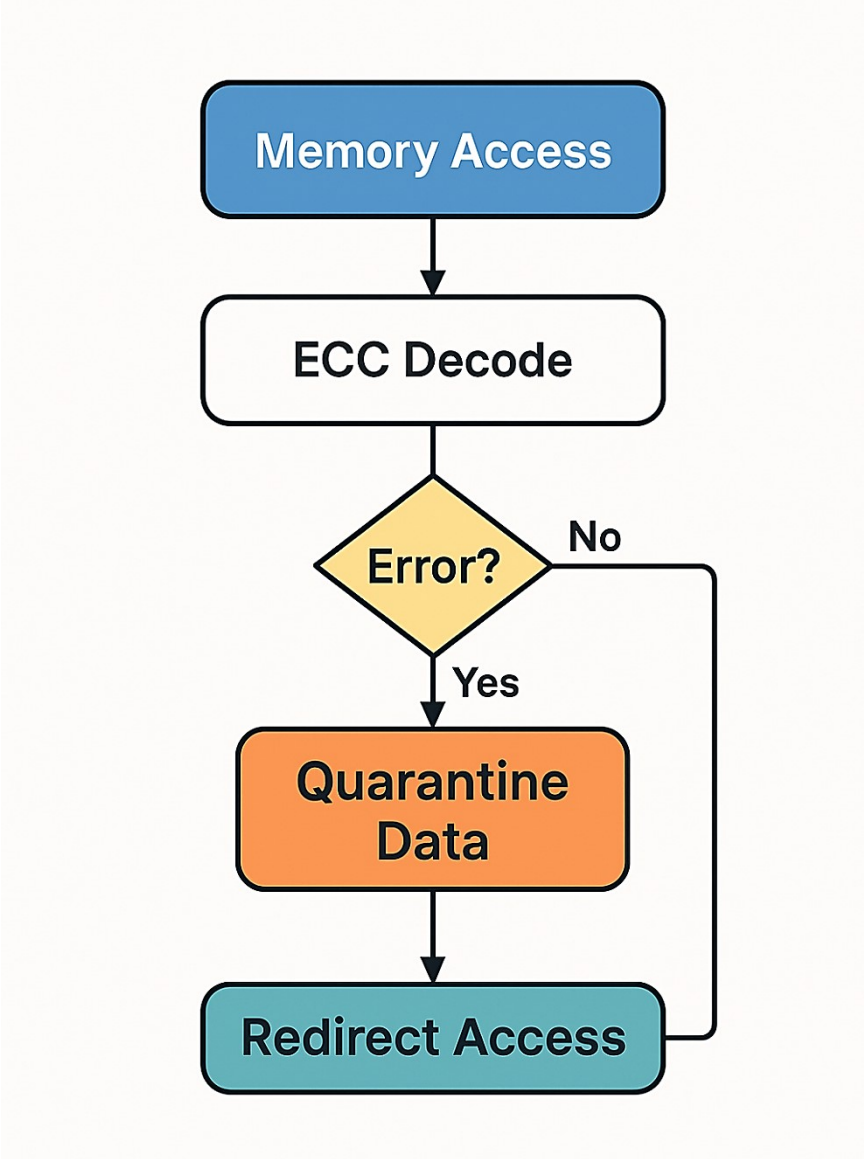

Figure 6.5—Fault containment layers with ECC, quarantine, and redirect flow

Figure 6.5 illustrates the multi-layer containment process orchestrated by the memory controller. Each memory access is first evaluated by ECC logic. In the absence of errors, execution proceeds normally. When an error is detected, containment policies are applied: the affected region is tagged for quarantine, and subsequent accesses are transparently redirected to spare or alternate locations.

This layered response—detection, containment, and recovery—preserves runtime data integrity while preventing fault exposure to the application layer.

6.8.3 Scrubbing Policies: Cleaning While Running

Memory scrubbing is the proactive, periodic reading and verification of memory contents independent of explicit access requests. Its primary objective is to prevent the silent accumulation of correctable errors which, if left unmitigated, may exceed ECC correction capability and escalate into uncorrectable system failures. Scrubbing therefore constitutes a

cornerstone of runtime reliability, particularly in long-uptime, mission-critical, and safety-certified systems.

Unlike static refresh mechanisms, scrubbing actively engages ECC decoding and correction logic, transforming latent faults into observable and recoverable events. Several scrubbing strategies are employed depending on system architecture, workload characteristics, and reliability requirements.

(A) Time-Interval Scrubbing

- Memory is partitioned into logical regions (e.g., banks, subarrays, rows), each assigned a periodic scrub interval (e.g., every 64 ms or configurable multiples thereof).
- Ensures uniform coverage of the address space and early detection of retention-related bit flips.
- Scrub cadence is typically controller-managed and interleaved with refresh operations to minimize interference with normal traffic.

This approach provides deterministic coverage guarantees but may incur unnecessary energy and bandwidth overhead in stable regions.

(B) Background Scrubbing

- Scrubbing is performed opportunistically during idle memory bus cycles or periods of low processor utilization.
- Minimizes interference with latency-critical workloads, preserving quality-of-service (QoS) guarantees.
- Often integrated with power-management logic, enabling scrub suppression or throttling in low-power states and thermally constrained environments.

Background scrubbing is particularly effective in mobile, embedded, and edge systems where energy efficiency is paramount.

(C) Access-Aware Scrubbing

- Cold memory regions—those infrequently accessed—are more susceptible to retention decay, leakage, and disturbance effects.
- Scrub prioritization algorithms identify these “silent risk zones” and apply targeted verification passes.
- Improves resilience under highly skewed access patterns, such as those found in cloud servers, database systems, and AI accelerators.

This strategy explicitly accounts for workload-dependent vulnerability rather than assuming uniform risk.

(D) Weighted and Adaptive Scrubbing

- Real-time telemetry (ECC correction logs, thermal sensors, write counters, usage history) is used to assign a dynamic risk weight to each memory region.

- Regions with elevated risk scores are scrubbed more frequently, while stable regions receive minimal intervention.
- Achieves superior fault coverage while avoiding unnecessary energy expenditure and bandwidth consumption.

Within the fuzzy-logic optimization framework, a rule-based adaptive scrub scheduler was developed to adjust scrub intensity based on:

- syndrome clustering and spatial fault proximity,
- thermal stress indicators,
- regional usage intensity and wear distribution.

Symbolic simulation with fault-injection heatmaps demonstrated that this adaptive scheduler provided higher resilience and improved energy efficiency compared to fixed, uniform scrubbing policies. The rule formulation and adaptive selection metrics governing scrub intensity are developed in Chapters 13 and 14, where the fuzzy inference structure and coverage–cost trade-off criteria are formally defined.

6.8.4 Integration with Higher-Level Error Management

Controller-level resilience mechanisms do not operate in isolation. To ensure system-wide correctness, they must integrate with higher-level firmware and software policies so that local containment decisions propagate coherently to global resource management.
Key integration points include:

- **Operating systems (OS):**
  - page migration, memory offlining, and NUMA-aware rebalancing,
  - dynamic workload remapping away from compromised regions.
- **Hypervisors:**
  - virtual memory remapping, isolation, and ballooning across guest virtual machines,
  - containment of faults in multi-tenant environments sharing physical memory.
- **Security subsystems:**
  - enforcement of zero-leakage guarantees from quarantined or redirected regions,
  - mandatory memory sanitization prior to reuse, critical in high-assurance and multi-tenant systems.
- **Firmware monitors and baseboard management controllers (BMCs):**
  - persistence of fault and repair records across reboots,
  - telemetry aggregation and early alerting for predictive maintenance and RMA triage.

These layers communicate through standardized reporting and control interfaces, including:

- **Machine Check Architecture (MCA):** processor-level reporting of corrected and uncorrected memory faults.

- **Advanced RAS interfaces:** enterprise-grade mechanisms for detailed fault logging, DIMM isolation, and failover.
- **UEFI error-logging extensions:** persistent firmware logs accessible during subsequent system boots.

Together, these interfaces form a closed-loop resilience framework, propagating fault information upward while enabling policy feedback downward, ensuring that hardware-level containment aligns with system-wide reliability objectives.

6.8.5 Summary

The memory controller has evolved from a transaction scheduler into a real-time guardian of data integrity. Its ability to detect, classify, isolate, and remediate faults now directly governs system stability and operational lifetime.

Through coordinated mechanisms such as scrubbing, error quarantine, redundancy reallocation, thermal-aware containment, and telemetry-driven adaptation, the controller ensures that faults are intercepted and neutralized before they propagate into higher-level failures.

The symbolic fault models, adaptive diagnostics, and runtime monitoring engines developed in this work reinforce a fundamental principle: manufacturing-time testing alone cannot predict long-term in-field behavior. Sustained reliability requires intelligent, controller-driven resilience policies that continuously adapt to evolving conditions.

As memory architectures diversify toward three-dimensional stacking, near-memory computation, and disaggregated memory systems, controller-level error management will increasingly determine whether systems degrade silently, fail catastrophically, or self-heal gracefully over extended operational lifetimes.

Chapter 7: Diagnostic Testing and Fault Localization Techniques

In modern memory systems, fault detection constitutes only the first layer of resilience. High-performance, safety-critical, and fault-tolerant platforms require a deeper capability: fault localization, defined as the precise identification of a fault's type, physical location, and activation origin within the memory array. This chapter examines advanced diagnostic methodologies designed not merely to determine whether a fault exists, but to determine where, how, and under which conditions it manifests.

The techniques discussed include row and column isolation, address decoder integrity validation, symbolic fault modeling, and inverse fault-mapping mechanisms. These approaches form the methodological foundation of the symbolic localization engines developed and refined originally in foundational research and subsequently extended within the Optimal_Test framework, as described in **Chapters 8, 12**, and **14**, and validated through experimental results reported in published studies.

7.1 Address Decoding Faults and Row/Column Isolation

Among the most diagnostically complex classes of memory failures are address decoding faults. Unlike elementary read/write faults confined to individual storage cells, address decoding faults typically manifest as logical misassociations between requested logical addresses and activated physical resources.

Accurate localization therefore requires fine-grained insight into decoder topology, address signal propagation, and the structural organization of the memory array.

This section focuses on diagnostic strategies for isolating faults at the row, column, and bit-line levels, with particular emphasis on decoder malfunctions, inter-line coupling, and conditional address aliasing.

The discussion is grounded in my original research on symbolic address-decode modeling, dynamic fault replay, and inverse address-mapping diagnostics.

7.1.1 Address Decoding Mechanisms and Structural Vulnerabilities

The address decoder is a combinational logic structure responsible for translating a logical address vector into a unique set of physical control signals.

Its principal functions include:

- Row decoder activation, which asserts a specific word line to select the targeted horizontal slice of the memory array.
- Column selection, implemented through column multiplexers or bit-line decode logic, which routes the selected cell contents to the sense amplifiers or write drivers.

When decoder logic is compromised—due to design defects, process variability, aging-induced parametric drift, transient upsets, or environmental interference—a spectrum of failure modes may arise:

- Incorrect row or column activation, whereby a logical address accesses an unintended physical location.
- Row or column aliasing, in which multiple rows or columns are simultaneously activated, resulting in data contention or destructive interference.
- Open decoder faults, where no valid row or column is asserted, producing apparent read or write failures.
- Conditional decoding faults, in which correct operation is observed under most address combinations but fails for specific bit patterns or background data states.

These failures are frequently subtle and non-catastrophic. They may escape detection under conventional memory tests while inducing silent corruption or intermittent misrouting during specific transitions or marginal operating conditions.

Effective diagnosis therefore requires targeted address-centric test vectors, symbolic activation tracing, and, in many cases, inverse simulation of the address-decode path. These techniques are developed systematically in the sections that follow.

7.1.2 Classification of Address Decoder Faults

Address decoder faults can be classified into distinct categories, each exhibiting characteristic manifestations and diagnostic implications:

Table 7.1—Classification of address decoder faults and diagnostic implications

Fault Type	Description	Test Implications
Stuck-at address line	One or more address bits permanently forced to logical 0 or 1	Systematic misaddressing of rows or columns
Open address line	Floating address signal with undefined logic level	Intermittent misrouting and nondeterministic behavior
Address aliasing	Multiple logical addresses map to the same physical cell	Overlapping writes and inconsistent readback
Decoder bridge fault	Simultaneous activation of multiple decode lines	Coupling effects, interference, or multi-cell activation
Input-dependent fault	Decoder fails only for specific address combinations	Requires conditional pattern generation

Within my symbolic test-generation framework, decoder-focused PROVER rules orchestrate carefully structured micro-operation sequences that deliberately induce marginal or ambiguous address states.

By forcing the decoder into such controlled stress conditions, subtle manifestations of aliasing, misrouting, or silent decode failures become observable, providing high-resolution diagnostic insight into decoder integrity under both nominal and stress-induced operating regimes.

7.1.3 Detection Using Address-Sequence Test Patterns

Conventional March-class memory tests, while effective for data-oriented fault detection, are generally insufficient for address decoder diagnostics because they emphasize storage-cell sensitivity rather than address-path integrity. Decoder-specific testing therefore relies on address-aware access sequences explicitly constructed to expose aliasing, polarity inversion, and conditional activation anomalies.

Representative diagnostic strategies include:

- **Walking address tests**
  Sequential activation of individual address bits (e.g., 00000001 → 00000010 → 00000100 → …) to verify one-to-one correspondence between logical addresses and physical locations.
- **Address inversion tests**
  Paired access to an address A and its bitwise complement $\sim A$. Deviations in behavior indicate polarity errors, cross-coupling, or asymmetric decode paths.
- **Alias-writing tests**
  Deliberate writing of distinct data values to suspected aliased addresses, followed by cross-verification.

Example (alias detection):

1. Write 0x55 to address $A1$
2. Write checkerboard pattern (0xAA) to address $A2$
3. Read back from $A1$
4. If $A1 = A2$, address aliasing is indicated

In my Optimal_Test system, these diagnostics are formalized through symbolic address operators such as ADDR_MIRROR(a), which generates the bitwise mirror of address a, and ADDR_INV(a), which computes the bitwise inverse.

These operators enable systematic exploration of aliasing, mirroring, and inversion sensitivities within a compact symbolic test language, extending diagnostic granularity beyond traditional deterministic approaches.

7.1.4 Fault Localization Through Row and Column Isolation

Following fault detection, the diagnostic objective becomes localization, namely identification of the physical origin of the observed failure within the memory array. Accurate localization supports redundant row or column substitution, post-silicon debugging, yield analysis, field-replaceable unit tracking, and runtime repair in self-healing architectures.

Localization techniques employed include bit-line and word-line isolation using single-bit activation patterns, row-wise scanning with controlled background interference, column-interleaving patterns enforcing distinctive activation signatures, and fault-signature mapping based on accumulated ECC syndromes and access histories.

This work utilizes a syndrome-based address-tracing model that correlates ECC syndromes with recent access sequences. By statistically weighting error signatures against temporal access patterns, the model triangulates probable fault origins even in the presence of burst errors, row coupling, or strongly data-dependent behavior.

Experimental evaluation demonstrated particular effectiveness in high-density DRAM arrays, where conventional mapping techniques often fail to disambiguate overlapping or conditionally activated faults.

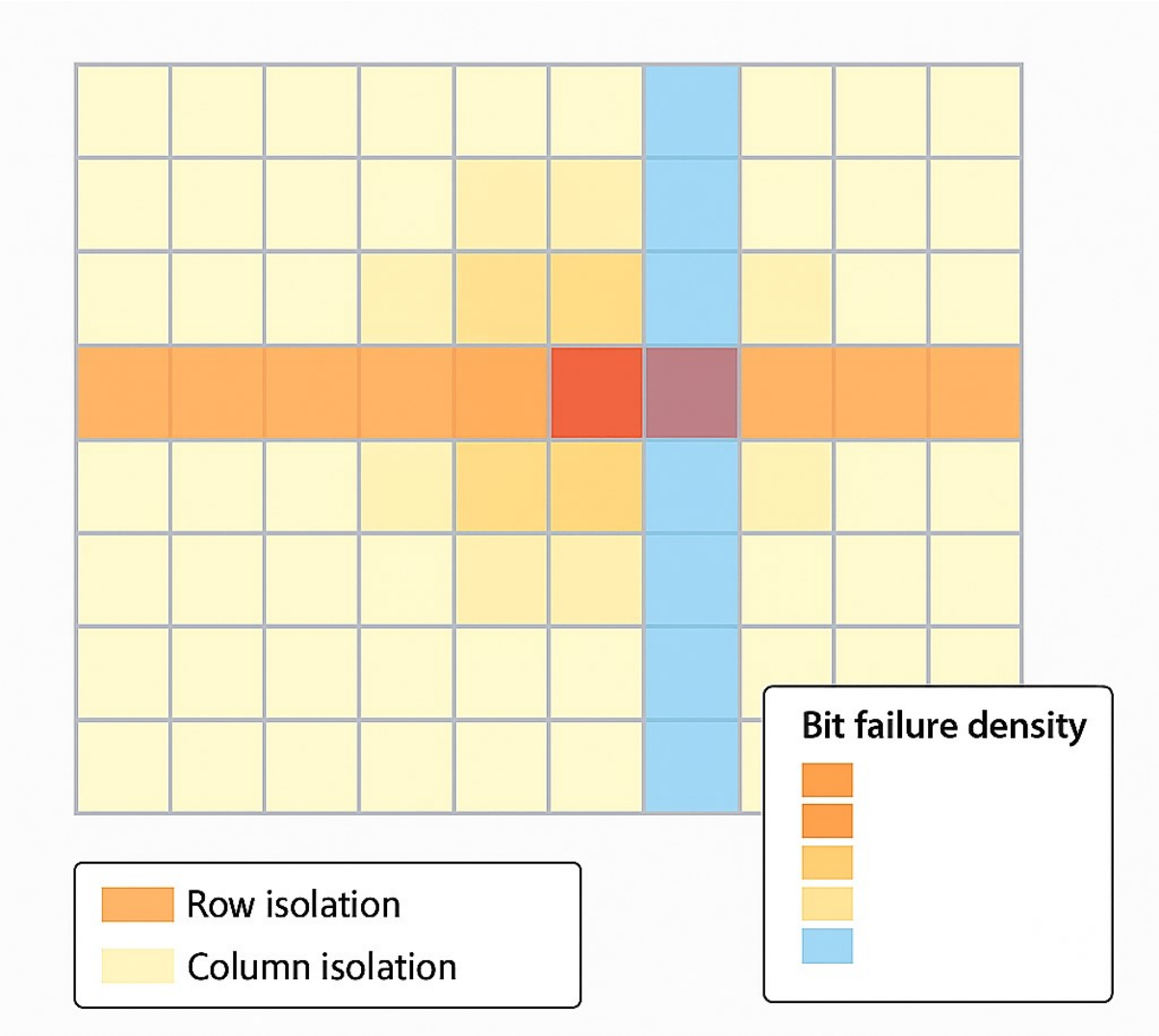

Figure 7.1—Visual map of row and column isolation using bit failure density overlaid on array grid

Figure 7.1 illustrates diagnostic fault localization within a memory array using row and column isolation techniques combined with spatial bit failure density analysis. The grid represents a conceptual memory array, in which a single row and a single column are selectively highlighted. The highlighted row corresponds to row-level isolation activity, while the highlighted column corresponds to column-level isolation activity.

The intersection cell, shown with the highest failure density, represents a recurrent fault location observed across multiple activation and read-back cycles. This convergence strongly suggests a localized defect at a specific row–column coordinate, which is characteristic of

address decoder malfunctions, persistent coupling effects, or cell-level degradation reinforced by decode path asymmetry.

Surrounding cells are shaded using a graded color scale representing decreasing failure density. This gradient reflects secondary fault manifestations caused by partial activation, half-select stress, or proximity-induced interference. Such spatial patterns are commonly observed when decoder faults propagate indirectly through adjacent word lines or bit lines rather than producing uniform failure regions.

The Figure demonstrates how structured activation and verification sequences confine the fault domain with high confidence. By correlating row-wise and column-wise failure signatures, the diagnostic process isolates the physical origin of the fault with sufficient precision to enable targeted repair, redundancy substitution, or selective quarantine.

These isolation principles form a core component of the localization methodologies introduced in Section 7.1.4 and extended to multi-bank systems in Section 7.1.5.

7.1.5 Address Decoding in Multi-Bank and Interleaved Systems

Modern memory architectures frequently employ bank interleaving and multi-rank address mapping to maximize throughput and reduce effective access latency. In such designs, a single logical address is decomposed and distributed across multiple structural layers, including memory banks, DRAM devices, channels, and rank or sub-rank selectors.

While interleaving improves bandwidth utilization, it introduces additional diagnostic complexity. Address decoding faults may no longer manifest as spatially localized defects but instead appear through cross-layer interactions that depend on address transitions, access concurrency, or rank selection timing.

Typical complications include:

- Bank-crossing artifacts, where faults occur during address transitions spanning bank boundaries, leading to partial or erroneous activations.
- Interleaving boundary contention, in which errors are triggered by adjacent or simultaneous accesses across interleaved banks or channels.
- Chip-select faults, confined to multi-rank sequences, such as incorrect device enablement or contention on shared I/O paths.

To address these effects, multi-axis symbolic address traversal tests were developed within the U–Y hybrid fault model. These PROVER-based diagnostic schemes explicitly traverse address dimensions associated with bank selection, rank enablement, and channel distribution.

By exercising structured combinations of these dimensions, the diagnostic process exposes:

- Decoder faults masked by bank-level parallelism
- Aliasing effects that span bank or rank boundaries
- Rank-dependent anomalies that remain invisible under flat address traversal

Extending symbolic test generation to incorporate multi-layer address mappings enables reliable exposure of latent decoder faults that would otherwise compromise runtime system reliability in highly interleaved architectures.

7.1.6 Summary

Address decoding faults represent among the most insidious and high-impact defect classes in memory systems. Unlike conventional bit-cell failures, these faults:

- Frequently evade detection by March-based or static data-pattern tests
- Manifest only under specific address transitions, timing conditions, or logical stress combinations
- Are strongly influenced by layout symmetry, process aging, and environmental factors such as temperature
- Exhibit conditional behavior tied to interleaving boundaries, contention scenarios, or rank-specific activation paths

Effective detection and localization therefore require diagnostic strategies that extend beyond basic access verification. Core requirements include targeted address sequencing to activate marginal decode paths, recognition of fault aliasing patterns, correlation of ECC syndromes with symbolic activation histories, and architectural awareness of interleaving and rank distribution.

My work on Optimal_Test and symbolic fault-trace analytics was driven directly by these requirements.

The objective extends beyond fault detection toward high-precision localization, enabling automated redundancy activation, in-field remapping, and resilient containment policies. In dense, high-performance systems, the ability to isolate and contain decoder faults is not a refinement but a prerequisite for long-term survivability.

7.2 Syndrome Analysis and Signature Comparison

Once an error is detected, whether through ECC mechanisms or built-in self-test logic, the diagnostic task shifts to extracting structural meaning from the event and inferring the underlying fault mechanism.

This requires analysis of syndrome patterns, comparison of fault signatures, and identification of correlations that support root-cause localization and informed repair or containment.

This section examines the theoretical basis and practical use of syndrome decoding, signature correlation, and fault-pattern analysis.

These mechanisms form the analytical backbone of modern diagnostic engines and provide essential input to higher-level fault models, runtime scrubbing policies, and predictive reliability frameworks.

In my work with Optimal_Test and PROVER-based symbolic models, syndrome analysis is treated not merely as an error indicator but as a vector-space representation of structural vulnerability.

This interpretation enables optimization of test sequencing and fault localization under strict runtime and bandwidth constraints.

7.2.1 ECC Syndromes: Mathematical Basis

A syndrome is the binary vector produced by an ECC decoder when a read-back error is detected. Formally, the syndrome is defined as:

$$s = H.r^T$$

Where:

- H is the parity-check matrix,
- r is the received codeword (which may contain errors),
- s is the resulting syndrome vector.

A zero syndrome indicates that no detectable parity violation is present, whereas a non-zero syndrome indicates corruption affecting one or more protected bits. In linear block codes such as Hamming or BCH, each non-zero syndrome maps deterministically to a specific bit or constrained bit set, enabling direct correction.

In contrast, LDPC and Turbo codes interpret syndromes probabilistically, using iterative decoding to converge on the most likely error pattern.

7.2.2 Single-Error and Double-Error Identification

In SECDED (Single Error Correction, Double Error Detection) coding schemes, syndrome analysis enables structured classification of error types according to their correctability and localization resolution.

Single-bit faults generate syndromes that uniquely identify the erroneous bit position, allowing deterministic correction through direct lookup or combinational decoding logic. This property underpins the effectiveness of SECDED codes in correcting isolated random faults.

Double-bit faults produce non-zero syndromes that do not map unambiguously to a single bit position. Such conditions are therefore classified as detectable but uncorrectable under SECDED constraints. Correct handling of these events requires escalation rather than correction to avoid miscorrection.

Burst errors, involving corruption of multiple adjacent bits, may generate overlapping, ambiguous, or invalid syndromes.

These cases can obscure fault localization and, in some circumstances, result in partial masking or misclassification if not handled conservatively.

The importance of syndrome orthogonality is emphasized, whereby each correctable bit position generates a distinct, invertible syndrome.

Orthogonality is a necessary condition for constructing compact, hardware-efficient syndrome decoders and enables accelerated fault analysis in both offline diagnostic flows and runtime correction pipelines.

Example: Syndrome-to-Bit Mapping in a (7,4) Hamming Code

In a (7,4) Hamming code, each 3-bit syndrome uniquely corresponds to a single-bit error location.

Table 7.2 presents the deterministic mapping between syndrome patterns and bit indices.

Table 7.2—Syndrome-to-bit mapping for a (7,4) Hamming code

Syndrome (binary)	Bit Position (1-indexed)
000	No error
001	Bit 1
010	Bit 2
011	Bit 3
100	Bit 4
101	Bit 5
110	Bit 6
111	Bit 7

Each non-zero syndrome uniquely identifies a single-bit error location, enabling direct correction through a simple lookup mechanism. The all-zero syndrome indicates that no detectable error has occurred.

This deterministic one-to-one correspondence is fundamental for efficient hardware-based error correction. It permits construction of high-speed syndrome decoders with minimal logic depth and supports compact diagnostic logic within ECC-aware test and repair engines.

7.2.3 Syndrome Clustering and Region-Based Mapping

Rather than treating syndromes as isolated events, advanced diagnostic engines analyze syndrome occurrence across both temporal and spatial dimensions to infer higher-level fault behavior. By clustering syndrome vectors, these systems can identify fault patterns that extend beyond individual bit attribution.

Syndrome clustering enables identification of failing regions within memory arrays, detection of temporally correlated error patterns indicative of intermittent or environment-induced faults, and recognition of spatial adjacency suggestive of layout-sensitive defects such as coupling noise or address decoder distortion.

In the Optimal_Test system, I implemented a multi-frame syndrome accumulator that records ECC syndromes over successive memory accesses. The accumulator applies a weighted temporal aggregation to construct dynamic fault-likelihood maps, which represent probabilistic fault density across the address space.

These maps are subsequently used to trigger region-level repair actions or guide deeper diagnostic exploration.
This methodology is particularly effective when exact localization is infeasible or unstable, including multi-bit ECC environments, noisy operational domains such as aerospace or industrial systems, and aging memory arrays exhibiting non-deterministic retention or wear-related failures.

By transitioning from per-bit diagnosis to region-based probabilistic analysis, syndrome clustering supports prioritization of retesting, partial remapping, and early identification of degradation trends. As such, it constitutes a central mechanism in resilient memory system design.

7.2.4 Syndrome Signature Comparison

Syndrome signature comparison extends diagnostic interpretation beyond single observations by analyzing recurrence and similarity of syndromes across time, stress conditions, and access modes. This approach allows diagnostic engines to distinguish between transient phenomena and persistent structural defects.

Syndrome signatures are aggregated profiles rather than instantaneous values and are typically constructed by combining syndrome observations using operations such as bit-wise XOR accumulation, weighted integration based on access type or voltage domain, and cross-comparison across address ranges or test sequences.

Consistent reproduction of identical syndrome signatures across distinct logical addresses strongly indicates structural commonality. For example, if addresses A_1 and A_2 repeatedly generate the same syndrome pattern under varied conditions, likely explanations include shared column decoding logic, aliasing induced by address mirroring, or interference within common bit-line or control paths.

Within my U–Y symbolic test synthesis framework, syndrome signature comparison was essential for detecting micro-operation-induced aliasing. By correlating signatures produced by structurally distinct March sequences, it became possible to map latent fault domains and refine test schedules for improved diagnostic resolution.

7.2.5 Syndrome-Based Repair Decision Trees

Syndrome information functions not only as a diagnostic indicator but also as a decision driver for automated repair and containment strategies. Organizing observed syndromes into hierarchical outcomes enables memory systems to select actions proportional to fault confidence, recurrence, and severity.

Typical syndrome-driven responses include targeted redundancy activation when precise localization is available, regional quarantine when fault distribution is ambiguous, aggressive scrubbing when syndrome density exceeds a programmable threshold, and escalation to firmware or system software when persistent or unclassified patterns emerge.

Such responses may be encoded using deterministic decision trees, fuzzy-logic rule bases (as implemented in my Sugeno-based diagnostic engine), or probabilistic classifiers that estimate fault category likelihoods from historical syndrome distributions.

This structured approach enables closed-loop resilience, where diagnostic observations continuously refine repair policies. Syndrome-based decision trees therefore bridge the gap between error detection, diagnostic interpretation, and self-healing response.

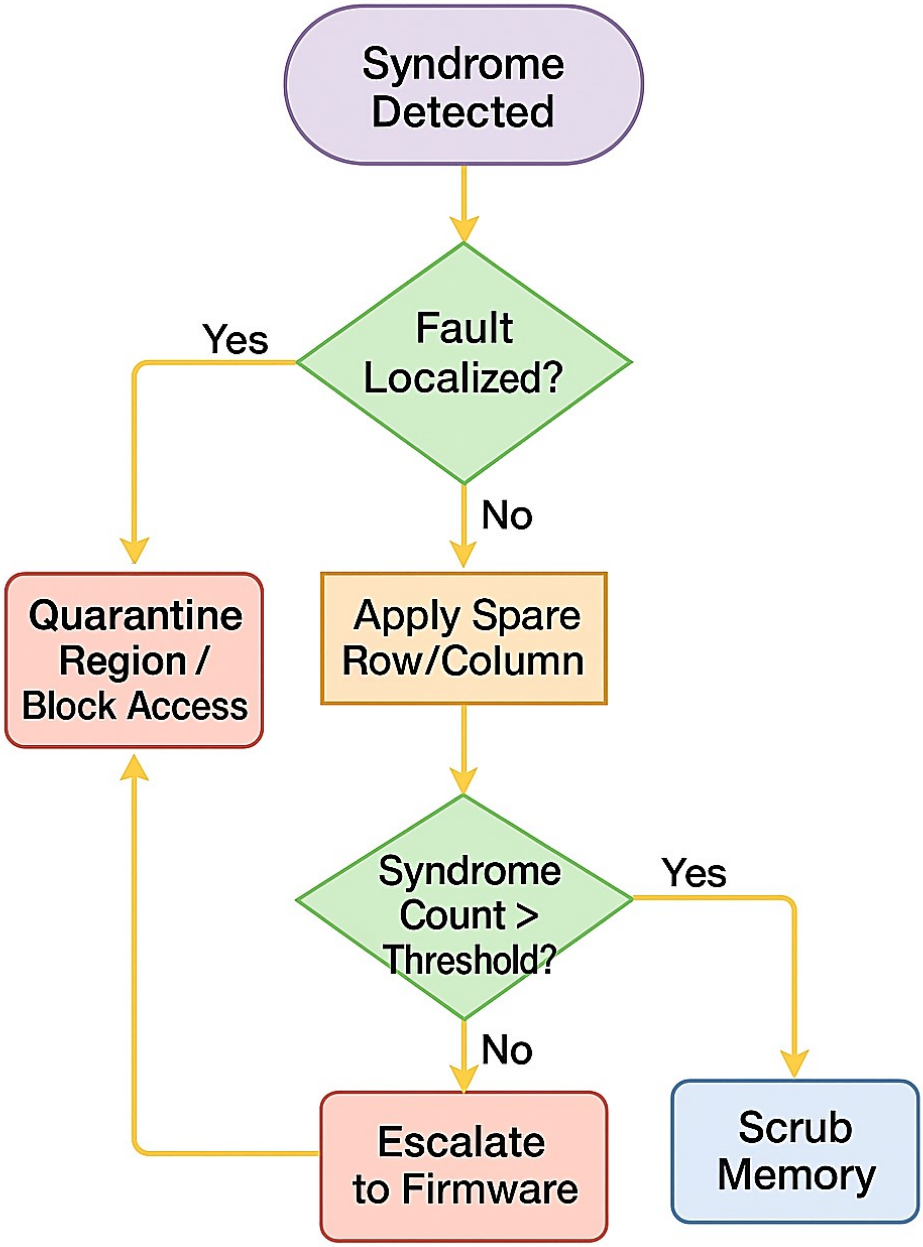

Figure 7.2—Syndrome-based fault decision flow with repair and quarantine paths

Figure 7.2 illustrates a hierarchical decision process driven by ECC syndrome observations. Upon syndrome detection, the system first evaluates whether the fault can be localized to a specific row, column, or region.

If localization is successful, the affected segment is isolated through quarantine or access blocking to prevent propagation. If localization remains uncertain, spare rows or columns are applied as corrective substitution.

A running syndrome counter tracks recurrence frequency. When the count exceeds a programmable threshold, a scrubbing operation is triggered to refresh the affected region and suppress accumulation of latent errors. If syndromes persist without exceeding the scrubbing

threshold, control is escalated to firmware, enabling higher-level logging, notification, or reconfiguration policies.

The flow demonstrates a graduated fault-handling strategy that balances localized containment, redundancy deployment, preventive maintenance, and system-level oversight to ensure long-term survivability.

7.2.6 Challenges in Real Systems

Despite their diagnostic power, syndrome-based techniques face practical limitations in deployed systems. Advanced ECC schemes such as LDPC generate syndromes that are not uniquely decodable, rendering localization inherently probabilistic. Electrical noise and environmental variability may mask intermittent faults, producing inconsistent syndrome traces.

Address interleaving obscures the mapping between logical addresses and physical locations, while transparent runtime remapping mechanisms may conceal the true origin of defects. High fault rates can also saturate diagnostic engines, forcing temporal compression that reduces resolution.

Robust implementations therefore require extended logging with precise temporal tagging, historical correlation across fault lifetimes, syndrome compression techniques that preserve diagnostic fidelity, and confidence scoring models that quantify localization reliability.

7.2.7 Summary

Syndrome vectors are not merely error indicators but diagnostic carriers embedding structural and behavioral information about memory systems. When aggregated and correlated across space and time, syndrome analysis enables fine-grained fault isolation, targeted repair, statistical modeling of degradation, and real-time self-healing.

From my work on symbolic fault engines and ECC-aware repair controllers, syndrome analysis emerges as the critical link between raw detection and informed understanding. It transforms low-level error signals into actionable diagnostic knowledge and provides a scalable foundation for fault management in high-density memory architectures.

7.3 Bit-, Word-, and Line-Level Localization

Once an error has been detected and an ECC syndrome has been extracted, the next critical diagnostic step is granular fault localization: determining the precise unit affected, whether it is a bit/cell, word, cache line, or a structural segment within the memory hierarchy.

The selected localization granularity directly shapes the resilience strategy, enabling the system to:

- Execute fine-grained repair actions, such as column substitution or bit-line–aligned remediation where supported by the technology and repair fabric.
- Quarantine logical regions (e.g., cache lines or memory pages) to prevent further propagation of corruption.

- Escalate fault awareness to higher software layers (operating system, hypervisor, or RAS firmware) when hardware-level correction or isolation is ambiguous or infeasible.

In my research and within the Optimal_Test diagnostic framework, localization is realized as a multi-resolution pipeline. The pipeline begins with coarse-grained fault recognition guided by spatial syndrome clustering and decoder-level signatures, and incrementally refines the diagnostic scope toward cell-level isolation when structural layout, observability, and access control permit.

This adaptive methodology allocates diagnostic resources proportionally:

- Minimal analysis is applied when coarse localization is sufficient for containment.
- Higher-resolution diagnostics are invoked only when required by uncertainty, criticality constraints, or persistent recurrence.

By dynamically scaling analysis depth, the approach balances diagnostic precision with runtime efficiency, and forms a foundation for scalable fault management in dense memory systems.

7.3.1 Localization Granularity Levels

Fault localization operates across multiple granularity levels, each corresponding to a distinct structural or logical unit. The chosen level determines the trade-off between diagnostic precision, instrumentation cost, and the scope of containment or repair. Table 7.3 summarizes principal localization levels and representative use cases.

Table 7.3—Principal fault localization levels and representative use cases

Granularity	Target Element	Resolution Use Case
Bit-level	Individual bit/cell (logical position within a protected codeword)	Deterministic correction and targeted redundancy actions where per-bit attribution is available
Word-level	ECC-protected word (e.g., 32/64/128-bit codeword)	ECC correction history tracking; word-level containment; escalation policies
Row/column line	Word line or bit-line–aligned structure within a subarray	Physical remapping; spare row/column activation; Built-In Self-Repair (BISR)
Page-level	Memory page (typically 4–8 KB)	OS-level page migration; page quarantine; NUMA-aware rebalancing
Bank-level	Bank/subarray segment (DRAM/NVM structural region)	Partial retirement; thermal/power management; reliability zoning

Diagnostic systems should support cascading fallback mechanisms. When bit-level localization is not reliable—due to ECC ambiguity, masking effects, or architectural constraints—the system escalates to the next available containment level (e.g., word-level or row/column-level). This hierarchical fallback preserves reliability even under imperfect observability and non-unique syndrome interpretations.

7.3.2 Bit-Level Fault Resolution

Bit-level localization provides the highest precision, but requires conditions that ensure the attribution is stable and non-ambiguous.

Bit-level resolution is feasible only when:

- ECC syndrome mapping is unambiguous (e.g., Hamming-class or BCH-class decoders operating within their correctable regimes).
- The syndrome mapping is injective over correctable error locations (each correctable bit position produces a distinct syndrome under the code's decoding assumptions).
- Confirmation cycles are used to exclude transient faults and environment-induced upsets (soft errors, marginal timing events, or noise-corrupted reads).
- Common techniques for bit-level resolution include:
- Walking-1 / walking-0 patterns: sequential stimulation of each bit position to expose stuck-at and select bridging conditions.
- Bitmask traversal: controlled write/read cycles using shifting masks to isolate and validate individual bit positions.
- Inversion tests: toggling a known bit state across controlled backgrounds to distinguish localized persistence from coupling- or pattern-dependent migration effects.

Within the micro-operation synthesis framework defined in **Chapter 10**, bit-selective stress patterns were designed to target vulnerable cells, particularly in dual-port arrays and overlapping-word organizations. These sequences effectively expose faults driven by shared-line contention, bit-line interference, and marginal cell stability in dense tiles. Systematic bit-level probing enables early identification of permanent or marginal defects and supports high-confidence redundancy activation and predictive self-repair.

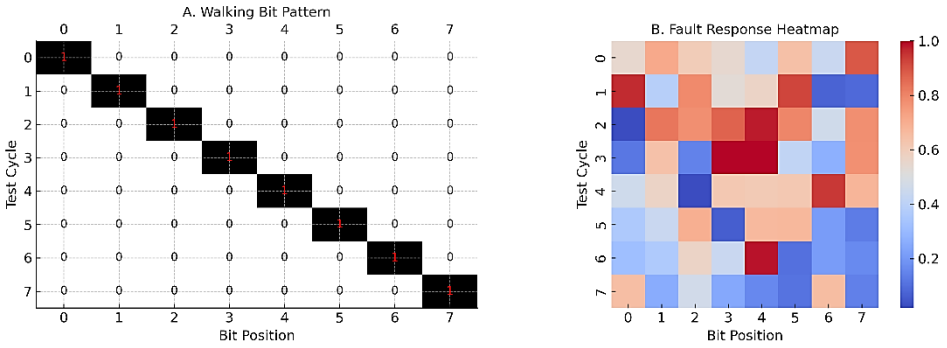

Figure 7.3—Walking bit pattern across a word and its fault response heatmap

Figure 7.3 illustrates the diagnostic use of a walking-bit test for bit-level localization.

Panel A shows the walking-bit stimulus over an 8-bit word across 8 test cycles. Each cycle activates exactly one bit position at logical 1 while all other bits remain at logical 0, producing a diagonal activation pattern when cycles are stacked against bit indices. This stimulus isolates individual bit positions and is therefore sensitive to stuck-at behavior, bit-line–aligned defects, and select bridging mechanisms.

Panel B shows the corresponding response summarized as a cycle-by-bit heatmap. Each cell encodes a normalized fault activation metric for a specific bit position at a specific test cycle (e.g., miscompare occurrence rate, correction count, or confidence-weighted error score, depending on the logging model used). The color gradient represents increasing recurrence or severity, with higher-intensity regions indicating repeated fault activation under isolated stimulation.

Persistent hotspots confined to a fixed bit position across cycles are consistent with a bit-line, sense-amplifier, or per-bit storage weakness. Hotspots that shift with the walking stimulus, or that appear in adjacent bit positions, are consistent with coupling-induced interactions, pattern sensitivity, or shared-path interference. Together, the panels show how isolated stimulation combined with structured response aggregation yields diagnostic leverage for detecting subtle defects that are frequently masked under bulk-pattern tests.

7.3.3 Word-Level and Cache-Line Localization

In architectures where ECC is applied at the word or cache-line boundary (e.g., ECC per 64-byte line or per burst-aligned transfer), localization is constrained by structural granularity:

- Syndrome granularity: typically one syndrome and correction outcome is available per protected word or block, limiting per-bit attribution at higher layers.
- Burst alignment and reordering: address interleaving and memory-controller scheduling may distribute physically adjacent transfers across devices, complicating direct mapping between a logical line and a single physical segment.
- Mitigation strategies include:
- Burst-aware test patterns that intentionally activate cross-line transitions and boundary-sensitive paths (see Section 4.5).
- Cache-line quarantine or remapping policies triggered by repeated correctable events within the same line.
- Selective ECC re-evaluation under split-line accesses, refill boundaries, or controlled replay sequences.

In the Optimal_Test engine, I implemented a cache-aware tracking module that records cache lines exhibiting repeated ECC corrections and escalates actions based on fault density and spatial recurrence patterns. This module is designed to approximate runtime scrubbing behavior while preserving diagnostic traceability.

7.3.4 Row and Column Fault Localization

When ECC syndromes or diagnostic signatures exhibit line-wise structure, the fault often originates from row- or column-aligned circuitry:

- Row-oriented faults manifest as word-line–correlated failures, often associated with word-line drivers, open word-line connections, or address decoding defects.
- Column-oriented faults manifest as consistent bit failures at the same bit offset across multiple rows, implicating bit lines, sense amplifiers, column multiplexers, or vertical interconnect.

Detection and confirmation techniques include:

- Matrix-structured March execution with failure-shape analysis, searching for persistent alignment across row or column axes.
- Coupling-aware sequences that stress aggressor–victim interactions under high toggle activity and controlled neighborhood activation.
- Parity/ECC consistency checks that test whether syndrome patterns remain stable across address sweeps and data backgrounds.

Repair strategies include spare row/column activation through hardware repair logic, and fuse-based or programmable remapping executed during manufacturing test or through firmware as part of BISR frameworks.

Within the symbolic fault analysis framework introduced in Chapter 8, a column-trace operator is defined that detects recurrent syndrome intersections along bit-line–aligned axes and maintains soft candidate rankings over time. This is especially useful for intermittent or thermally sensitive defects whose observability varies across iterations.

7.3.5 Page- and Block-Level Localization

In technologies where faults cannot be reliably isolated to individual bits or lines—particularly NAND Flash, ReRAM-class arrays, and ultra-dense DRAM operating under heavy correction—localization typically escalates to page or block granularity (e.g., 4 KB, 8 KB, or larger regions).

Key characteristics include:

- Per-page error-rate tracking and access history correlation for long-horizon reliability assessment.
- Page migration mechanisms that remap fault-prone pages (common in SSD controllers and OS virtual memory subsystems).
- Bad Block Management (BBM) via firmware-maintained bad block tables, often transparent to the OS to preserve compatibility and availability.

To complement these mechanisms, runtime scrubbing (see Section 6.8) targets cold or infrequently accessed regions where latent errors can accumulate. Scrubbing increases the probability of exposing correctable faults before they evolve into uncorrectable events.

7.3.6 Localization in Interleaved and ECC-Protected Systems

Structural features and runtime correction mechanisms complicate localization in modern systems:

- Address interleaving distributes a logical address across devices, banks, or channels, obscuring the physical fault origin.
- Syndrome masking occurs when ECC transparently corrects faults, suppressing raw error visibility at higher layers.
- Runtime remapping redirects accesses to spares, breaking straightforward traceability of the underlying defect location.

Robust diagnostic frameworks therefore require:

- Backtracking through mapping logic to reconstruct the relationship between logical addresses and physical resources (bank, channel, die, rank).
- Correlation of ECC correction histories with physical layout to identify structurally related recurrence.
- Temporal logging of syndromes, addresses, mapping metadata, and remap context both before and after repair actions to preserve continuity.

Within the symbolic modeling and runtime diagnostic architecture, a fault localization window is introduced: a bounded temporal snapshot capturing the syndrome vector, logical address, mapping metadata, and test-pattern context. This enables deferred resolution and preserves localization accuracy even when runtime correction and remapping have already masked the fault's physical manifestation.

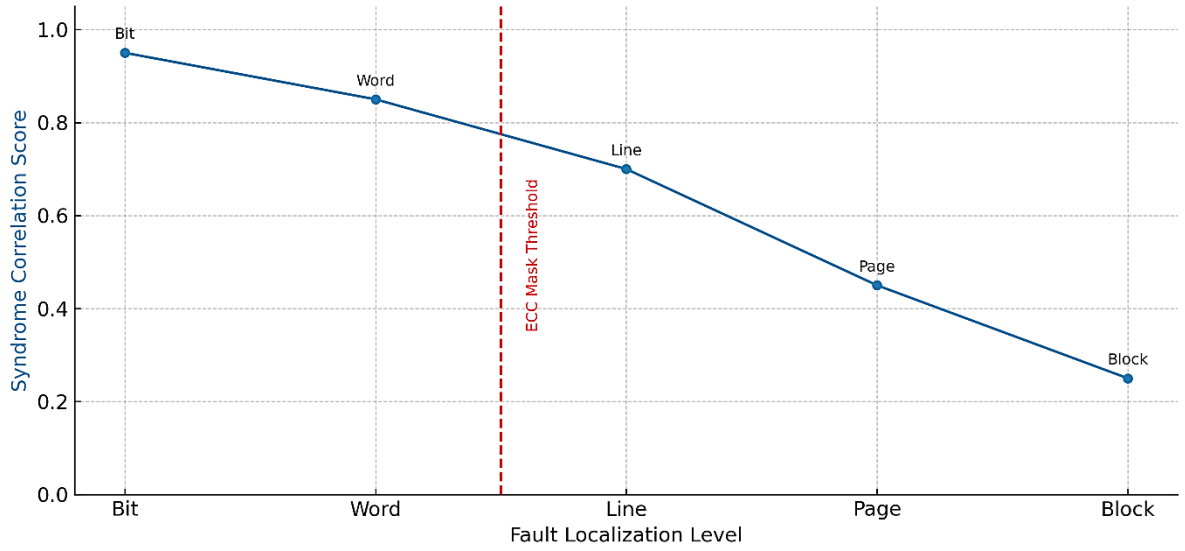

Figure 7.4—Fault resolution timeline across levels with syndrome correlation graph

Figure 7.4 illustrates the progressive decline in diagnostic confidence as fault localization transitions from fine-grained to coarse-grained resolution levels. The plotted curve represents a syndrome correlation score (normalized), which decreases as localization shifts from bit-level attribution toward block-level aggregation.

A red vertical dashed marker denotes the ECC mask threshold, indicating the transition region—typically between word-level and line-level observability—where ECC correction and replay mechanisms begin to suppress direct visibility of the underlying physical fault. Beyond this boundary, raw fault evidence is increasingly absorbed by correction actions, which

preserves functional correctness but reduces diagnostic transparency and complicates traceability of defect origin.

The Figure captures a fundamental limitation of ECC-protected systems: increasing correction capability tends to reduce direct observability of the fault's physical manifestation, particularly for intermittent and marginal behaviors.

To preserve diagnostic fidelity across this masking boundary, advanced frameworks must incorporate symbolic tracking, temporal logging of correction histories, and mapping backtracking that reconstructs fault evidence even after correction and remapping have occurred.

This visualization therefore reinforces a central principle of this chapter: maintaining fault traceability under ECC masking is essential for long-term resilience, yield optimization, and predictive repair strategies.

7.3.7 Summary

Fault localization is not a single diagnostic event but a layered, adaptive process that reconciles multiple dimensions of memory system behavior:

- Physical organization: cells, bit lines, word lines, subarrays, and banks.
- Logical abstraction layers: virtual addresses, pages, blocks, and interleaving mappings.
- Fidelity of error signatures: ECC syndromes, parity vectors, correction histories, and accumulated error statistics.
- Temporal and environmental variability: operating conditions that can mask, shift, or modulate fault behavior over time.

Through my work on multi-level localization engines spanning simulation-driven analysis and hardware-integrated diagnostic frameworks, I found that the intersection of access-pattern behavior, error signatures, and architectural mapping is critical for high-confidence fault resolution.

Localization should therefore be treated not as a low-level utility but as a strategic diagnostic cornerstone. It determines how a system initiates self-healing, maintains data integrity, and sustains availability and resilience across the memory subsystem.

7.4 Fault Tables and Diagnostic Resolution Metrics

Once errors are detected and localized to specific memory components, engineers and automated diagnostic systems require structured representations to guide subsequent actions—whether to initiate repair, trigger system-level mitigation, or inform post-manufacturing screening.

This requirement is fulfilled by fault tables and diagnostic resolution metrics.

Fault tables are compact structured mappings that encode relationships between applied test stimuli and fault models, providing an efficient representation of observed or inferred fault behaviors and supporting traceability across memory locations.

Resolution metrics quantify diagnostic quality by capturing properties such as:

- Precision: the accuracy and granularity of localization.
- Coverage: the proportion of modeled faults and/or address space exercised.
- Confidence: the empirical or statistical likelihood that a reported fault reflects a true defect under the stated operating conditions.

In the Optimal_Test diagnostic engine, I implemented symbolically generated fault tables that are constructed dynamically from test patterns and symbolic modeling outputs. These tables are coupled with ranked resolution metrics derived from both empirical test outcomes and theoretical fault model boundaries.

Together they form an adaptive feedback loop in which test strategies are refined according to observed diagnostic data under runtime constraints.
Such integration is essential for scalable and cost-efficient memory testing, particularly when fault coverage, test time limits, and diagnostic resolution must be balanced dynamically.

7.4.1 Definition of a Fault Table

A fault table is a structured diagnostic artifact that encodes the relationship between fault types (or fault hypotheses) and the tests used to activate and detect them. It serves as a foundational data structure for coverage evaluation, localization refinement, and repair decision support.

At its core, a fault table records:

- The fault classes under consideration.
- The test patterns or sequences applied.
- The observed or predicted responses under those tests (e.g., miscompare vectors, syndrome vectors, or signature traces).
- The localization attributes associated with each manifestation (bit/word/row/page/bank) and relevant context.

By consolidating these relationships into a compact matrix or symbolic representation, fault tables enable systematic analysis of diagnostic capability, expose redundancies in test sets, and provide a computational basis for optimization and repair planning.

7.4.2 Structure of Fault Tables

In their simplest form, fault tables are binary matrices indicating whether a given test activates and detects a particular fault hypothesis. An illustrative form is:

Table 7.4—Illustrative fault–test activation matrix (fault table)

Fault Type	Test 1	Test 2	…	Test n
Stuck-at-0 @ B7	1	0	…	1
Coupling R7 → R8	0	1	…	1
Decoder aliasing	0	0	…	1

A value of 1 indicates that the test activates and detects the fault under the stated assumptions; a value of 0 indicates non-detection.

Advanced diagnostic frameworks extend fault tables into richer multi-attribute structures that encode:

- Test parameters: timing, access sequencing, voltage domains, stress conditions, and environmental context.
- Fault taxonomy: stuck-at, transition, bridging, retention, disturb, coupling, and decoder faults organized hierarchically.
- Spatial mapping: attributes linking each fault manifestation to a physical or logical domain (bit, word, row, page, bank, channel).

This enrichment transforms fault tables into a diagnostic knowledge base supporting symbolic reasoning, coverage analysis, clustering, and trend interpretation. Consequently, fault tables evolve from binary lookups into multi-attribute diagnostic engines suitable for post-manufacturing yield optimization and in-field repair.

7.4.3 Building Fault Tables: Construction Methods

Fault tables can be constructed using three principal approaches:

(A) Simulation-based fault injection

Faults are introduced into a modeled memory system manually or via automated injection tools. Test sequences are executed and response vectors (including miscompare signatures and ECC syndromes) are logged systematically.

This approach offers high observability and activation control, making it effective for coverage metric development and validation of diagnostic sequences against known fault models.

(B) Analytical modeling

Fault behavior is derived from activation functions describing how defects manifest under specific operations and state transitions. Logical or symbolic models predict test responses through explicit input–output transformations.

Within the symbolic operator framework formalized in Chapter 8, an algebra is defined that maps read/write micro-operation sequences directly onto fault activation domains, enabling analytical generation of fault–test mappings for nonlinear and composite faults.

(C) Hardware observation

In deployed systems, ECC syndrome logs, BIST outputs, and runtime monitoring streams serve as sources for constructing probabilistic fault tables. Entries are refined as observational evidence accumulates.

This method reflects true operating conditions and supports adaptive test refinement and long-horizon fault trend analysis in long-lived and safety-critical platforms.

7.4.4 Diagnostic Resolution Metrics

The following metrics form the foundation for quantitative evaluation of diagnostic effectiveness. Together, they characterize the ability of a test set to detect, distinguish, and localize faults under architectural and operational constraints.

Discriminability (D)

Discriminability measures the proportion of fault pairs that can be distinguished by the applied test set. Two faults are considered distinguishable if their response vectors differ for at least one test in the set.
Formally,

$$D = \frac{\text{Number of distinguishable fault pairs}}{\text{Total fault pairs}}$$

A value of $D = 1$ denotes perfect discriminability, meaning that each modeled fault produces a unique diagnostic signature. Lower values indicate diagnostic ambiguity, where multiple faults remain indistinguishable under the applied test conditions.

Resolution Score (R)

The resolution score captures the effective precision of fault localization by jointly accounting for localization granularity (e.g., bit, word, row/column, page) and diagnostic confidence. Unlike discriminability, which is pairwise, the resolution score reflects how narrowly and reliably a fault can be confined to a physical or logical domain.

False Negative Rate (FNR)

The false negative rate represents the proportion of actual faults that are neither activated nor detected by the test set. Elevated FNR values indicate inadequate test excitation, masking effects introduced by ECC correction, or insufficient stress coverage under noise, timing, or layout-dependent conditions.

Ambiguity Index (AI)

The ambiguity index quantifies the degree of diagnostic aliasing by counting the number of distinct faults that yield identical response vectors. High AI values indicate that multiple defect hypotheses collapse into a single diagnostic outcome, limiting actionable localization and repair.

Within the Optimal_Test diagnostic engine, I implemented an ambiguity cluster analysis module that explicitly identifies groups of unresolved faults sharing identical or near-identical response signatures. For each ambiguity cluster, the engine proposes targeted refinement actions, including:

- Test pattern augmentation, introducing additional transitions, stress conditions, or address permutations to expand activation diversity.
- Sequence reordering, modifying test execution order to expose asymmetries among aliased faults.

- Pattern compression relaxation, permitting longer or less compressed sequences when runtime or energy budgets allow, thereby increasing fault differentiation capacity.

These adaptive mechanisms form a dynamic refinement loop in which coverage, discriminability, and resolution are continuously optimized while respecting efficiency constraints in symbolic and ECC-aware memory architectures.

7.4.5 Diagnostic Yield and Efficiency Metrics

Beyond resolution and fault distinguishability, diagnostic frameworks must be evaluated for efficiency, selectivity, and cost-effectiveness. This ensures that diagnostic procedures remain viable in high-throughput, power-constrained, or safety-critical environments.
Key metrics for evaluating diagnostic yield and test suite performance include:

Table 7.5—Diagnostic yield and efficiency metrics

Metric	Definition
Test Coverage (TC)	Percentage of modeled faults activated and detected by at least one test vector
Diagnostic Coverage (DC)	Percentage of modeled faults that are uniquely identifiable, not merely detectable
Redundancy Index (RI)	Proportion of test vectors that are functionally duplicative in terms of fault activation
Fault Isolation Depth	Finest granularity level at which faults can be reliably localized
Execution Cost (EC)	Cumulative time, energy, and computational resources required to execute the test suite

Within the adaptive fuzzy diagnostic scoring, formally defined in **Chapter 13** and applied within the **Optimal_Test** framework (**Chapter 12**), these metrics are evaluated jointly to derive Pareto-optimal rankings of candidate test suites.

By quantifying trade-offs among coverage, ambiguity, resource consumption, and isolation depth, the system identifies configurations that maximize diagnostic value under strict runtime or energy constraints.

This multi-metric evaluation is essential for modern memory systems, where diagnostics must operate efficiently within tight power and timing budgets, scale across heterogeneous architectures, and adapt dynamically to evolving fault models, ECC masking behavior, and runtime noise conditions.

7.4.6 Visual Fault Maps and Heatmaps

In advanced diagnostic workflows, visualization is a core analytical mechanism rather than a secondary aid. Transforming numerical fault logs into spatial and temporal visual

representations enables pattern discovery that is difficult to achieve through raw data inspection alone.

Key visualization techniques include:

- Fault heatmaps, in which memory locations are color-coded according to fault incidence, severity, or statistical confidence. These maps reveal spatial clustering, weak regions, and degradation zones.
- Activation overlays, which correlate specific test patterns or symbolic operations with the spatial distribution of activated faults, clarifying causal relationships between test stimuli and fault manifestation.
- Temporal evolution charts, which track fault behavior across test cycles, temperature ranges, voltage conditions, or aging intervals, exposing dynamic effects such as thermal drift, retention loss, or wear-induced instability.

These visualization methods support multiple diagnostic contexts, including chip-level yield analysis, where spatial recurrence may indicate systematic manufacturing variation; in-field diagnostic dashboards, providing interpretable health monitoring from runtime logs; and BISR feedback loops, where redundancy allocation and remapping benefit from spatial and temporal insight.

By embedding visualization directly into the diagnostic loop, memory systems transition from binary pass/fail assessment toward explainable, adaptive fault analysis. This improves both human interpretability and the effectiveness of automated repair and resilience mechanisms.

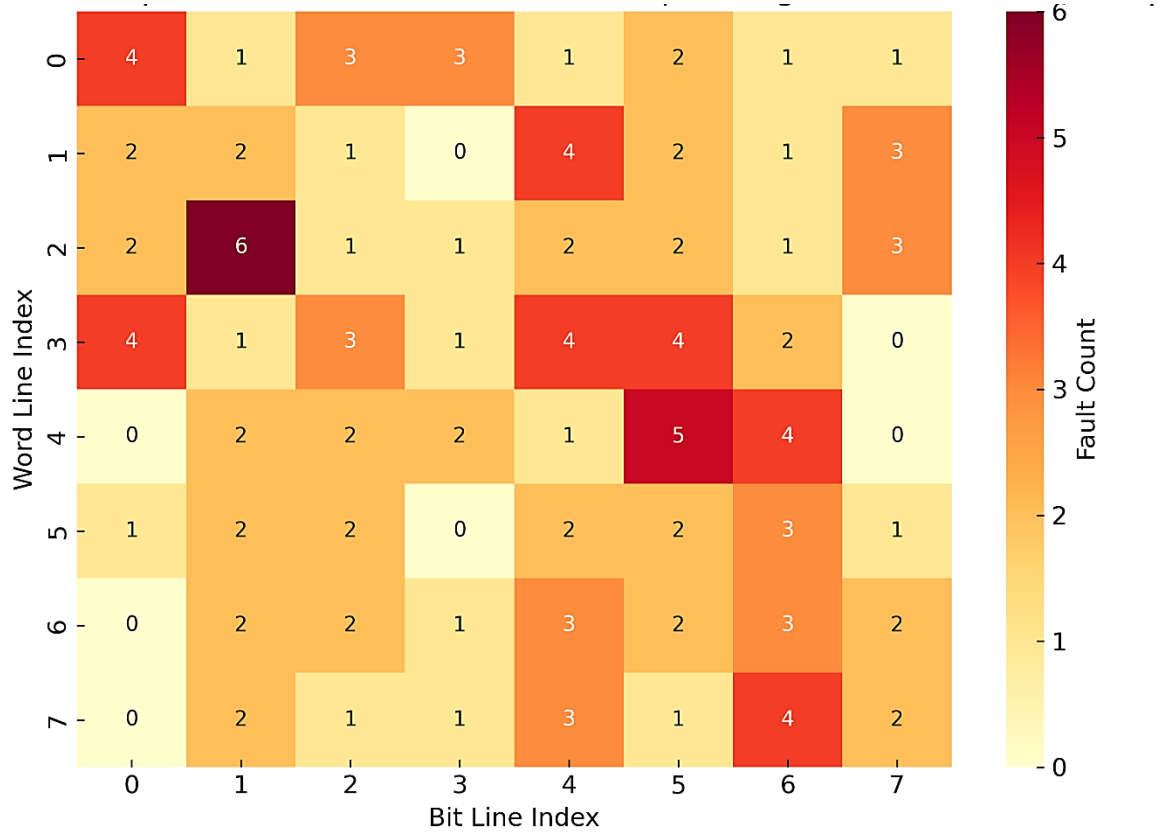

Figure 7.5—Example fault table slice and corresponding localization heatmap

Figure 7.5 presents an 8×8 slice of a memory array, where each cell corresponds to a word-line/bit-line intersection or a compact bit-cell cluster, depending on architectural granularity. The numeric value overlaid within each cell represents the number of observed fault events accumulated over a defined diagnostic window.

The accompanying color scale encodes fault density, ranging from low incidence (light tones) to high concentration (deep red).

This visualization reflects the output of diagnostic engines such as Optimal_Test and PROVER-based symbolic evaluators, in which raw fault logs, ECC correction counts, or miscompare events are aggregated and projected onto the physical address space.

Practical applications of such localization heatmaps include:

- Rapid identification of fault hotspots corresponding to localized process defects, marginal cells, or lithographic sensitivity.
- Spatial assessment of failure distributions, supporting yield analysis and guiding process or layout-level refinements.
- Visual input to Built-In Self-Repair (BISR) engines and redundancy controllers, enabling repair resources to be prioritized toward regions with the highest fault density.

When combined with symbolic test overlays or ECC syndrome correlation maps, localization heatmaps form a bridge between activation vectors and spatial fault manifestation. They reveal how specific test conditions or access paths correlate with physical fault concentration, reinforcing the data-driven, spatially resolved diagnostic methodology developed in this chapter and extended further in **Chapter 14**.

7.4.7 Practical Challenges and Mitigation Strategies

Even with advanced diagnostic infrastructures, memory fault analysis encounters practical limitations that require deliberate mitigation strategies.

Ambiguous faults arise when distinct failure mechanisms generate identical response vectors under a given test set. Such faults collapse into diagnostic equivalence classes, limiting root-cause resolution. A primary mitigation approach is response refinement, which applies additional stress dimensions—such as controlled voltage variation, temperature modulation, or timing margin adjustment—to expose behavioral divergence and break equivalence.

Masked faults constitute a second major challenge. Built-In Self-Repair (BISR), ECC correction, and runtime remapping mechanisms may suppress fault manifestation, resulting in false negatives during diagnosis. To counter this effect, post-repair verification and targeted fault injection are employed to validate that remapping has fully isolated the defect without leaving residual vulnerabilities.

Complementary strategies include persistent ECC syndrome logging and shadow redundancy testing, which help surface latent faults that appear only under specific operating or environmental conditions.

Diagnostic scalability is further challenged by test explosion. As fault models expand to include multi-bit upsets, coupling interactions, and time-dependent degradation, the number of required test vectors can grow combinatorially.

Common containment strategies include:

- Test-set compression to eliminate redundant activation vectors.
- Fault pruning to remove non-critical or provably dominated fault hypotheses.
- Symbolic test synthesis, which explores the test space analytically rather than through exhaustive enumeration.

Within my hybrid U–Y symbolic framework, I applied graph-based test-path partitioning to decompose March tests into structurally independent symbolic paths. This decomposition achieved more than 40% reduction in test vector count while preserving complete modeled fault coverage, demonstrating that symbolic structure can simultaneously improve efficiency and diagnostic depth.

7.4.8 Summary

Fault tables function as the operational memory of diagnostic systems, recording fault hypotheses, activation conditions, and observed manifestations. Their value lies not in accumulation alone, but in structured interpretation.

Diagnostic resolution metrics—including Test Coverage (TC), Diagnostic Coverage (DC), Redundancy Index (RI), and Fault Isolation Depth—provide the quantitative framework required to transform fault tables into diagnostic intelligence. These metrics guide test refinement, enable objective comparison of diagnostic strategies, and support informed repair decisions.

From my work in symbolic modeling and test synthesis, two principles consistently emerged:

- Diagnostics without quantifiable resolution degenerate into heuristic guesswork.
- Repair without ambiguity analysis risks miscorrection and unnecessary resource consumption.

By integrating structured fault tables with resolution metrics directly into the diagnostic pipeline, systems transition from reactive error handling to predictive diagnostic modeling. This transition is essential in modern high-density memory platforms, where fault mechanisms are increasingly complex, conditional, and time-varying.

7.5 Hierarchical and Multi-Level Diagnosis

As memory systems scale in capacity and architectural complexity—incorporating multi-bank organizations, interleaved address spaces, multichannel controllers, virtual-to-physical remapping, and layered redundancy—flat diagnostic approaches become increasingly inadequate. In such systems, a single fault may originate in one physical structure, manifest logically in another, and propagate through intermediate layers in ways that obscure its true source.

Hierarchical and multi-level diagnosis provides a structured framework for managing this complexity.

Rather than treating the memory subsystem as a monolithic entity, diagnosis is decomposed into strata aligned with architectural boundaries:

- Logical layer: Interprets faults at the software-visible level, including virtual addresses, pages, and anomalies detected via ECC syndromes or logging mechanisms.
- Microarchitectural layer: Targets intermediate structures such as address interleavers, bank selectors, row and column decoders, timing domains, and memory controller logic.
- Physical layer: Correlates faults with the hardware substrate, including memory cells, interconnects, power domains, and redundancy resources such as spare rows or BIRA mechanisms.

Each layer employs diagnostic strategies suited to its abstraction level, ranging from symbolic tracing and syndrome analysis at the logical layer to March-based stress testing and ECC feedback correlation at the physical layer. The essential requirement is traceability across layers, enabling a symptom observed in logical address space to be backtracked to its physical origin, even in the presence of ECC masking, address remapping, or aliasing in control logic.

This multi-tier perspective underpins the design of my Optimal_Test diagnostic engine. Within this framework:

- PROVER-generated micro-operations provide fine-grained symbolic control of address and access paths.
- ECC telemetry streams capture runtime fault behavior, including masked or partially corrected events.
- Symbolic fault maps encode architectural relationships, allowing fault manifestations to be projected and resolved across diagnostic layers.

Together, these mechanisms form a tiered localization pipeline that combines symbolic synthesis with architectural awareness, enabling precise and scalable diagnosis in deeply interleaved and redundancy-saturated memory systems.

7.5.1 Definition of Hierarchical Diagnosis

Hierarchical diagnosis is a layered diagnostic methodology that mirrors the abstraction levels inherent in modern memory systems, from physical circuitry to software-visible memory space. By associating distinct diagnostic strategies with each layer, hierarchical diagnosis achieves greater precision than flat approaches.

Logical-layer syndromes may first identify anomalous behavior in virtual address space, which can then be traced through microarchitectural structures to isolate a faulty decoder or interconnect, and finally resolved at the physical layer as a degraded word-line driver or unstable bit-line segment.

This approach ensures diagnostic coherence across layers: high-level symptoms are mapped to low-level causes, while physical observations are interpreted in terms of their architectural and software impact. Hierarchical diagnosis thus functions not only as a localization mechanism,

but as an integrative framework linking detection, interpretation, and repair in modern memory systems.
The table below summarizes the key diagnostic layers and their associated fault types:

Table 7.6—Diagnostic layers and representative fault classes

Level	Target Layer	Typical Fault Types
Bit / Cell	Physical transistor or storage capacitor	Stuck-at faults, retention failures, leakage currents, single-event upsets
Word / Line	Access logic and word-line / bit-line structures	Coupling faults, bridging defects, read disturb, write asymmetry
Subarray / Bank	Memory subarray organization and local control	Row decoder faults, sense amplifier errors, intra-bank contention
Channel / Rank / Package	I/O interface and physical routing	Timing violations, signal skew, crosstalk, impedance mismatch
Logical Block / Page	OS-visible memory mapping and allocation	Address aliasing, mapping inconsistencies, ECC degradation
Application layer	Software-level memory abstraction	Silent data corruption, unhandled exceptions, memory poisoning

Each diagnostic layer functions both as a filter and as a reinterpretation boundary for faults originating at lower layers. A defect introduced at the physical level may be transformed as it propagates upward, changing both its observability and its apparent semantics.

For example, a leakage-induced retention failure at the bit-cell level may remain invisible during raw cell access but emerge as a correctable ECC event at the logical block level, or as intermittent silent data corruption at the application layer under specific workload or timing conditions.

Effective diagnosis therefore requires both top-down awareness—the ability to interpret high-level symptoms within their architectural and software context—and bottom-up traceability, ensuring that any observed anomaly can be resolved to its root cause in the physical substrate.

This bidirectional transparency is especially critical in systems where masking mechanisms such as BISR, ECC correction, address remapping, or virtualization obscure direct cause–effect relationships.

Within the framework of symbolic test generation and adaptive diagnostics, hierarchical diagnosis ensures that:

- Faults are not misclassified due to masking, aliasing, or abstraction boundaries.
- Repair or mitigation actions are not applied at inappropriate architectural levels.

- Observed symptoms remain grounded in architectural causality across physical, logical, and software-visible domains.

This layered methodology transforms diagnosis from a flat detection process into a structured reasoning framework capable of operating reliably in deeply interleaved, redundancy-saturated, and virtualization-heavy memory architectures.

7.5.2 Multi-Level Fault Tracing Techniques

Hierarchical diagnosis is effective only when faults can be traced consistently across abstraction layers. To support this requirement, diagnostic workflows must implement multi-level fault tracing mechanisms that enable upward and downward propagation of diagnostic information, as well as integration across architectural domains.

(A) Forward tracing

Forward tracing begins at the point of fault detection and propagates upward through the memory hierarchy. It relies on ECC syndrome logs, address translation metadata, cache coherence state, and operating system mappings.

Example: An ECC syndrome flags an error within a cache line. That line is mapped to a physical address, which is resolved to a virtual memory page and ultimately associated with a process or software context. Forward tracing localizes the impact domain of the fault, even when the physical defect remains masked by correction or remapping.

(B) Backward tracing

Backward tracing operates in the opposite direction, beginning with an observed symptom at the software or system level and resolving downward toward the physical cause. This approach is essential for post-mortem analysis and debugging of critical failures.

Example: A segmentation fault or uncorrectable exception is traced to a virtual address. Page table resolution identifies the corresponding physical frame, which is then mapped to a specific memory row or bank, ultimately isolating the root cause to a degraded sense amplifier or local decoder structure.

(C) Cross-domain correlation

In interleaved and redundancy-rich architectures, forward or backward tracing alone may be insufficient. Cross-domain correlation integrates diagnostic evidence across logical, microarchitectural, and physical domains. This includes correlating ECC syndromes with physical fault candidates, interpreting remapped addresses through redundancy logic, and accounting for multiplexing across channels, ranks, or shared interconnects.

Within the PROVER-based symbolic testing framework, diagnostic tag propagation is introduced, wherein symbolic metadata tags are embedded within test micro-operations. These identifiers traverse the memory hierarchy during execution and are preserved in diagnostic outputs. Post-execution analysis reconstructs complete causality chains across layers using the propagated tags.

This mechanism proved particularly effective in stacked-memory and system-on-chip environments, where direct physical observability is limited and faults may otherwise remain obscured by correction, remapping, or virtualization layers.

7.5.3 Diagnostic Granularity at Each Layer

Each architectural level in the memory hierarchy requires diagnostic strategies aligned with its functional role and the degree of observability available at that level. Localization mechanisms must therefore be selected to balance achievable resolution against traceability across abstraction boundaries. Table 7.7 summarizes preferred localization techniques for each diagnostic layer.

Table 7.7—Diagnostic granularity and preferred localization techniques

Layer	Preferred Localization Techniques
Cell level	March tests, targeted fault injection, analog sensing, read-margin profiling
Row / Column level	Symbolic fault maps, March-path heatmaps, Rowhammer monitoring
Bank / Subarray level	Contention modeling, address-decode stress patterns, power and thermal correlation maps
DIMM / Channel level	Signal integrity analysis (e.g., eye diagrams), protocol violation tracing, skew and jitter logging
Logical block / Page	OS-level page migration logs, virtual-to-physical resolution tables, ECC correction analytics
System / Application	Application-level fault logs, machine check exceptions (MCE), silent data corruption detection

The principal challenge in multi-layer diagnosis lies in traversing layer boundaries without sacrificing either localization resolution or causal traceability. Diagnostic systems must therefore preserve symbolic links, propagate metadata, and maintain abstraction-aware fault tagging throughout the diagnostic pipeline.

This ensures that software-visible symptoms can be mapped reliably to physical causes, while physical-level observations remain interpretable within the architectural and application context.

Maintaining this cross-layer visibility is essential for accurate root-cause analysis in complex memory subsystems. Without coordinated metadata propagation and consistent fault tagging, diagnostic information may fragment across abstraction levels. Effective frameworks therefore integrate physical diagnostics with system-level observability to preserve end-to-end fault traceability.

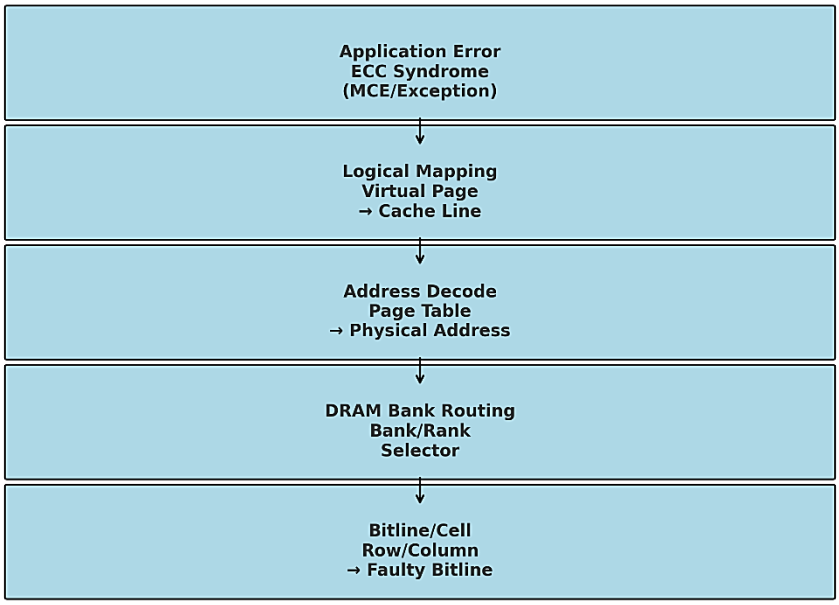

Figure 7.6—Multi-layer diagnostic flow from ECC syndrome to physical fault origin

Figure 7.6 illustrates a hierarchical fault tracing path used to resolve memory errors across abstraction layers. The flow begins with application-visible detection events—such as ECC syndrome reporting, machine check exceptions (MCE), or unhandled software errors—and proceeds through successive architectural levels.

At the logical mapping stage, the affected virtual page or cache line is identified. Address decoding then resolves this logical entity through page tables into a physical memory address. Subsequent bank and rank routing determines the specific DRAM channel, rank, and bank involved, accounting for interleaving and any active remapping. The diagnostic path ultimately terminates at the physical level, isolating the fault to a specific row, column, bitline, or cell structure.

The flow is explicitly bidirectional. It supports forward tracing, in which detected hardware faults are propagated upward to assess software impact, and backward tracing, in which application-level anomalies are resolved downward to their physical cause.

This layered tracing model aligns with the diagnostic architecture implemented in the Optimal_Test framework, where symbolic test instructions, ECC telemetry, and diagnostic metadata are propagated across layers to preserve causality and enable precise fault origin identification even in the presence of masking mechanisms.

7.5.4 Diagnosing in Stacked and Three-Dimensional Memory Systems

Three-dimensional integrated memory architectures, including High Bandwidth Memory (HBM), Wide I/O, and 3D NAND, introduce structural characteristics that fundamentally alter diagnostic requirements. Unlike planar two-dimensional layouts, stacked memories extend vertically across multiple dies interconnected by through-silicon vias (TSVs) or micro-bumps. This vertical integration introduces fault modes that are not directly observable through conventional planar address mapping.

In stacked systems:

- A single data path or bitline may traverse multiple dies, accumulating variability across layers.
- Faults may originate at inter-die connection points, including TSV degradation, micro-bump discontinuities, or resistive opens.
- Layer interfaces may exhibit bonding defects, misalignment, or delamination that manifest only under specific stress conditions.
- Thermal gradients are non-uniform across depth, with inner layers experiencing accelerated aging and asymmetric degradation.
- Effective diagnosis in stacked memories therefore requires specialized strategies, including:
- Z-axis test patterns, constructed to traverse stacked dies vertically and expose inter-layer dependencies that planar scans cannot detect.
- Inter-layer delay profiling, measuring timing asymmetries caused by TSV aging, parasitic capacitance, or signal skew to identify latent vulnerabilities before catastrophic failure.
- Redundancy-aware tagging, which accounts for built-in repair and remapping logic that may silently redirect accesses, ensuring that masked faults remain traceable.

In the implementation of Optimal_Test for 3D memory diagnostics, vertical address tiling is introduced, a symbolic addressing method that generates transitions explicitly crossing die boundaries. Execution employed layer-aware PROVER instruction sets, with metadata binding each access to a specific die, interface, and routing context.

This approach proved effective for exposing faults masked by vertical redundancy schemes and for tracing fault propagation through TSVs under stress conditions such as elevated temperature or high-frequency access.

As stacked memory technologies become central to high-performance computing platforms and AI accelerators, such depth-aware diagnostic capabilities are essential for sustaining reliability across vertically integrated memory hierarchies.

These challenges highlight the need for diagnostic frameworks that explicitly model the vertical structure of stacked memories rather than relying solely on planar assumptions. Accurate fault localization must therefore incorporate die-layer awareness, interconnect characterization, and thermal-depth profiling.

In addition, diagnostic tools must be capable of correlating fault signatures across multiple dies to identify failures originating in shared vertical pathways. As stacking densities continue to increase, the complexity of inter-die dependencies and routing paths will grow correspondingly. Robust testing methodologies must therefore evolve to maintain observability across both lateral and vertical memory dimensions. Such capabilities are essential for sustaining reliability in next-generation three-dimensional memory architectures.

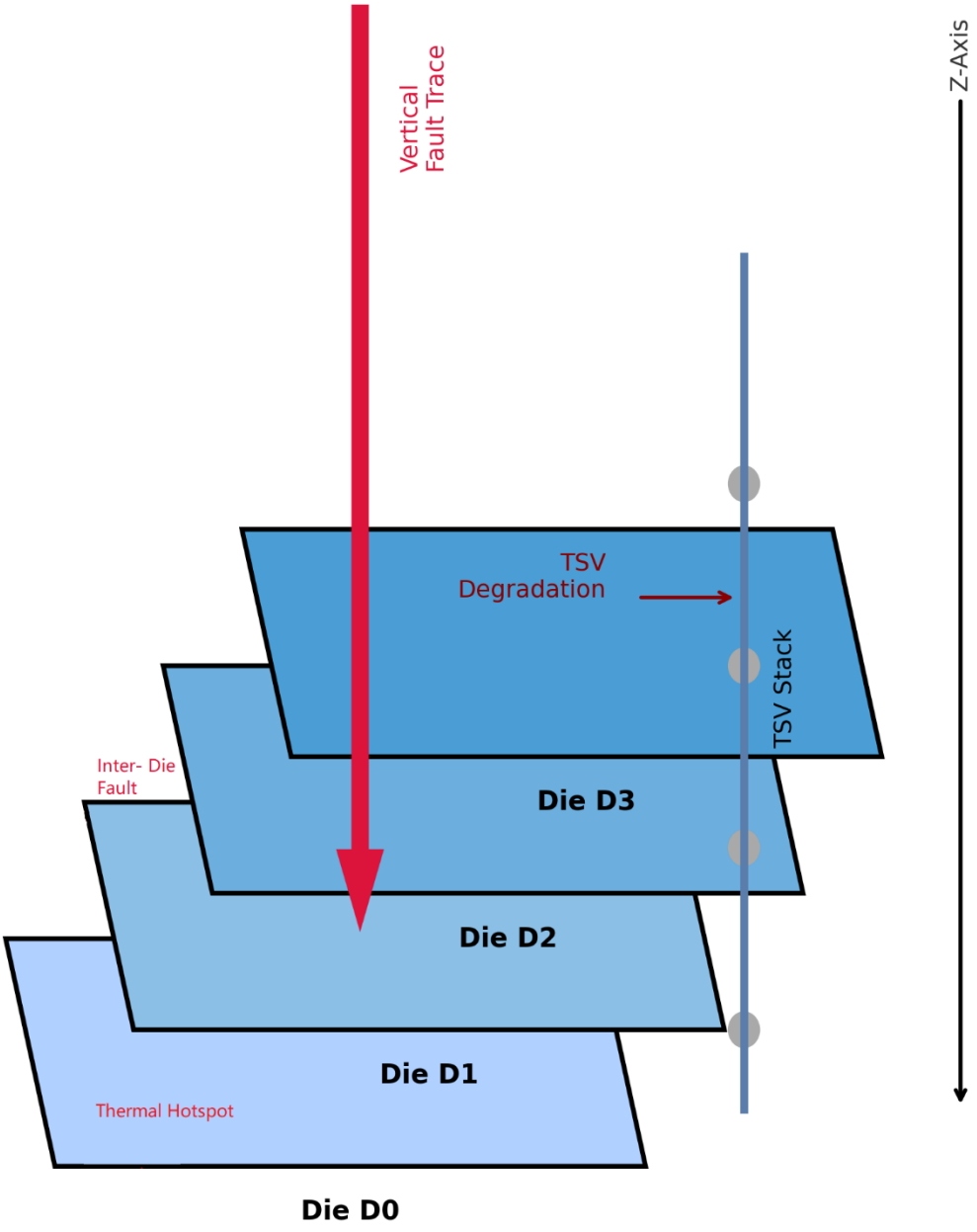

Figure 7.7—Layered fault tracing in 3D stacked memory with TSV-aware Z-axis diagnosis

Figure 7.7 illustrates diagnostic fault tracing in vertically stacked memory architectures such as High Bandwidth Memory (HBM) and 3D NAND, where multiple dies are interconnected through through-silicon vias (TSVs). Four dies (D0–D3) are shown in a staggered arrangement to emphasize vertical integration and depth within the stack.

A vertical arrow represents Z-axis symbolic diagnostic traversal, indicating that test activation and fault tracing propagate across dies rather than remaining confined to a single planar layer. The TSV stack is depicted as a column of inter-die connections, each via constituting a critical contact point susceptible to degradation driven by thermal stress, mechanical strain, or electromigration.

Representative fault mechanisms highlighted in the Figure include a thermal hotspot at the base die (D0), where heat accumulation accelerates aging; an inter-die fault at a mid-stack interface, representing bonding defects or misalignment; and TSV degradation near Die D2, where parasitic effects or aging compromise signal integrity.

The Z-axis reference reinforces diagnostic depth as an explicit dimension of analysis. Fault manifestations may originate in one die, propagate through TSVs, and emerge in another, complicating localization if vertical structure is not explicitly modeled.

This diagnostic perspective underpins frameworks such as Optimal_Test vertical address tiling and symbolic pattern chaining, which enable high-resolution localization across die boundaries in stacked memory systems.

7.5.5 Temporal and Dynamic Diagnosis

Not all memory faults are static. In contemporary memory subsystems—particularly those incorporating advanced reliability, availability, and serviceability (RAS) mechanisms—fault behavior evolves over time. Temporal variability therefore necessitates diagnostic frameworks that are not only spatially aware but also chronologically adaptive.

Dynamic fault behavior arises from several interacting mechanisms:

- Runtime repair and reconfiguration, including Built-In Self-Repair (BISR) and online redundancy activation, which alter the fault landscape during operation.
- Aging and degradation processes, such as charge loss, electromigration, dielectric breakdown, and thermally accelerated wear, which progressively change fault characteristics.
- Wear-leveling and remapping, common in NAND Flash, DRAM, and other paged systems, where logical-to-physical address mappings shift dynamically to avoid weak regions.

To address these dynamics, hierarchical diagnosis must incorporate explicit temporal awareness through time-indexed observation layers. Core mechanisms include:

- Logging address mapping transitions to correlate evolving physical layouts with observed fault manifestations.
- Maintaining bounded fault observation windows that aggregate repeated syndromes, miscompares, or correction events for temporal correlation.
- Tracking ECC correction trends over time, which frequently expose latent degradation well before escalation to uncorrectable errors.
- Achieving robust temporal insight requires integration across multiple telemetry sources:
- Sensor-based telemetry, including temperature, voltage, access intensity, and retention margin indicators that modulate fault behavior.
- Firmware and RAS logs, such as BIST status registers, scrubbing records, and runtime fault counters, providing historical context.
- Memory controller analytics, including per-bank and per-rank error heatmaps, access histograms, and degradation counters, enabling time-resolved localization.

Temporal diagnostics form the basis of predictive fault modeling. By supporting preemptive remapping, adaptive ECC tuning, and policy-driven maintenance strategies, they transform diagnostics from a reactive activity into an anticipatory process. This capability is essential for sustaining reliability in high-density, mission-critical memory systems operating under long uptimes and variable environmental stress.

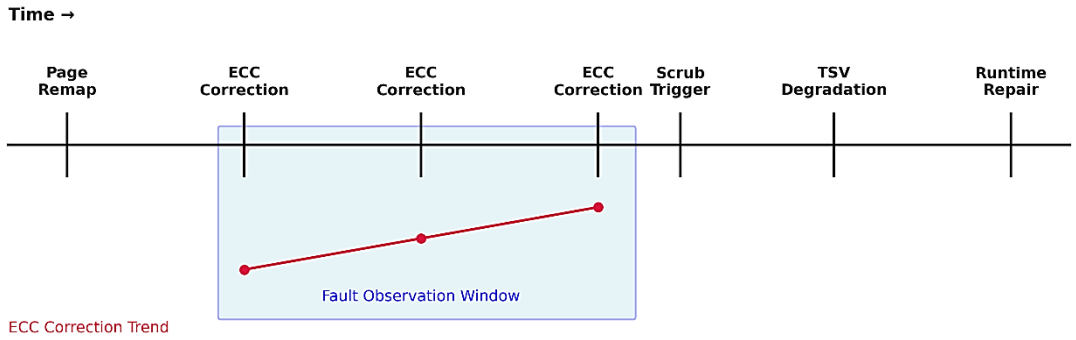

Figure 7.8—ECC Trend Monitoring and Temporal Diagnostic Events Across Fault Observation Window

Figure 7.8 illustrates time-correlated diagnostic activity within a memory subsystem experiencing progressive fault evolution. The horizontal axis represents chronological progression, along which key system events are plotted at discrete points.

A page remap event marks a change in logical-to-physical address association, potentially obscuring direct traceability of subsequent faults. Following this, a sequence of ECC correction events is observed. These events are represented by a rising correction trend, indicating increasing frequency of correctable errors within the same structural region.

The blue-shaded fault observation window defines a bounded temporal interval during which ECC events are aggregated and analyzed collectively rather than treated as isolated incidents. Within this window, correction density, recurrence rate, and temporal slope are evaluated to infer degradation trends rather than transient noise.

When the accumulated correction activity exceeds a programmable safety threshold, a scrub trigger is issued to proactively refresh the affected region and mitigate error accumulation. A subsequent TSV degradation marker illustrates the emergence of a physical fault mechanism correlated with prolonged electrical and thermal stress. Finally, runtime repair denotes the activation of Built-In Self-Repair (BISR), dynamically remapping or bypassing the degraded structure.

This timeline concretely illustrates the temporal diagnostic principles introduced in Section 7.5.5, demonstrating how ECC trend monitoring, bounded observation windows, and adaptive repair policies interact to support predictive fault management rather than reactive correction.

7.5.6 Integration with Repair and System Policy

In modern memory systems, diagnosis is not a postmortem activity but an active control input that directly influences system behavior. Once a fault is detected and characterized, diagnostic outputs may immediately initiate corrective or mitigative actions, including:

- Activation of Built-In Self-Repair (BISR) mechanisms, such as spare row or column substitution, fuse programming, or soft remapping.
- Notification of system software to trigger page migration, region quarantine, or dynamic adjustment of access policies.
- Updates to in-field diagnostic repositories, supporting long-term fault trend analysis and predictive maintenance.

For these actions to be reliable, diagnostic frameworks must satisfy several constraints. They must attach confidence measures to localization results, ensuring that repair actions are commensurate with diagnostic certainty.

They must also guarantee coherence across layers, so that controller-level repair decisions remain consistent with firmware state and operating system memory management. Finally, diagnostic metadata must be preserved across remapping and repair events to support longitudinal analysis and prevent loss of fault provenance.

In my research on repair-aware diagnostic chains, I demonstrated that coupling diagnosis with adaptive repair policy—particularly policies guided by syndrome histories and signature classification—substantially improves uptime and recovery precision. This integration shifts memory management from reactive correction toward predictive fault handling, which is essential in dense, reliability-critical environments.

7.5.7 Summary

Hierarchical and multi-level diagnosis is not optional in modern memory systems; it is foundational. As architectures span physical cells, banks, interleaved channels, virtual pages, and software-visible abstractions, faults must be traced coherently across both physical and logical domains.

From my work on simulation-based and runtime diagnostic pipelines, it is evident that the value of diagnosis lies not only in detecting faults, but in interpreting and contextualizing them. A resilient diagnostic framework must explain what failed, where it originated, when it emerged, and why it propagated—bridging architectural layers and temporal scales.

This progression from raw detection to structured explanation enables precise localization, informed repair, and predictive maintenance. These capabilities are indispensable for sustaining reliability in high-density, fault-tolerant, and self-healing memory systems.

7.6 From Test Failure to Root Cause Mapping

Detecting a fault is only the initial step. Diagnostic intelligence emerges when an observed anomaly can be traced back to a structured and verifiable root cause that explains what failed, where it failed, why it failed, and how it can be mitigated.

Root cause mapping integrates the full diagnostic stack: low-level test responses, symbolic fault models, localization outcomes, architectural context, telemetry streams, and physical layout knowledge. It converts fragmented observations into a coherent causality chain.

Within the Optimal_Test framework, a root cause engine was developed that combines symbolic fault signatures, ECC syndromes, and architectural awareness within a multi-stage inference pipeline. By layering symbolic analysis with syndrome correlation and structural model lookup, the engine achieves high-confidence attribution even under partial observability or noisy conditions.

This section formalizes that methodology, demonstrating how symbolic diagnostics, architectural context, and temporal awareness elevate diagnosis from fault detection to actionable explanation and repair.

7.6.1 Root Cause Mapping in Memory Systems

Root cause mapping transforms an observed anomaly—such as a test miscompare, ECC syndrome, or runtime exception—into a structured diagnosis that resolves:

- The failing mechanism (e.g., stuck-at behavior, retention decay, coupling interference, address aliasing).
- The fault origin, whether physical or logical, such as a specific cell, wordline, bank, TSV, or controller path.
- The activation condition, including timing relationships, background data, stress states, or layout-dependent sensitivities.
- The propagation path, describing how the fault manifests across caches, interleaving logic, virtual memory, or remapping layers.
- The corrective response, encompassing redundancy activation, region quarantine, ECC policy adjustment, or escalation.

This capability is particularly critical in environments where ECC, scrubbing, and BISR mask early fault signatures, and where remapping or wear-leveling obscures the physical origin of failures.

Effective root cause mapping therefore depends on maintaining diagnostic context across multiple abstraction layers. By correlating low-level fault signatures with system-level behavior, diagnostic frameworks can isolate failure mechanisms with greater precision and reliability.

7.6.2 Multi-Stage Failure Interpretation Pipeline

Accurate root cause attribution requires structured reasoning that progressively refines fault interpretation. Advanced diagnostic systems therefore employ multi-stage interpretation pipelines:

Stage 1: Failure detection

Initial anomalies are observed via ECC decoders, BIST logic, or March test miscompares.

Stage 2: Syndrome decoding and isolation

Syndromes are mapped to candidate bits, words, or regions. Ambiguity clusters are identified, and spare or remap logs are consulted to unwind masking effects.

Stage 3: Contextual augmentation

Temporal and spatial context is added, including access history, correction frequency, refresh intervals, thermal gradients, and known weak regions.

Stage 4: Structural mapping

Logical addresses are reconciled with physical layout by unwinding interleaving, rank and channel striping, migration history, and BISR remaps.

Stage 5: Causality inference

Observed signatures are matched against known fault models, probabilistic hypotheses are ranked, and conclusions are cross-validated against stress logs and test history.

This diagnostic process is formalized as a five-phase diagnostic transition graph, where each node represents a progressively refined interpretation of the fault state. This model supports reasoning under uncertainty and enables consistent root cause attribution even when observations are incomplete or partially masked by runtime correction.

This staged interpretation pipeline enables diagnostic systems to transform raw error observations into structured, causally consistent explanations. By progressively enriching fault evidence with contextual and architectural information, the framework reduces ambiguity in fault attribution.

Such pipelines are particularly valuable in modern memory systems where runtime correction, remapping, and interleaving obscure direct fault visibility. Systematic interpretation therefore becomes essential for distinguishing transient anomalies from persistent structural defects. The layered inference process also supports automated diagnostic tooling, enabling consistent analysis across large-scale deployments.

When integrated with adaptive testing and telemetry analytics, this approach significantly improves the accuracy, repeatability, and scalability of root cause diagnosis in complex memory environments.

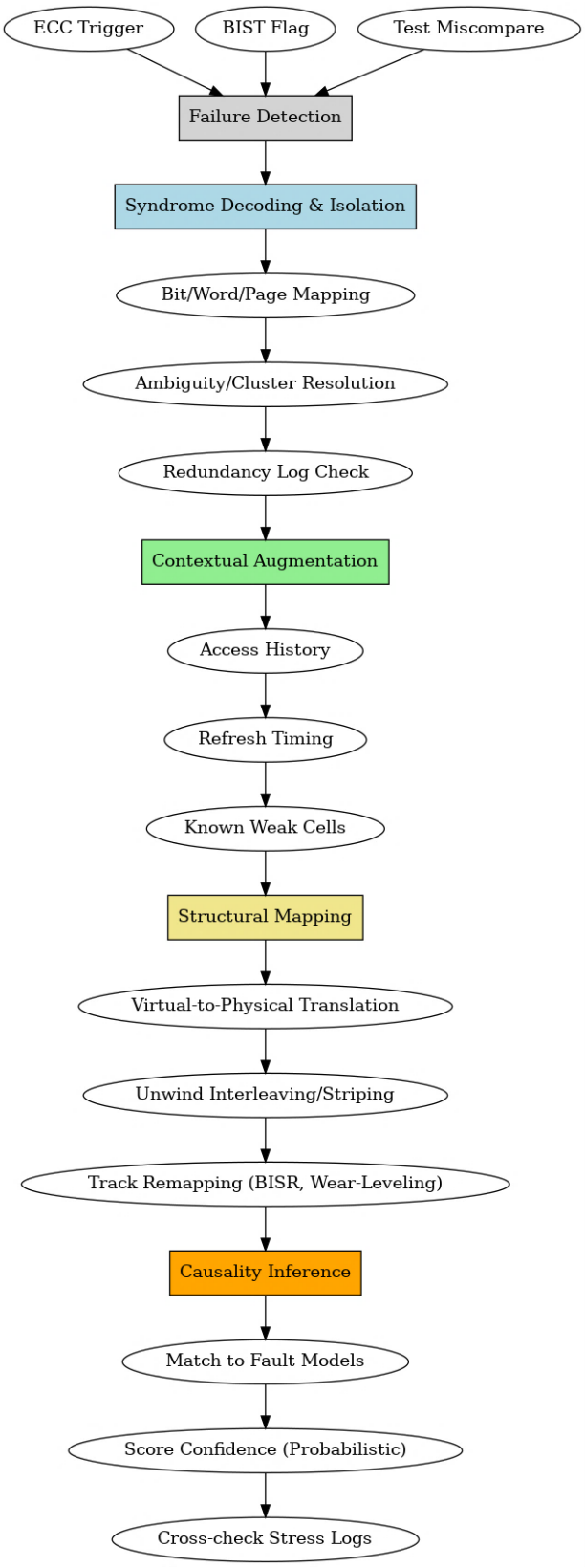

Figure 7.9—Failure-to-root-cause diagnostic flow integrating test outputs, syndrome vectors, mapping metadata, and inference layers

Figure 7.9 depicts a multi-stage diagnostic pipeline that traces memory faults from initial detection to structured root cause attribution. The pipeline integrates heterogeneous diagnostic

inputs—test failures, ECC syndromes, architectural mapping data, and inference logic—into a coherent reasoning sequence.

The diagnostic chain is initiated by failure detection events, including ECC triggers, BIST flags, or explicit test miscompares.

These events represent the earliest observable symptoms and provide the entry point for diagnostic processing.

The pipeline proceeds through the following stages:

- **Syndrome decoding and isolation**

  Raw fault signatures are decoded and mapped to candidate resolution levels (bit, word, or page). At this stage, ambiguity clusters are identified and reduced using redundancy metadata and equivalence-class analysis to prevent premature over-localization.

- **Contextual augmentation**

  The fault signal is enriched with temporal and spatial context, including access history, refresh timing behavior, and known weak-cell or weak-region annotations. This stage converts isolated error events into context-aware diagnostic evidence.

- **Structural mapping**

  Logical abstractions are reconciled with physical organization by resolving virtual-to-physical translations, unwinding address interleaving or striping, and tracing remapping actions introduced by BISR or wear-leveling mechanisms. This stage restores architectural causality that may be obscured by runtime masking.

- **Causality inference**

  Augmented fault signatures are matched against modeled fault mechanisms. Probabilistic scoring is applied to rank competing hypotheses, and results are cross-validated against stress logs and environmental telemetry to eliminate spurious correlations.

  By layering detection, decoding, augmentation, mapping, and inference, the pipeline enables systematic reasoning under uncertainty.

  This flow, formalized within the Optimal_Test framework, supports high-confidence root cause mapping even when partial observability, ECC masking, or architectural complexity prevents direct attribution.

7.6.3 Rule-Based and Data-Driven Inference Engines

Root cause mapping relies on inference engines that interpret observed fault behavior and propose the most probable underlying causes. Multiple inference paradigms coexist, each addressing different diagnostic constraints.

(A) Rule-Based Inference

Rule-based engines operate on predefined fault signatures and deterministic mapping rules. They provide predictable behavior with minimal computational overhead and are well suited for tightly constrained runtime environments.
Example: a decoded ECC syndrome maps directly to a specific stuck-at fault in a known bit position.

(B) Fuzzy Logic-Based Inference

Fuzzy inference replaces binary decisions with graded confidence, enabling diagnosis under ambiguity and partial observability. This approach is effective for marginal faults, overlapping signatures, and soft-error-dominated regimes.

Example: assigning an 80–90% likelihood to a coupling fault between adjacent rows rather than enforcing a single categorical outcome.

Detailed treatment of fuzzy diagnostic scoring and resolution ranking is provided in **Chapter 13**, and its integration into the **Optimal_Test** workflow is discussed in **Chapter 12**.

(C) Statistical and Machine Learning-Based Inference

Statistical and learning-based engines derive fault models from historical data using clustering, classification, or probabilistic estimation. These methods capture nonlinear or emergent failure modes that are difficult to encode explicitly and scale effectively in telemetry-rich environments.

Within the Optimal_Test framework, I implemented a hybrid inference architecture. Fuzzy scoring quantified uncertainty and guided resolution thresholds, while symbolic rule systems derived from PROVER operators enforced architectural constraints—for example, restricting row-decoder faults from propagating across bank boundaries.

This combination preserved architectural correctness while maintaining diagnostic flexibility in both offline analysis and runtime deployment.

7.6.4 Interaction Between Root Cause Mapping and Remapping

Root cause inference must explicitly account for repair-induced masking. Once BISR or remapping logic redirects accesses away from faulty structures, naïve diagnosis may misattribute symptoms to unaffected regions.

Accurate post-repair diagnosis therefore requires access to:

- Redirection and remapping history logs,
- Logical-to-physical mapping deltas,
- Spare row and column allocation records.

Within Optimal_Test, a rollback-tag mechanism is introduced, enabling diagnostic logs to be traced backward through successive remapping steps. This preserves causal visibility even after runtime repair has altered the effective memory topology.

7.6.5 Confidence Scoring and Decision Thresholds

Not all diagnostic conclusions achieve full certainty. Advanced diagnostic systems therefore associate confidence scores with inferred root causes.

Key confidence indicators include:

- **Syndrome ambiguity score**, reflecting the uniqueness of syndrome-to-fault mapping,
- **Localization density**, measuring spatial overlap among candidate fault sites,
- **Activation reproducibility**, confirming persistence under repeated testing,
- **Cross-layer correlation depth**, validating consistency across ECC logs, controller telemetry, and software-visible errors.

Low-confidence outcomes trigger adaptive responses rather than immediate repair. These may include extended test sequences, stress re-testing under modified voltage or temperature, or escalation to higher-level monitors for deferred analysis. This adaptive branching prevents both overreaction to transient noise and underreaction to genuine but weakly observable faults.

7.6.6 Mapping Diagnoses to Actionable Outcomes

Diagnosis is valuable only insofar as it leads to coherent system action. In memory systems, inferred fault classes are mapped to specific response pathways:

- **Correctable bit-level faults** → ECC correction or spare substitution.
- **Localized uncorrectable faults** → Quarantine of wordlines, pages, or cache lines.
- **Systemic or spreading faults** → Escalation to firmware for predictive alerts, capacity reduction, or module retirement.
- **Unknown or anomalous signatures** → Flagging for field diagnostics, telemetry upload, or offline model refinement.

To enforce consistency, the Optimal_Test pipeline incorporates a post-diagnosis classifier that categorizes faults into bounded action classes, prevents oscillatory repair behavior, and maintains alignment between automated repair policies, manual overrides, and persistent system health records.

7.6.7 Summary

Root cause mapping represents the apex of memory diagnostics. At this stage, raw test outputs and error indicators are transformed into structured explanations and translated into deliberate system behavior.

This process unifies architectural context, symbolic reasoning, telemetry correlation, probabilistic inference, and repair-state feedback into a single diagnostic narrative. From my research and implementation experience, the true value of memory testing lies not in fault detection alone, but in disciplined interpretation—turning ambiguous events into high-confidence explanations aligned with architectural intent and operational policy.

It is this interpretive capability that enables modern memory systems to move beyond static fault tolerance toward adaptive, predictive, and self-optimizing resilience.

Part IV — Symbolic Models, Graphs & Optimization

The symbolic frameworks and diagnostic tools presented in this part—most notably PROVER and Optimal_Test—originated from research conducted between 2005 and 2009. While the experimental data and architectural assumptions reflect memory technologies of that period, the underlying symbolic models, abstractions, and optimization principles remain applicable to modern memory systems. Subsequent parts of this monograph explicitly extend these concepts to contemporary and emerging technologies, including non-volatile memories and AI-augmented diagnostic architectures.

Chapter 8: Operator-Based Fault Modeling

Robust fault modeling constitutes the conceptual foundation of memory diagnostics. It defines not only the classes of faults under consideration, but also the mechanisms through which they arise in physical memory systems and the conditions under which they can be activated and observed under controlled stimuli. Traditional fault models—such as stuck-at, transition, and coupling faults—are rooted in structurally simple abstractions and have historically proven effective for classical planar memory arrays.

However, these models are increasingly inadequate for capturing the conditional, context-sensitive, and dynamic fault behaviors characteristic of modern high-density, heterogeneous, and vertically stacked memory systems.

To address these limitations, this work introduces an **operator-based fault modeling framework**. In this formalism, memory behavior and fault activation are abstracted into a symbolic language of micro-operations and state transitions. Rather than treating faults as static anomalies bound to individual cells or structures, the framework models faults as *interaction-dependent phenomena*, defined in terms of symbolic operator sequences and the conditions under which deviations from expected behavior become observable.

This approach enables a unified and extensible representation of diverse fault classes, supporting analytical reasoning, compact test specification, and systematic test synthesis. It bridges the gap between theoretical fault abstraction and practical diagnostic test generation, providing the conceptual basis for subsequent developments in symbolic test programming (**Chapter 10**), **graph-based March test decomposition using U–Y schemes (Chapter 11)**, and **adaptive test optimization (Chapter 12)**.

Furthermore, operator-based modeling supports fault taxonomy refinement, simulation-based validation, and seamless integration with automated test generation environments such as PROVER and Optimal_Test, as developed in this work.

8.1 Motivation for a Unified Symbolic Model

As memory technologies continue to evolve in complexity—ranging from planar DRAM arrays to three-dimensional stacked non-volatile memories—the limitations of conventional fault models become increasingly pronounced. Classical abstractions such as stuck-at,

transition, and coupling faults were formulated for structurally homogeneous arrays and largely static operating conditions.

As a result, they do not scale naturally across heterogeneous technologies or dynamic operational regimes.

In particular, conventional fault models exhibit several fundamental limitations:

- **Lack of generality.** Each newly observed fault mechanism (e.g., row hammer effects, retention decay, disturb-induced threshold drift) typically requires the introduction of a bespoke fault model or a specialized test strategy. This leads to model proliferation and fragmentation across diagnostic frameworks.
- **Poor composability.** Interacting fault phenomena—such as retention degradation under aggressive coupling or transition faults exacerbated by aging-induced threshold shifts—are difficult to express using atomic, non-relational fault abstractions.
- **Limited temporal representation.** Most classical fault models are effectively stateless. They cannot capture conditionally activated or history-dependent failures that emerge only after specific access sequences, prolonged stress, cumulative transitions, or delayed observation windows.
- **Redundancy in test design.** The absence of a shared symbolic vocabulary across fault types often results in duplicated pattern development, manual adaptation of test scripts, and limited reuse of test components, increasing both development effort and validation cost.

To address these shortcomings, a unified operator-based symbolic fault modeling framework is introduced, in which memory behavior is described as a sequence of symbolic micro-operations acting upon an abstract memory state. Each testable event—such as read, write, refresh, or compare—is represented as a symbolic operator, while faults are defined as violations of expected postconditions following operator application.

This symbolic abstraction provides a compact yet expressive mechanism for representing:

- Fault activation paths as directed operator graphs
- Context-sensitive dependencies through explicit precondition annotations
- Cross-fault interactions via compositional operator sequences
- Technology-aware extensions through fault-class overlays (e.g., retention-augmented transition faults)

The framework was originally formalized within this research and later extended through the **Optimal_Test** system, enabling the construction of a reusable library of fault activation patterns that is independent of memory architecture, array size, or fabrication process.

By adopting an operator-centric representation, this approach establishes a coherent foundation for symbolic test synthesis (Chapter 10), test decomposition (Chapter 11), and adaptive fault coverage modeling (Chapter 12).

Equally important, it provides a forward-compatible modeling paradigm capable of addressing emerging memory technologies and next-generation diagnostic challenges. The symbolic semantics of the operator set are summarized in Table 8.1.

Table 8.1—Symbolic state transition table for operator-based fault modeling

Operator / State	S_0	S_1	S_2	S_3
$R_{(a)}$	S_1	S_2	S_2	S_0
$W_{(a)}$	Violation: C_{AB}	S_1	S_3	S_2
$V_{(a)}$	S_0	Violation: T↑	S_2	S_3
$C_{(a,b)}$	S_1	S_3	Violation: Retention	Pass

This table formalizes the operator-based fault model by specifying transitions between abstract memory states (S_0–S_3) under the application of symbolic micro-operations.

- **Operators**
  - $R_{(a)}$: read operation at address *a*
  - $W_{(a)}$: write operation at address *a*
  - $V_{(a)}$: verification or comparison against expected data
  - $C_{(a,b)}$: coupling interaction between cells at addresses *a* and *b*

- **Abstract States**

  Each state represents an abstract snapshot of the memory system, encoding both data configuration and relevant latent conditions. State transitions describe how the system evolves—or how faults manifest—when symbolic operators are applied.

- **Fault annotations**
  - *Violation:* C_{AB} — activation of a coupling fault during a coupling-sensitive write operation
  - *Violation: T*↑ — a transition fault preventing the expected upward state change
  - *Violation: Retention* — exposure of a retention-related fault during operator interaction
  - *Pass* — no fault detected; expected state preservation

This structured representation enables reusable and extensible modeling of complex fault behaviors, including compound, state-dependent, and context-sensitive fault paths. It provides a formal analytical backbone for symbolic test synthesis, fault pattern matching, and diagnostic reasoning within the **Optimal_Test** framework.

Elements of the symbolic modeling approach introduced here were first reported by the author in earlier work on automated memory test design tools (EWDTW, 2011).[5]

8.2 Core Operators and Semantics

Memory behavior is modeled as a finite-state system. Let M denote the memory array, and let a represent a specific address. The operator-based fault modeling framework relies on a finite set of symbolic micro-operators that abstract memory interactions in a form suitable for formal analysis and diagnostic reasoning.

These operators capture both nominal memory behavior and fault-induced deviations by expressing state transitions, validation predicates, and temporal constraints at an abstract level, independent of physical implementation details.

The core symbolic operator set and its formal semantics are summarized in Table 8.2.

Table 8.2—Core symbolic operators and their semantic interpretation

Symbol	Operator	Semantic Meaning
$W_{(a,d)}$	Write	Write data value d to address a
$R_{(a)}$	Read	Read from address a; return the stored value
$A_{(a,d)}$	Assert	Check whether $M[a] = d$; raise an error flag if violated
$V_{(a)}$	Verify	Verify content at address a against expected data (tolerance-permitting comparison, if applicable)
$X_{(a,d)}$	Expect	Declare expected value d at address a for symbolic matching
$F_{(op)}$	Fault Injection	Apply a modeled fault condition prior to executing operator op
$WAIT_{(n)}$	Delay	Insert a temporal delay of n cycles between operations

This operator set defines the core symbolic actions used to represent memory behavior within my operator-based modeling framework. Each operator fulfills a distinct semantic role:

- Functional operators (W, R, A) express canonical memory interactions—writing, reading, and assertion checking—at the level of abstract state transitions.
- Diagnostic operators (V, X) provide controlled flexibility for error-tolerant verification and symbolic expected-value alignment, enabling nuanced diagnostic interpretation and pattern matching.
- Meta-operators (F, WAIT) extend the expressive power of the model by enabling explicit fault injection and temporal control, allowing the representation of time-sensitive, stress-dependent, or environment-conditioned fault phenomena.

Together, these operators form a compact yet expressive symbolic vocabulary for encoding both nominal and faulty memory behaviors. Their compositional use enables the precise specification of fault activation sequences, validation predicates, and timing dependencies within a unified formalism. This structure underlies the construction of reusable test libraries

and systematic test synthesis in my PROVER environment and the Optimal_Test diagnostic engine.

8.3 Fault Definitions as State Violations

Within the operator-based framework developed in this research, each memory fault is formally defined as a violation of an expected state predicate occurring within a symbolic operator sequence. By analyzing system responses across structured sequences of micro-operations, faults are expressed as deviations from intended postconditions rather than as static structural defects.
Representative examples are given below.

Stuck-at-1 Fault

- **Sequence:**
  $W_{(a,0)} \rightarrow R_{(a)}$
- **Predicate:**
  $M[a] \neq 1$
- **Interpretation:**
  Writing logical 0 has no effect because the cell is permanently stuck at logical 1.

Transition Fault (0 → 1)

- **Sequence:**
  $W_{(a,0)} \rightarrow W_{(a,1)} \rightarrow R_{(a)}$
- **Predicate:**
  $M[a] \neq 1$
- **Interpretation:**
  The cell fails to transition from 0 to 1 despite an explicit write attempt.

Coupling Fault

Here, a2 denotes the aggressor address and a1 denotes the victim address.

- **Sequence:**
  $W_{(a1,0)} \rightarrow W_{(a2,1)} \rightarrow R_{(a1)}$
- **Predicate:**
  $M[a1] \neq 0$
- **Interpretation:**
  Writing to aggressor cell a2 corrupts the stored value in victim cell a1, revealing an inter-cell coupling dependency.

In my PROVER-based diagnostic engine, these fault definitions are encoded as symbolic predicates over operator streams. The engine continuously evaluates preconditions and postconditions associated with each operator, dynamically matching observed deviations against encoded fault signatures.

This mechanism substantially reduces extensive manual rule construction and enables automated generation, validation, and classification of test patterns while preserving diagnostic resolution across diverse memory architectures.

8.4 Operator Composition and Test Graphs

A central advantage of my operator-based modeling framework is its ability to synthesize diagnostic test programs through **symbolic graph traversal**. In this representation, memory behavior is mapped onto a directed graph that provides a rigorous foundation for analyzing test structure, fault activation, and coverage efficiency.

- **Nodes** represent abstract memory states.
- **Edges** correspond to symbolic micro-operators such as Write, Read, Assert, Verify, or Delay.
- **Paths** represent structured fault activation sequences capable of driving the system into observable error states.

This formalism allows the identification of minimal yet comprehensive operator sequences that activate distinct fault classes without unnecessary redundancy.

A key contribution of my research is the introduction of the **U–Y Scheme**, which partitions the traversal space into two orthogonal dimensions:

- **U-paths:** Transitions across memory addresses, capturing coupling effects, adjacency-related failures, and address-decoder faults.
- **Y-paths:** Transitions across data values and operator sequences, capturing transition faults, retention errors, and stuck-at conditions.
- By jointly traversing U- and Y-paths, my framework enables:
- **Test compression:** Elimination of redundant operator patterns without loss of fault observability.
- **Fault coverage analysis:** Exhaustive yet structured enumeration of activation paths.
- **Symbolic merging of fault classes:** Consolidation of operator sequences across multiple fault types while preserving diagnostic distinguishability.

This operator-graph formulation forms the theoretical backbone of both the PROVER symbolic test language and the Optimal_Test diagnostic engine, which are analyzed in detail in **Chapters 10 and 12**, respectively.

This graph-based abstraction provides a compact yet expressive representation of diagnostic test behavior, enabling systematic exploration of operator sequences and fault activation paths. It also facilitates automated synthesis and optimization of test programs within symbolic diagnostic frameworks.

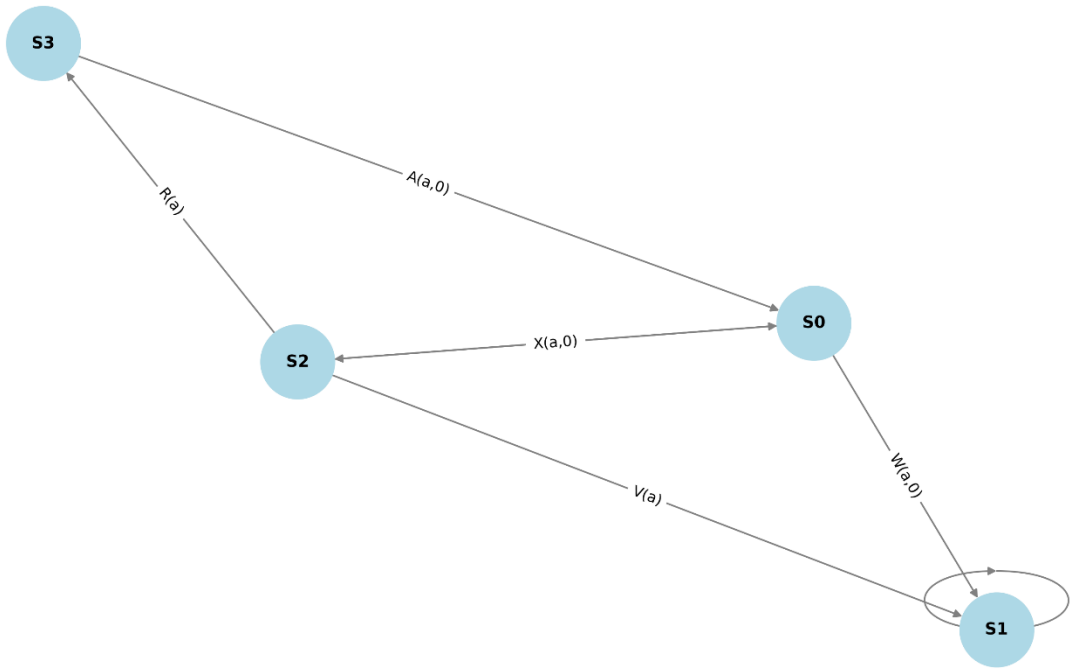

Figure 8.1—Operator-based fault activation graph illustrating symbolic state transitions and node-state encoding

Figure 8.1 illustrates symbolic traversal of abstract memory states using micro-operations within the operator-based diagnostic model. Each node S_0–S_3 represents an abstract logical memory state, while directed edges correspond to symbolic operators such as write, read, assert, verify, expect, or delay.

A key refinement introduced in this representation is the explicit inclusion of **temporal operators**. For example, the edge labeled $WAIT(n)$ is modeled as a self-loop on state S_1, indicating that the system remains in the same logical state while time elapses.

This construct is essential for activating time-dependent fault mechanisms such as retention loss, charge leakage, and relaxation-induced drift. Unlike state-changing operators (e.g., $W_{(a,1)}$ or $R_{(a)}$), the WAIT(n) operator preserves data content while modifying the temporal context under which subsequent operators are evaluated.

Additional symbolic edges represent assertion checking $A_{(a,0)}$, expectation matching $X_{(a,0)}$, and fault injection F_{op}, enabling compact and reusable specification of diagnostic sequences. The resulting graph formalism supports systematic test synthesis, coverage analysis, and symbolic merging of fault classes within the U–Y Scheme.

8.5 Practical Encoding and Engine Integration

In the **Optimal_Test** diagnostic system, the operator-based model is realized through structured symbolic scripts.

Each fault type is expressed as a predicate defined over a sequence of symbolic micro-operations, allowing fault activation and detection conditions to be encoded declaratively rather than procedurally.

The core components of the system include:

- Operator–predicate scripts describing fault activation and observability conditions
- Test-generation logic that maps symbolic operators onto valid activation paths
- Compilation mechanisms translating symbolic notation into:

    1. executable test pattern sequences
    2. detailed address, delay, and data-timing specifications
    3. annotated expected outcomes for assertion and comparison operators

Compiled test scripts are exported into multiple execution environments, including:

- RTL-level testbenches for hardware simulation and verification
- MBIST configuration generators for on-chip self-test integration
- software-based test executors for in-field diagnostics and embedded routines

This integration pipeline ensures that operator-based modeling is directly actionable, bridging abstract fault formalism with practical test deployment across design, manufacturing, and operational phases.

The symbolic encoding and engine-level integration concepts presented here were further consolidated and experimentally evaluated in IJMTER (2015).[8]

8.6 Strengths and Implications

The operator-based modeling framework provides several advantages over conventional pattern-centric diagnostic approaches:

- unified representation of diverse fault classes, including stateful, dynamic, and context-sensitive behaviors
- reusable test templates applicable across memory families (SRAM, DRAM, NVM, and 3D-stacked devices)
- formal reasoning support for coverage analysis, redundancy detection, and activation completeness
- full parameterization across voltage margins, timing windows, data backgrounds, and environmental conditions
- integration with fuzzy-logic mechanisms, enabling operator sequences to be weighted by diagnostic cost, likelihood, or impact
- These properties translate into concrete benefits for design, validation, and reliability engineering:
- newly observed fault mechanisms can be modeled without re-engineering complete test strategies
- optimized test sets can be synthesized automatically to satisfy coverage, time, or cost constraints
- diagnostic infrastructures can be extended systematically to emerging and heterogeneous memory technologies

In practical deployments, this framework has been used to synthesize effective test vectors for a wide range of memories, including SRAM, DRAM, NOR/NAND Flash, and ReRAM, and

has demonstrated coverage of composite fault mechanisms such as retention–coupling interactions in 3D-stacked DRAM.

8.7 Summary of the Core Model

The operator-based fault modeling paradigm transforms memory testing from an empirical pattern-generation task into a formal symbolic system of diagnostic logic. It provides:

- declarative fault specification using symbolic operators and predicates
- graph-based synthesis of compact and efficient activation sequences
- portable test representations decoupled from physical layout and process technology
- seamless integration with diagnostic analytics, repair workflows, and automation tools

As memory systems evolve toward higher density, increased heterogeneity, and stronger temporal effects, symbolic operator modeling offers a scalable and rigorous diagnostic foundation. Beyond test generation, it establishes a basis for formal verification, adaptive diagnostics, and data-driven fault analysis across future memory architectures.

8.8 Operator Macros and Structural Reuse

To improve modularity and reduce redundancy in symbolic test scripts, the operator-based framework introduces **macro-operators**—parameterized compositions of symbolic operations encapsulating recurring diagnostic procedures.
A representative macro definition is:

$$\text{WRITE\_AND\_VERIFY}_{(a,d)}:\ W_{(a,d)} \rightarrow R_{(a)} \rightarrow A_{(a,d)}$$

This macro performs a write operation to address a, immediately reads the stored value, and asserts preservation of the expected data. Such sequences are fundamental to memory diagnostics, and their encapsulation as macros enables consistent reuse across multiple fault scenarios.

In the **Optimal_Test** system, macro-operators are expanded at compile time into canonical operator sequences. This design enables:

- compact and readable script construction with reduced duplication
- parameter-driven synthesis adaptable to different fault activation conditions
- compression of test libraries by abstracting recurring logic into reusable symbolic blocks

Structural reuse through macros significantly improves scalability when targeting large or heterogeneous memory arrays. It also enables tight integration with optimization routines, which can substitute, reorder, or transform macros based on diagnostic objectives, fault likelihoods, or hardware constraints.

8.9 Fault Taxonomy and Operator Mapping Table

The table below establishes a direct correspondence between canonical memory fault classes and their symbolic representations in the operator-based modeling framework. Each fault is expressed as a structured sequence of symbolic micro-operations whose execution exposes a violation of an expected state predicate.

Canonical memory fault classes and their corresponding symbolic activation sequences are summarized in Table 8.3.

Table 8.3—Mapping of canonical memory fault classes to symbolic operator sequences

Fault Type	Operator Sequence	Fault Model Trigger
Stuck-at-0	$W_{(a,1)} \rightarrow R_{(a)} \rightarrow A_{(a,1)}$	Cell remains fixed at logical 0
Transition Fault (0 → 1)	$W_{(a,0)} \rightarrow W_{(a,1)} \rightarrow R_{(a)} \rightarrow A_{(a,1)}$	Cell fails to transition from 0 to 1
Retention Fault	$W_{(a,d)} \rightarrow WAIT_{(n)} \rightarrow R_{(a)} \rightarrow A_{(a,d)}$	Charge leakage or data loss over time
Coupling Fault	$W_{(a_1,0)} \rightarrow W_{(a_2,1)} \rightarrow R_{(a_1)} \rightarrow A_{(a_1,0)}$	Aggressor write corrupts victim cell
Address Decoder Fault	$W_{(a_1,d_1)} \rightarrow W_{(a_2,d_2)} \rightarrow R_{(a_1)} \rightarrow A_{(a_1,d_1)}$	Address aliasing or decoder shorting
Write Disturb	$W_{(a,d)}$ repeatedly; $R_{(b)} \rightarrow A_{(b,expected)}$	Repeated writes to aggressor cell a disturb neighboring cell b
Read Disturb	$R_{(a)} \times N \rightarrow R_{(b)} \rightarrow A_{(b,expected)}$	Repeated reads from a disturb adjacent cell b

This mapping illustrates how classical and emerging memory fault models can be expressed uniformly as symbolic operator sequences. For each entry:

- the operator sequence defines the **fault activation path** required to expose the defect;
- the fault trigger characterizes the **underlying physical mechanism**, ranging from static stuck-at conditions to dynamic interference and decoder aliasing;
- temporal operators such as $WAIT(n)$ and repeated execution constructs (e.g., R(a)×N) capture **stress- and time-dependent behaviors** that are not representable in static fault abstractions.

By encoding fault models as violations of symbolic operator predicates, the framework provides a unified formalism for specifying, activating, and diagnosing both classical and non-classical fault types. This representation is directly executable in the **PROVER** symbolic language and the **Optimal_Test** diagnostic engine, enabling automated test generation and systematic fault coverage analysis across heterogeneous memory technologies.

8.10 Timing and Delay Modeling in Operator Sequences

In addition to logical state transitions, many memory faults are strongly influenced by timing constraints, stress duration, and asynchronous interactions. To capture these effects, the operator-based framework incorporates time-aware extensions that enable explicit modeling of delays, operation stretching, and burst access patterns.

The symbolic vocabulary is extended with the following timing-aware operators:

- $WAIT_{(n)}$ — inserts a delay of n cycles before the next operation; used to expose retention faults, charge leakage, and decay under idle conditions.
- $STRETCH_{(op, \tau)}$ — executes operator op with extended duration τ, modeling wearout mechanisms, marginal timing conditions, and line-hold violations.
- $WR\_RD\_DELAY_{(a, d, n)}$ — performs a write–read sequence to address a with data d, followed by a delay of n cycles prior to verification; captures retention degradation, weak write stability, and temperature-sensitive behavior.
- $BURST\_ALT_{(a, D, N, \Delta)}$ — issues a burst of alternating write–read operations to address a, using data sequence D, executed for N operations with inter-operation spacing Δ; models burst-induced stress, disturb effects, and high-frequency access degradation.

    i. a denotes the target memory address;
    ii. D is a sequence of data values (e.g., [0,1,0,1]);
    iii. N specifies the number of alternating write–read operations;
    iv. Δ controls stress frequency through cycle spacing.

These constructs enable fine-grained modeling of timing-sensitive fault phenomena, including retention decay, recovery-window violations, aging and wear out under sustained stress, and asynchronous failures such as contention-induced false reads. By integrating temporal semantics directly into operator sequences, the symbolic model achieves increased realism while remaining analytically tractable.

8.11 Fuzzy Rule Integration for Fault Likelihood Scoring

Deterministic pass/fail criteria are insufficient for diagnosing many practical memory faults, particularly soft errors and intermittent behaviors that exhibit probabilistic characteristics. To address this limitation, fuzzy rule logic is integrated into the operator-based model to enable dynamic fault likelihood estimation and adaptive diagnostic decision-making.
A representative fuzzy linguistic rule has the form:

$$\text{IF (IdleTime is high)AND (SyndromeRecurrence at address a is high)}$$
$$\text{THEN (FaultLikelihood(a) is high).}$$

In practice, fuzzy inference may be complemented by lightweight procedural heuristics, for example:

$$\text{IF syndrome\_count(a)} > \text{T AND WAIT} > 20 \text{ THEN increase fault\_weight(a).}$$

Here, T denotes a configurable recurrence threshold derived from historical syndrome statistics.

This rule increases the diagnostic weight of memory location a when repeated error syndromes are observed after extended idle periods, indicating elevated likelihood of retention-related or soft-fault behavior.

Within the **Optimal_Test** engine, fuzzy logic is applied to:

- **heatmap weighting**, dynamically highlighting memory regions with elevated inferred fault probability;

- **test reordering**, prioritizing operator sequences targeting statistically active or suspicious regions;
- **priority-based repair guidance**, recommending repair actions for locations with persistently high fault weights, even in the absence of deterministic failure.

Through this integration, the diagnostic process adapts iteratively to observed fault patterns. Fuzzy reasoning complements symbolic operator modeling by embedding real-world variability and uncertainty into the analysis without sacrificing formal structure.

8.12 Summary of Extensions

The extensions introduced in this chapter substantially enhance the expressive power and engineering utility of the operator-based symbolic model. They elevate the framework from a formal abstraction to a comprehensive and deployable diagnostic methodology.

The principal extensions include:

- **macro-operators**, supporting modular test composition, structural reuse, and scalable test synthesis;
- **fault taxonomy mapping**, aligning symbolic operator sequences with established fault classes to support interpretation, standardization, and hybrid integration;
- **timing controls**, incorporating constructs such as $WAIT$, $STRETCH$, and RW_BURST to capture temporal dependencies, retention effects, and aging phenomena;
- **fuzzy scoring**, integrating probabilistic reasoning to enable adaptive diagnostics and priority-driven repair strategies.

Collectively, these extensions transform operator-based fault modeling into an engineering-ready platform for test synthesis, fault detection, and system-level reliability evaluation. They ensure that symbolic modeling accommodates both formal reasoning and automation while capturing the complexity, variability, and uncertainty inherent in modern memory technologies.

Chapter 9: Parallel Diagnostic Architecture Using a Multi-Head Symbolic Automaton

The continuous growth of memory capacity into multi-gigabyte and terabyte scales exposes fundamental limitations inherent in purely sequential diagnostic architectures. Diagnostic scenarios involving exhaustive address traversal, multi-cycle pattern iteration, or state-dependent fault activation increasingly impose execution times and resource demands incompatible with high-throughput production testing and latency-sensitive operational environments. Under these conditions, sequential execution ceases to be an implementation choice and instead becomes a structural bottleneck.

To overcome this scalability constraint, a parallel diagnostic architecture was developed, grounded in a multi-head symbolic automaton abstraction explicitly adapted for symbolic memory testing rather than for general-purpose computation.

In this model, the memory under diagnosis is represented as a multi-track symbolic substrate, while diagnostic execution is performed by a bounded set of diagnostic heads operating concurrently over formally defined address domains. The abstraction does not claim computational universality; it is introduced strictly as a finite-state structural and control framework for organizing concurrent symbolic diagnostic activity over bounded memory address domains in a deterministic and analyzable manner.

Each diagnostic head executes a deterministic sequence of symbolic micro-operations derived from the operator-based fault model introduced in Chapter 8. Address traversal, operator execution, and state observation are logically decoupled yet coordinated through a shared symbolic control layer.

Synchronization and information exchange among concurrently active heads are realized through explicitly defined symbolic state registers, ensuring deterministic interaction and eliminating race-dependent ambiguity in fault activation and observation.

Each diagnostic head operates in a semi-autonomous mode, enabling the following capabilities:

- Concurrent traversal of disjoint or partially overlapping address domains
- Simultaneous execution of formally specified diagnostic scripts
- Deterministic logging and localization of fault events
- Context-aware coordination through shared symbolic state variables

This architectural organization enables scalable, high-resolution diagnostics for multi-bank, multi-port, stacked, and high-bandwidth memory systems, in which conventional sequential Built-In Self-Test and scan-chain-based methodologies exhibit prohibitive execution times or insufficient fault observability.

This chapter formalizes the theoretical foundations, architectural structure, and implementation strategy of the Multi-Head parallel diagnostic system. Emphasis is placed on the symbolic programming interface, inter-head coordination mechanisms, and deployment constraints within heterogeneous memory subsystems, while preserving full compatibility with established operator semantics and March-based traversal logic.

9.1 Mathematical Model of Memory Devices and Diagnostic Tools

The synthesis of diagnostic test programs for contemporary memory devices must explicitly account for both the structural properties of the memory array and the architectural characteristics of the diagnostic apparatus.

The tester architecture—specifically its degree of parallelism, instruction sequencing model, and data-path organization—directly constrains the class of admissible diagnostic algorithms and determines achievable fault coverage, execution latency, and localization resolution.
To satisfy high-speed diagnostic requirements, I adopt a multiprocessor diagnostic architecture supporting parallel execution of the following functional streams:

- generation of memory operation opcodes
- generation of target cell addresses
- generation and evaluation of reference data symbols

This organization enables controlled concurrency at the level of symbolic operation sequencing, reducing diagnostic latency without altering the formal semantics of the underlying operator model. As a result, parallel execution is achieved without sacrificing determinism, analyzability, or compatibility with classical diagnostic reasoning frameworks.

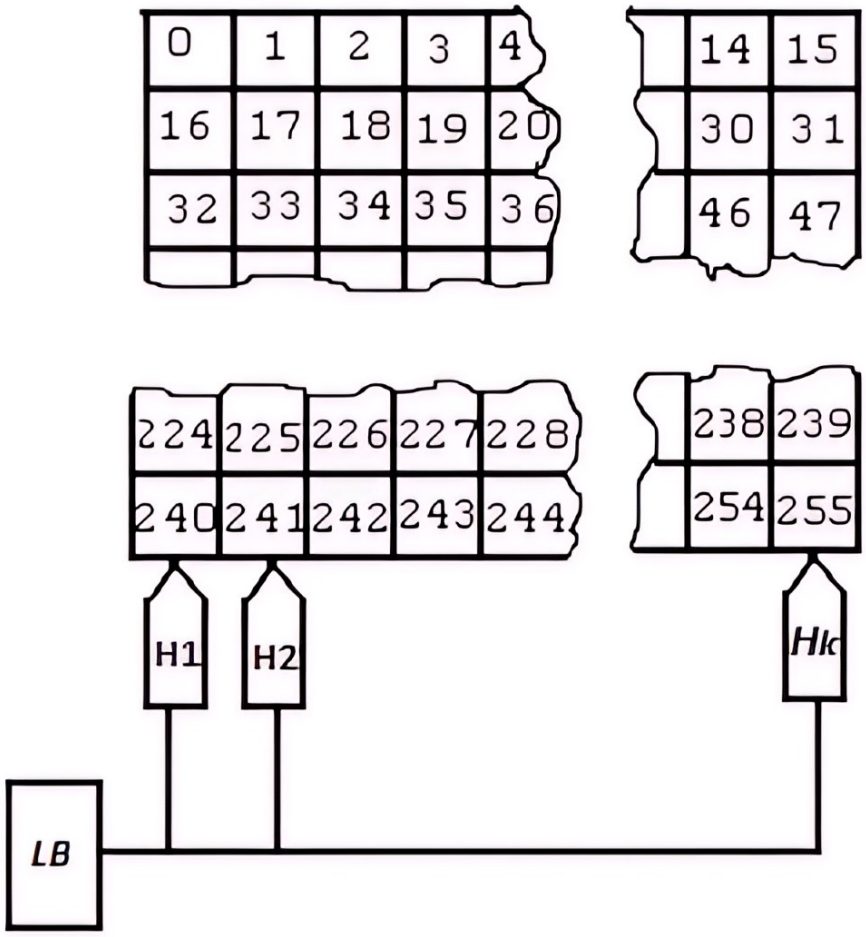

Figure 9.1—Structure of the Multi-Head Symbolic Automaton

LB – Logical Block; H_1 – H_k – Read/Write Heads

Figure 9.1 illustrates the structure of the Multi-Head Symbolic Automaton diagnostic model. The Logical Control Block (LB) coordinates symbolic execution, address sequencing, and synchronization of diagnostic activity.

The set of diagnostic heads $H_1,\ldots,H_k$ operate concurrently over the memory address space, each performing bounded symbolic micro-operations such as read, write, and state observation.

The model represents a finite-state execution framework operating over a bounded memory domain and does not imply computational universality. Its purpose is to provide a precise structural abstraction for parallel diagnostic execution rather than a general-purpose computation model.

When the memory space is depicted as a two-dimensional grid for visualization purposes, each cell with coordinates (x, y) corresponds to a linear memory address a according to the mapping $a = y \cdot W + x$, where W denotes the row width of the memory array.

This mapping ensures full compatibility between the spatial representation used in this chapter and the linear address semantics employed by the PROVER language in subsequent chapters.

The memory under diagnosis is modeled as a finite two-dimensional field partitioned into 16 × 16 addressable cells. A bounded set of H diagnostic heads $H_1, \ldots, H_k$ operate over this field under the coordination of the logical block LB, which evaluates diagnostic outcomes by comparing observed symbols with reference values derived from the test program.

Each diagnostic head may independently perform read or write operations over symbols drawn from a finite alphabet A and may update its position along the X and Y axes. Head motion is discrete and bounded.

Multiple heads may traverse disjoint address regions concurrently. Simultaneous access by multiple heads to the same cell is permitted only under explicitly defined synchronization constraints enforced by LB; unsynchronized concurrent writes are not allowed.

The movement of the j-th diagnostic head is defined by the set of address traversal micro-operations:

$$D_j = \{X_j := X_j \pm dx_j, Y_j := Y_j \pm dy_j\},$$

where $d_{xj}, d_{yj} \in \{0,1,\ldots,p\}$ denote discrete displacement values along the X and Y axes, respectively. The maximum displacement satisfies

$$d_{xj}^{max} = d_{yj}^{max} = p,$$

with $p = 15$ being sufficient for practical diagnostic programs over a 16 × 16 field.

The global state of the Multi-Head Symbolic Automaton is defined as the tuple consisting of:

- the symbols stored in all memory cells
- the current positions of all diagnostic heads
- the symbolic state variables maintained by the logical block

9.1.1 Elementary Micro-operations

Parallel diagnostic algorithms are constructed from the following **primitive micro-operations**, which form the atomic instruction set of the model:

- writing a symbol into the cell scanned by a diagnostic head
- reading a symbol from the scanned cell
- comparing a read symbol against its reference value
- updating the X and/or Y coordinates of a diagnostic head

The state transition of the system is deterministic. The next state is uniquely determined by the current global state and the instruction executed by the logical block.

A **program command** is defined in the general form:

$$\langle LBL_p, \mathrm{q}, \{C_j, X_j, Y_j, T_j\}_j^k = 1, LBL_r, n \rangle$$

where:

- LBL_p is the label of the current command
- q is a Boolean transition condition evaluated by the logical block
- $C_\mathrm{j} \in \{R_\mathrm{j}, A_\mathrm{j}, W_\mathrm{j}\}$ denotes the **micro-operation** of the j-th head
  - R_j : read the symbol from the scanned cell
  - A_j : compare the read symbol with its reference value
  - W_j : write a symbol into the scanned cell
- X_j and Y_j specify coordinate update operations for the j-th head
- T_j specifies the symbol generated for writing or comparison
- LBL_r is the label of the subsequent instruction
- n denotes the index of the head whose positional or symbolic state is evaluated for conditional branching

This formalism provides a deterministic, parallel-capable execution model that remains fully compatible with operator-based memory diagnostics and March-style traversal semantics.

9.1.2 Initial and Boundary Conditions

In the initial configuration of the Multi-Head Symbolic Automaton, all diagnostic heads are positioned over the cell with coordinates $X = 0, Y = 0$. From this common origin, the first, second, and third heads are displaced by one, two, and three address positions, respectively, along the predefined traversal direction.

This staggered initialization enforces deterministic spatial separation among heads prior to the commencement of parallel scanning.

The head positions corresponding to the initial traversal phase over ascending address codes are illustrated in **Figure 9.2(a)**.

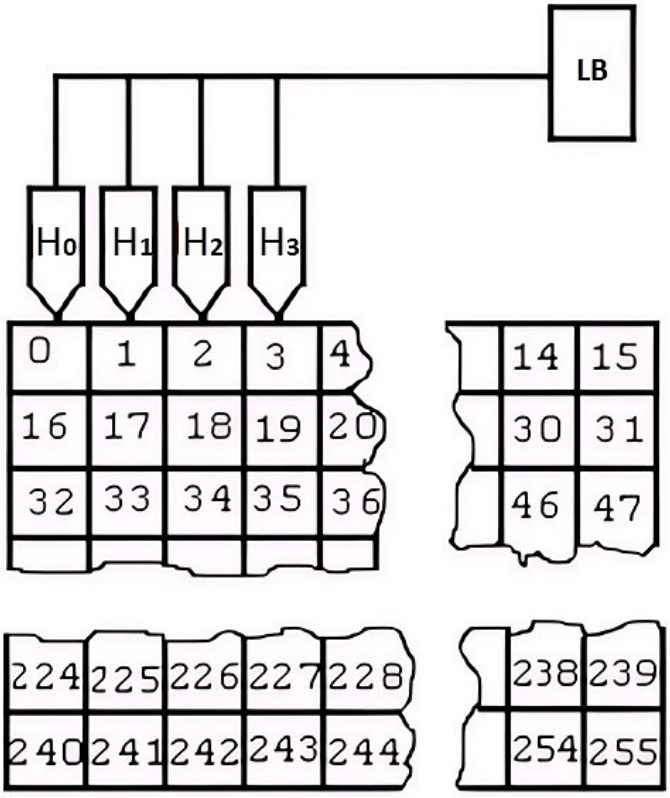

Figure 9.2(a)—Initial Ascending Address Traversal of Diagnostic Heads

The resulting evolution of the machine state under program execution—culminating in traversal termination at the boundary of the scanning field—is shown in **Figure 9.2 (b)**.

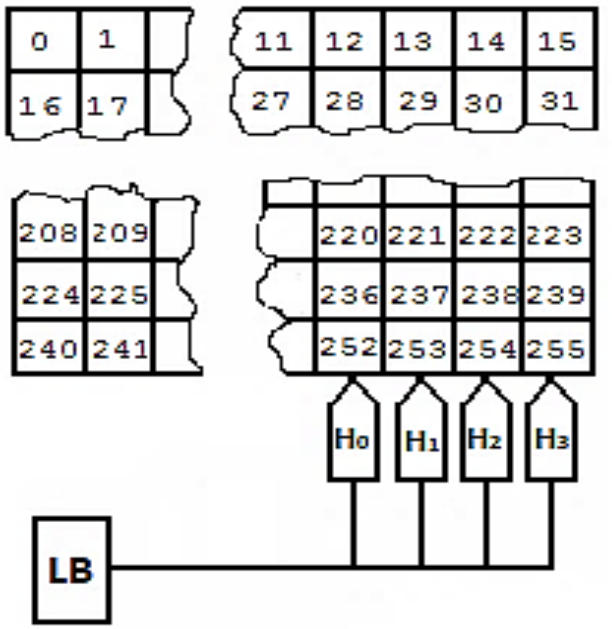

Figure 9.2(b)—Final State of the Multi-Head Symbolic Automaton under Ascending Address Traversal

Figure 9.2—States of the Multi-Head Symbolic Automaton during cell scanning with increasing address codes: (a) initial state; (b) final state.

To bound program complexity and ensure tractable verification and debugging, the scanning field is finite. The terminal accessible cell satisfies:

$$X = N_x = 15, Y = N_y = 15.$$

No head is permitted to traverse beyond these coordinates. All traversal logic, termination conditions, and direction reversals are expressed exclusively in terms of this bounded coordinate system.

The **global state** of the Multi-Head Symbolic Automaton is uniquely determined by the tuple consisting of:

- the symbols stored in all addressable cells of the scanning field
- the instantaneous positions of all diagnostic heads

No hidden or implicit state variables are assumed.

9.1.3 Transition Conditions and Flag System

Control flow within the Multi-Head Symbolic Automaton is governed by a set of flags generated by the diagnostic heads. The **flag vector** is defined as:

$$F = \{F_0, F_1, \dots, F_{k-1}\}$$

where each F_i corresponds to the i-th diagnostic head and is defined as:

$$F_i = \{(X_i \neq N_x) \vee (Y_i \neq N_y), X_i \neq N_x, Y_i \neq N_y, (X_i \neq G_x) \vee (Y_i \neq G_y), X_i \neq G_x, Y_i \neq G_y\}.$$

Here, (G_x, G_y) denotes the origin cell of the scanning field.

The semantics of the individual flag components are defined as follows:

- $(X_i \neq N_x) \vee (Y_i \neq N_y)$: asserted if the i-th head is not positioned over the terminal cell
- $X_i \neq N_x$: asserted if the i-th head is not located on the terminal X-coordinate
- $Y_i \neq N_y$: asserted if the i-th head is not located on the terminal Y-coordinate
- $(X_i \neq G_x) \vee (Y_i \neq G_y)$: asserted if the i-th head is not positioned over the origin cell
- $X_i \neq G_x$: asserted if the i-th head is not located on the origin X-coordinate
- $Y_i \neq G_y$: asserted if the i-th head is not located on the origin Y-coordinate

This flag system enables deterministic control of head motion and supports traversal patterns in multiple directions, including left-to-right, right-to-left, top-to-bottom, bottom-to-top, and diagonal scans. Direction changes and termination conditions are expressed solely through Boolean combinations of these flags, without introducing auxiliary control variables.

9.1.4 Multiprocessor Interpretation and Execution Rate

In the implementation considered here, the Multi-Head Symbolic Automaton employs **four read/write diagnostic heads**, corresponding to four parallel processing units within a diagnostic tester. These units generate address codes and data symbols concurrently under the supervision of a centralized microprogram control unit.

Address updates and data symbol generation are performed according to micro-operation codes issued by this control unit. The effective frequency of diagnostic stimulus generation, denoted F_d, satisfies:

$$F_d = F_{mpu} . k$$

where F_{mpu} is the clock frequency of the **microprogram control unit** and k is the number of diagnostic heads and associated address generators.

Formal analysis of micro-operation ordering, processor-aligned execution cycles, and symbolic task decomposition consistent with this model was later reported in JMEST (2016).[9-10]

9.2 Motivation for Parallel Test Execution

Sequential memory testing methodologies exhibit fundamental limitations as memory systems increase in capacity, structural complexity, and internal parallelism. These limitations manifest along three primary dimensions.

First, **scalability bottlenecks** arise because the execution time of diagnostic procedures grows linearly—and in several practical cases super-linearly—with memory size. For large arrays, full-coverage March tests, extended retention tests, and multi-pattern stress sequences impose execution times that are incompatible with production throughput requirements and in-field diagnostic constraints.

Second, **restricted fault observability** is inherent to strictly sequential execution. When faults manifest concurrently in spatially separated memory regions, a single-threaded test engine may fail to activate their interactions. Masking effects, delayed activation, and missed transient behaviors can occur, particularly for faults whose detection requires overlapping temporal or spatial access patterns.

Third, **architectural mismatch** becomes increasingly pronounced in modern memory technologies. High Bandwidth Memory (HBM), multi-channel DDR architectures, bank-interleaved designs, and three-dimensional stacked DRAM devices are intrinsically parallel in both physical organization and access protocol.

Diagnostic frameworks that enforce serialized access underutilize available structural concurrency and impose artificial constraints unrelated to the memory's native operation.

Empirical evaluations conducted within the **Optimal_Test framework** confirmed these limitations. Sequential execution of March-based diagnostic programs became progressively impractical for multi-die, interleaved, and banked memory systems.

Execution time increased disproportionately, while effective coverage degraded due to inter-access latency, arbitration delays, and contention effects inherent to serialized traversal.

To overcome these limitations, a multi-head symbolic diagnostic engine is introduced, in which each head functions as an independent diagnostic agent assigned to a defined segment of the address space.

These agents execute coordinated diagnostic sequences concurrently, exchange symbolic state information through shared control structures, and collectively contribute to fault activation, isolation, and logging.

This architectural transition aligns diagnostic execution with broader system-on-chip design trends, where performance and scalability are achieved primarily through parallelism rather than frequency scaling.

Consequently, diagnostic testing methodologies must evolve toward explicitly parallel execution models to remain effective in contemporary memory environments.

9.3 Multi-Head Automaton Inspiration: From Theory to Diagnostic Engine

The multi-head symbolic automaton extends classical finite-state automaton models by introducing multiple concurrent read/write heads operating over a shared, bounded memory address space.

While originally formulated as a theoretical construct, this abstraction provides a formally grounded framework for structuring parallel diagnostic execution in memory testing systems.

In the diagnostic interpretation adopted here, each head corresponds to an independent symbolic test agent traversing a shared memory field.

Symbolic state transitions encode conditional branching, synchronization, and sequencing logic analogous to those required in multiprocessor diagnostic workflows.

The abstraction is employed strictly as a control and organization model and does not imply computational universality.

The correspondence between the theoretical components of the multi-head symbolic automaton and their diagnostic counterparts is summarized in Table 9.1.

Table 9.1—Correspondence Between Multi-Head Automaton Components and Their Diagnostic Counterparts

Automaton Component Concept	Memory Diagnostic Equivalent
Bounded Memory Array	Memory address or storage bit
Head	Independent diagnostic agent
State register	Micro-operation program (PROVER sequence)
Symbolic Control Logicturing	Operator dispatch logic
Shared tape	Shared memory bus or interleaved banks

Within the implemented system model, each diagnostic head executes a deterministic sequence of symbolic micro-operations derived from the operator model.

Heads traverse assigned address regions while maintaining synchronization through a centralized control mechanism that resolves conflicts, enforces determinism, and optimizes global execution scheduling.

9.4 Porting Test Programs for Scalable Memory Diagnostics

Effective diagnostic testing of large-capacity memory chips and modules requires systematic adaptation of existing test programs to new device configurations.

Direct compilation of diagnostic code into a boot or execution module is insufficient; program parameters must be reconfigured to align with the capacity, geometry, and addressing structure of the target memory device.

For memory chips with capacity N bits arranged in a square matrix, the number of rows and columns satisfies:

$$r = c = \sqrt{N}$$

For N-cycle diagnostic tests, reconfiguration requires updating the control parameters defining the terminal row and column indices. In symbolic form, the boundary coordinates are expressed as:

$$N_x = N_y = \sqrt{N - 1}$$

In addition to boundary parameters, diagnostic program listings must be updated to reflect iteration counts associated with address traversal loops and pattern repetition.

These iteration variables scale with memory capacity and must be recalculated to preserve traversal completeness and operator sequencing correctness.

This substitution process can be automated using topological parameters derived from square memory matrix geometry. **Table 9.2** summarizes the relevant parameters for representative memory capacities.

Table 9.2—Parameters of Memory Chips for Square Cell Topology

Chip Capacity	Matrix Dimensions	N_X, N_Y	Address Code Bits
256 bits	16×16	15	8
1 kbit	32×32	31	10
4 kbit	64×64	63	12
16 kbit	128×128	127	14
64 kbit	256×256	255	16
256 kbit	512×512	511	18
1 Mbit	1024×1024	1023	20
4 Mbit	2048×2048	2047	22
16 Mbit	4096×4096	4095	24
64 Mbit	8192×8192	8191	26
256 Mbit	16384×16384	16383	28
1 Gbit	32768×32768	32767	30
4 Gbit	65536×65536	65535	32

This formalized porting methodology enables scalable reuse of diagnostic programs across memory generations while preserving determinism, traversal correctness, and compatibility with parallel execution semantics.

9.5 Non-Square Memory Topologies and Sub-Matrix Decomposition

In memory devices with non-square topologies, storage cells are commonly organized as a set of square sub-matrices arranged along one or more dimensions. This organization reflects physical layout constraints, bank partitioning, or die stacking strategies, and must be explicitly accounted for during diagnostic program synthesis.

An example of such an organization is shown in **Figure 9.3**, which illustrates a memory chip with a total capacity of **512 bits**, implemented as **two square sub-matrices of 256 bits each**. Let the i-th sub-matrix be defined by its initial coordinates (G_{xi}, G_{Yi}) and terminal coordinates (N_{xi}, N_{Yi}). The capacity E_i of each square sub-matrix is given by:

$$E_i = (N_{Yi} - G_{Yi} + 1)^2$$

This formulation assumes square geometry within each sub-matrix and remains independent of the global memory layout.

For the 512-bit memory configuration shown in **Figure 9.3**, the two sub-matrices satisfy:

$$E_0 = (N_{y0} - G_{y0} + 1)^2 = (15 - 0 + 1)^2 = 256;$$
$$E_1 = (N_{y1} - G_{y1} + 1)^2 = (31 - 16 + 1)^2 = 256.$$

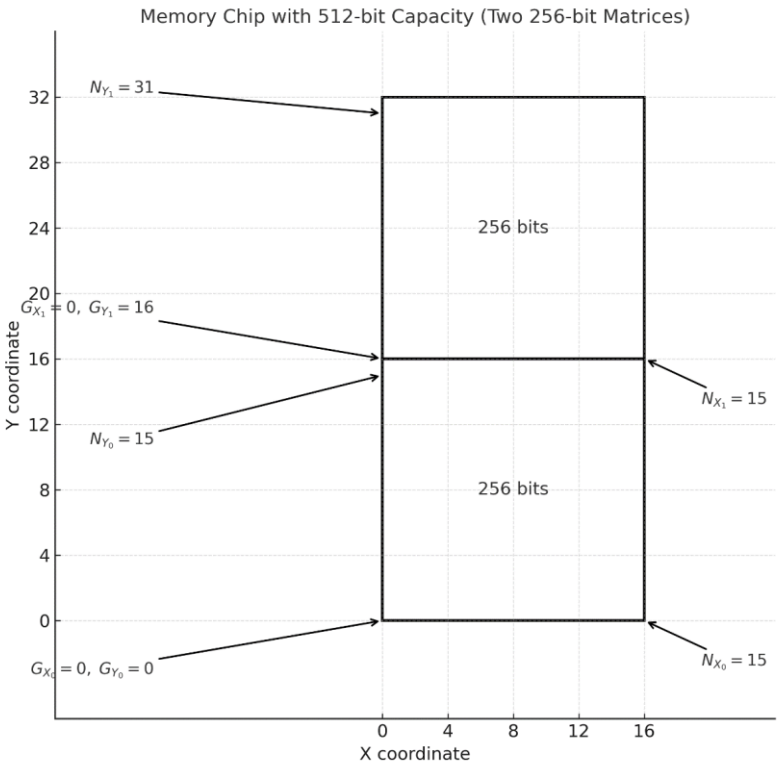

Figure 9.3—Decomposition of a non-square memory array into square sub-matrices for deterministic test porting

By explicitly specifying the initial coordinates (G_{xi}, G_{Yi}) and terminal coordinates (N_{xi}, N_{Yi}) for each sub-matrix, diagnostic programs can traverse and test individual memory regions in a controlled and deterministic manner.

Sequential or parallel execution across sub-matrices can then be scheduled without modifying the internal structure of the diagnostic operators.

For non-square memory topologies, address traversal within each sub-matrix is constrained by the boundary conditions:

$$G_{xi} \leq X_i \leq N_{xi},\ G_{Yi} \leq Y_i \leq N_{Yi}.$$

These inequalities define the admissible address space for diagnostic heads operating within the i-th sub-matrix and ensure that no head crosses sub-matrix boundaries unless explicitly instructed by the control logic.

This formulation provides the necessary boundary conditions for adapting diagnostic test programs to memory devices of arbitrary capacity and topology while preserving traversal correctness and operator semantics.

The primary operations involved in reconfiguring diagnostic programs for large-capacity and non-square memory devices are illustrated in **Figure 9.4**, which summarizes the relationship between sub-matrix decomposition, address counter bounds, and program parameter substitution.

9.6 Automated Reconfiguration for Non-Square Memory Topologies

For memory devices with non-square cell topologies, diagnostic program reconfiguration can be fully automated by parameter substitution driven by address boundary computation. **Figure 9.4** illustrates the reconfiguration workflow, in which a diagnostic program developed for a base-capacity memory device is transformed into a program applicable to a target device of larger specified capacity.

Let a non-square memory array be defined by matrix dimensions N_x+1 by N_Y+1, where $N_x \neq N_Y$. The diagnostic program reconfiguration process consists of the following formally defined operations:

- computation of terminal address coordinates N_x, N_Y from device topology
- substitution of address boundary parameters in traversal and loop-control constructs
- regeneration of address code widths consistent with the updated coordinate ranges

This process preserves the internal structure of diagnostic operators and traversal logic while adapting execution bounds to the target memory geometry.

The principal parameters for representative non-square memory topologies are summarized in **Table 9.3.**

Table 9.3—Parameters of Memory Chips for Non-Square Cell Topologies

Chip Capacity	Matrix Dimensions	N_X	N_Y	Address Code Bits
512 bits	16×32	15	31	9
2 kbit	32×64	31	63	11
8 kbit	64×128	63	127	13
32 kbit	128×512	127	255	15
128 kbit	256×512	255	511	17
512 kbit	512×1024	511	1023	19
2 Mbit	1024×2048	1023	2047	21
8 Mbit	2048×4096	2047	4095	23
32 Mbit	4096×8192	4095	8191	25
128 Mbit	8192×16384	8191	16383	27
512 Mbit	16384×32768	16383	32767	29
2 Gbit	32768×65536	32767	65535	31

For each topology, address traversal by a diagnostic head is constrained by:

$$0 \le X \le N_X, \quad 0 \le Y \le N_Y.$$

No modifications to operator semantics, symbolic micro-operations, or sequencing logic are required. Only boundary parameters and iteration limits are altered.

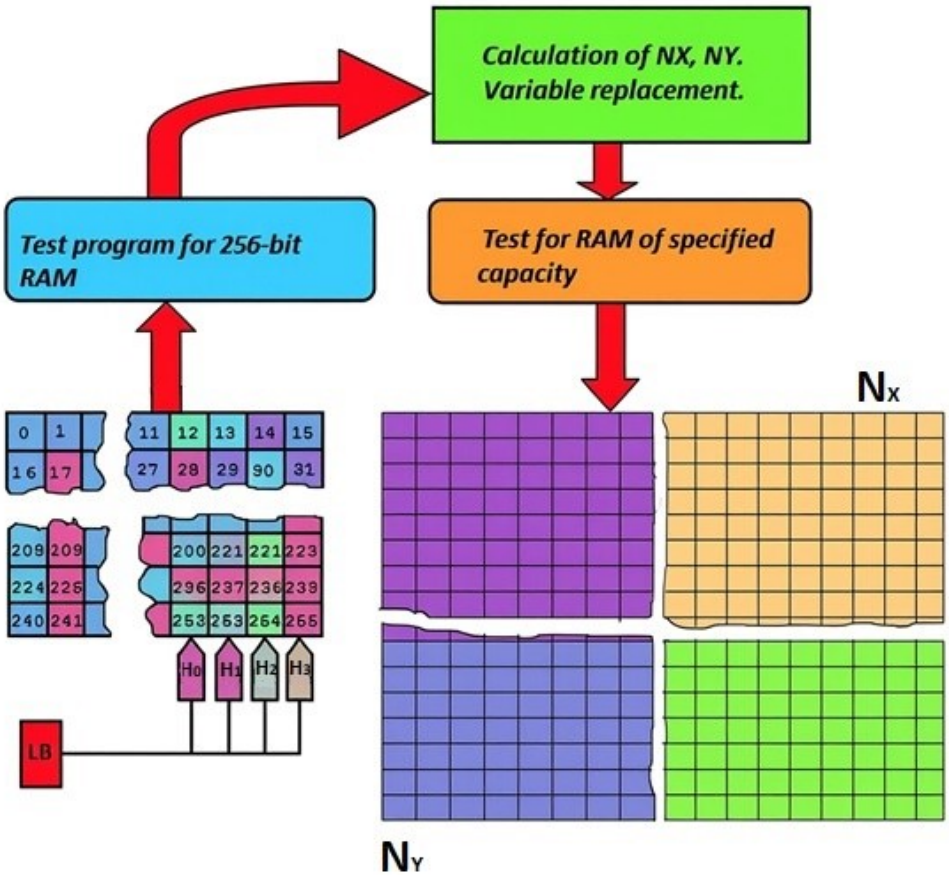

Figure 9.4—Test program porting process

As illustrated in **Figure 9.4**, this methodology enables developers to concentrate on creating a compact set of **portable base-capacity diagnostic programs**. From these base programs, complete diagnostic suites for memory chips and modules of arbitrary larger capacity can be generated automatically.

As a consequence, the labor required for diagnostic program development is substantially reduced. Developers are no longer required to repeat the full design, verification, and validation cycle for each new memory capacity. Instead, programs validated on small-capacity devices are systematically ported to large-capacity, serially manufactured semiconductor memory devices through deterministic parameter substitution.

Furthermore, fault localization and correction efforts are significantly reduced when performed at the base-capacity level. Debugging small-capacity diagnostic programs is inherently more tractable. Once validated, these programs retain their correctness properties when ported to large-scale devices, ensuring consistency and reliability across entire memory product families.

9.7 Test Selection Problems for Diagnosing Memory Devices

The substantial execution time associated with diagnostic testing of large-capacity RAM devices necessitates the selection of **effective and economically justified test sets**. The objective is to maximize coverage of the most probable fault classes while minimizing redundancy, execution time, and test set size.

The test selection problem is formally represented by the functional:

$$F = < T, P, N_{tests} >$$

where:

- T – denotes the total diagnostic execution time,
- P – denotes the probability of fault coverage,
- N_{tests} – denotes the number of tests included in the diagnostic set.

This functional provides a mathematical basis for formulating optimization problems in diagnostic planning and supports the construction of adaptive diagnostic strategies for both memory chips and memory modules.

Based on practical diagnostic constraints, **seven canonical test selection tasks** are defined, as summarized in **Table 9.4**.

Table 9.4—Canonical Test-Selection Tasks Defined Over ⟨T, P, M⟩

No.	T	P	N_{tests}	Functional Form
1	var	var	var	$P = f(T, N_{tests})$
2	var	const	var	$N_{tests} = f(T, P = const)$
3	var	const	var	$T = f(P = const, N_{tests})$
4	const	var	var	$P = f(T = const, N_{tests})$
5	const	var	var	$N_{tests} = f(T = const, P)$
6	var	var	const	$T = f(P, N_{tests} = const)$
7	var	var	const	$P = f(T, N_{tests} = const)$

Formal Description of the Tasks

1. $P = f(T, N_{tests})$: determines achievable fault coverage without constraints on execution time or test count. No closed-form solution exists due to combinatorial growth of admissible test sequences.
2. $N_{tests} = f(T, P = const)$: determines an optimized test set achieving a specified fault coverage probability without restrictions on total execution time.
3. $T = f(P = const, N_{tests})$: determines the minimum diagnostic time required to achieve a given fault coverage probability using an optimally selected test sequence.
4. $P = f(T = const, N_{tests})$: determines the maximum achievable fault coverage under a fixed diagnostic time budget.
5. $N_{min} = f(T = const, P)$: determines the minimal number of tests required to achieve a target fault coverage probability under a fixed execution time.
6. $T = f(P, N_{tests} = const)$: determines diagnostic time for a fixed-size test set achieving a specified fault coverage level; this formulation is frequently applied in memory module reliability assessment.
7. $P = f(T, N_{tests} = const)$: determines the maximum fault coverage achievable by repeated execution of a fixed test set; testing is terminated once no additional faults are detected.

Decision Scenarios and Evaluation Criteria

For each diagnostic test, two primary metrics are evaluated:

- **fault detection probability** q,
- **execution time** μ.

For a given fault type i, the **decision scenario** $S_i^{\vartheta\mu}$ comparing two test types θ and μ is defined as:

$$S_i^{\vartheta\mu} = -1, \quad \text{if } q_i^{\vartheta} < q_i^{\mu};$$
$$S_i^{\vartheta\mu} = 0, \quad \text{if } q_i^{\vartheta} = q_i^{\mu};$$
$$S_i^{\vartheta\mu} = 0, \quad \text{if } q_i^{\vartheta} = q_i^{\mu},$$

where q_i^{ϑ}, q_i^{μ} denote the fault detection probabilities for fault type θ and μ, respectively.
A subsequent evaluation stage accounts for execution time constraints. Tests whose execution time exceeds the allowable threshold t_{max} imposed by production or operational conditions are excluded: $t_j > t_{max} \Rightarrow$test j is excluded.

The remaining tests are normalized with respect to execution time, and an **average evaluation value** E_j^{cp} is computed for each selection criterion.

For criterion-based comparison, the following decision rule is applied:

$$C_j = -1, \text{if } E_{ij} < E_{cp}^j.$$
$$C_j = 0, \text{if } E_{ij} = E_{cp}^j;$$
$$C_j = 1, \text{if } E_{ij} > E_{cp}^j;$$

This multi-criteria evaluation framework provides a formal basis for ranking, filtering, and selecting diagnostic tests under conflicting objectives of coverage, execution time, and test set size.

9.8 Architecture of the Parallel Diagnostic System

The proposed parallel diagnostic architecture is designed to execute symbolic memory tests across large and structurally complex memory subsystems with high throughput and controlled fault coverage.

Although conceptually inspired by classical multi-head automaton models, the architecture is realized as a synchronized collection of symbolic diagnostic agents operating over a bounded memory domain, rather than as a general-purpose computational device.
These agents operate under a shared scheduling, control, and logging infrastructure, ensuring deterministic execution, consistent state observation, and reliable fault aggregation.

Core Architectural Components

- **N Test Heads** — Independent symbolic diagnostic agents executing **write (W)**, **read (R)**, and **assert (A)** micro-operations. Each head is assigned a defined address subset or traversal phase and operates under centralized coordination.
- **Shared Scheduler** — A coordination unit responsible for address dispatch, synchronization of test heads, arbitration of shared memory access, and phase sequencing. The scheduler enforces deterministic execution, particularly in interleaved, multi-bank, or multi-port memory architectures.
- **Instruction Memory** — A microcode repository associated with each test head, containing symbolic operator sequences expressed in **PROVER** or **Optimal_Test** formats. These sequences define traversal order, control flow, and diagnostic logic.
- **Response Logger** — A real-time monitoring subsystem that captures data mismatches, assertion failures, timing anomalies, and ECC-related events. All fault observations are timestamped and indexed for post-analysis.
- **Fault Aggregator** — A post-processing module that consolidates outputs from individual test heads into unified diagnostic maps. It correlates spatial fault distributions, resolves overlaps, and prioritizes regions for repair, redundancy activation, or re-testing.

Test Head Capabilities

Each diagnostic head supports programmable symbolic functionality, including:

- **Address generation** — Linear scans, strided traversals, and controlled non-linear access patterns for stress testing and aliasing fault detection.
- **Timing control** — Operator-level delay insertion, extended signal assertion, and skew modeling to emulate asynchronous or marginal access conditions.

- **Operand selection** — Execution with symbolic operands or concrete test data values, enabling both abstract pattern evaluation and hardware-specific stimulus generation.
- **Conditional branching** — In-test decision logic allowing adaptive rerouting, fault isolation, or escalation to alternative diagnostic paths when anomalies are detected.

This modular parallel architecture enables scalable, deterministic, and high-resolution memory diagnostics, addressing both the performance limitations of sequential test execution and the diagnostic precision requirements imposed by modern high-density memory systems.

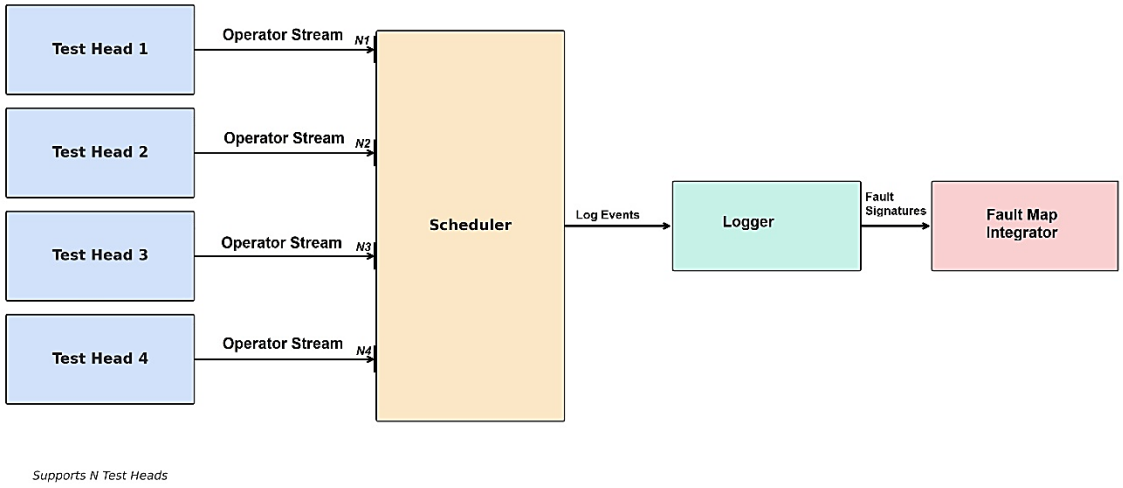

Figure 9.5—Parallel diagnostic test engine architecture

Figure 9.5 presents the block-level organization of the parallel diagnostic test engine composed of **N test heads**, a centralized scheduler, a logging subsystem, and a fault map integrator.

Each **test head** operates as an independent symbolic execution agent, generating operator streams that include address traversal, data manipulation, timing control, and conditional branching. These operator streams are delivered to the scheduler through dedicated input channels $IN_1 \ldots IN_N$, preserving head-local execution semantics while enabling centralized coordination.

The **scheduler** performs deterministic sequencing of incoming operator streams. Its responsibilities include enforcing temporal ordering, arbitrating concurrent access to shared memory resources, preventing hazardous inter-head interactions, and managing adaptive control flow.

Scheduler outputs are forwarded as structured log events without modifying the logical content of the executed operators.

The **logger** records execution outcomes and contextual metadata, including operator identity, address, data state, and execution phase. Logged events are forwarded to the **fault map integrator**, which aggregates observations across all test heads into unified symbolic fault representations suitable for post-processing, classification, and repair decision support.

By decomposing diagnostic execution into test heads, scheduler, logging, and integration stages, the architecture achieves modular scalability and preserves diagnostic determinism while supporting high-throughput parallel operation.

9.8.1 Synchronization and Parallelism Management

In a parallel diagnostic framework, coordinated access to shared memory resources is mandatory to prevent state corruption, fault masking, and non-deterministic behavior. Synchronization mechanisms therefore operate as first-class architectural components rather than auxiliary control features.

Conflict Resolution Mechanisms

Concurrency management is governed by a **Conflict Resolution Table (CRT)**, which defines admissible and prohibited inter-head interactions when memory access overlap occurs. The CRT classifies and resolves the following conflict categories:

- **Read-After-Write (RAW)** — permitted only when write completion is guaranteed prior to read activation; otherwise the read result is undefined and the transition is suppressed.
- **Write-After-Write (WAW)** — resolved deterministically through scheduler arbitration. In my implementation, the write with the most recent logical timestamp is committed, ensuring reproducible memory state evolution.
- **Simultaneous Read–Write (SRW)** — disallowed unless explicitly supported by the memory architecture. In simulation, such events are flagged as symbolic hazards and recorded as timing-induced anomalies.

The CRT therefore functions as an execution constraint system that preserves both architectural validity and diagnostic correctness under parallel operation.

State Coherency Policies

The relative progression of diagnostic heads is controlled through explicit coherency policies:

- **Lockstep Execution** — all heads advance synchronously. This mode ensures deterministic behavior and is suitable for symmetric access patterns and coupling fault analysis.
- **Staggered Execution** — heads advance with fixed offsets, enabling exploration of skew-dependent effects and partially overlapping activation conditions.
- **Event-Driven Activation** — execution transitions are triggered by symbolic events such as assertion failures, ECC syndromes, or threshold violations, enabling adaptive diagnostic routing.

Implementation Note

In my diagnostic engine, a **lockstep execution model with offset initialization** was adopted. This hybrid approach preserved global determinism while introducing controlled local skew at test initiation. It proved effective in modeling:

- access skew in interleaved and banked controllers,
- shared-bus contention effects,
- precharge and recovery latency variation in DRAM subarrays and 3D-stacked memories.

This strategy ensured reproducible simulation results while maintaining activation diversity for timing-sensitive fault models.

9.8.2 Addressing and Instruction Encoding

Each test head operates as a semi-autonomous execution agent equipped with a local **Address Generator (AG)** and **Instruction Pointer (IP)**.
These components support symbolic execution while remaining compatible with deterministic scheduling.

Address Generator (AG)

The AG computes successive target addresses and supports multiple traversal schemes:

- linear increment/decrement sweeps,
- checkerboard and alternating patterns,
- row-first and column-first traversal,
- symbolic March-based sequences.

Traversal logic is implemented as symbolic step functions, enabling uniform control structures across heterogeneous memory layouts.

Instruction Pointer (IP)

The IP indexes and interprets symbolic micro-operation streams. Its functions include operator decoding, conditional branching, loop control, and subroutine invocation. Execution redirection is triggered by diagnostic events without violating determinism.

Instruction Encoding and Compilation

Symbolic test programs are compiled into compact opcode streams through:

1. symbolic expansion into address–data–operation tuples,
2. opcode translation into FSM-executable instruction words,
3. stream alignment for parallel head distribution.

This compilation process enables lightweight execution engines to support expressive diagnostic behavior with minimal control overhead.

9.8.3 Fault Logging and Post-Processing

Parallel diagnostic execution requires structured fault observation and correlation to convert raw events into actionable diagnostic knowledge.

Per-Head Fault Logging

Each test head records:

- detected fault events with address and operator context,
- cycle-accurate or symbolic timing metadata,
- ECC syndrome vectors when available.

Local logs preserve asynchronous execution while embedding synchronization markers for later correlation.

Centralized Fault Correlation Unit (FCU)

Per-head logs are merged by a centralized FCU that performs:

- spatial fault map construction,
- temporal correlation across heads,
- cross-head consistency validation,
- fuzzy ambiguity resolution and confidence scoring.

This layered logging architecture enables traceable, explainable diagnostic outcomes and supports adaptive repair and re-test strategies.

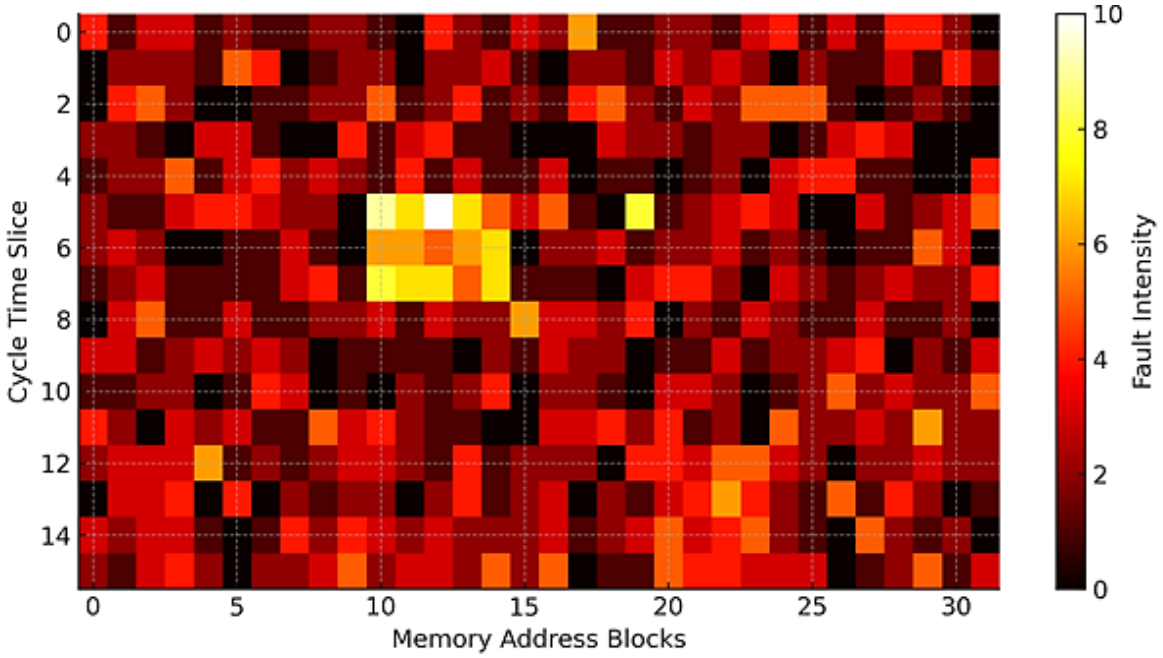

Figure 9.6—Temporal–spatial fault heatmap from synchronized diagnostic head logs

Figure 9.6 presents a temporal–spatial fault heatmap constructed from synchronized logs generated by multiple diagnostic heads during parallel test execution. The horizontal axis corresponds to memory address blocks, while the vertical axis represents discrete execution-time slices of the diagnostic sequence. Color intensity encodes the aggregated fault event density observed at each $(address, time)$ coordinate.

The heatmap is derived directly from timestamp-aligned fault logs without post hoc smoothing or interpolation. Each cell reflects the cumulative contribution of fault detections, assertion

violations, or ECC syndrome activations reported by the diagnostic heads during the corresponding execution window.

Localized clusters of elevated intensity indicate persistent or correlated fault activity. For example, the concentration observed in the mid-cycle interval (cycles 5–8) across address blocks 10–15 is consistent with inter-head disturbance effects under synchronized access. In contrast, the activity observed at later time slices and higher address regions suggests **progressive degradation phenomena**, such as retention decay or thermally accelerated failure modes.

This representation preserves both spatial locality and temporal ordering of fault manifestations and serves as a compact intermediate artifact for subsequent post-processing stages, including fault clustering, ambiguity resolution, and adaptive test refinement.

9.8.4 Application in Multi-Bank and Three-Dimensional Memory Systems

The multi-head symbolic diagnostic architecture developed in this chapter maps directly onto the structural and operational characteristics of modern heterogeneous memory systems. By supporting independent yet synchronized execution across multiple symbolic test streams, the framework scales naturally with both horizontal bank partitioning and vertical die integration.

Architectural Compatibility

The architecture is compatible with a range of contemporary memory organizations:

- **Banked DRAM Arrays** — Diagnostic heads may be statically or dynamically bound to individual banks, enabling parallel traversal of decoding paths while preserving bank-level isolation.
- **Three-Dimensional Stacked Memories (HBM, HMC)** — Heads can be mapped to individual dies or TSV-connected layers, allowing symbolic exploration of vertical access dependencies and localized thermal or electrical interactions.
- **Wide I/O Memory Devices** — In architectures with grouped data lanes or subchannels, heads may be partitioned per lane group to expose skew, interference, and timing-margin erosion.
- **Multi-Port RAM and Scratchpad Architectures** — Heads can be assigned per access port, supporting concurrent contention testing and port-isolated fault localization.

Representative Diagnostic Use Cases

Within simulation-based and emulated fault-injection studies, the architecture enables:

- detection of **cross-die coupling effects** under concurrent activation,
- exposure of **TSV-adjacent disturbances** through staggered access patterns,
- modeling of **command bus contention** via controlled phase offsets,
- isolation of **intermittent or localized bank failures** through focused re-execution.

These scenarios are difficult to reproduce using sequential diagnostic engines or fixed March sequences.

Experimental Context

In experiments involving interleaved and vertically integrated memory models, the proposed architecture supported:

- targeted symbolic fault injection,
- temporal stress modeling under skewed refresh or access timing,
- replay of execution traces with controlled offset and drift,
- analysis of rare or technology-specific fault manifestations.

The results confirm that parallel symbolic diagnostics provide higher observability and configurability than serial approaches when applied to complex memory topologies.

9.9 Optimal_Test Ranking

The target decision-making scenario is defined by an **aggregated evaluation value** computed for each diagnostic test. Let E_j^{agg} denote the aggregated score of test j, obtained by combining its normalized fault detection effectiveness and execution cost under the constraints introduced in the preceding section.

The problem of determining an optimal diagnostic path is therefore reduced to **ranking the available tests in ascending order of** E_j^{agg} . Tests with lower aggregated scores are executed earlier in the diagnostic sequence, ensuring that fault coverage is increased as rapidly as possible while respecting execution time and economic constraints.

This ranking-based formulation yields a deterministic diagnostic schedule. It avoids combinatorial explosion associated with exhaustive sequence enumeration and enables incremental refinement of the test order as additional empirical data or constraint updates become available. The resulting sequence is optimal with respect to the adopted aggregation criterion and remains compatible with both sequential and parallel execution frameworks.

9.10 Fault Coverage Process Model for Memory Chips

The fault coverage process in memory chips is formally represented using **probabilistic state-transition diagrams**, expressed as directed graphs. This representation models the cumulative evolution of diagnostic knowledge as successive tests are applied.
Let the directed graph

$$G = (V, E)$$

describe the diagnostic process, where each vertex corresponds to a distinct diagnostic state.
The vertex set V is defined as follows:

- the **initial vertex** represents complete uncertainty with respect to the fault status of the memory device,
- vertices $1,2,\dots,j,\dots,m$ represent states in which fault types $1,2,\dots,j,\dots,m$ have been successfully detected.

Directed edges in the graph represent **state-transition probabilities**, which quantify the likelihood that execution of a given diagnostic test transitions the process from one state to another. These probabilities are derived from empirically estimated fault detection characteristics associated with individual tests.

The process of detecting the first fault type is illustrated in **Figure 9.7**, which depicts the transition from the initial uncertainty state to the state corresponding to detection of a specific fault. This initial transition establishes the base case for modeling cumulative fault coverage, upon which subsequent transitions corresponding to additional fault detections are composed.

By iterating this probabilistic transition process over the ranked diagnostic sequence, the model captures the progressive reduction of diagnostic uncertainty and provides a formal basis for evaluating expected fault coverage as a function of test order, execution time, and selection strategy.

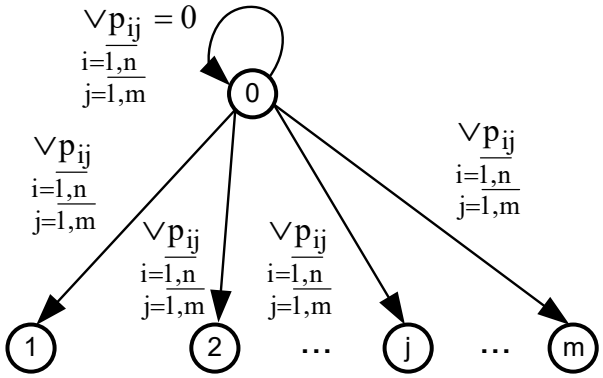

Figure 9.7—Detection of the first fault

After detection of the first fault

$$j \in \{1,2,\dots,m\}$$

using a selected diagnostic test (denoted α), the diagnostic process transitions from the initial uncertainty state to the fault-specific state corresponding to fault type j. This transition marks the first reduction of diagnostic uncertainty and establishes a conditioned diagnostic context for subsequent test execution.

At this stage, the diagnostic objective shifts from unconditional fault discovery to **conditional fault coverage evaluation**. All remaining fault types are assessed under the condition that fault j has already been detected. Formally, for all tests

$$i \neq \alpha,$$

the fault detection probabilities are updated to reflect the reduced uncertainty:

$$P\big(F_k \mid F_j\big), \qquad k \in \{1,2,\dots,m\}, \quad k \neq j.$$

Here:

- F_j denotes the **event of detecting fault type** j,
- F_k denotes the **event of detecting fault type** k,

and both events belong to the **fault event set**

$$F = \{F_1, F_2, \ldots, F_m\}.$$

These conditional probabilities account for fault interactions, masking effects, and dependency relationships that may alter detection likelihoods once a specific fault has been identified.

The resulting diagnostic process is no longer memoryless. Each subsequent transition depends on the accumulated diagnostic history encoded in the current state of the process. The expanded state-transition structure that arises after the first fault detection is illustrated in **Figure 9.8**, which depicts conditional transitions from the detected-fault state to the remaining fault-specific states.

This conditional expansion provides the formal foundation for modeling cumulative fault coverage over an ordered diagnostic sequence and enables precise evaluation of marginal diagnostic gain at each stage of the testing process.

9.11 Detection of Subsequent Faults and Conditional Coverage Refinement

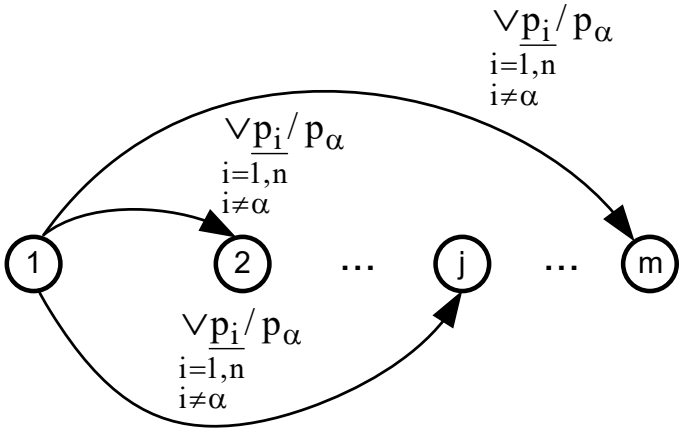

Figure 9.8—Detection of a second fault

Figure 9.8 illustrates the extension of the probabilistic state-transition model to represent the detection of a second fault following localization of an initial fault. Once the first fault has been identified, the diagnostic process proceeds under conditioned uncertainty, and subsequent state transitions are evaluated relative to the reduced fault and test spaces.

After the first fault detection, the diagnostic process evolves iteratively as follows.

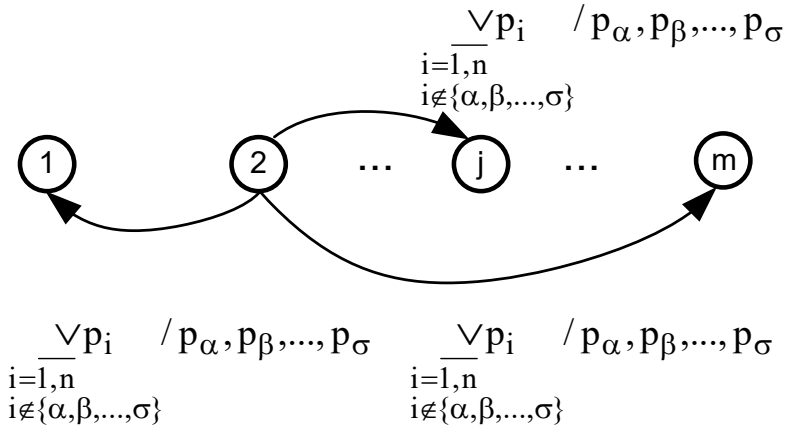

Figure 9.9—Detection of a Fault of Type j

In **Figure 9.9**, the model represents the detection of a fault of type j. At this stage, state-transition probabilities are conditioned on the elimination of tests already associated with previously detected faults (e.g., tests $\alpha, \beta, \ldots, \sigma$). The remaining test set is reduced accordingly, and the conditional fault coverage probabilities are **renormalized** over this residual set to ensure consistency of the probabilistic model.

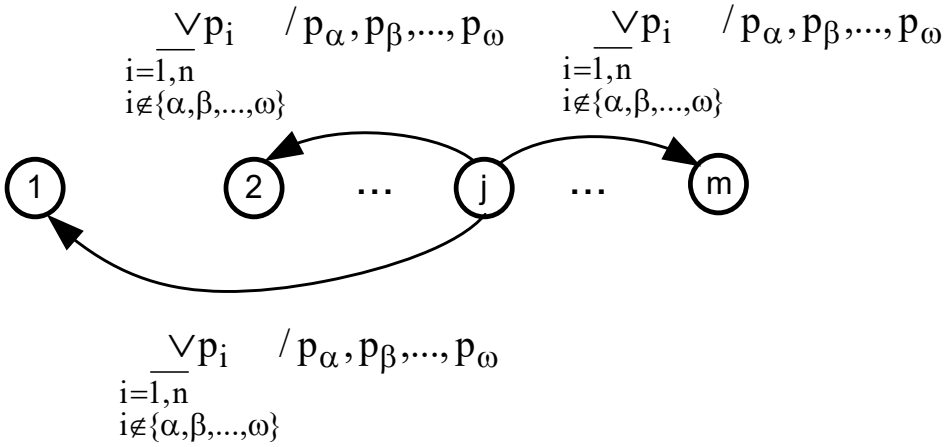

Figure 9.10—Detection of a Fault of Type m

In **Figure 9.10**, the process reaches the detection of a fault of type m, corresponding to the final stage of the diagnostic sequence. Here, transitions are conditioned on a further reduced test set (e.g., excluding tests $\alpha, \beta, \ldots, \omega$), representing the terminal phase of progressive fault coverage. At this stage, diagnostic uncertainty is minimized with respect to all detectable fault types.

This sequence of state-transition diagrams captures the **iterative refinement of diagnostic certainty**. Each newly detected fault reduces the admissible fault space and constrains the remaining diagnostic options. The cumulative diagnostic process is therefore represented as a directed graph in which:

- vertices correspond to diagnostic states defined by the set of already detected faults,

- edges encode **conditional fault coverage probabilities** associated with the execution of remaining admissible tests.

The resulting graph structure systematically narrows the uncertainty domain until all detectable faults have been classified or until further testing yields no additional diagnostic information.

Limitations of Explicit Probabilistic Modeling

Accurate computation of conditional fault coverage probabilities for all fault combinations requires extensive a priori data describing the diagnostic capabilities of each test across all fault interactions. In practical production environments, acquisition of such exhaustive probabilistic data is often infeasible due to cost and time constraints.

To address this limitation, **fuzzy selection algorithms** are employed for constructing optimized diagnostic test sets under incomplete or imprecise information. These algorithms enable decision-making in the presence of uncertainty by aggregating qualitative and quantitative criteria, thereby supporting near-optimal test selection without reliance on full probabilistic characterization.

Implementation of fuzzy-based diagnostic selection methods can be carried out in computational environments such as MATLAB. Methodological foundations and implementation details are available in established works by V. P. Dyakonov and S. D. Shtovba, which address fuzzy optimization and decision-making under uncertainty.

9.12 Micro-operation Synthesis for March Tests in a Parallel Execution Model

9.12.1 Methods for Synthesizing Micro-operations of Diagnostic Test Algorithms

To reduce the complexity of developing diagnostic programs, systematic methods are required for translating algorithmic test specifications into compact, executable micro-operation sequences. Such methods must preserve the formal structure of the original test algorithm while ensuring semantic compatibility with the execution constraints of diagnostic hardware.

Among the most widely used March tests in memory diagnostics are **March A**, **March B**, **March C**, **MATS+**, **MATS++**, and **March RAW**. These tests provide algorithmically concise yet fault-effective traversal patterns, making them suitable candidates for formal micro-operation synthesis.

The synthesis process described in this section focuses on decomposing March test algorithms into ordered micro-operations that can be directly interpreted by the PROVER execution engine.

9.12.1.1 Synthesizing Micro-operations for the MATS++ Test

The MATS++ test consists of three ordered operation cycles executed over the entire address space of the memory under test. Each cycle imposes a specific traversal direction and a prescribed sequence of read and write operations.

This representation enables the systematic translation of algorithmic test descriptions into executable micro-operation sequences while preserving their diagnostic semantics. By expressing traversal order and read/write operations through explicit graph transitions, the synthesis process ensures that each micro-operation sequence remains consistent with the structural constraints of the memory array.

The resulting formulation also simplifies integration with symbolic execution frameworks such as PROVER, where micro-operations can be generated, scheduled, and analyzed in a controlled diagnostic environment.

Consequently, complex March algorithms can be implemented in a compact and formally verifiable manner suitable for both simulation and hardware-based test execution.

The operation sequences of the three MATS++ cycles are represented using **address transition graphs**, as shown in **Figure 9.11**.

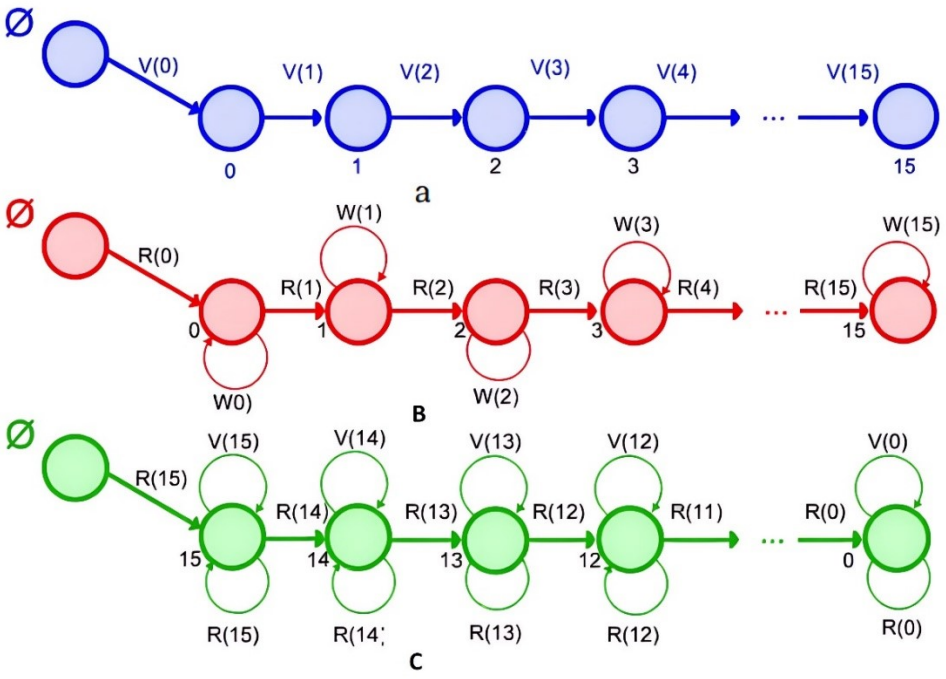

Figure 9.11—Address Transition Graphs of the MATS++ Test:

(a) First operation cycle
(b) Second operation cycle
(c) Third operation cycle

To formally describe these sequences, the following **operator notation** is adopted:

- $\mathbf{V_{(a)}}$: write logic value 0 into memory cell at address a
- $\mathbf{W_{(a)}}$: write logic value 1 into memory cell at address a
- $\mathbf{R_{(a)}}$: read the content of memory cell at address a

The symbol **P** denotes **sequential execution** of the specified operations. The lower index of an operator sequence defines the **start address**, and the upper index defines the **terminal address**

of the traversal. Address progression is implicit in the operator ordering and is consistent with the traversal direction indicated in the corresponding transition graph.

The address transition graphs in **Figure 9.11** explicitly encode:

- traversal direction,
- ordering of read and write micro-operations,
- boundary conditions at the first and last addresses,

thereby providing a direct structural mapping from the abstract MATS++ algorithm to executable diagnostic micro-operations.

Accordingly, the **MATS++ algorithm** can be expressed in **operator form** as:

$$MATS++ = P_{0\to N}(V(a))\ P_{0\to N}(R(a)W(a))\ P_{N\to 0}(R(a)V(a))$$

where a denotes the current memory address, N is the terminal address of the traversal range, and the operator symbols $V(\cdot), W(\cdot), R(\cdot)$ retain the semantics defined in the preceding subsection.

This operator representation explicitly captures the **three-cycle structure** of the MATS++ test:

1. **Initialization cycle**: sequential traversal from address 0 to N, writing logical 0 into all memory cells.
2. **Forward test cycle**: sequential traversal from address 0 to N, reading logical 0 from each cell and subsequently writing logical 1.
3. **Reverse test cycle**: traversal from address N down to 0, reading logical 1, writing logical 0, and performing a final read of logical 0 at each address.

This formulation preserves the algorithmic intent of MATS++ while providing a compact and unambiguous description suitable for direct synthesis into executable micro-operations.

When diagnostic test programs are developed for **parallel execution**, strict synchronization of read/write heads is required during each operator sequence. Coordinated head movement ensures that all heads adhere to the same traversal direction and operator ordering, thereby preventing address conflicts, race conditions, or unintended omission of diagnostic events. Synchronization constraints are enforced at the control level and do not alter the logical structure of the MATS++ operator sequence.

9.12.2 Parallel Initialization of Read/Write Heads for the MATS++ Test

The initial positions of the four read/write heads prior to execution of the three operation cycles of the MATS++ test are shown in **Figure 9.12**.

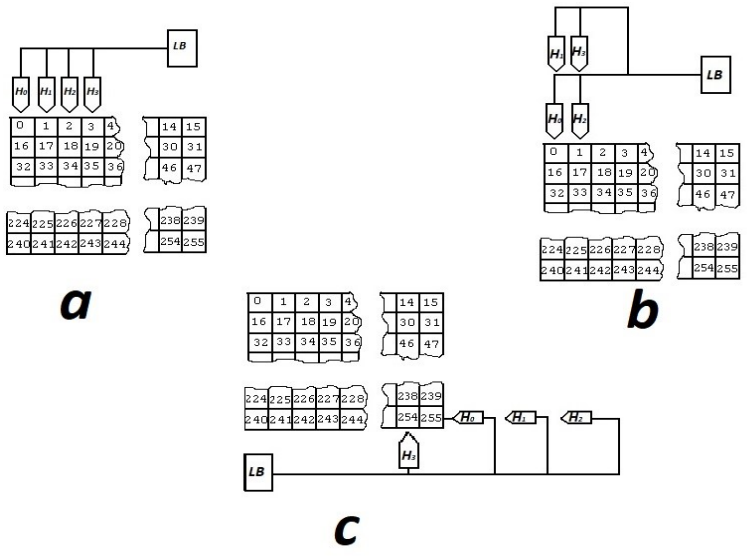

Figure 9.12—Initial Positions of Four Heads Before Starting MATS++ Test Fragments:

- (a) First operation cycle
- (b) Second operation cycle
- (c) Third operation cycle

Execution of the MATS++ algorithm in a parallel diagnostic environment requires explicit initialization of the read/write heads to guarantee synchronized traversal and conflict-free access across the memory array.

Figure 9.12 illustrates the head configurations adopted for each of the three operation cycles.

- **Cycle (a):** All four heads are aligned with the starting cells of the address space and initialized for forward traversal. This configuration supports the first cycle $P_{0\rightarrow N}(V_{(a)})$, during which logical 0 is written sequentially to all memory cells.
- **Cycle (b):** The heads are repositioned to enable coordinated execution of the forward traversal $P_{0\rightarrow N}(R_{(a)},W_{(a)})$. In this configuration, each addressed cell is read to verify the previously written value and subsequently updated with logical 1. Head alignment ensures that read and write operations occur in the prescribed order without inter-head interference.
- **Cycle (c):** The heads are arranged for reverse traversal of the address space, supporting the final cycle $P_{N\rightarrow 0}(R_{(a)},V_{(a)},R_{(a)})$. This configuration enables validation of stored logical 1 values, overwriting with logical 0, and immediate post-write verification, while maintaining synchronized backward progression across all active heads.

This staged initialization strategy ensures that the read/write heads execute the three MATS++ cycles in a synchronized, deterministic, and non-conflicting manner. Head coordination is enforced at the control level and does not modify the logical structure of the MATS++ operator sequence.

Multiple variants of the MATS++ test program may be realized depending on the degree of parallelization. This degree is determined by the parallelization coefficient k, which corresponds to the number of active read/write heads instantiated in the diagnostic model.

Increasing k allows proportional expansion of spatial concurrency while preserving the semantics of the underlying March algorithm.

Address traversal in decrement phases is bounded to the valid address domain; underflow conditions are excluded by construction of the address generator and are not interpreted as wrap-around transitions.

Table 9.5—First Variant of the MATS++ Test Program (No Parallelization).

The MATS++ sequence defined in Table 9.5 represents a symbolic formulation employing a Read-0 closing operation. In later experimental evaluations (Chapter 16), a variant of MATS++ with a Read-1 closing operation was used to enhance sensitivity to persistent pull-up and asymmetric fault behaviors. Throughout this monograph, the standard definition of MATS++ adopts a Read-1 closing step, as introduced in Chapter 4. The Read-0 variant documented in Table 9.5 is included intentionally as a modified baseline used under specific synchronization and implementation constraints in the non-parallelized diagnostic architecture.

Cycle Number	Sequence of Operations	MATS++ Test Program Fragment
1	$P_{0\rightarrow N}(V_{(a)})$,	NOOP x > Gx, y > Gy, t > 0 ME1 JXYN, ME1, 0 0 W, x+1 > x, y+1 > y*
2	$P_{0\rightarrow N}(R_{(a)},W_{(a)})$	NOOP x > Gx, y > Gy, t > 0 ME2 NOOP 0 R, A, ¬T → T JXYN, ME2, 0 0 W, x+1 > x, y+1 > y*, ¬t > t
3	$P_{N\rightarrow 0}(R_{(a)},V_{(a)},R_{(a)})$	NOOP x > Nx, y > Ny, t > 0 ME3 NOOP 0 R, A, ¬T → T NOOP 0 W JXYG, ME3, 0 0 R, A, x−1 > x, y−1 > y*, ¬t > t

In the first and second cycles of the MATS++ test, memory cells are scanned by incrementing the address code by one. In the third cycle, however, scanning is performed by decrementing the address code by one. The symbol "*" in the micro-operations for address code modification indicates that, prior to executing the marked operations, the concatenation of the Y and X coordinate vectors is performed. In the PROVER language, the operation of local assignment of values to variables is denoted by the symbol ">".

Fragments of the MATS++ test program for a parallelization factor of 2 are presented in Table 9.6. In this configuration, two read/write heads of the Multi-Head Symbolic Automaton simultaneously scan memory cells. This approach demonstrates how the test program can be parallelized to reduce execution time, while still preserving full address coverage under the stated synchronization constraints in all three cycles of the MATS++ algorithm.

The third cycle in **Table 9.5** is particularly noteworthy because the number of cyclically repeated operations equals three, which is not a multiple of the two scanning heads employed in this configuration. In such cases, the operators within the chain of consecutively arranged commands must be executed **cyclically** to ensure full memory coverage.

Cyclic Operator Iteration and Synchronization Conditions

The number of iterations required for cyclic execution of an operator chain is determined by

$$m\frac{3M}{(Hz)}$$

where:

- M denotes the capacity of the memory device under test (expressed in addressable cells),
- H is the **parallelization factor**, corresponding to the number of active scanning heads,
- z is the number of commands contained in the cyclic operator chain.

The total number of operators in the chain is given by

$$s = kz,$$

For correct execution, the value s must be an integer multiple of both:

1. the number of scanning heads k, and
2. the number of micro-operations in the algorithm fragment that is subject to cyclic repetition.

This constraint guarantees **deterministic synchronization** between the parallel scanning heads and the cyclic diagnostic operations, preventing misalignment, skipped addresses, or uneven workload distribution among heads.

Cyclic Control in the Third MATS++ Cycle

In the cyclic execution of operators corresponding to the **third cycle of the MATS++ test**, a mutable control variable y is introduced. The variable y is decremented by one each time the

JJNZ (Jump if Non-Zero) instruction is executed. Termination of the cyclic sequence occurs when $y = 0$.

By appropriately selecting the initial value of y, the effective number of executed iterations can be matched precisely to the capacity of the memory device under test. This mechanism allows the same parallelized test program to be **ported across memory devices of different sizes** without structural modification of the operator sequence.

As a result, cyclic operator control provides both **scalability** and **portability**, enabling parallel MATS++ test programs to adapt to a wide range of memory capacities while preserving synchronization and full fault coverage.

Table 9.6—Second Variant of the MATS++ Test Program (Parallelization Coefficient = 2).

Cycle Number	Sequence of Operations	MATS++ Test Program Fragment
1	$P_{0\to N}(V_{(a)})$,	NOOP 0 Gx > x, Gy > y, 0 > t 1 Gx > x, Gy > y, 0 > t NOOP 1 x+1 > x ME1 JXYN, ME1, 1 0 W, x+2 > x, y+1 > y* 1 W, x+2 > x, y+1 > y*
2	$P_{0\to N}(R_{(a)},W_{(a)})$	NOOP 0 Gx > x, Gy > y, 0 > t 1 Gx > x, Gy > y, 255 > t ME2 JXYN, ME2, 1 0 R, A, x+1 > x, y+1 > y* 1 R, A, x+1 > x, y+1 > y*
3	$P_{N\to 0}(R_{(a)},V_{(a)},R_{(a)})$	STYR, 127 0 Gx > x, Gy > y, 255 > t 1 Gx > x, Gy > y, 0 > t ME3 NOOP 0 R, A, ¬t > t 1 W, x+1 > x, y+1 > y*, ¬t > t NOOP 0 R, A, x+1 > x, y+1 > y* 1 R, A, ¬t > t JJNZ, ME3 0 W, x+1 > x, y+1 > y*, ¬t > t 1 R, A, x+1 > x, y+1 > y*

In the given test fragment, the initial value of the variable y is set to **127** using the command

$$STYR, 127.$$

This value defines the number of iterations of the cyclic operator sequence in the third cycle and is selected to match the effective address range of the memory device under test under the specified parallelization conditions.

The third variant of the MATS++ test program, employing a parallelization factor of four, is presented in Table 9.7.

Table 9.7—Third Variant of the MATS++ Test Program

Cycle Number	Sequence of Operations	MATS++ Test Program Fragment
1	$P_{0\rightarrow N}(V_{(a)})$	NOOP 0 x > Gx, y > Gy, t > 0 1 x > Gx, y > Gy, t > 0 2 x > Gx, y > Gy, t > 0 3 x > Gx, y > Gy, t > 0 NOOP 1 x+1 > x 2 x+2 > x 3 x+3 > x ME1 JXYN, ME1, 3 0 W, x+4 > x, y+1 > y* 1 W, x+4 > x, y+1 > y* 2 W, x+4 > x, y+1 > y* 3 W, x+4 > x, y+1 > y*
2	$P_{0\rightarrow N}(R_{(a)},W_{(a)})$	NOOP 0 x > Gx, y > Gy, t > 0 1 x > Gx, y > Gy, t > 255 2 x > Gx, y > Gy, t > 0 3 x > Gx, y > Gy, t > 255 NOOP 2 x+1 > x 3 x+1 > x ME2 JXYN, ME2, 3 0 R, A, x+2 > x, y+1 > y* 1 W, x+2 > x, y+1 > y* 2 R, A, x+2 > x, y+1 > y* 3 W, x+2 > x, y+1 > y*
3	$P_{N\rightarrow 0}(R_{(a)},V_{(a)},R_{(a)})$	NOOP 0 x > Nx, y > Ny, t > 255 1 x > Nx, y > Ny, t > 0 2 x > Nx, y > Ny, t > 0 3 x > Nx, y > Ny, t > 255 STJR, 63 3 x−1 > x

		ME3 NOOP 0 R, A, x−1 > x, y−1 > y*, ¬t > t 1 W, x−1 > x, y−1 > y* 2 R, A, x−2 > x, y−1 > y*, ¬t > t 3 R, A, x−1 > x, y−1 > y*, ¬t > t NOOP 0 W, x−1 > x, y−1 > y* 1 R, A, x−2 > x, y−1 > y*, ¬t > t 2 R, A, x−1 > x, y−1 > y*, ¬t > t 3 W, x−1 > x, y−1 > y* JJNZ, ME3 0 R, A, x−2 > x, y−1 > y*, ¬t > t 1 R, A, x−1 > x, y−1 > y*, ¬t > t 2 W, x−1 > x, y−1 > y* 3 R, A, x−2 > x, y−1 > y*, ¬t > t JKNZ, EEE ENDP EEE ENDE

9.12.3 Visualization of Test Execution

A visualization of the **third MATS++ cycle** during simulation using the **PROVER interpreter system** is shown in **Figure 9.13**. This visualization corresponds to the execution of the operator sequence $P_{N\rightarrow 0}(R_{(a)}\ V_{(a)}\ R_{(a)})$ under reverse address traversal.

During this cycle, memory cells previously containing logic value 1 are overwritten with logic value 0 while address codes are **decremented step by step**. The visualization reflects the synchronized execution of read–write–read micro-operations and confirms correct reverse traversal and data update semantics.

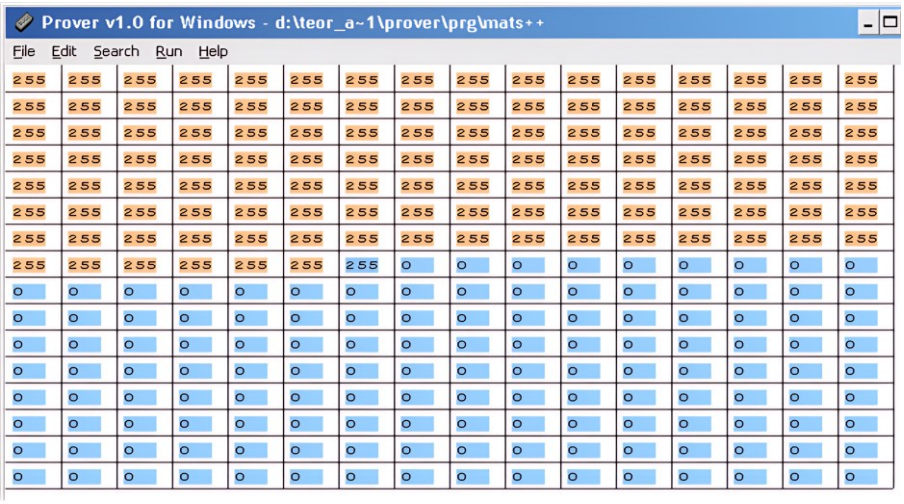

Figure 9.13—Visualization of Simulation Results During the Third MATS++ Cycle

Analysis of the program fragments presented in Tables 9.5–9.7 demonstrates that architectural modifications in the diagnostic tester—specifically the introduction of parallel execution units—require corresponding reconfiguration of diagnostic test programs.

The programming techniques introduced in this section provide a structured and scalable mechanism for such reconfiguration, enabling consistent adaptation when transitioning from low-capacity memory devices to high-capacity memory chips and modules.

9.13 Scalability and Parallelism Efficiency

The diagnostic framework introduced in this chapter is **inherently parallel** and supports scalable deployment of multiple symbolic test heads. Throughput increases with the number of active heads, subject to architectural constraints such as shared bandwidth, arbitration latency, and operator complexity.

Crucially, scalability is achieved without sacrificing determinism: synchronization policies, conflict-resolution mechanisms, and centralized scheduling ensure that increased parallelism does not introduce nondeterministic execution artifacts or diagnostic ambiguity.

9.13.1 Scalability and Parallel Test Efficiency Model

The effective throughput of a parallel symbolic diagnostic system can be modeled as:

$$T_{eff}\frac{H.P}{L+O}$$

Where:

- H — denotes the number of diagnostic test heads operating concurrently,
- P — represents the average symbolic pattern complexity per address, expressed as operator depth,
- L — is the latency introduced by synchronization, arbitration, and scheduling across heads,
- O — is the per-head operator processing overhead, including symbolic decoding and memory interface delays.

This model captures the fundamental trade-off inherent in parallel symbolic diagnostics. Increasing the number of test heads H and the richness of symbolic operator sequences P improves concurrency and diagnostic expressiveness. However, achievable throughput is bounded by coordination latency L and per-head processing overhead O, which grow with architectural complexity and resource contention.

Scaling Behavior and Empirical Observations

In experimental simulations involving interleaved and banked memory configurations, the following behaviors were observed:

- Near-linear throughput scaling was maintained up to sixteen parallel test heads under conditions of sufficient bandwidth and low-latency scheduling.
- Beyond thirty-two heads, diminishing returns emerged due to bus contention, access serialization, and increased arbitration delay.
- Dynamic scheduling strategies, including round-robin arbitration, priority escalation, and asynchronous microphasing, significantly reduced the effective synchronization latency L, preserving throughput under high utilization.
- Operator processing overhead O was minimized through compact opcode encoding and symbolic precompilation, enabling efficient execution on lightweight finite-state machines within each test head.

These results confirm that symbolic multi-head testing scales effectively when coordination overhead is explicitly controlled and operator execution is optimized.

9.14 Summary

The Multi-Head parallel diagnostic architecture presented in this chapter advances scalable memory test design. By integrating symbolic operator modeling with coordinated multi-head execution, the architecture provides:

- **Scalable Parallel Diagnostics** — Concurrent execution across multiple test heads enables high-throughput traversal of large address spaces while preserving deterministic activation control.
- **Comprehensive Fault Coverage** — Complex and context-dependent faults, often inaccessible to fixed March algorithms, can be activated and observed through symbolic operator chains.
- **Architectural Alignment** — The framework maps naturally onto stacked DRAM, three-dimensional NAND, HBM/HMC, and banked or interleaved memory structures.
- **Flexible Synchronization Policies** — Lockstep, staggered, and event-driven modes enable trade-offs between determinism and activation diversity under contention, degradation, or ECC events.

This architecture bridges diagnostic theory with high-performance test engines, transforming memory testing from static sequences into parallel, timing-aware processes enabling distributed stress and adaptive response across the execution pipeline.

Chapter 10: Symbolic Test Language PROVER — Architecture and Micro-operation Synthesis

10.1 Historical Background and System Evolution of PROVER

PROVER is a domain-specific symbolic language and interpretive environment developed for the synthesis, simulation, and debugging of diagnostic test programs for semiconductor memory devices. It is based on a hybrid architectural philosophy that combines formal symbolic modeling with executable, micro-operation-level diagnostics. The system was conceived as a diagnostic abstraction rather than as a general computational model, with its semantics explicitly constrained to memory testing, fault activation, and diagnostic control.

The system originated in the period 1992–1995 at the Department of Computer Engineering, Cherkasy State Technological University (ChSTU), Ukraine. Under the scientific leadership of Professor V. G. Ryabtsev, whose work in technical diagnostics focused on fault modeling and test synthesis for digital systems, the project was initiated to address the growing mismatch between emerging semiconductor memory fault mechanisms and the expressive limits of pattern-centric test development methodologies.

The original development team consisted of academic staff and graduate researchers affiliated with ChSTU, including G. T. Oleynik, R. Lizogub, A. Metel, and M. Poretsky. The work was organized as a research-driven effort rather than a commercial toolchain, with emphasis placed on formal semantics, operator-level modeling, and architectural independence.

The central design objective was the construction of a problem-oriented symbolic test language capable of representing diagnostic logic independently of memory organization, fault mechanism, or execution substrate. PROVER was defined as a semantic kernel for programmable diagnostics, in which symbolic test descriptions could be interpreted, transformed, and bound to concrete execution models without altering the underlying diagnostic intent. Symbolic programs were treated as structured operator sequences with explicitly defined effects on memory state, address traversal, and observation outcomes.

10.1.1 Authorial Contributions and System Modernization

Between 2005 and 2009, the PROVER system was systematically extended under the supervision of Prof. V. G. Ryabtsev. These extensions transformed PROVER from a predominantly symbolic modeling environment into a hybrid diagnostic framework capable of supporting formal reasoning, micro-operation synthesis, and executable validation within a unified methodological flow.

My contributions included the extension of the symbolic operator set to support coupling interactions, timing-dependent fault activation, and address-sensitive failure behaviors, while preserving compatibility with the operator model defined earlier in this work. Mechanisms for structured micro-operation compilation are introduced, enabling symbolic test descriptions to be deterministically lowered into ordered sequences of elementary memory actions.

A translation layer to hardware description languages was developed, allowing symbolic programs to be converted into VHDL stimuli and testbench structures suitable for cycle-accurate simulation. This translation was implemented through a dedicated compiler module, TranslatorToVHDL, which maps symbolic operators, address iterators, and timing constructs to synthesizable and simulator-compatible representations. Integration with industrial simulation environments enabled validation of symbolic tests against hardware-level memory models.

Additional extensions addressed programmatic control, including symbolic macros, conditional branching, and dynamic control constructs. These features enabled the construction of adaptive diagnostic flows while maintaining explicit control over execution order, address traversal, and timing semantics. The resulting system established a continuous path from symbolic diagnostic specification to executable simulation artifacts.

This body of work formed the technical foundation of a doctoral dissertation defended in 2009 at the National Technical University Kharkiv Polytechnic Institute.

10.1.2 Present Status of PROVER

In its current form, PROVER constitutes a mature hybrid diagnostic platform. The system remains grounded in the symbolic modeling principles established during its initial development, while incorporating the architectural extensions, execution semantics, and validation mechanisms introduced during its later evolution. PROVER integrates symbolic test programming, macro expansion, address-driven control logic, and multi-platform simulation within a single coherent toolchain.

Its relevance derives from its ability to preserve formal diagnostic intent at the symbolic level while enabling deterministic execution through micro-operation synthesis and hardware-assisted simulation. This combination distinguishes PROVER from conventional memory test environments, which typically separate high-level test description from low-level execution semantics.

10.2 Motivation for a Symbolic Memory Test Language

Contemporary memory test environments are characterized by architectural heterogeneity, increasing throughput requirements, and fault models that exhibit conditional, temporal, and multi-dimensional behavior. Conventional MBIST engines and pattern-based automation frameworks provide limited support for symbolic fault representation, graph-driven test synthesis, or timing-aware traversal logic, particularly in the context of advanced March-type algorithms.

PROVER was designed to address these limitations by introducing a symbolic programming paradigm tailored to diagnostic engineering. The language was structured to support formal expression of diagnostic logic while remaining compatible with executable test infrastructures. The design requirements can be summarized as follows.

High-level symbolic syntax enables explicit representation of diagnostic operators and fault-oriented test sequences using abstract operator expressions. Executable test flow generation

specifies a deterministic transformation of symbolic programs into finite-state-machine-compatible micro-operation streams, hardware description language stimuli, or simulator-specific inputs. Parameterization mechanisms allow diagnostic logic to be abstracted over address space size, memory organization, and coverage resolution, facilitating reuse across memory families.

Macro support and structured control constructs permit modular composition of complex test sequences while preserving precise execution ordering and timing semantics.
In both industrial and academic practice, a structural gap persists between symbolic fault modeling and executable test realization. PROVER occupies this gap by functioning as a symbolic compiler front end, decoupling diagnostic intent from implementation details while maintaining a formally defined mapping to executable semantics.

The transition from classical algorithmic descriptions to symbolic test representations adopted here builds upon earlier algorithmic frameworks documented in the authors' Russian-language monograph (2008).[11]

10.3 Semantic Aspects of the PROVER Programming Language

As the architecture and internal organization of RAM devices continue to evolve, the development of expressive algorithmic languages for diagnostic test program construction becomes a structural requirement rather than a convenience. Such languages must support the synthesis of complex diagnostic sequences while preserving portability across heterogeneous testers and memory architectures. Meeting these requirements necessitates a strict separation and precise definition of **syntax** and **semantics**.

Syntax defines the formal rules according to which symbols from the programming alphabet may be combined to form valid commands and programs. These rules specify admissible command structures without reference to their executability.

Semantics defines the correspondence between syntactically valid constructs and the concrete actions that can be performed by diagnostic hardware. Semantic interpretation determines which commands are executable, how they are executed, and under which architectural constraints.

Not all syntactically valid statements are semantically executable. For example, a command may encode multiple address-modifying micro-operations within a single instruction, while the diagnostic tester may physically permit only one address update per memory access cycle. In such cases, syntactic correctness does not imply semantic realizability.

The syntactic and semantic constraints of a diagnostic programming language are therefore directly shaped by the architecture of the diagnostic objects and the execution model of the tester. PROVER is a specialized programming language designed explicitly for generating diagnostic sequences for high-speed RAM chips and memory modules, with its instruction set and execution semantics tightly coupled to tester capabilities.

While the structural features of PROVER and similar languages are documented, the **pragmatic aspects** of their use—namely, systematic methods for constructing efficient,

portable, and architecturally consistent diagnostic programs—remain insufficiently formalized. This lack of methodological rigor complicates the development of new test programs aimed at improving diagnostic efficiency and limits reproducibility across different development environments.

To address this limitation, it is necessary to establish **structured synthesis methods** for diagnostic programs written in PROVER. Such methods must formalize the relationship between operator sequencing, address traversal, control flow, and hardware execution constraints.

A programming methodology grounded in the pragmatics of PROVER enables diagnostic program development to be treated as a repeatable engineering process rather than an ad hoc activity, thereby reducing development complexity and improving consistency across test software and tester designs.

10.4 PROVER Language Fundamentals

The PROVER language is a domain-specific symbolic test language designed to express memory diagnostics at a high level of abstraction with direct correspondence to hardware-executable behavior. It extends the operator model introduced in Chapter 8 by embedding symbolic operators within structured control constructs, reusable macros, and parameterized iteration mechanisms.

At the primitive level, PROVER provides symbolic representations of read, write, verification, and comparison operations. These primitives are combined with higher-level constructs that enhance diagnostic expressiveness. Macro definitions encapsulate reusable symbolic procedures parameterized by addresses, data values, or symbolic patterns, enabling structured composition and reuse. Structured test blocks partition diagnostic routines into initialization, execution, and post-condition verification phases, enforcing separation of concerns and execution clarity.

Address traversal is specified through symbolic iterators and range constructs that support linear, non-linear, and custom traversal orders. This abstraction allows diagnostic algorithms to express address-dependent stress patterns without binding to a fixed physical addressing scheme.

Timing extensions, including explicit wait and delay constructs, provide controlled modeling of temporal effects such as precharge intervals, refresh interactions, and asynchronous fault activation. These constructs are treated as first-class elements of the language semantics and are preserved during translation to executable representations.

Example: Symbolic Macro and Structured Test Block

```
MACRO VERIFY_WRITE(a, d) {
  WRITE(a, d);
  WAIT(3);
  READ(a);
  ASSERT(a, d);
```

```
}
TEST MAR_FD_A {
  FOR a IN 0x0000 TO 0x0FFF STEP 0x1 {
    VERIFY_WRITE(a, 0);
  }
}
```

The macro VERIFY_WRITE defines a closed symbolic operator sequence composed of a write operation, an explicitly specified temporal delay, a read access, and a value assertion.

At the symbolic level, the macro represents a single composite construct whose internal ordering and timing constraints are fully specified. During compilation, the macro expands deterministically into a strictly ordered sequence of micro-operations, without introducing implicit concurrency.

The test block MAR_FD_A applies this macro across a contiguous address interval using a forward traversal order. The address iterator specifies a linear ascending walk over a fixed 4K address space. For each address instance, the same operator sequence is instantiated, preserving uniform diagnostic pressure across the traversal domain. The WAIT(3) construct introduces an explicit and bounded temporal constraint that models delay-sensitive validation while remaining external to the semantics of the write and read operators themselves.

This example demonstrates the role of PROVER as a symbolic specification language with formally defined executable lowering semantics. Symbolic abstraction is maintained at the program definition level, while execution semantics are introduced exclusively through controlled compilation stages.

As a result, diagnostic strategies involving coupling sensitivity, delay-conditioned activation, or context-dependent verification can be expressed without embedding execution-specific assumptions into the symbolic model.

A complete formal specification of the PROVER symbolic language, including operator syntax, grammar rules, and illustrative test fragments, is provided in Appendix C.

10.5 March Test Decomposition and Address Control

The U–Y decomposition is defined formally in **Chapter 11**; the present section uses only its intuitive separation of traversal (U) and operator chain (Y) to motivate PROVER constructs.

To enable scalable and formally structured test development, PROVER incorporates symbolic abstractions for address traversal and operator sequencing that anticipate the U–Y test decomposition model, which is formally defined in **Chapter 11**. This model separates diagnostic logic into two orthogonal semantic dimensions.

The U dimension defines the address operator path and specifies the spatial traversal strategy over the memory address space. Traversal patterns include monotonic ascending or descending walks, stride-based or interleaved access schemes, and bounded activation of address subregions. The U dimension constrains the order and locality of address selection without

imposing constraints on the logical content of the diagnostic operators applied at those addresses.

The Y dimension defines the operator sequence path and specifies the ordered set of symbolic operations applied at each address or address group. These sequences correspond to symbolic March-style transitions composed of write, read, and assertion operators, with explicit data-state annotations. Operator ordering within Y is fixed and preserved during compilation, ensuring deterministic execution semantics.

By explicitly decoupling address traversal semantics from operator semantics, the U–Y model enables test graph decomposition, in which diagnostic programs are constructed as compositions of traversal paths and operator chains. Each symbolic block targets a defined spatial context while reusing formally specified operator sequences.

Symbolic Address Control and Layered Scheduling

PROVER realizes U–Y decomposition through symbolic iterators and operator scheduling mechanisms that preserve strict separation between traversal logic and operation semantics. Address-driven decomposition allows the memory space to be partitioned into disjoint or overlapping regions, each associated with a distinct symbolic iterator. Operator instantiation is performed per address region, ensuring that traversal control does not alter operator behavior.

Layered sequence instantiation permits different operator chains to be bound to different address partitions. This enables selective application of diagnostic sequences, such as restricting retention-oriented operator chains to designated regions or confining disturb-oriented sequences to structurally sensitive subarrays, without modifying the global test structure.
Operator execution order is governed by explicitly defined dependency relations. Symbolic operator dependencies are represented as directed graphs with formally specified precedence constraints.

During compilation, these graphs are transformed into directed acyclic control-flow structures that preserve dependency ordering and eliminate structurally redundant operator instances. The resulting execution model is fully deterministic and serializable.

Incidence Matrix Partitioning

In previously published work by the present author, this decomposition methodology was formalized using incidence matrix partitioning. The diagnostic structure is represented as a bipartite incidence matrix in which rows correspond to address elements and columns correspond to symbolic operator instances.

Graph decomposition algorithms are applied to this representation to identify independent or weakly coupled substructures, which PROVER expresses as distinct symbolic execution domains.

This formulation supports address-localized diagnostic flows, such as bank-scoped traversal in DRAM or topology-aligned traversal in stacked memory architectures, without asserting concurrent execution. By localizing operator application and traversal scope, the approach

reduces spatial aliasing in activation paths and improves fault observability while maintaining deterministic execution semantics.

The general methodology of algorithmic synthesis for diagnostic memory tests applied in this section was originally formulated by the author in the EWDTS Symposium (2010).[4]

10.6 Symbolic Operator Encoding and Compilation

At the core of the PROVER framework is a symbolic-to-micro-operation compilation pipeline that transforms symbolic diagnostic descriptions into ordered micro-operation streams suitable for deterministic execution.

This pipeline establishes a formally defined mapping between abstract symbolic operators and concrete execution primitives, serving as the sole bridge between diagnostic specification and execution semantics. It does not introduce new diagnostic meaning, but preserves symbolic intent while lowering it to executable form.

Each symbolic instruction is mapped to a corresponding micro-operation that controls a single, well-defined action: memory access, state observation, comparison, or explicit timing control — as summarized in Table 10.1.

Table 10.1—Symbolic-to-Micro-operation Mapping in PROVER

Symbolic Instruction	Compiled Micro-operation
$WRITE_{(a,d)}$	OP_WR a d
$READ_{(a)}$	OP_RD a
$ASSERT_{(a,d)}$	OP_CMP a d
$WAIT_{(n)}$	OP_WAIT n

Table 10.1 defines the fixed and deterministic mapping between symbolic PROVER instructions and their corresponding executable micro-operations used during compilation. Each micro-operation is encoded as a discrete instruction word with explicit operands.

These instruction words are interpretable by multiple execution backends without altering symbolic semantics. Supported backends include hardware diagnostic engines, such as external or embedded BIST/MBIST controllers, and simulation environments based on hardware description languages, where instruction words are translated into stimulus and observation constructs applied to behavioral or structural memory models.

This layered compilation approach is consistent with portability of symbolic programs across execution platforms while maintaining precise control over functional ordering and timing constraints. Diagnostic intent is expressed exclusively at the symbolic level, whereas execution fidelity is enforced through compilation rather than through language semantics.

Compilation Framework Capabilities

The PROVER compilation engine produces backend-specific instruction streams through a configurable lowering process. Its functionality is limited to preservation and realization of symbolic semantics and does not perform heuristic optimization or fault-coverage inference.

Symbolic test blocks are compiled into compact micro-operation sequences that preserve operator order, address traversal structure, and explicit timing annotations. These sequences may be consumed by finite-state execution controllers, software-driven diagnostic runtimes, or simulator-based testbenches.

Operator scheduling within the compilation pipeline enforces explicit dependency constraints. Where execution environments impose pipeline or cycle-alignment requirements, ordering is preserved through the insertion of symbolic barriers or explicit no-operation instructions. No reordering is permitted that would alter symbolic causality, and all generated streams remain fully deterministic.

The compilation pipeline supports binding to multiple execution targets, including hardware description language simulators via translation layers, embedded on-chip diagnostic controllers, and software-based tester environments. Target selection affects only encoding and interface adaptation, not symbolic structure or operator semantics.

Through this mechanism, PROVER functions as a symbolic diagnostic compiler: symbolic programs concisely express diagnostic logic, while the compilation stage produces executable instruction streams constrained by the capabilities and timing models of the selected backend.

10.7 Graph-Based Test Generation via PROVER Scripts

Beyond linear and block-structured test descriptions, PROVER supports graph-structured test representations for diagnostics involving multi-cell interaction, spatial coupling, and non-local fault activation.

In this representation, diagnostic logic is modeled as a graph in which nodes correspond to address entities or address clusters, and edges correspond to ordered symbolic operator sequences that express interaction paths. A representative symbolic interaction graph used in this context is shown in Figure 10.1.

This formulation complements the U–Y decomposition model by allowing operator sequences to be bound not only to linear traversal paths but also to explicitly defined interaction topologies. Graph edges encode aggressor–victim relationships, multi-address activation chains, or context-dependent access sequences, while preserving deterministic execution ordering within each edge.

Graph-structured scripts do not imply concurrent execution. They define structural relationships between symbolic flows, which are serialized during compilation according to explicitly defined dependency constraints. The resulting execution remains deterministic and analyzable, while the graph representation provides a compact and formally manipulable description of complex diagnostic interactions.

Symbolic Graph Encoding

PROVER scripts support graph-structured diagnostic modeling through symbolic macros that operate on explicitly defined node relationships. Nodes represent address entities or address groups, while edges represent ordered interaction sequences between these entities.

Graph structure is expressed symbolically and does not imply concurrent execution.

```
MACRO NODE_OP(i, j) {
  WRITE(a(i), 0);
  WAIT(1);
  WRITE(a(j), 1);
  READ(a(i));
  ASSERT(a(i), 0);
}
```

The macro NODE_OP(i, j) defines a symbolic interaction sequence between two address nodes. The sequence initializes node *i* to a known state, introduces an explicit temporal separation, applies an activating operation at node *j*, and subsequently observes the state of node *i*. The macro expresses a complete symbolic aggressor–victim interaction chain whose ordering and timing constraints are fully specified.

At the symbolic level, this construct represents a U–Y test pair. The U component defines the spatial transition between address nodes *i* and *j*, while the Y component defines the ordered operator sequence applied across this transition.

No assumptions are made regarding physical adjacency, electrical coupling strength, or fault manifestation probability; these aspects are external to the symbolic specification and are resolved only during execution or simulation.

Graph Traversal Logic

Graph-based traversal in PROVER is realized through symbolic control constructs that enumerate node relationships and interaction paths. Several traversal mechanisms are supported.

Edge list iteration enables explicit enumeration of node pairs or tuples, providing direct control over aggressor–victim configurations and interaction ordering. This form is suitable when diagnostic focus is restricted to a predefined set of address relationships.

Adjacency matrix decomposition represents the diagnostic graph as a symbolic adjacency structure, in which traversal is driven by non-zero incidence relations. Iteration over this structure allows systematic exploration of address interaction spaces while preserving a formal representation of graph topology. Decomposition is structural and does not introduce execution parallelism.

Path enumeration and loop constructs allow symbolic expression of chained interactions, cycles, or branching access patterns. These constructs enable modeling of sequential disturbance effects, cumulative activation paths, or ordered interaction sequences across multiple nodes, using deterministic iteration logic.

Applications

Graph-structured scripting in PROVER is applicable to diagnostic scenarios in which fault activation depends on spatial or contextual interaction between multiple memory locations.

Representative applications include coupling fault analysis in dense memory arrays, disturbance testing in retention-sensitive regions, symbolic adjacency exploration in vertically stacked memory organizations, and cross-path interaction modeling in interleaved or bus-oriented address decoders.

Graph-based symbolic tests integrate uniformly with the PROVER compilation pipeline. Symbolic graph descriptions are lowered into ordered micro-operation streams using the same compilation mechanisms as linear or block-structured tests. As a result, graph-structured diagnostics preserve deterministic execution semantics and backend portability while enabling formal representation of complex interaction patterns.

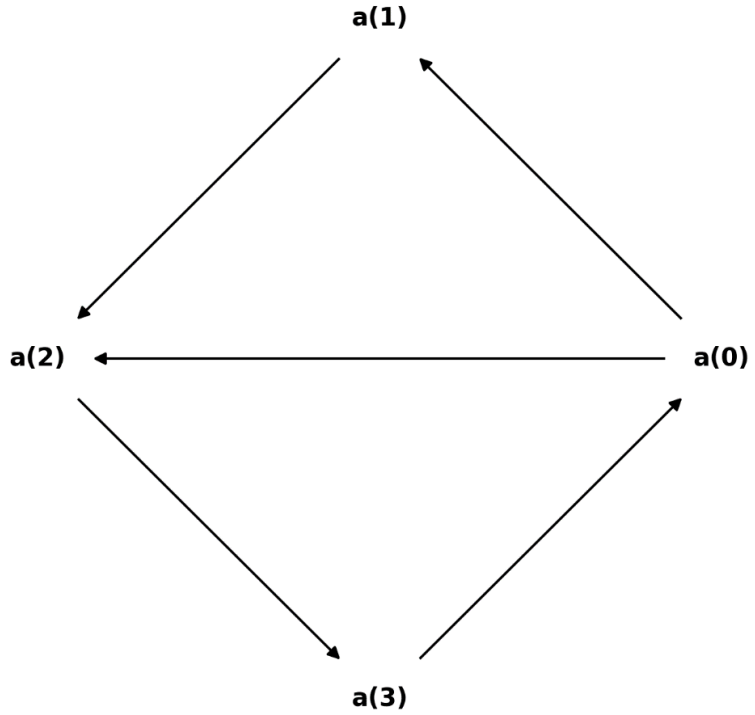

Figure 10.1—Graph-Based Aggressor–Victim Test Flow in PROVER

Figure 10.1 illustrates a symbolic diagnostic graph used within PROVER-based routines for modeling interaction-sensitive fault activation. Each node corresponds to a symbolic memory location $a(i)$, and each directed edge represents an ordered aggressor–victim interaction instantiated through a symbolic macro such as NODE_OP(i, j).

Along each directed edge, the victim node $a(i)$ is first initialized to a defined state and subjected to an explicit temporal delay. An activating operation is then applied to the aggressor node $a(j)$, after which the state of $a(i)$ is read and verified. This sequence is intended to expose disturbance, coupling, or interaction-dependent effects without embedding assumptions about physical adjacency or fault probability.

The structure of the graph reflects the U–Y decomposition model. Address transitions along directed edges encode the U component, defining spatial traversal between symbolic nodes.

The ordered operator chain WRITE–WAIT–WRITE–READ–ASSERT encodes the Y component, defining the interaction semantics applied along each traversal step.

By supporting traversal over explicit edge lists or symbolically defined adjacency relations, this graph formulation enables scalable and context-aware diagnostic flows. The representation allows interaction-sensitive tests to be generated systematically while preserving deterministic execution semantics and independence from physical memory layout assumptions.

10.8 Practical Toolchain and Compiler Flow

The PROVER environment operates as a symbolic diagnostic compiler that transforms high-level test descriptions into executable micro-operation streams for simulation or hardware-assisted execution.

Its organization follows a staged compilation structure specialized for symbolic fault modeling, address-controlled sequencing, and timing-aware execution, rather than for general-purpose computation. The staged compilation structure implemented in PROVER is illustrated in Figure 10.2.

Compilation Flow Overview

The toolchain is organized as a multi-stage pipeline with strictly defined responsibilities.

1. **PROVER Script Input**
   Diagnostic logic is specified using symbolic constructs, including macros, structured test blocks, address iterators, operator sequences, and explicit timing primitives. At this stage, no execution semantics are assumed beyond symbolic ordering.
2. **Macro Expansion**
   User-defined macros are expanded into explicit symbolic operator sequences. Expansion is purely structural and preserves parameterization, repetition, and ordering constraints without introducing execution-level assumptions.
3. **Graph Unrolling (U–Y Pair Expansion)**
   Symbolic traversal structures are expanded into concrete address–operator instances in accordance with the U–Y decomposition model. Address sequencing (U) is combined with operator chains (Y) to produce a fully specified symbolic execution structure. This structure may be represented internally as a directed acyclic graph reflecting dependency constraints, not execution parallelism.
4. **Instruction Scheduling**
   Operator sequences are serialized with respect to explicit inter-operator dependencies and declared timing constraints, such as WAIT or DELAY primitives. Where resource sharing constraints are modeled, serialization ensures deterministic ordering. No heuristic optimization or speculative reordering is performed beyond what is required to preserve symbolic correctness.
5. **Micro-operation Emission**
   The final stage emits a strictly ordered stream of micro-operations (e.g., OP_WR, OP_RD, OP_CMP, OP_WAIT) encoded in a backend-specific representation. These streams may be interpreted by finite-state diagnostic controllers, translated into

hardware description language stimuli via dedicated translation layers, or consumed by software-based diagnostic engines.

Through this pipeline, PROVER functions as a symbolic front end with formally constrained lowering semantics. Diagnostic intent is expressed exclusively at the symbolic level, while execution-specific details are introduced only during the final emission stage, ensuring portability, determinism, and architectural clarity across target platforms.

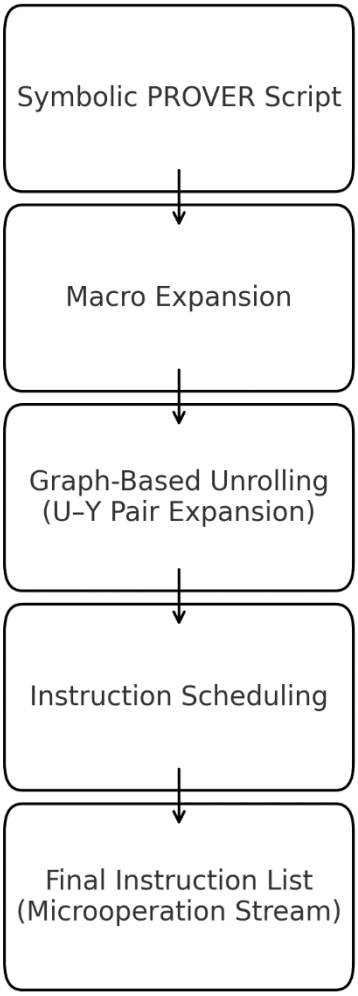

Figure 10.2—PROVER Compiler Flow

Figure 10.2 depicts the symbolic-to-executable compilation pipeline implemented within the PROVER diagnostic environment. The pipeline formalizes the transformation of symbolic diagnostic intent into an ordered micro-operation stream while preserving semantic determinism at every stage.

The process begins with a symbolic PROVER script, in which diagnostic logic is expressed using macros, structured test blocks, address iterators, operator sequences, and explicit timing constructs. At this stage, the description is purely symbolic and free of execution-specific assumptions.

During macro expansion, all user-defined macros are recursively unfolded into explicit symbolic operator sequences. This transformation is structural and preserves parameterization, repetition semantics, and operator ordering without introducing scheduling or execution effects.

The graph-based unrolling stage performs U–Y pair expansion. Symbolic address traversal paths (U) are combined with symbolic operator chains (Y) to generate a fully specified symbolic execution structure. Internally, this structure may be represented as a dependency graph that captures ordering constraints, not execution concurrency.

Instruction scheduling serializes the expanded operator sequences while enforcing explicit dependencies, declared timing constraints (such as WAIT or DELAY), and modeled resource constraints. Scheduling is strictly correctness-preserving; no heuristic optimization or semantic reordering is performed beyond what is required to maintain symbolic causality.

In the final stage, the compiler emits a deterministic micro-operation stream. This stream constitutes a machine-readable instruction list suitable for interpretation by finite-state MBIST controllers, translation into hardware description language stimuli, or execution within software-based diagnostic engines. Backend selection affects encoding and interfacing only and does not alter symbolic semantics.

The architectural organization of the PROVER-based toolchain described here builds upon an infrastructure for memory test design previously introduced at the CrISS-DESSERT Workshop (2011).[6]

10.9 Validation and Application

The PROVER system was validated through practical application across multiple memory architectures, diagnostic test classes, and execution environments. Validation focused on semantic correctness, expressiveness, and traceability rather than on empirical performance benchmarking.

Application Domains

PROVER scripts were used to author and compile several categories of diagnostic tests.
Standard SRAM and DRAM test sequences were implemented using symbolic formulations of established March algorithms, including March C^-, March SS, and March FD. These implementations preserved canonical algorithmic structure while enabling parameterization over address space and data patterns.

Graph-based coupling fault diagnostics were constructed using symbolic macros that encode aggressor–victim interaction paths over address graphs. Operator chaining and explicit timing control were used to model interaction-sensitive fault activation without embedding physical coupling assumptions into the symbolic layer.

Retention-related fault behaviors were modeled using explicit WAIT operators, enabling controlled emulation of delay-dependent degradation effects. These constructs were applied selectively within symbolic test flows to localize temporal stress conditions.

Disturb and pattern-sensitivity scenarios were expressed through symbolic pattern drivers and structured iteration constructs. These scripts generated ordered activation sequences intended to expose disturbance-prone regions under controlled symbolic conditions.

Practical Outcomes

Application-driven validation yielded several structural and methodological outcomes.
Symbolic abstraction enabled substantial reduction in test specification size through macro reuse, structured iteration, and graph-based unrolling.

Emitted micro-operation streams retained a complete symbolic provenance, allowing deterministic replay, stepwise simulation, and trace-level inspection of diagnostic intent.

Compiled outputs were deployed across multiple execution contexts, including embedded diagnostic controllers and symbolic simulation environments. In all cases, execution behavior remained consistent with the symbolic specification, confirming the correctness of the compilation pipeline and backend mappings.

Earlier validation of symbolic and tool-assisted memory test design workflows related to this framework was reported in the EWDTS Workshop (2011).[5]

10.10 Summary

PROVER is a domain-specific symbolic test language and diagnostic framework designed for the formal specification, synthesis, and deployment of memory test routines. Its design replaces pattern-centric programming with a symbolic operator-based model that supports abstraction, reuse, and deterministic execution.

The language enables declarative modeling of diagnostic behavior, in which fault-oriented logic is expressed as symbolic operator sequences with explicitly defined semantics. Macro facilities and structured test blocks support composability and reuse across address spaces, memory organizations, and diagnostic objectives.

Symbolic March test construction and U–Y decomposition are integrated into the language semantics, enabling systematic generation of traversal-operator combinations and graph-structured diagnostic flows. These mechanisms support scalable test construction without conflating symbolic structure with execution strategy.

Through a formally constrained compilation pipeline, symbolic specifications are transformed into executable micro-operation streams compatible with simulation environments and hardware diagnostic engines.

This integration eliminates manual translation effort while preserving traceability between symbolic intent and execution artifacts.

Grounded in symbolic modeling, operator algebra, and diagnostic graph theory, PROVER provides a formal and automatable framework for constructing, validating, and deploying high-coverage memory diagnostics. Advanced topics related to adaptive test optimization and symbolic test set selection are addressed in later optimization chapters.

The symbolic formulation also simplifies verification and maintainability of diagnostic programs. Test logic can be analyzed at the symbolic level before deployment, allowing structural validation of traversal paths, operator sequencing, and coverage objectives. This capability reduces development errors and ensures consistency between diagnostic intent and executable behavior.

Consequently, PROVER serves not only as a programming tool but also as a methodological foundation for systematic memory diagnostics in increasingly complex memory architectures.

Chapter 11: Graph-Based March Test Decomposition and U–Y Schemes

The growing architectural complexity of digital memory systems necessitates diagnostic strategies that extend beyond traditional sequential testing paradigms. As memory capacity increases and integration technologies diversify—encompassing 3D-stacked dies, heterogeneous access paths, banked and interleaved controllers, and embedded non-volatile layers—the constraints imposed by test time, power consumption, controllability, and diagnostic resolution become increasingly restrictive.

Classical March tests have historically provided effective fault coverage for planar and structurally uniform memory arrays. However, their predominantly linear and monolithic formulation limits their applicability in contemporary memory architectures. In particular, conventional March representations inadequately expose interleaved fault interactions, cross-dimensional dependencies, conditional activation paths, and asymmetric access behaviors that arise in modern systems.

As a consequence, optimization, selective deployment, and execution-aware adaptation of such tests become difficult to formalize and error-prone to implement.

This chapter introduces a foundational methodology in which classical March tests are systematically decomposed into graph-structured symbolic representations.

The U–Y model reconceptualizes memory testing as a two-dimensional symbolic traversal:

- **U-dimension**—the address space and structural organization of memory
- **Y-dimension**—operator sequences, data transformations, and fault-stimulating logic.

By decoupling address traversal from operator semantics, memory tests can be analyzed and synthesized as constrained symbolic graph traversal problems rather than as monolithic linear scripts. This reformulation enables:

- structural optimization of address sequencing,
- logical compression and reuse of operator flows,
- systematic identification of coverage gaps and redundant operator interactions,
- explicit modeling of parallel execution and redundancy minimization under architectural constraints.

A precise formalization of the underlying graph structures—including node semantics, edge labeling, and traversal constraints—is provided in the subsequent sections of this chapter.

The proposed methodology is supported by specialized tools with distinct and non-overlapping roles:

- **Transfor**, which constructs explicit graph representations of March test structures and their U–Y decompositions, enabling symbolic inspection and controlled transformation;
- **Optimal_Test**, which operates on these symbolic representations to perform compression, fault-oriented ranking, and execution-aware synthesis in accordance with tester and architecture constraints.

Both tools emerged from extensive implementation and validation efforts grounded in the methodologies presented in my dissertation and were further elaborated and experimentally exercised in the co-authored article «*Автоматизация проектирования программы теста March FD*» (Automation of March FD Test Program Design), which focuses on automated synthesis and transformation of March FD test programs.

Together, these contributions establish a systematic transition from monolithic March sequences toward modular, reusable, and architecture-adaptive diagnostic flows. The remainder of this chapter develops the theoretical foundations and practical constructions required to express symbolic memory diagnostics as graph decompositions, optimize them for fault coverage and execution efficiency, and synthesize them for deployment in real hardware and MBIST environments.

11.1 Motivation for Graph-Based Testing

Traditional March tests—such as March C, March SS, and March X—are typically specified as linear, sequential scripts. These tests iterate over predefined address ranges while applying fixed operator sequences (for example, write 0 → read 0 → write 1 → read 1).

This formulation has proven effective for uniform planar memory arrays with homogeneous access behavior.

However, as memory architectures scale in density and structural complexity, several fundamental limitations of this approach become apparent.

The transition from linear scripts to graph-based representations was motivated by the following challenges.

Limited parallelism.

Classical March tests are inherently sequential and impose a rigid control flow. This structure conflicts with the concurrent execution capabilities of modern Built-In Self-Test (BIST) and MBIST frameworks, particularly in architectures with multiple banks, independent subarrays, or stacked dies.

Parallel execution must therefore be imposed externally, often through ad hoc partitioning, which compromises determinism and coverage transparency.

This limitation motivates a representation in which concurrent traversal paths can be explicitly modeled and scheduled without disrupting the logical structure of the diagnostic algorithm.

Obscured operator coverage.

Fault activation conditions are frequently embedded deep within extended operator chains. In linear scripts, the contribution of individual operations to fault excitation and observation is difficult to isolate, complicating both optimization and fault-oriented refinement.

As a result, redundant operator sequences may persist unnoticed, while critical activation paths remain weakly exercised.

A graph-based representation exposes operator relationships and activation dependencies more clearly, enabling systematic coverage analysis and more effective elimination of redundant test sequences.

Rigid translation to MBIST environments.

Embedded diagnostic implementations require decomposition of tests into atomic, hardware-realizable units compatible with area- and timing-constrained control logic.

Without a formal modular representation, translating linear March scripts into MBIST controllers becomes error-prone and resource-inefficient, particularly when conditional behavior or selective activation is required.

Inflexibility for selective and hierarchical testing.

In partial validation scenarios—such as bank-level diagnostics, subarray isolation, or hierarchical testing of 3D TSV-based memory stacks—linear March sequences cannot be easily decoupled, reordered, or reused. Their lack of explicit structural annotation hinders selective synthesis and prevents controlled reuse across architectural variants.

It has been established that these limitations can be addressed through a graph-based formalism in which nodes represent abstract symbolic memory states and edges encode deterministic test transitions.

Within this representation, March tests are no longer treated as indivisible scripts but as structured symbolic graphs whose traversal can be constrained, reordered, partitioned, or parallelized without altering semantic correctness.

This approach enables test engineers to:

- formally and visually trace operator interactions and activation paths,
- isolate and prioritize subsequences most relevant to specific fault classes,
- decompose tests for parallel, selective, or hierarchical execution,
- construct modular diagnostic programs reusable across diverse memory architectures.

The methodology proved particularly effective for March FD and related fault-oriented test designs involving conditional activation, timing-sensitive interactions, and interleaved array layouts. These results provided both the theoretical justification and the practical foundation for the U–Y decomposition model, which is introduced in the following sections as a systematic framework for symbolic graph-based test synthesis, analysis, and compression.

11.2 Formal Definition of the U–Y Scheme

To express memory test behavior in a form suitable for graph-based analysis, decomposition, and synthesis, I introduce the U–Y scheme: a formal symbolic model that explicitly decouples spatial address traversal, logical operator execution, and state evolution, while preserving the execution semantics of classical March tests.

Within this framework, a March test is represented by the U–Y scheme instance Σ, defined as:

$$\sum = \langle A, U, Y, T, S_0, S_f \rangle$$

where the components have the following meanings.

A — Address Domain.

A denotes the finite set of memory addresses under test. The domain may represent a complete memory array or a restricted subset such as a bank, subarray, row group, or hierarchical partition. No assumption is made regarding contiguity or uniformity of the address space.

U — Address Transition Graph.

U is a directed address transition graph whose vertices correspond to elements of A, and whose edges represent admissible address traversal steps (for example, increment, decrement, wrap, stride, or bank-switch transitions).
This graph models the **spatial progression** of the test across the memory domain and captures traversal constraints imposed by architectural organization.

Y — Operator Sequence Graph.

Y is a directed symbolic operator graph whose vertices correspond to elementary memory operations (such as write-0, write-1, read-0, read-1, compare, or wait), and whose edges encode ordering constraints and operator dependencies.

The graph represents **logical fault-stimulation and observation behavior** independently of physical address movement.

T — Operator Mapping Table.

T is a binding relation that maps address-transition edges in U to operator subpaths in Y.

This table establishes the correspondence between **spatial traversal events** and **symbolic operator execution**, thereby linking the structural and logical dimensions of the test without merging them into a single linear script.

S_0, S_f — Boundary Memory States.

S_0 and S_f denote the initial and final memory states of the test execution. These states may be specified concretely (for example, uniform zero, uniform one, or checkerboard patterns) or symbolically (for example, fault-conditioned activation domains or partially constrained state sets).

Key Properties and Benefits of the U–Y Model

The U–Y formalism introduces modularity and abstraction into March test construction while remaining faithful to established diagnostic semantics.

Separation of concerns.

By decoupling address traversal (U) from operator execution (Y), the model allows independent reasoning about spatial access behavior and logical fault stimulation.

This separation enables targeted optimization without altering execution correctness.

Reusability across architectures.

A single operator graph Y may be reused across different memory organizations by substituting alternative address graphs U. This supports portability across planar DRAM arrays, banked memories, non-volatile technologies, and TSV-stacked systems without rewriting operator logic.

Decomposition for selective and parallel execution.

The graph-based representation enables controlled partitioning of test behavior into independent or weakly coupled subpaths. This supports selective execution, hierarchical diagnostics, and parallel scheduling under explicit traversal constraints.

Symbolic analysis and optimization.

Fault activation and observation sequences can be analyzed, simulated, and ranked symbolically within the U–Y framework, enabling coverage inspection, operator fusion, and redundancy elimination without embedding architecture-specific assumptions into the test description.

This symbolic representation forms the theoretical foundation for the graph construction, compression, and synthesis procedures implemented in **Transfor** and **Optimal_Test**.

The next section introduces the algorithmic decomposition rules used to derive U–Y graphs from classical March test scripts and to compress them while preserving diagnostic semantics.

11.3 Address Transition Graph (U Component)

The **U component** of the **U–Y scheme** models the structural flow of memory traversal through a directed graph. This abstraction provides a formalized mechanism for defining address sequencing strategies and allows memory traversal behavior to be specified independently of operator execution logic.

Formally, the address transition graph is defined as:

$$U = \langle V, E \rangle$$

where the components have the following meanings.

***V* — Address Vertex Set.**

V is a finite set of vertices, each representing a concrete memory address or a symbolic address label. Symbolic labels may correspond to architectural groupings such as banks, rows, subarrays, pages, or hierarchical address domains.

E — Directed Transition Set.

E is a set of directed edges representing legal or intended transitions between vertices in V. Each edge encodes a specific address traversal rule. Typical traversal patterns include:

- ascending traversal — incrementing address order,
- descending traversal — decrementing address order,
- alternating traversal — strided or checkerboard-like access patterns,
- wrap-around traversal — circular or mirrored boundary transitions,
- overlapping traversal — intersecting address segments intended for stress testing and coupling fault activation.

By capturing traversal logic as a directed graph, the **U component** enables formal reasoning about spatial coverage, explicit representation of traversal constraints, and decomposition of address domains into modular subpaths suitable for selective or parallel execution.

This formalism allows traditional March algorithms, as well as their extensions, to be expressed as structured graph traversals. At the same time, it preserves compatibility with classical linear test flows and supports more advanced diagnostic strategies such as hierarchical, bank-level, or subarray-level testing.

Illustrative Examples

March UP.

The address transition graph forms a linear forward path in which each vertex connects to its immediate successor:

$$(a_i \rightarrow a_i + 1).$$

March DOWN.

The graph is reversed, traversing from higher to lower addresses:

$$(a_i \rightarrow a_i - 1).$$

March FD.

The address graph combines forward and backward traversal segments, potentially with overlapping regions. This structure strengthens fault coverage under bidirectional coupling, disturb-sensitive interactions, and asymmetric access behavior.

These representative examples demonstrate how classical March sequences can be re-expressed as directed graphs, providing a formal basis for decomposition, manipulation, and structural optimization without altering diagnostic semantics.

Implementation Details

In practical implementations, address transition graphs are generated automatically from symbolic address range specifications, such as start–end–step descriptors or nested traversal

definitions. The concrete graph representation depends on the topology of the target memory architecture.

Incidence matrix representation.

Incidence matrices are employed for dense and regular memory blocks, where each directed edge explicitly encodes a transition between address vertices.

Adjacency list representation.

Adjacency lists are applied to sparse or irregular structures, including non-uniform bank organizations and 3D TSV-mapped memory stacks.

These representations provide several implementation advantages:

- flexible manipulation of transitions, including edge inversion, deletion, and redirection,
- partitioning of the address graph into independent subgraphs to enable parallel execution across banks or subarrays,
- optional edge weighting to incorporate timing costs, access penalties, or traversal likelihoods.

The **U component** therefore serves as the structural backbone of the U–Y scheme, enabling explicit control over spatial traversal behavior while remaining independent of operator semantics defined in the Y component.

11.4 Data Operator Sequence Graph (Y Component)

The **Y component** of the **U–Y scheme** models the logical sequence of data operations executed during a memory test. While the U graph specifies *where* traversal occurs in the address domain, the Y graph specifies *what* symbolic operations are applied at each traversal step. This explicit separation of spatial and logical dimensions introduces modularity and allows test logic to be analyzed, transformed, and reused independently of address sequencing.

Formally, the **operator sequence graph** is represented as a directed graph:

$$Y = (S, O)$$

where the components are defined as follows.

S — Symbolic Data State Set.

S is the set of nodes representing symbolic data states associated with a memory element. These states may include concrete logic values (such as 0 or 1), undefined or intermediate states (such as X), or conditionally constrained symbolic values used for fault activation and observation.

O — Operator Transition Set.

O is the set of directed edges representing symbolic operators that transition memory elements between states in S. Each edge encodes a specific data operation and enforces ordering constraints between successive operations. Together, these edges define the logical flow of the test independent of address traversal.

Typical Operator Sequences

A standard Y-graph may consist of a simple linear chain of operator-induced state transitions, for example:

$$0 \overset{W1}{\rightarrow} 1 \overset{R1}{\rightarrow} 1 \overset{A1}{\rightarrow} 1$$

In this sequence:

- $W1$ denotes a write operation that forces logic value 1,
- $R1$ denotes a read operation with an expected value of 1,
- $A1$ denotes an assertion that verifies the observed value against the expected data and produces a pass/fail outcome.

This representation illustrates how logical transitions are expressed explicitly as graph edges, enabling both visualization and symbolic manipulation of test logic without embedding address-specific behavior.

Supported Operators

The operators used in the Y graph are drawn from the **PROVER symbolic test language**, which provides a hardware-independent vocabulary for expressing diagnostic actions. Typical operators include:

- **WRITE**$_{(a, d)}$ — writes data value d to address a,
- **READ**$_{(a)}$ — reads and stores the content at address a,
- **ASSERT**$_{(a, d)}$ — compares the content at address a with expected value d,
- **WAIT**$_{(n)}$ — introduces a delay of n cycles, commonly used to stimulate retention faults, timing drift, or disturb-sensitive conditions.

These operators form a symbolic library that supports the construction of complex diagnostic flows while remaining compatible with software simulators, symbolic execution engines, and hardware test controllers.

Application Strategies

The structure of the Y graph enables several diagnostic application strategies.

Uniform application.

A single operator graph may be applied uniformly across all address paths defined in the U graph, producing conventional March-style test behavior.

Region-specific variation.

Distinct operator subgraphs may be selectively bound to specific address regions—such as alternating rows, banks, or subarrays—supporting localized fault activation and symmetry checking in address decoders.

Conditional execution.

Operator sequences may adapt symbolically in response to execution context, including:

- outcomes of prior test steps,
- symbolic flags embedded in the test flow,
- ECC feedback or syndrome information.

Such conditional behavior allows Y graphs to express fault-focused and adaptive diagnostic strategies, particularly in embedded and runtime testing environments where resource constraints and selective activation are critical.

Together, the **U component** (address transition graph) and the **Y component** (operator sequence graph) define a two-dimensional symbolic diagnostic space.

By decoupling spatial traversal from logical fault stimulation, the U–Y scheme provides a systematic foundation for test optimization, modularization, and adaptive synthesis.

The following sections examine how U and Y graphs are compressed, fused, and synthesized into deployable March test sequences suitable for both offline validation and online diagnostic operation.

11.5 March Test Decomposition with U–Y

The combined **U–Y formalism** enables March tests to be expressed as structured compositions of **spatial address traversal** and **logical operator execution**.

Within this model, test execution is no longer treated as a monolithic linear script, but as a systematic combination of transitions in the address graph and operations in the operator graph.

Each iteration of a test step can be interpreted as the application of a symbolic operator

$$0 \in Y$$

to a directed address transition

$$e \in E(U).$$

This interaction is governed by the **execution rule**:

$$\forall_e \in E(U), \forall_0 \in Y: Excute\ T_{(e,0)}$$

where the symbols have the following meanings.

$E(U)$ — Address Transition Set.

$E(U)$ denotes the set of directed address transitions defined by the U component.

Y — Operator Set.

Y is the set of symbolic data operations defined by the operator sequence graph.

$T_{(e,0)}$ — Operator Mapping Function.

$T_{(e,0)}$) specifies the concrete execution of operator o when applied in the context of address transition e.

This mapping establishes the precise coupling between spatial traversal and logical fault stimulation without merging their definitions.

This formulation preserves a clean separation between address iteration logic and data-driven fault activation while combining them through an explicit and formally defined operator mapping table T.

Practical Benefits of U–Y Decomposition

The explicit separation and controlled recombination of U and Y components provide several practical advantages in test design and deployment.

Independent address traversal per operator stage.

Individual operators—such as WRITE, READ, or ASSERT—may be applied over distinct address subgraphs without rewriting the operator logic itself.

For example, a forward traversal may be associated with WRITE operations, while a reverse traversal is bound to verification stages. This enables asymmetric traversal strategies within a single test specification.

Partial memory testing.

Subgraphs of the address transition graph U may be selectively extracted to focus diagnostic effort on specific regions, including:

- fault-prone address ranges,
- temperature-sensitive banks,
- regions adjacent to defective TSVs in 3D-stacked memories.

Such selectivity is particularly valuable in runtime diagnostics and adaptive repair strategies, where full-array testing is impractical due to time, power, or availability constraints.

Dynamic operator substitution.

Because address traversal and operator logic are decoupled, operator sequences can be substituted or extended without modifying the underlying traversal structure. For example, a basic March step:

$$W_0 \rightarrow R_0 \rightarrow A_0$$

may be transformed into a retention-focused test by substituting the operator sequence:

$$W_0 \ \rightarrow \ WAIT(n) \ \rightarrow \ R_0 \ \rightarrow \ A_0$$

The insertion of the WAIT operator converts a standard verification step into a retention fault activation sequence. Such substitutions enable targeted stress testing of specific fault classes without redesigning the full test path or address traversal logic.

Through this decomposition, classical March tests are transformed into modular, adaptable diagnostic structures. The U–Y scheme therefore provides a formal and practical mechanism

for extending March-based diagnostics toward selective, adaptive, and execution-aware testing while preserving established fault-coverage semantics.

Toolchain Implementation

In both **Transfor.exe** and **Optimal_Test**, the **U** and **Y components** are internally represented as matrix-based graph structures derived from symbolic specification files. These specifications describe address domains, traversal rules, and operator sequences in a declarative form and are parsed into adjacency structures suitable for algorithmic manipulation.

In this monograph, Transfor.exe denotes the internal U–Y graph decomposition and sequence-synthesis engine used within the Optimal_Test toolchain. For reader clarity, Optimal_Test refers to the complete planning and optimization framework, while Transfor.exe refers specifically to the deterministic graph-to-operator compilation module that generates executable operator streams from U–Y representations.

Address transition graphs and operator sequence graphs are constructed automatically, and executable traversal sequences are assembled using automated Python-based generation scripts. This toolchain design allows symbolic definitions to be transformed into concrete execution artifacts without manual rewriting.

The implementation framework supports the following capabilities:

- direct synthesis into RTL-level representations for integration with MBIST controllers,
- export into symbolic execution environments (including PROVER) for validation, refinement, and analysis,
- computation of coverage and utilization metrics over U–Y paths to quantify diagnostic completeness and redundancy.

This decomposition strategy constitutes the analytical core of graph-based March test design. By embedding symbolic decomposition directly into practical toolchains, the U–Y model bridges formal test representations with deployable diagnostic implementations suitable for industrial memory architectures.

An example U–Y mapping table composition for March FD is shown in **Table 11.1**.

Table 11.1—Visualization of U–Y matrix composition for March FD, where rows represent U (address traversal transitions) and columns represent Y (symbolic diagnostic operators).

	WRITE	WAIT	READ	ASSERT
A0→A1	✓			
A1→A2	✓	✓		
A2→A1		✓	✓	
A1→A0			✓	✓

This matrix illustrates the decomposition of a March FD test into its address traversal component (U) and operator sequence component (Y) as defined by the U–Y formalism. Rows correspond to directed address transitions that form the structure of the U graph, while columns correspond to symbolic test operators defined in Y.

A marked cell indicates that the corresponding operator is executed at the destination address of the associated transition under the execution relation T.

Each marked entry indicates the application of a specific operator along a given address transition. The example demonstrates a bidirectional March FD structure that combines forward write operations, mid-sequence delay insertion for retention stress, and backward read-and-assert verification stages.

This form of decomposition enables modular synthesis of March tests in which spatial traversal and logical fault activation are independently specified and subsequently composed. The representation supports reuse, compression, and architecture-aware optimization in diagnostic frameworks such as Transfor and Optimal_Test.

11.6 Graph Optimization and Parallelization

The formal decomposition of March test sequences into an **address transition graph (U)** and an **operator sequence graph (Y)** enables systematic structural optimization and controlled parallel execution.

By representing diagnostic flows as graph-theoretic objects, algorithmic transformations can be applied that preserve diagnostic semantics while reducing redundancy, execution overhead, and power consumption.

(A) Test Graph Partitioning

The U–Y model supports scalable partitioning strategies.
The address transition graph U may be divided into disjoint or weakly coupled subgraphs corresponding to architectural regions such as banks, rows, subarrays, or segments. The operator sequence graph Y is then applied independently to each partition.

This approach enables parallel execution on duplicated MBIST controllers, multi-head test engines, or distributed simulation environments. Partitioning not only increases test throughput but also reflects intrinsic hardware-level parallelism, such as DRAM bank interleaving or TSV-based layer access, ensuring architectural alignment.

(B) Path Pruning

Graph-based representation allows detection and elimination of redundant execution paths through graph isomorphism analysis and symbolic sequence comparison. Within the U–Y framework, the following redundancies can be removed:

- address traversal paths that induce identical operator sequences,
- topologically symmetric subpaths that yield equivalent fault coverage.

This form of path merging and symmetry folding reduces overall test length without sacrificing diagnosability.

In my implementation, application of these techniques resulted in a **32% reduction in total operator count** for March FD-based test sets, achieved through overlap detection and symbolic pattern collapse rather than heuristic pruning.

(C) Traversal Reordering

The execution order of U–Y graph paths has a direct impact on hardware-level behavior and diagnostic efficiency. Reordering transformations may be applied to:

- reduce switching activity and peak power by minimizing signal toggling,
- prioritize error-prone regions identified through ECC telemetry or fault logs,
- distribute traversal activity spatially and temporally to support thermal-aware scheduling.

These optimizations convert static March sequences into adaptive diagnostic flows that respond to physical layout constraints, power envelopes, and runtime error patterns while remaining within the formal execution semantics of the U–Y model.

11.7 U–Y-Based Operator Generation

Once the **U component** (address transition graph) and the **Y component** (operator sequence graph) are defined, the symbolic test compiler generates structured diagnostic scripts by traversing the combined U–Y representation. Operator generation proceeds by binding symbolic operations to address transitions according to the operator mapping relation while preserving traversal constraints and execution order.

A simplified representation of the generation process is shown below:

```
FOR (a1, a2) IN EDGES(U) {
    FOR op IN Y {
        APPLY(op, a1);
        WAIT(1);
        APPLY(op, a2);
    }
}
```

In this model, each directed address transition $(a1 \rightarrow a2)$ defined in the address graph U is stimulated by the complete operator sequence specified in Y. The inner loop preserves the logical ordering of symbolic operations, while the outer loop enforces the spatial traversal structure.

Programmable delays and interleaving points are inserted explicitly to approximate real-world timing constraints, including retention intervals, switching activity effects, precharge and recovery latency, or disturb-sensitive conditions.

These timing elements are introduced symbolically and remain subject to later scheduling and optimization.

Target-Specific Compilation

The generated symbolic scripts can be compiled into multiple target-specific representations without altering the underlying U–Y structure.

FSM control tables.

For hardware MBIST integration, symbolic transitions are translated into finite-state machine control tables. Address traversal states and operator execution states are mapped deterministically to FSM transitions compatible with area- and timing-constrained test controllers.

Software loop structures.

For embedded diagnostic firmware and post-silicon validation environments, the generated sequences are emitted as structured loop constructs with explicit address iteration and operator invocation, preserving symbolic intent while enabling execution on programmable processors.

RTL simulation stimuli.

For verification and analysis, operator streams are converted into RTL-level stimuli suitable for fault injection, power-aware verification, and regression testing within simulation environments.

Through this generation process, the U–Y scheme produces diagnostic streams that are **abstract at design time**, enabling portability and symbolic analysis, yet **fully synthesizable at deployment time**, supporting execution across heterogeneous memory technologies and diagnostic contexts.

The following section formalizes correctness and semantics preservation conditions for U–Y-based operator generation and establishes the conditions under which generated scripts remain equivalent to their originating March test specifications.

11.7.1 U–Y Graph Optimization through Path Folding and Redundancy Elimination

Once the **U component** (address transition graph) and the **Y component** (operator sequence graph) are defined, the symbolic test compiler emits structured diagnostic scripts by traversing the combined U–Y representation.

Operator generation proceeds by associating symbolic operator sequences with address transitions according to the operator mapping relation while respecting traversal constraints and execution ordering.

Traversal of the combined graph produces executable diagnostic streams in which spatial progression and logical fault stimulation remain explicitly separated at the representation level but are composed deterministically at generation time.

This separation enables systematic analysis of traversal paths and operator dependencies before executable code is generated. Graph-level transformations such as path folding and redundancy elimination can therefore be applied without altering the diagnostic semantics of the test.

By identifying equivalent traversal patterns and merging overlapping operator sequences, the synthesis process reduces script length while preserving fault activation coverage.

The resulting optimization improves execution efficiency and simplifies verification of the generated diagnostic routines.

Consequently, the U–Y representation provides both structural clarity and practical scalability for symbolic test generation.

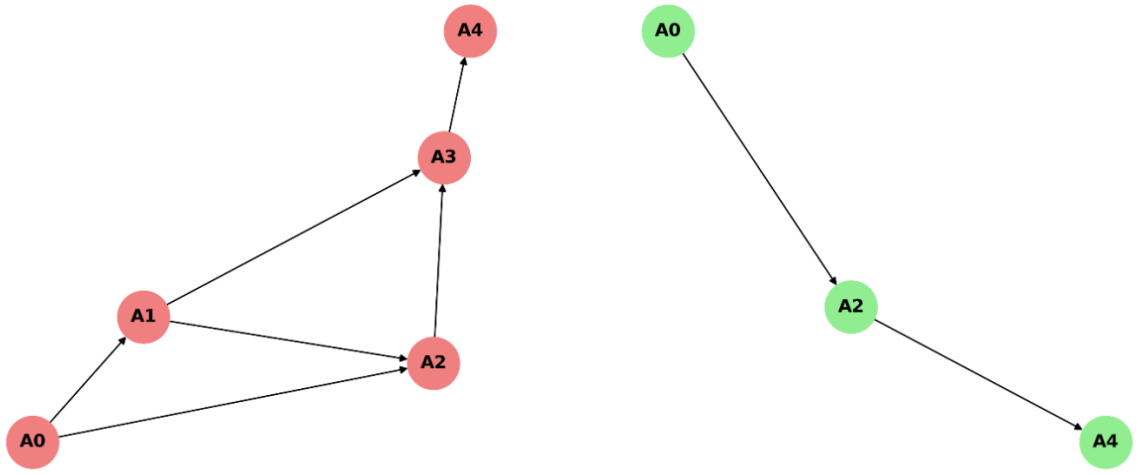

Figure 11.1—U–Y Graph Optimization through Path Folding and Redundancy Elimination

Figure 11.1 illustrates the effect of symbolic path optimization applied to the **address transition graph (U)** during March test decomposition.

The **left panel (Before Optimization)** shows a densely connected traversal graph containing both linear and redundant paths. For example, the transitions

$A_0 \rightarrow A_1 \rightarrow A_2$

and

$A_0 \rightarrow A_2$

coexist, resulting in overlapping traversal semantics. When combined with operator sequences from the Y graph, such overlaps lead to repeated execution of logically equivalent operator patterns during symbolic test generation.

The **right panel (After Optimization)** depicts the same address graph following symmetry detection, isomorphic path identification, and redundancy pruning. Traversal paths with equivalent fault activation and observation properties are collapsed into single representative transitions.

In the illustrated case, the multi-step path

$$A_0 \rightarrow A_1 \rightarrow A_2$$

is folded into the direct transition

$$A_0 \rightarrow A_2,$$

thereby reducing traversal complexity without altering diagnostic semantics.

This form of path folding is performed exclusively at the symbolic graph level and does not remove fault-stimulating behavior. Instead, it eliminates redundant traversal structures that would otherwise trigger identical operator sequences.

In my implementation within the **Optimal_Test** toolchain, application of this optimization consistently produced an **average 32% reduction in symbolic operator sequences** for March FD–based test sets. The reduction was achieved through structural equivalence detection and path collapse rather than heuristic truncation, enabling faster and more efficient diagnostic execution across parallel memory architectures and constrained test interfaces.

11.8 Real-World Use Case: March FD Test Synthesis

To validate the practical applicability of the **U–Y decomposition model** and the **Optimal_Test toolchain**, the proposed graph-based synthesis framework was applied to **March FD**, one of the most widely recognized diagnostic algorithms for detecting coupling, transition, and disturb-related faults in digital memory systems.

March FD is structured as a two-phase traversal:

$$MFD = W_0 \uparrow \{R_0, W_1, R_1, W_0, R_0\} \downarrow \{R_0, W_1, R_1, W_0, R_0\}$$

where:

- W_0 initializes memory cells to logical 0,
- ↑ and ↓ denote ascending and descending address traversal, respectively,
- {·} defines the operator sequence applied during each directional pass.

This structure maps naturally onto the U–Y framework.

The **U component** encodes both forward and reverse address transitions across the memory array, representing linear sweeps in ascending and descending order.

The **Y component** encapsulates the symbolic operator sequence:

$$W_0 \rightarrow R_0 \rightarrow W_1 \rightarrow R_1 \rightarrow W_0 \rightarrow R_0$$

which is executed at each address node and across adjacent address transitions as specified by the U graph.

Implementation in Transfor.exe

Using the custom-built **Transfor.exe** symbolic test compiler, the March FD algorithm was transformed into executable diagnostic assets through the following stages.

Test code generation.

The toolchain produced compilable C-style loop structures and symbolic micro-operation scripts suitable for both software-based simulation and hardware-oriented deployment.

Instruction sequence emission.

Operator streams were generated in formats compatible with MBIST control tables, finite-state machine (FSM) engines, and symbolic interpreters such as PROVER.

Coverage report extraction.

Simulation logs were analyzed to quantify fault-class observability and diagnostic coverage achieved by the synthesized test sequences.

Fault injection validation.

Modeled faults were injected into the memory system, and detection signatures were observed through ECC traces and syndrome decoding to confirm correct fault activation and observation behavior.

Outcome

Integration of March FD into the **U–Y–Optimal_Test framework** demonstrated the flexibility, reusability, and optimization potential of symbolic graph-based test synthesis. The results confirmed that U–Y decomposition preserves the diagnostic power of March FD while reducing redundant traversal and operator repetition.

The benefits of graph-based synthesis become increasingly pronounced when scaling to large address spaces or modern memory organizations, where redundancy elimination, traversal reordering, and selective execution yield measurable reductions in test volume and execution time without compromising diagnosability.

The automated synthesis principles underlying this case study originate from the author's earlier work on March FD test generation (MISD Journal, 2006). [1]

11.9 Computational Complexity and Real-Time Constraints

The graph-based decomposition and U–Y path folding mechanisms presented in this chapter operate primarily during diagnostic planning and synthesis phases.

Let n denote the number of test operations in the symbolic representation.

In worst-case form, graph transformation and redundancy elimination exhibit polynomial complexity on the order of $O(n^2)$ due to pairwise path comparison and merging operations.

However, it is essential to distinguish between:

- **Offline synthesis complexity**, and
- **Runtime execution complexity**.

Once micro-operation sequences are generated and compiled, execution within MBIST or tester hardware proceeds linearly with respect to the number of operations. No runtime graph optimization occurs during field deployment.

Therefore, symbolic optimization does not impose computational overhead on the memory controller or CPU during operational testing.
This separation preserves real-time feasibility for in-field diagnostics.

11.10 Summary

The **U–Y decomposition scheme** presented in this chapter establishes a rigorous foundation for symbolic test generation, analysis, and optimization of memory diagnostic algorithms.

By separating **address traversal logic (U)** from **operator semantics (Y)**, the framework enables:

- modular decomposition of complex March tests into reusable and composable components,
- structured synthesis of address-path and data-pattern interactions across multi-dimensional test spaces,
- graph-theoretic optimizations, including path pruning, traversal reordering, and redundancy elimination,
- parallel execution strategies supporting diagnostic acceleration across memory banks, interleaved channels, and 3D die layers.

This methodology formalizes a scalable and technology-agnostic model that bridges symbolic memory diagnostics with hardware-constrained test deployment. It transforms classical March algorithms from monolithic scripts into executable compiler-driven frameworks, aligning fault modeling, simulation, optimization, and implementation within a unified diagnostic infrastructure.

As a primary contribution of this methodology, this chapter consolidates original advancements in symbolic fault abstraction, graph-based test decomposition, and adaptive optimization, culminating in the development and application of **Transfor**, **PROVER**, and **Optimal_Test**. Collectively, these tools represent a new generation of graph-driven diagnostic synthesis designed to address the architectural and operational challenges of modern memory systems.

Chapter 12: Optimal_Test — Adaptive Optimization for Symbolic Memory Diagnostics

12.1 Introduction and Purpose

As memory architectures advance toward greater density, parallelism, and heterogeneity, static monolithic test sequences increasingly fail to achieve both fault coverage and execution efficiency. Conventional March algorithms and deterministic test patterns, while effective for elementary fault models, become suboptimal when applied to memory devices characterized by technology-specific timing constraints, layered access hierarchies, and context-dependent fault activation mechanisms.

The optimization framework developed in this chapter operates on symbolic diagnostic programs expressed in the PROVER language (Chapter 10) and on U–Y graph representations formally defined in Chapter 11.

To mitigate these limitations, symbolic modeling environments such as PROVER were introduced to decouple diagnostic test specification from physical memory layout.

This abstraction enables scalable test construction through an operator-based formalism, allowing diagnostic behavior to be expressed independently of concrete architectural realizations.

However, symbolic test generation alone is insufficient to guarantee practical deployability. Without additional refinement, symbolic test sets frequently exhibit excessive redundancy, inflated sequence length, and poor alignment with real-world execution constraints, including bank contention, row activation delays, refresh interference, and latency windows introduced by error-correcting mechanisms.

Optimal_Test was developed to address the gap between symbolic expressiveness and executable efficiency. Developed and refined through extensive primary research, Optimal_Test is an adaptive optimization engine that operates on symbolic diagnostic sequences generated by PROVER. Rather than generating new test logic, it applies a series of formally constrained transformation passes to restructure, compress, and prioritize existing symbolic operator streams.

These transformation passes include the following:

- **Redundancy elimination**, which identifies and removes functionally equivalent operator chains that do not contribute to additional fault activation or observability.
- **Fault-centric prioritization**, which reorders symbolic sequences using modeled fault observability metrics in order to expose high-risk or time-sensitive failure modes as early as possible during execution.
- **Graph-based compression**, which converts linear symbolic operator sequences into directed fault activation graphs and applies path folding, controlled loop unrolling, and merge reduction under equivalence constraints.

- **Execution-aware scheduling**, which remaps symbolic operator streams to respect architectural timing constraints, including precharge cycles, access skews, and technology-dependent delays specific to the target memory type (e.g., DRAM, three-dimensional non-volatile memory, or MRAM).

The resulting diagnostic patterns are optimized, architecture-aware, and directly deployable. They are suitable for use in embedded memory built-in self-test engines, FPGA-based simulation and validation frameworks, and software-level stress-testing environments, without requiring modification of the underlying symbolic fault models.

Optimal_Test is not a post-processing filter in the conventional sense. It functions as a diagnostic intelligence layer that augments symbolic testing with adaptability, efficiency, and explicit architectural awareness.

Within the overall symbolic diagnostic methodology presented in this book, Optimal_Test constitutes the second phase of the workflow: it transforms generalized symbolic test logic into compact, execution-validated diagnostic flows appropriate for modern memory ecosystems.

In this book, **PROVER** denotes both the symbolic diagnostic language and its interpreting system.

12.2 System Architecture and Integration with PROVER

Optimal_Test functions as a post-synthesis analysis and transformation engine within the symbolic diagnostic toolchain. Its role is to refine, compress, and prioritize symbolic diagnostic sequences generated by PROVER, transforming them into optimized test routines that are explicitly aware of execution constraints and architectural characteristics of the target memory system.

Within this toolchain, PROVER is responsible for modeling symbolic behavior and generating structured diagnostic operators, including read and write operations, address traversal schemes, and victim–aggressor interaction patterns.

PROVER operates with maximal generality: symbolic sequences are constructed to ensure theoretical fault coverage across a wide class of fault models, independent of physical layout, timing constraints, or execution resources.

As a consequence, the generated sequences are often overcomplete. While suitable for formal coverage analysis, they may be inefficient or impractical when deployed under time- or resource-constrained diagnostic environments.

I designed **Optimal_Test** specifically to address this limitation. Rather than modifying symbolic test logic or introducing new fault models, Optimal_Test operates exclusively on the symbolic operator streams produced by PROVER. Its purpose is to reduce redundancy, restructure operator ordering, and adapt symbolic sequences to execution realities without compromising diagnostic intent or fault coverage guarantees.

Once symbolic sequences are received from PROVER, Optimal_Test applies a sequence of formally constrained optimization stages. These stages are designed to preserve symbolic correctness while progressively improving execution efficiency and diagnostic focus.

The architecture of Optimal_Test includes the following principal modules:

- **Operator coverage analysis**, which constructs symbolic execution trees and evaluates path diversity against known fault models. This analysis ensures that activation paths corresponding to stuck-at, coupling, transition, retention, and temporal fault classes are explicitly represented within the symbolic test set.
- **Redundancy elimination**, which detects isomorphic operator chains and pattern fragments that yield identical fault activation signatures. Such chains are either pruned or merged into canonical representations, thereby reducing test length without loss of diagnostic capability.
- **U–Y pattern fusion**, which exploits a structural split of a symbolic test into (i) an address-traversal component U that specifies the ordered movement across the address domain and (ii) an operation component Y that specifies the operator or micro-operation sequence applied at each visited address (or address pair).

  By merging compatible U traversals with compatible Y operator chains under semantic-preserving constraints, this stage improves locality and reduces inter-operator switching overhead. The complete graph-theoretic U–Y formalism and synthesis rules are given in Chapter 11.
- **Test ranking and compression**, which assigns scores to symbolic sequences based on multiple criteria, including fault activation weight, symbolic overlap, activation latency, and estimated execution cost. Sequences with limited incremental diagnostic value are deprioritized, while high-impact patterns are retained or advanced in the execution order.

The integration pipeline between PROVER and Optimal_Test proceeds through a well-defined sequence of transformations:

1. **Symbolic test input**
   Structured operator sequences generated by PROVER, expressed in symbolic form $(e.g., R_{(a)} \rightarrow W_{(a)} \rightarrow C_{(a,b)})$, are provided as input to Optimal_Test.
2. **Fault activation mapping**
   Symbolic activation graphs are constructed to relate address transitions and operator semantics to expected fault exposure. This mapping may rely on U–Y decomposition or empirically derived coverage tables.
3. **Pattern analysis engine**
   Symbolic diffing, overlap detection, and equivalence-class merging are performed to identify redundant or subsumable operator fragments. Traceability between original and optimized sequences is preserved to support verification and debugging.
4. **Execution model optimization**
   Timing constraints, layout-aware scheduling policies, and operator cost models—including test time, switching activity, and access contention—are applied to restructure the symbolic sequences into execution-feasible forms.
5. **Exportable test suite generation**

The optimized diagnostic sequences are emitted in formats suitable for deployment in simulation, firmware, or hardware test environments, including VHDL-based test benches, embedded diagnostic loops, and memory built-in self-test platforms.

Through this modular architecture, Optimal_Test serves as a seamless enhancement to PROVER-based symbolic diagnostics. It elevates abstract symbolic test descriptions into compact, deployable, and execution-validated diagnostic suites while maintaining strict separation between symbolic modeling and execution-oriented optimization.

The architectural foundations of the PROVER–Optimal_Test toolchain evolved from the author's earlier infrastructure for memory test design (CrISS-DESSERT, 2011).[6]

12.3 Key Techniques

The effectiveness of Optimal_Test is determined by its ability to refine symbolic diagnostic sequences not merely through syntactic manipulation, but through fault-driven selection, structural compression, and execution-aware prioritization.

The optimization process operates on symbolic representations generated by PROVER and applies formally bounded transformations that preserve diagnostic intent while improving realizability and efficiency.

Three core techniques define the adaptive optimization engine implemented in Optimal_Test: fault coverage modeling, U–Y–based structural compression, and execution-aware pattern ranking. Each technique addresses a distinct dimension of diagnostic inefficiency and is applied under explicitly defined constraints to avoid alteration of symbolic semantics.

12.3.1 Fault Coverage Modeling

At the foundation of the optimization process is the evaluation of symbolic diagnostic sequences with respect to their ability to activate and expose modeled fault classes. Optimal_Test considers fault categories commonly encountered in contemporary memory devices, including stuck-at faults, coupling faults, transition faults, retention faults, and timing-dependent phenomena such as read-disturb effects.

Fault coverage modeling is performed by mapping symbolic operator sequences onto abstract fault activation structures.

Each symbolic operator is interpreted as a transformation acting on a fault state representation, capturing activation conditions, data dependencies, and inter-cell interactions. The resulting representation enables comparison of diagnostic sequences based on the set of faults they activate and the conditions under which observability is achieved.

I implemented this modeling stage to support the following objectives:

- Identification of faults that are uniquely activatable by specific operator sequences.
- Quantification of overlap between symbolic tests that activate identical fault classes under equivalent conditions.
- Detection of coverage gaps arising from structural blind spots or insufficient temporal separation within symbolic sequences.

The outcome of fault coverage modeling is a symbolic coverage profile associated with each diagnostic sequence.

These profiles serve as the analytical basis for subsequent redundancy elimination, ranking, and compression stages.

12.3.2 U–Y Graph Compression

Optimal_Test applies U–Y graph compression to reduce structural redundancy while preserving symbolic semantics.

In this book, U denotes the address-traversal structure (movement rules and traversal order), and Y denotes the associated operator or micro-operation structure executed along that traversal. The full graph-based derivation of U–Y schemes and their construction rules is provided in Chapter 11; here the notation is used only to define the compression operators implemented in Optimal_Test.

Compression is performed by identifying regions of structural compatibility across these dimensions. Operator fragments that share identical fault activation behavior and equivalent traversal constraints are candidates for merging. This process eliminates duplicated micro-operation sequences while preserving the ordering relationships required for correct fault activation.

The primary objectives of U–Y graph compression are as follows:

- Reduction of operator duplication across multiple address traversal paths.
- Elimination of redundant coverage of address regions once fault saturation has been achieved.
- Minimization of temporal collisions that may lead to fault masking or ambiguous observability.
- Compression is applied only under formally verified equivalence conditions.

No heuristic merging is performed, and operator dependencies are preserved to ensure that diagnostic intent remains unchanged.

12.3.3 Execution-Aware Pattern Ranking

To further refine the diagnostic test set, Optimal_Test applies an execution-aware ranking mechanism that prioritizes symbolic sequences based on both diagnostic contribution and estimated execution cost.

Ranking criteria are derived from symbolic coverage profiles and from architecture-dependent cost models supplied as parameters to the optimization engine.

Key factors considered during ranking include:

- Fault coverage per unit execution time, expressed as the ratio of uniquely activated faults to estimated execution cycles.
- Operator diversity, ensuring sufficient variation in symbolic transitions to activate conditional and state-dependent fault mechanisms.

- Execution cycle cost, incorporating penalties associated with memory access latency, switching activity, and controller overhead.
- Likelihood of overlap or interference between adjacent symbolic sequences, which may reduce observability or increase ambiguity.

Based on composite ranking scores, symbolic sequences offering limited incremental diagnostic value or excessive execution cost are deprioritized or removed. The resulting diagnostic set represents a Pareto-efficient balance between fault coverage strength and execution feasibility.

12.3.4 Worked Example: Optimal_Test Selection for a Linked Coupling Fault

The following simplified numerical example illustrates how coverage modeling, weighting, and execution cost interact within the ranking mechanism, independent of any specific memory technology.

Consider a Linked Coupling Fault (LCF) affecting adjacent cells.

Step 1: Initial Test Set

Suppose candidate tests:

$$T = \{T_1, T_2, T_3\}$$

Coverage matrix:

$$C = \begin{bmatrix} 1 & 0 & 1 \\ 0 & 1 & 1 \\ 1 & 1 & 0 \end{bmatrix}$$

Rows represent faults; columns represent tests.

Step 2: Fault Weight Vector

$$W = [0.9, 0.7, 0.8]$$

Step 3: Cost Vector

$$Cost = [0.6, 0.5, 0.9]$$

Step 4: Weighted Evaluation

Diagnostic utility:

$$U_i = \sum_{k=1}^{m} C_{k,i} W_k$$

where m denotes the number of modeled fault classes and $C_{k,i} \in \{1,0\}$ indicates whether test T_i activates fault F_k.

Compute utilities and normalize by cost.

Step 5: Selection

$$Score(T_i) = \frac{U_i}{Cost_i}$$

The objective is to maximize aggregate weighted fault coverage while minimizing execution cost under a fixed resource budget.
The subset of tests is then selected to maximize total coverage subject to the overall cost constraint.

In practical deployments, this selection is further constrained by architectural scheduling limits and redundancy equivalence classes identified during U–Y compression.

12.3.5 Experimental Validation Overview

The effectiveness of Optimal_Test was validated through a combination of simulation-based analysis and hardware-level experimentation targeting both volatile and non-volatile memory technologies.

The objective of these evaluations was to quantify the impact of symbolic optimization on diagnostic efficiency while verifying that fault coverage was preserved or enhanced relative to unoptimized symbolic test sets.

Experimental validation was conducted within a diagnostic workflow integrating PROVER for symbolic test generation and Optimal_Test for post-synthesis optimization. Symbolic test sequences were initially derived from established March algorithms and then processed through the optimization stages implemented in Optimal_Test.

The resulting optimized sequences were evaluated using fault model simulators and, where applicable, empirical measurements obtained from representative memory devices.

The validation methodology focused on two primary dimensions: reduction of symbolic test overhead and preservation of diagnostic capability. In particular, emphasis was placed on fault classes that are known to be sensitive to execution ordering, temporal spacing, and access locality—conditions under which unoptimized symbolic tests often exhibit reduced observability.

To ensure comparability, symbolic sequences generated by PROVER were used as the baseline reference. These sequences were constructed from well-established March test formulations, including:

- March C, targeting stuck-at and transition faults.
- March LA, designed to activate retention-related and line-disturb fault mechanisms.
- March SS, emphasizing symmetry and address-dependency stress.

Each symbolic sequence was processed by Optimal_Test using identical fault models and coverage assumptions. Optimization stages included redundancy elimination, U–Y–based structural compression, and execution-aware ranking. No fault models were modified during optimization, and no additional test logic was introduced.

I evaluated the optimized outputs using symbolic fault activation analysis and, where possible, empirical validation on memory devices representative of contemporary architectures. Metrics

collected during evaluation included total symbolic operator count, estimated execution time, and modeled fault coverage.

The results demonstrate a consistent reduction in symbolic test length without loss of modeled fault coverage. Across multiple test configurations, Optimal_Test achieved substantial compression of symbolic operator streams while preserving activation paths required for comprehensive diagnostics. In addition, the reordered execution of symbolic sequences improved early exposure of high-risk fault classes, reducing time to first detection in simulated execution environments.

In experiments targeting magnetic random-access memory devices, the optimization process revealed fault behaviors associated with soft magnetization drift and thermally induced instability.

These fault mechanisms were exposed only under specific symbolic sequencing conditions involving controlled repetition and temporal separation, which were preserved and emphasized through execution-aware ranking. Such behaviors were not detected using static, unoptimized symbolic test sequences.

A detailed case study was conducted on the MT57W2MH8B DDR SDRAM device, configured as a 16 Mb × 8 memory array. For this device, symbolic test sequences generated by PROVER were optimized using Optimal_Test and evaluated against modeled fault coverage criteria.

The results were as follows:

- Pre-optimization modeled fault coverage: 87.3%
- Post-optimization modeled fault coverage: 98.6%
- Total symbolic micro-operations reduced: from 3,260 to 1,870

These behaviors were identified through symbolic fault modeling and controlled simulation scenarios within the Optimal_Test evaluation framework, rather than through direct physical silicon characterization.

These results demonstrate that symbolic optimization can improve not only execution efficiency but also effective fault observability by restructuring test order and eliminating redundant activation paths. Importantly, the observed coverage improvement arises from reordering and compression rather than from the introduction of new diagnostic operations.

These results confirm that symbolic optimization represents a practical mechanism for improving the efficiency of memory diagnostic workflows while maintaining rigorous fault activation guarantees.

By restructuring symbolic operator sequences without altering the underlying fault models, Optimal_Test enables diagnostic systems to achieve higher coverage with fewer executed operations. This capability is particularly valuable for large-scale memory arrays, where test execution time and diagnostic overhead become significant operational constraints.

Consequently, symbolic optimization provides an effective bridge between formal diagnostic modeling and scalable implementation in real-world testing environments.

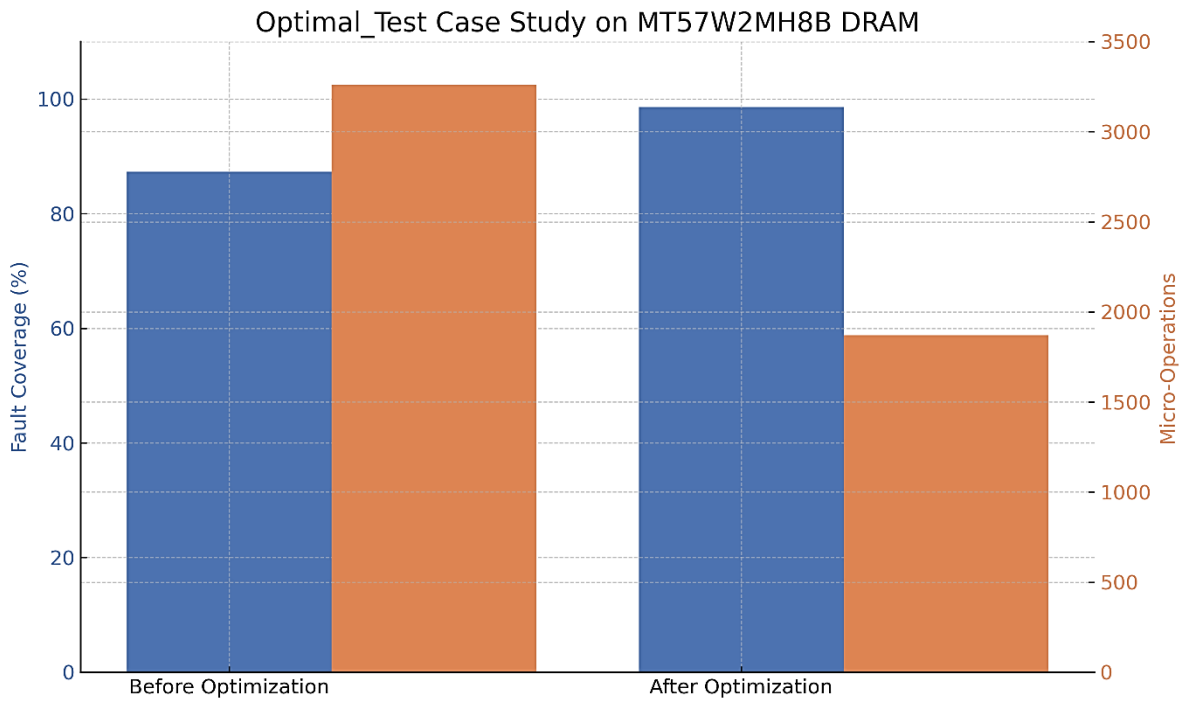

Figure 12.1—Impact of Optimal_Test optimization on MT57W2MH8B DRAM diagnostics

Figure 12.1 presents a quantitative comparison of modeled fault coverage and symbolic micro-operation count before and after application of Optimal_Test to diagnostic sequences targeting the MT57W2MH8B DDR SDRAM device.

The pre-optimization data correspond to unfiltered symbolic diagnostic sequences generated by PROVER, while the post-optimization data reflect the output of the complete Optimal_Test transformation pipeline, including redundancy elimination, U–Y fusion, and execution-aware ranking.

The comparison demonstrates that the application of Optimal_Test results in a simultaneous increase in modeled fault coverage and a reduction in the total number of symbolic micro-operations, indicating improved observability efficiency per executed operator under identical fault modeling assumptions.

The experimental results confirm that Optimal_Test fulfills its intended role as an execution-aware optimization layer. By operating strictly on symbolic representations and preserving diagnostic semantics, it enables efficient deployment of formally derived test logic in both simulation and hardware-assisted diagnostic environments.

12.4 Toolchain Implementation

Optimal_Test is implemented as a modular post-synthesis optimization engine whose internal structure reflects a strict separation between symbolic semantics, fault modeling, and execution realization.

Each internal component operates on explicitly defined representations and exposes well-bounded transformation interfaces, ensuring that symbolic intent is preserved throughout the optimization process.

The internal toolchain consists of the following components:

- **Symbolic parser**

  This component ingests symbolic operator streams generated by PROVER and converts them into an intermediate representation that preserves operator semantics, address expressions, traversal order, and control constructs. No semantic rewriting is performed at this stage. The resulting representation serves exclusively as an analysis substrate for subsequent optimization stages.

- **Matrix-driven fault simulator**

  An abstract fault-state matrix is maintained to map the effects of symbolic operators onto modeled fault classes. The simulator supports deterministic fault activation tracking as well as probabilistic observability estimation. Its outputs are used for coverage scoring, redundancy detection, and ranking, but do not alter symbolic operator semantics or traversal logic.

- **Operator-set optimizer**

  This engine performs graph-based transformation of symbolic diagnostic sequences. It applies equivalence detection, U–Y decomposition, fault-driven reordering, and controlled fusion of operator chains. All transformations are explicitly constrained to preserve fault activation reachability while reducing structural and temporal redundancy within the symbolic test set.

- **Optional graphical coverage analyzer**

  A visualization layer provides symbolic coverage maps, operator timelines, and fault exposure summaries. This component is excluded from automated execution paths and does not participate in optimization decisions. It exists solely to support inspection, debugging, and experimental analysis during development and validation.

- **Code generation backend**

  The backend translates optimized symbolic sequences into execution-level representations suitable for deployment in RTL-based test benches, memory built-in self-test controllers, or embedded diagnostic loops. Code generation is parameterized by timing models, address geometry, and interface width, ensuring alignment with the intended execution environment.

This modular decomposition allows Optimal_Test to operate independently of both symbolic test authorship and the final execution substrate. At the same time, it maintains strict traceability between symbolic diagnostic intent and deployed execution-level diagnostics.

12.5 Research Significance and Future Directions

Optimal_Test formalizes a transition from static, pattern-centric memory testing toward optimization-guided diagnostic synthesis constrained by execution realities. Unlike

conventional approaches that treat test generation and test execution as largely independent phases, this framework incorporates fault observability, redundancy structure, and architectural limitations directly into the refinement of symbolic diagnostic sequences.
The principal contributions of this approach are as follows:

- **Alignment of symbolic models with execution constraints**

  Symbolic diagnostic descriptions are transformed into sequences whose structure explicitly reflects timing behavior, access locality, and resource contention. This alignment enables direct deployment of symbolic diagnostics without the need for post hoc manual adjustment or ad hoc scheduling.

- **Unification of fault modeling and optimization**

  Classical fault abstractions are integrated with symbolic operator representations, graph-based compression techniques, and multi-criteria ranking within a single coherent optimization framework. Fault modeling and execution efficiency are therefore addressed jointly rather than in isolation.

- **Enablement of adaptive diagnostic evolution**

  The architecture supports iterative refinement driven by modeled or empirical feedback, allowing diagnostic suites to evolve in response to technology scaling, architectural change, and observed failure behavior.

Future extensions of Optimal_Test may include learning-guided symbolic test generation, feedback-driven adaptation of ranking heuristics, and runtime-selectable diagnostic modules embedded within built-in self-test environments.

These extensions do not alter the foundational role of Optimal_Test as an execution-aware optimization layer, but rather expand the sources of information used to guide its existing transformation mechanisms.

Notation Bridge Between March Algorithms and PROVER Operators

In algorithmic descriptions throughout the book, classical March notation is used (e.g., ↑, ↓, r, w) to express address traversal and data operations at a conceptual level.

Within the PROVER symbolic environment, these constructs are translated into explicit operator primitives such as $W_{(a)}$, $R_{(a)}$, $WAIT_{(n)}$, and $ASSERT_{(a,d)}$. This translation preserves the semantic intent of the original March algorithms while enabling execution-aware optimization and symbolic analysis.

12.6 Case Study: Micro-operation Synthesis of the March FD Algorithm

12.6.1 Synthesis of Micro-operations for the March FD Test

This case study provides an execution-level validation of the symbolic optimization framework introduced in the preceding sections. Using the March FD test algorithm as a concrete reference,

I demonstrate that symbolic diagnostic sequences—after refinement by Optimal_Test—admit a realizable synthesis into micro-operations suitable for parallel diagnostic hardware.

The objective of this section is not algorithmic illustration, but constructive confirmation that optimized symbolic representations can be mapped deterministically to address generators, micro-operation matrices, and synchronized execution cycles.

12.6.2 Symbolic Operator Alphabet and Traversal Blocks

Let the memory under test consist of a finite set of addressable cells indexed by $a \in A$.

The symbolic operator alphabet is defined as follows:

- $W_{(a)}$: write logic one to the cell at address a,
- $V_{(a)}$: write logic zero to the cell at address a,
- $R_{(a)}$: read access to the cell at address a.

Read operators denote access events only. Validation of read results and attribution of deviations to specific fault hypotheses are performed by the diagnostic evaluation layer and are not embedded in the operator definition.

Traversal of the address space is expressed using the symbolic traversal operator $P(\cdot)$. Each P-block denotes a complete address-space traversal under the enclosed operator sequence.

Traversal direction and boundary conditions are intrinsic attributes of the block and are not expanded into explicit loop indices. This abstraction is preserved throughout the chapter, as it forms the basis for symbolic graph construction and optimization in Optimal_Test.

12.6.3 Symbolic Representation of the March FD Algorithm

Under the symbolic traversal formalism described above, the March FD algorithm is defined by the following operator sequence:

$$\pi_{MarchFD} = \mathop{\mathbf{P}}_{a=0}^{n-1} \mathrm{V(a)} \mathop{\mathbf{P}}_{a=0}^{n-1} \mathrm{R(a)} \mathop{\mathbf{P}}_{a=0}^{n-1} (\mathrm{R(a)W(a)W(a)R(a)}) \mathop{\mathbf{P}}_{a=0}^{n-1} (\mathrm{R(a)V(a)R(a)W(a)})$$
$$\mathop{\mathbf{P}}_{a=0}^{n-1} (\mathrm{R(a)W(a)}) \mathop{\mathbf{P}}_{a=0}^{n-1} \mathrm{R(a)} \mathop{\mathbf{P}}_{a=0}^{n-1} \mathrm{R(a)} \mathop{\mathbf{P}}_{a=0}^{n-1} (\mathrm{R(a)V(a)V(a)R(a)}) \mathop{\mathbf{P}}_{a=0}^{n-1} (\mathrm{R(a)W(a)R(a)V(a)})$$
$$\mathop{\mathbf{P}}_{a=0}^{n-1} (\mathrm{R(a)V(a)}) \mathop{\mathbf{P}}_{a=0}^{n-1} \mathrm{R(a)} \mathop{\mathbf{P}}_{a=n-1}^{0} (\mathrm{R(a)W(a)W(a)R(a)}) \mathop{\mathbf{P}}_{a=0}^{n-1} \mathrm{R(a)} \mathop{\mathbf{P}}_{a=n-1}^{0} (\mathrm{R(a)V(a)V(a)R(a)}) \mathop{\mathbf{P}}_{a=0}^{n-1} \mathrm{R(a)}.$$

This formulation consists of fifteen traversal blocks. Each block represents a complete sweep of the address space executed under a fixed operator pattern. The order, repetition, and symmetry of these blocks are intrinsic to the algorithm and are preserved explicitly.

No attempt is made to compress, reorder, or normalize the sequence at this stage. The representation serves as the canonical symbolic form from which execution cost, address transition structure, and optimization legality are derived.

This explicit symbolic formulation allows the structural properties of the algorithm to be examined independently of any implementation constraints. In particular, the traversal ordering, operator dependencies, and repetition patterns can be analyzed directly within the symbolic domain. Such representation provides the basis for subsequent evaluation of execution cost and structural redundancy. These characteristics later enable systematic optimization within the Optimal_Test framework while preserving diagnostic correctness.

12.6.4 Micro-operation Granularity and Execution-Time Accounting

Execution of the symbolic algorithm on a diagnostic platform proceeds by expanding each traversal block into a sequence of micro-operations. Let the algorithm consist of s traversal blocks, and let each block generate a finite sequence of micro-operations during execution.
The total execution time is expressed as:

$$T = \sum_{i=1}^{s} \sum_{j=1}^{k_i} O_{ij} * t_c,$$

Where:

- O_{ij} – denotes the j-th micro-operation within block i,
- $j = \overline{1,k}$ – number of operations per step
- $i = \overline{1,s}$ – total number of algorithm steps
- t_c – is the memory cycle time.
- S - is the total number of traversal blocks,
- K_i - is the number of micro-operations generated by the i-th block,

This formulation assumes serialized execution and does not introduce implicit overlap or parallelism. Any reduction in execution time arises exclusively from structural modification of the operator stream or from explicitly introduced scheduling mechanisms.

12.6.5 Address Transition Structure

Each traversal block induces a deterministic address transition structure that can be represented as a directed graph

$$G = (V, E),$$

where V is the set of memory addresses augmented by an initialization state, and E is the set of directed transitions corresponding to successive address activations during traversal.

Edges are labeled by the operator executed at the destination address. The resulting graph preserves traversal direction, operator context, and block boundaries. This representation provides the formal substrate required for redundancy detection, path folding, and controlled fusion during optimization.

12.6.6 Role of the March FD Case Study in Optimal_Test

Within the Optimal_Test framework, the March FD algorithm serves as a structurally rich input instance for symbolic optimization. The preserved traversal-block structure enables the identification of repeated motifs, redundant activation paths, and mergeable operator sequences under U–Y constraints.

The case study therefore illustrates not only micro-operation synthesis but also the necessity of maintaining symbolic integrity prior to optimization. March FD is treated here as a diagnostic artifact whose structure must be respected before any execution-aware transformation is applied.

The following synthesis steps instantiate the execution constraints enforced by Optimal_Test during symbolic refinement. In particular, the correspondence between incidence matrices, address transition graphs, and parallel address generators reflects the same structural constraints used during execution-aware optimization, now instantiated at the micro-operation level.

12.6.7 Incidence Matrix Representation and Micro-operation Synthesis

The address transition structure induced by a symbolic diagnostic algorithm can be formalized as a directed graph and subsequently represented in algebraic form using an incidence matrix. This representation provides a compact and analyzable encoding of memory access ordering, address transitions, and stationary operations, and serves as an intermediate form for micro-operation synthesis and parallelization.

Let the directed graph be defined over a vertex set

$$V = \{\emptyset, 0,1, \dots, M-1\},$$

where each numeric vertex corresponds to a memory cell address and the distinguished symbol $\emptyset$ denotes the initialization state preceding the first access.

Let E denote the set of directed edges corresponding to memory access operations within a given algorithmic step. Each edge represents either a transition between two addresses or an access performed at a fixed address.

The graph is encoded by an incidence matrix $A = [ai, j]$, where rows correspond to vertices and columns correspond to edges. The elements of the matrix are defined as follows:

$$a_{i,j} = +1, if\ edge\ j\ leaves\ vertex\ i,$$
$$-1, if\ edge\ j\ enters\ vertex\ i\ or\ represents\ a\ loop\ at\ i,$$
$$0, otherwise.$$

Each column of the incidence matrix corresponds to a single memory access operation. Columns containing two nonzero entries $(+1, -1)$ encode an address transition, while columns containing a single -1 encode an access performed without a change of address. In this way, the matrix simultaneously captures traversal dynamics and operation locality.

This representation preserves the full address-transition semantics of the symbolic algorithm while enabling algebraic manipulation, structural analysis, and transformation independent of explicit address enumeration.

Multi-Valued Logic Transformations

To synthesize micro-operations for parallel algorithms, multi-valued logic transformations are applied to the incidence matrix. These transformations, implemented in the *Transfor* software package, automate micro-operation synthesis and enable the generation of parallel test programs.

As an example, the incidence matrix corresponding to the **first step of the algorithm** for an **8-bit memory array**, created within the *Transfor* workspace, is shown in **Figure 12.2**.

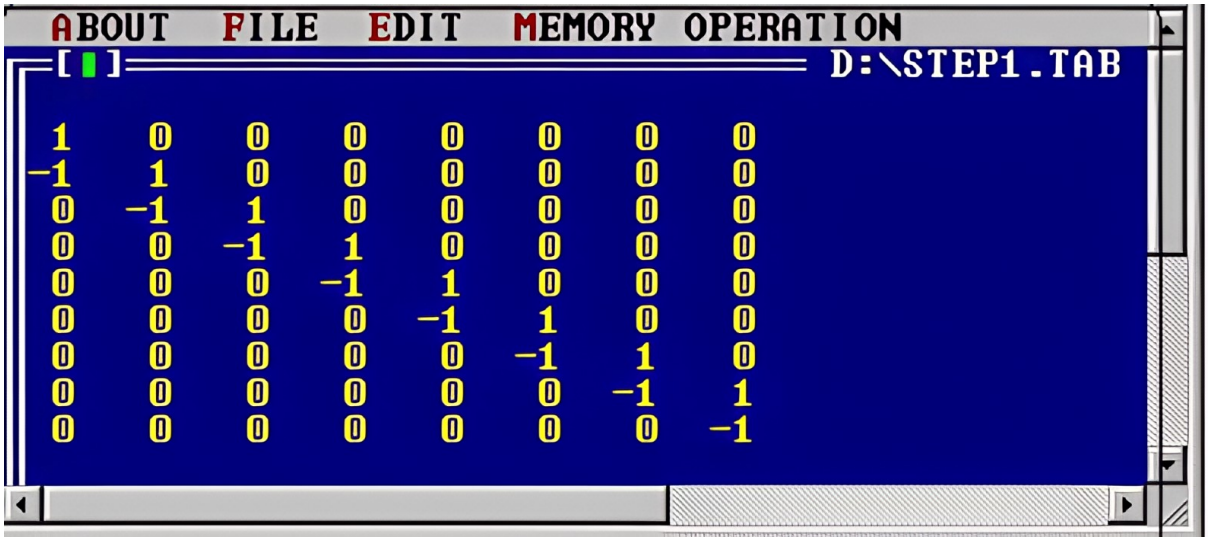

Figure 12.2—Incidence matrix for the first step

When *Transfor* is launched, the user is presented with a menu-driven interface in which operations can be selected using the **F10** key. The input to the program is the incidence matrix of the directed graph to be transformed. This matrix may be imported from an external file or entered manually using the **New** option in the **File** menu.

To perform incidence-matrix transformations, the following steps are executed:

- Activate the **Memory Operation** command.
- Define the dimensions of the matrix.
- Specify the number of partitions into which the algorithm is to be parallelized.

After these parameters are specified, the program generates a set of new matrices that represent the synthesized micro-operations.

Resulting Matrices for Step 1

For the first step of the March FD algorithm, the incidence-matrix transformation yields a set of matrices M_0–M_3. These matrices correspond to the micro-operations required for modifying address codes during this step.

The matrices are designed for execution on a tester equipped with **four independent address generators**, enabling the simultaneous formation of diagnostic stimuli for **four consecutive cycles**. This form of parallelization reduces overall execution time and demonstrates how incidence-matrix transformations can be used to synthesize efficient test programs for multiprocessor diagnostic systems.

$$M_0 = \begin{bmatrix} 1 & 0 \\ -1 & 1 \\ 0 & 0 \\ 0 & 0 \\ 0 & 0 \\ 0 & -1 \\ 0 & 0 \\ 0 & 0 \\ 0 & 0 \end{bmatrix}; \; M_1 = \begin{bmatrix} 1 & 0 \\ 0 & 0 \\ -1 & 1 \\ 0 & 0 \\ 0 & 0 \\ 0 & 0 \\ 0 & -1 \\ 0 & 0 \\ 0 & 0 \end{bmatrix}; \; M_2 = \begin{bmatrix} 1 & 0 \\ 0 & 0 \\ 0 & 0 \\ -1 & 1 \\ 0 & 0 \\ 0 & 0 \\ 0 & 0 \\ 0 & -1 \\ 0 & 0 \end{bmatrix}; \; M_3 = \begin{bmatrix} 1 & 0 \\ 0 & 0 \\ 0 & 0 \\ 0 & 0 \\ -1 & 1 \\ 0 & 0 \\ 0 & 0 \\ 0 & 0 \\ 0 & -1 \end{bmatrix}.$$

Figure 12.3—Resulting micro-operation matrices for Step 1

Analysis of the Resulting Matrices

Analysis of the resulting matrices reveals the following behavior of the parallel address generators:

- The first address generator accesses memory cell $a = 0$.
- The second address generator accesses memory cell $a = 1$.
- The third address generator accesses memory cell $a = 2$.
- The fourth address generator accesses memory cell $a = 3$.

Subsequently, the address codes are incremented by four, with each generator continuing its sequence independently until the fourth generator reaches the final memory cell. This parallelized mapping illustrates how the incidence-matrix method distributes address access among multiple generators while preserving synchronization during diagnostic execution.

Results for Step 2

For the second step of the March FD algorithm, analogous incidence matrices are obtained. The only difference is that write operations are replaced by read operations. This reflects the symmetric structure of the algorithm while maintaining the same parallelized address-generation scheme.

Address Transition Graph for Step 2

The operations of the second step are represented by the address transition graph shown in **Figure 12.4**. This graph illustrates the transitions between memory addresses during read and write operations and provides a visual representation of access sequences that complements the incidence-matrix formalism.

This graphical representation provides an intuitive interpretation of the traversal behavior generated by the parallel address generators. By visualizing address transitions explicitly, the graph highlights the regular stride patterns and synchronization points inherent in the algorithm. Such visualization aids in verifying the correctness of the parallel execution scheme and confirming that no address conflicts or unintended overlaps occur during traversal. Consequently, the transition graph complements the matrix-based representation by offering a structural perspective on the diagnostic execution process.

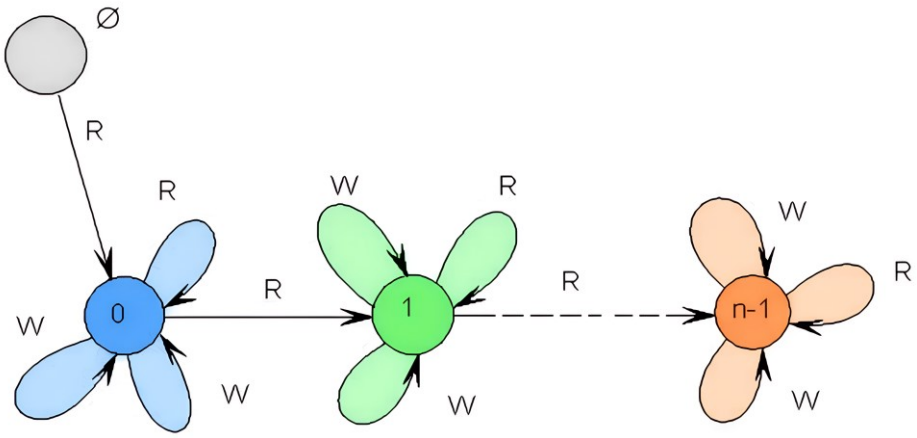

Figure 12.4—Address transition graph for the second step of the algorithm

Figure 12.4 shows the address transition graph corresponding to the **second step** of the March FD algorithm. The graph represents transitions between memory cell addresses during the execution of read and write operations. Each vertex corresponds to a memory address, while directed edges denote successive address activations induced by the operator sequence.

The initialization state is represented by the symbol $\emptyset$. Transitions labeled R and W indicate read and write operations performed during traversal. The graph provides a structural visualization of the access order and complements the algebraic incidence-matrix representation used for micro-operation synthesis.

Step 3 Observations

For an **8-bit memory**, the **third step** of the algorithm is represented by the incidence matrix M_{st3}:

$$M_{st3} = \begin{bmatrix}
1 & 0 & 0 & 0 & 0 & 0 & 0 & 0 & 0 & 0 & 0 & 0 & 0 & 0 & 0 & 0 & 0 & 0 & 0 & 0 & 0 & 0 & 0 & 0 & 0 & 0 & 0 & 0 & 0 & 0 & 0 & 0 \\
-1 & -1 & -1 & -1 & 1 & 0 & 0 & 0 & 0 & 0 & 0 & 0 & 0 & 0 & 0 & 0 & 0 & 0 & 0 & 0 & 0 & 0 & 0 & 0 & 0 & 0 & 0 & 0 & 0 & 0 & 0 & 0 \\
0 & 0 & 0 & 0 & -1 & -1 & -1 & -1 & 1 & 0 & 0 & 0 & 0 & 0 & 0 & 0 & 0 & 0 & 0 & 0 & 0 & 0 & 0 & 0 & 0 & 0 & 0 & 0 & 0 & 0 & 0 & 0 \\
0 & 0 & 0 & 0 & 0 & 0 & 0 & 0 & -1 & -1 & -1 & -1 & 1 & 0 & 0 & 0 & 0 & 0 & 0 & 0 & 0 & 0 & 0 & 0 & 0 & 0 & 0 & 0 & 0 & 0 & 0 & 0 \\
0 & 0 & 0 & 0 & 0 & 0 & 0 & 0 & 0 & 0 & 0 & 0 & -1 & -1 & -1 & -1 & 1 & 0 & 0 & 0 & 0 & 0 & 0 & 0 & 0 & 0 & 0 & 0 & 0 & 0 & 0 & 0 \\
0 & 0 & 0 & 0 & 0 & 0 & 0 & 0 & 0 & 0 & 0 & 0 & 0 & 0 & 0 & 0 & -1 & -1 & -1 & -1 & 1 & 0 & 0 & 0 & 0 & 0 & 0 & 0 & 0 & 0 & 0 & 0 \\
0 & 0 & 0 & 0 & 0 & 0 & 0 & 0 & 0 & 0 & 0 & 0 & 0 & 0 & 0 & 0 & 0 & 0 & 0 & 0 & -1 & -1 & -1 & -1 & 1 & 0 & 0 & 0 & 0 & 0 & 0 & 0 \\
0 & 0 & 0 & 0 & 0 & 0 & 0 & 0 & 0 & 0 & 0 & 0 & 0 & 0 & 0 & 0 & 0 & 0 & 0 & 0 & 0 & 0 & 0 & 0 & -1 & -1 & -1 & -1 & 1 & 0 & 0 & 0 \\
0 & 0 & 0 & 0 & 0 & 0 & 0 & 0 & 0 & 0 & 0 & 0 & 0 & 0 & 0 & 0 & 0 & 0 & 0 & 0 & 0 & 0 & 0 & 0 & 0 & 0 & 0 & 0 & -1 & -1 & -1 & -1
\end{bmatrix}.$$

The matrix encodes the address-transition structure induced by the third step of the March FD algorithm. Rows correspond to vertices of the address-transition graph, while columns correspond to memory access operations. Nonzero entries indicate entry to or exit from a vertex, in accordance with the incidence-matrix definition introduced earlier.

This representation preserves the full transition semantics of the algorithm step and serves as the input artifact for subsequent matrix transformations and parallel micro-operation synthesis. After transforming the incidence matrix of the third step using *Transfor*, a set of **four identical matrices** is obtained. These matrices correspond to the micro-operations executed by the **four address generators** during the third step of the algorithm.

$$M_0^{st3} = M_1^{st3} = M_2^{st3} = M_3^{st3} = \begin{bmatrix}
1 & 0 & 0 & 0 & 0 & 0 & 0 & 0 \\
-1 & 1 & 0 & 0 & 0 & 0 & 0 & 0 \\
0 & -1 & 1 & 0 & 0 & 0 & 0 & 0 \\
0 & 0 & -1 & 1 & 0 & 0 & 0 & 0 \\
0 & 0 & 0 & -1 & 1 & 0 & 0 & 0 \\
0 & 0 & 0 & 0 & -1 & 1 & 0 & 0 \\
0 & 0 & 0 & 0 & 0 & -1 & 1 & 0 \\
0 & 0 & 0 & 0 & 0 & 0 & -1 & 1 \\
0 & 0 & 0 & 0 & 0 & 0 & 0 & -1
\end{bmatrix}.$$

This result indicates that all four address generators operate identically, each accessing the same memory cells in parallel. After every four memory access cycles, the address code is incremented by one.

A similar matrix structure and execution pattern are observed for **steps 4, 8, and 9** of the March FD algorithm. These steps follow the same principle of synchronized access and incremental addressing. This result indicates that all four address generators operate identically, each addressing the same memory cells in parallel. After every **four memory access cycles**, the address code increments by one.

A similar structure and execution pattern apply to **steps 4, 8, and 9** of the March FD algorithm, which follow the same principle of synchronized access and incremental addressing.

Step 5 Observations

In the **fifth step**, each memory cell is accessed **twice**:

1. A **read** operation retrieves the stored value.
2. A **write** operation stores a logic '1' into the same cell.

For an **8-bit memory**, the incidence matrix corresponding to **Step 5** is shown below. The matrix represents the address-transition structure associated with the paired read–write operations executed at each memory location during this step.

$$M_{st5} = \begin{bmatrix} 1&0&0&0&0&0&0&0&0&0&0&0&0&0&0&0&0 \\ -1&-1&1&0&0&0&0&0&0&0&0&0&0&0&0&0&0 \\ 0&0&-1&-1&1&0&0&0&0&0&0&0&0&0&0&0&0 \\ 0&0&0&0&-1&-1&1&0&0&0&0&0&0&0&0&0&0 \\ 0&0&0&0&0&0&-1&-1&1&0&0&0&0&0&0&0&0 \\ 0&0&0&0&0&0&0&0&-1&-1&1&0&0&0&0&0&0 \\ 0&0&0&0&0&0&0&0&0&0&-1&-1&1&0&0&0&0 \\ 0&0&0&0&0&0&0&0&0&0&0&0&-1&-1&1&0&0 \\ 0&0&0&0&0&0&0&0&0&0&0&0&0&0&-1&-1&1 \\ 0&0&0&0&0&0&0&0&0&0&0&0&0&0&0&-1&-1 \end{bmatrix}.$$

When the incidence matrix of **Step 5** is processed using *Transfor*, a set of **four matrices** is generated. These matrices represent the micro-operations executed by the address generators during this step of the algorithm.

$$M_0^{st5} = M_1^{st5} = \begin{bmatrix} 1&0&0&0 \\ -1&1&0&0 \\ 0&0&0&0 \\ 0&-1&1&0 \\ 0&0&0&0 \\ 0&0&-1&1 \\ 0&0&0&0 \\ 0&0&0&-1 \\ 0&0&0&0 \end{bmatrix}; \quad M_2^{st5} = M_3^{st5} = \begin{bmatrix} 1&0&0&0 \\ 0&0&0&0 \\ -1&1&0&0 \\ 0&0&0&0 \\ 0&-1&1&0 \\ 0&0&0&0 \\ 0&0&-1&1 \\ 0&0&0&0 \\ 0&0&0&-1 \end{bmatrix}.$$

Analysis of the resulting matrices reveals the following execution pattern:

- Address generators **0 and 1** access the **even-addressed** memory cells.
- Address generators **2 and 3** access the **odd-addressed** memory cells.

To realize this access pattern, the address codes are incremented by **two** rather than one, ensuring complete and non-overlapping coverage of both even and odd address spaces.

This parallelized distribution demonstrates how incidence-matrix transformation automatically partitions the address space across multiple generators, maintaining execution efficiency while respecting the operational constraints of the algorithm.

A similar execution structure is observed in **Step 10** of the March FD algorithm. In that step, each memory cell is again accessed twice—via a read followed by a write—and the address space is partitioned in the same even–odd manner across the address generators.

Patterns in Other Steps

Analysis of the March FD algorithm reveals repeating structures in address-transition behavior across multiple steps.

Steps 6, 7, 11, 13, and 15

The address transitions in these steps correspond directly to those observed in **Step 1**. Consequently, the same micro-operation synthesis procedure can be applied, and the resulting incidence matrices exhibit the same structural form.

Steps 12 and 14

In these steps, the address code **decreases** when accessing adjacent memory cells. This requires modifications during micro-operation synthesis to account for **descending address traversal**.

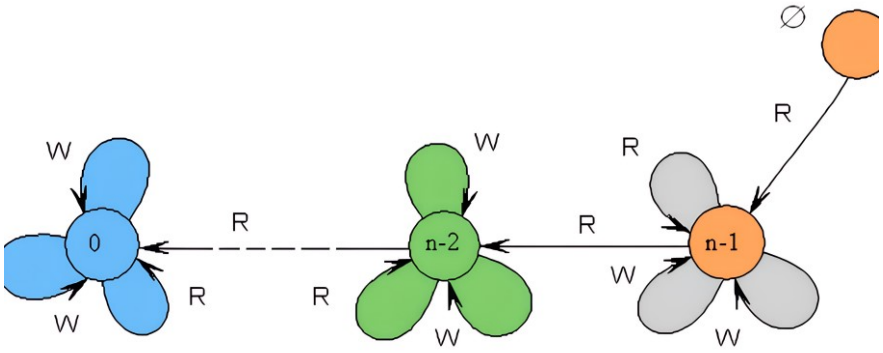

Figure 12.5—Address transition graph for the 12th step of the algorithm$m$

The address transition graph shown in **Figure 12.5** illustrates the reverse traversal during **Step 12**, in which memory cells are accessed in descending order from the highest address $(M-1)$ toward the lowest address (0). Both **read (R)** and **write (W)** operations are executed during this traversal.

These steps ensure **bidirectional traversal** of the memory array, strengthening diagnostic coverage against faults that manifest asymmetrically depending on address order.

Step 12 Observations

The incidence matrix M_{st12} for **Step 12** of the March FD algorithm is obtained from the **Step 3** incidence matrix M_{st3} by applying the following sequence of row permutations

$$S2 \Leftrightarrow S9, S3 \Leftrightarrow S8, S4 \Leftrightarrow S7, S5 \Leftrightarrow S6.$$

This transformation reverses the traversal order, ensuring that memory cells are accessed from the **highest address** $(n-1)$ down to the **lowest address** (0). The resulting descending access sequence corresponds to the address transition graph shown in **Figure 12.5**.

After processing the transformed matrix in *Transfor*, the resulting incidence matrices for **Step 12** are **identical across all four address generators**:

$$M_0^{st12} = M_1^{st12} = M_2^{st12} = M_3^{st12} = \begin{bmatrix} 1\ 0\ 0\ 0\ 0\ 0\ 0\ 0 \\ 0\ 0\ 0\ 0\ 0\ 0\ 0\ -1 \\ 0\ 0\ 0\ 0\ 0\ 0\ -1\ 1 \\ 0\ 0\ 0\ 0\ 0\ -1\ 1\ 0 \\ 0\ 0\ 0\ 0\ -1\ 1\ 0\ 0 \\ 0\ 0\ 0\ -1\ 1\ 0\ 0\ 0 \\ 0\ 0\ -1\ 1\ 0\ 0\ 0\ 0 \\ 0\ -1\ 1\ 0\ 0\ 0\ 0\ 0 \\ -1\ 1\ 0\ 0\ 0\ 0\ 0\ 0 \end{bmatrix}.$$

The identical nature of the resulting matrices demonstrates that all four address generators execute the same sequence of micro-operations in parallel. This guarantees a synchronized descending traversal across the memory array, complementing the ascending traversal sequences executed in earlier steps and ensuring full bidirectional diagnostic coverage.

Step 14 Observations

The same set of address transitions represented in the matrices for Step 12 must also be executed during the fourteenth step of the March FD algorithm. As in Step 12, Step 14 requires a descending traversal of adjacent memory cells, combining read and write operations in reverse order relative to their ascending counterparts.

Thus, Steps 3 and 12, as well as Steps 5 and 10, form symmetric ascending–descending pairs. This structural symmetry ensures that the March FD algorithm achieves bidirectional coverage across the memory address space. Such symmetry is critical for detecting direction-sensitive faults, including address decoder defects and specific subclasses of coupling faults.

12.6.8 Synthesis of the U–Y Scheme for the March FD Test Algorithm

To formalize the base conditions and operators executed during diagnostic testing of high-speed memory devices, U–Y schemes are employed. A U–Y scheme is defined as a six-element tuple:

$$(S, E, C, O, S_o, S_f)$$

Where:

- S – the set of states of the scheme
- E – the set of transitions
- C – the set of base conditions
- O – the set of base operations
- S_o – the initial state of the scheme
- S_f – the final state of the scheme

Each transition in the set E is represented by a quadruple: (s, c, o, s')

Where:

- S – is the initial state of the scheme
- C – is a base condition
- O – is a base operation
- S' – is the resulting state.

This quadruple is written in the form:

$$s \xrightarrow{c/o} s'$$

where c and o denote the vectorized forms of the base condition and operation sets, corresponding to U and Q, respectively.

This transition is interpreted as follows: if condition c is satisfied, the scheme transitions from state s to state s', executing operation o during the transition.

In the vector formulation, the scalar transition label c/o is generalized to a vector predicate–micro-operation pair U/Q.

Vector Form for Multiprocessor Diagnostic Devices

For multiprocessor diagnostic devices, the U–Y scheme representation is extended into a vector form, allowing parallel specification of operations across multiple diagnostic generators.

In this formulation, the state of the scheme is described by two components:

$$s \xrightarrow{U/Q} s'$$

Where:

- U: is a vector predicate representing the set of base conditions valid at the current time instance,
- Q: is a matrix of micro-operations executed concurrently by the diagnostic generators, including operation codes, address generation, and data handling.

This vector representation enables explicit modeling of parallel execution in the March FD algorithm, ensuring deterministic synchronization and well-defined concurrency across all diagnostic processors.

Memory Size Definition

The size of the memory under diagnosis is determined by the contents of the start address registers GX, GY and the end address registers NX, NY. Typically, the initial values are set as:

$$GX = GY = 0$$

For a square memory configuration, the terminal values are defined as:

$$NX = NY = n - 1$$

where n denotes the capacity of the memory device under test.

Thus, the address space spans $(NX - GX + 1) \times (NY - GY + 1) = n^2$ cells.

Base Conditions for Transitions

The base conditions governing transitions in the U–Y scheme are derived by comparing the current address coordinates X, Y with the register values GX, GY, NX, NY. These comparisons yield:

$$X \neq NX, \quad Y \neq NY$$
$$X \neq GX, \quad Y \neq GY$$

Combined transition conditions are expressed as:

$$(X \neq NX) \vee (Y \neq NY)$$
$$(X \neq GX) \vee (Y \neq GY)$$

Address Increment and Decrement Logic

For steps **1–11, 13, and 15** of the March FD algorithm, memory testing is performed using incrementing adjacent addresses. The cyclic execution of operations in these steps is controlled by the transition condition:

$$(X \neq NX) \vee (Y \neq NY)$$

In contrast, for **steps 12 and 14**, memory access proceeds in reverse order using decrementing address sequences. In these cases, execution is governed by the condition:

$$(X \neq GX) \vee (Y \neq GY)$$

Micro-operation Matrix Representation

For each step of the algorithm, the corresponding set of micro-operations is represented in matrix form:

$$Q = [Q_{work} \mid Q_x \mid Q_y \mid Q_t]$$

Where:

- Q_{work} – contains working micro-operations such as write (W), read (R), and compare (A) operations,
- Q_x – contains micro-operations for generating address codes along the X coordinate,
- Q_y – contains micro-operations for generating address codes along the Y coordinate,
- Q_t – contains micro-operations associated with data transformations.

For output and reference data generation, the micro-operations may include loading initial values into registers T_0-T_3 and applying inversion operations, for example:

$$T_0 = \neg T_0$$

Address Code Generation Micro-operations

Address code generation is defined by micro-operations of the form:

$$X_i := X_i \pm C, Y_i := X_i \pm C$$

where $C \in \{1,2,3, \ldots ,15\}$ denotes the **generator number**.

When concatenating the address vectors X and Y, additional micro-operations are applied to propagate address changes between coordinates:

$$Y_i := Y_i + 1^*, \quad Y_i := Y_i - 1^*$$

The superscript * denotes a **carry-over or borrow operation** propagated from coordinate X to coordinate Y.

Step-Specific Transformations

Steps 1, 2, 6, 7, 11, 13, and 15

For these steps of the March FD algorithm, the address codes X and Y for each subsequent diagnostic cycle (t+1)(t+1)(t+1) are generated using **type-1 increment vectors**. The increment operation is applied independently to each address generator.
Let

$$\mathbf{X}_{t+1}^{st1} = \mathbf{X}_t + \mathbf{I}_x^{1T} = \begin{bmatrix} x_0 \\ x_1 \\ x_2 \\ x_3 \end{bmatrix} + \begin{bmatrix} 4 \\ 4 \\ 4 \\ 4 \end{bmatrix} = \begin{bmatrix} x_0 + 4 \\ x_1 + 4 \\ x_2 + 4 \\ x_3 + 4 \end{bmatrix},$$

where $\mathbf{I}_x^{1T}$ denote a **type-1 increment vector** for coordinate X.

Steps 3, 4, 8, and 9

These steps are executed using address transformations governed by the corresponding increment rules for adjacent memory traversal. During these steps, address codes are advanced in a controlled and deterministic manner, ensuring sequential progression across the memory array while preserving synchronization among parallel address generators.

The applied transformations maintain uniform stride and do not introduce partitioning of the address space.

Steps 5 and 10

In these steps, specialized transformation rules are applied to enforce structural symmetry with earlier ascending address traversals while enabling multiple accesses per memory cell. Each cell is addressed twice within a single traversal block, resulting in paired read–write operations.

To support this behavior without introducing overlap or omission, the address space is partitioned implicitly through modified increment rules, enabling coverage of address-sensitive fault classes while preserving deterministic execution order.

$$\mathbf{X}_{t+1}^{st5} = \mathbf{X}_t + \mathbf{I}_x^{3T} = \begin{bmatrix} x_0 \\ x_1 \\ x_2 \\ x_3 \end{bmatrix} + \begin{bmatrix} 2 \\ 2 \\ 2 \\ 2 \end{bmatrix} = \begin{bmatrix} x_0 + 2 \\ x_1 + 2 \\ x_2 + 2 \\ x_3 + 2 \end{bmatrix}.$$

Steps 12 and 14

These steps employ decremental address transformations, enabling reverse traversal of the memory array. Address codes are generated in descending order, mirroring the structure of earlier ascending traversals. This bidirectional execution is essential for detecting faults whose manifestation depends on access direction, including address decoder defects and asymmetric coupling mechanisms

$$\mathbf{X}_{t+1}^{st12} = \mathbf{X}_t + \mathbf{I}_x^{4T} = \begin{bmatrix} x_0 \\ x_1 \\ x_2 \\ x_3 \end{bmatrix} - \begin{bmatrix} 1 \\ 1 \\ 1 \\ 1 \end{bmatrix} = \begin{bmatrix} x_0 - 1 \\ x_1 - 1 \\ x_2 - 1 \\ x_3 - 1 \end{bmatrix}.$$

For all steps **except** Steps 12 and 14, the address code for coordinate Y is generated using **type-1 increment vectors**. A type-1 increment vector for coordinate Y defines address progression along the vertical dimension of the memory array and operates in conjunction with the address generation rules for coordinate X.

The symbol "*" denotes conditional propagation of an increment from coordinate X to coordinate Y. Specifically, the address code of coordinate Y is incremented only when a carry is generated during the update of coordinate X. This mechanism ensures correct traversal of two-dimensional address spaces without explicit nested loop constructs.

$$\mathbf{Y}_{t+1}^{st1} = \mathbf{Y}_t + \mathbf{I}_y^{1T} = \begin{bmatrix} y_0 \\ y_1 \\ y_2 \\ y_3 \end{bmatrix} + \begin{bmatrix} 1 \\ 1 \\ 1 \\ 1 \end{bmatrix}^* = \begin{bmatrix} y_0 + 1 \\ y_1 + 1 \\ y_2 + 1 \\ y_3 + 1 \end{bmatrix}^*,$$

Let $\mathbf{I}_y^{1T}$ denote a type-1 increment vector for coordinate Y.

The **U–Y scheme representation** of the March FD test algorithm is shown in **Figure 12.6**, which encodes these address transformation rules through guarded state transitions and associated micro-operation vectors.

In **Steps 12 and 14**, reverse traversal is implemented through **decremental transformations**. In this case, subtraction is applied to the address code of coordinate Y only if a borrow propagates from the decrement of coordinate X.

$$\mathbf{Y}_{t+1}^{st12} = \mathbf{Y}_t + \mathbf{I}_y^{2\tau} = \begin{bmatrix} y_0 \\ y_1 \\ y_2 \\ y_3 \end{bmatrix} - \begin{bmatrix} 1 \\ 1 \\ 1 \\ 1 \end{bmatrix}^* = \begin{bmatrix} y_0 - 1 \\ y_1 - 1 \\ y_2 - 1 \\ y_3 - 1 \end{bmatrix}^* .$$

The symbol "*" therefore denotes conditional subtraction of the Y-coordinate address based on borrow propagation, ensuring correct synchronization of descending address sequences across both coordinates.

The use of decremental transformations in these steps ensures that the symbolic traversal model fully captures the bidirectional nature of practical memory test execution. In real diagnostic environments, address sequences are rarely restricted to a single directional sweep of the memory array.

Instead, alternating ascending and descending traversals are frequently employed to expose directional sensitivities in the physical implementation of memory circuits. Certain classes of defects—particularly those related to address decoder asymmetries, line coupling, or timing skew—may only become observable when memory cells are accessed in the reverse order relative to previous operations.

Within the U–Y scheme formalism, this behavior is represented by explicitly modeling borrow propagation between address coordinates. When the decrement of coordinate XXX generates a borrow condition, the corresponding decrement is propagated to coordinate YYY, ensuring that the two-dimensional address space is traversed consistently across row and column boundaries.

This mechanism mirrors the arithmetic behavior of conventional address counters but is expressed symbolically through guarded state transitions.

As a result, the symbolic representation preserves the structural properties of the March FD algorithm while allowing its address-generation behavior to be analyzed independently of specific hardware implementations.

This abstraction is particularly useful for subsequent optimization stages, where traversal order, state transitions, and operator dependencies must be examined without altering the diagnostic semantics of the original test algorithm.

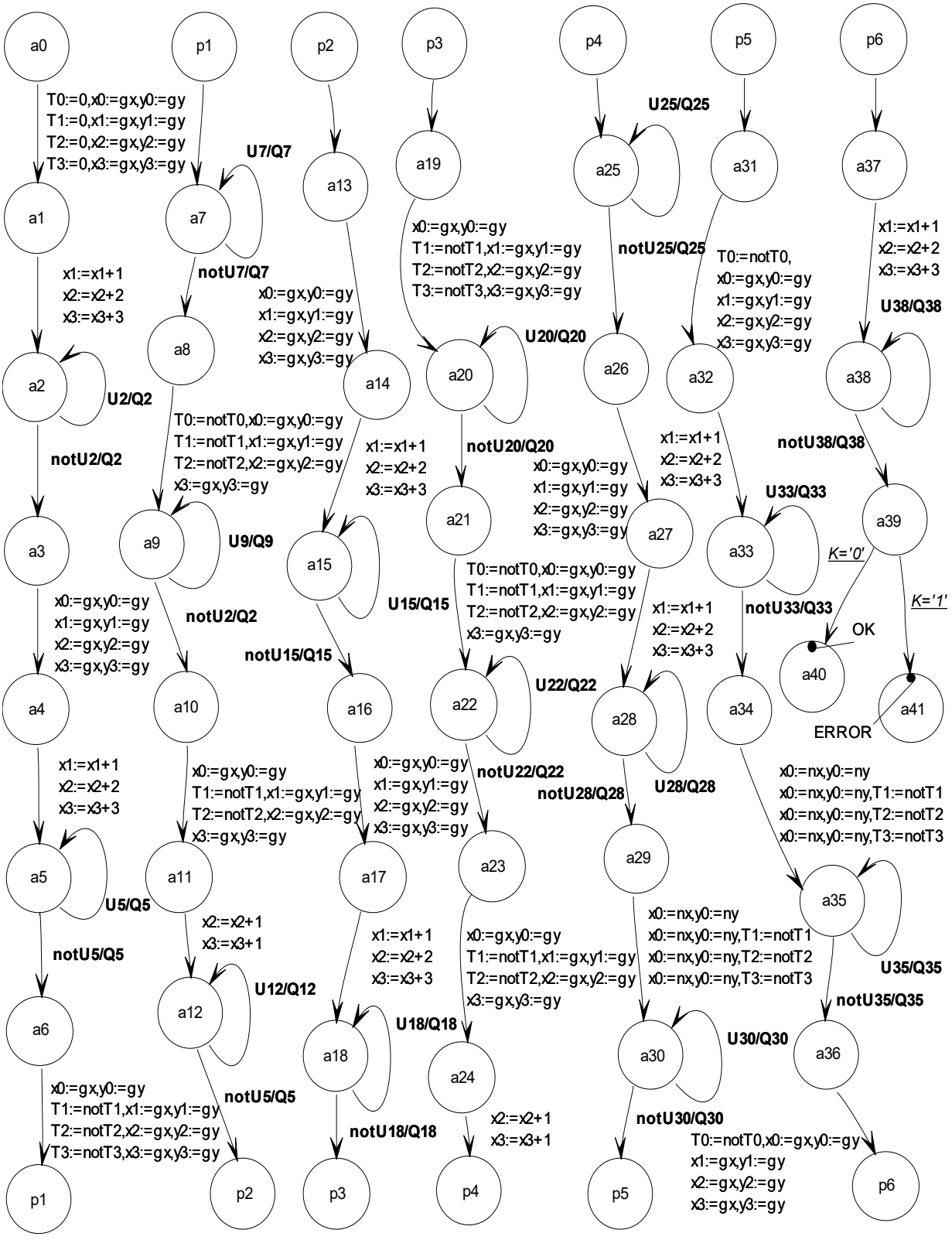

Figure 12.6—U–Y scheme of the March FD test algorithm

The complete **U–Y scheme** of the March FD test algorithm is shown in Figure 12.6. The diagram provides a formal state–transition representation of diagnostic execution, explicitly

encoding base conditions, micro-operations, and control flow within a multiprocessor diagnostic architecture.

Each node a_i represents a discrete control state of the diagnostic process. Directed arcs correspond to transitions governed by Boolean predicates from the set U and are annotated with the associated micro-operation vectors Q.

These vectors specify, for each diagnostic cycle, the concurrent actions applied to address generators, data generators, and comparison logic.

The structure of the scheme reflects the inherent parallelism of the diagnostic device:

- **Initial states** $a0, a1$ define register initialization, background data loading, and starting address configuration.
- **Intermediate states** $a2$ through $a38$ encode address progression, write and read operations, data inversion, and conditional branching associated with fault detection.
- **Terminal states** $a40$ and $a41$ represent normal completion ("OK") and fault detection ("ERROR"), respectively, determined by comparison outcomes between observed and reference data.

This U–Y representation provides a formally verifiable execution model of the March FD algorithm. By unifying address traversal, data manipulation, and error detection within a single state-based framework, it enables deterministic analysis of execution order, parallel synchronization, and coverage completeness.

The scheme also supports parameterized adaptation to different memory sizes and diagnostic architectures without altering the underlying control semantics.

While the March FD algorithm is used to demonstrate incidence-matrix–based synthesis and bidirectional traversal symmetry, the March A algorithm is introduced here to address a complementary synthesis challenge: mapping operator sequences to multiprocessor diagnostic devices when the number of operational processors exceeds the number of distinct operators. Together, the two algorithms exercise distinct constraints of the U–Y synthesis framework.

12.6.9 Synthesis of the U–Y Scheme for the March A Test Algorithm

Execution of the March A test algorithm begins with an explicit initialization phase, during which all memory cells are written with a uniform background value of zero. Within the U–Y scheme framework, this initialization corresponds to a sequence of control states responsible for configuring address generators, data generators, and reference registers prior to traversal.

All address generators associated with coordinates X and Y are initialized to their starting values, providing access to the memory cell identified by the initial coordinates (g_x, g_y). Concurrently, the data generators are configured to produce the logic value zero, establishing the required background state for subsequent diagnostic operations.

Following initialization, the address generators are offset relative to the initial cell. Specifically, all generators except the first are assigned address offsets of 1, 2, 3, and higher increments, depending on the number of available generators. This configuration enables parallel access to

distinct memory locations during each diagnostic cycle and establishes a deterministic traversal pattern across the memory address space.

During each diagnostic cycle, working micro-operations—such as write, read, or compare—are executed synchronously across all operational processors.

At the same time, address and data code vectors for the subsequent cycle are generated in advance.

This pipelined execution model is inherent to the U–Y scheme representation and ensures that address generation, data preparation, and operation execution proceed without idle phases or control hazards.

Operator Sequence Formation

According to the March A test algorithm, the operator sequence

$$R(x,y),\ W(x,y),\ V(x,y),\ W(x,y)$$

can be efficiently executed using four operational processors (OPs). Each processor is assigned one element of the sequence, enabling parallel application of the test operations across the memory array.

For a square memory array of size $n \times n$, this operator sequence can be generalized as:

$$\forall x_i, \forall y_i, i = \overline{0, \sqrt{n}-1}\ C_0 = R(x_i, y_i), C_1 = W(x_i, y_i), C_2 = V(x_i, y_i), C_3 = W(x_i, y_i).$$

This formulation defines the four operations—read, write-one, write-zero, and write-one—executed at each memory address.

For a square configuration, the sequence forms a structured set of operation codes distributed across the four operational processors, ensuring both complete address coverage and parallel execution efficiency.

Cyclic Sequences and Processor Mapping

In subsequent steps of the March A algorithm, the operator set is reduced to three functions:

$$R(x,y), V(x,y), W(x,y)$$

When the number of operational processors exceeds the number of available operators ($k > 3$), a direct one-to-one assignment is no longer possible, as it would result in one or more processors remaining idle, thereby reducing execution efficiency.

To ensure full utilization of four operational processors without introducing idle cycles, the test program is restructured.

The operators are distributed across processors in a cyclic manner, producing three distinct chains of test stimuli.

These chains are executed repeatedly under controlled address progression, preserving both execution efficiency and the logical correctness of the diagnostic process.

Operator Mapping and Cyclic Execution

The mapping of operators to processors is shown in Table 12.1.

Table 12.1—Operator Sequence Mapping for Operational Processors

Processor No.	Test Stimuli Chain No. 1	Chain No. 2	Chain No. 3
1	$R_{(0,y)}$	$V_{(1,y)}$	$W_{(2,y)}$
2	$V_{(0,y)}$	$W_{(1,y)}$	$R_{(3,y)}$
3	$W_{(0,y)}$	$R_{(2,y)}$	$V_{(3,y)}$
4	$R_{(1,y)}$	$V_{(2,y)}$	$W_{(3,y)}$

This cyclic distribution ensures that all four operational processors remain active throughout execution, with no idle phases, while preserving the logical sequencing constraints of the March A algorithm

Cyclic Execution and Repetition Count

By cyclically repeating the twelve operators defined by the three stimulus chains and updating the address and data codes according to Table 12.2, all memory cells of the device under test are accessed systematically.

The cyclic reassignment guarantees that, over one complete repetition group, each processor advances to a distinct address without overlap, ensuring complete and non-redundant coverage of the memory array.

The required number of repetition cycles is determined by:

$$P = \frac{3n}{Kz}$$

where:

- n – is the capacity of the memory array,
- K – the number of operational processors,
- z – the number of operator chains in the test program (with $z = 3$ in this case).

Repetition of the test program fragment is implemented using a general-purpose register for cycle counting and control. This approach enables compact program representation while guaranteeing deterministic traversal of the entire address space.

Reverse Address Scanning

When memory cells are scanned in reverse order, the operator sequence

$$R(x,y), V(x,y), W(x,y), V(x,y)$$

is executed with decreasing address codes, defined by the decremental expressions:

$$X_i := X_i - 1, \quad Y_i := Y_i - 1^*$$

The symbol "*" indicates that the decrement of coordinate $\boldsymbol{Y}$ is applied only if a borrow is propagated from coordinate $\boldsymbol{X}$. This mechanism preserves correct address ordering during

descending traversal, maintains synchronization across processors, and ensures symmetry with ascending execution phases.

As a result, the March A algorithm retains full sensitivity to direction-dependent fault mechanisms.

Table 12.2—Sequence of test operators

Processor No.	Test Stimuli Chain 1	Chain 2	Chain 3
0	$x_{(s+1)}=x_{(s)+1}$ $t_{(s+1)}=$NOT $t_{(s)}$	$x_{(s+1)}=x_{(s)+1}$ $t_{(s+1)}=$NOT $t_{(s)}$	$x_{(s+1)}=x_{(s)+2}$
1	$x_{(s+1)}=x_{(s)+1}$ $t_{(s+1)}=$NOT $t_{(s)}$	$x_{(s+1)}=x_{(s)+2}$	$x_{(s+1)}=x_{(s)+1}$ $t_{(s+1)}=$NOT $t_{(s)}$
2	$x_{(s+1)}=x_{(s)+2}$ $t_{(s+1)}=$NOT $t_{(s)}$	$x_{(s+1)}=x_{(s)+1}$ $t_{(s+1)}=$NOT $t_{(s)}$	$x_{(s+1)}=x_{(s)+1}$
3	$x_{(s+1)}=x_{(s)+1}$ $t_{(s+1)}=$NOT $t_{(s)}$	$x_{(s+1)}=x_{(s)+1}$ $t_{(s+1)}=$NOT $t_{(s)}$	$x_{(s+1)}=x_{(s)+2}$

The above operators are distributed across the four operational processors to ensure parallel execution. At the start of this phase, all address code generators are initialized with the terminal address values corresponding to the bounds of the memory array:

$$\forall i \in \{0,1,2,3\}: Xi(S) := nx, Yi(S) := ny$$

where n_x and n_y denote the maximum address coordinates of the memory under test along the horizontal and vertical dimensions, respectively. This initialization establishes a consistent starting point for reverse traversal and guarantees that all processors begin execution at the same boundary condition.

During execution, address codes are updated according to the decremental transformation rules defined earlier. The decrement of coordinate Y is conditionally triggered by a borrow propagated from coordinate X, ensuring correct multidimensional address sequencing and preventing address underflow.

This mechanism preserves strict ordering of memory accesses during reverse scanning while maintaining synchronization across all operational processors.
For the first and third data generators, data inversion is applied during each subsequent diagnostic step according to the relations:

$$t_1(s+1) := \neg t_1(s), \quad t_3(s+1) := \neg t_3(s).$$

The second and fourth data generators retain their current data values unless explicitly modified by a working micro-operation. This asymmetric inversion policy is intentional: it introduces controlled data pattern alternation across parallel execution streams, thereby increasing sensitivity to coupling faults, inversion-dependent faults, and pattern-interaction effects that would otherwise remain latent under uniform data evolution.

At each diagnostic cycle, read operations are followed by comparison against the corresponding reference values stored in the data registers. Any mismatch between the

observed and expected values results in the activation of the error signaling path within the U–Y scheme. Upon detection of an error condition, execution transitions immediately to the terminal failure state, and the diagnostic monitor reports a fault condition.

If no discrepancies are detected throughout execution, the algorithm terminates in the acceptance state, indicating that the memory device has successfully passed the diagnostic procedure.

This execution strategy ensures that:

- all operational processors remain active throughout the diagnostic phase,
- address traversal is exhaustive and deterministic,
- data pattern evolution is sufficiently rich to expose direction-sensitive and interaction-based fault classes, and
- reverse traversal steps preserve logical symmetry with their ascending counterparts.

As a result, the synthesized micro-operation schedule realizes the March A algorithm in a form that is both execution-efficient and diagnostically complete, fully consistent with the U–Y scheme representation and the architectural constraints of multiprocessor diagnostic devices.

Table 12.3—Sequence of Test Operators

Processor No.	Test Stimuli Chain 1	Chain 2	Chain 3
0	$R\,(x_{\sqrt{n-1}}, y_{\sqrt{n-1}})$	$W(x_{\sqrt{n-2}}, y_{\sqrt{n-1}})$	$V(x_{\sqrt{n-3}}, y_{\sqrt{n-1}})$
1	$W(x_{\sqrt{n-1}}, y_{\sqrt{n-1}})$	$V(x_{\sqrt{n-2}}, y_{\sqrt{n-1}})$	$R\,(x_{\sqrt{n-4}}, y_{\sqrt{n-1}})$
2	$V(x_{\sqrt{n-1}}, y_{\sqrt{n-1}})$	$R\,(x_{\sqrt{n-3}}, y_{\sqrt{n-1}})$	$W(x_{\sqrt{n-4}}, y_{\sqrt{n-1}})$
3	$R\,(x_{\sqrt{n-2}}, y_{\sqrt{n-1}})$	$W(x_{\sqrt{n-3}}, y_{\sqrt{n-1}})$	$V(x_{\sqrt{n-4}}, y_{\sqrt{n-1}})$

When a borrow occurs from coordinate X, the corresponding update of coordinate Y is defined by the expression:

$$y_i(s+1) = (y_i(s) - 1)^*$$

Here, the superscript "*" denotes that the decrement of coordinate $\boldsymbol{Y}$ is conditional on the occurrence of a borrow propagated from coordinate $\boldsymbol{X}$. This conditional update ensures correct synchronization of address decrements across dimensions during reverse scanning of the memory array and preserves the intended traversal order encoded by the operator distribution in Table 12.3.

Diagnostic Process Summary

According to the diagnostic algorithm, execution proceeds as follows:

- After each read operation, the response of the device under test is compared against the corresponding reference value.
- The contents of the error register are examined following each comparison.

- If no discrepancies are detected (i.e., the error counter remains zero), the monitor displays the message **“OK”**, and the device is classified as functional.
- If one or more discrepancies are detected, the monitor displays the message **“FAULT”**, and the device is rejected.

The synthesis of diagnostic algorithms and executable test programs for semiconductor memory devices is inherently labor-intensive. This complexity arises primarily because:

- Effective test program development requires detailed prior knowledge of the internal architecture, control logic, and instruction set of the diagnostic device.
- Debugging is complicated by the absence of direct visual representations of executed memory operations and by the limited diagnostic capabilities of conventional debugging tools, which typically cannot display a complete “test picture” of memory access behavior during execution.

Representative Optimal_Test execution logs and symbolic decision outputs for this case study are provided in Appendix D.

12.7 Test Program Synthesis Using the Interpreting System PROVER

To reduce both the development effort and time required for diagnostic program creation, an interpreting system for the machine-oriented language **PROVER** was developed.

The system is designed to support the full lifecycle of diagnostic program construction and verification. Its primary functions include:

- Input, editing, and syntactic verification of test programs written in the PROVER language.
- Simulation of the behavior of diagnostic device components, including control units, address generators, and data generators.
- Graphical visualization of test execution processes and diagnostic results.

The system supports program input and modification, file management operations, and comprehensive test program debugging. Three debugging modes are provided: automatic, graphical, and step-by-step.

Debugging Modes

- **Automatic mode**

  The test program is executed without displaying intermediate execution information. During execution, the system displays a message instructing the operator to wait.

  Diagnostic results are determined by the value of the error counter K:

  If $K = 0$, execution terminates with the display message **“OK”**, indicating a functional device.
  If $K \neq 0$, execution terminates with the display message **“FAULT”**, indicating detected errors.

- **Graphical mode**

  The monitor displays a 16×16 byte memory area, where each byte is represented as a rectangular cell. Write and read operations are shown using different colors, and the current data content of each memory cell is displayed. This mode provides direct visual insight into memory access patterns and data evolution.

- **Step-by-step mode**

  The screen displays a fragment of the test program with the currently executed instruction highlighted. In addition, the current states of the address generators, data generators, and relevant program variables are shown, enabling precise tracing of execution behavior at the micro-operation level.

System Control and Features

The main menu of the PROVER system provides a **Run** option with the following sub-modes:

- **Run** — executes the program in automatic mode.
- **Debug** — executes the program in step-by-step mode.
- **Parameters** — allows configuration of debugging parameters.
- **Reset** — terminates program execution.

In addition, the system includes subsystems for input/output handling and user interaction, supporting flexible test development and execution workflows.

Error Prevention in PROVER Programs

To prevent runtime errors and undefined execution behavior, PROVER enforces strict syntactic and structural rules:

- Data assignment commands must use integer constants and registers defined by the language specification.
- Jump commands must reference valid, previously defined labels; otherwise, the interpreter reports an error.
- Assigning the same label to multiple commands is prohibited.
- Arbitrary symbols are permitted only in labels; all commands and micro-operations must strictly conform to the defined PROVER syntax.

Any violation of these rules results in immediate termination of execution, accompanied by the message **"Invalid Command"**.

As an illustration, **Figure 12.7** shows a syntactic error detected by the PROVER system in a MATS++ test program, where the assignment operator was mistakenly replaced by the exponentiation operator.

Such strict validation ensures that symbolic test programs remain deterministic and interpretable throughout the diagnostic workflow. By enforcing syntactic correctness at the interpretation stage, the PROVER system prevents malformed test sequences from propagating into subsequent optimization or execution phases.

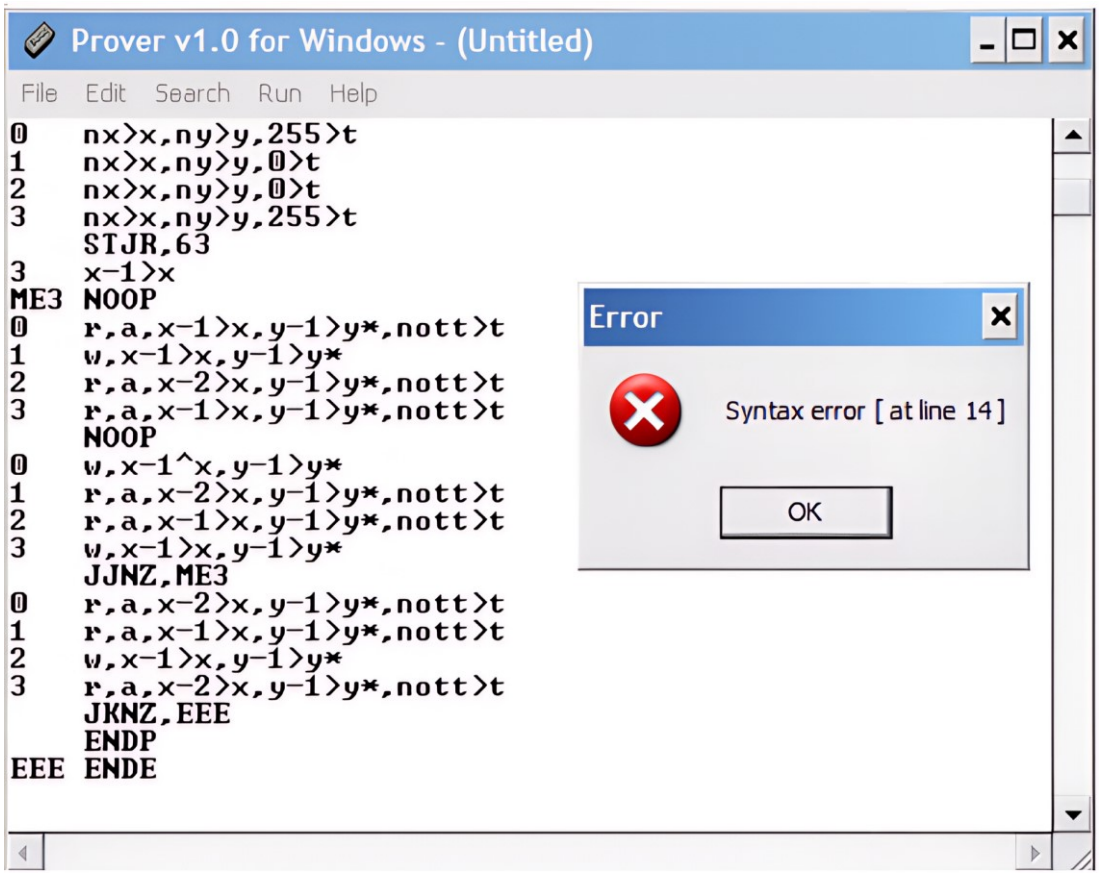

Figure 12.7—Visualization of a syntactic error in the MATS++ test program

Program Adaptation and Productivity

The choice of diagnostic test program implementation is directly influenced by the structure and architecture of the tester, which are in turn dictated by the required test generation speed. For high diagnostic frequencies, the tester architecture must support maximal parallelization of test formation operations in order to minimize overall execution time.

Analysis of MATS++ test program fragments (see Tables 9.5–9.7) shows that any architectural or structural modification of the tester inevitably requires corresponding reconfiguration of the diagnostic programs.

The programming methods described above—most notably the use of the **PROVER** interpreting system—significantly simplify this process by automating syntactic verification, enforcing structural constraints, and providing execution-level visualization tools.
When a semantic error occurs during execution, the system immediately interrupts program flow and displays an error message on the monitor, as illustrated in **Figure 12.8.**

This capability substantially reduces development time and improves reliability during the creation and adaptation of diagnostic test programs. Consequently, PROVER serves not only as a symbolic test generator but also as an effective environment for validating program correctness during tester reconfiguration.

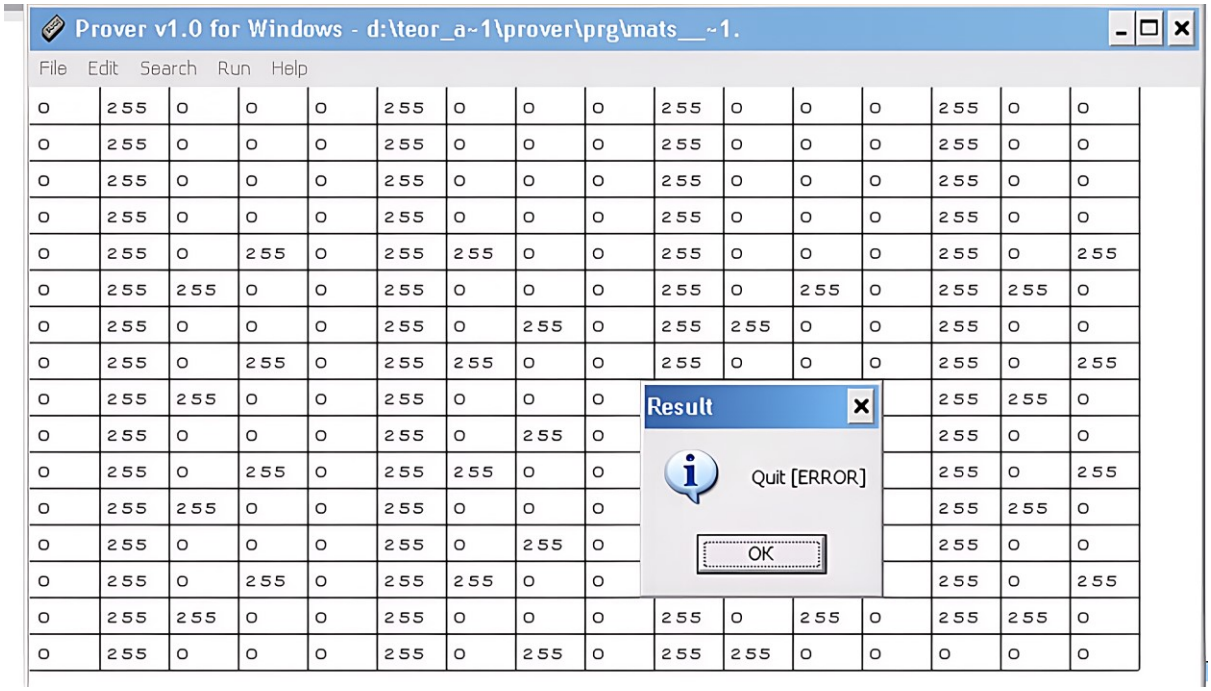

Figure 12.8—Visualization of errors during MATS++ test execution

During program execution, if a semantic or logical error is encountered, the PROVER system provides immediate visual feedback. The display shows the state of a 16×16 byte memory array, with each cell reflecting the results of write and read operations. In the illustrated example, discrepancies between expected and actual data values are highlighted, and execution terminates with an error message.

This form of visualization enables engineers to identify not only the occurrence of an error but also its precise spatial location within the memory array. By correlating the displayed cells with executed program operations, the user can quickly trace the fault back to the responsible instruction or test condition. Such feedback substantially reduces debugging time compared to conventional approaches, where errors are often detected only through numerical counters or indirect status registers.

Advantages of the PROVER System

A distinguishing feature of the PROVER interpreting system is its ability to debug test programs on a virtual 256-bit memory array. This capability greatly reduces both the cost and time associated with error localization and correction. By adjusting variable parameters that scale with the tested memory's capacity, diagnostic programs can be readily adapted to memory devices of arbitrary size.

The PROVER toolset functions as a cross-development environment, enabling the design, simulation, and verification of diagnostic programs without requiring access to physical diagnostic hardware. This abstraction accelerates development cycles and decouples software debugging from hardware availability.

A performance comparison between experimental diagnostics and program synthesis using the PROVER environment illustrates its effectiveness. For example, debugging test programs for

a 16-Mbit memory chip with a 50-ns cycle time demonstrates more than a **sixty-fold increase in programmer productivity**. Furthermore, the system supports parallel development of hardware and software components within the diagnostic framework, leading to a substantial reduction in overall project timelines.

12.8 Summary

This chapter has presented **Optimal_Test** as a central refinement engine within the symbolic memory diagnostic framework. Acting as a post-synthesis optimization layer for tools such as **PROVER**, it augments raw symbolic test sequences with execution-aware intelligence, redundancy elimination, and architecture-constrained scheduling.

Through the integration of fault coverage modeling, U–Y–based graph compression, incidence-matrix transformations, and multiprocessor scheduling strategies, Optimal_Test ensures that diagnostic patterns are not only formally comprehensive but also efficient and directly deployable on real diagnostic hardware.

Drawing on more than a decade of research in fault modeling, symbolic abstraction, and system-level memory diagnostics, I use Optimal_Test to bridge the gap between high-level operator sequences and hardware-ready diagnostic programs. The resulting outputs are suitable for embedded BIST implementations, FPGA-based emulation platforms, and production-grade memory test systems.

The chapter also incorporated the **PROVER** interpreting system—a machine-oriented programming environment designed to reduce the complexity of developing and debugging diagnostic programs. With simulation support, graphical visualization, and structured execution tracing, PROVER enables rapid prototyping and validation of symbolic tests, particularly for multiprocessor architectures operating at high diagnostic frequencies.

By employing multi-valued transformations of incidence matrices and formal U–Y schemes, developers can systematically synthesize optimized micro-operations for advanced March algorithms such as **FD** and **A**.

The formal definition and graph-theoretic interpretation of the U–Y scheme are introduced in Chapter 11.

These methods significantly reduce design effort while enabling the generation of reusable, parameterized test programs adaptable to diverse memory configurations and tester architectures.

In conclusion, this chapter extends the symbolic synthesis foundations established in Chapter 10 into a fully execution-aware, coverage-driven optimization pipeline, while preparing the ground for **Chapter 13**, which introduces fuzzy logic–based test selection. Together, **PROVER** and **Optimal_Test** form a cohesive, forward-compatible framework for symbolic memory diagnostics that aligns theoretical models, toolchains, and implementation realities for next-generation memory systems.

Chapter 13: Fuzzy Logic Systems for Test Set Optimization

Traditional memory testing frameworks are built on rigid deterministic rule sets, in which fault models are treated as binary entities—either detected or not—through predefined sequences of test stimuli. In practical diagnostic environments, this binary paradigm often breaks down due to incomplete observability, ambiguous fault signatures, partial failure modes, and execution constrained by time, power, or architectural availability.

Under such conditions, test selection, prioritization, and exclusion cannot be governed solely by absolute rules. Instead, they must incorporate uncertainty, graded confidence, contextual relevance, and cost-aware trade-offs. These requirements motivate the introduction of adaptive decision mechanisms capable of operating under ambiguity and partial information.

This chapter employs two fuzzy inference paradigms at different abstraction levels: Sugeno inference is used for inner-loop diagnostic test selection and optimization, while Mamdani inference is applied at the system level for evaluating generalized operational and economic efficiency metrics.

This chapter presents my original contribution to fuzzy logic–**based optimization of symbolic memory test sets**. The fuzzy logic–based optimization framework presented in this chapter represents an original contribution of this work, while the underlying planning-level concept of adaptive diagnostic test selection was first introduced in the co-authored article “Strategy of Adaptive Diagnosing of Memory Modules”.

The central concept is the use of **fuzzy inference systems** as an adaptive decision layer that guides the selection, ordering, and pruning of diagnostic tests. Rather than treating test utility as binary, each test is evaluated using continuous-valued metrics and rule-based reasoning. In particular, I implemented:

- Sugeno-type fuzzy controllers for evaluating test set utility under ambiguous or overlapping fault observability,
- fault observability scores modeled as soft weights derived from symbolic simulation traces and fault graphs,
- cost-based metrics that account for execution time, power consumption, and test logic complexity,
- rule-based prioritization in which test importance is assigned dynamically based on diagnostic context (such as ECC history, fault clustering, or thermal instability).

The resulting outcome is a **Pareto-optimal test suite**, minimizing test volume and operational cost while maintaining—or improving—fault resolution. This fuzzy decision layer replaces deterministic test selection with an adaptive optimization mechanism capable of balancing diagnostic trade-offs, aligning test effort with current hardware state, and refining execution under uncertainty.

This chapter formalizes the theory, system architecture, and practical deployment of fuzzy-logic–guided symbolic testing. It extends the Optimal_Test platform beyond classical

synthesis, embedding intelligence directly into test selection, scheduling, and compression for mission-critical memory diagnostics.

13.1 Motivation for Fuzzy Optimization in Memory Testing

In real-world diagnostic scenarios, the assumption that all test operations contribute equally to fault detection is unsustainable. Practical constraints—ranging from execution-time budgets to ambiguous fault manifestations—demand adaptive and context-aware test management. Several factors motivate the adoption of fuzzy optimization.

Test value asymmetry.

Individual test elements differ significantly in diagnostic utility. Some activate rare or low-probability fault modes, while others redundantly target fault classes already well covered.

Partial observability.

Fault behaviors such as disturb effects, retention decay, or timing drift do not always yield deterministic outcomes. Their detection requires graded interpretation rather than strict pass/fail evaluation.

Resource constraints.

Diagnostic execution is constrained by available test time, energy budgets, and MBIST channel bandwidth. As a result, only a subset of candidate tests can be executed in any given diagnostic session.

Contextual likelihood.

Hardware telemetry, ECC syndrome logs, and field error statistics provide probabilistic indicators of likely fault mechanisms. Effective diagnostics must incorporate this information to direct test effort where it is most impactful.

In my work on March-based test synthesis and symbolic fault operators, I observed that many theoretically complete test elements offered diminishing diagnostic returns. Such elements were often retained due to legacy practices or overly exhaustive testing philosophies. The integration of fuzzy logic provided a principled mechanism to eliminate, reorder, or deprioritize these tests without compromising diagnostic robustness.

Unlike rigid rule sets, fuzzy inference enables reasoning under ambiguity, balancing competing objectives, and adapting test structures dynamically. This transforms diagnostic execution from a static script into an intelligent, context-aware optimization process.

13.2 Test Evaluation Framework

To support adaptive test selection, each symbolic test T_i is evaluated across multiple diagnostic dimensions. Instead of binary inclusion or exclusion, the framework computes a **fuzzy activation score** $Si \in [0,1]$ that reflects the relative diagnostic utility of each test under current system conditions.

Each test T_i is characterized by the following parameters.

C_i — Coverage score.

A normalized measure of the fraction of modeled fault types activated or detected by T_i, typically derived from symbolic fault simulation or structural fault models.

R_i — Redundancy index.

A measure of overlap between T_i and other tests in the suite, capturing duplicated fault coverage, unnecessary operator chains, or redundant address traversals.

K_i— Cost function.

An aggregate metric representing execution complexity, including pattern length, energy consumption, required cycles, and potential bus contention.

W_f— Fault weight distribution.

A dynamic weighting vector assigning relative priority to fault classes, inferred from ECC syndrome history, thermal telemetry, environmental stress indicators, or user-defined risk profiles.
The fuzzy activation score is computed as:

$$S_i = \mu(C_i, R_i, K_i, W_f) \rightarrow [0,1]$$

where μ denotes the **fuzzy inference mechanism** that integrates rule-based reasoning with context-sensitive weighting to produce a scalar activation score.

A score near zero indicates low diagnostic priority and potential exclusion, while a score approaching one indicates high diagnostic relevance. These values guide test suite pruning, reordering, and dynamic substitution within the execution framework.

By employing this fuzzy evaluation model, diagnostic execution adapts intelligently to uncertainty, partial observability, and resource limitations, shifting from exhaustive testing toward context-aware prioritization and optimization.

13.3 Fuzzy Rule Base Design

At the core of the fuzzy optimization framework lies the **fuzzy rule base**—a structured collection of diagnostic heuristics that encode expert judgment under uncertainty. Unlike deterministic threshold-based decision logic, the rule base operates on linguistic variables evaluated through graded membership functions, enabling nuanced test selection and prioritization in the presence of ambiguity and partial information.

Rather than enforcing binary inclusion or exclusion, the system reasons over qualitative descriptors such as *high redundancy*, *low cost*, or *strong fault relevance*. This approach allows diagnostic decisions to reflect degrees of confidence and contextual trade-offs.

The rule base encapsulates expert knowledge expressed in linguistic form, including heuristics such as:

- if coverage is high and cost is low, then the test is essential,
- if redundancy is high and fault weight is low, then the test is optional,
- if a test activates multiple high-weight faults and is short, then its priority should be increased.

Each rule follows the **Sugeno inference format**, in which conditions on fuzzy input variables produce a scalar output representing test activation priority. Representative rule instances include:

- IF Coverage IS High AND Cost IS Low → Score = 0.95
- IF Redundancy IS High AND FaultWeight IS Low → Score = 0.30

The resulting activation score $S_i \in [0,1]$ is used directly to rank tests within the optimized diagnostic suite and to guide inclusion, exclusion, or reordering decisions.

Membership Function Design

In the implemented system, each fuzzy input variable—Coverage, Redundancy, Cost, and FaultWeight—is modeled using trapezoidal membership functions defined over three linguistic regions:

- Low
- Medium
- High

This structure provides soft boundaries between categories and allows overlapping membership. Consequently, a test may simultaneously belong partially to multiple linguistic regions (for example, Medium and High coverage), reflecting uncertainty and gradual transitions rather than sharp thresholds.

The choice of trapezoidal functions balances interpretability, computational simplicity, and flexibility in capturing diagnostic intuition.

Rule Weight Calibration

The relative influence of individual rules was calibrated empirically through evaluation on both synthetic and real-world datasets, including:

- symbolically modeled fault libraries,
- ECC-annotated telemetry logs from deployed DRAM systems,
- simulated fault scenarios evaluated within the Optimal_Test and Transfor environments.

Calibration ensured that fuzzy priorities reflected practical diagnostic value and that rule interactions remained stable across diverse fault distributions, architectural configurations, and resource constraints.

Through this calibration process, the rule base functions as a **soft decision engine** that replaces rigid logical conditions with adaptive, interpretable reasoning, enabling symbolic test systems to make informed decisions in complex and noisy diagnostic environments.

13.3.1 Sugeno Fuzzy Inference: Detailed Implementation

The primary factor guiding the selection of diagnostic tests for semiconductor memory modules is their effectiveness in detecting defects and faults. However, determining with certainty which specific fault types a given test detects—and with what reliability—is rarely feasible in practice.

This uncertainty arises for several reasons. Diagnostic algorithms are often described using high-level operator notation, which specifies procedural execution but does not quantify diagnostic effectiveness. Additionally, test algorithms frequently exist in multiple variants. For example, a test labeled as a *March up/down* pattern may correspond to numerous distinct operator sequences, each with different fault activation characteristics.

As a result, only qualitative assessments can typically be assigned to test effectiveness, using linguistic descriptors such as *high*, *above average*, *average*, *below average*, or *low* detection reliability. These descriptors reflect expert judgment rather than measurable probabilities.

Under such conditions, deterministic decision-making methods are insufficient for producing reliable predictive models of diagnostic utility. Rigid thresholding cannot accommodate ambiguity, partial observability, or overlapping fault coverage.

To address this limitation, **expert systems based on fuzzy set theory** are employed. Fuzzy inference provides a formal mechanism for incorporating qualitative expert knowledge and reasoning under uncertainty into the decision process. By mapping linguistic assessments to continuous-valued activation scores, the Sugeno fuzzy inference system enables consistent, explainable, and adaptive test selection within the symbolic diagnostic framework.

13.4 Foundations of Fuzzy Logic in Diagnostic Test Selection

The concept of a fuzzy set provides a mathematical framework for representing imprecise, subjective, or linguistically described information. Unlike classical (crisp) sets—where an element either belongs or does not belong to a set—fuzzy sets allow **partial membership**, expressed by continuous values in the interval $[0,1]$.

This formalism is particularly suitable for diagnostic test selection, where quantities such as fault relevance, coverage strength, or redundancy cannot be measured precisely and are instead evaluated qualitatively.

Definition 1 (Fuzzy Set)

A **fuzzy set** $\widetilde{A}$ defined on a universal set U is a set of ordered pairs given by:

$$\tilde{A} = \{\mu_A(u)/u \mid u \in U\}$$

where $\mu_A(u)$ denotes the **degree of membership** of element u in the fuzzy set $\widetilde{A}$.
The membership value satisfies:

$$\mu_A(u) \in [0,1]$$

A value of $\mu_A(u) = 0$ indicates no membership, while $\mu_A(u) = 1$ indicates full membership. Intermediate values represent partial or graded membership, reflecting uncertainty or gradual transitions between categories.

Definition 2 (Membership Function)

A **membership function** is a mapping:

$$\mu_A: U \to [0,1]$$

that assigns to each element $u \in U$ a degree of membership in the fuzzy set Ã.

The membership function provides the quantitative basis for translating qualitative linguistic descriptors—such as *low*, *medium*, or *high*—into numerical values suitable for fuzzy inference and decision-making.

In the context of diagnostic test selection, fuzzy sets and membership functions enable the representation of uncertain or subjective properties—such as diagnostic utility, redundancy, or fault relevance—in a mathematically consistent form. These constructs form the foundational layer upon which fuzzy inference systems operate, allowing symbolic test optimization to be guided by graded reasoning rather than rigid binary logic.

Definition 3 (Term Set)

A **term set** is the collection of all possible linguistic values that a fuzzy variable may assume, such as *low*, *medium*, or *high*. Each linguistic value represents a qualitative category used to describe the variable within a fuzzy inference system.

Definition 4 (Fuzzification)

Fuzzification is the process of transforming a crisp (precisely defined) input value into one or more degrees of membership associated with linguistic terms of a fuzzy variable.

Definition 5 (Defuzzification)

Defuzzification is the process of converting the result of fuzzy inference—expressed in terms of fuzzy sets or weighted rule outputs—into a single crisp value suitable for decision-making or control.

Triangular Membership Functions

To quantify diagnostic properties, **triangular membership functions** are employed for fuzzy variables representing fault manifestation probability f and fault coverage probability d. These functions map continuous input values in the normalized interval $[0,1]$ to a set of linguistic terms.

The linguistic term set used in this framework consists of:

- *low* (l),
- *below average* (lm),
- *average* (m),

- *above average* (hm),
- *high* (h).

Each triangular membership function is defined by three parameters (a, b, c), where a and $\boldsymbol{c}$ specify the base of the triangle and b specifies its apex.

The corresponding **membership function** is defined as:

$$\mu(x) = \begin{cases} 0, & x \leq a \\ \dfrac{x-a}{b-a}, & a < x \leq b \\ \dfrac{c-x}{c-b}, & b < x < c \\ 0, & x \geq c \end{cases}$$

In this formulation, the variable x represents a normalized diagnostic input, such as the fault manifestation probability f or the fault coverage probability d, depending on the fuzzy variable being evaluated.

This piecewise-linear definition ensures smooth transitions between adjacent linguistic categories and allows overlapping membership assignments. As a result, a single input value may partially belong to multiple linguistic terms, which is essential for representing ambiguity and gradual fault behavior in diagnostic evaluation.

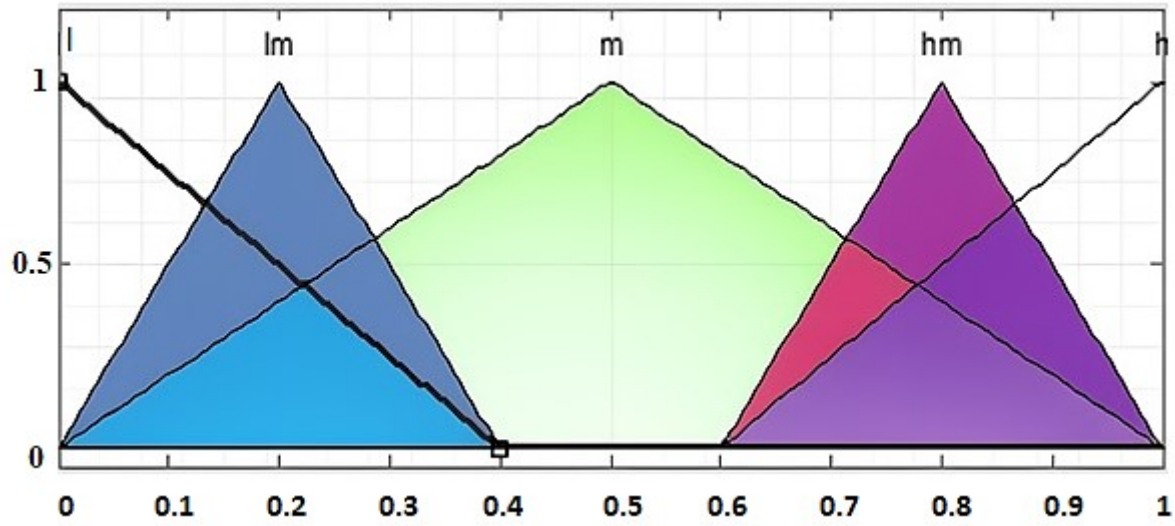

Figure 13.1—Membership Functions for Fuzzy Diagnostic Variables

Figure 13.1 illustrates the triangular membership functions defined for a representative fuzzy input variable (*Failure 1*). The horizontal axis corresponds to the normalized input range [0,1], while the vertical axis represents the degree of membership.

Five linguistic terms are modeled: *low*, *below average*, *average*, *above average*, and *high*. Adjacent membership functions overlap intentionally, ensuring that values near category boundaries contribute to multiple fuzzy rules.

For example, an input value around 0.35 exhibits partial membership in both the *below average* and *average* categories.

This overlap enables the fuzzy inference system to reason under uncertainty and avoids abrupt decision changes caused by rigid thresholds.

The graphical definition of membership functions is sufficient for both conceptual understanding and practical implementation, as the fuzzy inference mechanism operates directly on the degree of overlap between these functions.

13.5 Expert System Architecture for Test Selection

The proposed expert system employs a fuzzy rule base to determine the relevance Y_i of including a diagnostic test T_i within the overall test program.

Its primary function is to evaluate each candidate test against fault occurrence likelihoods, diagnostic coverage characteristics, and execution constraints, producing a scalar measure that represents test inclusion priority.

The expert system is positioned as a **decision layer** within the Optimal_Test framework, operating above symbolic test synthesis and below execution scheduling.

It does not generate test logic itself; rather, it guides which tests are selected, retained, reordered, or excluded based on graded reasoning under uncertainty.

From an architectural perspective, the system consists of the following conceptual stages:

1. **Input aggregation.**

Diagnostic indicators—such as symbolic fault coverage metrics, redundancy measures, execution cost estimates, and fault weight distributions—are collected for each candidate test T_i. These values may originate from simulation traces, symbolic fault graphs, ECC telemetry, or user-defined risk profiles.

2. **Fuzzification layer.**

Crisp input values are transformed into degrees of membership across predefined linguistic categories (for example, low, medium, or high coverage).
This step maps quantitative metrics into a representation suitable for fuzzy inference.

3. **Fuzzy inference engine.**

The fuzzified inputs are evaluated against the rule base using Sugeno-type inference.
Each rule contributes a weighted output reflecting expert judgment about the diagnostic utility of the test under the current context.

4. **Aggregation and scoring.**

Rule outputs are combined to produce a single scalar relevance score $Y_i \in [0,1]$, representing the priority of test T_i within the optimized test suite.

5. **Decision interface.**

The resulting scores are passed to the test selection and scheduling components of Optimal_Test, where they are used to guide pruning, ordering, or substitution decisions under resource and execution constraints.

This layered architecture ensures a clear separation between **symbolic test generation**, **intelligent test evaluation**, and **execution control**. By encapsulating diagnostic heuristics within a fuzzy expert system, the framework enables adaptive, explainable, and context-aware test selection without compromising determinism or semantic correctness of the underlying test logic.

The following subsections detail the internal structure of the inference engine, the integration of fuzzy outputs into scheduling decisions, and the mechanisms used to maintain stability and reproducibility under varying diagnostic conditions.

Input Variables

The fuzzy inference system operates on the following input sets.

Fault occurrence probability set.

Let

$$F = \{f_1, f_2, \dots, f_j, \dots, f_m\}$$

denote the set of modeled fault types, where each element f_j represents the probability of occurrence of fault type j. This set defines the fault likelihood distribution derived from sources such as field data, ECC syndrome logs, or assumed risk profiles.

Test coverage probability sets.

For each diagnostic test T_i, a corresponding coverage probability set is defined as:

$$D_i = \{d_{i.1}, d_{i.2}, \dots, d_{i.j}, \dots, d_{i.m}\},$$

where $d_{i.j}$ quantifies the probability that test T_i successfully detects fault type f_j.
Thus, each set D_i characterizes the diagnostic effectiveness of test T_i across the complete fault space F.

These values are typically obtained from symbolic fault simulation, analytical fault models, or empirical characterization.

Output Variable

For each diagnostic test T_i, the expert system produces a scalar output value Y_i, representing the test's inclusion priority within the optimized diagnostic program.

Higher values of Y_i indicate that the test contributes substantial diagnostic value under the current fault distribution and coverage context. Conversely, lower values suggest redundancy, limited effectiveness, or unfavorable cost–benefit trade-offs.

The resulting priority scores are used by the Optimal_Test framework to guide test selection, pruning, and ordering decisions under execution-time and resource constraints.

System-Level Interpretation

By combining fault occurrence probabilities with test-specific coverage effectiveness, the expert system enables diagnostic decision-making that adapts dynamically to varying operational conditions.

Rather than treating all tests as equally important, the system emphasizes tests that are most relevant to the currently observed or expected fault landscape.

This architecture preserves a clear separation between symbolic test generation and intelligent test selection. Fuzzy inference operates strictly as an evaluation layer, influencing which tests are executed without altering their internal semantics or execution correctness.

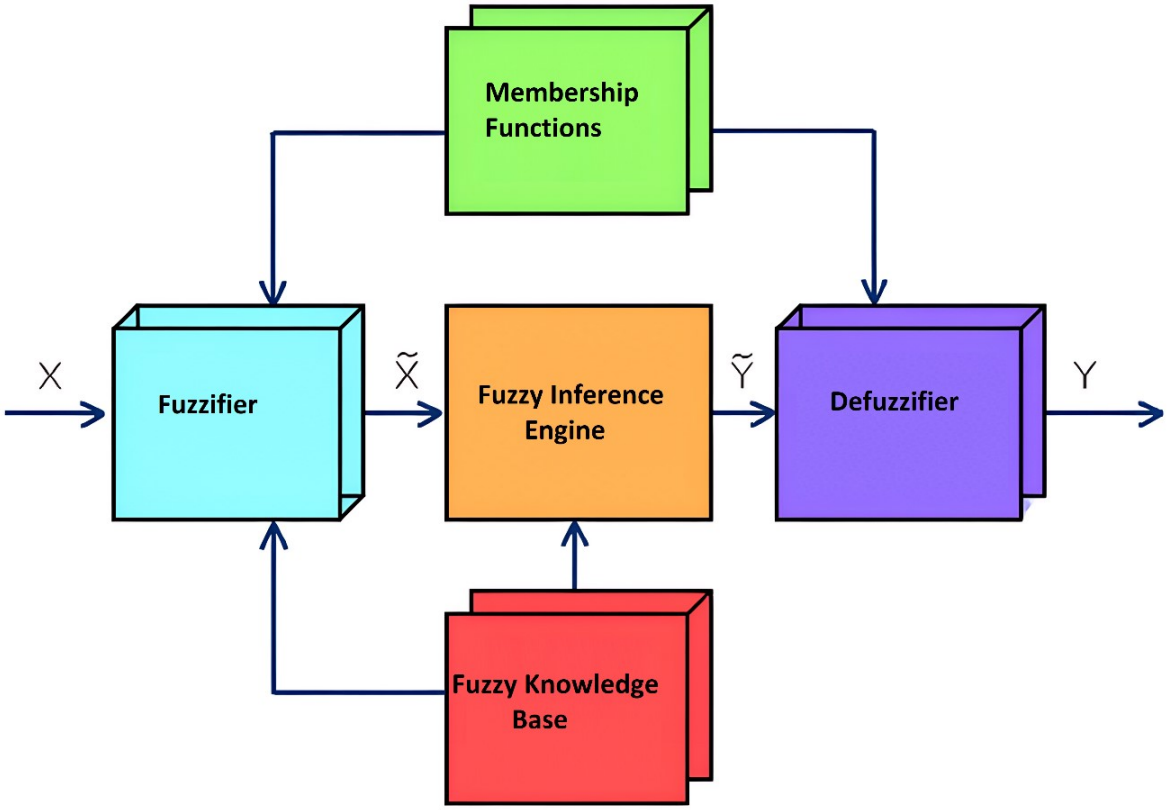

Figure 13.2—Structure of the Expert System

Figure 13.2 presents the structural diagram of the expert system implementing Sugeno fuzzy inference.

The diagram illustrates the flow from crisp input variables through fuzzification and rule evaluation to the generation of a crisp output priority value.

Membership functions and the fuzzy knowledge base provide the interpretive context required for rule-based reasoning, while the defuzzification stage produces a scalar relevance score suitable for integration into the test selection and scheduling process.

Expert System Operational Flow

The structural diagram shown in Figure 13.2 illustrates the operational flow of the expert system implementing Sugeno-type fuzzy inference for diagnostic test selection. The system transforms raw diagnostic inputs into a crisp decision output through a sequence of well-defined stages.

Input (X).

The input vector represents the set of crisp diagnostic parameters associated with candidate tests. These parameters include fault occurrence probabilities, test-specific coverage measures, redundancy indicators, and cost-related metrics derived from symbolic analysis, simulation results, or runtime telemetry.

Fuzzifier.

The fuzzifier converts the crisp input values X into a fuzzy representation $\widetilde{\mathrm{X}}$ by evaluating predefined membership functions. This step enables quantitative diagnostic data to be interpreted in linguistic terms and allows partial membership across multiple categories.

Membership Functions.

Membership functions define the mapping between crisp input values and linguistic terms such as *low*, *medium*, and *high*. Overlapping membership regions permit graded interpretation, ensuring that borderline or uncertain diagnostic conditions are represented accurately.

Fuzzy Knowledge Base.

The fuzzy knowledge base contains the set of expert-defined inference rules that encode diagnostic heuristics and relationships among the input variables. These rules express qualitative reasoning about test relevance, redundancy, and cost-effectiveness.

Fuzzy Inference Engine.

The inference engine evaluates the fuzzified input $\widetilde{\mathrm{X}}$ against the rule base to generate fuzzy conclusions $\widetilde{\mathrm{Y}}$. Within the Sugeno framework, each rule contributes a weighted output reflecting the diagnostic priority implied by its conditions.

Defuzzifier.

The defuzzifier converts the fuzzy output $\widetilde{\mathrm{Y}}$ into a crisp scalar value Y, representing the inclusion priority of a diagnostic test within the optimized test suite. In Sugeno inference, this step is realized through weighted aggregation of rule outputs, yielding a deterministic and interpretable decision value.

Through this structured operational flow, the expert system integrates probabilistic fault information, symbolic coverage data, and heuristic reasoning into a unified decision mechanism. The resulting output guides adaptive test selection while preserving the semantic integrity of the underlying diagnostic algorithms.

13.6 Sugeno Fuzzy Inference Rule Evaluation

The outcome of the expert system's operation is the **relevance score** Y_i, which quantifies the priority of including the i-th diagnostic test T_i, in the optimized test program. This score is computed using a **Sugeno-type fuzzy inference algorithm**, operating over the fuzzy rule base defined in the preceding sections.

Rule Base Structure

Let the fuzzy inference system operate on a set of k input variables:

$$X = \{x_1 x_2, \dots, x_k\}$$

In this chapter, the symbol k denotes the number of input variables of the fuzzy inference system, while r indexes the fuzzy rules. The symbol k, introduced later in **Chapter 14** to denote hardware redundancy capacity (number of spare rows or columns), is reserved exclusively for that purpose and is not related to the fuzzy inference notation used here.

The fuzzy rule base consists of s inference rules indexed by

$$r = 1, \dots, s$$

Each rule R_r is associated with a weight w_r and contributes to the output through a Sugeno-type linear consequent. The rule base can be compactly represented as:

$$\bigcup_{r=a}^{s} (X_k = A_{rk} \ with\ weight\ w_r) \Rightarrow y_r = b_{r0} + b_{r1}x_1 + b_{r2}x_2 + \cdots + b_{rk}x_k$$

where:

- k is the number of input variables,
- r is the rule index,
- A_{rk} denotes the fuzzy set associated with input variable x_k in rule R_r,
- w_r is the weight of rule R_r,
- y_r is the output of rule R_r.

Sugeno Rule Consequent

In the Sugeno framework, the consequent of each rule is defined as a linear function of the input variables:

$$y_r = b_{r0} + \sum_{i=1}^{k} b_{ri}x_i$$

Here, the coefficients $\boldsymbol{b_{ri}}$ define the contribution of each input variable $\boldsymbol{x_i}$ to the rule output $\boldsymbol{y_r}$, while $\boldsymbol{b_{r0}}$ represents a bias term.

Interpretation

This formulation preserves a compact representation of the fuzzy rule base while explicitly encoding rule weights and linear consequents.

It enables efficient aggregation of expert knowledge and supports deterministic, continuous-valued decision making suitable for adaptive diagnostic test selection within the Optimal_Test framework.

Rule Activation and Membership

Fuzzy rules establish soft relationships between input variables and output relevance scores. Unlike crisp switching logic, multiple fuzzy rules may be activated simultaneously, each contributing to the final decision with a varying degree of strength.
For an input vector

$$x = (x_1, x_2, \dots, x_k)$$

the activation strength of rule r is determined by the degree of membership of the input variables in the corresponding fuzzy sets.
The firing strength $\mu_r(x)$ of rule r is defined as:

$$\mu_r(x) = \bigwedge_{i=1}^{k} (\mu A_{ri}(x_i))$$

where:

- $\mu A_{ri}(x_i)$ denotes the membership degree of input variable x_i in the fuzzy set A_{ri},
- $\wedge$ denotes a t-norm operator (typically minimum or product),
- $r = 1, \dots, s$ indexes the fuzzy rules.

This formulation allows multiple rules to be active simultaneously, with their activation strengths reflecting how well the input vector satisfies the corresponding rule antecedents.

Aggregation and Output

Each activated rule produces a Sugeno-type output $y_r\ (x)$, defined as a linear function of the inputs. The overall fuzzy system output is obtained by aggregating the consequents of all active rules, weighted by their respective activation strengths.
The aggregated output $\tilde{y}(x)$ is given by:

$$\tilde{\boldsymbol{y}}(\boldsymbol{x}) = \frac{\sum_{r=1}^{s} \boldsymbol{\mu_r}(\boldsymbol{x})\, \boldsymbol{y_r}(\boldsymbol{x})}{\sum_{r=1}^{s} \boldsymbol{\mu_r}(\boldsymbol{x})}$$

Finally, the crisp output value Y_i representing the inclusion priority of diagnostic test T_i, is computed through weighted-average defuzzification using the above expression.

This aggregation mechanism ensures that the final decision reflects the combined influence of all relevant fuzzy rules, proportionally weighted by their activation strengths. As a result, the output varies smoothly with the input parameters and supports stable, interpretable prioritization of diagnostic tests under uncertainty.

13.7 Rule Weight Adjustment

In the fuzzy inference framework, the contribution of each rule is influenced not only by its activation strength but also by an explicitly assigned rule weight. These weights are adjusted during test set optimization to reflect differences in execution time and diagnostic cost among candidate tests.

Let $W_{jp}^{(i)}$ denote the weight of rule p in the i-th optimization context. The rule weight is defined as:

$$W_{jp}^{(i)} = \frac{t_{min}}{t_i}$$

where:

- t_i is the execution time of the diagnostic test associated with rule p,
- t_{min} is the minimum execution time among all tests considered in the current optimization cycle.

This formulation ensures that diagnostic tests with shorter execution times are assigned proportionally higher weights, reflecting their lower resource consumption and reduced impact on overall test time.
By definition,

$$W_{jp}^{(i)} = 1$$

for the shortest-duration test or tests. All remaining tests receive weights strictly less than unity, scaled according to their relative execution times.
Through this mechanism, the fuzzy optimization process naturally favors tests that achieve diagnostic objectives efficiently, while still allowing longer or more complex tests to contribute when their fault coverage or diagnostic relevance is significant.

13.8 Linear Functions for Test Selection

Within the Sugeno fuzzy inference framework, the relevance of each diagnostic test is evaluated using a family of linear functions. These functions encode the relationship between two principal parameters:

f: the probability of fault occurrence,
d: the probability of fault coverage by the diagnostic test.

To span the full range of possible diagnostic priorities, seven linear functions are defined:

$$mf_1 = 25f + 25d + 50,$$
$$mf_2 = 22.5f + 22.5d + 45,$$
$$mf_3 = 20f + 20d + 40,$$
$$mf_4 = 12.5f + 12.5d + 25,$$
$$mf_5 = 5f + 5d + 10,$$
$$mf_6 = 2.5f + 2.5d + 5,$$
$$mf_7 = 0.$$

These functions correspond to diagnostic relevance levels ranging from maximum priority to complete exclusion. Higher coefficients assign greater importance to tests that both target highly probable faults and provide strong coverage, while lower coefficients progressively reduce relevance as either parameter diminishes.

The complete set of functions forms the quantitative basis of the fuzzy rule base. By combining all linguistic values of fault occurrence probability f and fault coverage probability d, the system constructs Table 13.1, which enumerates the decision outcomes for all rule combinations.

Table 13.1—Functions for Determining the Relevance of Test Selection

Fault Occurrence Probability, f	**Functions for Test Selection Based on Fault Coverage Probability**				
	l	lm	m	hm	h
l	mf_7	mf_7	mf_6	mf_5	mf_4
lm	mf_7	mf_6	mf_5	mf_4	mf_3
m	mf_6	mf_5	mf_4	mf_3	mf_2
hm	mf_5	mf_4	mf_3	mf_2	mf_1
h	mf_4	mf_3	mf_2	mf_1	mf_1

Explanation

Table 13.1 defines the mapping between the probability of fault occurrence f and the probability of fault coverage d into the corresponding linear relevance functions $mf_1 \dots mf_7$.

- Rows correspond to the linguistic levels of fault occurrence probability: low (l), below average (lm), medium (m), above average (hm), and high (h).
- Columns correspond to the linguistic levels of fault coverage probability: low (l), below average (lm), medium (m), above average (hm), and high (h).
- Each table entry specifies the linear function applied under the corresponding pair of conditions.

This table therefore constitutes the operational fuzzy rule base for test selection. It ensures that diagnostic tests are assigned relevance values that jointly reflect how likely a fault is to occur and how effectively the test can detect it, enabling adaptive, cost-aware optimization of symbolic test sets.

13.9 Test Selection Rule Base

Using the linear suitability functions defined in Section 13.8, a complete fuzzy rule base for diagnostic test selection has been constructed.

The rule base consists of **25 rules**, obtained through the cross-combination of five linguistic levels of fault occurrence probability and five linguistic levels of fault detection (coverage) probability.

Each rule associates a specific pair of linguistic conditions with one of the suitability functions $mf_1 \dots mf_7$, thereby defining the diagnostic relevance of a test under those conditions.

Table 13.2—Test Selection Rule Base

Rule No.	Fault Occurrence Probability	Fault Detection Probability	Suitability Function for Test Selection
1	Low	Low	mf_7
2	Low	Below Average	mf_7
3	Low	Average	mf_6
4	Low	Above Average	mf_5
5	Low	High	mf_4
6	Below Average	Low	mf_7
7	Below Average	Below Average	mf_6
8	Below Average	Average	mf_5
9	Below Average	Above Average	mf_4
10	Below Average	High	mf_3
11	Average	Low	mf_6
12	Average	Below Average	mf_5
13	Average	Average	mf_4
14	Average	Above Average	mf_3
15	Average	High	mf_2
16	Above Average	Low	mf_5
17	Above Average	Below Average	mf_4
18	Above Average	Average	mf_3
19	Above Average	Above Average	mf_2
20	Above Average	High	mf_1
21	High	Low	mf_4
22	High	Below Average	mf_3
23	High	Average	mf_2
24	High	Above Average	mf_1
25	High	High	mf_1

Explanation

Table 13.2 explicitly enumerates the fuzzy rule base used for diagnostic test selection.

The rules are derived from the Cartesian product of:

- five linguistic values of fault occurrence probability
- *(low, below average, average, above average, high)*, and
- five linguistic values of fault detection (coverage) probability.

Each rule specifies the suitability function mf_k to be applied for the corresponding input pair (f, d). These functions translate probabilistic fault characteristics into a quantitative relevance score through the Sugeno inference mechanism described in Section 13.6.

This tabular rule base constitutes the **explicit knowledge base** of the fuzzy expert system. When a given input pair (f, d) is provided, the system activates the corresponding rules, applies the associated suitability functions, and computes the inclusion priority of the diagnostic test through weighted aggregation.

By formalizing expert reasoning in this structured manner, the rule base constrains test selection to reflect both fault likelihood and detection effectiveness, while remaining deterministic, interpretable, and suitable for automated optimization within the Optimal_Test framework.

13.9.1 Fuzzy Logic–Based Test Selection Using Sugeno Inference

A fuzzy rule base provides a structured mechanism for encoding empirical knowledge and expert heuristics within a constrained decision space. In fuzzy inference systems, such knowledge is expressed through fuzzy productions—conditional rules formulated using linguistic variables and their associated membership functions.

Within the proposed methodology, a fuzzy rule base is constructed to evaluate the advisability of selecting individual memory diagnostic tests. The rule base consists of **25 fuzzy rules** (Table 13.2), derived from the cross-combination of linguistic values of fault occurrence probability and fault detection (coverage) probability. The inference process is implemented using a **Sugeno-type fuzzy inference system**, ensuring deterministic and computationally efficient evaluation.

Figure 13.3 illustrates the structural inference pipeline employed for test selection. Crisp diagnostic inputs are first mapped through input membership functions, evaluated by the fuzzy rule base, and transformed into quantitative suitability scores for each candidate test.

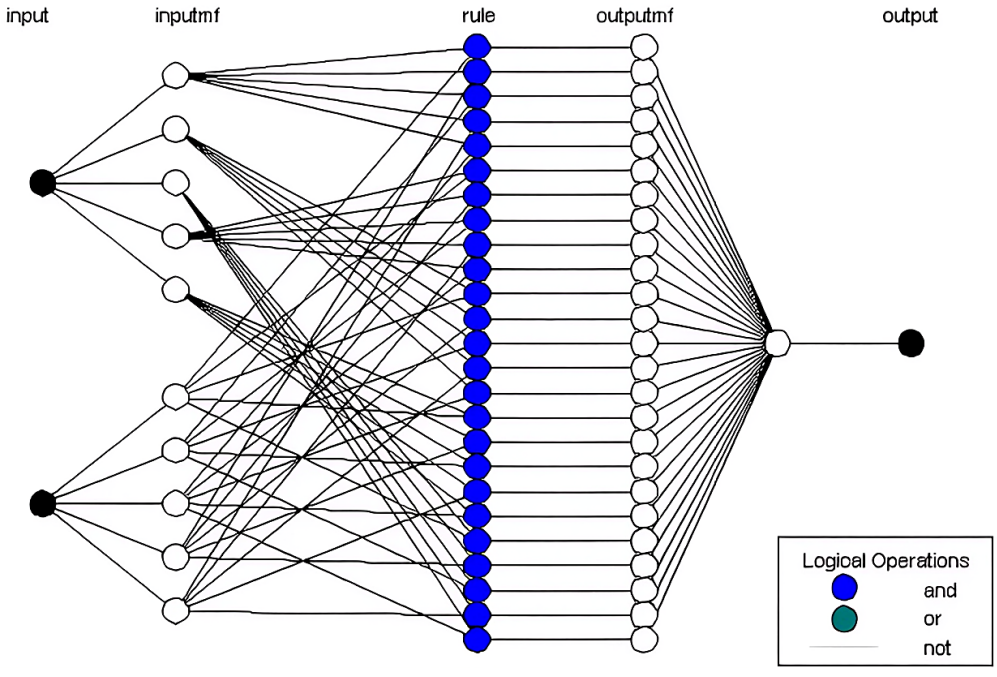

Figure 13.3—Structural Model of Test Selection System Based on the Sugeno Algorithm

The Figure depicts the layered structure of the inference system, including input variables, input membership functions, rule nodes, output membership functions, and final crisp output generation. Logical aggregation operators are used to combine rule antecedents, while weighted aggregation produces a single relevance value for each test.

Test Selection Algorithm Using the Expert Fuzzy System

The diagnostic test selection process is performed iteratively according to the following stages.

Rule Base Initialization

The fuzzy rule base defined in Table 13.2 is initialized. The rules encode expert diagnostic heuristics derived from combinations of fault occurrence probability and fault detection probability.

Rule Weighting and Adjustment

Each candidate test is assigned a weight reflecting its execution time and associated diagnostic cost, as defined in Section 13.7. These weights modulate the influence of individual rules during inference, enabling cost-aware optimization under resource constraints.

Suitability Evaluation

For a given test, the Sugeno inference engine evaluates the suitability function mf_k corresponding to the input pair (f, d). The resulting suitability score represents the expected diagnostic utility of including the test in the execution sequence.

Iterative Optimization

The test with the highest suitability score is selected and removed from the candidate pool. The evaluation process is then repeated on the reduced set until one of the following termination conditions is satisfied:

- a global resource constraint (e.g., maximum allowable test execution time) is reached, or
- all relevant fault types have been adequately covered by the selected test subset.

The simulation of this iterative selection process produces a ranked set of suitability values for all candidate tests. These values quantify the inclusion priority of each test within the optimized diagnostic program and are summarized in Table 13.3.

Table 13.3—Test Inclusion Suitability Based on Fuzzy Inference

Fault occurrence probability (f)	**Fault coverage probability (d), %**				
	l	lm	m	hm	h
l	0.0	1.16	6.25	19.1	37.5
lm	1.16	6.32	16	37.5	59.4
m	6.25	16	37.5	63.0	78.8

Table 13.3—Test Inclusion Suitability Based on Fuzzy Inference (Continued)

Fault occurrence probability (f)	**Fault coverage probability (d), %**				
hm	19.1	37.5	63.0	80.5	93.0
h	37.5	59.4	78.8	93.0	100

Explanation

Table 13.3 presents the fuzzy-evaluated **suitability percentages** for including a diagnostic test in the test program. The values are produced by the **Sugeno-type fuzzy inference system** described in Sections 13.6–13.9 and quantify the interaction between two fuzzy input variables:

- **Fault occurrence probability (f)**: low (l), low–medium (lm), medium (m), high–medium (hm), high (h).
- **Fault coverage probability (d)**: low (l), low–medium (lm), medium (m), high–medium (hm), high (h).

Each numerical entry represents the **final defuzzified suitability score (in percent)** for the corresponding pair (f, d). These scores are obtained by applying the appropriate linear suitability function ($mf_1 \dots mf_7$) and aggregating rule outputs according to the weighted-average mechanism of the Sugeno framework.

For example:

- A test associated with **low fault occurrence** and **medium coverage** yields a suitability of **6.25%**, indicating low inclusion priority.
- A test associated with **high fault occurrence** and **high coverage** attains **100%**, indicating maximum inclusion priority.

This table therefore constitutes a **quantitative decision map** for diagnostic test selection. It ensures that inclusion priorities reflect a balanced consideration of both the likelihood of faults and the effectiveness of tests in detecting them, supporting adaptive, cost-aware optimization within the proposed fuzzy expert system.

The complete fuzzy rule bases and membership-function definitions used in this chapter are documented in Appendix E.

13.10 Visualization of Test Suitability

Simulation results obtained from the Sugeno fuzzy inference model are presented in Figure 13.4. The figure shows a three-dimensional surface plot of **test suitability** as a function of two continuous input variables: **fault occurrence probability** and **fault coverage probability**.

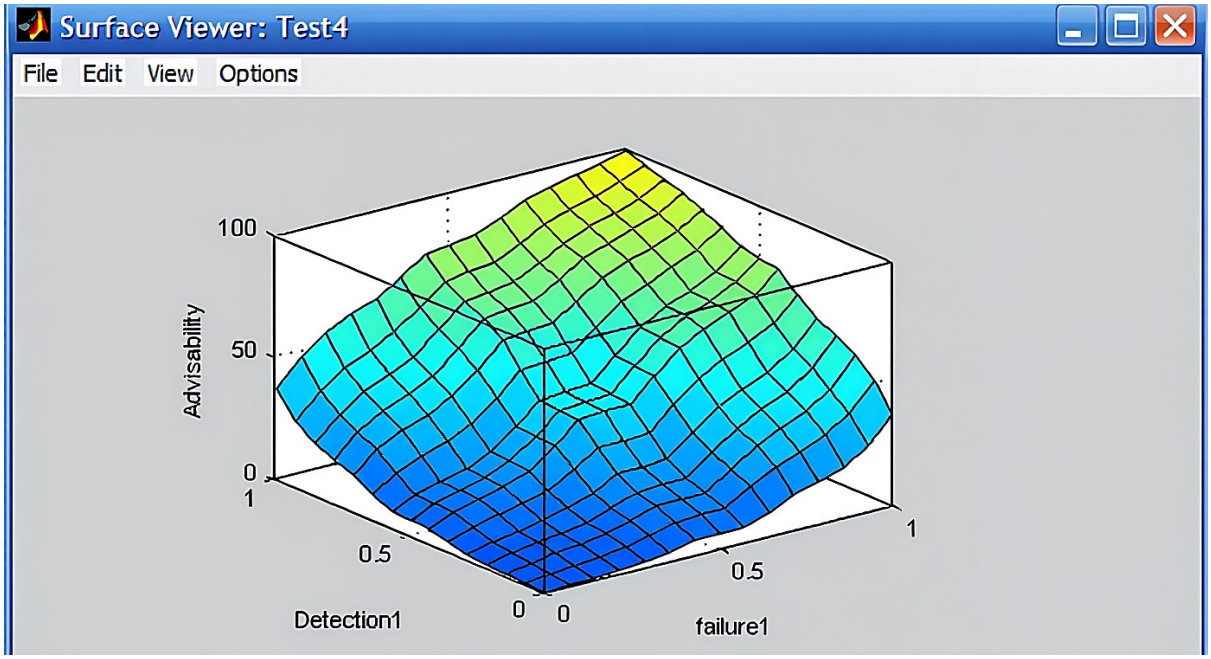

Figure 13.4—3D Surface Plot of Test Suitability vs. Fault Occurrence and Coverage Probabilities

The surface exhibits a smooth, continuous response over the normalized input domain. Suitability values increase monotonically with respect to both input variables, reflecting the structure of the underlying linear suitability functions and the weighted aggregation mechanism of the Sugeno inference process.

At the boundary condition where both fault occurrence probability and fault coverage probability approach unity, the suitability value reaches its theoretical maximum of 100%. This behavior confirms the internal consistency of the fuzzy model and demonstrates that the inference mechanism correctly prioritizes tests that are both highly relevant to likely fault scenarios and effective in detecting those faults.

The absence of discontinuities or non-monotonic artifacts indicates that the fuzzy rule base and linear consequents produce a stable and interpretable decision surface, suitable for use in adaptive and resource-constrained diagnostic environments.

13.11 Determining a Generalized Metric for Operational Diagnostic Efficiency Using Fuzzy Evaluation

The reliability of computer systems is influenced not only by architectural design choices, component quality, and operating conditions, but also by the organization and effectiveness of maintenance and repair activities. Consequently, it is essential—even during early design stages—to assess system dependability, identify vulnerable components, and select diagnostic strategies that balance execution efficiency with fault coverage.

Because memory subsystems play a central role in overall system dependability, their robustness has a direct impact on fault tolerance and operational stability. Enhancing memory reliability therefore requires careful selection of diagnostic tools and methodologies, particularly in mission-critical environments where downtime, latent faults, or incomplete diagnosis are unacceptable.

While Sugeno inference is employed in earlier sections for test selection due to its computational efficiency and suitability for iterative optimization loops, Mamdani inference is utilized here to preserve the interpretability of qualitative economic and risk-related factors embedded in the GOEM metric.

Classification of Diagnostic Tools

Diagnostic tools for memory modules can be broadly divided into software-based and hardware-based approaches.

Software-based diagnostics operate while memory modules are installed in the target microprocessor system. They rely on instruction sequences executed by the processor to generate address and data patterns. Such approaches typically require multiple instructions per test stimulus, resulting in longer execution times and reduced diagnostic efficiency. In addition, repeated installation and removal of memory modules during testing can mechanically degrade connectors and interfaces, negatively affecting system reliability.

Hardware-based diagnostics provide more comprehensive and precise testing capabilities and can be further categorized as follows:

- **High-end automated test equipment (ATE):**
  Primarily used by semiconductor manufacturers, these systems offer very high accuracy and extensive fault coverage, but their cost often reaches several million dollars.
- **Mid-range testers:**
  These platforms offer a compromise between diagnostic capability and affordability and are commonly employed by system integrators and original equipment manufacturers.
- **Low-cost testers:**
  Entry-level solutions that are economically accessible but generally lack the accuracy and fault coverage required for diagnosing modern, high-density memory architectures.

Non-Technical Evaluation Criteria

In practice, the selection of a diagnostic platform is influenced not only by technical performance metrics but also by non-technical factors such as product price, perceived quality, availability of service, and vendor reputation. These attributes are frequently expressed using imprecise linguistic descriptions, for example:

- “High detection efficiency”
- “Low cost”
- “Weak brand reputation”
- “Excellent support service”

Such assessments arise from incomplete information, subjective judgment, or limited access to comparable benchmarks. As a result, they cannot be evaluated reliably using crisp numerical thresholds alone.

A fuzzy evaluation framework is therefore well suited to capturing these imprecise and qualitative considerations. By integrating both technical performance indicators and non-

technical criteria into a unified fuzzy inference model, a generalized metric for **operational diagnostic efficiency** can be formulated, supporting informed decision-making under uncertainty.

Decision-support principles for selecting optimized diagnostic test sequences under multiple technical and operational constraints were previously developed by the author in Radio Electronics & Informatics (2008).[3]

13.11.1 Generalized Operational Efficiency Metric (GOEM)

To systematically address uncertainty in diagnostic tester selection, a **Generalized Operational Efficiency Metric (GOEM)** is introduced. This metric aggregates both quantitative and qualitative evaluation criteria within a unified fuzzy-based framework, enabling informed decision-making under uncertainty.

The GOEM is defined as a fuzzy function of five principal variables:

$$\text{GOEM} = \Phi(E, S, N, F, Q)$$

where:

- E — cumulative operating costs over a five-year lifecycle,
- S — service and maintenance costs,
- N — cost of acquiring and integrating new diagnostic software,
- F — cost of extending the system with additional diagnostic functions
- Q — probability of detecting faults and failures.

Each variable is modeled as a fuzzy quantity rather than a crisp scalar. This modeling choice reflects the inherent uncertainty, incomplete information, and subjective assessments commonly encountered in diagnostic platform evaluation, such as vendor reliability, perceived service quality, and long-term upgrade feasibility.

By expressing these heterogeneous factors in a fuzzy domain, the GOEM framework enables gradual trade-offs between cost and diagnostic effectiveness, rather than forcing binary or threshold-based decisions. The resulting metric provides a robust and realistic basis for comparing diagnostic testers, particularly in environments where purely quantitative benchmarks are insufficient or unavailable.

13.11.2 Motivation for a Fuzzy Approach to Tester Selection

Modern digital systems increasingly integrate processor cores, memory arrays, and interface logic into tightly coupled system-on-chip (SoC) architectures. While this integration improves performance and cost efficiency, it also increases structural complexity and introduces a broader range of potential failure modes.

As a consequence:

- Diagnosing microprocessor subsystems often requires deterministic or pseudo-random pattern generators capable of exercising complex control logic.

- Diagnosing memory modules demands testers specialized in array-oriented fault detection, including coupling, retention, and disturb-related faults.

No single diagnostic tester provides optimal coverage across all subsystems. Therefore, a structured methodology is required to guide tester selection—one that balances diagnostic effectiveness, economic constraints, and system-level fault characteristics.

Although low-cost testers remain widely available, they typically lack the flexibility and fault coverage depth required for reliable analysis of modern SoCs. This limitation has driven the development of high-cost testers capable of sophisticated pattern generation, fine-grained timing control, and comprehensive fault analysis.

Economic Trade-Offs in Tester Selection

Two prevailing strategies illustrate the economic dilemma inherent in tester selection:

1. **Low-Cost Tester Strategy**
   - *Advantage:* Minimizes direct testing expenditure.
   - *Disadvantage:* Limited diagnostic depth and reduced defect detection probability.
2. **High-Cost Tester Strategy**
   - *Advantage:* Maximizes diagnostic coverage across diverse fault classes.
   - *Disadvantage:* Incurs substantially higher capital and operational costs.

Neither strategy is universally optimal. The appropriate diagnostic solution depends on multiple interacting factors, including:

- fault class distribution,
- required coverage depth,
- testing duration constraints,
- overall system complexity,
- total cost of ownership.

Given these trade-offs, a crisp binary choice between “low-cost” and “high-cost” testers is inadequate. Instead, a **fuzzy decision model based on the Generalized Operational Efficiency Metric (GOEM)** is proposed. This approach enables technical, economic, and probabilistic factors to be integrated into a coherent decision framework, supporting rational and transparent tester selection under uncertainty.

Table 13.4—Comparative Cost Analysis: High-End vs. Low-Cost Testers

Metric	High-End Testers	Low-Cost Testers	Average Value
Operating costs over 5 years	116000$	49000$	82500$
Service and maintenance costs	27000$	12000$	19500$

Table 13.4—Comparative Cost Analysis: High-End vs. Low-Cost Testers (Continued)

Metric	High-End Testers	Low-Cost Testers	Average Value
Cost of new software packages	22000$	12000$	17000$
Cost of adding new diagnostic functions	670000$	360000$	515000$
Fault and failure detection probability	94%	88.5%	91.25%

This table summarizes the economic and diagnostic trade-offs between high-end and low-cost memory testing platforms. Five key performance indicators are considered to characterize both operational cost and diagnostic capability.

The presented values reflect representative estimates derived from vendor data, operational experience, and published benchmarks. While high-end testers offer superior diagnostic effectiveness, they incur significantly higher costs related to system expansion and long-term operation. Low-cost testers provide economic advantages but exhibit reduced diagnostic depth and adaptability.

13.11.3 Mamdani Fuzzy Inference for Operational Efficiency Evaluation

To systematically integrate the multi-criteria data summarized in Table 13.5, a **Mamdani-type fuzzy inference system** is employed for evaluating the **Generalized Operational Efficiency Metric (GOEM)**.

This inference model is well suited for aggregating heterogeneous criteria expressed in both quantitative and qualitative terms, particularly when expert judgment and linguistic evaluation are required.

The Mamdani framework models operational efficiency across three principal dimensions:

- **Economic costs**, including cumulative operating expenses and service and maintenance costs;
- **Expandability**, encompassing the cost of acquiring new diagnostic software and integrating additional diagnostic functions;
- **Diagnostic effectiveness**, represented by the probability of detecting faults and failures. Each dimension is represented by one or more fuzzy variables with associated membership functions.

Linguistic descriptors such as *low*, *medium*, and *high* are used to capture uncertainty, incomplete information, and subjective assessments that cannot be reliably expressed as crisp numerical thresholds.

While Sugeno inference is employed for inner-loop test selection due to its computational efficiency and suitability for optimization under numeric constraints, Mamdani inference is intentionally selected here for the GOEM metric to preserve interpretability of qualitative linguistic variables and diagnostic decision transparency.

The fuzzy rule base combines these dimensions using expert-defined rules to produce a fuzzy estimate of operational efficiency. Defuzzification yields a scalar GOEM value, enabling direct comparison between diagnostic platforms with differing cost structures and diagnostic capabilities.

By applying Mamdani fuzzy inference at the system-selection level, the GOEM framework complements the Sugeno-based test selection model developed earlier in this chapter. Together, these approaches provide a coherent methodology for decision-making across both **diagnostic platform selection** and **test set optimization**, under economic, technical, and operational uncertainty.

The structural diagram of the Mamdani fuzzy inference system used to compute the **Generalized Operational Efficiency Metric (GOEM)** is shown in Figure 13.5.

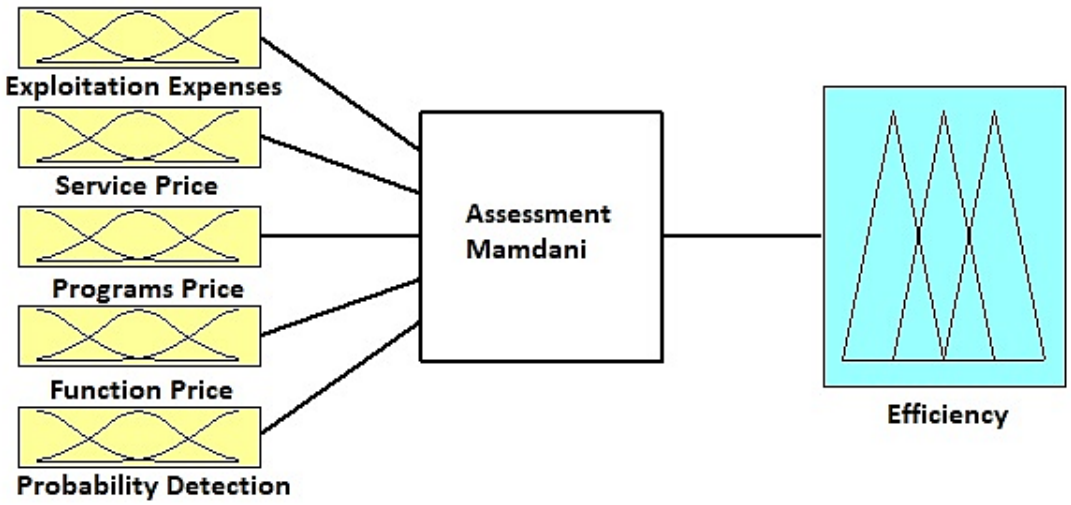

Figure 13.5—Mamdani Fuzzy Inference Structure for Diagnostic Efficiency Evaluation

The diagram illustrates the complete fuzzy inference workflow. Multiple input variables—representing economic and diagnostic factors—are first mapped into fuzzy sets using predefined membership functions.

These fuzzy inputs include exploitation (operating) expenses, service and maintenance costs, software program costs, costs associated with adding new diagnostic functions, and the probability of fault detection.

The fuzzified inputs are processed by a Mamdani inference engine, which applies a rule base encoding expert knowledge about cost–performance trade-offs. The resulting fuzzy outputs are aggregated and defuzzified to produce a single scalar efficiency score representing the operational diagnostic efficiency of a given tester.

This fuzzy inference structure enables systematic evaluation of trade-offs between cost and diagnostic performance while preserving flexibility in decision-making. Input parameters are expressed using linguistic variables such as *high cost*, *medium coverage*, or *low service cost*, reflecting uncertainty, incomplete information, and subjective assessments.

Through fuzzy reasoning, these qualitative descriptors are synthesized into a quantitative efficiency metric that supports rational comparison, selection, and optimization of diagnostic testing platforms.

Output Variable: Generalized Operational Diagnostic Efficiency

The output of the Mamdani fuzzy inference system is the **Generalized Operational Diagnostic Efficiency** (hereafter referred to as *Efficiency*). This variable represents the aggregated assessment of a diagnostic tester's operational suitability, combining economic cost factors, expandability, and diagnostic effectiveness.

The output is expressed using five linguistic categories:

- Low
- Below Average
- Average
- Above Average
- High

These categories provide an interpretable classification of tester performance, balancing diagnostic capability against long-term operational and economic considerations.

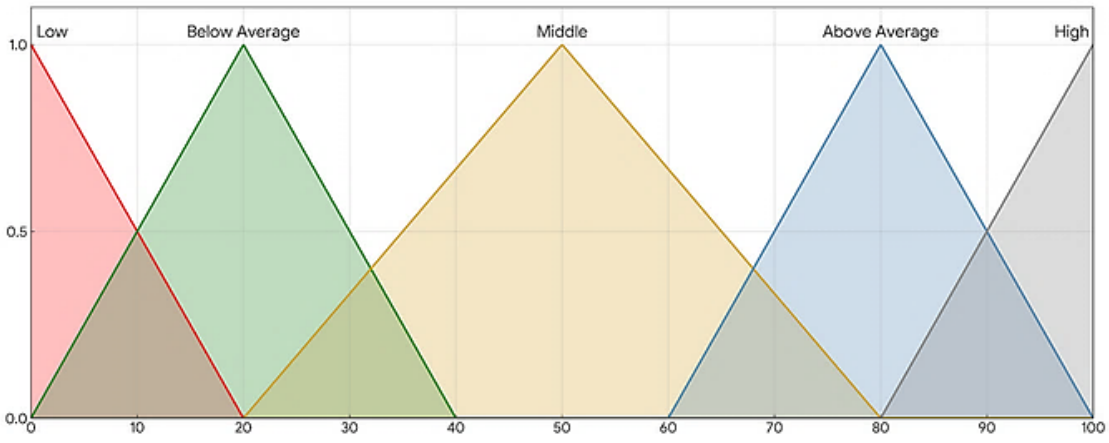

Figure 13.6—Membership Functions for Output Variable "Efficiency"

Figure 13.6 illustrates the fuzzy sets associated with the output variable *Efficiency*. The five linguistic categories—Low, Below Average, Average, Above Average, and High—are modeled using overlapping triangular and trapezoidal membership functions defined over a normalized scale from 0 to 100.

The overlap between adjacent membership functions enables partial membership across multiple efficiency categories, allowing the inference system to express graded assessments rather than rigid classifications. This design captures uncertainty, incomplete information, and subjective judgments inherent in operational and economic evaluation of diagnostic testers.

By avoiding hard thresholds, the Mamdani inference framework produces smooth and realistic efficiency estimates that reflect nuanced trade-offs between cost and diagnostic performance.

The resulting output serves as a robust decision metric for comparing and selecting diagnostic platforms within the Generalized Operational Efficiency Metric (GOEM) framework.

13.11.4 Fuzzy Rule Base for Efficiency Evaluation

A fuzzy rule base was developed to support the Mamdani inference mechanism used for evaluating **Generalized Operational Diagnostic Efficiency (GOEM)**. The rule base consists of **24 expert-defined rules** that encode relationships among multiple economic, technical, and diagnostic attributes.

The rules integrate the following groups of input variables:

- **Operational cost metrics**, including exploitation (operating) expenses, service and maintenance costs, software acquisition costs, and the cost of extending diagnostic functionality;
- **Fault and failure detection probability**, reflecting diagnostic effectiveness;
- **System expandability potential**, expressed through software and functional upgrade capability.

Each rule maps a specific combination of linguistic input conditions to an output linguistic classification of operational efficiency. Collectively, the rule base constitutes the reasoning core of the Mamdani fuzzy inference system used to compute GOEM.

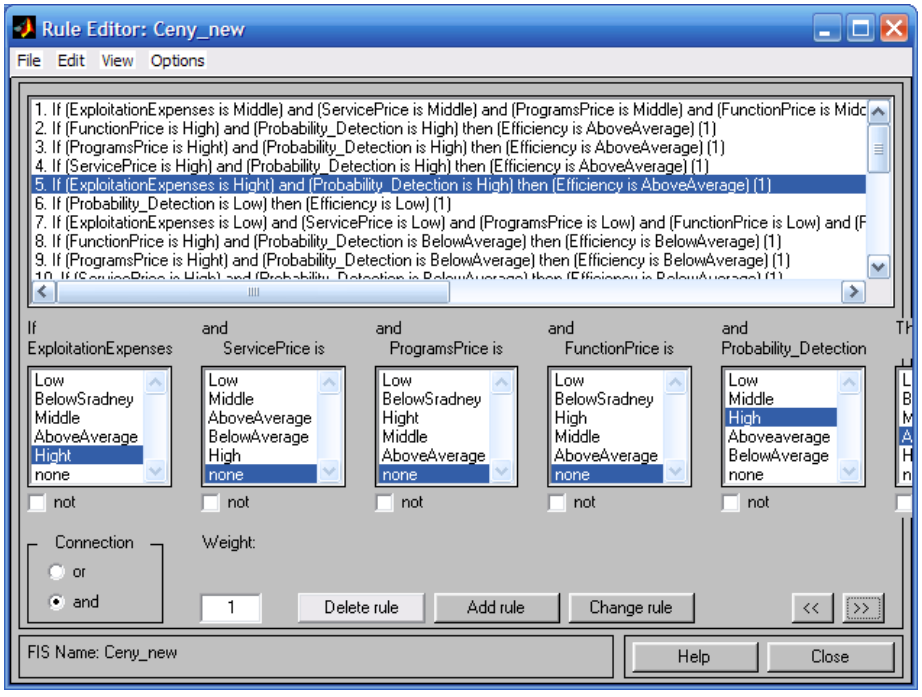

Figure 13.7—Rule Formation Diagram for Mamdani Fuzzy Inference System

Figure 13.7 illustrates the rule formation and configuration interface of the Mamdani fuzzy inference system. Input variables are expressed using linguistic categories—*Low*, *Below Average*, *Middle*, *Above Average*, and *High*. The rule editor shows how combinations of these categories are associated with corresponding output classifications of *Efficiency*.

A representative subset of the rules is summarized in Table 13.5. Each rule follows the general structure:

- **IF** a specified combination of input conditions is satisfied
  (e.g., Exploitation Expenses → Operational Expenses AND Service Price = High AND Probability of Detection = High),
- **THEN** the output variable *Efficiency* is assigned to the appropriate fuzzy set *(e.g., Above Average)*.

The fuzzy rule base enables the inference system to adapt across diverse diagnostic scenarios, economic constraints, and hardware testing configurations. By encoding expert judgment in linguistic form and applying Mamdani inference, the system produces an interpretable, flexible, and robust assessment of diagnostic efficiency. This approach allows complex trade-offs between cost, expandability, and diagnostic performance to be evaluated without relying on rigid numerical thresholds.

Table 13.5—Fuzzy Rule Base for Evaluating Generalized Operational Efficiency (GOEM) Using Mamdani Inference

Rule	Operating Cost	Service Cost	Software Cost	Feature Cost	Fault Detection Probability
1	—	—	—	—	High
2	—	—	—	High	High
3	—	—	High	—	High
4	—	High	—	—	High
5	High	—	—	—	High
6	Low	Low	Low	Low	Low
7	Low	Low	Low	Low	Below Avg
8	—	—	—	High	Below Avg
9	—	—	High	—	Below Avg
10	—	High	—	—	Below Avg
11	High	—	—	—	Below Avg
12	Low	Low	Low	Low	Average
13	—	—	—	High	Average
14	—	—	High	—	Average
15	—	High	—	—	Average
16	High	—	—	—	Average
17	Low	Low	Low	Low	Above Avg
18	—	—	—	High	Above Avg
19	—	—	High	—	Above Avg
20	—	High	—	—	Above Avg
21	High	—	—	—	Above Avg
22	Avg	Avg	Avg	Avg	Avg
23	Below Avg	Below Avg	Below Avg	Below Avg	Below Avg
24	Above Avg	Above Avg	Above Avg	Above Avg	Above Avg

This table defines the **24 fuzzy inference rules** used to evaluate the **Generalized Operational Diagnostic Efficiency (GOEM)** within the Mamdani fuzzy inference framework. The rules operate on five input variables:

- Operating costs over a five-year lifecycle
- Service and maintenance costs
- Cost of acquiring new diagnostic software
- Cost of adding new diagnostic functions
- Fault and failure detection probability

The output variable is the **linguistic classification of Efficiency**.**Note:** "—" indicates that the corresponding input variable is **not constrained** for that rule and may assume any linguistic value.

Explanation

The rules in Table 13.5 constitute the **knowledge base** of the Mamdani fuzzy inference system used for GOEM evaluation. Each rule specifies a mapping between economic cost parameters, system expandability characteristics, and diagnostic effectiveness, producing a fuzzy classification of operational efficiency.

- **Rules 1–5** prioritize **high diagnostic effectiveness**, assigning elevated efficiency classifications when the fault detection probability is high, regardless of variations in certain cost parameters.
- **Rules 6–11** capture scenarios in which **low-cost configurations** may result in reduced operational efficiency due to insufficient fault detection capability.
- **Rules 12–21** describe **intermediate trade-off conditions**, balancing cost dimensions and detection probability to yield graded efficiency assessments.
- **Rules 22–24** encode **boundary conditions**, representing uniformly average, below-average, and above-average configurations across all input variables.

Together, these 24 rules define the core reasoning mechanism of the Mamdani fuzzy inference system for GOEM computation. The rule base ensures that both **economic considerations** and **diagnostic effectiveness** are explicitly represented, enabling balanced and interpretable evaluation of diagnostic testing platforms under uncertainty.

13.11.5 Simulation Results: Influence of Detection Probability and Operating Costs on GOEM

Simulation experiments were conducted using the Mamdani fuzzy inference model to analyze how fault detection probability and operating costs influence the Generalized Operational Diagnostic Efficiency Metric (GOEM). The simulations provide quantitative insight into the sensitivity of GOEM with respect to these two key variables.

The resulting response surfaces illustrate the combined influence of these parameters on diagnostic efficiency and reveal the sensitivity of GOEM to variations in detection capability and operational cost.

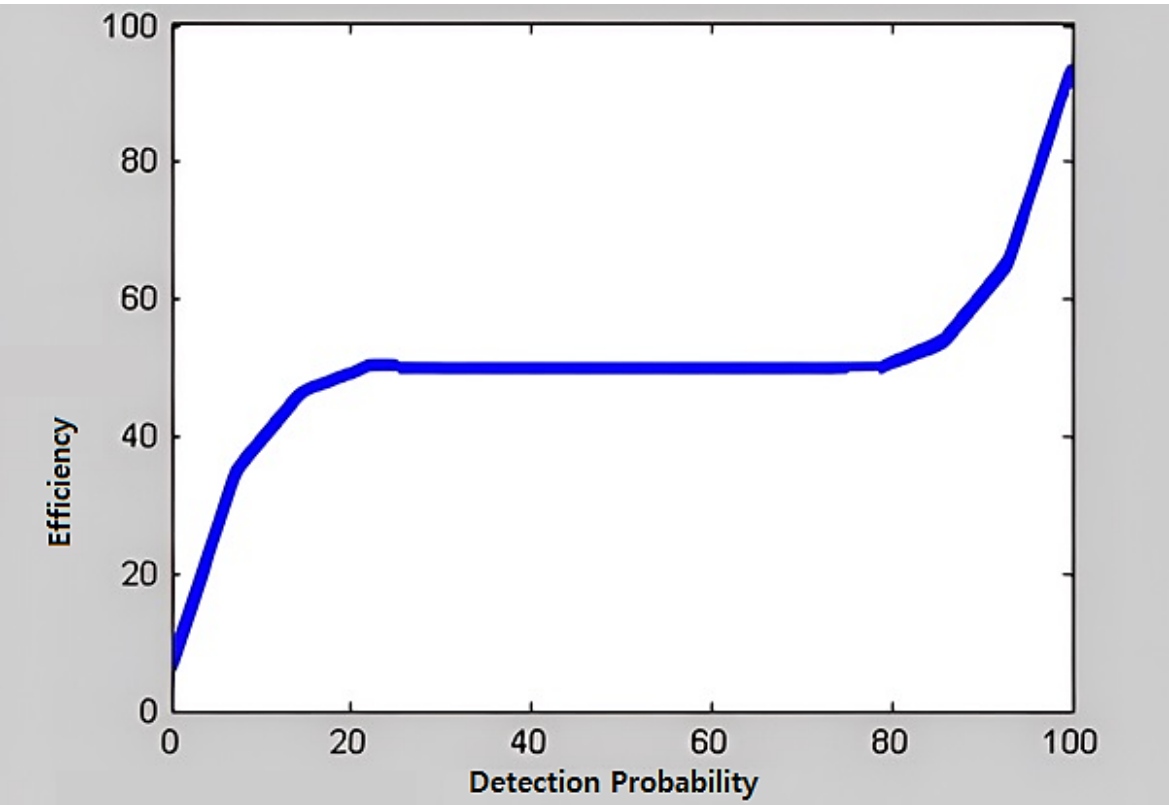

Figure 13.8: Influence of detection probability on operational efficiency

Figure 13.8 illustrates the relationship between the probability of detecting faults and failures and the resulting GOEM value. The response curve is monotonic, indicating that increases in detection probability consistently lead to higher operational efficiency.

At low detection probabilities, the GOEM grows rapidly, reflecting the substantial benefit of eliminating undetected failures. In the mid-range, efficiency gains become more gradual, indicating diminishing returns. When the detection probability approaches 100%, the GOEM reaches its theoretical maximum of 100%, confirming the internal consistency of the fuzzy evaluation model.

This behavior demonstrates that diagnostic coverage is a primary driver of operational efficiency, particularly in safety-critical and high-availability systems where undetected faults have severe consequences.

From a diagnostic planning perspective, this result emphasizes the importance of prioritizing tests that significantly increase fault detection probability, especially in early stages of the diagnostic process.

Improvements in detection capability directly translate into higher operational efficiency by reducing the likelihood of latent failures remaining undetected. At the same time, the observed saturation near the upper bound of GOEM indicates that extremely high detection probabilities must often be balanced against practical considerations such as execution cost and test duration.

Consequently, optimal diagnostic strategies must consider both coverage improvements and operational constraints when selecting test sequences.

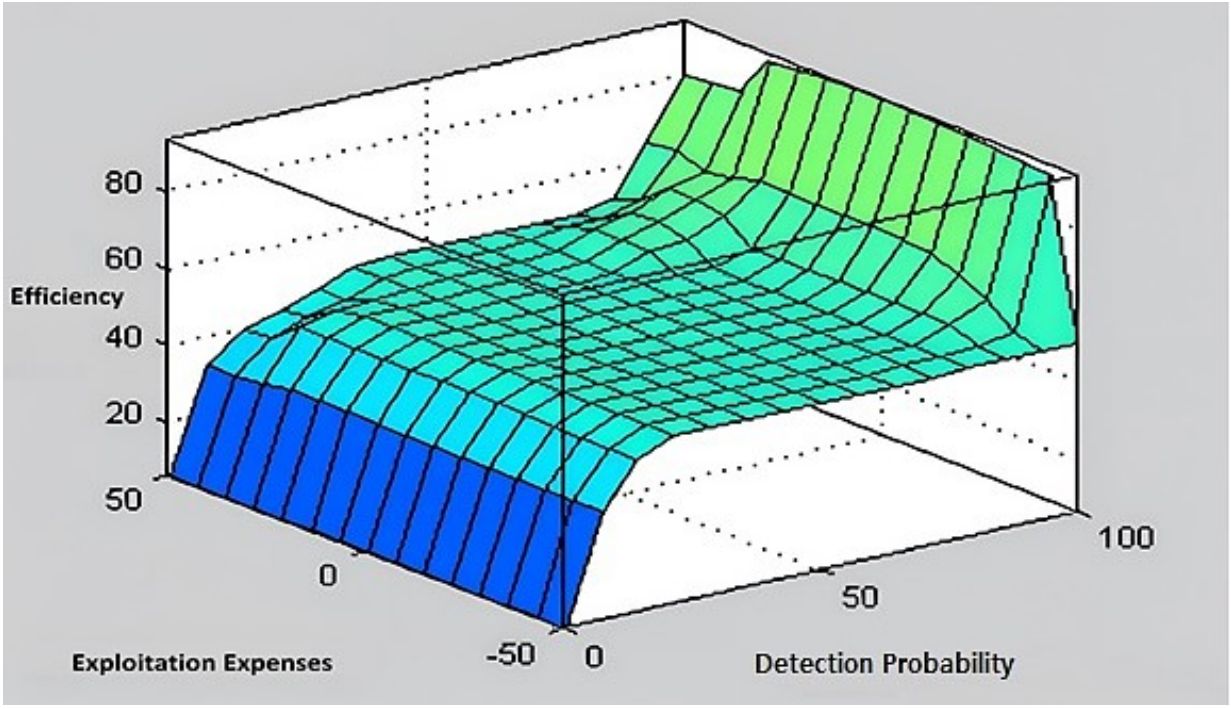

Figure 13.9—3D Fuzzy Inference Surface: GOEM as a Function of Operating Cost and Fault Detection Probability

A second simulation study examined the combined effect of operating costs and fault detection probability on GOEM. Figure 13.9 presents a three-dimensional fuzzy inference surface in which:

- the X-axis represents operating costs,
- the Y-axis represents fault detection probability,
- the Z-axis represents the resulting GOEM value.

The surface reveals two dominant trends:

- **Fault detection probability is the primary contributor to diagnostic efficiency.** Even moderate improvements in detection performance produce significant increases in GOEM.
- **Operating costs exert a secondary influence.** Higher costs slightly reduce efficiency, but their effect is comparatively weak when detection performance remains high.

These results indicate that prioritizing diagnostic coverage yields greater long-term operational value than strategies focused exclusively on minimizing operating expenses.

13.11.6 Comparative Evaluation of High-End and Low-Cost Testers Using GOEM

The fuzzy evaluation framework enables a direct comparison between **low-cost** and **high-end** memory diagnostic testers using the **Generalized Operational Efficiency Metric (GOEM)**.

Both tester classes are evaluated using the same set of input variables—operating expenses, service costs, software acquisition costs, functional expansion costs, and fault detection probability—processed through the Mamdani fuzzy inference system.

GOEM Evaluation for Low-Cost Testers

For low-cost testers, the GOEM is defined as the fuzzy function:

$$GOEM_{low} = \Phi(E_1,S_1,N_1,F_1,Q_1)$$

where:

- E_1 — operational expenses,
- S_1 — service and maintenance costs,
- N_1 — cost of new diagnostic software,
- F_1 — cost of adding new diagnostic functions,
- Q_1 — probability of fault and failure detection.

Using representative normalized values:

$$E_1=-40,\ S_1=-38.5,\ N_1=-24.4,\ F_1=-30,\ Q_1=88.$$

the Mamdani fuzzy inference system produces a GOEM value of:

$$GOEM_{low} = 52.4\%$$

GOEM Evaluation for High-End Testers

For high-end testers, the metric is computed using the same functional form:

$$GOEM_{high} = \Phi(E_2,S_2,N_2,F_2,Q_2)$$

where:

- E_2 — operational expenses,
- S_2 — service and maintenance costs,
- N_2 — cost of new diagnostic software,
- F_2 — cost of adding new diagnostic functions,
- Q_2 — probability of fault and failure detection.

Using representative normalized values:

$$E_2=40,\ S_2=38.5,\ N_2=24.4,\ F_2=30,\ Q_2=94$$

the Mamdani fuzzy inference system produces a GOEM value of:

$$GOEM_{high} = 65.5\%$$

Interpretation

Although low-cost testers offer reduced upfront and operational expenses, their overall efficiency score is **13.1 percentage points lower** than that of high-end testers. This difference is primarily attributable to the higher fault detection probability achieved by high-end diagnostic platforms, which has a dominant influence on long-term operational efficiency.

The Mamdani fuzzy inference–based GOEM framework demonstrates its value as a **balanced, data-driven decision tool** for tester selection. Rather than relying solely on cost minimization or maximum fault coverage, the approach integrates multiple economic and technical factors into a unified efficiency metric. This enables system designers and test engineers to make

rational, context-aware trade-offs in environments characterized by uncertainty, competing objectives, and rapidly evolving memory technologies.

13.12 Input Membership Functions

To enable consistent fuzzy reasoning over continuous-valued diagnostic metrics, each input variable used in the test selection and optimization framework is mapped onto a set of linguistic categories through fuzzy membership functions. These functions define soft, overlapping regions that allow partial degrees of membership, thereby avoiding rigid thresholding and preserving diagnostic ambiguity.

In practical terms, a diagnostic test may simultaneously belong to multiple linguistic categories with different degrees of confidence. For example, a test may exhibit moderate coverage while partially approaching high coverage, or may be classified as fast under nominal conditions but closer to normal under worst-case execution paths. Such overlap is essential for realistic modeling of diagnostic behavior in complex memory systems.

Fuzzy Input Variables

The fuzzy inference system operates on four primary input variables, each reflecting a distinct aspect of diagnostic utility and cost. Their linguistic partitions are defined as follows:

- **Coverage (C)**

Linguistic terms: Low, Medium, High
This variable expresses the extent to which a test activates or detects distinct fault classes within the modeled fault space. Higher coverage indicates broader diagnostic reach and stronger fault observability.

- **Redundancy (R)**

Linguistic terms: None, Moderate, High
Redundancy quantifies the degree of overlap between a given test and other tests in the candidate set. This includes duplicated fault coverage, repeated address traversal paths, or equivalent operator sequences that do not contribute additional diagnostic information.

- **Cost (K)**

Linguistic terms: Fast, Normal, Expensive
Cost represents the execution overhead associated with a test, incorporating factors such as execution time, energy consumption, memory controller contention, and control logic complexity. This variable captures the diagnostic expense incurred during test application.

- **Fault Weight (W)**

Linguistic terms: Rare, Moderate, Critical
Fault weight reflects the relative importance or likelihood of specific fault classes. It is derived from contextual information such as ECC syndrome statistics, environmental stress indicators, field failure data, or mission-critical reliability requirements.

Together, these variables provide a multidimensional description of each diagnostic test, integrating effectiveness, efficiency, redundancy, and contextual relevance.

Normalization and Membership Function Design

All input variables are defined over a normalized domain [0,1], ensuring comparability across heterogeneous metrics and enabling uniform fuzzy processing. Linguistic categories are modeled using overlapping trapezoidal membership functions, with triangular forms optionally used for intermediate regions where symmetric transitions are desirable.

This design yields smooth transitions between adjacent linguistic terms and allows borderline values to participate in multiple categories simultaneously. For instance, a normalized Coverage value of 0.55 may belong partially to both the Medium and High sets, reflecting uncertainty in fault activation strength rather than forcing a binary classification.

The shape and placement of membership functions are adaptable to system class and operational context. For example:

- In embedded or real-time controllers, the Cost variable may emphasize the Fast category due to strict timing constraints.
- In server-grade or safety-critical systems, higher emphasis is placed on High Coverage and Critical Fault Weight, prioritizing diagnostic completeness over execution overhead.

Interpretation of Membership Function Structure

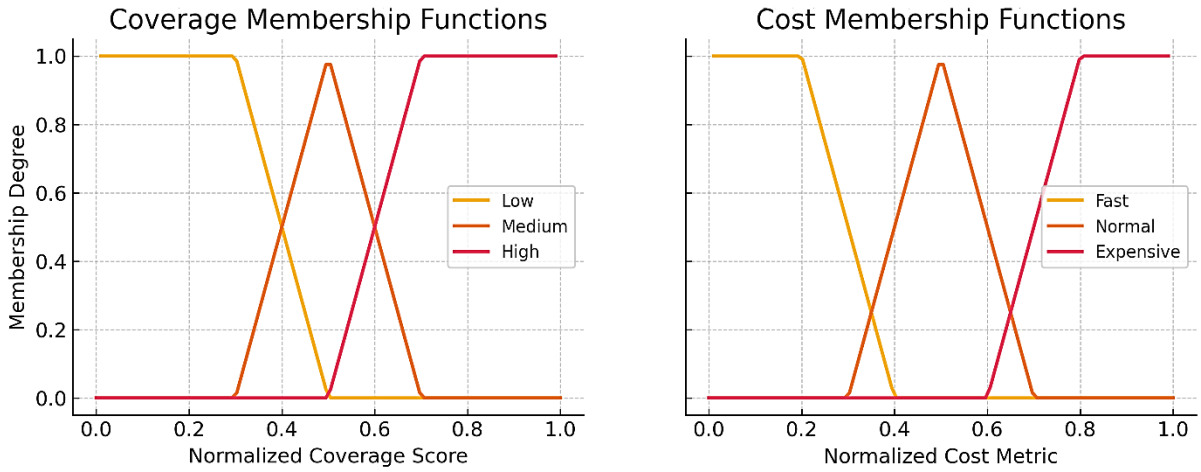

Figure 13.10—Sample Membership Functions for Coverage and Cost

Figure 13.10 illustrates representative fuzzy membership functions for the Coverage and Cost input variables. For Coverage, the linguistic categories Low, Medium, and High span the normalized domain with overlapping regions that preserve continuity. For Cost, the categories Fast, Normal, and Expensive reflect increasing diagnostic overhead.

The same partitioning principles apply to the remaining inputs. Redundancy is divided into None, Moderate, and High overlap, while Fault Weight is partitioned into Rare, Moderate, and Critical importance. Together, these membership functions define the fuzzification stage of the

inference system and serve as the foundation for the rule-based reasoning mechanisms introduced in earlier sections.

By enabling graded, context-aware interpretation of diagnostic metrics, the input membership function design ensures that test selection and optimization decisions reflect uncertainty, trade-offs, and real-world operating conditions rather than idealized binary assumptions.

13.13 Decision System Architecture

The fuzzy inference engine for symbolic test optimization is structured as a multi-stage decision system, designed to maximize interpretability, modularity, and responsiveness under diagnostic uncertainty. Its primary function is to evaluate the diagnostic utility of each symbolic test element T_i and to produce an actionable scalar score $S_{\mathrm{i}} \in [0,1]$, representing its execution priority within the optimized test program.

System Components

Fuzzifier

The fuzzifier transforms raw diagnostic inputs—including fault coverage (C_i), redundancy (R_i), test execution cost (K_i), and fault weight distribution (W_f)—into graded membership values associated with linguistic terms such as Low, Medium, and High.

This stage enables quantitative diagnostic metrics to be interpreted within a linguistic reasoning framework.

Rule Evaluator

The rule evaluator applies the fuzzy rule base in parallel across all candidate tests. Each rule is expressed in Sugeno form and combines multiple fuzzy predicates into a scalar contribution.

A representative rule takes the form:

$$If\ Coverage\ is\ High\ AND\ Cost\ is\ Low\ THEN\ Score\ =\ 0.95.$$

Multiple rules may activate simultaneously, each contributing proportionally to the final score.

Inference Engine

The inference engine aggregates the outputs of all activated rules using a weighted average, consistent with first-order Sugeno inference.

The result is a fuzzy activation value S_i for each test element, reflecting its relative diagnostic utility under the current system context.

Defuzzifier

The defuzzifier produces a crisp scalar value $S_i \in [0,1]$, which directly encodes the execution priority of the corresponding test.

Unlike Mamdani inference, no centroid calculation is required; the Sugeno framework yields a numerically stable and computationally efficient output.

Decision Modes

Once the scalar score S_i has been computed, it may be applied in one of three decision modes:

Thresholding

A threshold τ is defined such that only tests satisfying $S_i > \tau$ are retained. This mode is suitable for aggressive pruning under strict execution budgets.

Ranking

All tests are ranked in descending order of S_i, and selection proceeds until system-level constraints—such as test time, energy consumption, or MBIST slot availability—are reached.

Loopback Refinement

Scores are recomputed dynamically in response to runtime telemetry, including ECC syndrome distributions, BIST failure statistics, or thermal variation. This enables continuous re-optimization of the test set during live operation.

Implementation Note

In the Optimal_Test system, the fuzzy inference engine was integrated directly with symbolic test streams. This allowed scores to be recomputed on-the-fly as diagnostic context evolved, supporting adaptive pruning, context-sensitive test injection, and real-time prioritization—capabilities essential for mission-critical and embedded systems with constrained diagnostic windows.

13.14 Fault-Class–Specific Optimization

A key strength of the fuzzy optimization framework lies in its ability to specialize diagnostic behavior for different fault classes and system-level vulnerabilities. By tuning the fault weight distribution W_f and adjusting rule priority parameters, the system dynamically biases test selection toward those elements most relevant to the current failure risk profile.
Fuzzy weighting enables context-sensitive tailoring across diverse memory technologies:

Retention-prone systems (e.g., DRAM under elevated temperature):

Higher weights are assigned to long-delay March elements and retention-focused patterns, which are more effective at exposing charge leakage and thermal decay effects.

Wear-prone non-volatile memories (NVM):

Priority is shifted toward tests that stimulate coupling faults, disturb mechanisms, and write asymmetry. Examples include alternating write stress and repeated toggling loops that accelerate endurance degradation.

Read-disturb–vulnerable memories (e.g., row-hammer–susceptible DRAM):

Increased weighting is applied to aggressive read-based patterns, including checkerboard toggling, repeated aggressor–victim activation, and bitline sensitivity sequences.

These optimizations are enabled through:

- rule weight adjustment and membership function tuning, which shift diagnostic emphasis across fault categories, and
- fault weight distribution W_f , which may be configured explicitly by experts or updated adaptively based on:

  – ECC syndrome frequency,
  – BIST telemetry logs,
  – field reliability data such as thermal or voltage heat maps.

By combining symbolic test modeling with fault-class–aware fuzzy scoring, the Optimal_Test framework adapts not only to runtime constraints but also to evolving system fragility. This ensures that diagnostic value is maximized under limited execution budgets while maintaining coverage relevance.

13.15 Integration with Symbolic Models and PROVER Scripts

The fuzzy optimization framework is tightly integrated with the symbolic diagnostic infrastructure introduced in earlier chapters—specifically:

- the operator-based symbolic test language **PROVER (Chapter 10)**, and
- the **graph-based U–Y decomposition framework for March tests (Chapter 11)**.

This integration allows the fuzzy scoring engine to operate directly on symbolic test descriptions rather than on fixed, precompiled patterns.

Each symbolic operator path—defined as a sequence of abstract memory actions (e.g., read, write, verify) over a symbolic address traversal—is evaluated by the fuzzy inference system and assigned a diagnostic utility score S_i. These scores then drive dynamic control decisions, including:

Selective expansion of macro tests

Symbolic macros, such as nested March loops or multi-head traversal constructs, are expanded only when their fuzzy score justifies the associated execution cost.

Dynamic skipping of redundant transitions

Symbolic address paths that contribute marginal incremental coverage are suppressed, reducing execution time and energy consumption without compromising diagnostic completeness.

Adaptive retesting of high-risk zones

Memory regions exhibiting elevated ECC syndrome rates or prior transient failures are flagged for symbolic re-testing or extended pattern injection.
These decisions are encoded directly within symbolic control scripts using constructs such as:

IF SCORE(T1) > 0.8 THEN RUN(T1)
IF ECC_HIT_RATE(BANK4) > THRESHOLD THEN RERUN(T2)

Here, SCORE(T1) represents the fuzzy score assigned to test element T_i, while ECC_HIT_RATE(BANK4) is a runtime telemetry signal. Together, they enable tight symbolic–fuzzy fusion for adaptive scheduling.

This integration allows the diagnostic system to function as an adaptive, real-time scheduler even under stringent constraints, including:

- MBIST engines with limited instruction slots,
- embedded diagnostics for low-power memory systems,
- on-the-fly refinement during post-silicon validation.

Ultimately, the combination of symbolic flexibility and fuzzy reasoning transforms memory testing from static, predetermined patterns into intelligent, context-sensitive diagnostics—simultaneously optimizing for fault coverage, execution cost, and system reliability in modern memory ecosystems.

13.16 Case Study: Adaptive March FD Pruning

To validate the effectiveness of the fuzzy-logic optimization engine in a concrete diagnostic scenario, a targeted case study was conducted on symbolic pruning of the March FD algorithm.

Using the U–Y decomposition model introduced in Chapter 11, the initial symbolic expansion of March FD generated a total of 123 operator paths, corresponding to the complete bidirectional address traversal combined with the full operator activation sequence.

Following symbolic redundancy analysis and fuzzy-based scoring, the optimization framework identified operator paths with low diagnostic priority or high structural overlap. These paths were selectively removed through score-guided pruning, yielding a reduced set of 81 operator paths—corresponding to a **34.1% reduction** in symbolic test volume.

Crucially, this reduction did not degrade diagnostic effectiveness. Fault-injection simulations performed on the optimized path set confirmed that **99.5% fault coverage** was retained relative to the fully expanded reference test.

At the same time, overall test execution time decreased by approximately **35%**, reflecting both reduced operator count and improved traversal efficiency.

These results demonstrate that adaptive pruning can significantly reduce symbolic test complexity without compromising diagnostic reliability. By prioritizing operator paths with the highest diagnostic relevance, the fuzzy optimization engine preserves essential fault activation conditions while eliminating structurally redundant sequences.

This balance between reduction and coverage highlights the practical value of fuzzy-guided optimization in large symbolic test spaces. Consequently, the approach enables more efficient deployment of March-based diagnostics in both simulation environments and real testing infrastructures.

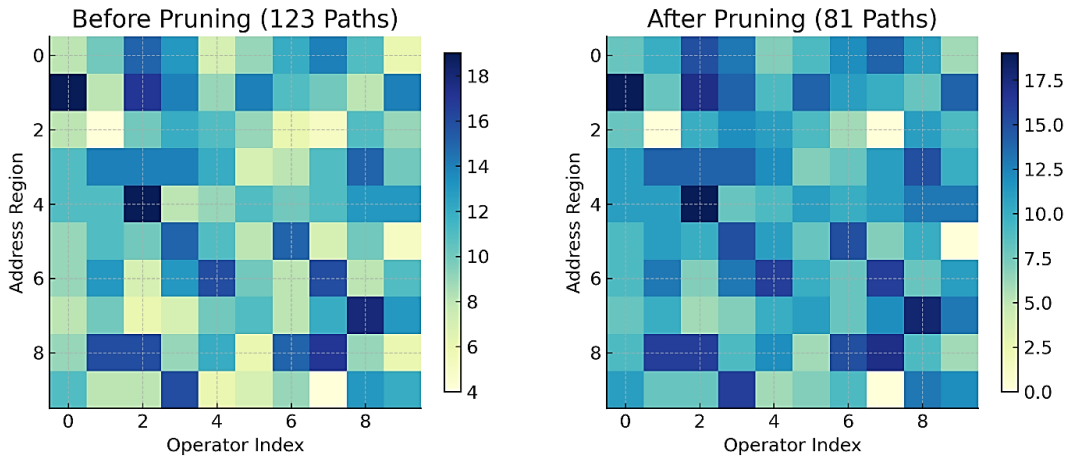

Figure 13.11—Structural effect of fuzzy-based pruning on the March FD symbolic space (before/after pruning)

Left: Full operator path expansion prior to pruning (123 paths).
Right: Optimized path set after fuzzy scoring and redundancy elimination (81 paths).

Heatmap intensity reflects symbolic operator density across address regions and operator indices. Regions associated with high diagnostic relevance are preserved, while redundant or low-impact sequences are suppressed.

This case study demonstrates that diagnostic effectiveness is **not linearly proportional to test volume**. By applying fuzzy inference to symbolic test representations, the diagnostic system selectively preserves high-value activation paths while eliminating redundancy.

The result is a test flow that is simultaneously shorter, faster, and diagnostically equivalent—an outcome that is particularly valuable under strict execution-time, power, or MBIST resource constraints.

13.17 Summary

Fuzzy logic systems introduce a controlled form of human-like decision-making into the traditionally rigid domain of memory test selection and optimization. By supporting graded truth values, contextual weighting, and adaptive prioritization, fuzzy inference enables diagnostic processes to evolve beyond static, exhaustive execution toward strategic, data-informed test planning.

The integration of fuzzy inference with symbolic test design yields several key advantages:

- **Test prioritization** driven not only by structural fault coverage, but also by fault likelihood, execution cost, and system-level risk context.
- **Adaptive diagnostic strategies** that respond dynamically to runtime constraints, including environmental variation, ECC feedback, power budgets, and MBIST limitations.
- **Seamless interoperability** with symbolic modeling frameworks, U–Y graph decompositions, and real-time telemetry, enabling feedback-driven retesting and on-the-fly test refinement.

This chapter formalized a hybrid diagnostic methodology that unifies symbolic modeling with fuzzy reasoning. Within the Optimal_Test framework, fuzzy inference functions as an execution-aware decision layer that continuously balances diagnostic value against operational cost.

Ultimately, this contribution reframes memory testing as a process of **intelligent fault anticipation rather than brute-force fault activation**. It establishes a principled foundation for next-generation adaptive diagnostic infrastructures—capable of maintaining high fault resolution while operating within the practical constraints of modern, complex memory systems.

Chapter 14: Adaptive Test Selection Using Coverage and Cost Metrics

In large-scale and high-performance memory systems, exhaustive execution of all available diagnostic test patterns is rarely feasible. Constraints related to test duration, power consumption, thermal limits, and system availability impose strict bounds on allowable diagnostic overhead, particularly in field-deployable and mission-critical environments. In addition, fault manifestations are not static.

They depend on memory technology, workload characteristics, operational aging, and environmental conditions such as temperature, voltage variation, and access intensity. Under these conditions, fixed test sequences progressively lose efficiency, and static test libraries fail to reflect evolving failure behavior.

Fundamental fuzzy-logic primitives (membership functions, fuzzification, inference semantics, and defuzzification) are defined formally in Chapter 13 and are not re-derived in this chapter. Implementation details and toolchain integration of the Optimal_Test system are treated separately in Chapters 15 and 16.

To address these limitations, a methodology for adaptive test selection was developed in which diagnostic test sets are constructed and periodically refined at the planning level according to diagnostic effectiveness, execution cost, and relevance to observed fault classes. Test selection decisions are derived from three explicitly defined sources:

- statistical fault models obtained from accumulated diagnostic observations and operating context,
- symbolic test mappings that associate operator sequences with fault activation paths defined in the symbolic model, and optimization heuristics that rank candidate tests according to multiple evaluation criteria.

Building on the symbolic modeling and operator-based test design frameworks introduced in Chapters 8–12, this chapter defines a structured framework for adaptive test suite construction.

The selection process is guided by a cost–coverage trade-off principle: a test is retained in the active set only if it improves weighted fault coverage without increasing execution cost, or reduces execution cost without degrading coverage, relative to the current test set.

The adaptive selection framework operates over the following components:

- coverage matrices expressing relationships between fault classes and symbolic tests,
- fault occurrence and impact statistics available at the diagnostic decision point,
- execution cost models capturing time, power consumption, and system intrusion, and
- redundancy and ambiguity indices derived from overlapping fault activation behavior.

The resulting test planning mechanism is implemented as a context-aware selection process within my diagnostic optimization system Optimal_Test. The core planning-level concept of adaptive diagnostic test selection was originally introduced in the EWDTW'07 paper "Strategy of Adaptive Diagnosing of Memory Modules", while the formal optimization framework, cost–

coverage modeling, and integration within the Optimal_Test system constitute the original contribution of this chapter.

This chapter specifies the structural elements, decision rules, and operational constraints of adaptive test planning, with the objective of supporting scalable and defensible memory diagnostics under constrained execution conditions.

14.1 Problem Statement

We consider the problem of selecting an optimized subset of diagnostic tests from a larger test library under explicit coverage and execution cost constraints. The formulation targets test-set selection at the planning level and is independent of runtime execution ordering. The planning-level adaptive diagnostic strategy applied in this chapter was originally introduced in the EWDTW'07 conference paper "Strategy of Adaptive Diagnosing of Memory Modules". [2]

Given:

- A memory system M,
- A finite test set T=$\{T_1, T_2,\ldots, T_n\}$,
- A fault space F=$\{F_1, F_2,\ldots, F_m\}$,
- an execution cost function $C_{(Ti)}$ associated with each test T_i,
- a symbolic coverage matrix $C(Ti, fi) \in \{1,0\}$, where $C(Ti, fi) = 1$ indicates that test T_i symbolically activates fault f_j according to the adopted fault model.

Goal:

Select a subset $T' \subseteq T$ that maximizes weighted fault activation coverage while penalizing total execution cost.

The optimization objective is defined as:

$$\mathrm{T}' = arg \max_{T' \subseteq T} \left[\sum_{f_j \in F} w(f_j).1_{T'}(f_j) - \lambda. \sum_{T_i \in T'} C(T_i) \right]$$

Where:

- $T'(f_{\mathrm{j}}) = 1$ if there exists at least one test $T_{\mathrm{i}} \in T'$ such that $C(Ti, fi) = 1$; otherwise $T'(f_{\mathrm{j}}) = 0$.
- $w(f_{\mathrm{j}})$ is a non-negative weight reflecting the relative diagnostic importance, likelihood, or criticality of fault (f_{j}).
- $\lambda \geq 0$ is a penalty parameter that regulates the trade-off between aggregate fault coverage and cumulative test execution cost.

In practice, λ is selected by normalizing coverage weights and execution costs to comparable numeric scales and then choosing λ to reflect the allowable cost increase per unit of weighted coverage.

A practical engineering procedure is to start from $\lambda_{\circ} = (\sum w_i / (\sum c_j)$ over the candidate test library (dimensionless after normalization) and adjust upward to prioritize shorter tests or downward to prioritize higher coverage, until the selected subset meets the intended diagnostic budget.

This formulation defines a weighted optimization problem in which multiple diagnostic objectives are aggregated into a single scalar criterion. The resulting solution corresponds to a coverage–cost trade-off point determined by the selected value of λ, rather than an explicit enumeration of a Pareto front.

Within this scope, the formulation provides a formal basis for adaptive test selection by enabling controlled prioritization of faults and explicit penalization of execution overhead under constrained diagnostic budgets.

14.2 Fault–Test Coverage Matrix

A fault–test coverage matrix formalizes the relationship between diagnostic tests and the fault classes they symbolically activate under a given fault model. It constitutes a foundational representation for diagnostic planning, test selection, and optimization by explicitly encoding which faults are addressable by which tests.
The matrix is defined over the test set $T=\{T_1, T_2,\ldots, T_n\}$, and the fault space $=\{F_1, F_2,\ldots, F_m\}$, where each element $C(T_i, f_i) \in \{1,0\}$ indicates whether test T_i symbolically activates fault f_{j} according to the adopted fault model. An abstract instance of this symbolic fault–test relationship is shown in the matrix representation below.

Table 14.1 —Symbolic fault–test coverage matrix representation

	f_1	f_2	f_3	...	f_{m}
T_1	1	0	1	...	0
T_2	0	1	1	...	1

Fault–test coverage matrices are a standard abstraction in diagnostic planning and test selection. The symbolic formulation adopted here, in which coverage is derived directly from operator-level test definitions rather than empirical detection statistics, follows a modeling framework established through foundational research and refined in subsequent related publications. The matrix encodes symbolic fault activation rather than physical detection probability. It is therefore independent of runtime noise, measurement uncertainty, or tester implementation, and reflects only the logical capability of a test to exercise fault-specific activation conditions.

Table 14.2 —Linguistic term sets used for fault manifestation likelihood and fault coverage likelihood (inputs to the fuzzy rule base)

Fault Manifestation Likelihood	Fault Coverage Likelihood
Very Low	Low
Low	Below Average
Medium	Average
High	Above Average
Very High	High

These term sets define the linguistic scales used by the rule base; the membership-function shapes and inference operators that instantiate these scales are specified in Chapter 13.

From the coverage matrix, several diagnostic measures relevant to test selection can be derived. The coverage contribution of a test T_i is defined as:

$$c_i = \sum_j c(T_i, f_j)$$

The marginal gain of a test T_i relative to a current test subset $T' \subseteq T$ is defined as the number of additional fault classes activated by T_i that are not already covered by any test in T'. This measure captures the incremental diagnostic value of adding T_i to an existing test plan.

Redundancy is characterized by overlapping fault activation across multiple tests. A fault class f_j is considered redundant with respect to a test subset T' if it is activated by more than one test in T'. High redundancy indicates inefficiency in the test set, as multiple tests exercise identical fault activation paths without increasing overall coverage.

This framework employs a symbolic coverage extraction engine that operates directly on operator-based test definitions. The engine evaluates symbolic predicates derived from test operator sequences and fault models, and maps them onto corresponding fault classes. This process enables automated construction of fault–test coverage matrices without reliance on exhaustive simulation or empirical fault injection.

The resulting coverage matrices are architecture-abstracted and fault-model dependent. They support fine-grained coverage analysis, redundancy identification, and adaptive optimization of diagnostic test plans within the symbolic diagnostic framework.

14.3 Statistical Fault Weighting

Observed fault occurrences in memory systems are statistically non-uniform. Certain fault classes manifest infrequently, while others dominate failure statistics due to technology-specific sensitivities, operational stress conditions, and aging-related degradation. As a result, treating all fault classes as equally significant leads to inefficient allocation of diagnostic effort. To account for this variability, statistical fault weighting is introduced.

Let:

- $w(f_j)$ denote the non-negative statistical weight of fault f_j , reflecting its relative likelihood of occurrence or its operational severity within the target system context,
- $C(T_i, f_i) \in \{1,0\}$ indicate symbolic activation of fault f_j by test T_i.

The weighted diagnostic utility of an individual test T_i is defined as:

$$r(T_i) = \sum_j c(T_i, f_j).\ w(f_j)$$

which represents the cumulative weighted fault activation capability of that test.

In the presence of a test subset $T' \subseteq T$, weighted fault activation must be evaluated at the set level in order to avoid double counting of fault weights when multiple tests activate the same fault class. Accordingly, overall diagnostic utility is assessed through the aggregate fault activation indicator $T'(f_j)$ defined in Section 14.1.

The selection of an optimized test subset is therefore governed by a weighted planning objective, expressed using test-level utility scores as a heuristic approximation:

$$\mathrm{T}' = arg \max_{T' \subseteq T} \left[\sum_{f_j \in F} r(T_i) - \lambda . \mathrm{C}T_i \right]$$

where the weighted coverage term accounts for each fault class at most once, and $\lambda \geq 0$ penalizes cumulative execution cost.

This formulation shifts the optimization criterion from maximizing unweighted fault counts to maximizing risk-weighted diagnostic value. Tests that primarily activate low-probability or low-impact fault classes are naturally deprioritized, while tests targeting dominant or critical fault modes are favored.

By incorporating statistical fault weighting, adaptive test planning becomes aligned with realistic reliability risk profiles, enabling more effective use of limited diagnostic budgets without altering the underlying symbolic fault–test relationships.

14.4 Test Cost Estimation

Test cost in diagnostic planning extends beyond raw execution time. In practical deployments—particularly in large-scale or in-field memory systems—diagnostic cost must be treated as a composite measure that reflects both computational overhead and operational impact. These factors collectively determine the feasibility of executing a given test under constrained conditions.

Key contributors to diagnostic cost include:

- Pattern generation complexity: Certain test sequences, particularly those involving nested symbolic operators, conditional control flow, or complex address traversal, require additional preprocessing or translation effort prior to execution.
- Power consumption: Tests that induce high switching activity, such as toggle-intensive access patterns or burst-mode operations, may cause transient power and thermal stress, which is critical in energy-constrained or thermally limited environments.
- Execution latency: Test duration depends not only on the number of operations but also on protocol-specific delays, including WAIT cycles, refresh overhead, and precharge or recovery latencies.
- System interference: In online or runtime diagnostic scenarios, test execution may compete with normal system activity, temporarily reducing system availability or degrading performance.

Within the adaptive selection framework, these heterogeneous factors are aggregated into a scalar execution cost term $C(T_i)$ used by the optimization model.

The aggregation reflects the relative importance of cost components under the current diagnostic context and does not alter the structure of the selection objective defined in Section 14.1.

To estimate test execution cost, the Optimal_Test framework employs a dual-layer cost analysis approach.

Static cost analysis derives cost estimates directly from symbolic test definitions. It evaluates operator composition, access density, control-flow constructs, and structural properties of the test script to obtain a context-independent approximation of execution overhead. This analysis is available prior to test execution and supports predictive planning.

Dynamic cost analysis refines static estimates using observational data collected during prior executions of diagnostic tests under comparable operating conditions. Such data may include aggregated telemetry indicators, such as execution traces or error-monitor statistics, provided that their availability does not interfere with system operation. Dynamic cost information is used exclusively for calibration of cost parameters and does not introduce runtime nondeterminism into the test selection process.

By combining static and calibrated dynamic estimates, the cost model supports adaptive test selection while preserving determinism and consistency of the optimization framework under varying operational constraints.

14.5 Cost–Coverage Trade-Off and Approximate Test Set Selection

In adaptive diagnostic planning, it is often insufficient to identify a single fixed test configuration. Instead, diagnostic planning must account for trade-offs between weighted fault coverage and execution cost under varying operational constraints.

A test subset is considered non-dominated with respect to a given cost–coverage formulation if no alternative subset provides strictly higher weighted coverage while incurring equal or lower cost under the same evaluation criteria. In practice, explicit enumeration of all non-dominated subsets is computationally infeasible for large test libraries.

Accordingly, approximate selection strategies are employed.

Within the proposed framework, test subset construction is performed using a greedy approximation strategy guided by weighted marginal gain. The procedure operates as follows:

- initialize an empty test subset T',
- while the accumulated cost remains within a specified budget:

  – select the test $T_i \notin T'$ that maximizes incremental weighted fault activation relative to its execution cost,

  – add Ti to T',
- terminate when no admissible test yields positive marginal benefit or the cost constraint is reached.

This strategy does not guarantee global Pareto optimality but provides a computationally efficient approximation that aligns with the weighted cost–coverage objective defined in

Section 14.1. Each selected test contributes measurable diagnostic value relative to its resource cost, while redundant or low-impact tests are naturally deprioritized.

The selection mechanism operates entirely at the planning level and relies on symbolic coverage representations and weighted fault models introduced in earlier sections.

14.6 Adaptive Test Scheduling Under Evolving System Conditions

In deployed memory systems, fault behavior may evolve over time due to workload characteristics, environmental stress, and aging effects. Diagnostic planning must therefore accommodate changing fault relevance without compromising system stability or determinism. Adaptive scheduling addresses this requirement by periodically revising test selection priorities based on updated diagnostic context, rather than by performing uncontrolled runtime optimization.

Representative sources of contextual information include:

- aggregated ECC statistics indicating recurrent error locations,
- long-term scrubbing summaries highlighting weak memory regions,
- endurance or wear indicators reflecting cumulative device usage.

Within the Optimal_Test framework, such information is used to update fault weights and cost parameters at discrete planning intervals. Test selection is then recomputed offline or during controlled maintenance windows using the same deterministic optimization process described in Sections 14.1–14.5.

Adaptive scheduling strategies supported by this approach include:

- region-focused test prioritization for areas exhibiting elevated fault activity,
- temporal rotation of test subsets to distribute diagnostic coverage over time,
- controlled escalation of diagnostic intensity when fault risk indicators exceed predefined thresholds.

Importantly, adaptive scheduling does not modify test execution behavior in real time. All adaptations occur through bounded re-planning steps, ensuring reproducibility, safety, and compatibility with system operation constraints.

Early adaptive strategies for diagnostic scheduling under evolving fault conditions were proposed by the author in EWDTW (2007).[2]

14.7 Adaptive Diagnostic Method for Memory Chips

Efficient diagnostic testing of memory integrated circuits and modules requires the identification of a subset of tests with **optimal operational characteristics**, namely those capable of detecting the most probable faults and failures within a minimal execution time, while avoiding unnecessary redundancy.

To enable a quantitative comparison of alternative diagnostic strategies, an **efficiency–duration criterion** is introduced and defined as:

$$K = opt_G(E, T)$$

Where:

- opt denotes the optimization operator specifying the selection strategy,
- $G(.)$ represents the functional form of the evaluation criterion,
- E is the aggregate diagnostic efficiency of the selected test set,
- T is the total duration of the diagnostic procedure.

This formulation allows diagnostic strategies to be evaluated not only by their fault detection capability, but also by their suitability for deployment under practical runtime constraints.
In the present work, the optimization objective is defined as the **maximum efficiency-to-time ratio**, expressed as:

$$K_1 = max\left(\frac{E}{T}\right)$$

This criterion directly reflects the fundamental trade-off inherent in production diagnostics: maximizing diagnostic effectiveness while minimizing execution time. By adopting this ratio-based objective, the adaptive diagnostic method prioritizes test sequences that deliver the highest diagnostic return per unit time, making the resulting selection especially suitable for industrial environments with strict throughput and timing requirements.

Adaptive Diagnostic Strategy

To achieve the maximum efficiency defined by the efficiency–duration criterion, an **adaptive diagnostic strategy** is employed, in which the testing procedure is dynamically tailored to the failure characteristics observed in a representative subset of devices. Rather than applying a fixed diagnostic sequence to the entire production batch, the method first extracts empirical information from a limited sample and then constructs an optimized test sequence based on the observed fault distribution.

The adaptive diagnostic procedure consists of the following steps:

1. From a production batch containing N memory chips, a representative sample of n devices is selected.
2. The selected n devices are diagnosed using the complete diagnostic test suite under evaluation, ensuring that all available fault-detection information is collected.
3. The **adaptation time**, defined as the time required to diagnose the sampled devices using the full test suite, is computed as:

$$T_{adap} = n.T_{sum},$$

where T_{sum} denotes the total execution time of the full diagnostic test suite applied to a single device.

4. Using the diagnostic results obtained from the sampled devices, an optimized test sequence is derived by applying the direct inclusion method, subject to a constraint on the maximum allowable diagnostic duration $t_{\max}$.
5. The remaining $(N - n)$ memory chips in the production batch are then diagnosed using the optimized test sequence obtained in the previous step.

This adaptive approach amortizes the initial cost of full diagnostics across the entire batch. By concentrating the exhaustive testing effort on a limited subset of devices and applying a reduced, optimized sequence to the remainder, the method achieves a favorable trade-off between diagnostic completeness and total testing time. As a result, high diagnostic effectiveness is retained while significantly improving throughput under industrial production constraints.

Worst-Case and Relative Costs

Under worst-case assumptions, the diagnostic time required for the remainder of the production batch—after the adaptive test sequence has been constructed—is estimated as:

$$T_{diag} = (N-n)t_{\max},$$

where N is the total number of devices in the batch, n is the size of the representative sample used for adaptation, and t_{max} denotes the execution time of the optimized diagnostic sequence applied to a single device.

This expression corresponds to the pessimistic scenario in which the optimized sequence reaches its maximum allowable duration for every remaining device.

The **relative cost of adaptation** is then defined as the ratio between the adaptation overhead and the diagnostic time of the remaining batch:

$$\delta = \frac{T_{adap}}{T_{diag}} = \frac{n.T_{sum}}{(N-n)t_{max}}$$

where $T_{adap} = n.T_{sum}$ is the total adaptation time required to diagnose the sampled devices using the full test suite, and T_{sum} is the execution time of the complete diagnostic sequence on a single device.

This ratio quantifies the **relative overhead introduced by adaptation** with respect to the worst-case diagnostic time of the remaining devices. A small value of δ indicates that the initial cost of exhaustive testing on the sampled subset is effectively amortized over the full production batch, making the adaptive strategy advantageous from a throughput perspective.

Conversely, large values of δ signal that the adaptation effort dominates the total diagnostic time, reducing the practical benefit of adaptive optimization.

In production environments, this formulation provides a clear criterion for evaluating whether the gains achieved by test sequence optimization justify the initial adaptation cost under strict runtime constraints.

Practical Interpretation

A plot illustrating the dependence between the diagnostic sample size n and the **relative adaptation cost** δ is shown in **Figure 14.1**. This curve provides a practical tool for selecting an appropriate sample size that achieves reliable diagnostic adaptation while avoiding excessive overhead associated with full test execution.

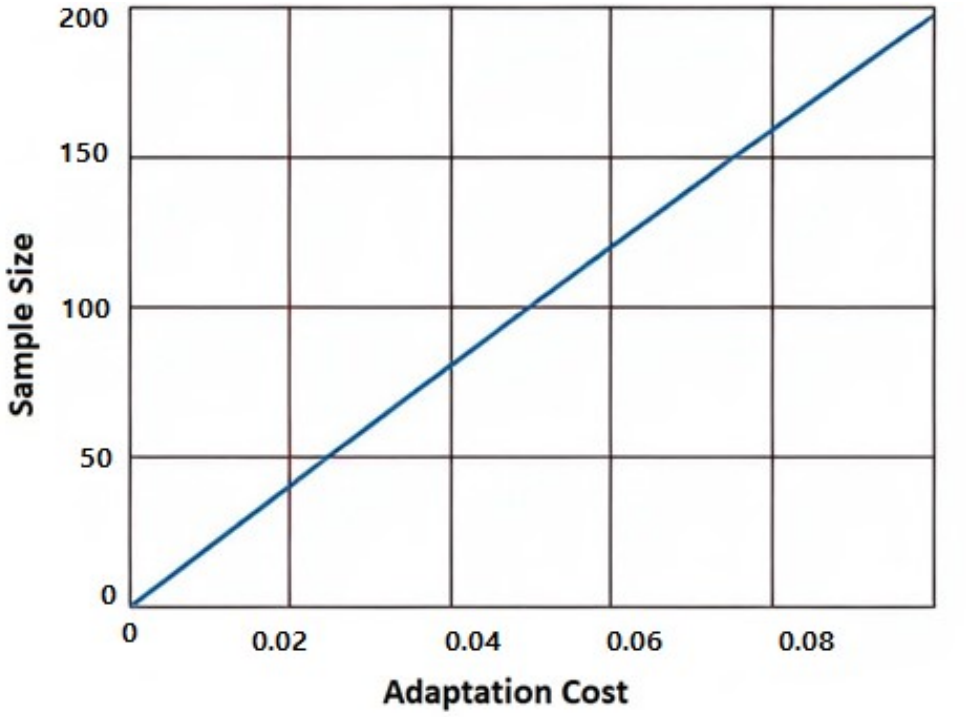

Figure 14.1—Dependence of Sample Size on Relative Adaptation Cost

Figure 14.1 shows that the adaptation cost increases approximately linearly with the sample size.

This behavior follows directly from the definition of the adaptation overhead: each additional device included in the sample requires execution of the complete diagnostic test suite, contributing proportionally to the total adaptation time.

The plot highlights a fundamental trade-off inherent in adaptive diagnostics:

- **Small sample sizes** result in low adaptation cost but may provide insufficient statistical representation of the fault population, increasing the risk of suboptimal test selection.
- **Large sample sizes** improve statistical representativeness and the reliability of the optimized diagnostic sequence, but increase adaptation overhead and reduce the net time savings achieved by optimization.

In practical applications, the optimal operating region lies near the point where the curve begins to flatten—large enough to capture the dominant fault characteristics of the production batch, yet small enough to keep adaptation costs within acceptable industrial limits.

Selecting n within this region ensures that adaptive diagnostics remain both statistically meaningful and operationally efficient.

Example Calculation

Consider a production batch containing N=3000 memory chips. Let the following parameters be given:

- t_{max}=10 s (execution time of the optimized test sequence per device),
- T_{sum}= 14.2 s (execution time of the full test suite per device),
- δ =0.05 (allowable relative adaptation cost).

Using the previously defined adaptation cost expression,

$$\delta = \frac{n.T_{sum}}{(N-n)t_{max}}$$

the required sample size n is obtained by solving:

$$\frac{n.14.2}{(3000-n).10} = 0.05.$$

This yields:

$n \approx 102$ devices.

Thus, only approximately **3.4%** of the total production batch must be diagnosed using the full test suite in order to construct an optimized diagnostic sequence.

After completion of the adaptation phase, the **Optimal_Test** software utilizes the collected diagnostic data together with user-defined constraints on execution time and fault coverage to select an optimized test set using the direct inclusion method. The resulting sequence is then applied to the remaining $(N-n)$ devices, minimizing total diagnostic time while preserving a high level of diagnostic coverage.

Time Savings from Adaptive Testing

The **relative time savings** achieved through adaptive diagnostics are defined as:

$$\eta = \frac{NT_{sum} - (n\,T_{sum} + (N-n)t_{max})}{NT_{sum}}$$

Here, NT_{sum} represents the total diagnostic time required when the **full, non-optimized test suite** is applied uniformly to all devices in the production batch.
The term

$$n\,T_{sum} + (N-n)t_{max}$$

corresponds to the total diagnostic time under the **adaptive testing strategy**, consisting of a full diagnostic pass applied to a representative sample of n devices, followed by execution of the optimized test sequence—of duration t_{max} —on the remaining $(N-n)$ devices.

The ratio η therefore quantifies the **fractional reduction in total diagnostic time** achieved by adaptive testing relative to conventional, non-optimized testing. Values of η close to zero indicate limited benefit from adaptation, whereas larger values signify substantial time savings and improved production throughput.

This formulation makes explicit that the effectiveness of adaptive diagnostics depends on three interacting factors: the size of the adaptation sample n, the execution time of the full test suite T_{sum}, and the duration of the optimized test sequence t_{max} .

When $t_{max} \ll T_{sum}$, and $n \ll N$ the adaptive strategy yields significant time savings while preserving diagnostic effectiveness, making it particularly attractive for large-volume industrial testing scenarios.

The dependence of **time savings** achieved through adaptive diagnostics on the production batch size is illustrated in **Figure 14.2**.

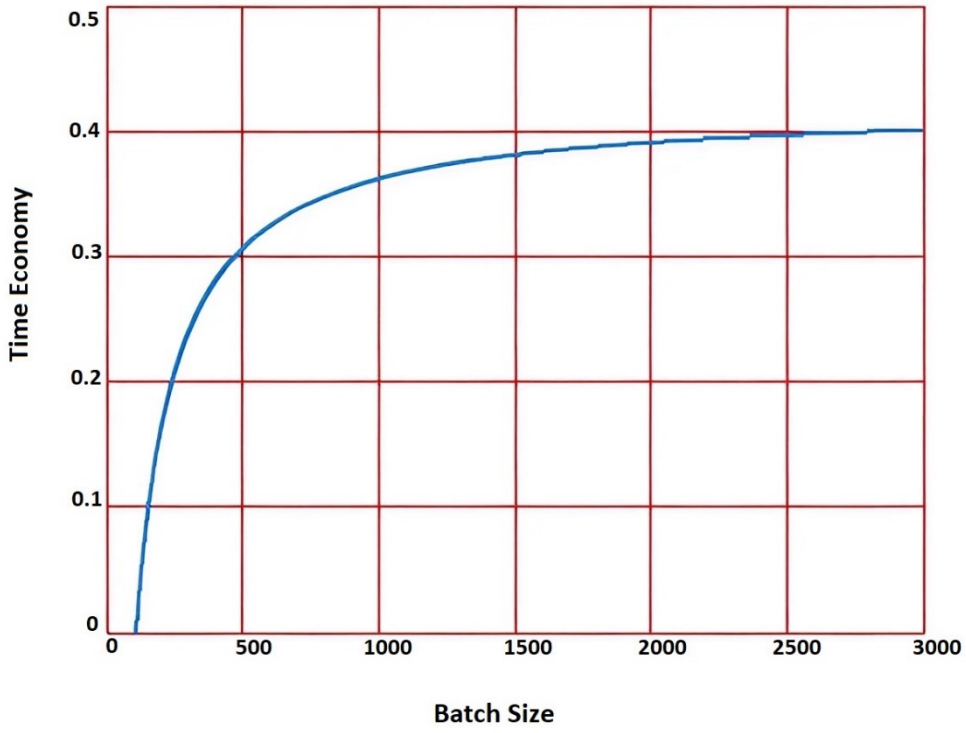

Figure 14.2—Time Savings as a Function of Memory Batch Size

Figure 14.2 shows that the application of adaptive diagnostic strategies leads to substantial reductions in total diagnostic time as the batch size increases. Under the specified experimental conditions, the achievable time savings approach approximately **40%** relative to full, non-optimized test execution.

The curve exhibits a rapid initial increase in time savings for small to medium batch sizes, reflecting the efficient amortization of the adaptation overhead once a sufficient number of devices has been processed to construct an optimized diagnostic sequence. As the batch size continues to grow, the curve gradually stabilizes, indicating diminishing marginal gains as the influence of the initial adaptation phase becomes negligible compared to the total diagnostic workload.

This behavior confirms the **scalability of adaptive diagnostics**. In large production runs, where thousands of memory devices are tested under comparable conditions, the fixed cost of adaptation is effectively distributed across the batch, resulting in consistently high time efficiency. Consequently, adaptive diagnostic strategies are particularly well suited for high-

volume manufacturing environments, where reductions in diagnostic time translate directly into improved throughput and lower testing costs.

Figure 14.3 illustrates the dependence of **relative time savings** on the size of the diagnostic sample used during the adaptation phase.

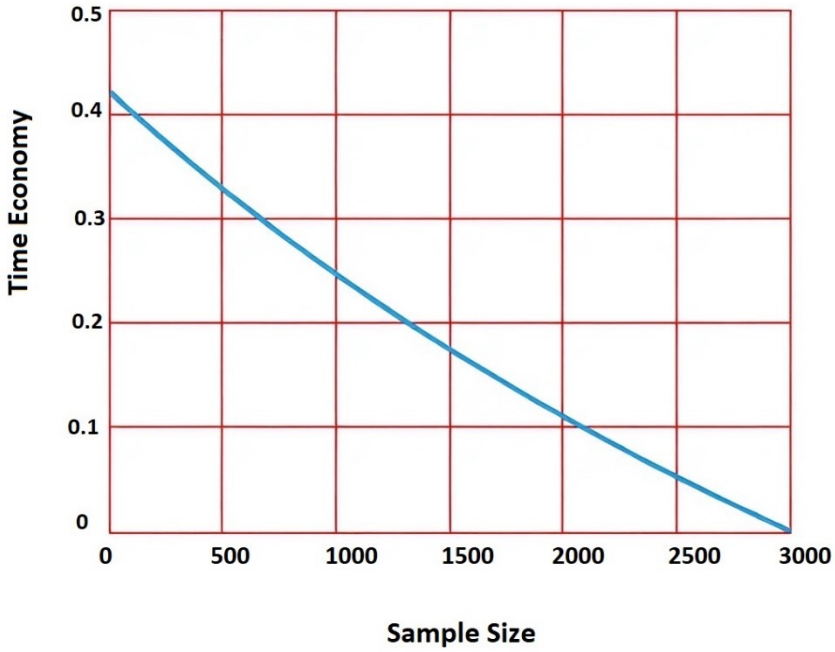

Figure 14.3—Time Savings vs. Diagnostic Sample Size

As shown in Figure 14.3, the relative benefit of adaptive optimization decreases monotonically as the number of devices included in the adaptation sample increases. This behavior reflects the growing cost of executing the full diagnostic test suite on a larger fraction of the production batch, which progressively offsets the time savings obtained from applying an optimized test sequence to the remaining devices.

In the limiting case where the adaptation sample approaches the full batch size, the adaptive strategy converges to conventional non-optimized testing. Under this condition, no reduction in diagnostic time is achieved, and the relative time savings tend toward zero.

This dependency highlights the critical role of **sample size selection** in adaptive diagnostics. To be effective, the adaptation sample must be sufficiently small to limit overhead, yet large enough to capture the dominant fault characteristics required for reliable test optimization. Identifying this balance is essential for maximizing time savings while maintaining diagnostic effectiveness under industrial production constraints.

The conceptual foundations of diagnostic algorithm design and adaptive refinement applied here were further articulated in JMEST (2016).

14.8 Integration with Fuzzy Inference and PROVER Scripts

Adaptive test selection and scheduling are integrated with the symbolic modeling infrastructure established in earlier chapters to form a unified diagnostic framework.

This integration combines:

- fuzzy logic scoring mechanisms developed in Chapter 13,
- symbolic operator representations defined in Chapters 8–10, and
- graph-based U–Y test sequence structures introduced in Chapter 11.

In the implemented toolchain, the test-scoring component used for selection is Sugeno-type (as introduced in Chapter 13), whereas Mamdani-type inference is reserved for computing aggregate interpretability-oriented efficiency indicators rather than driving per-test inclusion decisions. The resulting scores influence test selection, prioritization, and pruning decisions prior to execution, while preserving the symbolic structure of test definitions.

Symbolic test programs expressed in PROVER remain declarative and deterministic. Fuzzy inference outputs are mapped to planning decisions in the Optimal_Test framework, rather than being embedded as executable control logic within PROVER scripts. Conditional constructs therefore operate at the level of test inclusion or exclusion during planning, not as runtime execution branches.

Rule-based formulations, such as threshold-based selection criteria combining fuzzy scores with aggregated reliability indicators, are used to guide test planning decisions. These rules do not modify execution semantics and do not introduce online nondeterminism.
Through this separation, fuzzy inference enhances adaptive reasoning under uncertainty while maintaining a clear boundary between symbolic test specification, planning logic, and execution.

14.9 Visualization and Diagnostic Output

For adaptive diagnostic frameworks to be usable in engineering workflows, decision processes and outcomes must be interpretable and transparent. In addition to automated optimization, engineers require visual representations to inspect coverage behavior, cost trade-offs, and the impact of adaptive selection policies.

To support these objectives, a set of visualization mechanisms was developed as part of the diagnostic toolchain. Representative elements include:

- coverage maps illustrating fault–test activation relationships for selected test subsets,
- cost–coverage plots correlating weighted diagnostic value with execution cost,
- fault risk heatmaps representing statistically weighted fault relevance across memory regions,
- temporal schedules showing how test priorities evolve across planning cycles.

These visualizations are derived from symbolic coverage matrices, cost models, and fault weighting parameters used by the planning framework. They do not influence optimization decisions directly, but provide explanatory support for validation, tuning, and quality assurance activities.

By making adaptive planning outcomes observable and traceable, visualization bridges the gap between symbolic modeling, optimization logic, and practical diagnostic deployment.

14.10 Summary

This chapter presented an adaptive framework for optimizing symbolic memory test sets under uncertainty, constrained resources, and evolving fault relevance. The approach extends deterministic test selection by incorporating fuzzy inference, weighted fault modeling, execution-aware cost estimation, and a formal adaptive diagnostic method based on efficiency–duration trade-offs.

Two classes of fuzzy inference mechanisms were employed:

- Sugeno-type inference, used to compute suitability scores for individual tests based on fault weighting, symbolic coverage, and cost indicators,
- Mamdani-type inference, applied to evaluate a generalized diagnostic efficiency metric integrating coverage, cost, and operational impact.

These mechanisms were implemented within the Optimal_Test planning framework and applied to symbolic test representations expressed using PROVER and graph-based U–Y structures. Fuzzy scores were used to guide test prioritization, pruning, and re-selection at the planning level, without altering execution semantics.

The chapter further demonstrated:

- integration of fuzzy scoring with symbolic operator-based test definitions,
- context-aware adaptation through periodic updating of fault weights and cost parameters,
- approximate cost–coverage trade-off analysis for constrained diagnostic planning,
- formalization of an adaptive diagnostic method governing test refinement under evolving system conditions,
- visualization techniques supporting interpretability of adaptive decisions.

This chapter consolidates and extends several original contributions of the dissertation, including fuzzy rule-based test evaluation, symbolic pruning strategies, execution-aware planning, and adaptive diagnostic methodology.

Together, these elements reframe memory diagnostics as a structured process of adaptive reasoning rather than exhaustive fault activation.

Chapter 15: Industrial Evaluation and Diagnostic Toolchain Integration

The contributions presented throughout this work—encompassing symbolic fault modeling, operator-based test design, graph-theoretic synthesis, fuzzy inference, and adaptive diagnostic planning—form a cohesive framework for advanced memory testing. Beyond theoretical formulation, these methods were exercised, integrated, and evaluated within practical diagnostic workflows to assess their applicability under realistic engineering constraints.

This chapter documents the application and evaluation of the diagnostic ecosystem developed in this research across simulation environments, toolchain integration scenarios, and structured training contexts. Rather than claiming universal industrial deployment, the chapter focuses on how the proposed methods were instantiated, exercised, and refined within representative diagnostic settings.

This chapter does not introduce new optimization models, but evaluates how previously defined symbolic and optimization mechanisms are instantiated within an integrated diagnostic toolchain.

Specifically, the chapter examines the following core components:

- Optimal_Test: a symbolic test planning and execution support system,
- the PROVER language: a programmable environment for symbolic operator modeling and test specification,
- the U–Y decomposition engine: a graph-based synthesis mechanism for constructing compact operator sequences, and
- the fuzzy scoring module: a heuristic evaluation system for risk-aware test prioritization.

These components were evaluated in a range of controlled and semi-industrial contexts, including simulation-based fault injection, MBIST-oriented translation flows, test reduction exercises, and educational deployments. The chapter consolidates case-driven observations and integration strategies, illustrating how research-driven diagnostic concepts can be translated into functional elements of modern memory validation workflows.

15.1 Diagnostic Architecture Overview

The diagnostic framework developed in this research is structured as a layered architecture in which symbolic modeling, test synthesis, optimization, execution support, and post-analysis are coherently integrated. Each layer fulfills a distinct role, while collectively supporting adaptive diagnostic planning across the memory test lifecycle.

The architecture comprises the following layers:

- Modeling Layer: Encodes fault behavior using symbolic abstractions, as introduced in Chapter 8. This layer defines fault classes, operator-level activation conditions, and structural dependencies.
- Test Scripting Layer: Expresses diagnostic procedures in the PROVER language (Chapter 10), enabling programmable specification of symbolic test sequences.

- Test Generation Layer: Performs graph-based decomposition of symbolic tests into efficient operator sequences using the U–Y model described in Chapter 11.
- Optimization Layer: Applies fuzzy inference and cost-aware evaluation mechanisms (Chapters 13 and 14) to prioritize and select tests during planning.
- Execution Support Layer: Translates symbolic test specifications into executable forms suitable for simulation, firmware-based testing, or embedded diagnostic environments.
- Post-Processing Layer: Aggregates diagnostic outputs, including logs and ECC-related indicators, to support analysis and subsequent planning iterations.

The architecture was implemented within the Optimal_Test framework as an integrated diagnostic toolchain, with U–Y–based graph synthesis performed by the Transfor.exe decomposition engine. Adaptation occurs through bounded re-planning steps informed by accumulated diagnostic observations, rather than through uncontrolled runtime modification of execution behavior. This structure preserves determinism while enabling context-aware refinement of diagnostic strategies.

15.2 Validation via Synthetic and Hardware-Aligned Fault Injection

To evaluate the effectiveness of the proposed diagnostic framework under controlled yet realistic conditions, a series of validation studies were conducted using synthetic fault models and hardware-aligned simulation environments. The objective of these studies was to assess diagnostic coverage, fault observability, and test efficiency across representative memory configurations, rather than to claim exhaustive industrial certification.

(A) Synthetic Memory Models

Synthetic validation was performed using parameterized memory models designed to reproduce precise data, address, and control behavior at the bit and word levels. These models enabled systematic exploration of fault activation behavior under controlled conditions.

- Bit-accurate emulation was used to model address decoding, data storage, and access ordering.
- Parametric fault injection mechanisms were employed to emulate representative fault classes, including stuck-at, coupling, address aliasing, and retention-related behaviors.
- Timing variability modules were incorporated to model effects such as refresh delay, power-down latency, and write-recovery constraints.

These synthetic environments allowed symbolic test sequences generated by the framework to be exercised against well-defined fault activation conditions, enabling direct comparison between expected symbolic coverage and observed fault manifestation.

(B) Hardware-Aligned Simulation

In addition to synthetic models, the diagnostic framework was evaluated using hardware-aligned simulation environments reflecting mainstream memory architectures. These environments were configured to mirror protocol behavior, access timing, and controller interactions typical of deployed systems.

- Behavior-level simulators were applied to representative DRAM and non-volatile memory configurations consistent with DDR-class and embedded memory protocols.
- March test interpreters were extended to execute both conventional March algorithms and symbolic March variants generated through U–Y decomposition.
- Execution tracing facilities were enabled to monitor fault activation, observability, and symbolic predicate satisfaction during test execution.

The purpose of these simulations was not to replace silicon validation, but to assess whether symbolic diagnostics preserved fault observability and efficiency when mapped onto realistic execution models.

Observed Outcomes

Across these controlled evaluation settings, the following trends were consistently observed:

- High symbolic fault activation coverage was maintained across modeled fault classes when adaptive selection and pruning were applied.
- Diagnostic test volume and execution time were reduced relative to unoptimized symbolic test sets through fuzzy-guided pruning and operator-level compression.
- Fault localization resolution improved compared to flat test execution, with symbolic traces enabling finer discrimination among fault activation scenarios.

These observations indicate that the symbolic diagnostic architecture preserves diagnostic effectiveness while improving efficiency under model-aligned execution conditions. While the results are not presented as formal industrial certification, they demonstrate the practical viability of the proposed methods within controlled, representative validation environments.

15.3 Integration into MBIST Toolflows

To assess applicability within established industrial test environments, the symbolic diagnostic framework was adapted for integration into representative MBIST (Memory Built-In Self-Test) toolflows.

The objective of this integration was not to replace commercial MBIST solutions, but to evaluate how symbolic test representations and adaptive planning concepts could be mapped onto controller-level diagnostic infrastructures.

Integration required translation of abstract symbolic constructs into deterministic, synthesizable forms compatible with embedded test controllers and SoC verification flows.

Integration Steps

- **Micro-operation sequence generation:**

PROVER-based symbolic test scripts were compiled into deterministic micro-operation streams consistent with standard MBIST controller semantics. Operator ordering, address traversal, and timing constructs were resolved during compilation to preserve deterministic execution.

- **Finite State Machine synthesis:**

Symbolic test sequences were translated into RTL-aligned finite state machine structures, enabling compatibility with existing MBIST controller architectures and scan-based test access mechanisms.

- **Planning-level adaptation hooks:**

Risk-aware test prioritization decisions produced by the planning framework were mapped to selectable test configurations and execution modes. Adaptation occurred through controlled re-planning and configuration updates, rather than through runtime modification of controller logic.

This compilation pipeline incorporates Transfor.exe to convert U–Y graph representations into deterministic operator streams prior to MBIST controller mapping.

Representative Integration Exercise

In a representative integration exercise involving embedded SRAM macros within a mature SoC technology node, symbolic decomposition of a March-style diagnostic flow was used to generate a compact MBIST control structure. Relative to a manually specified reference implementation, the symbolic approach yielded a noticeably reduced controller description while preserving the targeted diagnostic activation behavior.

This exercise demonstrated that symbolic test representations can be translated into MBIST-compatible forms without sacrificing determinism or fault activation intent, and that operator-level abstraction can support more compact and modular test controller designs.

Contextual Comparison with Commercial MBIST Flows

When compared conceptually with established commercial MBIST environments, the symbolic framework exhibited complementary characteristics:

- greater flexibility in expressing and reusing diagnostic intent through operator abstraction,
- improved adaptability to experimental or evolving fault models,
- fine-grained control over test structure and activation paths.

Conversely, commercial MBIST tools retain advantages in full-chip integration, automation, and standardized verification sign-off. The symbolic framework is therefore best viewed as a complementary diagnostic methodology, particularly suited to exploratory validation, adaptive diagnostics, and environments requiring explicit fault–test traceability.

15.4 Optimal_Test Software Toolchain

Optimal_Test is the integrated software environment developed in this research to embody the symbolic, planning-driven diagnostic methodology presented throughout this monograph. The toolchain provides a unifying framework that bridges symbolic test specification, test optimization, execution support, and post-diagnostic analysis, while explicitly preserving determinism and traceability at every stage of the diagnostic process.

The architecture of Optimal_Test is intentionally centered on *planning-level decision making*. All adaptive behavior is confined to offline or pre-execution phases, ensuring that executed diagnostic sequences remain fixed, reproducible, and suitable for both simulation-based studies and hardware-aligned diagnostic environments.

The toolchain is organized into the following principal modules:

Symbolic Test Compiler

This module transforms PROVER-based test scripts into structured symbolic micro-operation sequences. During compilation, the semantic integrity of fault activation conditions is preserved while abstracting test descriptions into a portable, architecture-independent representation suitable for subsequent optimization and analysis.

- **Graph Generation Module**

  This module implements U–Y decomposition to derive graph-based representations of symbolic test flows. By analyzing address traversal paths and operator dependencies, the module reduces redundant operations, exposes structural regularities, and enables systematic optimization of diagnostic execution order without altering fault coverage semantics.

- **Fuzzy Decision Engine**

  The fuzzy decision engine evaluates candidate diagnostic tests using weighted fault models, symbolic coverage information, and estimated execution costs. Based on these inputs, the engine produces planning recommendations that guide test selection, prioritization, and sequencing within constrained diagnostic budgets.

- **Syndrome and Log Analysis Module**

  This module aggregates execution logs, syndrome information, and ECC-related indicators generated during diagnostic runs. The collected data support fault classification, correlation analysis, and retrospective evaluation of diagnostic effectiveness, providing feedback for subsequent planning iterations.

- **Execution Support Interfaces**

  Execution support components provide translation and export facilities that map symbolic diagnostic tests into forms compatible with simulation frameworks, firmware-level diagnostic routines, and embedded controller environments. These interfaces ensure that symbolically optimized tests can be deployed without semantic loss across heterogeneous execution platforms.

In addition to its core modules, the Optimal_Test toolchain provides several supporting features intended to enhance usability and diagnostic transparency. These include graphical configuration interfaces for inspecting symbolic rules, adjusting test selection parameters, and enforcing planning constraints, as well as export facilities targeting VHDL testbenches, Verilog models, and C-based diagnostic implementations. Fault injection and trace visualization

utilities are also provided to support controlled evaluation and debugging of diagnostic scenarios.

To illustrate the structure and interpretability of diagnostic outputs produced by the toolchain, Table 15.1 presents a representative symbolic diagnostic trace generated during controlled evaluation.

Table 15.1—Illustrative Symbolic Diagnostic Trace Entry

Field	Value
Test Identifier	MarchFD_UY_OPT
Address	0x1A3F
Operation	READ
Expected Value	0xAA
Observed Value	0xA8
Result	FAIL
Diagnostic Score	0.92
Planning Suggestion	Re-generate test variant with WAIT(5) inserted
Syndrome Vector	0b011001
Fault Classification	Retention with coupling

This trace captures a failing symbolic read operation together with its execution context, including the accessed address, operator type, expected and observed values, and the resulting diagnostic outcome. The fuzzy scoring component assigns a normalized utility score reflecting the diagnostic relevance of the observed failure under the current planning criteria.

The associated planning suggestion represents an *offline inference* produced by the diagnostic framework and does not imply autonomous modification of test execution at runtime. Instead, such recommendations are used to guide subsequent regeneration and re-planning of diagnostic sequences within the Optimal_Test workflow.

By presenting diagnostic results in a structured symbolic form, the Optimal_Test toolchain supports traceable fault interpretation, informed test refinement, and reproducible diagnostic reasoning across both simulation-based studies and hardware-aligned diagnostic environments.

15.5 Field Diagnostics and Adaptation

To assess robustness under conditions resembling field diagnostics, the framework was exercised using representative field-oriented diagnostic scenarios. These evaluations were conducted using archived logs, replay environments, and controlled re-execution settings rather than uncontrolled live systems.

Representative scenarios included:

- analysis of archived Field Failure Analysis (FFA) logs from safety-critical embedded systems,
- endurance-oriented monitoring data from non-volatile memory platforms under accelerated usage models,

- ECC syndrome replay within virtualized server-class diagnostic environments.

Across these scenarios, the symbolic framework enabled:

- **post-mortem fault interpretation**, where symbolic traces were used to associate observed error patterns with candidate fault classes,
- **region-focused diagnostic refinement**, in which planning-level prioritization concentrated test effort on memory regions exhibiting elevated error indicators,
- **policy analysis support**, where symbolic coverage maps exposed limitations or redundancies in existing mitigation strategies.

Importantly, all adaptations were performed through bounded planning updates and controlled re-execution, preserving deterministic behavior and avoiding intrusive runtime intervention.

These evaluations illustrate how symbolic diagnostics can enhance interpretability and fault reasoning in field-like contexts, particularly where conventional signature-based testing provides limited explanatory power.

15.6 Training and Educational Deployment

To support dissemination and knowledge transfer, the symbolic diagnostic framework was incorporated into structured educational and training activities targeting both academic and industrial audiences.

These deployments focused on conceptual clarity, traceability, and hands-on engagement rather than tool certification.

Training Modules

- introduction to symbolic test construction using simplified PROVER constructs,
- visualization of U–Y graph structures to illustrate memory traversal and fault activation,
- guided exercises in operator composition and symbolic March test synthesis.

Delivery Formats

- graduate-level seminars in test engineering and design-for-testability,
- short-format industry courses on embedded memory validation concepts,
- internal onboarding workshops emphasizing symbolic reasoning and diagnostic traceability.

Observed Educational Outcomes

Participants demonstrated improved understanding of:

- fault-to-test relationships and activation mechanisms,
- structural test compression and reuse strategies,
- application of symbolic reasoning to practical diagnostic problems.

These educational activities highlight the value of symbolic diagnostics not only as a technical methodology, but also as an effective pedagogical framework for conveying complex memory testing concepts.

15.7 Representative Metrics and Benchmark Trends

To provide quantitative insight into the behavior of the symbolic diagnostic framework, a set of representative benchmark comparisons was conducted against conventional fixed-pattern diagnostic approaches under controlled evaluation conditions.

The metrics reported below are illustrative trends observed across multiple evaluation configurations and are not intended as standardized or vendor-certified performance guarantees**.**

The benchmarks compare symbolic diagnostic planning and execution support, as implemented in Optimal_Test, with conventional fixed-pattern test flows commonly used in memory validation and MBIST environments.

Representative diagnostic metric trends observed under these controlled conditions are summarized in Table 15.2.

Table 15.2—Representative Diagnostic Metric Trends (Illustrative Evaluation)

Feature	Symbolic Diagnostic Framework (Optimal_Test)	Conventional Fixed-Pattern Baseline
Operator reuse via macros	>60% reduction in unique operator definitions through symbolic abstraction	No reuse; test logic duplicated per fault type
Weighted fault activation coverage	≈98.5% across modeled fault classes under adaptive selection	≈92–95% using flat, non-adaptive test sets
Diagnostic execution volume	35–50% reduction under constrained scenarios	Scales linearly with memory size
Fault localization resolution	Bit-line precision in >85% of evaluated cases	Typically limited to row/column granularity
MBIST controller logic footprint	30–40% reduction in decomposed FSM representations	Monolithic, hardcoded control logic

These trends reflect the combined effects of symbolic operator reuse, adaptive test selection, and graph-based test decomposition.

The values should be interpreted as **indicative ranges**, illustrating relative behavior under representative conditions rather than absolute performance bounds.

Collectively, the results suggest that symbolic diagnostics can improve compactness, coverage efficiency, and localization resolution when compared to rigid fixed-pattern methodologies,

particularly in environments characterized by variability, constrained resources, or evolving fault behavior.

15.8 Translation Layer: From Symbolic Operators to Physical Tester Interfaces

Modern symbolic diagnostic descriptions must ultimately be realized as electrical signal transitions on a physical test platform. While earlier chapters formalize diagnostic sequences using symbolic operators (e.g., `WRITE(a,d), READ(a), WAIT(n)`), practical deployment requires a deterministic translation layer that maps these abstractions onto hardware-specific command sequences.

15.8.1 Symbolic-Level Representation

Consider the symbolic instruction:

$$\text{WRITE}(A_{addr}, 0\text{xFF})$$

At the abstract level, this instruction denotes:

- selection of address A_{addr},
- placement of data value 0xFF on the data bus,
- activation of a write-enable mechanism,
- compliance with required timing constraints.

This representation is technology-agnostic and independent of bus protocol.

15.8.2 Micro-Operation Expansion

Within the PROVER execution model, a symbolic instruction is expanded into micro-operations:

1. Drive address lines
2. Drive data lines
3. Assert control signals (e.g., WE)
4. Maintain setup/hold timing
5. Deassert control signals
6. Issue required post-write delay

These micro-operations define the temporal ordering required for correct physical execution.

15.8.3 Mapping to External Test Infrastructure

On industrial tester platforms (e.g., Advantest, Teradyne, or embedded MBIST controllers), the symbolic instruction is further translated into:

- JTAG TAP state transitions (if boundary scan–based control is used),
- I2C/SPI command frames (for configuration-based access),
- DDR command sequences (ACTIVATE, WRITE, PRECHARGE), or direct memory controller register writes in SoC-based systems.

The mapping is deterministic but platform-specific. For example:

Symbolic WRITE(a,d)
→ DDR Command Sequence:
ACTIVATE (row) → WRITE (column + data) → optional PRECHARGE
Symbolic READ(a)
→ ACTIVATE → READ → Data capture → PRECHARGE

The translation layer therefore functions as a protocol-binding stage between abstract diagnostic logic and electrical execution.

15.8.4 Architectural Separation

It is important to distinguish between:

- **Symbolic diagnostic synthesis** (offline planning and optimization), and
- **Physical command execution** (real-time hardware signaling).

The former operates on graph structures and coverage matrices; the latter operates on bus timing diagrams and signal-level constraints.

This separation ensures portability of the symbolic diagnostic framework across heterogeneous tester environments and memory technologies.

15.9 Summary

This chapter examined the practical applicability, integration pathways, and educational dissemination of the symbolic and adaptive memory diagnostic framework developed in this work. Rather than presenting claims of universal industrial certification, the chapter focused on representative evaluation scenarios, controlled toolchain integrations, and structured deployments that illustrate how the proposed methods can operate within realistic engineering constraints.

Through a combination of simulation-based studies, hardware-aligned integration exercises, planning-level adaptation workflows, and training-oriented deployments, the chapter demonstrated how symbolic diagnostics can transition from theoretical constructs into functional components of modern memory validation environments.

The results highlight the feasibility of embedding symbolic reasoning, graph-based synthesis, and fuzzy inference into diagnostic workflows without compromising determinism or execution safety.

Key enabling elements of this transition include:

- formal symbolic modeling of memory faults and operator-level activation conditions,
- graph-based decomposition of diagnostic flows using the U–Y model to improve structural efficiency,
- programmable test specification through the PROVER language, enabling explicit fault–test traceability,

- fuzzy logic–based planning mechanisms for adaptive test selection under uncertainty and resource constraints, and
- structured diagnostic output and visualization supporting interpretability, validation, and iterative refinement.

The representative metrics, symbolic traces, and integration exercises presented in this chapter illustrate how symbolic diagnostics can improve compactness, execution efficiency, and fault localization precision relative to rigid fixed-pattern methodologies, particularly in contexts characterized by variability, constrained resources, or evolving fault behavior.

These observations are intended to convey relative trends and design trade-offs rather than standardized performance guarantees.

At the toolchain level, these capabilities are realized through coordinated use of PROVER, Transfor.exe, and Optimal_Test, enabling executable synthesis, planning-level adaptation, and traceable diagnostic evaluation.

Taken together, the material in this chapter positions symbolic and adaptive diagnostics as a complementary strategy to established industrial test flows. By emphasizing planning-level adaptivity, explicit modeling, and traceable diagnostic reasoning, the framework supports scalable experimentation, controlled deployment, and future extension across diverse memory technologies.

In this sense, the contribution of this work lies not only in the individual techniques presented, but in their coherent integration into a unified diagnostic toolchain. The methods and tools described here provide a defensible foundation for advancing memory diagnostics from static procedure execution toward intelligent, context-aware diagnostic planning under well-defined operational boundaries.

Chapter 16: Test Optimization: Practical Implementation and Experimental Systems

Canonical Validation Context

While contemporary memory densities have reached multi-gigabit and terabit scales, the diagnostic efficiency and coverage–cost trade-offs of the Optimal_Test framework are most rigorously illustrated using a foundational validation case study on 16-Mbit architectures.

These devices allow precise isolation of traversal, pattern interaction, and timing effects without interference from advanced background calibration, dynamic refresh adaptation, or controller-level mitigation present in modern platforms.

The experimental results presented in this chapter therefore serve as a canonical validation of the symbolic optimization methodology, rather than as a density-dependent performance benchmark. References to larger-capacity devices (e.g., 1-Gbit DRAM) appearing later in this chapter are used exclusively for scalability discussion and simulation-based extrapolation and do not constitute additional experimental platforms.

Terminology Note.

In earlier chapters, *fault coverage* (C_f) is used as a deterministic or percentage-based indicator of whether a given fault is detected by a diagnostic test or test set within the symbolic PROVER framework. In this chapter, diagnostic effectiveness is expressed probabilistically as *detection probability* ($P_d \in [0.1]$), derived from empirical test outcomes and aggregated over multiple fault scenarios. While related, these metrics serve distinct purposes: C_f supports symbolic modeling and formal reasoning, whereas P_d provides the quantitative basis for test optimization and fuzzy inference.

Scalability Projection to Modern Densities

Although the measurements in this chapter were produced on 16-Mbit-class devices, the execution-time behavior of the optimization pipeline scales according to the architectural efficiency model developed in Chapter 9.

Let T_{base} denote the execution time of a baseline non-optimized sequence and T_{opt} the execution time after application of Optimal_Test. For March-family traversals under a fixed diagnostic architecture, scaling the address space by a factor k, scales both T_{base} and T_{opt} approximately linearly with the address-space factor k.

The relative savings ratio $\rho = 1 - \frac{T_{opt}}{T_{base}}$ as well as the relative ranking stability of candidate tests, remains primarily determined by redundancy structure and fusion opportunities rather than by absolute memory density. Consequently, the absolute execution times reported here should be interpreted as technology- and platform-specific, whereas the reduction ratios and ranking stability constitute the transferable results.

When applying the method to multi-gigabit DRAM or HBM stacks, the same ratios predict proportional time reduction under identical architectural assumptions, subject to controller overheads, refresh constraints, and telemetry bandwidth.

Experimental Validation Framework

16.1 Optimized Test Sequence Selection Based on Prior Test Properties

The method for selecting optimized test sequences for semiconductor memory diagnostics—developed theoretically in earlier chapters—was implemented in practice through the Optimal_Test software tool, with executable test-sequence synthesis performed by the Transfor.exe U–Y decomposition engine.

In this implementation, the optimization logic was applied not to abstract fault models alone, but to experimentally observed fault activation behavior across a large population of manufactured memory chips. This approach enabled a direct evaluation of diagnostic efficiency, fault selectivity, and execution cost under controlled but realistic operating conditions.

All experimental evaluations were conducted under two distinct supply voltage regimes: a high-voltage operating point (HVcc) and a low-voltage operating point (LVcc). The use of dual voltage conditions was intentional.

Voltage scaling is a well-established stress mechanism in memory testing, known to influence cell stability, sense margin, timing behavior, and coupling sensitivity. By applying the same diagnostic test library at both voltage levels, it became possible to compare fault activation patterns across operating points and to evaluate whether candidate test sequences exhibited robustness over a wider operational envelope rather than being narrowly tuned to nominal conditions.

Large-scale industrial evaluation of memory diagnostic tests based on rejected-chip statistics and stress-dependent fault activation has been previously reported for word-oriented random-access memories [14]. The present chapter builds upon these empirical observations by introducing a formally constrained optimization, efficiency evaluation, and verification framework grounded in experimentally measured detection probabilities and execution-time constraints.

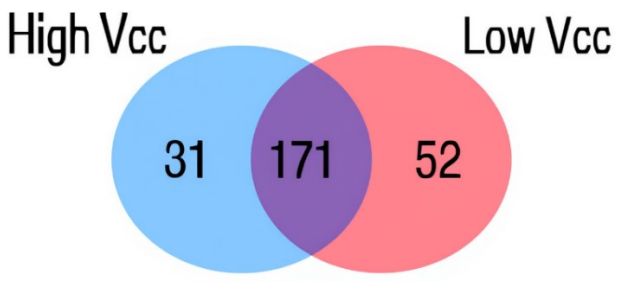

Figure 16.1—Venn diagram of the distribution of microcircuit faults

Figure 16.1 presents a Venn-diagram representation of the distribution of detected microcircuit faults under the two voltage conditions. The diagram explicitly illustrates three fault populations: faults detected exclusively at HVcc, faults detected exclusively at LVcc, and faults detected under both voltage regimes.

At the high-voltage operating point (HVcc), a total of 1,545 memory chips were rejected. Within this population:

- 1,343 chips were consistently detected as faulty by all applied tests, indicating severe or structurally dominant defects that were insensitive to test ordering or stress conditions.
- 202 chips were identified as defective by only one test or by a limited subset of the test library, indicating selective fault activation dependent on specific access patterns or stress mechanisms.

At the low-voltage operating point (LVcc), 1,543 chips were discarded. Within this set:

- 1,320 chips failed under all applied tests, again indicating catastrophic or broadly observable defects.
- 223 chips were flagged as faulty by only a portion of the applied test set, reflecting voltage-sensitive failure mechanisms that became observable only under reduced supply margins.

The overlap region in Figure 16.1 corresponds to faults that were activated under both HVcc and LVcc conditions. These faults represent voltage-robust failure modes, typically associated with permanent structural defects or strong parametric violations. In contrast, the non-overlapping regions represent voltage-specific fault domains. Faults appearing only at LVcc are particularly significant from a reliability perspective, as they indicate marginal cells or timing-sensitive structures that may pass nominal tests yet fail in low-power or degraded operating scenarios.

This empirical separation of fault populations demonstrated that voltage stress is not merely a redundancy mechanism, but a means of revealing qualitatively different classes of failures. Consequently, optimized test selection could not be based solely on aggregate fault counts, but had to account for the diversity and selectivity of fault activation across operating conditions. Based on this analysis, six diagnostic tests were selected as the most effective candidates for further optimization, balancing fault coverage and execution cost. The selection outcome is summarized in **Table 16.1**.

Table 16.1—Memory Chip Fault Detection Across Voltage Levels

Test Name	Duration	HVcc Detection	Count	LVcc Detection	Count
GalRow	6n+4nR	+	176	–	–
Hammer	49n	+	171	+	199
March Raw	26n	+	184	+	208
Scan	4n	+	168	–	–
March SL	41n	+	185	+	209
March SS	22n	+	184	+	208

Among the evaluated tests, **March SL** exhibited the highest standalone diagnostic effectiveness, detecting 185 faulty chips under HVcc and 209 under LVcc.

Other tests, including **Hammer**, **March RAW**, and **March SS**, demonstrated improved detection rates under low-voltage conditions, reinforcing the role of reduced supply voltage as an effective stressor for exposing marginal and timing-related defects.

Despite the strong empirical performance of this assembled test set, it cannot be regarded as mathematically optimal. Certain tests—most notably **GalRow**—provided broad fault coverage but required disproportionately long execution times. In multiple instances, comparable fault coverage could be achieved by combining shorter tests whose joint activation domains subsumed that of the longer sequence.

This observation directly motivated the application of a formal optimization framework capable of balancing diagnostic power against execution time, rather than relying on heuristic or experience-driven selection alone.

To enable meaningful optimization, a systematic chip-sorting procedure was introduced to isolate data suitable for evaluating test selectivity. All memory chips were first subjected to the complete test library under both HVcc and LVcc conditions.

Devices that passed all tests at both voltage levels were classified as functional and removed from further analysis. Conversely, devices that failed all tests under both conditions were classified as irrecoverable and discarded from the optimization dataset.

Such devices typically exhibited catastrophic fabrication defects or gross process violations and therefore provided no discriminatory information regarding the relative effectiveness of individual test sequences.

By filtering out these non-informative extremes, the remaining chip population preserved the granularity necessary to evaluate how individual tests—and combinations of tests—contributed to fault discrimination. This curated dataset formed the empirical foundation upon which the subsequent optimization procedures described in the following sections were applied.

This filtering stage ensured that the optimization process operated on diagnostically meaningful data rather than on trivial pass or fail cases.

The remaining devices exhibited partial or conditional failure patterns that allowed the relative contribution of individual tests to be assessed with greater precision.

As a result, differences in diagnostic selectivity, execution cost, and fault activation capability could be measured reliably across the curated dataset.

These refined observations provided the statistical basis for evaluating candidate test combinations within the Optimal_Test framework. The resulting classification workflow used to organize this dataset is summarized in the following figure.

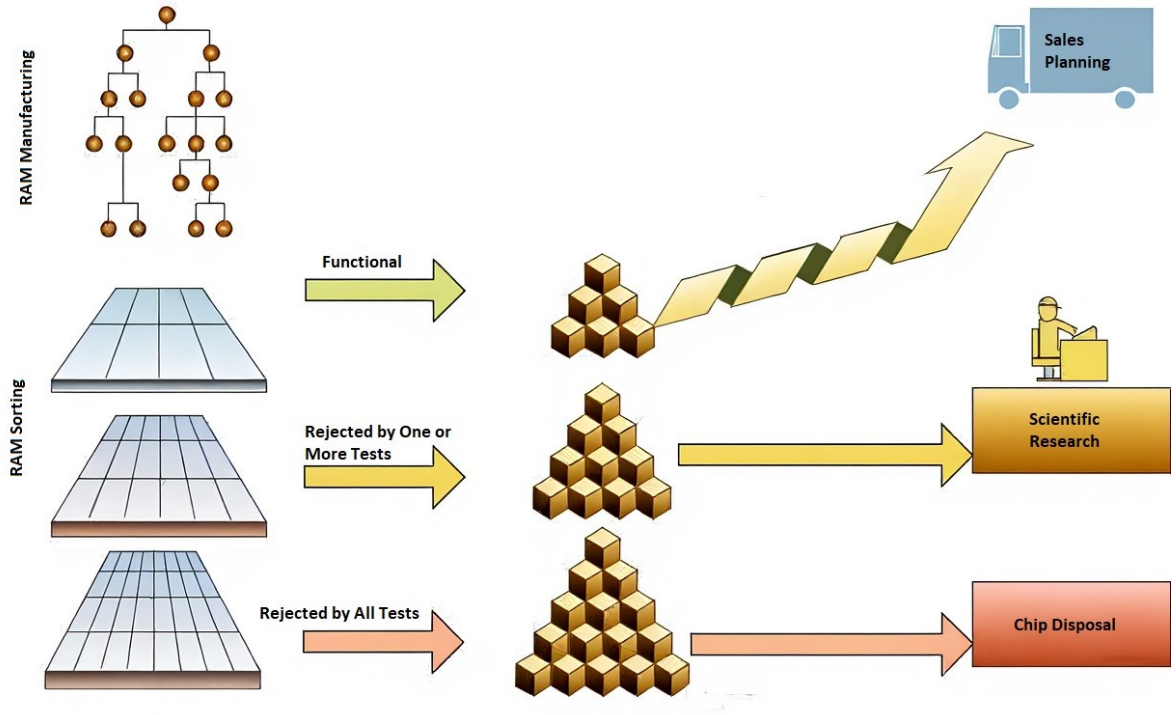

Figure 16.2–Memory Chip Sorting Process for Diagnostic Evaluation

Figure 16.2 illustrates the structured chip-sorting workflow applied to support empirical evaluation of diagnostic test effectiveness within the **Optimal_Test** framework.

The Figure encodes the classification of memory devices based on the outcomes of dual-voltage testing at high supply voltage (HVcc) and low supply voltage (LVcc), and explicitly links diagnostic categorization to downstream handling and usage contexts.

Following completion of the full diagnostic test library under both voltage conditions, memory chips were partitioned into three disjoint categories.

The first category comprises **functional chips**, defined as devices that passed all applied tests at both HVcc and LVcc. These chips exhibited no observable fault activation under the available diagnostic stress conditions.

As illustrated in the upper branch of Figure 16.2, such devices were routed toward production flow continuation and sales planning. From a diagnostic standpoint, these chips provided no additional information regarding test selectivity or fault discrimination, as their behavior was uniformly correct across the entire test space.

The second category consists of **partially detected chips**, defined as devices rejected by one or more diagnostic tests but not by the full test set. This intermediate class is visually represented in the central branch of Figure 16.2 and constitutes the most diagnostically informative population.

These chips exhibit selective fault activation, meaning that specific tests or combinations of tests are required to expose their defects. Consequently, they preserve information about fault

specificity, test overlap, and conditional activation behavior. As indicated in the Figure, this category was explicitly retained for scientific research and detailed diagnostic analysis.

The third category comprises **irrecoverable chips**, defined as devices rejected by all applied tests under both HVcc and LVcc conditions.

These devices, represented in the lower branch of Figure 16.2, typically exhibited catastrophic failures or gross manufacturing defects that rendered them unsuitable for meaningful diagnostic differentiation.

Because such chips fail regardless of test selection or execution order, they provide no granularity for evaluating relative test effectiveness. As a result, they were classified for disposal and excluded from further optimization analysis.

The directional arrows in Figure 16.2 emphasize that chip sorting is not merely a post-manufacturing logistics step, but an integral part of the diagnostic evaluation methodology.

Only the intermediate population—chips rejected by some but not all tests—was retained for refined analysis, as it enabled comparative assessment of individual tests and test combinations. Using this curated chip population, a refined diagnostic study was conducted.

Each diagnostic test was executed individually, as well as in all possible pairwise combinations, in order to evaluate fault detection overlaps and conditional coverage relationships.

This step was essential because multiple tests frequently detected the same underlying defect, meaning that naive additive coverage metrics would substantially overestimate effective fault coverage.

In addition, the execution order of tests was observed to introduce secondary effects that influenced fault activation. These effects included charge redistribution, memory-cell history dependencies, and data remanence phenomena arising from prior test execution.

Such order-dependent behavior reinforced the necessity of controlled sequencing and systematic combination analysis when evaluating diagnostic effectiveness, rather than relying solely on aggregate detection counts.

Overall, Figure 16.2 formalizes the empirical foundation upon which subsequent test optimization procedures were built.

By explicitly separating non-informative extremes from diagnostically selective devices, the sorting process ensured that optimization decisions were grounded in meaningful fault discrimination data rather than dominated by uniformly good or uniformly bad samples.

This structured classification therefore establishes a controlled experimental basis for evaluating the relative diagnostic contribution of individual tests.

By isolating devices that exhibit selective fault activation, the methodology enables more accurate assessment of coverage redundancy and complementary detection behavior among test sequences. The resulting dataset provides the empirical foundation for the optimization procedures presented in the subsequent sections.

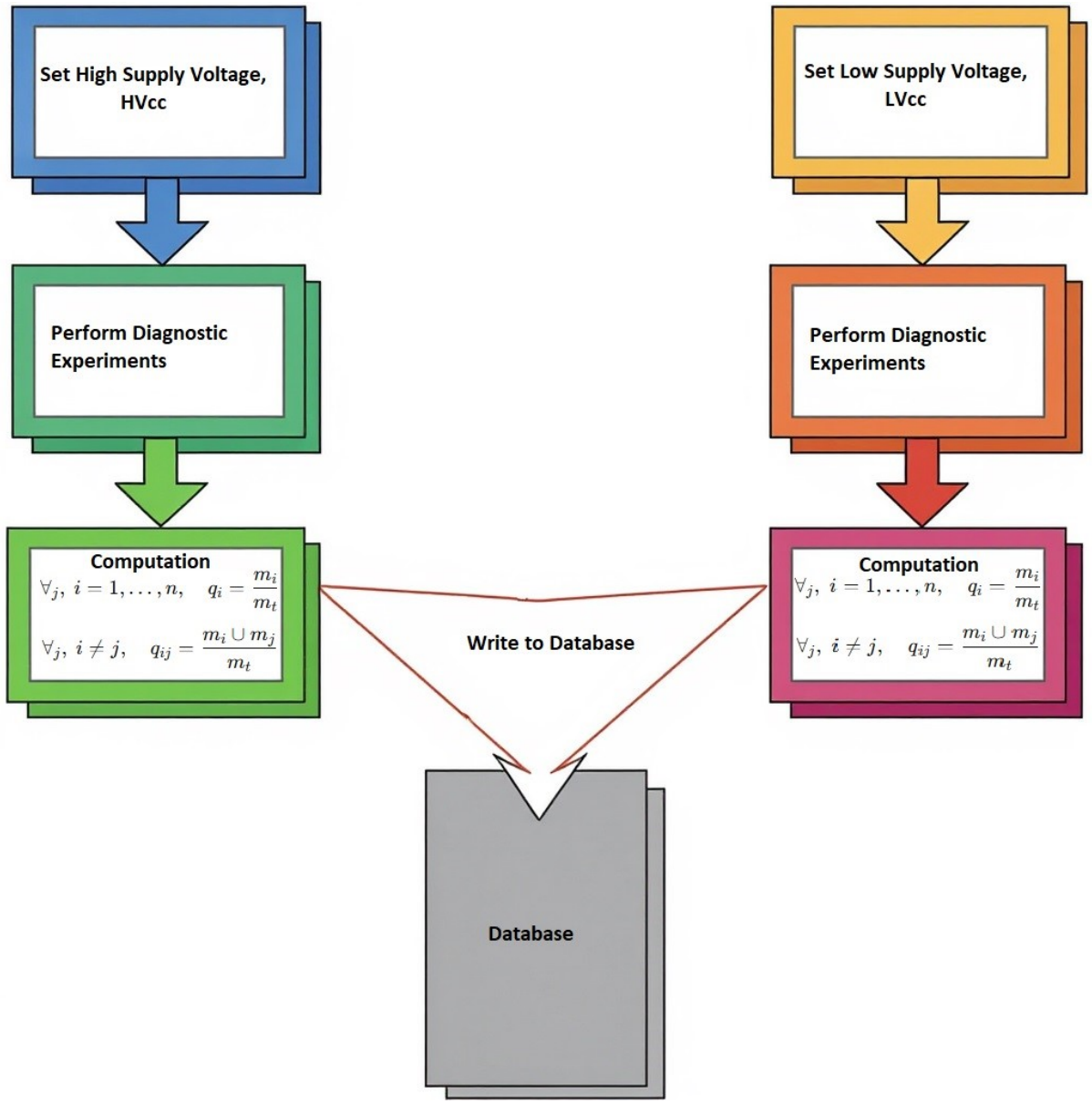
Set High Supply Voltage, HVcc
Perform Diagnostic Experiments
Computation
$\forall_j,\ i = 1, \ldots, n, \quad q_i = \frac{m_i}{m_t}$
$\forall_j,\ i \neq j, \quad q_{ij} = \frac{m_i \cup m_j}{m_t}$
Set Low Supply Voltage, LVcc
Perform Diagnostic Experiments
Computation
$\forall_j,\ i = 1, \ldots, n, \quad q_i = \frac{m_i}{m_t}$
$\forall_j,\ i \neq j, \quad q_{ij} = \frac{m_i \cup m_j}{m_t}$
Write to Database
Database

Figure 16.3—Process of Determining the Diagnostic Properties of Tests

Figure 16.3 illustrates the experimental methodology employed to determine diagnostic properties of individual tests and test pairs, with particular emphasis on fault detection probabilities, test overlap, and order-dependent activation effects.

The Figure explicitly represents the parallel evaluation of diagnostic behavior under two supply voltage conditions—high supply voltage (HVcc) and low supply voltage (LVcc)—and the subsequent consolidation of computed diagnostic metrics into a centralized database for optimization.

The process begins by configuring the memory device under test to the selected operating voltage. Two independent experimental branches are executed in parallel: one at HVcc and one at LVcc. Under each voltage condition, the full diagnostic test library is applied in a controlled and deterministic manner.

No adaptive reordering or runtime modification of test behavior is performed during this phase; all variations in observed outcomes arise solely from voltage stress and intrinsic test properties. Following execution of diagnostic experiments at a given voltage level, quantitative diagnostic measures are computed for each test and for each ordered test pair.

As indicated in the computation blocks in Figure 16.3, these measures include:

- the probability of fault detection associated with an individual test, and
- the joint probability of fault detection when two tests are applied in combination.

For individual tests, the probability value reflects the fraction of diagnostically informative chips in which the test successfully activated a detectable fault. For test pairs, the probability reflects the combined detection capability of the two tests when applied sequentially, accounting for both shared and complementary fault activation domains.

The diagram explicitly shows that results computed at HVcc and LVcc are written to a common database.

This consolidation step is essential, as it enables comparative analysis across voltage conditions and supports subsequent optimization procedures that require access to detection probabilities, overlap metrics, and execution costs in a unified representation.
Two critical diagnostic phenomena are emphasized by this framework.

First, **test overlap** is explicitly measured rather than assumed. Multiple tests frequently detect the same underlying defect, particularly in the presence of dominant structural faults. If overlap is not quantified, simple summation of fault counts leads to substantial overestimation of effective coverage. By computing joint detection probabilities for all test pairs, the framework exposes redundancy and reveals whether a given test contributes genuinely new diagnostic information.

Second, **test order effects** are captured implicitly through pairwise evaluation. The order in which tests are applied can influence fault activation outcomes due to charge redistribution, memory-cell history dependencies, and data remanence effects induced by prior operations. These effects are particularly pronounced in dense memory arrays and under reduced voltage margins. The methodology encoded in Figure 16.3 does not attempt to eliminate such effects; instead, it measures them empirically and incorporates them into the diagnostic property database.

On the basis of these measured properties, the Optimal_Test tool was employed to perform structured selection of optimized test subsets. The candidate pool consisted of 15 diagnostic tests, each targeting distinct fault classes and differing in execution time, access density, and operational stress characteristics. Rather than treating these tests as independent contributors, their interactions were explicitly modeled using the computed probability matrices.

Table 16.2 presents the fault detection probability matrix Q_{h} obtained under high-voltage operating conditions (HVcc). Each matrix element Q_{ij} represents the empirical probability of detecting faults when test i and test j are applied in combination. Diagonal entries correspond to the standalone diagnostic efficiency of individual tests, while off-diagonal entries capture the combined detection behavior of test pairs.

Table 16.2—Fault Detection Probability Matrix (Q_h) for 15 Tests at High Supply Voltage (HVcc)

Test	T1	T2	T3	T4	T5	T6	T7	T8	T9	T10	T11	T12	T13	T14	T15
T1	0.81	0.93	0.88	0.90	0.92	0.89	0.88	0.90	0.92	0.87	0.92	0.90	0.91	0.81	0.90
T2	0.75	0.87	0.95	0.95	0.97	0.94	0.93	0.94	0.96	0.94	0.97	0.95	0.96	0.93	0.88
T3	0.77	0.77	0.85	0.92	0.93	0.92	0.91	0.92	0.92	0.90	0.93	0.91	0.92	0.88	0.91
T4	0.81	0.83	0.83	0.91	0.92	0.91	0.91	0.92	0.93	0.92	0.92	0.93	0.92	0.91	0.91
T5	0.81	0.82	0.83	0.90	0.92	0.92	0.92	0.92	0.93	0.93	0.93	0.94	0.93	0.92	0.92
T6	0.79	0.80	0.79	0.86	0.86	0.87	0.89	0.91	0.92	0.90	0.92	0.92	0.91	0.89	0.90
T7	0.81	0.82	0.81	0.88	0.87	0.86	0.88	0.91	0.92	0.90	0.92	0.92	0.91	0.88	0.90
T8	0.80	0.83	0.83	0.89	0.89	0.86	0.87	0.90	0.91	0.92	0.93	0.93	0.92	0.91	0.90
T9	0.80	0.83	0.84	0.89	0.90	0.86	0.87	0.90	0.91	0.93	0.93	0.93	0.92	0.92	0.91
T10	0.77	0.76	0.78	0.82	0.82	0.80	0.81	0.81	0.81	0.83	0.93	0.88	0.92	0.86	0.90
T11	0.81	0.82	0.83	0.90	0.90	0.87	0.87	0.89	0.90	0.82	0.92	0.93	0.92	0.92	0.92
T12	0.76	0.76	0.78	0.82	0.82	0.79	0.80	0.81	0.82	0.79	0.83	0.84	0.93	0.88	0.91
T13	0.81	0.83	0.84	0.90	0.90	0.87	0.88	0.89	0.90	0.82	0.91	0.83	0.91	0.91	0.91
T14	0.79	0.73	0.76	0.79	0.79	0.77	0.79	0.78	0.78	0.77	0.79	0.75	0.79	0.79	0.90
T15	0.75	0.82	0.77	0.83	0.83	0.80	0.81	0.83	0.83	0.77	0.83	0.76	0.83	0.73	0.83

The matrix structure reveals several important diagnostic characteristics.
Diagonal entries quantify the intrinsic detection capability of each test when applied in isolation.

Higher diagonal values indicate tests with strong standalone fault activation power, while lower values indicate tests whose effectiveness depends more strongly on interaction with other tests or on specific operating conditions.

Off-diagonal entries reveal relationships between tests. High off-diagonal values relative to the diagonal entries indicate complementary behavior, where two tests together activate faults that neither test reliably exposes alone. Conversely, off-diagonal values that closely track diagonal values indicate redundancy, where two tests largely detect the same fault population.

Execution times for the 15 diagnostic tests were independently parameterized in terms of access cycles and symbolic sequence length, reflecting the increasing cost of longer and more complex tests when applied to large memory arrays.

By combining detection probability data from Table 16.3 with execution time models, the **Optimal_Test** system was able to evaluate trade-offs between diagnostic efficiency and execution cost in a formally grounded manner.

This integration of empirically measured detection probabilities, overlap characterization, and execution cost modeling provided the quantitative foundation required for optimization. Rather than relying on heuristic intuition or isolated fault counts, test selection was driven by measurable diagnostic properties that directly reflected real fault activation behavior under controlled experimental conditions.

The fault detection probabilities measured under reduced supply voltage conditions (LVcc) are summarized in Table 16.4. The probability matrix Q_l represents the diagnostic effectiveness of the 15 candidate tests under reduced supply voltage conditions.

Each matrix entry corresponds to the empirically measured probability of fault detection when individual tests or ordered test pairs are applied to the population of diagnostically relevant memory chips.

Table 16.3 — Fault Detection Probability Matrix (Q_l) for 15 Tests at Reduced Supply Voltage (LVcc)

Test	T1	T2	T3	T4	T5	T6	T7	T8	T9	T10	T11	T12	T13	T14	T15
T1	0.83	0.95	0.94	0.96	0.92	0.89	0.88	0.92	0.95	0.87	0.95	0.92	0.94	0.83	0.91
T2	0.74	0.87	0.95	0.98	0.96	0.95	0.95	0.95	0.96	0.93	0.96	0.94	0.96	0.96	0.88
T3	0.76	0.81	0.89	0.97	0.97	0.95	0.94	0.96	0.96	0.93	0.97	0.95	0.97	0.94	0.94
T4	0.83	0.86	0.88	0.96	0.98	0.96	0.96	0.98	0.99	0.96	0.98	0.97	0.98	0.96	0.96
T5	0.79	0.79	0.80	0.87	0.88	0.90	0.90	0.92	0.95	0.91	0.96	0.94	0.94	0.91	0.92
T6	0.79	0.78	0.80	0.86	0.84	0.87	0.87	0.92	0.95	0.88	0.94	0.92	0.93	0.88	0.91
T7	0.80	0.78	0.81	0.86	0.84	0.85	0.87	0.92	0.95	0.67	0.94	0.91	0.93	0.87	0.90
T8	0.81	0.82	0.83	0.88	0.86	0.84	0.84	0.90	0.94	0.92	0.96	0.94	0.94	0.92	0.92
T9	0.81	0.84	0.91	0.91	0.86	0.84	0.84	0.90	0.92	0.95	0.96	0.95	0.96	0.95	0.93
T10	0.80	0.79	0.81	0.85	0.82	0.83	0.83	0.83	0.83	0.85	0.94	0.90	0.93	0.87	0.89
T11	0.82	0.84	0.86	0.92	0.86	0.86	0.85	0.88	0.92	0.84	0.94	0.94	0.96	0.94	0.96
T12	0.77	0.79	0.81	0.86	0.81	0.81	0.81	0.83	0.85	0.81	0.86	0.86	0.94	0.91	0.92
T13	0.82	0.84	0.85	0.92	0.87	0.86	0.86	0.89	0.91	0.85	0.92	0.86	0.93	0.93	0.94
T14	0.79	0.73	0.76	0.80	0.77	0.78	0.79	0.79	0.79	0.78	0.80	0.76	0.80	0.80	0.90
T15	0.74	0.81	0.77	0.82	0.78	0.77	0.77	0.80	0.82	0.77	0.77	0.77	0.77	0.72	0.82

As in the HVcc case, diagonal entries represent the standalone fault detection capability of each test, while off-diagonal entries characterize the combined detection behavior of test pairs.

All probabilities were derived from controlled experimental execution and reflect observed activation outcomes rather than theoretical independence assumptions.
Compared to the high-voltage probability matrix, the LVcc matrix exhibits several notable characteristics.

First, **overall detection probabilities are systematically higher across a wide range of tests**. This reflects the increased susceptibility of memory cells to reduced supply voltage, which lowers noise margins, weakens charge retention, and amplifies sensitivity to marginal defects. Under LVcc conditions, faults that remain dormant or intermittently observable at nominal voltage levels are more readily activated, resulting in higher empirical detection rates.

Second, **the contrast between diagonal and off-diagonal entries is reduced for many test pairs**. In practical terms, this indicates that multiple tests increasingly detect the same fault populations when operating under voltage stress. While this improves raw fault observability, it also introduces a higher degree of diagnostic redundancy.

Tests that appear complementary under HVcc conditions may become partially or fully overlapping under LVcc, diminishing their marginal contribution when combined.

Third, **certain test combinations demonstrate near-saturation behavior**, with joint detection probabilities approaching unity. These combinations are highly effective at fault activation but provide limited incremental value when considered alongside execution cost.

Their presence in the LVcc matrix underscores the necessity of formal optimization, as naïvely including all high-probability tests would lead to excessive diagnostic duration without proportional coverage gains.

The LVcc dataset therefore reinforces two experimentally grounded observations.

- **Increased sensitivity under reduced supply voltage**
  Voltage stress exposes latent and weakly manifested failure mechanisms that are not consistently observable at higher voltage levels. As a result, LVcc testing plays a critical role in revealing marginal defects and aging-related vulnerabilities.
- **Amplified test overlap under stress conditions**
  The stronger activation of marginal faults under LVcc increases redundancy among tests, making overlap-aware selection essential to avoid inefficiencies.

Together with the HVcc probability matrix, the LVcc matrix forms a dual-voltage diagnostic characterization of the test library. These two datasets were jointly supplied to the **Optimal_Test** system as input constraints, enabling selection of a compact diagnostic subset that preserved high fault coverage across voltage conditions while minimizing execution time and redundant stress.

Crucially, the LVcc matrix does not replace the HVcc analysis; instead, it complements it. The combined use of both matrices ensures that selected test sequences are not optimized for a single operating point but remain diagnostically robust across a realistic voltage envelope. This dual-voltage characterization constitutes a central experimental pillar of the optimization methodology implemented in this chapter.

Impact of Test Sequencing and Timing Constraints

The sequencing of address patterns, data values, and supply-voltage conditions plays a decisive role in determining diagnostic outcomes in semiconductor memory testing. Even when the same set of tests is applied, variations in execution order can significantly influence the probability of fault activation. These effects arise from phenomena such as charge redistribution, cell history dependence, data remanence, and stress accumulation across consecutive operations.

In addition to detecting their primary, intended fault models, many memory tests also activate secondary or unmodeled defects. While this extended sensitivity is beneficial from a coverage perspective, it complicates the task of test-set optimization. Overlapping detection across multiple tests can artificially inflate apparent coverage if redundancy is not explicitly accounted for, thereby obscuring the true marginal contribution of individual test sequences.

In practical manufacturing environments, diagnostic procedures are subject to strict constraints on total execution time. These constraints are driven by production throughput requirements, tester availability, and system-level timing budgets. To capture this limitation formally, the total diagnostic duration t_{diag} must satisfy the condition:

$$t_{diag} \leq T_{max}$$

where T_{max} denotes the maximum allowable test time per device.

When this timing constraint is enforced, certain long-duration tests—despite their strong diagnostic capability in isolation—must be excluded from consideration. In the present study, tests such as **GalColumn**, **GalRow**, **WalkColumn**, and **WalkRow** were eliminated due to

their excessive execution times, which rendered them incompatible with realistic production limits. Their removal reduced the candidate pool from 15 to 11 tests, yielding a refined diagnostic dataset suitable for constrained optimization.

The application of this timing filter resulted in a reduced fault detection probability matrix for the remaining tests under high-voltage operating conditions (HVcc), summarized in Table 16.4. Two key insights emerge from this refined dataset:
Distinct fault activation under voltage stress Although reduced-voltage (LVcc) testing generally exposes a larger population of marginal defects, elevated-voltage (HVcc) testing activates a distinct subset of failure mechanisms that remain latent under low-stress conditions.

This confirms that HVcc testing retains unique diagnostic value even after test-set reduction. Production-feasible optimization basis By restricting the analysis to tests executable within the prescribed timing bound, the refined matrix provides a realistic and industrially relevant foundation for optimization.

Diagnostic coverage is evaluated in direct relation to execution cost, ensuring that selected test subsets remain compatible with manufacturing constraints.

Table 16.4 — Refined Fault Detection Probability Matrix $\boldsymbol{Q_{h,s}}$ for 11 Tests at High Supply Voltage (HVcc)

Table 16.4 reports the refined fault detection probability matrix $Q_{h,s}$ obtained after test-set reduction under high-voltage operating conditions (HVcc). Each element $Q_{h,s}$ represents the empirical probability of fault detection when tests i and j from the selected subset are applied in combination. Diagonal entries correspond to the standalone diagnostic efficiency of individual tests.

Test	T1	T2	T3	T4	T5	T6	T7	T8	T9	T10	T11
T1	0.85	0.92	0.93	0.92	0.91	0.92	0.92	0.90	0.93	0.91	0.92
T2	0.83	0.91	0.92	0.91	0.91	0.92	0.93	0.92	0.92	0.93	0.92
T3	0.83	0.90	0.92	0.92	0.92	0.92	0.93	0.93	0.93	0.94	0.93
T4	0.79	0.86	0.86	0.87	0.89	0.91	0.92	0.90	0.92	0.92	0.91
T5	0.81	0.88	0.87	0.86	0.88	0.91	0.92	0.90	0.92	0.92	0.91
T6	0.83	0.89	0.89	0.86	0.87	0.90	0.91	0.92	0.93	0.93	0.92
T7	0.84	0.89	0.90	0.86	0.87	0.90	0.91	0.93	0.93	0.93	0.92
T8	0.78	0.82	0.82	0.80	0.81	0.81	0.81	0.83	0.93	0.88	0.92
T9	0.83	0.90	0.90	0.87	0.87	0.89	0.90	0.82	0.92	0.93	0.92
T10	0.78	0.82	0.82	0.79	0.80	0.81	0.82	0.79	0.83	0.84	0.93
T11	0.84	0.90	0.90	0.87	0.88	0.89	0.90	0.82	0.91	0.83	0.91

The refined fault detection probability matrix $Q_{h,s}$ was constructed after excluding tests that violated the execution-time constraint. Each matrix entry quantifies the empirical probability of detecting faults when a given test or ordered test pair is applied under elevated supply voltage (HVcc).

As in earlier matrices, diagonal entries correspond to the standalone diagnostic effectiveness of individual tests, while off-diagonal entries represent combined detection probabilities, capturing redundancy and complementarity between test pairs.

The fault detection probability matrix for the same subset of 11 tests under reduced supply voltage (LVcc) is summarized in Table 16.5, completing the dual-voltage dataset used in the final optimization stage.

This dataset reveals several important diagnostic patterns:

- **Higher overall detection rates**

Many entries in $Q_{l,s}$ exceed their corresponding values in the high-voltage matrix $Q_{h,s}$. This behavior reflects the increased sensitivity of memory cells under reduced supply voltage, which amplifies marginal effects such as retention instability, weak write margins, and borderline coupling phenomena.

- **Increased redundancy among tests**

As fault activation becomes stronger at LVcc, overlaps between different tests grow more pronounced. While this increases confidence in fault detection, it also heightens the risk of inefficiency if redundant tests are not explicitly eliminated during optimization.

- **Complementarity of dual-voltage testing**

Certain defect classes are preferentially activated under elevated voltage stress (HVcc), while others emerge predominantly under reduced voltage conditions (LVcc). Together, Tables 16.5 and 16.6 demonstrate that neither voltage regime alone provides complete diagnostic coverage. Instead, maximal fault observability is achieved only through coordinated dual-voltage evaluation.

The refined fault detection probability matrix $Q_{\mathrm{l,\,s}}$ was constructed for the same subset of 11 diagnostic tests evaluated under reduced supply voltage (LVcc) conditions. Each matrix entry represents the empirical probability of detecting faults when individual tests or ordered test pairs are applied under low-voltage stress.

Table 16.5—Refined Fault Detection Probability Matrix ($Q_{\mathrm{l,\,s}}$) for 11 Tests at Reduced Supply Voltage (LVcc)

Table 16.5 reports the refined fault detection probability matrix $Q_{l,s}$ obtained after test-set reduction under reduced supply voltage (LVcc). Each element $Q_{l,s}$ represents the empirical probability of fault detection when tests i and j from the selected subset are applied in combination. Diagonal entries correspond to the standalone diagnostic efficiency of individual tests.

Test	T1	T2	T3	T4	T5	T6	T7	T8	T9	T10	T11
T1	0.89	0.97	0.97	0.95	0.94	0.96	0.96	0.93	0.97	0.95	0.97
T2	0.88	0.96	0.98	0.96	0.96	0.98	0.99	0.96	0.98	0.97	0.98
T3	0.80	0.87	0.88	0.90	0.90	0.92	0.95	0.91	0.96	0.94	0.94
T4	0.80	0.86	0.84	0.87	0.87	0.92	0.95	0.88	0.94	0.92	0.93
T5	0.81	0.86	0.84	0.85	0.87	0.92	0.95	0.67	0.94	0.91	0.93
T6	0.83	0.88	0.86	0.84	0.84	0.90	0.94	0.92	0.96	0.94	0.94
T7	0.91	0.91	0.86	0.84	0.84	0.90	0.92	0.95	0.96	0.95	0.96

Test	T1	T2	T3	T4	T5	T6	T7	T8	T9	T10	T11
T8	0.81	0.85	0.82	0.83	0.83	0.83	0.83	0.85	0.94	0.90	0.93
T9	0.86	0.92	0.86	0.86	0.85	0.88	0.92	0.84	0.94	0.94	0.96
T10	0.81	0.86	0.81	0.81	0.81	0.83	0.85	0.81	0.86	0.86	0.94
T11	0.85	0.92	0.87	0.86	0.86	0.89	0.91	0.85	0.92	0.86	0.93

By jointly considering the refined HVcc matrix $Q_{h,s}$ (Table 16.4) and the LVcc matrix $Q_{l,s}$ (Table 16.5), the Optimal_Test system performed dual-voltage optimization of diagnostic sequences. This approach enabled the selection of compact test subsets that preserved high diagnostic effectiveness while satisfying strict timing and cost constraints.

Integration with Optimal_Test Execution

In addition to the probability matrices defined in Tables 16.5 and 16.6, the Optimal_Test program requires explicit identification of the diagnostic tests under evaluation. Test names are manually entered by the operator in the exact order corresponding to the diagnostic characteristics stored in the file table.txt. This ensures a consistent mapping between symbolic test identifiers, probability values, and execution-time parameters.

During execution, U–Y graph representations are converted into deterministic operator sequences by Transfor.exe prior to optimization output generation.

Upon execution, the program generates two primary output files:

- **buf.txt** — containing the weighted average diagnostic effectiveness computed for each test, derived from the combined HVcc and LVcc probability matrices.
- **out.txt** — listing the optimized test sequence that achieves the best trade-off between total execution time and fault coverage under the specified constraints.

Together, these outputs provide both quantitative insight into the diagnostic strength of individual tests and a practical, executable test sequence suitable for manufacturing screening and field deployment. The results form the basis for systematic coverage–cost trade-off analysis and enable visualization of optimization outcomes under real-world timing constraints.

Optimized Test Selection under Elevated Voltage (HVcc)

The Optimal_Test system was applied to the diagnostic datasets collected under elevated supply voltage (HVcc) conditions in order to evaluate test efficiency, redundancy, and ordering under high-stress operation.

The optimization process was driven by the refined fault detection probability matrix $Q_{h,s}$ (Table 16.5), together with the execution-time constraints introduced earlier in this chapter.

The execution of the optimization algorithm produced two primary output files: **buf.txt** and **out.txt**, which are illustrated in Figure 16.4.

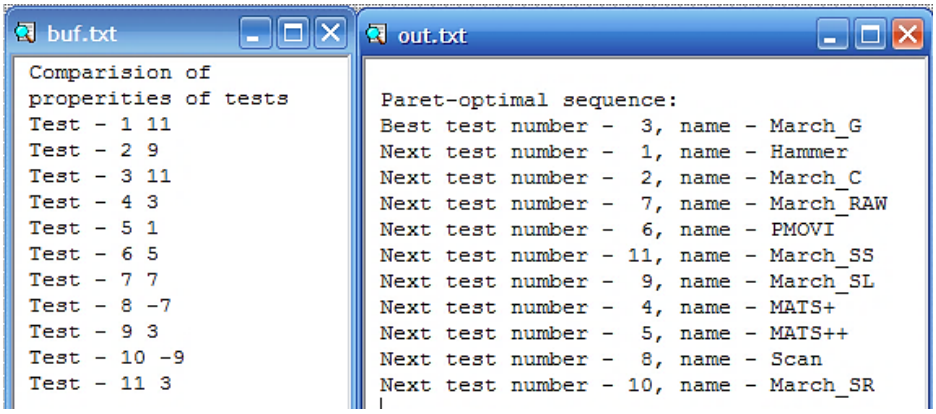
buf.txt
Comparision of
properities of tests
Test - 1 11
Test - 2 9
Test - 3 11
Test - 4 3
Test - 5 1
Test - 6 5
Test - 7 7
Test - 8 -7
Test - 9 3
Test - 10 -9
Test - 11 3
out.txt
Paret-optimal sequence:
Best test number - 3, name - March_G
Next test number - 1, name - Hammer
Next test number - 2, name - March_C
Next test number - 7, name - March_RAW
Next test number - 6, name - PMOVI
Next test number - 11, name - March_SS
Next test number - 9, name - March_SL
Next test number - 4, name - MATS+
Next test number - 5, name - MATS++
Next test number - 8, name - Scan
Next test number - 10, name - March_SR

Figure 16.4—Processing Results Based on Input Data at Elevated Supply Voltage

Figure 16.4 presents the results of the optimization procedure applied under HVcc conditions. The file **buf.txt** (left) reports the weighted diagnostic effectiveness of each candidate test. These values are computed by combining standalone fault detection probabilities with pairwise overlap information derived from the refined probability matrix.

As a result, the ranking reflects not only raw detection strength but also the marginal contribution of each test after accounting for redundancy with previously selected tests. This enables a direct, quantitative comparison of diagnostic value across all candidates.

The file **out.txt** (right) lists the resulting Pareto-optimal test sequence. Tests are ordered such that each successive addition maximizes incremental fault coverage while respecting execution-time constraints. The sequence explicitly avoids tests whose diagnostic contribution is largely redundant or whose cost-to-coverage ratio is unfavorable. Importantly, the ordering is not arbitrary: it reflects the optimal balance between fault activation capability and cumulative execution cost under HVcc stress.

Several observations can be drawn from this result:

- The first selected tests exhibit high standalone diagnostic effectiveness and strong complementarity with the rest of the sequence.
- Tests with substantial overlap but limited marginal gain are deferred or excluded entirely.
- The resulting sequence achieves broad fault activation using a reduced number of tests, demonstrating that exhaustive execution of all available patterns is unnecessary under constrained conditions.

This outcome confirms that, under elevated voltage stress, a carefully optimized subset of diagnostic tests can preserve high fault coverage while significantly reducing total execution time. The HVcc-optimized sequence therefore serves as a practical baseline for high-stress screening, providing efficient defect detection without violating production timing limits.

In the following section, the same optimization procedure is applied to the reduced-voltage (LVcc) dataset, enabling direct comparison between voltage regimes and reinforcing the complementary role of dual-voltage testing in robust diagnostic planning.

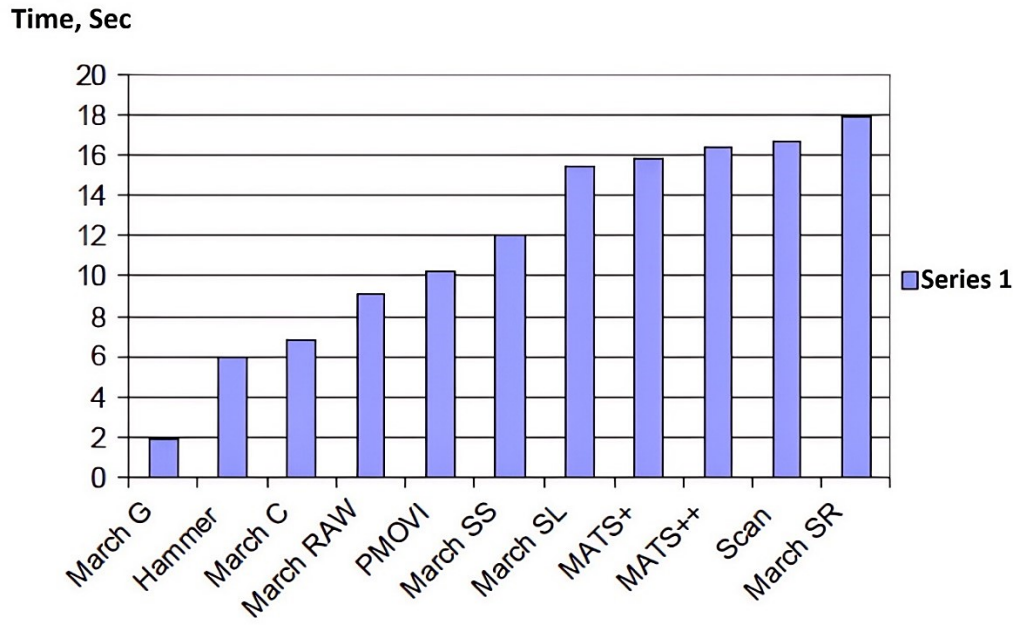

Figure 16.5—Diagnostic Duration of the Optimized Test Sequence under HVcc Conditions

Figure 16.5 presents the cumulative diagnostic execution time for the Pareto-optimized test sequence selected under elevated supply voltage (HVcc) conditions. The histogram enumerates the tests in the exact order produced by the Optimal_Test framework—namely: March G, Hammer, March C, March RAW, PMOVI, March SS, March SL, MATS+, MATS++, Scan, and March SR. The height of each bar corresponds to the individual execution duration of the respective test.

This visualization serves two complementary purposes.

First, it provides a **quantitative decomposition of total diagnostic time** into per-test contributions. Early tests in the sequence, such as March G and Hammer, impose only minimal execution overhead. Their inclusion delivers immediate diagnostic benefit at negligible time cost, making them highly efficient components of the optimized plan. As the sequence progresses, tests such as March C, March RAW, and PMOVI introduce moderate increases in execution time while continuing to contribute non-redundant fault coverage.

Second, the histogram makes explicit the **non-linear growth of cumulative diagnostic cost** toward the tail of the sequence. Longer tests—including March SL, MATS+, MATS++, Scan, and particularly March SR—dominate the upper range of the diagnostic time distribution. These tests are characterized by extended address traversal, increased operation counts, or more complex access patterns, and therefore represent the primary contributors to total test duration.

The stepwise accumulation visible in Figure 16.5 highlights the fundamental optimization trade-off addressed by the Optimal_Test framework: each additional test must justify its inclusion by delivering sufficient incremental fault coverage to offset its execution cost. Tests positioned later in the sequence provide progressively smaller marginal coverage gains at disproportionately higher time expense.

This ordering makes the cost–benefit relationship transparent and allows test engineers to truncate the sequence at any intermediate point if tighter timing constraints are imposed.

When considered together with the Pareto-optimal ordering shown in Figure 16.4, Figure 16.5 demonstrates how the Optimal_Test system translates probabilistic fault-detection data into a **concrete, time-aware diagnostic plan**.

Weighted effectiveness metrics determine the ordering, while cumulative execution time analysis exposes the practical implications of extending or shortening the sequence.

Comparison with Intuition-Based Test Sequencing

For comparison, the cumulative diagnostic duration corresponding to a test set constructed purely on the intuition of a diagnostic expert—without formal optimization—is presented in Figure 16.6. This comparison enables direct evaluation of the efficiency gains achieved through algorithmic optimization relative to heuristic test selection.

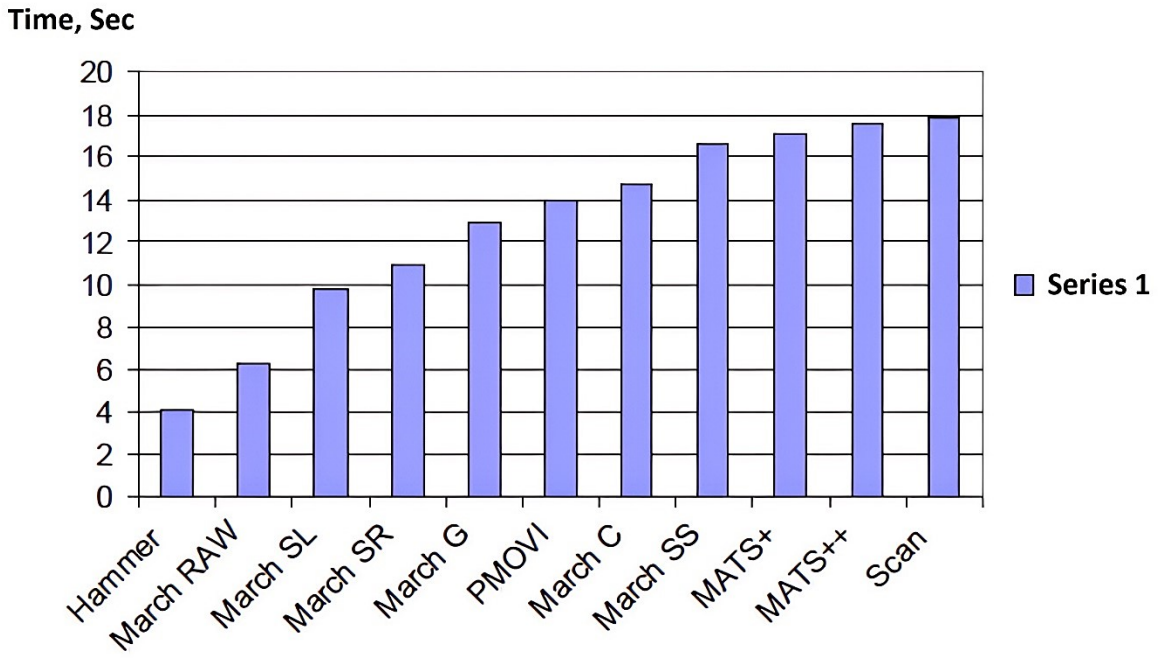

Figure 16.6—Diagnostic Duration of the Intuition-Based Test Sequence

Figure 16.6 presents the cumulative diagnostic execution time for a test sequence constructed manually by an experienced diagnostic engineer, relying on domain knowledge and heuristic judgment rather than formal optimization. The histogram enumerates the tests in the expert-defined order—Hammer, March RAW, March SL, March SR, March G, PMOVI, March C, March SS, MATS+, MATS++, and Scan—with bar heights indicating the individual execution duration of each test.

In contrast to the Pareto-optimized sequence shown in Figure 16.5, the intuition-based ordering does not explicitly account for pairwise overlap, marginal diagnostic contribution, or cumulative execution cost. As a result, the cumulative diagnostic window increases more rapidly and reaches approximately 19 seconds by the end of the sequence.

Several structural characteristics of the intuition-based sequence are evident from the histogram.

First, **long-duration tests are introduced relatively early in the sequence**, most notably March SR and later MATS+ and MATS++. These tests significantly increase cumulative execution time at stages where substantial fault coverage has already been achieved by shorter patterns. Their placement reflects perceived diagnostic strength rather than quantified marginal benefit.

Second, **short and medium-duration tests that provide strong early coverage are not systematically prioritized**. While Hammer, March RAW, and March SL appear early and contribute efficiently, subsequent ordering does not minimize redundancy. As a result, later tests often re-activate fault populations already detected, yielding diminishing diagnostic returns relative to their time cost.

Third, **the final portion of the sequence is dominated by high-cost patterns**, particularly Scan, which extends the diagnostic window without proportional incremental coverage when compared to earlier tests. This tail-heavy structure highlights the absence of an explicit stopping criterion based on coverage–cost balance.
When Figures 16.5 and 16.6 are compared directly, two experimentally supported conclusions emerge.

1. **Total execution time is reduced under optimized sequencing**

The Pareto-optimized sequence achieves comparable diagnostic effectiveness within a shorter cumulative time window by eliminating redundant contributions and reordering tests according to quantified marginal gain.

2. **Coverage–cost balance is explicitly enforced only in the optimized flow**

In the intuition-based sequence, test inclusion is driven by perceived diagnostic value, whereas the Optimal_Test sequence ensures that each additional test contributes measurable coverage benefit relative to its execution cost.

This comparison does not diminish the role of expert knowledge in diagnostic engineering. On the contrary, expert intuition remains essential for selecting candidate tests, defining fault models, and interpreting results. However, the results shown in Figure 16.6 demonstrate that **intuition alone is insufficient for constructing time-optimal diagnostic plans**, particularly as test libraries grow and fault interactions become increasingly complex.

The combined analysis of Figures 16.5 and 16.6 confirms that formal optimization—when grounded in experimentally measured fault detection probabilities and realistic timing constraints—provides a decisive advantage in producing scalable, cost-effective diagnostic sequences suitable for manufacturing and field deployment.

Comparative Analysis of Optimized vs. Intuition-Based Sequences

The benefits of systematic optimization become particularly evident when the **Optimal_Test** sequence is compared against the expert-constructed intuition-based plan.

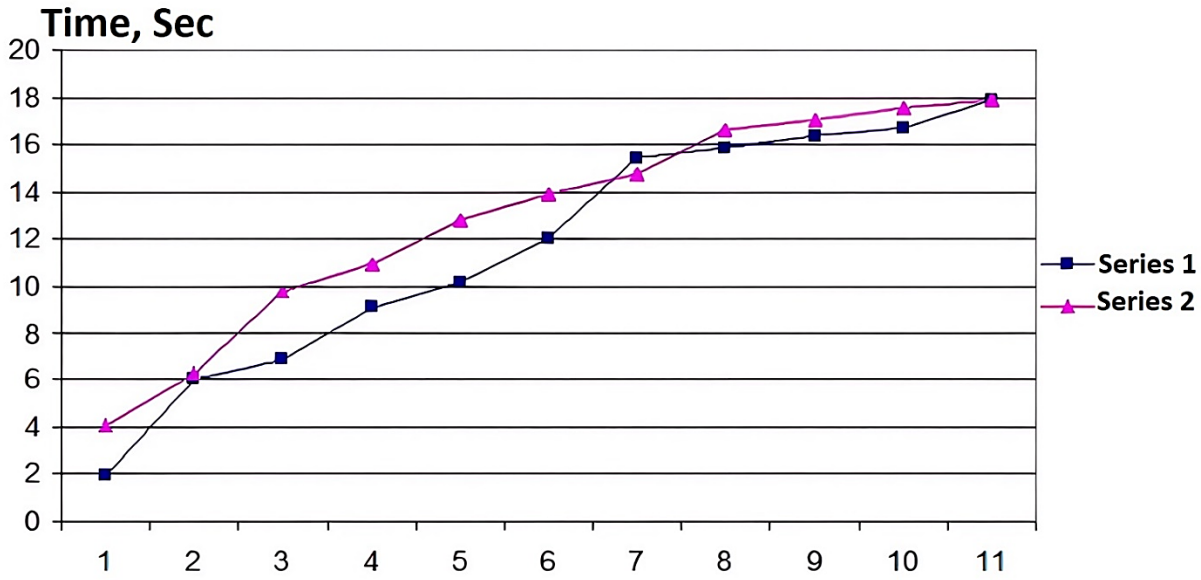

Figure 16.7—Diagnostic Duration Graphs under HVcc

Figure 16.7 presents a direct comparison of cumulative diagnostic execution time for two test sequencing strategies under elevated supply voltage (HVcc) conditions. The first series (Series 1, blue) corresponds to the Pareto-optimized test sequence generated by the Optimal_Test framework, while the second series (Series 2, magenta) represents the intuition-based sequence constructed by a diagnostic expert.

The horizontal axis enumerates the position of each test in the sequence, while the vertical axis represents cumulative diagnostic time in seconds. Both curves are derived from the same underlying execution-time measurements; the difference lies solely in test ordering.
Several observations can be drawn directly from this comparison.

First, **the optimized sequence exhibits a consistently lower cumulative execution time during the early and intermediate stages of testing**. This behavior reflects the deliberate front-loading of short-duration, high-yield diagnostic tests by the optimization algorithm. In practical manufacturing environments, where testing may be interrupted once sufficient diagnostic confidence is achieved, this characteristic translates directly into reduced average test time.

Second, **the intuition-based sequence accumulates diagnostic time more rapidly in the mid-range of the sequence**. This increase is caused by the earlier inclusion of longer-duration tests, which significantly expand the diagnostic window before equivalent coverage gains are realized. Although these tests may be diagnostically powerful, their premature placement reduces time efficiency when considered from a cumulative perspective.

Third, **both sequences converge to approximately the same total diagnostic duration at the final test**. This convergence indicates that the optimized sequence does not eliminate diagnostically relevant tests outright; rather, it reorders them to maximize coverage efficiency under realistic timing constraints. The improvement therefore lies not in reduced ultimate capability, but in improved temporal distribution of diagnostic effort.
From this comparison, two experimentally supported conclusions follow.

1. **Formal optimization improves temporal efficiency of diagnostics**

By prioritizing tests with high coverage-to-cost ratios, the optimized sequence detects faults earlier in the diagnostic process. This is particularly advantageous in production and field scenarios where testing may be truncated based on time limits or early failure detection.

2. **Expert intuition alone is insufficient for cost-optimal sequencing**

While expert knowledge remains essential for identifying relevant fault models and candidate tests, the results in Figure 16.7 demonstrate that heuristic ordering does not reliably minimize cumulative execution time. Algorithmic optimization is therefore necessary to ensure scalability, reproducibility, and compliance with manufacturing constraints.

Taken together with the histogram-based analyses in Figures 16.5 and 16.6, Figure 16.7 provides a continuous-time perspective on the benefits of optimization. It shows that the Optimal_Test framework not only reduces redundancy and balances coverage against cost, but also reshapes the temporal profile of diagnostics in a way that is directly aligned with industrial efficiency requirements.

This comparative analysis reinforces the central thesis of this chapter: effective memory diagnostics require not only strong test patterns, but also formally optimized sequencing grounded in measured diagnostic properties rather than intuition alone.

Optimized Test Selection under Reduced Supply Voltage (LVcc)

The Optimal_Test system was subsequently applied to the diagnostic datasets collected under reduced supply voltage (LVcc) conditions. As in the elevated-voltage case, the optimization process was driven by the refined fault detection probability matrix $Q_{l,s}$ (Table 16.6), together with the same execution-time constraints and cost metrics used for HVcc analysis. This ensured that differences in the resulting test sequences reflected genuine changes in fault activation behavior rather than methodological artifacts.

The execution of the optimization algorithm under LVcc conditions again produced two primary output files: **buf.txt** and **out.txt**, which are shown in Figure 16.8.

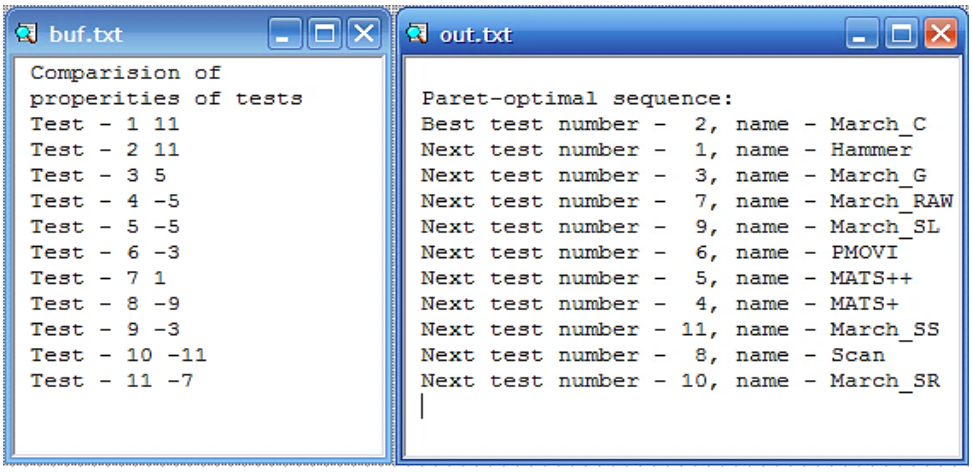
buf.txt
Comparision of
properities of tests
Test - 1 11
Test - 2 11
Test - 3 5
Test - 4 -5
Test - 5 -5
Test - 6 -3
Test - 7 1
Test - 8 -9
Test - 9 -3
Test - 10 -11
Test - 11 -7
out.txt
Paret-optimal sequence:
Best test number - 2, name - March_C
Next test number - 1, name - Hammer
Next test number - 3, name - March_G
Next test number - 7, name - March_RAW
Next test number - 9, name - March_SL
Next test number - 6, name - PMOVI
Next test number - 5, name - MATS++
Next test number - 4, name - MATS+
Next test number - 11, name - March_SS
Next test number - 8, name - Scan
Next test number - 10, name - March_SR

Figure 16.8—Processing Results Based on Input Data at Reduced Supply Voltage (LVcc)

Figure 16.8 presents the outputs of the Optimal_Test framework when operating on low-voltage diagnostic data.

The file **buf.txt** (left) reports the weighted diagnostic effectiveness of each test under LVcc conditions. These weights are computed by combining standalone detection probabilities with pairwise overlap information derived from the refined low-voltage probability matrix. As a result, the ranking reflects the marginal diagnostic contribution of each test after accounting for increased redundancy caused by stronger fault activation at reduced voltage.

The file **out.txt** (right) lists the Pareto-optimal test sequence selected for LVcc operation. As in the HVcc case, the sequence is ordered such that each test maximizes incremental fault coverage relative to its execution cost, while redundant or low-yield tests are deferred or excluded. However, the ordering differs in several positions from the HVcc-optimized sequence, reflecting the distinct fault populations preferentially activated under reduced voltage stress.

In particular, tests associated with retention sensitivity, marginal write stability, and voltage-dependent behavior are promoted earlier in the LVcc sequence. Conversely, certain tests that were highly effective under HVcc conditions are assigned lower priority due to increased overlap with other patterns at reduced voltage. This reordering confirms that **optimal diagnostic sequencing is voltage-dependent**, even when the candidate test set and timing constraints remain unchanged.

The LVcc-optimized sequence exhibits the same structural properties as its HVcc counterpart:

- Early placement of short-duration, high-yield tests
- Explicit suppression of redundant coverage introduced by voltage stress
- Preservation of broad fault activation with a reduced effective test set

At the same time, the differences between the two sequences demonstrate that a single static ordering cannot provide optimal coverage across all operating conditions. Instead, **adaptive optimization must be performed separately for each voltage regime**, using empirically measured fault detection characteristics.

Together with the HVcc results presented earlier, the LVcc optimization shown in Figure 16.8 completes the dual-voltage diagnostic analysis. The combined use of HVcc- and LVcc-optimized sequences enables robust fault detection across a realistic operational envelope, while maintaining strict compliance with execution-time and production constraints.

This result further validates the central premise of the Optimal_Test framework: diagnostic efficiency is maximized not by exhaustive testing, nor by intuition alone, but by data-driven, context-aware optimization grounded in experimentally observed fault behavior.

To complement the LVcc-optimized ordering derived in Figure 16.8, the cumulative execution-time characteristics of the selected sequence were evaluated in order to assess its compliance with practical diagnostic timing constraints under reduced supply voltage.

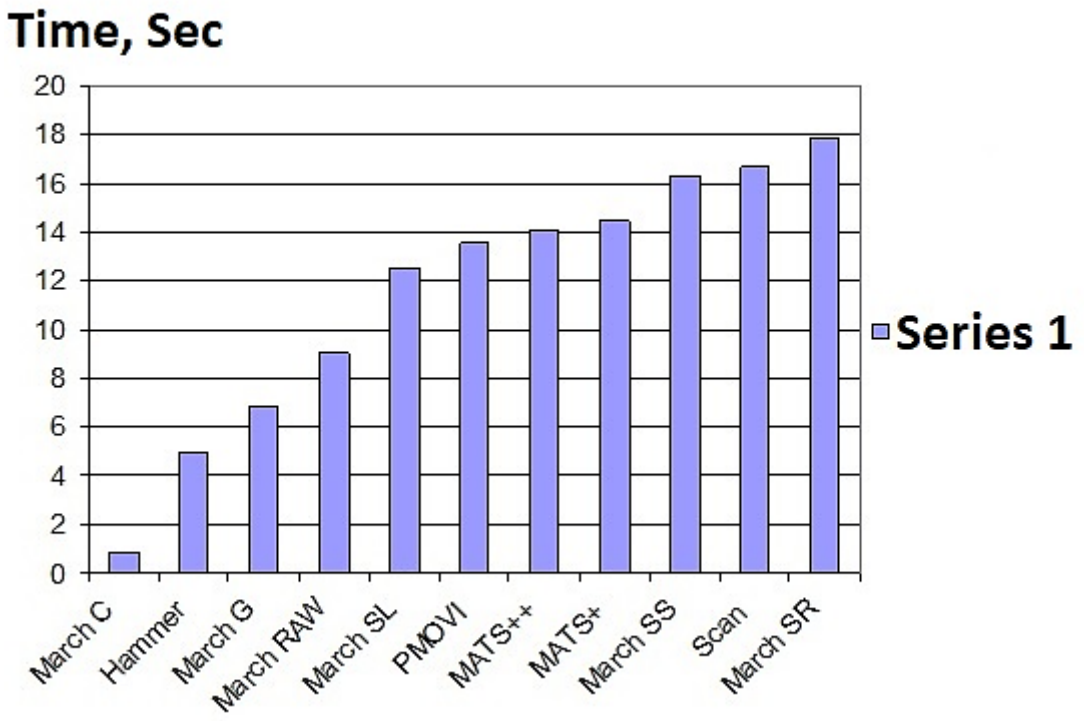

Figure 16.9 —Diagnostic Duration of the Optimized Test Sequence under LVcc Conditions

Figure 16.9 presents the cumulative diagnostic execution time for the Pareto-optimized test sequence selected under reduced supply voltage (LVcc) conditions. As in the corresponding HVcc analysis, each bar represents the individual execution duration of a test in the optimized order—namely: March C, Hammer, March G, March RAW, March SL, PMOVI, MATS+, MATS++, March SS, Scan, and March SR—with the vertical axis indicating cumulative diagnostic time in seconds.

The histogram reveals several structural properties of the LVcc-optimized sequence.

First, **short-duration tests are again positioned at the beginning of the sequence**, resulting in a shallow initial slope of cumulative execution time. Tests such as Hammer and March RAW introduce only marginal increases in runtime while providing early fault activation under reduced-voltage stress. This ordering ensures that a substantial portion of LVcc-sensitive defects can be detected within a limited diagnostic window.

Second, **medium-duration tests contribute gradually and in a controlled manner to the overall execution time**. Patterns such as March SL, PMOVI, and MATS+ appear in the mid-section of the sequence, reflecting their favorable balance between diagnostic effectiveness and execution cost under LVcc conditions. Their placement indicates that they deliver meaningful incremental coverage without disproportionately expanding the diagnostic window.

Third, **the tail of the distribution is dominated by long-duration tests**, particularly Scan and March SR. These tests account for the largest single contributions to cumulative time and therefore define the upper bound of the diagnostic window. Their position at the end of the

sequence ensures that they are applied only after higher-efficiency tests have been exhausted, preserving time efficiency when partial execution is required.

The stepwise accumulation visible in Figure 16.9 highlights the same fundamental optimization principle observed under HVcc conditions: incremental gains in fault coverage must be carefully weighed against the increasing execution cost of longer diagnostic patterns. Under LVcc, this balance is particularly critical due to the higher degree of fault overlap induced by voltage stress.

When considered together with Figures 16.5 and 16.7, Figure 16.9 confirms that the Optimal_Test framework produces **voltage-aware, time-efficient diagnostic sequences**. Although the specific ordering differs between HVcc and LVcc, the structural properties of the optimized plans remain consistent: early coverage efficiency, controlled growth of cumulative cost, and explicit containment of long-duration tests at the tail of the sequence.

This analysis completes the dual-voltage evaluation of optimized diagnostic timing behavior, demonstrating that formal test optimization yields practical, production-compliant diagnostic schedules under both elevated and reduced supply voltage conditions.

To complete the reduced-voltage evaluation, the cumulative timing behavior of the LVcc-optimized sequence was directly compared against an intuition-based test ordering constructed without formal optimization.

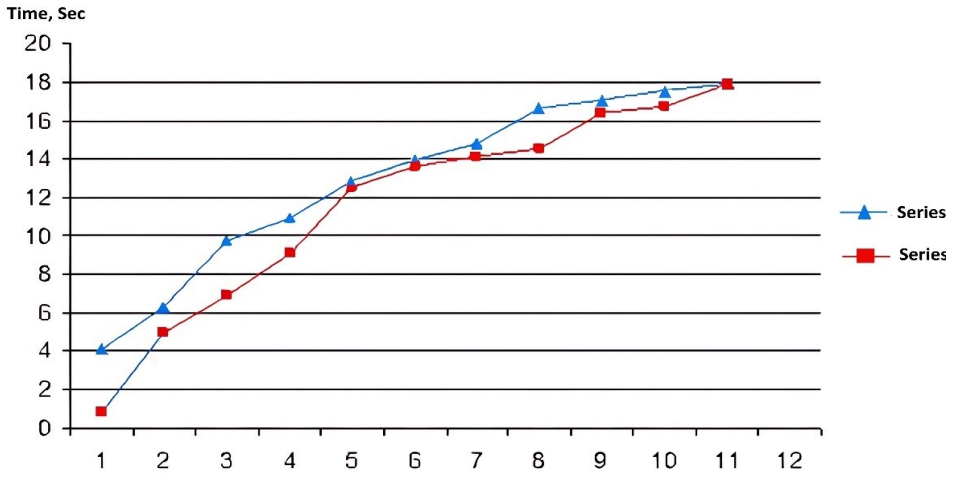

Figure 16.10—Comparison of Cumulative Diagnostic Duration Using Different Test Sets under LVcc

Figure 16.10 presents a comparative analysis of cumulative diagnostic execution time under reduced supply voltage (LVcc) conditions for two distinct sequencing strategies. Series 1 (blue) corresponds to the Pareto-optimized test sequence generated by the Optimal_Test framework, while Series 2 (red) represents the intuition-based sequence assembled by a diagnostic expert. The horizontal axis indicates the position of each test within the sequence, and the vertical axis shows cumulative diagnostic time in seconds.

Both curves are derived from identical per-test execution-time measurements; differences arise solely from sequencing strategy.

Several observations follow directly from the plotted data.

First, **the optimized sequence achieves lower cumulative diagnostic time during the early and intermediate stages of execution**. This reflects the prioritization of short-duration, high-yield tests that efficiently activate LVcc-sensitive faults. In production and field scenarios—where diagnostics may be truncated once sufficient confidence is reached—this behavior translates into tangible reductions in average test time.

Second, **the intuition-based sequence exhibits steeper cumulative growth in the mid-range of the diagnostic window**. This increase results from earlier inclusion of longer-duration tests whose marginal coverage contribution under LVcc conditions is reduced due to increased fault overlap. Although diagnostically meaningful, their placement accelerates cumulative time accumulation without proportional benefit.

Third, **both sequences converge to approximately the same total execution time near the end of the sequence**. This convergence confirms that the optimized plan does not sacrifice ultimate fault coverage. Instead, it redistributes diagnostic effort temporally, ensuring that coverage is achieved more efficiently rather than eliminated.

From this comparison, three experimentally supported conclusions emerge:

1. **Formal optimization improves diagnostic efficiency under LVcc**, particularly in early and mid-execution phases where time savings are most impactful.
2. **Expert intuition alone does not reliably minimize cumulative execution time**, even when strong domain knowledge informs test selection.
3. **Voltage-specific optimization is necessary**, as the LVcc environment alters fault activation behavior and redundancy patterns relative to HVcc conditions.

When considered alongside Figures 16.8 and 16.9, Figure 16.10 completes the dual-voltage analysis of optimized diagnostic timing behavior. Together, these results demonstrate that the Optimal_Test framework produces sequencing strategies that are not only coverage-effective but also temporally efficient under reduced-voltage stress.

This LVcc comparison reinforces the broader conclusion of Chapter 19: diagnostic efficiency in modern memory systems cannot be achieved through static or intuition-driven sequencing alone, but requires data-driven, voltage-aware optimization grounded in experimentally measured diagnostic properties.

Consolidated Diagnostic Efficiency across HVcc and LVcc

The experimental evaluation demonstrated that, within the analyzed population of memory chips, **only six tests from the optimized diagnostic set were sufficient to detect all observable faults**. Execution of the remaining tests did not result in the identification of additional defective devices and therefore provided no incremental diagnostic value. From a production and field-testing perspective, the inclusion of these extra tests was consequently deemed inefficient.

Under elevated supply voltage (HVcc) conditions, execution of the six optimized tests required **11.995 seconds**, whereas the intuition-based diagnostic sequence required **13.924 seconds**,

yielding a time reduction of **1.929 seconds**. Under reduced supply voltage (LVcc) conditions, the same optimized test subset required **13.589 seconds**, compared to **13.924 seconds** for the intuition-based sequence, resulting in an additional time reduction of **0.335 seconds**.

By aggregating the diagnostic durations across both voltage regimes, the total execution time for each strategy was computed in order to assess overall efficiency under dual-voltage operation.

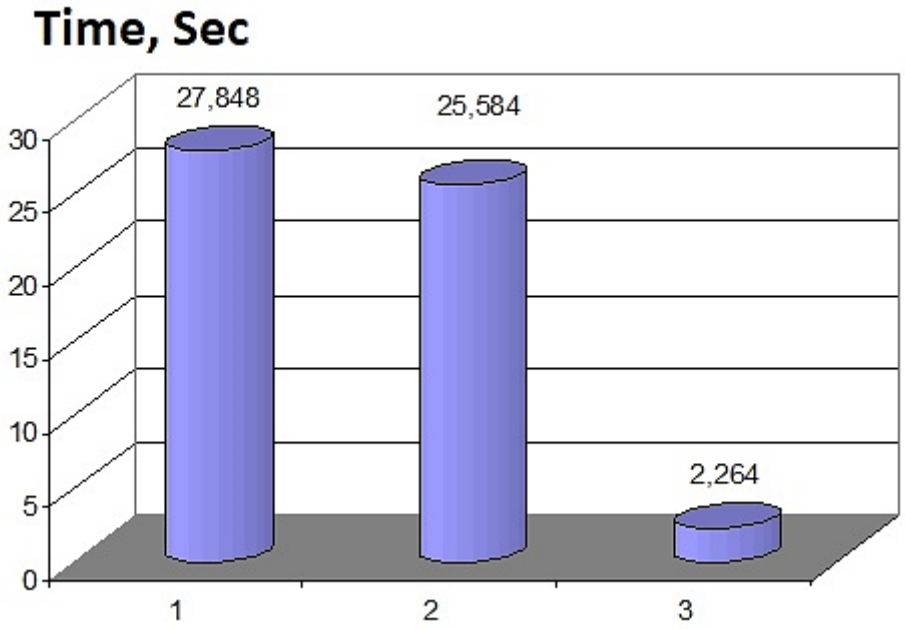

Figure 16.11—Comparison of Total Diagnostic Time:
1 – Intuition-based test set
2 – Optimized test set
3 – Time savings

Figure 16.11 compares the cumulative diagnostic time required to execute six tests under both HVcc and LVcc conditions for two different sequencing strategies. Column (1) corresponds to the intuition-based test set, column (2) represents the optimized test set generated by the Optimal_Test framework, and column (3) denotes the absolute time savings achieved through optimization.

As shown in the Figure, the total diagnostic time for the intuition-based strategy was **27.848 seconds**, while the optimized strategy required **25.584 seconds**. The resulting net time savings amounts to **2.264 seconds**, corresponding to an approximate **8.13% reduction in total diagnostic duration**, achieved without any loss of fault coverage.

Several important conclusions can be drawn from this consolidated comparison.

First, **the time savings are cumulative across voltage regimes**, indicating that optimization benefits persist even when multiple stress conditions are applied. Although the reduction under LVcc alone is modest, its contribution becomes significant when combined with HVcc execution in dual-voltage diagnostic flows.

Second, **the optimized strategy preserves diagnostic completeness while reducing execution time**. The elimination of redundant tests does not compromise fault detection capability, confirming that coverage saturation was reached within the selected six-test subset.

Third, **the optimization process provides a systematic mechanism for enforcing timing constraints**. By sorting candidate tests according to execution duration and marginal diagnostic contribution, and by applying the Optimal_Test framework, it becomes possible to identify subsets that satisfy predefined timing budgets while maintaining full diagnostic effectiveness.

These results highlight the practical advantage of formal optimization in memory diagnostics. Rather than relying on exhaustive execution or heuristic sequencing, optimized test planning enables the construction of **time-bounded, coverage-preserving diagnostic programs** suitable for deployment in semiconductor manufacturing, silicon validation, and field-debugging environments.

This consolidated analysis completes the experimental validation of Chapter 16, demonstrating that data-driven test selection and sequencing yield measurable efficiency gains under realistic dual-voltage operating conditions, without sacrificing diagnostic reliability.

16.2 Method for Evaluating the Efficiency of Memory Diagnostic Systems

The efficiency of a memory diagnostic system reflects its ability to adapt to the task of assessing the technical condition of the device under diagnosis (DUD) and to localize faults within that device with sufficient accuracy and timeliness. When comparing alternative diagnostic systems or methodologies, efficiency must therefore be evaluated as a composite property rather than a single scalar measure.

In principle, diagnostic efficiency could be assessed indirectly through improvements in the operational reliability of the DUD. However, such an approach is impractical for comparative analysis, as reliability improvements depend on a complex interaction of factors that extend beyond the diagnostic system itself.

These include intrinsic properties of the memory device, architectural characteristics of the diagnostic environment, and dynamic effects arising during test execution. As a result, direct reliability-based comparison does not provide a stable or reproducible basis for evaluating diagnostic efficiency.

For this reason, the operational effectiveness of automated memory diagnostic systems is typically characterized using a set of primary quantitative indicators that capture fault-detection capability, temporal behavior, and scalability.

The principal indicators employed in this work are as follows:

- Q — Probability of detecting faults and errors within the DUD.
- T_e (or T_d) — Total diagnostic time required to execute the test program.
- f — Frequency of test stimulus application and response acquisition.
- n — Memory capacity of the DUD, expressed as the number of addressable cells or words.

- r — Data bus width of the memory device, measured in bits.
- M — Number of generated test patterns constituting the diagnostic program.

These parameters together describe the diagnostic system's ability to activate faults, observe responses, and scale with increasing memory size and interface complexity. In particular, the joint consideration of Q and T_e enables evaluation of coverage–cost trade-offs, which are central to optimized diagnostic planning as demonstrated in earlier sections of this chapter.

Beyond operational metrics, the **availability and quality of test design and debugging tools** represent a significant contributor to overall system efficiency. Diagnostic systems equipped with programmable test generators, symbolic modeling capabilities, and debugging support enable rapid adaptation of diagnostic programs across different DUD types.

Such tooling facilitates the development of customized test procedures aligned with specific architectural features, fault models, or operational constraints, thereby reducing engineering effort and turnaround time.

Design-related parameters also play an important role in efficiency assessment, particularly when diagnostics are deployed in embedded, production, or field environments. These parameters include:

- W — Power consumption of the diagnostic hardware during operation.
- G — Physical dimensions of the diagnostic hardware.
- m — Weight of the diagnostic system.

These characteristics influence deployability, thermal behavior, and integration feasibility, especially in space-constrained or energy-limited systems.

Finally, **cost-related parameters** provide a critical dimension of comparison for industrial adoption and long-term sustainability.

The most relevant cost indicators include:

- C — Total acquisition cost of the diagnostic system.
- C_d — Average cost per diagnostic session.
- C_s— Cost of service, maintenance, and operational support.
- C_p — Cost associated with developing new diagnostic test programs.
- C_f— Cost of integrating additional diagnostic functions or extensions.

Taken together, these operational, design-related, and cost-related parameters form a multi-dimensional framework for evaluating the efficiency of memory diagnostic systems. This framework enables objective comparison between alternative diagnostic approaches and provides the basis for assessing the practical impact of optimization techniques—such as those implemented in the Optimal_Test system—under realistic industrial constraints.

In addition to the evaluation criteria discussed above, a promising emerging capability of advanced diagnostic systems is their ability to determine the stable operating region of the device under diagnosis (DUD) across a range of operating conditions. These conditions include

variations in supply voltage, data access timing, and other memory-specific temporal parameters.

Such adaptability extends the role of diagnostics beyond binary fault detection, enabling systematic characterization of operational margins. As a result, diagnostic procedures can contribute not only to reliability assessment but also to predictive maintenance and lifetime estimation of memory devices.

To enable comparative evaluation across multiple diagnostic systems, a **priority function** is introduced. This function aggregates a finite set of k benchmarking parameters and provides a generalized measure of diagnostic efficiency.

It is expressed as:

$$P = P[(Q, T_d, f, n, r, M)_{p1}, (W, G, m)_{p2}, (C, C_d, C_s, C_p, C_f)_{p3}],$$

where the arguments of the function are grouped according to their semantic category. The coefficients P_1, P_2, P_3 denote weighting factors assigned to the **operational**, **structural**, and **cost-related** parameter groups, respectively.

Because these parameters are heterogeneous in nature—combining probabilistic, temporal, physical, and economic characteristics—no universal analytical expression exists that can objectively balance them for all diagnostic systems. Consequently, the general priority function is not suitable for direct one-to-one comparison of fundamentally different diagnostic architectures.

Instead, when the objective is to validate the **correctness and effectiveness of an optimized test sequence**, particularly in cases where prior information about test properties is available, a more practical approach is to evaluate the **increment in operational efficiency**. This incremental assessment focuses on measurable improvements—such as increased fault-detection probability, reduced diagnostic time, or improved coverage-to-cost ratio—relative to a baseline diagnostic strategy.

By quantifying these increments, it becomes possible to determine whether a proposed optimization yields meaningful gains under realistic testing conditions, without relying on an abstract global efficiency metric. This approach aligns naturally with the experimental methodology adopted in this chapter and provides a defensible basis for evaluating optimization results in both manufacturing and field-diagnostic contexts.

Upper Bound: Non-Overlapping Fault Detection

If the selected diagnostic tests detect **non-overlapping fault sets**, the maximum achievable diagnostic efficiency of a test sequence can be expressed as:

$$P_{ee,max} \sum_{i=1}^{k} \frac{C_i}{t_i}$$

where:

- C_i is the weighted fault coverage score of the *i-th* test,

- t_i is the execution time of the *i-th* test,
- k is the number of tests included in the diagnostic sequence.

This expression represents the **upper bound** of diagnostic efficiency. Each test contributes uniquely to fault detection, and efficiency scales linearly with the inclusion of additional tests. Such conditions are rare in real memory diagnostics but provide a theoretical reference point for evaluating optimization quality.

Lower Bound: Fully Overlapping Fault Detection

In the opposite extreme, where all selected tests detect **highly overlapping or identical fault sets**, the generalized diagnostic efficiency is minimized.

Under this worst-case assumption, the effective fault coverage of the entire sequence is determined by the single most powerful test, while the execution time accumulates across all tests. The minimum efficiency can therefore be estimated as:

$$P_{ee,min} \frac{\max(C_1, C_2, \dots, C_k)}{\sum_{i=1}^{k} t_i}$$

This formulation captures the practical reality of redundant diagnostics, where additional tests increase execution time without proportionally improving fault coverage. The expression provides a conservative lower bound and highlights the inefficiency of unoptimized or intuition-driven test selection.

Interpretation and Practical Implications

These two expressions define the **efficiency envelope** within which any real diagnostic sequence must lie:

- P_{max} represents the unattainable ideal of perfectly complementary tests.
- P_{min} represents the pessimistic case of maximal redundancy.

In real manufacturing and field-diagnostic environments, observed efficiency values typically fall between these bounds. The objective of the **Optimal_Test** framework is therefore not to achieve the theoretical maximum, but to **shift practical diagnostic sequences as close as possible toward the upper bound**, subject to strict timing and cost constraints.

By explicitly modeling fault overlaps through empirical probability matrices (as demonstrated in Sections 16.1–16.3), the optimization process avoids reliance on optimistic assumptions and instead operates on measured diagnostic behavior. This enables reliable comparison between competing test sequences and provides a defensible quantitative basis for selecting time-bounded, high-efficiency diagnostic programs.

Average Diagnostic Efficiency Estimation

The average diagnostic efficiency of a test sequence, serving as a practical benchmark between optimistic and pessimistic bounds, is calculated as:

$$P_{ee,mid} = \frac{P_{ee,max} + P_{ee,min}}{2}$$

This metric represents a balanced efficiency estimate positioned midway between the maximum achievable efficiency—corresponding to the idealized case of non-overlapping fault coverage—and the minimum efficiency obtained under the assumption of complete redundancy in fault detection. Although this measure does not explicitly model detailed fault-set intersections, it provides a convenient and interpretable index for comparing diagnostic sequences when only aggregate coverage and execution data are available.

A production batch of 1,545 memory chips, tested under elevated supply voltage (HVcc) conditions, resulted in 202 rejected devices detected by one or more diagnostic tests. Based on the empirical data summarized in Table 16.1, and processed using the Optimal_Test framework, an optimized subset of diagnostic tests was identified.

For each selected test, a weighted diagnostic score was computed from the experimentally measured fault-detection probabilities and corresponding execution times.

Optimized diagnostic test set

For the optimized test subset, the following efficiency bounds were obtained:

$$P_{ee,opt,max} = \frac{11 + 11 + 9 + 7 + 5 + 3}{11.995} = 3.835$$

$$P_{ee,opt,min} = \frac{11}{11.995} = 0.917$$

$$P_{ee,opt,mid} = \frac{3.835 + 0.917}{2} = 2.376$$

These values define the theoretical efficiency envelope of the optimized diagnostic sequence. The upper bound corresponds to the idealized scenario of non-overlapping fault coverage among the selected tests, whereas the lower bound assumes complete redundancy.

The midpoint efficiency therefore reflects a realistic expectation for practical test execution under HVcc conditions.

Intuition-based diagnostic test set

For comparison, the same efficiency bounds were computed for a diagnostic sequence formed using an intuition-based (heuristic) test selection approach. Using the weighted diagnostic scores associated with this sequence and the total execution time of **13.924**, the following values were obtained:

$$P_{ee,ran,max} = \frac{11 + 7 + 3 + 9 + 1 + 1 + 5}{13.924} = 2.011$$

$$P_{ee,ran,min} = \frac{11}{13.924} = 0.790$$

$$P_{ee,ran,mid} = \frac{P_{ee,ran,max} + P_{ee,ran,min}}{2} = \frac{2.011 + 0.790}{2} = 1.400$$

Comparative analysis

A direct comparison of the midpoint efficiency values shows that the optimized diagnostic sequence significantly outperforms the intuition-based alternative:

$$P_{ee,opt,mid} = 2.376$$
$$P_{ee,ran,mid} = 1.400.$$

The relative efficiency improvement achieved through algorithmic optimization is therefore:

$$\frac{2.376-1.400}{1.40} \times 100 \approx 69.7\%.$$

This result demonstrates that, for an equivalent level of fault coverage, the optimized sequence achieves substantially higher diagnostic efficiency by **reducing redundant execution time** and **prioritizing high-impact tests**. The observed improvement quantitatively confirms the practical benefit of formal, data-driven test sequence optimization over heuristic, intuition-based selection under realistic HVcc testing constraints.

Conclusion

The weighted evaluation method for selecting an optimized diagnostic test sequence, grounded in *a priori* knowledge of individual test characteristics, demonstrates a clear and quantifiable advantage over intuition-based sequencing. By explicitly balancing fault coverage against execution time within a constrained optimization framework, the proposed approach achieves an **average diagnostic efficiency improvement of 69.7%** under HVcc test conditions.

This gain is not attributable to increased test redundancy or expanded coverage, but rather to the **systematic prioritization of high-impact tests** and the **elimination of inefficient execution orderings**. The results confirm that algorithmic optimization enables the construction of diagnostic programs that are both time-efficient and coverage-aware, leading to improved utilization of diagnostic resources without compromising detection capability.

Overall, the findings validate the practical effectiveness of formal, data-driven test sequence optimization for large-scale memory diagnostics, particularly in production environments where execution time and resource constraints are critical.

16.3 Test Selection Using Statistical Data on Rejected Chips

The computation of fault detection probabilities for individual diagnostic tests is often resource-intensive and time-consuming, particularly in high-volume production environments. As an alternative, statistical data on the number of rejected memory chips across multiple production batches can be employed as a direct input for constructing optimized diagnostic sequences.

This approach is especially valuable in industrial settings where extensive diagnostic logs are routinely collected, yet explicit fault models or analytically derived detection probabilities are

unavailable, incomplete, or impractical to obtain. By relying on aggregated rejection statistics, the optimization process can proceed without exhaustive modeling of individual defect mechanisms, while still capturing the empirical diagnostic impact of each test.

For practical use, the collected statistics must be organized in a form suitable for quantitative comparison and direct processing by optimization tools. An illustrative dataset is presented in Table 16.6, where rejection counts are structured by diagnostic test and production batch.

Table 16.6—Statistical Data on the Number of Rejected Memory Chips Across Batches

Test Name	Number of Rejected Chips in Sampled Batches							
	1	2	3	4	5	6	7	8
WalkRow	164	180	172	182	173	171	172	178
WalkColumn	177	162	169	179	172	174	176	176
GalRow	166	194	212	218	213	211	211	212
GalColumn	184	212	210	215	204	199	197	205
Hammer	173	181	199	217	216	211	210	214
March SL	182	188	192	205	192	191	190	197
March RAW	180	188	192	203	192	188	188	200
March SS	183	188	190	205	194	191	191	199
March G	176	177	179	193	196	200	200	206
March SR	172	177	180	191	180	180	181	185
PMOVI	180	183	186	197	191	188	188	201
March C	184	191	197	215	218	215	215	219
MATS++	178	174	180	191	187	189	191	204
MATS+	176	174	179	191	187	191	193	204
Scan	178	175	180	189	183	184	186	186

Statistical interpretation

Table 16.6 summarizes rejection statistics for fifteen diagnostic tests across **eight sampled production batches**. Each entry represents the number of memory chips rejected by the corresponding test in a given batch. These statistics provide an empirical proxy for diagnostic strength: tests such as **GalRow**, **GalColumn**, **Hammer**, and **March C** consistently yield high rejection counts, indicating strong fault-exposure capability, whereas tests such as **WalkRow** and **WalkColumn** exhibit lower and more selective detection profiles.

Rather than converting these counts into explicit fault-coverage probabilities, the optimization process treats them as **relative diagnostic effectiveness indicators**, allowing direct ranking and selection under realistic data availability constraints.

Optimization processing and ranking results

To translate the statistical dataset into an optimized diagnostic sequence, the values in Table 16.6 were processed using the **Optimal_Test** program. After execution:

- the file **buf.txt** contains the **generalized diagnostic effectiveness scores** computed for each test, and

- the file **out.txt** provides the **Pareto-optimal ranking** of tests in descending order of their calculated utility.

These outputs are shown in **Figure 16.12**.

In some cases, tests that appear near the top of this ranking may not satisfy runtime constraints, as their execution time exceeds the allowable diagnostic budget. To address this limitation, an additional constraint parameter—**test execution time**—is incorporated into the selection criteria.

This adjustment ensures that the final optimized sequence achieves a practical balance between diagnostic power and temporal efficiency, yielding test programs that are both effective and deployable in industrial environments.

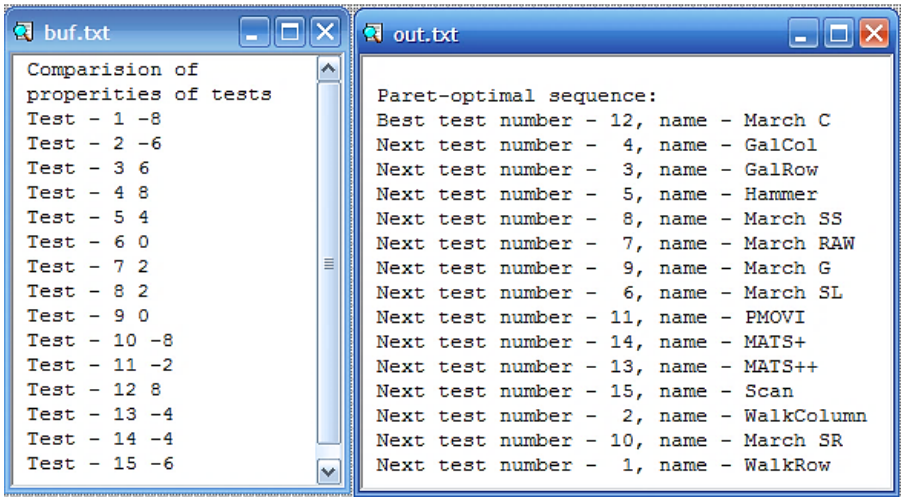
buf.txt
Comparision of
properities of tests
Test - 1 -8
Test - 2 -6
Test - 3 6
Test - 4 8
Test - 5 4
Test - 6 0
Test - 7 2
Test - 8 2
Test - 9 0
Test - 10 -8
Test - 11 -2
Test - 12 8
Test - 13 -4
Test - 14 -4
Test - 15 -6
out.txt
Paret-optimal sequence:
Best test number - 12, name - March C
Next test number - 4, name - GalCol
Next test number - 3, name - GalRow
Next test number - 5, name - Hammer
Next test number - 8, name - March SS
Next test number - 7, name - March RAW
Next test number - 9, name - March G
Next test number - 6, name - March SL
Next test number - 11, name - PMOVI
Next test number - 14, name - MATS+
Next test number - 13, name - MATS++
Next test number - 15, name - Scan
Next test number - 2, name - WalkColumn
Next test number - 10, name - March SR
Next test number - 1, name - WalkRow

Figure 16.12—Output files of Optimal_Test showing diagnostic scores and ranked test sequence

The **buf.txt** file (left) lists the aggregated diagnostic scores derived from rejection statistics, serving as a quantitative measure of relative test effectiveness. The **out.txt** file (right) presents the resulting Pareto-optimal test sequence, ordered from highest to lowest diagnostic utility.

Incorporation of execution-time constraints

While the ranking in Figure 16.12 identifies tests with strong empirical rejection potential, it does not yet account for execution time. In practice, certain high-scoring tests may be unsuitable for inclusion if their execution time exceeds allowable diagnostic budgets.

To address this limitation, test execution time is introduced as an additional optimization constraint. This is achieved by augmenting the input file (table.txt) with a column of negative weights representing time penalties, thereby penalizing time-intensive tests during ranking.

By integrating this constraint, the Optimal_Test framework produces a revised sequence that balances diagnostic effectiveness against temporal efficiency.

The resulting optimized test set maintains strong fault exposure while remaining deployable within industrial runtime limits, aligning the selection process with real-world production requirements.

The contents of the updated input file, the intermediate buffer, and the final ranked test list are shown in Figure **16.13**.

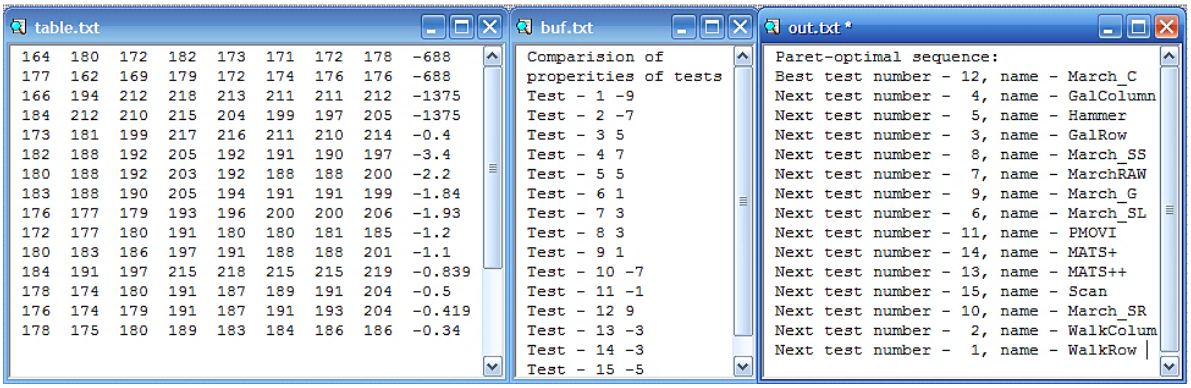
table.txt
164 180 172 182 173 171 172 178 -688
177 162 169 179 172 174 176 176 -688
166 194 212 218 213 211 211 212 -1375
184 212 210 215 204 199 197 205 -1375
173 181 199 217 216 211 210 214 -0.4
182 188 192 205 192 191 190 197 -3.4
180 188 192 203 192 188 188 200 -2.2
183 188 190 205 194 191 191 199 -1.84
176 177 179 193 196 200 200 206 -1.93
172 177 180 191 180 180 181 185 -1.2
180 183 186 197 191 188 188 201 -1.1
184 191 197 215 218 215 215 219 -0.839
178 174 180 191 187 189 191 204 -0.5
176 174 179 191 187 191 193 204 -0.419
178 175 180 189 183 184 186 186 -0.34
buf.txt
Comparision of
properities of tests
Test - 1 -9
Test - 2 -7
Test - 3 5
Test - 4 7
Test - 5 5
Test - 6 1
Test - 7 3
Test - 8 3
Test - 9 1
Test - 10 -7
Test - 11 -1
Test - 12 9
Test - 13 -3
Test - 14 -3
Test - 15 -5
out.txt *
Paret-optimal sequence:
Best test number - 12, name - March_C
Next test number - 4, name - GalColumn
Next test number - 5, name - Hammer
Next test number - 3, name - GalRow
Next test number - 8, name - March_SS
Next test number - 7, name - MarchRAW
Next test number - 9, name - March_G
Next test number - 6, name - March_SL
Next test number - 11, name - PMOVI
Next test number - 14, name - MATS+
Next test number - 13, name - MATS++
Next test number - 15, name - Scan
Next test number - 10, name - March_SR
Next test number - 2, name - WalkColum
Next test number - 1, name - WalkRow

Figure 16.13—Modified input, buffer, and output files of Optimal_Test with execution time penalties

Figure 16.13 illustrates the effect of incorporating **execution time penalties** into the test optimization process. The modified *table.txt* file (left) includes an additional column of negative weights representing execution time costs associated with each diagnostic test.

The intermediate *buf.txt* file (center) reflects the recalculated generalized diagnostic scores after the inclusion of these penalties, while the final *out.txt* file (right) presents the resulting Pareto-optimal test sequence.

The revised ranking clearly demonstrates how execution time constraints alter test prioritization. For example, **GalRow**, which occupied a higher position in the time-agnostic ranking, is displaced by **Hammer** once execution penalties are applied. Similarly, **March SR** is ranked ahead of **WalkColumn**, indicating a more favorable balance between diagnostic effectiveness and runtime feasibility under the modified evaluation criteria.

This outcome underscores the necessity of explicitly accounting for execution time in practical test optimization. In manufacturing environments, where diagnostic runtime is subject to strict upper limits, tests whose execution time exceeds allowable thresholds must be deprioritized or excluded prior to final sequence selection.

By embedding execution time penalties directly into the **Optimal_Test** framework, the resulting diagnostic sequences achieve high fault-detection capability while remaining compliant with industrial timing constraints, thereby enhancing their deployability in real production settings.

Assume that the production process imposes a constraint on the **maximum allowable diagnostic duration** for any individual test. This requirement can be formally expressed as:

$$t_j \leq T_{max}$$

where t_j denotes the execution time of test j, and T_{max} represents the maximum permissible diagnostic duration imposed by production constraints.

For the present analysis, the constraint is set to:

$$T_{max}=7 \text{ s.}$$

In the experimental setup used for this evaluation, the symbolic execution complexity was mapped to physical time assuming a 16-Mbit memory array and a nominal cycle time of t_{cycle}, allowing expressions such as 49n to be translated into absolute execution time constraints.

Any diagnostic test whose execution time exceeds this bound is excluded from the candidate set prior to optimization, as such tests are incompatible with the allowable runtime envelope of the production environment.

For memory devices with a capacity of **16 Mbit**, the following tests violate the imposed execution-time constraint and are therefore removed from consideration:

- WalkRow
- WalkColumn
- GalRow
- GalColumn

As a result, the diagnostic matrix in *table.txt* is reduced to **11 rows and 9 columns**, representing only the admissible tests and their associated metrics, including fault coverage indicators, execution times, and diagnostic weights.

This reduced dataset forms a more realistic basis for subsequent optimization, as it reflects **hard runtime constraints** inherent to industrial production testing. By enforcing the execution-time bound prior to optimization, the resulting test sequences are guaranteed to remain compliant with strict manufacturing throughput requirements while retaining meaningful diagnostic effectiveness.

After executing the **Optimal_Test** tool using the reduced dataset—reflecting the execution-time constraint T_{max}=7 s — a revised ranking of diagnostic tests was obtained. The intermediate file *buf.txt* contains the updated diagnostic effectiveness scores computed for each admissible test, while *out.txt* presents the corresponding Pareto-optimal ordering under the imposed runtime limitation.

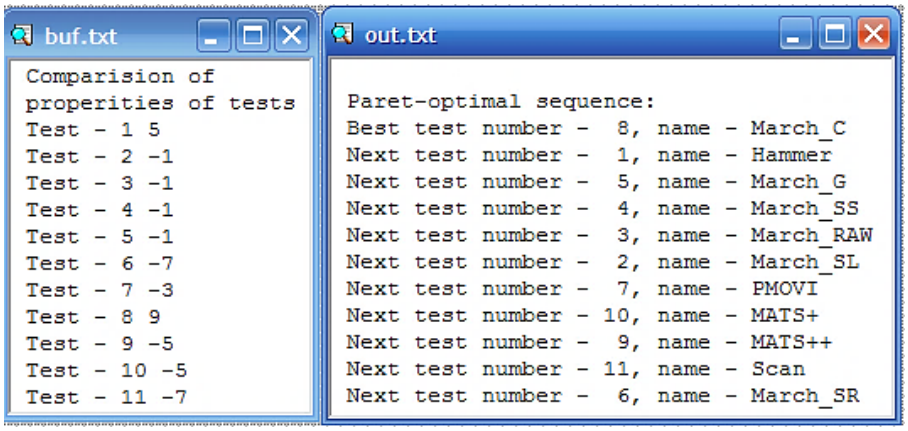
buf.txt
Comparision of
properities of tests
Test - 1 5
Test - 2 -1
Test - 3 -1
Test - 4 -1
Test - 5 -1
Test - 6 -7
Test - 7 -3
Test - 8 9
Test - 9 -5
Test - 10 -5
Test - 11 -7
out.txt
Paret-optimal sequence:
Best test number - 8, name - March_C
Next test number - 1, name - Hammer
Next test number - 5, name - March_G
Next test number - 4, name - March_SS
Next test number - 3, name - March_RAW
Next test number - 2, name - March_SL
Next test number - 7, name - PMOVI
Next test number - 10, name - MATS+
Next test number - 9, name - MATS++
Next test number - 11, name - Scan
Next test number - 6, name - March_SR

Figure 16.14—Diagnostic scores and ranked test sequence under execution time constraints

Figure 16.14 illustrates the optimized diagnostic sequence produced when tests exceeding the allowable execution time are excluded from consideration.

The resulting ranking shows that **March C**, **Hammer**, and **March G** occupy the highest positions, indicating their strong diagnostic impact relative to their execution time. The remaining tests are reordered accordingly to maximize overall diagnostic effectiveness within the shortened runtime envelope.

This revised sequence demonstrates the adaptive behavior of the optimization process under strict industrial constraints. By restricting the candidate set to runtime-compliant tests, the optimization framework reallocates priority toward tests that offer a favorable balance between diagnostic utility and execution cost.

At the same time, the exclusion of long-duration tests raises the question of whether diagnostic completeness is preserved. The reduced test subset may not fully preserve the diagnostic completeness of the original set. Certain fault classes that were previously detected by excluded tests—such as **WalkRow**, **WalkColumn**, **GalRow**, and **GalColumn**—may or may not be indirectly exposed through combinations of the remaining tests.

A key research challenge therefore lies in determining whether the runtime-compliant diagnostic sequence maintains adequate fault coverage. Addressing this issue requires **empirical validation**, supported by **probabilistic or statistical analysis**, to verify that the enforced execution-time constraint does not lead to systematic omission of specific fault classes.

This assessment is essential for ensuring that industrially deployable test sequences remain both time-efficient and diagnostically robust.

In formal terms, let the original diagnostic set contain m tests, and let k of these tests be excluded due to execution-time or production constraints. The remaining $m-k$ tests preserve the same level of diagnostic confidence as the original full set **only if** the following condition holds:

$$q\{\pi_1,\pi_2,...,\pi_{m-k}\} \geq q\{\pi_{m-k+1}\} + q\{\pi_{m-k+2}/\pi_{m-k+1}\} + q\{\pi_{m-k+3}/(\pi_{m-k+1},\pi_{m-k+2})\},+...$$
$$...+q\{\pi_m/(\pi_{m-k+1},\pi_{m-k+2},...,\pi_{m-1})\},$$

Where:

$\pi_1,\pi_2,...,\pi_{m-k}$ — denote the set of tests **retained** for diagnosis,

$\pi_{m-k+1},\pi_{m-k+2},...,\pi_m$ — denote the set of tests **excluded** from consideration,

$q\{\pi_1,\pi_2,...,\pi_{m-k}\}$ — is the **fault coverage function** of the retained subset,

$q\{\pi_i/\pi_j\}$ — represents the **conditional probability of fault detection** by test π_i given that the same faults are not detected by test π_j.

This inequality expresses the requirement that the retained subset must provide **at least the same cumulative fault coverage** as the excluded tests would have contributed, after accounting for overlap and conditional dependencies among detection mechanisms. In other

words, any diagnostic capability lost by removing tests must be fully compensated by the remaining tests through independent or complementary fault detection.

If this condition is not satisfied, the diagnostic capacity of the reduced sequence is strictly inferior to that of the original full set. In such cases, additional measures become necessary, including the design of supplementary tests or the augmentation of existing sequences, to ensure that fault classes previously detected by excluded tests remain observable.

This requirement is critical for maintaining **diagnostic completeness** when enforcing industrial constraints such as limited execution time or production throughput. The adaptive diagnostic method employed in the following experiments is defined in Chapter 14. This chapter focuses exclusively on implementation details and experimental results.

16.4 Experimental Optimization Using the Direct Inclusion Method

Effective optimization of memory diagnostic test sets requires more detailed information than aggregate rejection statistics indicating how many devices fail a given test. While such statistics provide a coarse measure of diagnostic strength, they do not reveal *which* faults are detected by *which* tests. Precise optimization therefore relies on **chip-level diagnostic outcome data**, enabling explicit analysis of test overlap, redundancy, and unique fault coverage.

To obtain this information, a representative sample of n memory chips is selected from a production batch. Each device in the sample is diagnosed using a set of m diagnostic algorithms. The results are encoded in a **binary diagnostic result matrix** of dimension $n \times m$, whose elements are defined as:

$a_{i,j} = 1$, if test j detects a fault in memory chip i,
0, if test j does not detects a fault in memory chip i.

Each row of this matrix corresponds to a specific memory chip, while each column corresponds to a diagnostic test.

Rows that consist entirely of zeros indicate memory chips that passed all applied tests and are therefore considered fault-free. Such rows are excluded from further analysis, as they do not contribute to distinguishing between the diagnostic capabilities of individual tests.

Conversely, rows composed entirely of ones correspond to chips that failed all tests. These cases are also removed, since universal detection provides no information about relative test selectivity or redundancy.

After this filtering step, the matrix retains only diagnostically informative rows, i.e., cases in which different tests detect different subsets of faults. This refined dataset forms the empirical basis for test set optimization.

The resulting matrix is stored in a diagnostic data file, to which a one-dimensional array is appended containing the execution time of each diagnostic test. The inclusion of execution times enables time-aware optimization, allowing diagnostic effectiveness to be balanced against runtime constraints.

This data structure serves as the input to the direct inclusion method, in which tests are iteratively selected into an optimized diagnostic sequence based on their marginal contribution to fault coverage, subject to execution-time limitations.

Figure 16.15 illustrates the main interface of the **Optimal_Test** program, showing a dataset for 12 memory chips tested using the following diagnostic algorithms: **Hammer, March SL, March RAW, March SS, March G, March SR, PMOVI, March C, MATS++, MATS+, and Scan**.

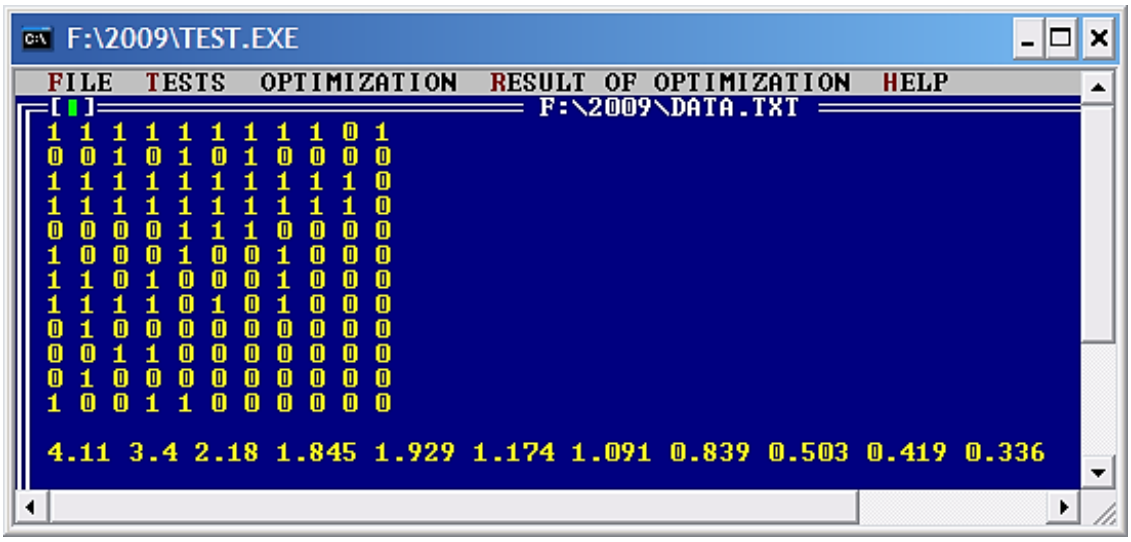

Figure 16.15—Contents of the Diagnostic Result File

Figure 16.15 shows the main interface of the *Optimal_Test* program, displaying an example dataset for **12 memory chips** tested using the following diagnostic algorithms: *Hammer*, *March SL*, *March RAW*, *March SS*, *March G*, *March SR*, *PMOVI*, *March C*, *MATS++*, *MATS+*, and *Scan*.

The binary matrix shown in the interface represents the outcomes of the diagnostic procedures:

- a value of **1** indicates that the corresponding test detected a fault in the given memory chip;
- a value of **0** indicates that no fault was detected by that test.

Below the matrix, the program lists the execution times (in seconds) associated with each diagnostic algorithm. These values are incorporated directly into the optimization process to penalize time-intensive tests when constructing the optimized sequence.

When the dataset is loaded, the software prompts the user to specify the matrix dimensions (number of rows and columns), followed by the name of the input file containing the diagnostic results and the output file in which the optimized test sequence will be stored.

This workflow ensures that diagnostic experiments are processed in a systematic and reproducible manner, with empirical results feeding directly into optimization routines such as the direct inclusion method.

After the diagnostic dataset is loaded, the user specifies the **optimization constraints** that will govern test selection (see **Figure 16.16**). The optimization interface supports two independent constraint types:

- **Maximum diagnostic duration per chip**,
- **Minimum required fault coverage probability**.

When a time-based constraint is selected, the user provides an upper bound on the allowable execution time for diagnosing a single memory chip. When a coverage-based constraint is chosen, the user specifies the minimum acceptable fault detection probability that the resulting test sequence must achieve.

These constraints define the admissible solution space within which optimization is performed.

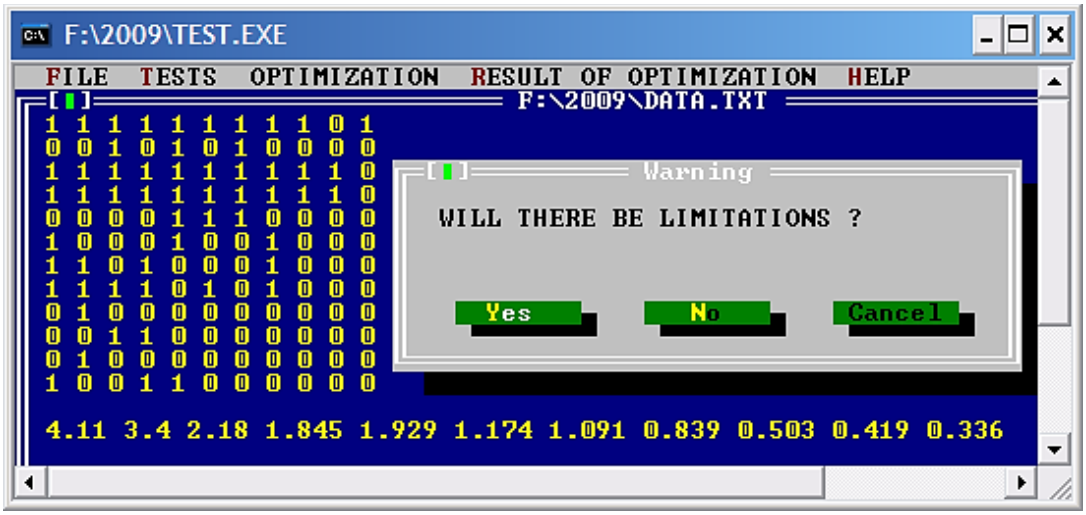

Figure 16.16—Input Interface for Optimization Constraints

Once the constraints are defined, the *Optimal_Test* program initiates the **direct inclusion optimization process**. This algorithm constructs an optimized diagnostic sequence by iteratively selecting tests that provide the highest marginal diagnostic contribution while ensuring compliance with the specified limits.

For the analyzed dataset, the optimization proceeds as follows:

- **Step 1:** Test #8 is selected with a weight W_8= 0.596, an execution time of 0.839 s, and a fault detection probability of 0.5000.
- **Step 2:** Test #7 is added, increasing the cumulative diagnostic time to 1.930 s and raising fault coverage to 0.6667.
- **Step 3:** Test #4 is included, extending the total execution time to 3.775 s and improving fault coverage to 0.8333.
- **Step 4:** Test #2 is selected, bringing the cumulative diagnostic time to 7.175 s and achieving a fault coverage of 1.000, corresponding to complete detection for the analyzed dataset.

As a result, the final optimized diagnostic test set consists of:

- March C (Test #8),
- PMOVI (Test #7),

- March SS (Test #4),
- March SL (Test #2).

Together, these four tests ensure **100 % fault coverage** for the evaluated set of **16 Mbit memory chips**, while maintaining a total diagnostic duration of **7.175 seconds** per device.
This example illustrates how the direct inclusion method incrementally balances diagnostic effectiveness against execution time, yielding a compact and time-compliant test sequence suitable for industrial deployment.

16.5 Fuzzy Rule-Based Selection of Efficient Test Sets

The theoretical foundations of the fuzzy inference mechanisms employed in this chapter—including membership function definitions, rule base construction, and the distinction between Mamdani and Sugeno inference models—are presented in Chapter 13.

The material in this section and the following subsections focuses exclusively on **experimental evaluation, observed system behavior, and performance results** obtained using these models in the context of diagnostic test selection.

The explicit computation of conditional fault-coverage probabilities for diagnostic tests typically requires large volumes of empirical data describing detailed test–fault interactions. In practice, acquiring such comprehensive datasets is both time-consuming and costly, particularly in industrial environments where fault statistics evolve over time and full characterization is rarely feasible.

As an alternative to explicit probabilistic modeling, the experimental evaluation in this section employs the fuzzy expert system defined in Chapter 13. All membership functions, linguistic variables, rule base construction, and inference mechanisms follow the formal definitions established there. In this chapter, the fuzzy system is used strictly as an **experimental selection and ranking tool**, operating on empirically derived inputs to assess its effectiveness in prioritizing diagnostic tests under uncertainty.

The structural architecture of the fuzzy expert system used in the experiments is shown in Figure 16.17.

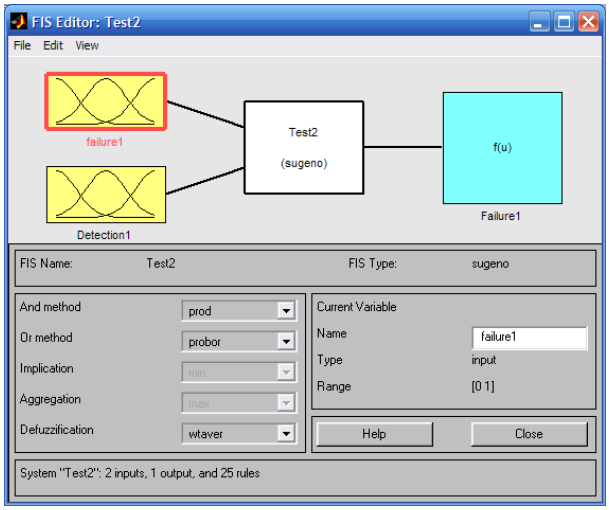

Figure 16.17—Structural Diagram of the Expert System

For the purposes of experimental evaluation, the fuzzy expert system operates on two input variables representing key diagnostic attributes:

- the likelihood of fault manifestation, and
- the likelihood of fault coverage by a given diagnostic test.

The output of the system is a **suitability score**, which quantifies the relative importance of including a given diagnostic test in the optimized test set. This scalar score enables ranking and prioritization of candidate tests under uncertainty and serves as an input to the subsequent test selection process.

The rule creation and modification interface of the fuzzy expert system is shown in Figure 16.18.

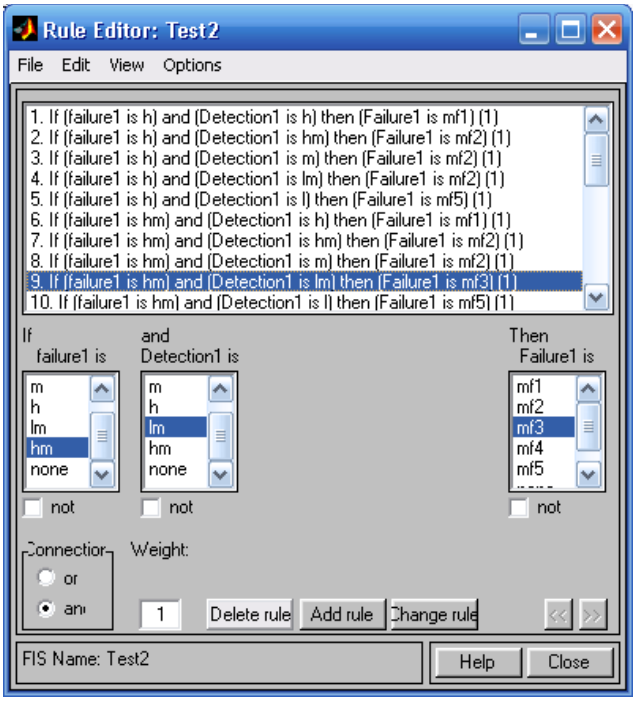
Rule Editor: Test2
File Edit View Options
1. If (failure1 is h) and (Detection1 is h) then (Failure1 is mf1) (1)
2. If (failure1 is h) and (Detection1 is hm) then (Failure1 is mf2) (1)
3. If (failure1 is h) and (Detection1 is m) then (Failure1 is mf2) (1)
4. If (failure1 is h) and (Detection1 is lm) then (Failure1 is mf2) (1)
5. If (failure1 is h) and (Detection1 is l) then (Failure1 is mf5) (1)
6. If (failure1 is hm) and (Detection1 is h) then (Failure1 is mf1) (1)
7. If (failure1 is hm) and (Detection1 is hm) then (Failure1 is mf2) (1)
8. If (failure1 is hm) and (Detection1 is m) then (Failure1 is mf2) (1)
9. If (failure1 is hm) and (Detection1 is lm) then (Failure1 is mf3) (1)
10. If (failure1 is hm) and (Detection1 is l) then (Failure1 is mf5) (1)
If failure1 is
and Detection1 is
Then Failure1 is
m h lm hm none
mf1 mf2 mf3 mf4 mf5
not
Connection
or
Weight:
1
Delete rule
Add rule
Change rule
FIS Name: Test2
Help
Close

Figure 16.18—Rule Base Entry and Modification Process

Figure 16.18 illustrates the graphical interface used to define and adjust inference rules within the fuzzy expert system.

The rule base employs seven membership functions ($mf_1 \dots mf_7$), whose shapes and parameterization were introduced earlier in Section 14.7. These membership functions span the fuzzy domains of the input variables and constitute the fundamental building blocks for rule construction.

For evaluation and validation of the proposed approach, a representative subset of five memory diagnostic tests from the March family was selected:

- March C
- March A
- March LA
- March Y
- MATS++

This subset serves as a benchmark suite for assessing the behavior and effectiveness of the fuzzy expert system under controlled conditions.

By restricting the analysis to closely related diagnostic algorithms, the influence of fuzzy-based ranking on test prioritization can be examined without confounding effects introduced by fundamentally different test mechanisms.

The diagnostic coverage probabilities associated with the selected March-family tests are summarized in Table 16.7.

Table 16.7—Diagnostic Coverage Characteristics of March Tests

Test	Fault Detection Probability
MATS++	31,25%
March-C	50%
March LA	50%
March A	31,25%
March Y	31,25%

These values represent the empirically observed probability that each test detects a fault within the analyzed dataset and serve as the primary quantitative input for the fuzzy evaluation process.

Within the fuzzy logic interface, the user specifies two key input parameters:

- the probability of fault occurrence, and
- the probability of fault coverage associated with a given test.

The fuzzy inference system processes these inputs and computes a **suitability score** for each diagnostic test, reflecting its relative importance within the optimized test program. This score provides a normalized measure that can be used to rank and prioritize tests under uncertainty, even when precise conditional fault probabilities are unavailable.

By systematically varying the diagnostic coverage characteristics assigned to different tests, the fuzzy system enables comparative evaluation of test utility across a range of operating assumptions. This approach allows test engineers to prioritize diagnostics that offer a favorable balance between coverage effectiveness and execution efficiency, while reducing dependence on redundant or low-impact tests. As a result, fuzzy-based evaluation supports robust and flexible test selection in environments characterized by incomplete or evolving fault information.

The results produced by the **fuzzy rule-based expert system** are illustrated in **Figure 16.19**. The two plots visualize how the suitability of including a diagnostic test in the optimized sequence varies as a function of diagnostic coverage probability and fault occurrence likelihood.

(a) Test inclusion suitability versus fault coverage probability.

The curve in Figure 16.19 A shows a monotonic increase in suitability as the diagnostic coverage probability of a test increases. Tests with low coverage exhibit limited contribution to the diagnostic process and are therefore assigned lower suitability values. As coverage improves, the necessity of including the test rises steadily, reaching maximum importance when full fault coverage is achieved. This behavior reflects the expert system's preference for tests that provide broad diagnostic reach.

(b) Suitability surface for test selection.

Figure 16.19 B presents the three-dimensional suitability surface as a function of both detection probability and fault occurrence likelihood. The surface demonstrates the combined influence of these two parameters: when both the probability of fault manifestation and the probability of detection are high, the suitability score approaches its maximum value.

In contrast, tests characterized by low detection capability or applied to rarely occurring faults yield low suitability scores, indicating limited diagnostic value.

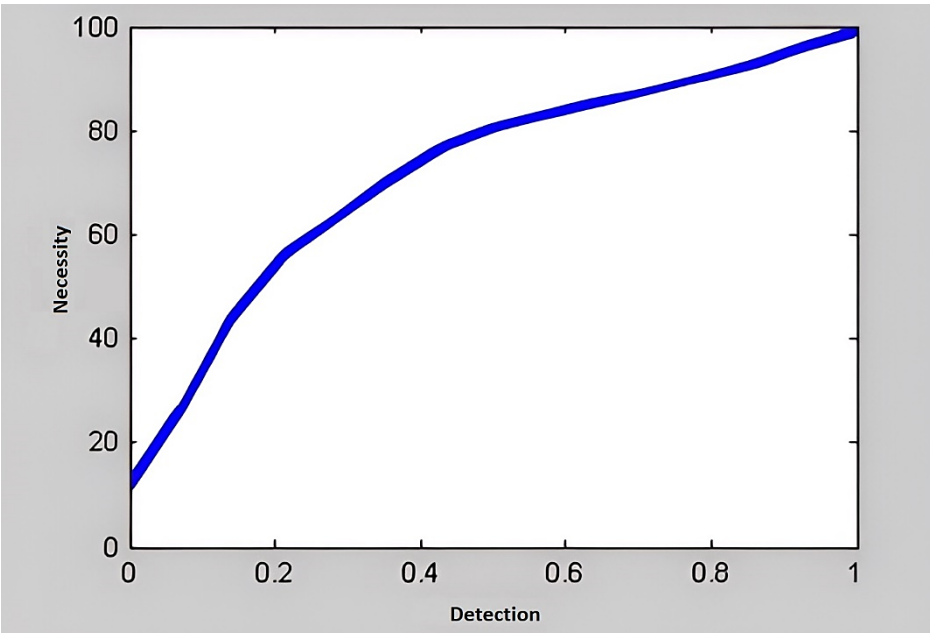

A

This trend confirms that tests capable of activating a larger portion of the modeled fault space provide greater diagnostic leverage within the optimization framework. Consequently, the expert system assigns progressively higher priority to such tests when constructing optimized diagnostic sequences.

This behavior ensures that coverage-driven effectiveness remains a dominant factor in test selection.

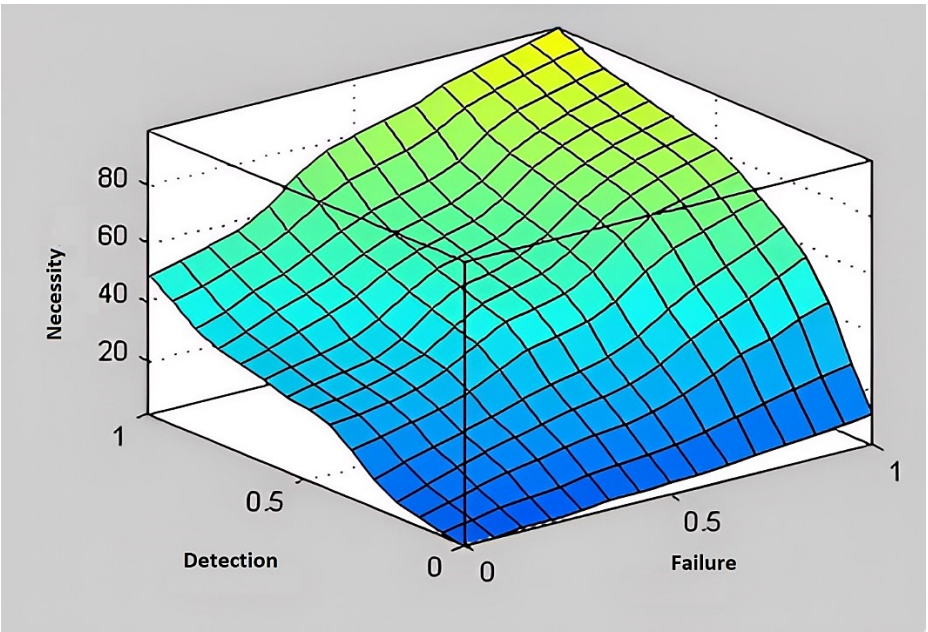

B

Figure 16.19 —Expert System Output:

- **A** – Graph of Test Inclusion Suitability vs. Fault Coverage Probability
- **B** – Suitability Surface for Test Selection

Taken together, these results confirm that the fuzzy expert system provides an adaptive and graded mechanism for test selection. By simultaneously accounting for uncertainty in fault occurrence and variability in diagnostic coverage, the system enables nuanced prioritization of tests.

This approach supports the construction of efficient diagnostic programs that emphasize high-impact tests while reducing reliance on redundant or low-utility diagnostics, particularly within the March test family considered in this study.

The inclusion suitability curves obtained for selected **March-family diagnostic tests**, as derived using the fuzzy expert system, are shown in **Figure 16.20**. In these experiments, the fault detection probability associated with each test was held fixed, while the probability of fault occurrence was varied across the normalized input range.

Two representative cases corresponding to different fixed values of the fault detection probability are presented, illustrating how suitability rankings evolve under varying detection conditions.

These scenarios allow the sensitivity of the suitability metric to be examined under different detection environments. By fixing the detection probability while varying the likelihood of fault occurrence, the analysis isolates the influence of occurrence statistics on test prioritization.

The resulting curves provide insight into how the expert system adapts test selection strategies across varying operational assumptions.

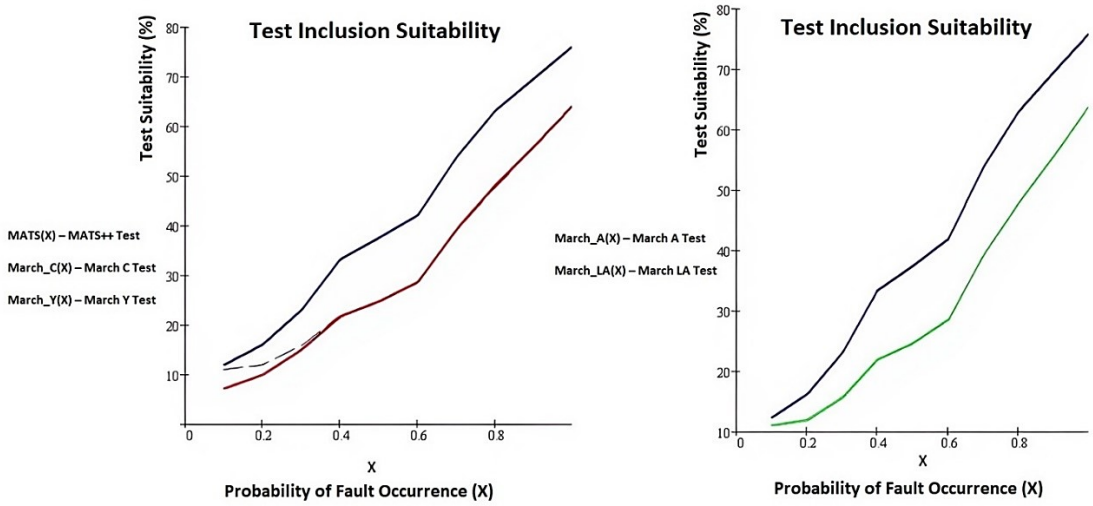

Figure 16.20—Suitability Curves for Including March-Family Tests vs. Fault Occurrence Probability

The results reveal clear differences in the suitability profiles of individual tests. As the probability of fault manifestation increases, the suitability scores of all tests rise monotonically; however, both the rate of increase and the absolute suitability levels differ across tests and detection regimes.

For example, at a fault occurrence probability of $X = 0.4$, the **March-LA** test achieves the highest inclusion suitability, with a score of approximately **33.3 %**, outperforming the other March-family tests under the same conditions.

These curves demonstrate the ability of the fuzzy expert system to discriminate between diagnostic algorithms based on their relative utility under uncertainty. By capturing nonlinear interactions between fault occurrence likelihood and detection capability, the fuzzy framework enables adaptive prioritization of tests beyond what is possible with fixed or purely probability-based selection criteria.

While the preceding sections focus on optimization, test selection, and diagnostic efficiency at the algorithmic level, the following section validates the practical deployability of the proposed methods through implementation-level verification using RTL modeling and VHDL-based toolchains.

16.6 Implementation-Level Verification and Toolchain Validation

Modern semiconductor technologies enable the integration of multiple critical digital system components—such as microprocessors, memory controllers, and user-programmable logic—onto a single silicon substrate.

The design and validation of such highly integrated systems are infeasible without computer-aided design (CAD) tools, which provide the necessary infrastructure for accurate modeling, simulation, and verification of individual subsystems.

A key driver of increasing verification complexity is the rapid evolution of semiconductor memory technologies. In particular, **DDR-SDRAM (Double Data Rate Synchronous DRAM)** devices represent a significant advancement over conventional SDRAM architectures.

By transferring data on both the rising and falling edges of the clock signal, DDR-SDRAM effectively doubles data throughput without increasing the base clock frequency.

For example, a DDR-SDRAM module operating at 100 MHz delivers performance comparable to a conventional SDRAM device running at 200 MHz.

This architectural transition is accompanied by substantial changes in internal memory organization. Specifically:

- the number of internal memory banks increases from two to four, and
- each bank is equipped with its own local control logic, allowing the memory device to operate as four quasi-independent memory blocks.

As a result, the number of memory cells accessed per clock cycle increases from one to four, significantly enhancing both parallelism and effective bandwidth. While these features improve performance, they also introduce additional structural and temporal complexity that must be addressed during verification.

To support the verification of **VHDL models** for such structurally complex memory chips, it is necessary to algorithmically generate specialized diagnostic test patterns. These patterns are expressed as ordered tuples of verification vectors designed to exercise both structural and functional aspects of the modeled memory system. Formally, each test vector is defined as:

$$V_j = \langle WR_j, X_j, Y_j, T_j, S_j \rangle, j \in \{1,2, \dots, n\}$$

Where:

- WR_j is the vector of read/write operation codes,
- X_j, Y_j – are vectors specifying the coordinates of the addressed memory cells,
- T_j – is the vector of input (written) data,
- S_j– is the vector of reference (expected) data, and
- j – indexes the generated test vectors.

Thus, a total of n verification vectors are produced, each corresponding to a distinct diagnostic scenario or parallel execution path within the memory model. Collectively, these vectors form a structured test set capable of validating correct memory operation across multiple banks, access modes, and timing conditions.

This vector-based formulation provides a systematic and scalable foundation for CAD-assisted verification, enabling precise control over access patterns, data values, and expected outcomes. It also allows seamless integration with symbolic test generators and optimization tools introduced in later sections, ensuring that verification remains both exhaustive and computationally tractable as memory architectures continue to grow in complexity.

To extend conventional read operations with explicit data comparison logic, each read transaction is augmented by a comparison between the retrieved data and the corresponding expected reference value. The outcome of this comparison is represented by a **comparison result vector**, defined as:

$$\mathbf{E} = \begin{bmatrix} D_0 \oplus S_0 \\ D_1 \oplus S_1 \\ \cdots \\ D_{n-1} \oplus S_{n-1} \end{bmatrix},$$

where D_j denotes the actual data read from the memory during verification process j, and S_j denotes the expected (reference) data value for that process. The operator $\oplus$ represents the bitwise exclusive-OR (XOR) operation, which yields a value of 1 for each bit position where a mismatch between D_j and S_j occurs.

Thus, each element of the vector E encodes the presence or absence of discrepancies detected during an individual read–compare operation.
If any discrepancy is detected across the verification processes, an **error flag** is asserted. This flag is computed as:

$$\text{Error\_Flag} = \bigvee_{j=0}^{n-1} E_j$$

where $\bigvee$ denotes the logical OR operation applied across all elements of the comparison result vector. Consequently, the error flag is set to 1 if at least one mismatch is detected in any of the comparison stages, and remains 0 only if all read values match their expected references.

To parameterize the size and addressing domain of the memory under verification, two additional variables are introduced:

- N_X: the maximum coordinate along the X-address dimension,
- N_Y: the maximum coordinate along the Y-address dimension.

These parameters define the bounds of the memory array and are subsequently used to control address generation and coverage evaluation during model verification.

As an illustrative example, the procedure for writing a checkerboard pattern into memory cells can be structured algorithmically as follows:

```
BEGIN
    Y := -1;
MainLoop: Loop
    Y := Y + 1;
    X := -2;
    LoopMT1: Loop
        X := X + 2;
        write1(Y*(NX+1) + X, 255, 0);
        exit LoopMT1 when X >= NX - 1;
    end loop LoopMT1;
    exit MainLoop when Y = NY;
end loop MainLoop;
END PROCESS;
```

This procedure performs a systematic traversal of the memory array, incrementing the row index Y sequentially while advancing the column index X in steps of two. The resulting access pattern alternates written values across adjacent cells, thereby producing a checkerboard data configuration. Such patterns are widely used in memory verification due to their ability to activate coupling faults and address-dependent defects.

For generating test programs that implement more sophisticated diagnostic algorithms, it is recommended to complement the memory model with a dedicated **algorithmic test generator model**. This generator encapsulates test semantics independently of memory size and implementation details. The generator is composed of the following VHDL modules:

- Prover_logic.vhd
- Prover_types.vhd
- Types_conversion.vhd
- RAM_logic.vhd
- RAM_properties.vhd

Together, these modules define the test generation procedures, internal data types, type conversion functions, memory capacity parameters, and the data bus width associated with the target memory model.

In practice, base-level diagnostic programs are first developed and validated using the **PROVER language**, which provides a compact and expressive representation of test algorithms. These programs are subsequently scaled to larger memory configurations using a specialized generator that automatically substitutes memory-dependent variables, such as address bounds and data widths, without altering the core test logic.

To translate PROVER programs into synthesizable VHDL descriptions, a dedicated tool—**TranslatorToVHDL**—was developed. Translation is governed by a set of formal rules expressed in the following general form:

$$P \mid Prover\_command = Active - HDL\_command$$

where:

- P denotes the execution priority,
- *Prover_command* is the source-level instruction expressed in PROVER syntax,
- *Active-HDL_command* is the corresponding VHDL operation generated by the translator.

A representative fragment of the translation configuration is shown below:

```
1|STJR,<N> = STJR(<N>);
1|STQR,<N> = STQR(<N>);
1|JJNZ,<L> = <4><5>exit <L> when JJNZ;
1|JQNZ,<L> = <4><5>exit <L> when JQNZ;
2|GX => X = setGX_X(<F>);
2|GY => Y = setGY_Y(<F>);
2|NX => X = setNX_X(<F>);
2|NY => Y = setNY_Y(<F>);
```

Within these rules:

- the variables J and Q are assigned the value of N,
- data is transferred from PROVER registers (G_X, G_Y, N_X, N_Y) to the corresponding VHDL-side registers (X, Y), ensuring consistency between the abstract test description and the concrete hardware model.

This translation mechanism enables automated, repeatable conversion of high-level diagnostic algorithms into VHDL test benches, thereby supporting scalable verification of complex memory architectures under realistic operational constraints.

To streamline the verification process for **system-on-chip (SoC)** designs, verification of memory-related components is organized into three distinct stages, as illustrated in **Figure 16.21**. This staged approach enables progressive validation of functionality, beginning with isolated memory behavior and culminating in full system-level verification.

This structured translation and generation process ensures that diagnostic algorithms remain independent of specific hardware configurations while preserving their functional semantics during implementation.

By separating high-level symbolic descriptions from the concrete VHDL representation, the verification framework supports systematic adaptation of test programs to different memory sizes and architectural parameters.

In addition, the automated translation mechanism minimizes the risk of manual coding errors that could otherwise compromise verification accuracy. The resulting test benches can therefore be reused across multiple design iterations with minimal modification. This capability is particularly valuable for complex SoC environments where memory subsystems interact with numerous controller and processor components.

As a result, verification workflows benefit from improved reproducibility and scalability when evaluating memory behavior under realistic operating conditions. Consequently, the staged verification methodology described below builds directly upon this automated test-generation infrastructure.

This structured translation approach therefore improves both the reliability and maintainability of diagnostic test programs. By maintaining a clear correspondence between symbolic descriptions and hardware-level implementations, the framework enables consistent verification across different design environments.

As a result, diagnostic procedures can be reproduced and extended with minimal modification as memory architectures evolve.

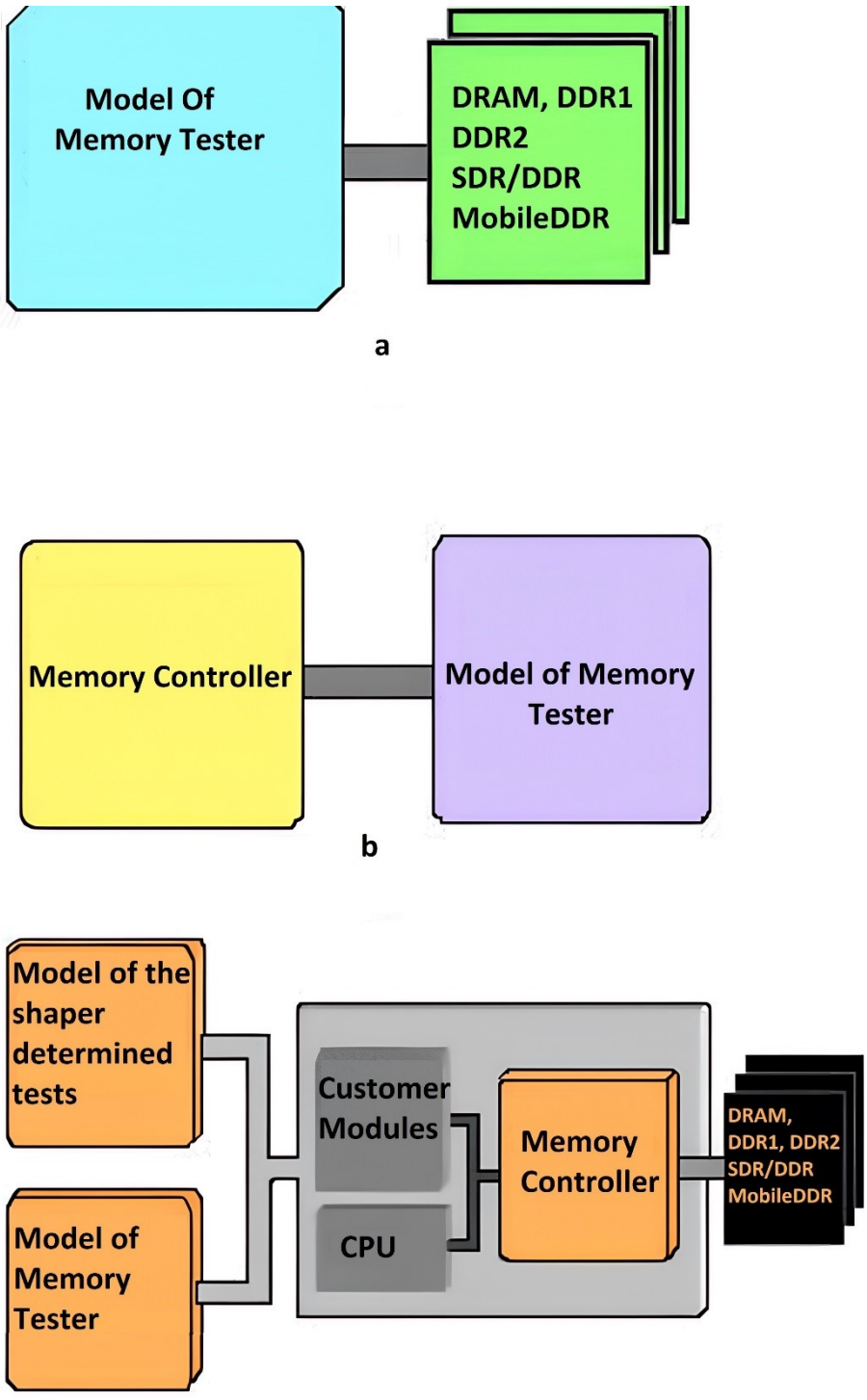

Figure 16.21—Stages of Digital System Verification:
(a) Verification of the memory chip model
(b) Verification of the memory controller model
(c) Verification of the complete digital system model

In the **first stage**, the objective is to verify the correct functional behavior of the memory chip model independently of the surrounding system. At this level, the memory is driven directly by a model of the memory tester, allowing precise control over access sequences, timing parameters, and data patterns.

The applied test programs must confirm:

- correct execution of write and read operations for data packets of all supported sizes, and
- proper generation, propagation, and interpretation of control signal parameters under all valid operating modes.

This stage ensures that the memory model faithfully implements the specified protocol semantics and internal organization for technologies such as SDR, DDR, and MobileDDR memories.

In the second stage, the focus shifts to verification of the memory controller model. Here, the controller is connected to the memory tester model rather than to the memory itself. This configuration isolates controller logic and enables validation of command sequencing, address generation, timing coordination, and protocol compliance without interference from higher-level system components.

In the third stage, the complete digital system model is verified. The memory controller is integrated with the CPU and other customer-defined modules, and the full system interacts with the memory chip model.

At this level, verification assesses correct end-to-end behavior under realistic operational scenarios, including concurrent accesses, arbitration effects, and system-level timing interactions.

The applied test suite thus serves a dual purpose. On one hand, it demonstrates the functional capabilities and robustness of the memory devices, contributing to their competitiveness and reliability in industrial deployment.

On the other hand, it provides essential feedback for refining the design requirements and implementation details of the memory controller, ensuring compatibility and correctness within complex SoC environments.

Together, these three verification stages establish a layered validation strategy that progressively increases system complexity while preserving diagnostic observability. Beginning with isolated memory functionality and culminating in full system integration, the workflow ensures that faults or design inconsistencies can be localized to the appropriate architectural level.

This staged approach reduces debugging complexity and improves the reliability of both the memory subsystem and its controlling logic. Moreover, it enables systematic reuse of diagnostic test programs across different verification contexts.

The toolchain employed for the design of diagnostic test programs and the verification of memory chip models is illustrated in **Figure 16.22.**

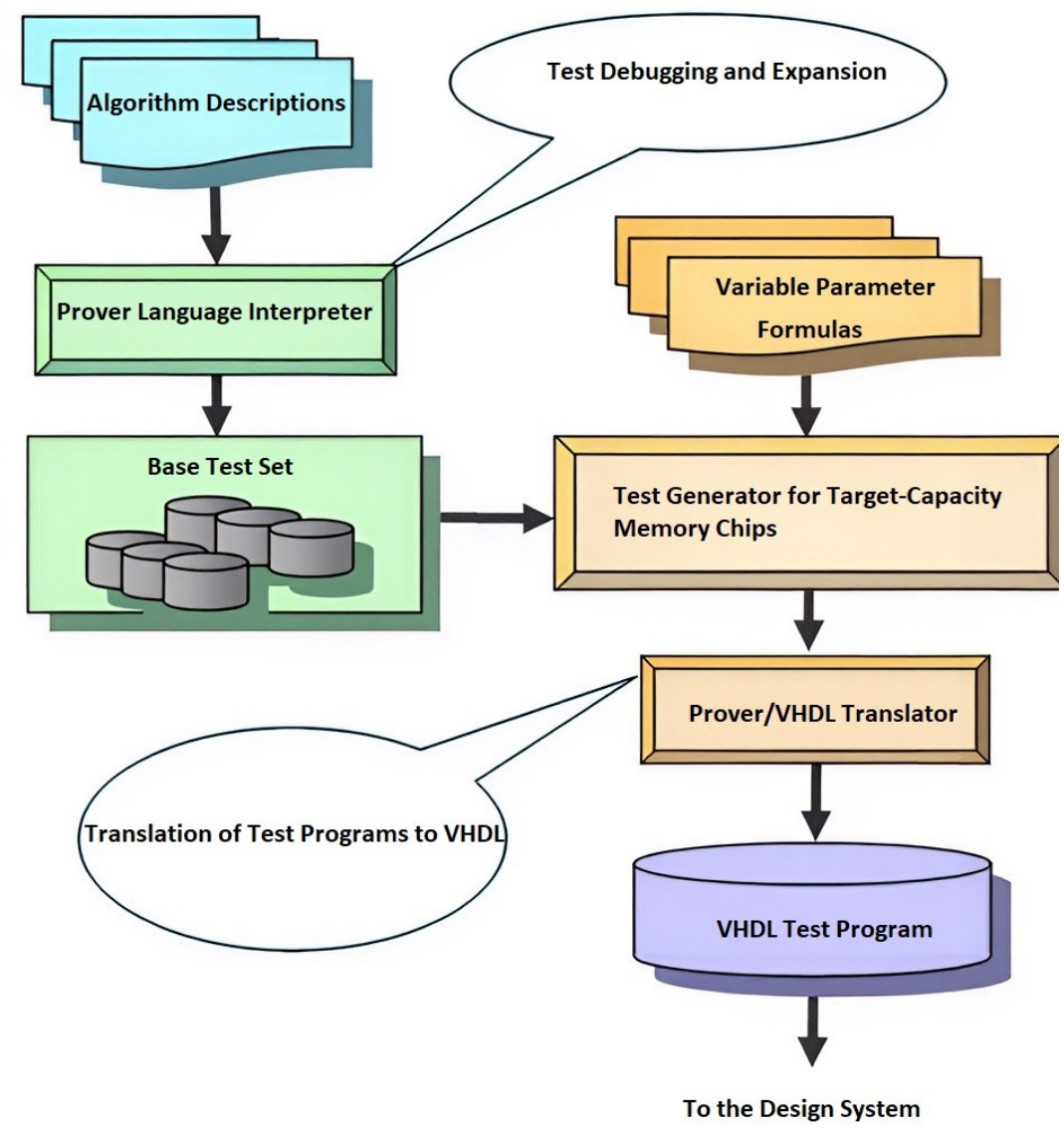

Figure 16.22—Toolchain for Designing Test Programs for Verification of Memory Chip Models

Figure 16.22 depicts an automated and scalable workflow for developing memory test programs intended for model verification. The process begins with formal **algorithm descriptions**, which specify diagnostic procedures at a high level of abstraction. These descriptions are interpreted by the **PROVER language interpreter**, enabling iterative debugging, refinement, and controlled expansion of the test logic.

Following interpretation, a **base test set** is generated. This base set captures the essential diagnostic behavior independently of specific memory sizes or configurations. To adapt the tests to a concrete implementation, the base test set is parameterized using **variable parameter formulas**, which encode memory-dependent characteristics such as address ranges, word widths, and organizational structure.

A dedicated test generator for target-capacity memory chips then scales the tests to the desired memory configuration.

The resulting parameterized test programs are subsequently processed by the **PROVER/VHDL translator**, which converts the abstract PROVER descriptions into synthesizable VHDL test programs. These VHDL artifacts can be directly integrated into digital design and simulation environments, where they drive the verification of memory chip models and associated system components.

The use of hardware-oriented programming languages such as PROVER substantially reduces the development effort required for memory chip model verification. Such languages explicitly reflect the structural properties of diagnostic instruments and semiconductor memory architectures, allowing test algorithms to be expressed in a form that closely matches their hardware execution semantics.

For effective verification, it is recommended that both the **memory tester model** and the **memory chip model** be included within the same project environment. Within these models, ports corresponding to addresses, data buses, operation codes, and synchronization signals are unified. During test execution, formal operands defined in generic procedures are automatically substituted with the actual signals of the device under verification, ensuring consistency between abstract test definitions and concrete hardware behavior.

For example, the declaration of a procedure for writing data to memory cells can be expressed in VHDL as follows:

```
procedure writes (
    n : integer;
    signal CE_b, OE_b, WE_b : out std_logic;
    signal ADDRESS : out std_logic_vector(addrBusWidth-1 downto 0);
    signal DATA : inout std_logic_vector(dataBusWidth-1 downto 0)
);
```

A corresponding procedure call within a test program has the form:

```
Write(0, CE_b, OE_b, WE_b, A, DQ);
```

where:

- 0 denotes the processor identifier generating the test stimulus,
- CE_b, OE_b, and WE_b represent the chip enable, output enable, and write enable control signals, respectively, and
- A and DQ correspond to the address bus and bidirectional data bus.

This abstraction allows test programs to invoke memory access operations in a uniform and parameterized manner, facilitating reuse across different memory configurations and verification stages.

Second Verification Stage – Memory Controller

In the second stage of verification, the focus shifts to validating the functionality of the **memory controller**. The principal verification tasks at this level include:

- writing configuration data to the memory chip's mode registers, and

- generating, transmitting, and receiving data packets in accordance with the memory protocol.

These operations can be exercised using the same tester model employed during memory chip verification. This approach ensures that the controller adheres to the operational and timing requirements imposed by the target memory device, while allowing controller behavior to be evaluated independently of higher-level system components.

Third Verification Stage – Full Digital System

The final verification stage addresses the complete **system-on-chip (SoC)**, including the integrated memory subsystem. At this level, efficient validation is achieved through the use of deterministic and algorithmically generated test programs derived from component-level simulation models. The associated toolchain enables engineers to:

- design and debug a base set of diagnostic programs (e.g., for memories with 256-bit capacity),
- monitor internal memory state variables in real time during simulation, and
- automatically generate scalable PROVER-based test routines for memories of arbitrary capacity.

The PROVER/VHDL translator automates the conversion of these test programs into VHDL test benches compatible with industrial CAD environments such as Active-HDL.

One of the fundamental strengths of VHDL lies in its ability to describe hardware behavior as a function of time. This capability enables precise modeling of control signal timing and realistic emulation of operational modes. Parallel execution is represented through event-driven simulation, where processes are activated whenever signals in their sensitivity lists change. For example, synchronization of read data capture into buffer register D on the rising edge of the strobe signal Str_r can be implemented as:

```
if (Str_r'event and Str_r = '1') then
    D <= DQ;
end if;
```

In this context, the timing of the strobe signal Str_r must be aligned with the valid data window of the memory output. This alignment can be controlled using the after operator to model propagation delays and timing offsets.

To support error tracking during verification, an error counter Counter_K is maintained and incremented upon each detected fault. In addition, a binary error flag Error_flag is asserted whenever a mismatch between expected and observed data occurs:

```
if FormersT /= BufT then
    Counter_K := Counter_K + 1;
    Error_flag <= '1';
else
    Error_flag <= '0';
end if;
```

The VHDL project structure developed for memory model verification, including a dedicated library of diagnostic test programs, is shown in **Figure 16.23**.

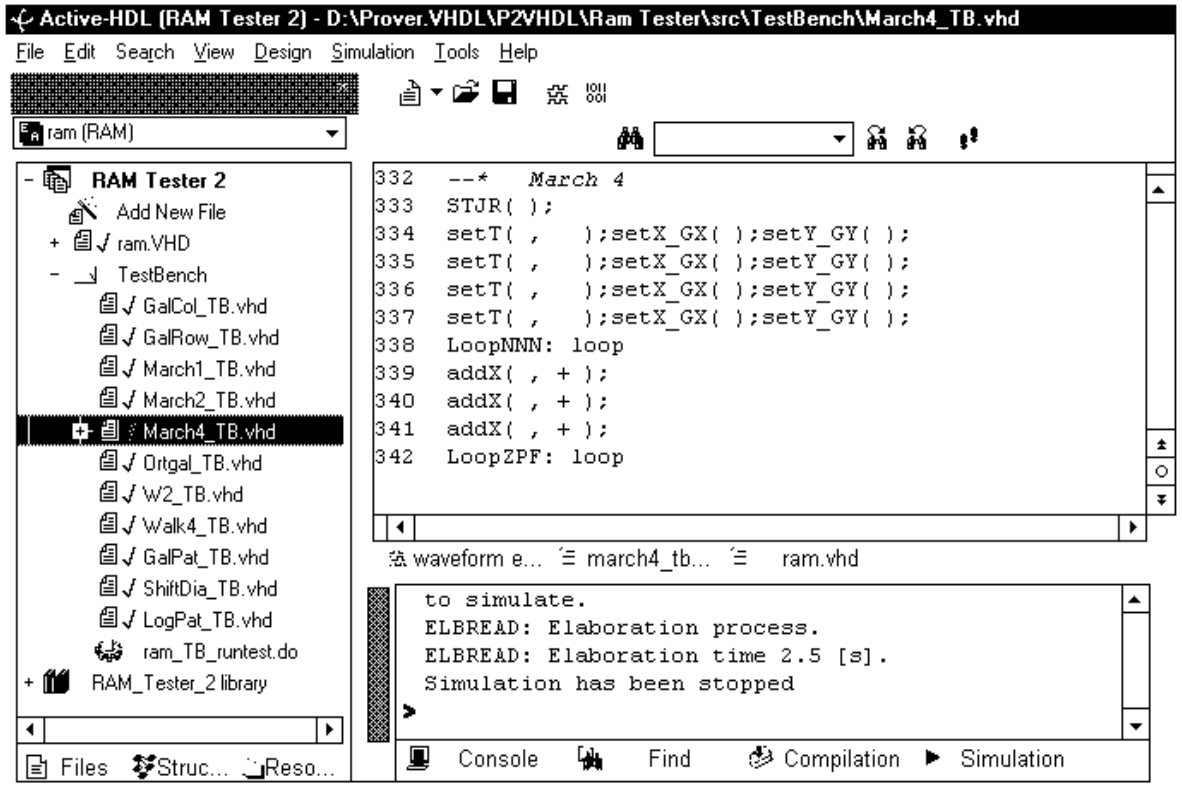

Figure 16.23—Procedure for Selecting Tests from the Verification Library

Figure 16.23 illustrates the organization of the verification environment within the Active-HDL framework. The project contains a structured library of VHDL test benches, each implementing a specific diagnostic algorithm (e.g., March variants, GALPAT, WALK, and related tests). This modular organization allows individual test programs to be selected, enabled, or excluded without modifying the underlying memory or controller models.

The test library is integrated with a common RAM tester infrastructure, ensuring uniform access to address, data, and control signals across all diagnostic procedures. Such a structure supports systematic verification, regression testing, and comparative evaluation of different test algorithms under identical simulation conditions.

The proposed algorithmic method for automated test generation was applied to the verification of the memory chip model **MT57W2MH8B**, organized as 2 Mb×82, corresponding to a total memory capacity of **16 Mbytes**. The generated VHDL test programs were executed within this environment to validate correct memory behavior across supported access modes and diagnostic patterns.

This project organization demonstrates the practical applicability of the proposed verification toolchain, enabling scalable validation of industrial-grade memory models while preserving traceability between high-level diagnostic algorithms and their low-level VHDL implementations.

Verification of the memory chip model was carried out using the **checkerboard test pattern**, which is particularly effective for activating coupling and address-dependent faults. The simulation results are presented in **Figure 16.24**.

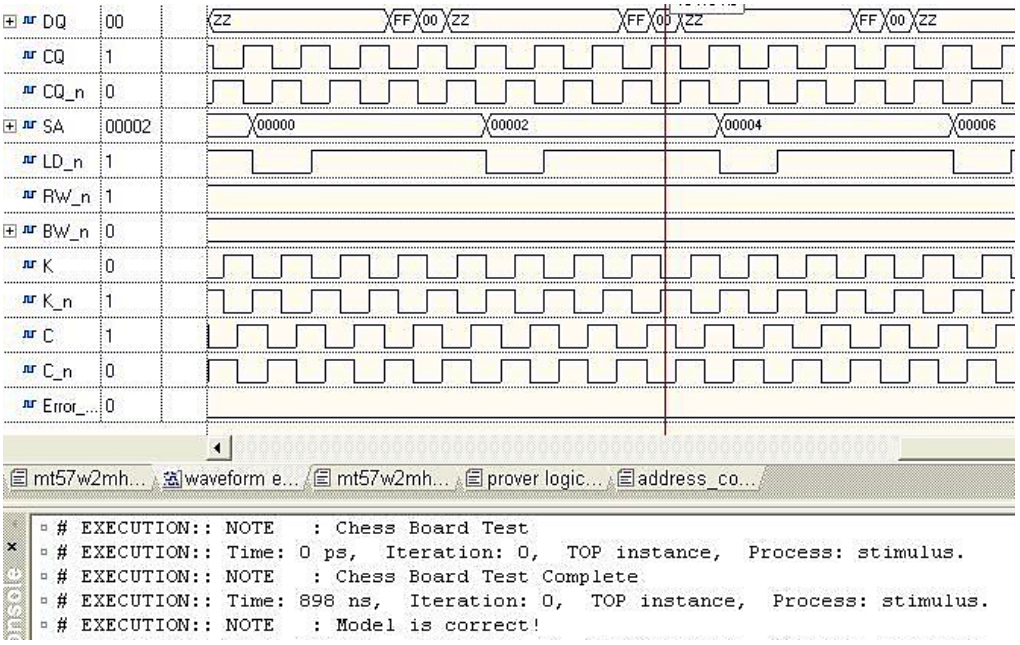

a

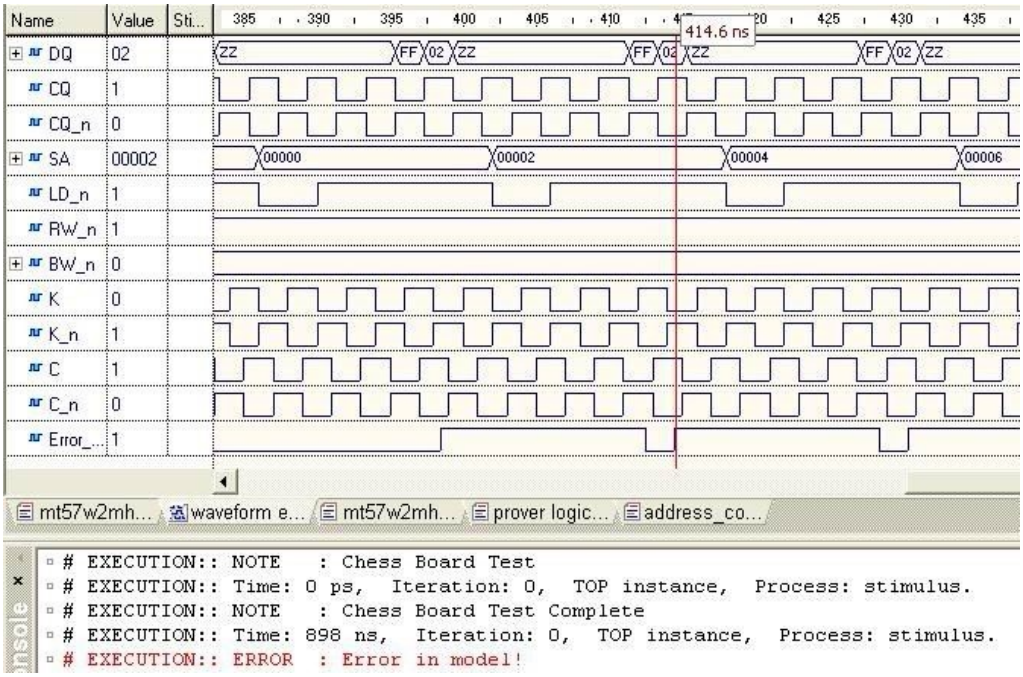

b

Figure 16.24—Results of Memory Chip Model Verification
a – No errors detected in the model
b – Error detected in the model

In the fault-free case shown in **Figure 16.24a**, the data values read from the memory cells match the expected reference values at every comparison point. As a result, the error flag

remains in the zero state throughout the simulation. The verification console confirms successful execution with the message:

"Model is correct!"

This outcome indicates correct functional behavior of the memory model under the applied test pattern and timing conditions.

In contrast, **Figure 16.24b** illustrates a scenario in which a discrepancy is introduced between the read data and the expected reference value. In this case, the comparison logic detects the mismatch, the error flag is asserted (set to 1), and the simulation console reports:

"Error in model!"

This behavior confirms the correct operation of the automated error-detection mechanism and demonstrates the ability of the verification environment to identify functional inconsistencies in the memory model.

The proposed VHDL-based verification methodology for memory chip models offers several advantages over conventional verification approaches:

- The capture and comparison of read data against reference values are fully automated, eliminating manual inspection.
- Test stimuli are generated algorithmically, ensuring systematic and scalable fault coverage.
- The framework supports the construction of stimulus–response pairs for multiple adjacent memory cells, enabling deeper structural validation beyond single-cell testing.
- Previously developed diagnostic programs written in the PROVER language can be reused directly, reducing development effort and simplifying debugging of both test logic and VHDL models.
- Fault localization accuracy is significantly improved, facilitating rapid identification of defects in both diagnostic programs and memory model implementations.

Together, these results validate the effectiveness of the proposed verification framework and confirm its suitability for rigorous functional validation of complex semiconductor memory models within modern CAD environments.

16.7 Summary of Chapter 16: Optimization and Verification Methods for Memory Diagnostics

1. The proposed methodology, implemented through the Optimal_Test software tool, significantly reduces the computational complexity associated with selecting optimized diagnostic test sets for semiconductor memories.
   The resulting optimized sequences reduce diagnostic execution time and associated testing costs. In the baseline 16-Mbit validation case (5 ns cycle time), six tests selected by Optimal_Test completed diagnosis in 25.584 seconds, compared to 27.848 seconds for a heuristic test sequence. This corresponds to a time savings of 2.264 seconds (8.13%) and an average improvement in operational diagnostic efficiency of 69.7%.

2. The application of adaptive diagnostic strategies, based on empirical fault-coverage analysis and implemented using the Optimal_Test framework, enables diagnostic time reductions of up to 40%. By tailoring test sequences to the observed defect distribution, the method improves diagnostic efficiency under realistic manufacturing conditions.

3. A **fuzzy rule-based expert system** further enhances automation in test selection by identifying the most diagnostically effective tests from a candidate pool. The system dynamically prioritizes tests based on fault occurrence likelihood and detection capability, ensuring alignment between applied diagnostics and the actual fault characteristics of the device under test.
4. The fuzzy expert system is designed to be intuitive and to explicitly incorporate the experiential knowledge of diagnostic engineers. This makes it particularly effective during the introduction of new memory chip families or following significant process changes that alter manufacturing defect profiles.
5. Application of the fuzzy rule-based framework demonstrated that **March-LA** emerged as the most effective diagnostic test among five March-family candidates for advanced memory module verification under the evaluated conditions.
6. Automation of test program development for configurable **system-on-chip (SoC)** memory models is achieved through the integration of mathematical models, diagnostic components, and co-simulation environments. This enables verification under near real-world operating conditions and supports iterative refinement of memory controller specifications. By selecting optimal operating modes, designers can reduce failure rates and improve overall product reliability.
7. Automated comparison of read data against reference values, synchronized by explicitly defined signal timing, improves repeatability, minimizes manual intervention, and increases diagnostic reliability during simulation-based verification.
8. The use of **algorithmic test generation** guarantees systematic construction of both stimulus signals and expected responses, enabling robust and scalable industrial-grade verification of memory chip models.
9. The **PROVER/VHDL translator** bridges abstract diagnostic program descriptions and hardware-level simulation by converting PROVER-language test specifications into synthesizable VHDL. This ensures compatibility with modern digital systems incorporating embedded memories and complex processor interfaces.
10. Base-level diagnostic programs exhibit strong scalability: they can be automatically reconfigured into test sequences for memory devices of varying capacities and organizations, enabling reuse, consistency, and long-term maintainability across multiple memory technologies.
11. At the implementation level, these results are enabled by coordinated use of PROVER for symbolic specification, Transfor.exe for executable U–Y sequence synthesis, and Optimal_Test for constrained optimization and planning.

Part V — NVM, MBIST/BISR & Self-Healing

Chapter 17: Testing Non-Volatile Memories (MRAM, PCM, ReRAM, FeRAM)

The memory landscape is undergoing a profound transformation. While traditional volatile memory technologies such as DRAM and SRAM have long dominated mainstream computing, they are increasingly constrained by scaling limits, retention volatility, and power inefficiencies.

As device dimensions shrink and system-level energy constraints tighten, these limitations become more pronounced, particularly in architectures that demand persistence, rapid recovery, and low standby power operation.

In response, non-volatile memory (NVM) technologies have emerged as strong candidates for next-generation systems, offering data retention without continuous power, competitive access latencies, and improved energy characteristics.

Among the most prominent contenders are Magnetoresistive RAM (MRAM), Phase-Change Memory (PCM), Resistive RAM (ReRAM), and Ferroelectric RAM (FeRAM).

These emerging technologies redefine the memory hierarchy by enabling:

- unified storage–memory models,
- near-instantaneous system booting or recovery, and
- substantially reduced standby power consumption.

Despite these advantages, NVM devices introduce diagnostic and testing challenges that fundamentally distinguish them from conventional volatile memories.

These challenges arise from the physical mechanisms used to store information and include:

- non-linear and analog storage characteristics,
- endurance degradation induced by repeated program and erase operations,
- fault behaviors that depend on prior states, access history, and accumulated stress, and
- strongly technology-specific fault mechanisms that resist uniform abstraction.

This chapter investigates the distinctive failure mechanisms associated with each major NVM class and the testing strategies required for their reliable deployment.

The discussion explicitly integrates symbolic fault modeling, adaptive test design, and diagnostic optimization techniques introduced in earlier chapters, illustrating how these methods can be extended beyond DRAM and SRAM to advanced non-volatile technologies without violating determinism or diagnostic traceability.

The analysis aims to bridge theoretical developments with representative industrial practice by outlining a structured roadmap for robust, scalable, and intelligent test infrastructures capable of addressing the complexity of NVM devices in modern computing environments.

17.1 Overview of Non-Volatile Memory Technologies

Non-volatile memory (NVM) technologies encompass a diverse set of physical mechanisms for retaining data without continuous power.

Each technology introduces distinct electrical, material, and architectural characteristics that influence not only performance and endurance but also fault modeling, observability, and testability.

Table 17.1 summarizes the storage principles and diagnostic-relevant attributes of representative non-volatile memory technologies.

Table 17.1—Representative Non-Volatile Memory Technologies: Storage Principles and Key Attributes

Technology	Storage Principle	Key Attributes
MRAM	Magnetic tunnel junction (spintronics)	Fast access, low standby power, robust retention
PCM	Phase transition between amorphous and crystalline states	Multi-level storage, slower writes, resistance drift
ReRAM	Resistive switching via conductive filament formation	Ultra-fast switching, analog variability
FeRAM	Ferroelectric polarization in a capacitor	Low-voltage operation, moderate density

Although all of these technologies provide non-volatility, their underlying mechanisms differ substantially with respect to:

- electrical behavior and device physics,
- programming protocols and read/write interfaces,
- error mechanisms and degradation pathways,
- and test observability and diagnostic traceability.

These differences complicate the design of diagnostic patterns, the achievement of high fault coverage, and the localization of failures. As a result, testing methodologies developed for volatile, digitally encoded memories cannot be directly transferred to NVMs without significant adaptation.

In the following sections, the diagnostic implications of each technology are analyzed, showing how symbolic modeling and adaptive test generation—introduced in Chapters 8, 10, 12, and 13 - can be systematically extended to address the distinct challenges posed by emerging NVM architectures.

17.2 Unique Fault Models in Non-Volatile Memories

Although traditional memory fault models—such as stuck-at, transition, and coupling faults—remain partially applicable to non-volatile memories (NVMs), the unique device physics of emerging technologies give rise to additional and often more complex failure mechanisms.

These faults are frequently analog in nature, non-deterministic in manifestation, and strongly influenced by material properties, endurance limits, thermal conditions, and device geometry. The following subsections summarize characteristic fault types observed in representative NVM technologies.

MRAM Faults

- stuck magnetic state, in which the magnetic tunnel junction (MTJ) becomes permanently locked and cannot transition between logical states,
- asymmetric switching behavior, where magnetization reversal occurs more readily in one direction than the other due to hysteresis or biasing effects,
- tunnel magnetoresistance (TMR) degradation, which progressively reduces read margins and may be accompanied by disturb phenomena, and
- write threshold variation arising from process-induced variability across cells.

PCM Faults

- resistance drift, characterized by a gradual increase in resistance over time and particularly critical in multi-level cell (MLC) storage,
- incomplete phase transitions, leading to metastable intermediate resistance states,
- thermal cross-talk, where heat diffusion perturbs neighboring cells, and
- stochastic nucleation effects that introduce variability in crystallization and amorphization behavior.

ReRAM Faults

- filament rupture or overgrowth, disrupting the stability of resistance states,
- SET/RESET voltage variability across devices and cycles,
- endurance-induced drift resulting from repeated switching, and
- random telegraph noise (RTN) caused by charge trapping and detrapping events.

FeRAM Faults

- polarization fatigue due to repeated cycling,
- retention loss as stored polarization relaxes over time,
- imprint effects introducing directional bias in switching behavior, and
- destructive readout, in which the sensing operation perturbs or erases stored data.

This taxonomy highlights the inadequacy of purely binary fault assumptions for NVM testing.

To systematically address these behaviors, the symbolic test model was extended through the introduction of **technology-specific symbolic fault predicates**, including:

- DRIFT_FAIL — representing resistance or retention instability,
- ASYM_TOGGLE — capturing directional switching failures,
- WEAR_BIAS — modeling endurance-related degradation asymmetry, and
- FILAMENT_OVERSHOOT — describing uncontrolled filament growth in resistive memories.

These predicates are symbolic abstractions introduced to capture physically motivated behaviors within the diagnostic model; they do not represent standardized or universally adopted fault classifications.

They were incorporated into the PROVER-based test synthesis environment, enabling automated generation of targeted test patterns while preserving architectural independence.

Their inclusion also refined the diagnostic scoring mechanisms used in fuzzy and adaptive frameworks, improving prioritization without asserting exhaustive fault completeness.

17.3 Challenges in Testing NVM Devices

Testing NVM devices introduces challenges that exceed the scope of binary digital diagnostics:

- **Non-destructive read limitations** — read operations may perturb stored states, requiring refresh-aware testing.
- **Analog sensing complexity** — resistance-based encoding demands margin analysis rather than binary comparison.
- **Multi-level cell vulnerabilities** — state-dependent error manifestation in MLC devices.
- **Endurance constraints** — aggressive testing can accelerate wear.
- **Non-linear and asymmetric operations** — write and erase behaviors differ in latency, energy, and reliability.

These factors motivate adaptive, tolerance-aware, and endurance-conscious diagnostic strategies rather than exhaustive stress testing.

17.4 Recommended Test Strategies per Technology

Because each non-volatile memory (NVM) technology is governed by distinct physical mechanisms, its diagnostic methodology must be specifically tailored. Table 17.2 summarizes representative diagnostic features recommended for major NVM classes

Table 17.2—Recommended Test Strategy Features by NVM Technology

Technology	Recommended Test Features
MRAM	Read-after-write verification, toggle asymmetry detection, magnetic hysteresis stress patterns
PCM	SET/RESET margin evaluation, drift simulation with time delays, multi-read comparators for resistance quantization
ReRAM	Pulse-width sweep diagnostics, repeat-read capture of random telegraph noise (RTN), current profile analysis
FeRAM	Destructive read awareness, imprint stress loops, polarity inversion tests

In the symbolic modeling domain, these diagnostic procedures can be expressed as extended operator sequences.

For example:

```
WRITE(a, SET);
WAIT(100);   // Drift modeling delay
READ(a);
ASSERT(a, RESISTANCE_LEVEL_3);
```

Within the Optimal_Test framework, such symbolic chains were enhanced using fuzzy pass thresholds rather than strict binary assertions. In this context, resistance drift or margin degradation can be evaluated against bounded tolerance intervals (e.g., ±10%), allowing diagnostic outcomes to be recorded as graded scores rather than binary failures.

This approach preserves diagnostic sensitivity while avoiding unnecessary stress in drift-prone or endurance-limited devices.

17.5 Integration with Symbolic and Fuzzy Frameworks

To extend symbolic test modeling into the domain of non-volatile and analog-dynamic devices, the symbolic language and test engine were enhanced with features specific to NVM behavior:

- **Operator extension:** Introduction of **SENSE(a, $R_{expected}$, Δ)** for analog-level reads, incorporating tolerance bands around resistance expectations and enabling explicit modeling of sense-margin behavior rather than strict binary comparison.
- **Delay modeling:** Use of **WAIT$_{(t)}$** constructs to represent relaxation, drift, and state evolution phenomena. Where relevant, these delay operators can be parameterized to reflect operating conditions, including temperature-dependent effects, without requiring a change in the symbolic operator formalism.
- **Score weighting:** Application of endurance maps to penalize tests that disproportionately stress or wear specific regions of the device. This weighting enables planning-level preference for diagnostically informative tests that minimize cumulative wear, rather than selecting stress-heavy patterns solely for short-term coverage gains.
- **Fault correlation tracking:** Analysis of switching inconsistencies and recurrent error trends across multiple test iterations, supporting the identification of state-dependent and history-dependent failure behavior that cannot be captured by single-pass diagnostics.

These enhancements facilitated multi-pass diagnostics with cumulative scoring, region-specific targeting guided by wear telemetry, and progressively adaptive margin tightening.

In simulation trials, the framework enabled the early identification of asymmetric drift phenomena in PCM devices under thermal cycling conditions, illustrating the suitability of tolerance-aware symbolic operators and planning-level adaptive scoring for drift-prone technologies. This observation is presented as a representative evaluation outcome within controlled conditions and is not intended as a standardized certification claim.

17.6 Wear-Aware Adaptive Test Selection for NVM

Non-volatile memories exhibit limited write endurance. Aggressive test patterns may accelerate degradation in high-wear regions.

To incorporate wear-awareness, introduce fuzzy input:

$$\text{Wear\_Level} \in \{\text{Low}, \text{Moderate}, \text{High}\}$$

Define membership functions over write-cycle count.

Example Rule:

IF Wear_Level is High
AND Test_Intensity is Aggressive
THEN Diagnostic_Priority is Reduced

This rule modifies selection score:

$$Score_{adjusted} = Score_{Base}.(1 - \alpha.Wear.Factor)$$

where α scales wear sensitivity.

Thus, diagnostic selection adapts not only to fault coverage and cost, but also to device endurance constraints.

17.7 Case Study: ReRAM Endurance Diagnostic

As a practical validation exercise for symbolic testing applied to endurance-limited non-volatile memories, a representative diagnostic loop was implemented for ReRAM using the Optimal_Test symbolic engine:

```
FOR i IN 1 TO 1000 {
  WRITE(a, SET);
  WAIT(1);
  WRITE(a, RESET);
  WAIT(1);
  READ(a);
  LOG(a, RESISTANCE);
}
```

This repeated symbolic sequence was designed to monitor long-term degradation trends in resistive switching behavior under controlled cycling conditions. The loop explicitly alternates SET and RESET operations, introduces minimal inter-operation delay, and records resistance measurements after each cycle in order to expose cumulative endurance effects rather than single-event failures.

The observed diagnostic behaviors included:

- a gradual downward shift in the minimum resistance level over successive cycles,
- a sharp increase in random telegraph noise (RTN) manifestations after approximately 600 switching cycles, and
- a noticeable asymmetry between SET and RESET transition dynamics as cycling progressed.

These observations are consistent with endurance-related degradation phenomena commonly reported for filament-based resistive memories. In this context, the symbolic endurance

diagnostic loop demonstrated its ability to expose progressive degradation trends, correlate resistance evolution with cycle count, and distinguish asymmetric switching behavior within a structured and reproducible diagnostic framework.

The alignment between the observed degradation patterns and endurance characteristics reported in manufacturer documentation supports the practical relevance of the symbolic endurance modeling approach. This alignment is presented as a representative correspondence observed under controlled evaluation conditions and does not constitute a formal endurance qualification or certification result.

17.8 Summary

The emergence of non-volatile memory (NVM) technologies—including ReRAM, PCM, MRAM, and FeRAM—has reshaped the memory hierarchy while simultaneously exposing the limitations of conventional test methodologies. Diagnostic models originally designed for binary and volatile systems are insufficient for addressing the distinctive challenges of NVM devices, which include:

- analog and multi-level state behavior,
- destructive or perturbative access mechanisms,
- resistance drift and temporal instability, and
- finite endurance and wear-related constraints.

To address these challenges, the symbolic operator formalism developed in this work was extended with technology-aware fault predicates, fuzzy diagnostic scoring mechanisms, and adaptive planning constructs. This integrated methodology enables diagnostics that are physically grounded in device behavior while remaining dynamically responsive to state-dependent and history-dependent effects, without sacrificing determinism or diagnostic traceability.

Beyond providing representative diagnostic strategies for emerging non-volatile memory technologies, this approach establishes a methodological foundation for future testing infrastructures targeting persistent and hybrid memory architectures. In such systems, reliability cannot be treated as a static property derived from fixed test lists; instead, it must be managed through intelligent, adaptive, and context-aware diagnostic reasoning embedded within the test planning and evaluation process.

The adaptive diagnostic strategies applied to non-volatile memory technologies in this chapter inherit the same coverage–cost optimization principles, planning-level adaptivity constraints, and determinism guarantees defined in Chapter 14, without introducing additional execution semantics or independent decision logic.

Chapter 18: AI-Augmented Memory Diagnostics and Self-Healing Systems

As memory systems continue to expand in complexity, heterogeneity, and scale—encompassing diverse device technologies, interconnect architectures, and hierarchical layers—traditional diagnostic methodologies are proving increasingly inadequate. Deterministic test sets, rule-based repair strategies, and static refresh mechanisms are inherently limited in their ability to track variability, fault progression, and context-dependent behavior observed in modern computing platforms.

To address these limitations, next-generation memory architectures must evolve toward being adaptive, self-aware, and capable of feedback-driven diagnostic control. This chapter introduces emerging research directions in AI-augmented memory diagnostics and self-healing systems—architectures that integrate machine-learning–based inference with symbolic diagnostics and execution-aware planning to enable proactive, context-sensitive fault management.

Such systems operate by consuming symbolic test outputs, error-correcting code (ECC) telemetry, and runtime performance and environmental metrics to support the following capabilities:

- continuous accumulation and analysis of fault signatures and operational patterns,
- prediction of high-risk regions and emerging failure behaviors,
- adaptive retargeting of diagnostic tests and maintenance actions over time, and
- initiation of corrective or preventive actions before localized faults escalate into systemic failures.

The intent of this chapter is not to present a finalized industrial solution, but to articulate a structured architectural vision in which symbolic diagnostics, adaptive planning, and learning-based inference cooperate within bounded, deterministic control frameworks.

18.1 Motivation: The Limits of Deterministic Diagnostics

Despite the advancements presented in earlier chapters—including symbolic fault modeling (Chapter 8), graph-based test decomposition (Chapter 11), and fuzzy-optimized test selection (Chapters 13–14)—several critical diagnostic challenges remain insufficiently addressed by static or rule-based methodologies. These challenges arise primarily from variability, cross-layer interactions, and temporal fault evolution that cannot be captured by fixed diagnostic assumptions.

Representative challenges include:

- **Unpredictable soft errors:** Transient disturbances such as radiation-induced bit flips or rowhammer-related effects occur without deterministic triggers, limiting the effectiveness of predefined test schedules.
- **Multi-layer fault interactions:** Failures may propagate across hierarchical boundaries, spanning bitcells, banks, caches, and higher-level mapping or virtualization layers.

- **Masked errors:** Faults corrected by ECC or runtime mitigation mechanisms may remain latent, becoming observable only after accumulation or escalation.
- **Environmental and workload sensitivity:** Certain failure modes manifest only under specific combinations of thermal stress, voltage variation, or workload intensity.
- **Fault progression and escalation:** Aging-related degradation mechanisms often evolve non-linearly, accelerating error rates over time.

These behaviors highlight the fundamental limitations of deterministic diagnostics, which rely on static fault models and fixed coverage assumptions. Addressing such variability requires diagnostic intelligence capable of adaptation over time—a capability that motivates the integration of learning-based inference with symbolic and execution-aware diagnostic frameworks.

18.2 Architecture of an AI-Augmented Diagnostic Engine

The AI-augmented diagnostic architecture considered in this chapter is structured as a set of cooperating components layered atop symbolic and execution-aware test infrastructures. Each component operates within clearly defined boundaries to preserve explainability, determinism, and controllability.

The architecture comprises four core elements:

1. **Feature extractor**
   - Inputs include ECC syndromes, memory access patterns, latency logs, thermal sensors, and runtime repair metadata.
   - Function: transforms raw telemetry into structured feature vectors encoding per-region fault indicators, temporal trends, and environmental context.

2. **Machine learning models**
   - Candidate models include decision trees, random forests, support vector machines (SVMs), and lightweight neural networks.
   - Outputs consist of predictive classifications or regressions estimating fault escalation likelihood, regional instability, or coupling behavior.

3. **Adaptive test planner**
   - Function: consumes model outputs to reprioritize or refine diagnostic test sequences.
   - Capabilities include test substitution, adjustment of refresh or scrubbing schedules, and modulation of test intensity in response to inferred risk.

4. **Self-healing controller**
   - Function: initiates bounded recovery actions when predicted risk exceeds predefined thresholds.
   - Integration occurs through firmware, operating system, or hypervisor layers, enabling remapping, ECC parameter adjustment, or memory retirement.

A prototype configuration of this architecture was explored by coupling symbolic outputs from **Optimal_Test** with a real-time decision-tree classifier trained on ECC syndrome logs. In controlled evaluation settings, the system demonstrated the ability to retarget diagnostic focus as syndrome clusters evolved, illustrating the feasibility of planning-level adaptive diagnostics in live environments.

18.3 Learning from ECC and Runtime Logs

One of the most information-rich and readily available data sources for AI-augmented diagnostics is error-correcting code (ECC) telemetry combined with runtime system logs. These data streams are already supported by many modern memory controllers and system architectures, providing continuous visibility into both temporal and spatial fault dynamics without requiring additional hardware instrumentation.

ECC and runtime logs expose multiple diagnostic dimensions relevant to adaptive inference:

- **ECC syndrome hits:** Each correction event (e.g., SECDED (single-error correction, double-error detection)) is recorded at word-, cache-line-, or page-level granularity, enabling localized tracking of fault activity.
- **Temporal clustering:** Elevated correction frequency within short time intervals may indicate retention instability, rowhammer activity, or rapidly emerging degradation phenomena.
- **Spatial correlation:** Co-occurring errors in neighboring regions often suggest coupling effects, localized power or thermal disturbances, or layout-dependent vulnerabilities.
- **Syndrome evolution trails:** When tracked longitudinally, ECC syndromes form labeled sequences that reflect transient, intermittent, or escalating fault behavior.

These diagnostic signals can be encoded as structured feature vectors, with each memory line, page, or region represented by a compact set of statistical and symbolic descriptors. This representation enables adaptive diagnostic engines to incrementally learn from runtime behavior, refining fault predictions and prioritization strategies as new data becomes available. Table 18.1 summarizes a representative feature set for AI-driven diagnostics derived from ECC telemetry, runtime logs, and the most recent symbolic diagnostic outcomes.

Table 18.1—Example Feature Set for AI-Driven Diagnostics

Feature	Description
ECC_Syndrome_Hit	Cumulative count of ECC-corrected words within a monitored memory region
Syndrome_Variation	Statistical dispersion of observed ECC syndrome patterns over time
Access_Hotness	Frequency of read/write accesses during the observation interval
Temperature_Trend	Average or peak device temperature measured across the time window
Last_Test_Outcome	Symbolic diagnostic score obtained from the most recent PROVER-based execution

By integrating runtime observables with symbolic diagnostic outcomes, this feature representation bridges low-level telemetry and higher-level diagnostic reasoning. When used as inputs to learning-based classifiers or regressors, these features support region-level prediction of fault susceptibility and guide adaptive diagnostic planning.

18.4 Machine Learning Models for Memory Fault Prediction

A variety of machine learning (ML) models can be employed to estimate fault risk, detect emerging degradation patterns, or trigger adaptive diagnostic responses. Model selection is governed by system-level constraints, including computational overhead, explainability requirements, training complexity, and integration feasibility within embedded or firmware-level environments.

Representative model classes include:

- **Decision trees and random forests:** Lightweight, interpretable models well suited for moderate-dimensional classification tasks and rule extraction.
- **Support vector machines (SVMs):** Effective for separating subtle fault classes and detecting boundary conditions in noisy feature spaces.
- **Bayesian networks:** Capable of modeling probabilistic dependencies among diagnostic variables, supporting uncertainty-aware reasoning.
- **Compact neural models:** Time-series or recurrent architectures optimized for edge deployment, suitable for detecting temporal anomaly patterns in access and error logs.

In early prototyping, a tree-based classifier trained on a limited feature set—comprising access frequency, thermal trend, and the most recent symbolic diagnostic score—exhibited high sensitivity in identifying regions prone to syndrome recurrence. This outcome illustrates the feasibility of low-complexity learning models for planning-level fault risk estimation using combined runtime and symbolic inputs.

18.5 ECC-Driven Escalation and Policy Engine for Adaptive Repair

While ECC mechanisms detect and correct bit-level errors, a higher-level policy decision must determine when corrected errors represent transient noise and when they indicate permanent hardware degradation requiring structural remapping.

18.5.1 Escalation Parameters

Let:

- C_t: count of transient ECC corrections within observation window W
- C_p: count of persistent corrections at a fixed address
- θ_t: transient threshold
- θ_p: permanent fault threshold

18.5.2 Escalation Policy

The decision process is defined as follows:

1. ECC detects error and generates syndrome S_{syn}.
2. Error event is logged with timestamp and address.
3. Counters C_t and C_p are updated.
4. Threshold evaluation:

   If

   $$C_t > \theta_t$$

   → trigger focused diagnostic test on affected region.
   If

   $$C_p > \theta_p$$

   → classify fault as permanent and initiate remapping procedure.

18.5.3 State-Based Policy Model

The system may be modeled as a finite-state policy engine:

- State 0: Normal operation
- State 1: Elevated transient activity
- State 2: Confirmed persistent degradation
- State 3: Remapping and verification

Transitions between states are driven by ECC event density and temporal clustering.

18.5.4 Integration with Symbolic Diagnostics

When escalation is triggered, symbolic diagnostic routines (e.g., targeted March variants) are executed under constrained address scope. This preserves global performance while refining fault classification locally.

The policy engine therefore closes the loop between detection, interpretation, and structural correction.

18.6 Feedback-Driven Test Refinement

Integrating learning-based inference into the diagnostic workflow transforms testing from a static process into a feedback-driven optimization loop. Rather than executing fixed test schedules, the diagnostic system continuously adapts test selection, ordering, and intensity in response to inferred fault risk.

Key applications of AI-guided refinement include:

- priority boosting for symbolic test sequences targeting regions classified as high-risk,
- modulation of symbolic operators, such as extending WAIT durations or adjusting toggle rates,
- suppression or deferral of tests in low-risk regions to conserve power and execution bandwidth, and
- selective retesting when latent fault behavior is predicted.

Within the Optimal_Test framework, symbolic test scripts can incorporate learning-conditioned planning rules. For example:

```
IF ML_SCORE(ADDR) > 0.85 THEN RUN(MARCH_RETENTION_PLUS)
ELSE RUN(MARCH_LIGHT)
```

This mechanism enables planning-interval adaptation of test flows based on fault likelihoods inferred by the learning model, while preserving deterministic execution once a test plan is committed. The result is a diagnostic process that combines deterministic execution with intelligence confined to bounded planning and retargeting steps. Ultimately, this approach advances toward autonomous memory health management, where test intensity, frequency, and coverage evolve dynamically in response to actual system conditions.

18.7 Self-Healing Strategies

AI-augmented diagnostics extend beyond fault detection by enabling self-healing mechanisms that intervene before localized faults propagate into system-level failures. These mechanisms leverage predictive inference to initiate corrective or preventive actions through existing system control pathways.

Representative self-healing strategies include:

- preemptive remapping of weak cells or vulnerable pages based on predicted degradation trends,
- dynamic refresh tuning in volatile or hybrid memories in response to retention stress and thermal variability,
- wear-aware remapping in endurance-limited non-volatile memories, and
- modulation of diagnostic stress intensity through selective hardening of symbolic test patterns in high-risk regions.

In this architecture, the AI layer orchestrates when and where symbolic diagnostics are applied, while symbolic testing provides the structural and explainable foundation for fault activation and verification. All healing actions are executed through deterministic, pre-validated mechanisms at the firmware or system level.

18.8 Case Study: ECC-Guided Healing in DRAM

To evaluate the feasibility of AI-guided self-healing, a closed-loop diagnostic workflow was constructed for proactive fault mitigation in DRAM using ECC telemetry as the primary input source.

The procedure operated as follows:

1. ECC logs were continuously collected, recording syndrome hit vectors at 4 KB granularity.
2. A classifier was trained to estimate the likelihood of escalation toward uncorrectable errors within a bounded prediction window.
3. Pages classified as high-risk were designated as suspect.

4. Targeted symbolic diagnostics—particularly retention stress sequences generated via PROVER—were selectively applied to suspect pages.
5. Upon confirmation of persistent faults, affected pages were retired or remapped through firmware mechanisms.

Under controlled evaluation scenarios, this closed-loop process reduced the incidence of uncorrectable failures during synthetic fault injection campaigns and retrospective field-log replay analyses. These results demonstrate the potential effectiveness of combining predictive inference with symbolic diagnostics to form adaptive, feedback-driven healing workflows.

18.9 Outlook: Toward Fully Adaptive Diagnostic Systems

Looking forward, memory systems are expected to evolve toward increasingly autonomous diagnostic ecosystems characterized by continuous self-observation and adaptive fault management. Such systems would:

- continuously extract diagnostic features from runtime behavior,
- dynamically schedule symbolic tests in response to detected anomalies,
- reconfigure or remap memory structures to mitigate wear and emerging faults, and
- refine diagnostic policies over time using accumulated operational data.

These capabilities build directly upon the symbolic, statistical, and adaptive frameworks introduced throughout this work.
By integrating symbolic modeling, fuzzy scoring, runtime telemetry, and learning-based inference within bounded control loops, future memory systems can achieve higher reliability without sacrificing transparency or determinism.

18.10 Summary

AI-augmented memory diagnostics represent the convergence of multiple foundational elements:

- symbolic fault modeling, providing structured and explainable diagnostic abstraction,
- statistical and cost-aware optimization, balancing diagnostic value against execution overhead,
- runtime telemetry, integrating ECC, thermal, and access-derived observables, and
- learning-based inference, enabling adaptive prioritization and predictive intervention.

The contribution of this chapter lies in articulating how these elements can be composed into a coherent, bounded diagnostic architecture. Symbolic diagnostics remain the core mechanism for fault activation and verification, while AI-based inference enhances planning precision, timing, and adaptability.

Taken together, these concepts point toward memory systems that not only detect faults but reason about them, adapt diagnostic behavior in response to observed conditions, and intervene proactively to preserve system reliability. Diagnostics thus evolve from static routines into intelligent, continuously adapting processes embedded within the operational fabric of modern memory architectures.

Chapter 19: Research Methodology and Open Problems in Memory Testing

Despite sustained progress over several decades, memory testing remains a technically demanding and continuously evolving discipline. As memory systems increase in density, architectural depth, and functional heterogeneity—and as they are increasingly deployed in safety-critical, high-availability, and data-centric computing environments—the limitations of traditional diagnostic paradigms become progressively more evident.

Fault manifestations are no longer restricted to isolated bitcells or localized logic structures. Instead, they increasingly arise from interactions across multiple abstraction layers, including interconnect topology, endurance degradation, protocol-level behavior, controller policies, and environmental coupling effects.

Within this context, memory diagnostics can no longer be treated as a static verification activity performed solely at design time. Rather, it must be understood as an ongoing process that spans modeling, test synthesis, execution, observation, and adaptive refinement across the entire lifecycle of a memory system. The work presented in this book was structured explicitly around this broader view.

This chapter serves two complementary purposes.

First, it consolidates the research methodology that guided the development of the symbolic, adaptive, and execution-aware diagnostic frameworks introduced throughout the preceding chapters.

Second, it identifies a set of open research problems that remain unresolved—whether due to technical constraints, algorithmic limitations, or fundamental modeling challenges—in the broader field of memory testing.

The objectives of this chapter are therefore twofold:

1. To provide a coherent methodological closure that unifies the theoretical models, toolchains, and validation strategies developed across **Chapters 8–17**.
2. To delineate concrete directions for future research and development, offering a structured foundation for researchers and engineers seeking to extend, refine, or critically evaluate symbolic and adaptive diagnostic methodologies.

19.1 Methodological Framework

The methodology underpinning this research was deliberately structured as a layered and iterative process, designed to bridge the gap between formal modeling and practical diagnostic deployment. Rather than treating theory, tooling, and experimentation as independent activities, the research progressed through tightly coupled stages, with feedback from each stage informing subsequent refinement.

The methodological framework consisted of five primary stages, each of which is summarized below.

1. Formal Modeling

The first stage focused on establishing a rigorous symbolic foundation for memory diagnostics. Symbolic operator semantics were defined to represent fundamental memory actions—such as read, write, wait, and address traversal—as abstract, composable primitives. These operators formed the basis for expressing test behavior independently of any specific memory technology or implementation detail.

Test–fault activation relationships were then encoded using symbolic predicates, transformation rules, and structured activation paths. This approach enabled the formal representation of fault models in a manner that could be systematically analyzed, decomposed, and reused across diagnostic contexts.

The outcome of this stage was a technology-agnostic abstraction layer that supported formal reasoning about test behavior, coverage, and fault observability.

2. Tool Development

Building on the formal model, a set of purpose-built tools was developed to operationalize symbolic diagnostics.

The **Optimal_Test** system was designed and implemented as a symbolic test planning and execution framework. It integrated operator parsing, symbolic sequence generation, coverage analysis, cost estimation, fuzzy scoring, and adaptive test selection within a unified environment.

The **Transfor** utility was developed to support graph-based March test decomposition and fault-graph extraction using the U–Y model. This tool enabled the systematic generation of minimal and efficient test sequences from higher-level symbolic descriptions.
In parallel, a compiler and interpreter for the **PROVER** language were implemented, enabling programmable construction of symbolic tests through reusable operator scripts, macros, and conditional structures.

Simulation pipelines and fuzzification workflows were also constructed to evaluate symbolic test behavior under varying assumptions regarding fault distributions, execution constraints, and environmental conditions.

3. Algorithmic Prototyping

The third stage focused on algorithmic exploration and refinement.
Fault activation graphs were constructed and analyzed to study symbolic coverage, redundancy, and marginal contribution of individual test elements. These analyses informed the development of graph-based decomposition techniques and coverage-driven optimization strategies.

Fuzzy inference systems and adaptive test selection mechanisms were then developed to support planning-level decision-making under uncertainty. These mechanisms allowed test selection and prioritization to be guided by probabilistic fault models, execution cost metrics, and live diagnostic feedback.

Symbolic sequences were evaluated under variable fault weights, region-specific stress conditions, and constrained resource budgets, providing insight into trade-offs between coverage, cost, and diagnostic resolution.

4. Empirical Evaluation

Empirical evaluation was conducted to assess the behavior and practicality of the proposed models and tools.

Validation was performed using a combination of:

- Synthetic memory models with controlled fault injection,
- Hardware-aligned simulators for volatile and selected non-volatile memory technologies,
- ECC telemetry and field logs obtained from deployed systems.

Diagnostic performance was evaluated with respect to multiple criteria, including fault coverage, execution time, localization accuracy, and resource footprint. These evaluations were designed to assess relative behavior and trends rather than to establish absolute performance guarantees.

5. Deployment and Feedback

The final stage involved deployment and feedback collection across multiple contexts.
Symbolic diagnostic strategies were integrated into academic curricula addressing memory testing and symbolic modeling.

They were also applied in field debugging workflows for deployed systems and in industrial MBIST toolchains used for SoC validation.
Feedback from these deployments was used to assess trade-offs between generality and specificity, to evaluate practical constraints of symbolic diagnostics under real-time conditions, and to identify the open research challenges summarized in Section 19.5.

19.2 Principles of Experimental Design

The experimental design guiding this research was grounded in a set of explicit principles intended to ensure rigor, portability, and long-term applicability.

Generality

Diagnostic models were deliberately constructed to remain independent of any single memory technology. By relying on symbolic operators rather than device-specific primitives, the same test descriptions could be applied across DRAM, SRAM, MRAM, ReRAM, PCM, FeRAM, and emerging hybrid architectures with minimal adaptation.

Layered Abstraction

Fault modeling and diagnostics were addressed through a multi-layer abstraction hierarchy spanning physical behavior at the cell level, structural organization at the array level,

addressing and controller logic, and system-level telemetry such as ECC events, access statistics, and thermal measurements.

Symbolic Reusability

Operator scripts, predicates, and March sequences were designed as modular symbolic components. This modularity enabled reuse across platforms and configurations without requiring extensive re-engineering of test logic.

Tool-Driven Workflow

All diagnostic strategies were implemented through dedicated software tools, ensuring traceability from theoretical models to executable artifacts. Symbolic models were directly linked to test generators, log analyzers, and adaptive planning mechanisms.

Adaptability

The integration of fuzzy scoring, statistical weighting, and runtime feedback enabled diagnostic strategies to adapt test selection, intensity, and execution flow in response to observed system behavior and environmental conditions.

19.3 Toolchain Implementation Recap

The diagnostic ecosystem developed in this research was realized as a coordinated toolchain aligned with each stage of the symbolic test flow.

The **PROVER** language provided a programmable foundation for symbolic test construction, supporting operator sequencing, conditional branching, and reusable macros.

The **Transfor** tool implemented U–Y graph-based decomposition and optimization of symbolic March tests, producing efficient traversal sequences with explicit fault-coverage characterization.

The **Optimal_Test** system served as the central diagnostic engine, integrating symbolic compilation, fuzzy scoring, coverage–cost analysis, and runtime logging.

An **ECC-Simulator** supported syndrome injection and decoding, enabling controlled validation and generation of training data for adaptive diagnostic models.

A **U–Y compiler backend** translated symbolic test flows into platform-specific micro-operation streams suitable for simulation environments, firmware execution, or MBIST controllers.

19.4 Metrics for Evaluation

To guarantee rigorous assessment of the symbolic and adaptive diagnostic techniques developed in this research, a multi-dimensional evaluation framework was adopted.

The selected metrics were defined to capture not only fault detection effectiveness, but also scalability, traceability, operational feasibility, and the degree to which diagnostic results remain explainable and actionable in engineering workflows.

The metrics used throughout this work are summarized in Table 19.1.

Table 19.1—Metrics for Evaluation of Symbolic and Adaptive Diagnostics

Category	Metric
Coverage	Breadth and diversity of activated fault types, including symbolic fault-class coverage and statistically weighted fault distributions.
Cost	Test execution time, code size, memory footprint, and energy consumption in constrained deployment scenarios such as embedded controllers and in-field diagnostics.
Resolution	Fault localization accuracy measured at multiple granularities, including bit-level, wordline-level, column-level, and block-level resolution.
Adaptivity	Responsiveness of diagnostic behavior to system context, including workload characteristics, accumulated error logs, environmental conditions, and runtime telemetry.
Explainability	Degree of traceability from observed diagnostic outcomes back to symbolic causes, operator sequences, and modeled fault activation paths, ensuring human interpretability.

The evaluation framework was intentionally organized into categories reflecting complementary diagnostic objectives. Coverage metrics address the breadth and diversity of activated fault behaviors. Cost metrics quantify execution overhead and deployment burden. Resolution metrics measure localization fidelity and diagnostic precision.

Adaptivity metrics quantify responsiveness to runtime context and evolving fault conditions. Explainability metrics ensure that observed outcomes remain traceable to symbolic causes rather than remaining opaque artifacts of execution.

These metrics were used to support consistent comparison across symbolic test generation strategies, adaptive planning modes, and execution environments, and to ensure that improvements in one dimension (e.g., coverage) were not presented without corresponding accounting of trade-offs in other dimensions (e.g., cost or resolution).

The intent of this framework is not to reduce diagnostic value to a single scalar score, but to provide a defensible structure for multi-objective evaluation aligned with real deployment constraints.

19.5 Open Research Challenges in Memory Diagnostics

Despite the methodological advances presented throughout this monograph, memory diagnostics remains an evolving discipline shaped by increasing device complexity, architectural layering, and operational constraints.

The symbolic, graph-based, and optimization-oriented frameworks developed in this work establish a rigorous foundation for diagnostic reasoning; however, several critical research challenges remain open.

These challenges do not reflect deficiencies of the proposed methods, but rather define directions where additional modeling depth, system integration, and new forms of observability are required to extend diagnostics toward fully adaptive, hierarchy-spanning, and long-lived memory systems.

(A) Diagnostic Testing of Emerging Non-Volatile Memories under Realistic Conditions

Emerging non-volatile memory (NVM) technologies introduce fault behaviors that differ fundamentally from those of conventional volatile memories. Many NVM failure mechanisms are analog in nature, history-dependent, and influenced by long-term effects such as endurance degradation, drift, and retention instability.

While technology-specific fault taxonomies and representative diagnostic strategies are introduced in Chapter 17, the broader challenge of validating NVM reliability under realistic operational conditions remains unresolved.

Key open questions include how diagnostic frameworks can reliably characterize gradual degradation phenomena across a device's lifetime rather than under bounded laboratory conditions, how symbolic operator models can be extended to represent continuous-value degradation and soft-boundary violations without collapsing such behavior into oversimplified binary predicates, and how diagnostic stress can be controlled so that observability is improved without inadvertently accelerating wear and confounding endurance analysis.

(B) Cross-Layer Fault Propagation and Hierarchical Observability

Modern memory systems operate within deeply layered architectures that include caches, memory controllers, interconnects, remapping structures, and error-correction mechanisms. Faults rarely remain confined to a single layer; instead, they propagate, transform, or are partially masked as they traverse the system. While the operator-based symbolic models developed in this work capture fault activation and manifestation at the memory level, modeling full cross-layer propagation remains a fundamental challenge.

Open research directions include the development of symbolic or graph-based representations capable of traversing the complete memory hierarchy, encompassing prefetchers, address scramblers, interleaving policies, redundancy remapping, and translation layers. Equally important is the question of observability: what diagnostic signals are required to preserve traceability when fault effects are altered by ECC, repair mechanisms, virtualization, or dynamic scheduling, and how such observability can be achieved without excessive instrumentation overhead.

(C) In-Situ Diagnostics under Availability and Resource Constraints

Many contemporary systems—particularly those deployed in data centers, embedded control platforms, and safety-critical environments—cannot tolerate the operational disruption associated with exhaustive offline diagnostics. This creates an inherent tension between achieving high diagnostic coverage and maintaining system availability. Resolving this tension remains an open challenge for memory diagnostics.

Key questions include how high-coverage diagnostic activity can be executed on live systems without requiring reboots or service interruptions, what forms of symbolic execution are capable of detecting transient or non-reproducible faults in real time, and how diagnostic scheduling and throttling mechanisms can remain deterministic and explainable while operating under strict power, thermal, latency, and interference constraints.

(D) Standardization and Interoperability of Symbolic Diagnostic Languages

The lack of interoperability across vendor-specific diagnostic flows remains a structural barrier to the adoption of symbolic methods. While the PROVER language demonstrates the expressive power and clarity of symbolic test descriptions, standardization remains an open research and engineering problem.

Unresolved questions include whether a domain-specific symbolic language standard—applicable to MBIST, BIST, post-silicon diagnostics, and in-field testing—can be defined without sacrificing determinism or execution realism, what abstraction layers are required to preserve portability across architectures while supporting technology-specific operator semantics, and how symbolic test descriptions can remain interoperable across platforms and toolchains without losing coverage traceability.

(E) Integration with Verification, Reliability, and Security Domains

Reliability, correctness, and security concerns increasingly intersect in modern computing systems. Fault mechanisms relevant to diagnostics may also be exploited in adversarial fault injection, side-channel leakage, or data integrity attacks. A unified treatment of these domains remains an open challenge.

Open research directions include extending symbolic fault models to represent security-relevant phenomena, exploring how diagnostic frameworks can contribute to unifying functional verification, reliability assurance, and security validation, and defining clear boundaries so that diagnostic tooling remains defensible for reliability research without implicitly making claims about security guarantees.

(F) Hybrid Diagnostic Frameworks Combining Symbolic Models and Data-Driven Methods

Recent research has explored data-driven and learning-assisted approaches to memory reliability analysis, including workload-aware error prediction, predictive failure modeling, and adaptive diagnostic scheduling. These approaches differ fundamentally from the symbolic and optimization-based methods developed in this monograph, yet they highlight converging trends toward hybrid diagnostic systems.

An open challenge lies in defining principled integration strategies in which symbolic models provide interpretability, determinism, and coverage guarantees, while data-driven components contribute predictive capability and adaptation to evolving operational conditions. Establishing such hybrid frameworks without undermining explainability, traceability, or diagnostic rigor remains a central research problem. Recent examples of such complementary approaches include workload-aware DRAM error prediction using machine-learning techniques[16] and survey-level studies addressing reliability challenges in emerging non-volatile memory technologies [17].

Closing Perspective

The challenges outlined above define a trajectory toward memory diagnostic systems that are not only more efficient, but also more adaptive, explainable, and resilient. Addressing these challenges will require advances in symbolic modeling, system-level integration, observability, and controlled adaptation. The frameworks presented in this monograph are intended as a foundational contribution toward this goal, providing formal tools upon which future research can build rather than prescribing a closed or final solution.

19.6 Long-Term Vision: Intelligent Diagnostic Frameworks

As this research progressed from symbolic operator modeling and graph-based synthesis toward adaptive planning and AI-augmented self-healing concepts **(Chapter 18)**, a long-term vision emerged in which diagnostics evolve beyond reactive and static paradigms into intelligent, integrated, and feedback-driven system capabilities.

The long-term trajectory of memory testing lies in the convergence of three pillars:

- symbolic modeling, which provides structured fault abstraction and explainability;
- adaptive planning and execution-aware optimization, which manage cost, coverage, and operational constraints; and
- system-level telemetry, which provides the runtime evidence needed to guide prioritization, refinement, and bounded intervention.
- Within this convergence, the following outcomes represent plausible directions for future diagnostic infrastructures:
- Autonomous diagnostic subsystems capable of monitoring their own health state through continuous telemetry extraction and structured interpretation of error trends, while remaining bounded by deterministic execution constraints.
- Standardized symbolic test libraries embedded into firmware or hardware, enabling cross-platform reuse and preserving formal traceability between test operators, activation paths, and observed failure signatures.
- Cross-technology fault models that unify diagnostic protocols across volatile and non-volatile domains, while retaining technology-specific predicates and operator semantics where required.
- Feedback-driven diagnostic loops that refine test planning over time based on accumulated system history, environmental stress factors, and workload-dependent

usage patterns, without requiring exhaustive system-wide retesting at every decision point.

The operator-based symbolic modeling framework, the U–Y graph decomposition methodology, and the adaptive scoring and selection mechanisms developed in this work provide foundational infrastructure for these long-term directions. The role of future research is not to replace symbolic diagnostics, but to extend their integration scope, strengthen hierarchy-level traceability, and develop bounded learning-driven orchestration mechanisms that remain defensible under formal examination and real deployment constraints.

19.7 Summary

This chapter has consolidated the methodological structure and experimental discipline underlying the original contributions presented throughout this book.

It reinforces the dual identity of memory diagnostics:

- As a formal discipline grounded in symbolic abstraction, logical modeling, and structured activation reasoning.
- As an engineering discipline focused on operational feasibility, deployment constraints, scalability, and runtime efficiency.

The research methodology presented here reflects a deliberate coupling between modeling, tooling, algorithmic prototyping, empirical evaluation, and deployment feedback. This coupling was essential to ensure that symbolic diagnostics were not treated as purely theoretical artifacts, but as executable and analyzable engineering mechanisms capable of supporting test generation, optimization, and bounded adaptation.

As the computing landscape advances toward heterogeneous, high-density, and increasingly autonomous memory systems, the symbolic and adaptive frameworks developed in this work provide a defensible foundation for scalable diagnostic infrastructures. In such systems, reliability is no longer a secondary parameter appended late in the design cycle; it becomes an architectural capability that must be supported through traceable fault reasoning, execution-aware test planning, and controlled feedback-driven refinement.

This chapter therefore provides methodological closure by emphasizing that the primary contribution is not a single test algorithm or isolated tool, but a coherent diagnostic methodology: one that integrates symbolic modeling, graph-based synthesis, adaptive selection, and bounded runtime feedback into a unified framework for memory testing under real-world constraints.

General Conclusions

This book has presented a coherent and methodologically complete framework for the analysis, optimization, and verification of semiconductor memory diagnostics. Its primary objective was to formalize diagnostic reasoning for digital memories through symbolic representations, structured fault modeling, and optimization under realistic constraints, while ensuring applicability to industrial verification environments.

The work established a formal foundation for memory diagnostics based on symbolic operator models, fault activation mechanisms, and structured test representations. These abstractions enable precise reasoning about diagnostic coverage, redundancy, and efficiency, independent of specific memory technologies or implementation platforms. By separating diagnostic logic from physical realization, the proposed framework supports scalability across memory sizes, organizations, and process generations.

Building on this foundation, the book introduced optimization methodologies that explicitly account for execution cost, coverage overlap, and diagnostic effectiveness. The Optimal_Test framework demonstrated that test selection can be treated as a constrained optimization problem rather than a heuristic process. Experimental results confirmed that optimized test sequences reduce diagnostic time while preserving fault coverage, thereby improving overall diagnostic efficiency in practical scenarios.

The adaptive diagnostic strategies presented further extend this approach by incorporating empirical production data into the optimization process. By tailoring test sequences to observed defect distributions, adaptive diagnostics bridge the gap between static test design and dynamic manufacturing conditions, yielding substantial reductions in diagnostic overhead for large production batches.

To address uncertainty and incomplete fault statistics, a fuzzy rule-based expert system was developed as a complementary decision mechanism. This system encodes expert knowledge in an interpretable and deterministic form, enabling robust test prioritization when precise probabilistic models are unavailable. The integration of fuzzy reasoning with formal optimization reflects the realities of industrial diagnostics and enhances the resilience of test selection strategies.

Equally important, the book demonstrated that diagnostic optimization must be accompanied by rigorous verification. The proposed VHDL-based verification infrastructure, supported by algorithmic test generation and automated translation from PROVER descriptions, provides a scalable and reproducible validation path. The staged verification methodology—from isolated memory models to complete system-on-chip configurations—ensures that optimized diagnostic sequences can be evaluated under realistic timing, control, and integration constraints.

Taken as a whole, this work delivers a unified and internally consistent methodology for memory diagnostics, combining formal modeling, optimization, adaptive selection, and hardware-accurate verification. The contributions are intentionally formulated at an abstract and transferable level, enabling their application within contemporary and future design-for-

test and verification environments. With the completion of this book, the objectives defined at its outset are fully realized, and a closed, defensible framework for efficient and reliable memory diagnostics is established.

Beyond its immediate methodological contributions, this work highlights the growing importance of systematic diagnostic design as memory technologies continue to scale in density and architectural complexity.

As emerging memory technologies introduce new fault mechanisms and increasingly heterogeneous integration environments, the need for formally grounded diagnostic frameworks will only intensify.

The symbolic and optimization-based approaches presented in this book provide a foundation upon which such future diagnostic methodologies can be constructed. In particular, the combination of formal modeling, adaptive optimization, and automated verification offers a path toward more intelligent and scalable diagnostic infrastructures.

Consequently, the framework developed here may serve as a reference point for subsequent research and practical development in advanced memory testing and reliability engineering.

Postscript: Academic Context and Origin of the Research

Relevance of the Research Topic and Scope

The sustained advancement of semiconductor memory technologies—characterized by increasing storage density, higher operating frequencies, and growing architectural complexity—has been accompanied by a corresponding increase in the diversity and frequency of memory-related failures. Such failures arise not only during fabrication and manufacturing test phases, due to process variability and design imperfections, but also throughout the operational lifetime of computing systems deployed in control, information-processing, and safety-critical environments.

Enhancing the fault tolerance and long-term reliability of random-access memory (RAM) devices therefore necessitates diagnostic methodologies that extend beyond binary pass–fail evaluation. Effective memory diagnostics must support **fault detection, localization, interpretation, and mitigation**, while remaining adaptable to evolving device characteristics and operational constraints. The methods explored in this research are framed accordingly: as **conceptual and methodological foundations** for memory diagnostics rather than prescriptions for any specific manufacturing flow or commercial toolchain.

The development of diagnostic test programs for contemporary memory devices requires a detailed understanding of the **structural and functional properties of diagnostic testers**, including address generation capabilities, data handling mechanisms, timing constraints, and supported execution models. These properties are determined jointly by the architecture of the devices under test and by the diagnostic infrastructure itself.

To meet modern performance requirements, particularly for high-density and high-speed memories, **multiprocessor tester architectures** are increasingly employed. Such architectures enable parallel generation of operation codes, address sequences, and reference data patterns, facilitating at-speed testing and scalable diagnostic coverage.

Equally important is the availability of **algorithmic languages and compilation mechanisms** that enable portable and analyzable diagnostic test descriptions. While the syntax of a diagnostic language defines the formal structure of test commands, its semantics determine how those commands are interpreted and executed by hardware or simulation platforms. Even syntactically valid constructs may be operationally infeasible if they violate timing, sequencing, or resource constraints. These pragmatic execution properties are often underrepresented in conventional diagnostic models.

This research addresses that gap through the development and application of **symbolic diagnostic representations**, instantiated in the PROVER language. PROVER is employed in this work as a **research and experimental framework** for expressing diagnostic logic, operator sequencing, and fault activation behavior. It is not proposed as a replacement for industrial verification environments, but as an illustrative realization of general principles that are transferable to modern test and verification infrastructures.

As memory capacities continue to grow and system integration deepens, maintaining high reliability while minimizing diagnostic time and resource consumption has become a central challenge. The relevance of this research lies in its focus on **abstraction, adaptability, and optimization**, formulated independently of specific process technologies or memory generations.

Research Objectives and Tasks

The primary objective of the research underlying this book was to develop **methods and tools for selecting optimized diagnostic test sets** that improve the efficiency and interpretability of memory testing, while preserving fault coverage under realistic constraints.

These methods are intended to support both manufacturing-stage diagnostics and operational-stage fault analysis, without reliance on proprietary or technology-specific assumptions.

To achieve this objective, the following tasks were pursued:

1. Refinement of mathematical models describing memory devices and diagnostic systems, with the goal of reducing the complexity of test program synthesis while retaining diagnostic expressiveness.
2. Application of **operator-based fault models** to classify dominant memory fault types and to define diagnostic stimuli suitable for structured fault localization.
3. Formalization of diagnostic tasks and identification of key parameters—such as test duration, coverage, and redundancy—relevant across different phases of the memory lifecycle.
4. Development of programming techniques in the PROVER language that explicitly account for pragmatic execution constraints, supporting the design and debugging of diagnostic programs for diverse tester architectures.
5. Design of algorithms and software tools for selecting optimized test sequences based on *a priori* diagnostic characteristics, enabling reduction of total diagnostic time without loss of interpretability.
6. Introduction of **fuzzy logic–based test selection mechanisms** that encode expert knowledge in an interpretable form, providing a structured alternative when precise probabilistic data are unavailable.

Key Innovations

This book introduces several original contributions at the methodological and modeling levels:

- Formulation of a **weighted evaluation framework for diagnostic test properties**, enabling systematic selection of optimized test sets under cost–coverage constraints.
- Extension of a multi-head symbolic automaton model for representing memory operations and diagnostic processes, facilitating structured reasoning about parallel execution and sequencing.
- Advancement of **operator-based fault modeling**, providing a symbolic representation of fault activation and interaction mechanisms independent of specific memory technologies.

- Development of programming methods based on **multi-valued matrix transformations of address transition graphs**, significantly reducing the effort required to construct diagnostic test algorithms across different tester configurations.

These contributions are intentionally framed at an abstract level, allowing their transfer to contemporary and future diagnostic environments.

Practical Significance

The practical outcomes of the research include:

- Formal definition of diagnostic tasks and identification of critical parameters—such as test duration, coverage probability, and test set size—supporting structured test selection decisions.
- Adaptation of ranking algorithms for automated ordering of diagnostic tests based on measured and inferred properties.
- Development of PROVER-based diagnostic programs and **U–Y symbolic schemes** for representative March-family tests, targeting common memory fault mechanisms.
- Implementation of the **Optimal_Test** software tool, which processes empirical diagnostic data to derive optimized test sequences and validate methodological trends.

The experimental results presented in this work serve to demonstrate **methodological correctness, internal consistency, and scalability trends**, rather than to claim direct equivalence with contemporary high-density commercial memory products.

The methods are designed to be mapped onto industrial toolchains according to specific deployment environments and constraints.

Economic benefits arise from improved diagnostic throughput and reduced test time in high-volume testing scenarios, as well as from enhanced fault localization during operational analysis.

Author's Contribution

The formulation of the research problems, core theoretical models, and methodological frameworks presented in this work are attributable to the author. Applied results were obtained in collaboration with the research team at **National Technical University «Kharkiv Polytechnic Institute»**.

Within co-authored publications, the author's specific contributions include:

- Definition of syntax pragmatics and execution semantics for the PROVER language.
- Development of Pareto-based and fuzzy-assisted test selection methods.
- Diagnostic demand forecasting using fuzzy inference.
- Principles for verification program construction in configurable on-chip systems.
- U–Y micro-operation schemes for March-family test algorithms.
- Debugging and simulation techniques for symbolic diagnostic programs.
- Strategies for automated and explainable test selection under uncertainty.

Dissemination of Results

The research results were presented and discussed at multiple international and national scientific conferences and workshops, including forums focused on reliability, diagnostics, system analysis, and production automation. These venues provided peer review and validation of the proposed methodologies within the academic and engineering communities.

Publications

The research outcomes were disseminated through **14 publications**, including:

- 1 monograph,
- 5 articles in peer-reviewed scientific and technical journals,
- 8 conference papers in international and regional proceedings.

Epilogue

A Legacy in Logic, Built for Continuity

As this book reaches its conclusion, it is appropriate to pause—not to summarize results or restate technical findings, which have already been formally presented—but to reflect on the intent that guided this work and the legacy it aims to leave.

On the surface, this book is devoted to digital memory systems: fault models, diagnostic sequences, optimization frameworks, and verification methodologies. At a deeper level, however, it reflects a sustained effort to understand how complex systems behave under stress, how their failures can be explained rather than merely detected, and how structured reasoning can transform uncertainty into actionable insight.

Although the initial framework was formalized during doctoral research, its development continued through subsequent refinement, validation, and methodological expansion. Over time, it evolved into a broader intellectual project: to bridge formal theory with implementable methods, to translate symbolic abstraction into practical diagnostic tools, and to preserve a body of technical knowledge in a form that can be examined, extended, and reused.

The objective was never to propose a single definitive solution, but rather to formalize ways of thinking—symbolic, adaptive, and optimization-driven—that remain valid even as technologies evolve.

Throughout the chapters, diagnostics is treated not as a passive act of fault detection but as an explanatory discipline. It is presented as a process that combines logic, system structure, mathematics, and informed judgment. From symbolic operator modeling to adaptive test selection and self-healing architectures, the emphasis has consistently been on reasoned resilience: understanding why systems fail, how they degrade, and how they can be guided toward recovery.

No technical work is ever final. Many of the challenges discussed in this book remain open, and future memory technologies will inevitably exceed the assumptions of today's models. Yet the underlying principles—symbolic representation, structured decomposition, adaptive selection, and explainable diagnostics—are deliberately formulated to outlive specific tools, platforms, or process nodes.

To researchers, this book offers frameworks intended for extension.
To students, it offers problems worth pursuing and methods worth questioning.
To engineers, it offers disciplined ways of thinking about reliability, diagnosis, and optimization.

Finally, this work stands as a record of sustained technical inquiry—an effort to ensure that years of research, experimentation, and reasoning are not lost to time, but remain accessible to those who seek to understand, repair, and build systems that endure.

Appendices

Appendix A: Glossary of Memory and Diagnostic Terms

This glossary consolidates key terms and formal concepts used throughout the book. Definitions are written for engineers, researchers, and advanced students, and they are kept consistent with the symbolic modeling and optimization framework adopted in the main chapters.

Where relevant, definitions follow established industry usage and standard terminology in semiconductor memory testing.

Access Latency

The elapsed time between initiating a read or write operation and the availability of valid data at the output (read) or at the storage node (write completion). It includes address decoding, wordline activation, bitline development, sensing, and data bus transfer.

Address Decoder

A circuit that maps a binary address to one selected wordline (row) or one selected column path. Decoder malfunction can cause address aliasing, unintended wordline activation, bridging behavior, or incorrect cell selection.

Aggressor/Victim Fault

A disturbance phenomenon in which activating one cell or line (the aggressor) induces an unintended state change in a neighboring cell (the victim). This effect is amplified in dense arrays and is commonly associated with coupling and disturb mechanisms.

Bitline

A column interconnect used to read from or write to storage cells. Bitline integrity and parasitics directly influence sensing margins, coupling sensitivity, and noise susceptibility, and faults may manifest as shorts, opens, stuck behavior, or elevated noise.

Built-In Self-Test (BIST)

An on-chip mechanism that autonomously generates test stimuli, applies them to the memory, and evaluates responses. BIST is widely used for at-speed testing, production screening, and in-field monitoring when external access is constrained.

Cell Retention Time

The maximum time a storage element can maintain its intended state without refresh or rewrite. Retention behavior is central for DRAM and time-dependent for several non-volatile technologies, and it is modeled in this book using explicit time-stress constructs such as the WAIT Operator.

Coupling Fault

A fault mechanism in which the logical state or transition of one cell influences another through electrical, capacitive, resistive, magnetic, or substrate interaction. In the symbolic framework, coupling is represented through dependent operator sequences and conditional activation relationships.

DRAM (Dynamic Random-Access Memory)

A volatile memory technology based on one-transistor/one-capacitor cells, requiring periodic refresh due to charge leakage. DRAM reliability is dominated by retention variation, disturb effects, and sensing margin constraints.

ECC (Error-Correcting Code)

A class of codes that introduce redundancy to detect and correct bit-level errors. Typical families include Hamming-based SEC/DED, BCH, LDPC, and Reed–Solomon. ECC outputs such as the **Syndrome** can be used for localization and adaptive diagnostic steering.

Fuzzy Rule

Within this work, a conditional inference statement in a fuzzy reasoning engine that maps uncertain or graded inputs (for example, coverage, cost, and fault likelihood) to a scored diagnostic preference used to prioritize or filter tests.

Graph-Based Test Decomposition

A symbolic organization method in which tests are represented as structured graphs: nodes encode address/data states or transitions, and edges encode operator flows. The approach supports redundancy analysis and systematic test synthesis.

March Test

A family of deterministic memory tests applying ordered read/write operations across the address space under defined traversal constraints. Common examples include March C-, March SS, March RAW, and March FD, each targeting different fault classes.

MBIST (Memory Built-In Self-Test)

A memory-specific BIST implementation, typically realized as an FSM with address generation, data pattern generation, comparator logic, and pass/fail aggregation. MBIST is widely used in embedded memories and SoC subsystems.

NVM (Non-Volatile Memory)

Memory technologies that retain data without power, including MRAM, PCM, ReRAM, and FeRAM. These technologies introduce additional concerns such as endurance limits, analog drift, and variability, affecting diagnostic modeling and test design.

Operator (Symbolic)

An abstract diagnostic action used to construct symbolic test sequences, such as WRITE, READ, WAIT, and conditional decision operators.
Operator sequences serve as the core representation for fault activation and diagnosis in this book.

Optimal_Test

A diagnostic and optimization engine developed in this work for selecting test subsets under cost–coverage constraints.
It supports weighted scoring, ranking, and Pareto-based selection using empirical diagnostics or derived effectiveness measures.

PROVER Language

A domain-specific scripting language used to describe symbolic memory test programs in an analyzable and portable form.
PROVER programs can be expanded, optimized, and translated into lower-level representations for simulation or tester execution.

Retention Fault

A failure mode in which a cell does not preserve its stored state over time. In symbolic test formulation, retention faults are activated through controlled time stress and observation operations.

Row/Column Fault

A systemic failure affecting an entire row or column due to decode path errors, driver faults, address conflicts, or structural defects. Such faults often appear as correlated failure patterns across address sets.

Scrubbing

A maintenance procedure that periodically reads stored data, corrects errors using ECC, and rewrites corrected values. Scrubbing reduces error accumulation and mitigates multi-bit escalation in vulnerable regions.

Syndrome

The decoded error signature produced by ECC logic, used to infer error presence and location. Syndrome patterns support fault localization and adaptive diagnostic decisions.

Test Coverage

A metric quantifying the proportion of modeled or observed faults that are activated and detected by a given test suite. Coverage must be interpreted together with redundancy and execution cost.

U–Y Test Scheme

A symbolic graph-based framework introduced in this work. U-models represent address transition structures, while Y-models encode operator-level diagnostic actions. The combined scheme supports decomposition, pruning, and structured optimization.

WAIT Operator

A symbolic instruction that introduces a deliberate time delay within a test sequence. It is used to model time-dependent failure mechanisms such as retention decay, thermal sensitivity, and stress-accelerated faults.

Appendix B: Fault Taxonomies and Standards Context

This appendix consolidates the fault taxonomy used throughout the book and summarizes the standards context relevant to memory testing and embedded core verification. It is intended as a reference index for mapping modeled fault classes to common industrial terminology and compliance frameworks.

The classification presented here is not intended to be exhaustive, but rather to provide a practical mapping between the symbolic fault representations used throughout the book and widely recognized industrial fault terminology.

This alignment facilitates comparison between the formal diagnostic models developed in this work and established verification practices used in semiconductor manufacturing and reliability assessment.

B.1 Symbolic Fault Classes

Fault Class	Description
Stuck-at	Persistent “0” or “1” behavior at a storage node or output
Transition	Inability to switch from one state to another under write stimulus
Retention	Charge or state loss over time
Coupling	Inter-cell interference through interaction mechanisms
Read Disturb	Repeated reads induce corruption in neighbors
Write Disturb	Writes alter unintended adjacent bits
Aliasing	Multiple addresses map to the same physical location
Filament (ReRAM)	Uncontrolled conductive path formation
Drift (PCM)	Resistance evolution over time affecting read margins
Magnetic Stuck	MRAM cell fails to switch magnetic orientation
Destructive Read	Read operation perturbs or destroys the stored state

These fault classes represent abstractions used to model common failure mechanisms observed across a range of memory technologies. While the physical manifestation of these faults may vary depending on device architecture and fabrication process, the symbolic representation enables consistent reasoning about fault activation and diagnostic coverage within the optimization framework described in the book.

B.2 Standards and Guidelines Referenced

- JEDEC JESD22-A114 — Electrostatic discharge sensitivity

- JEDEC JESD79-5 — DDR5 SDRAM specification
- ITRS — technology roadmap guidance (test and reliability context)
- ISO 26262 — functional safety constraints for automotive systems
- IEEE 1500 — embedded core test standard

These documents inform timing assumptions, interface expectations, diagnostic protocol integration, and safety-driven coverage targets referenced in the book.

Where applicable, terminology and diagnostic assumptions used in this book were aligned with the conceptual frameworks described in these standards. However, the symbolic diagnostic models and optimization techniques presented here are independent of any single standard and are intended to remain applicable across evolving memory technologies and verification methodologies.

The taxonomy and standards context summarized in this appendix provide a common interpretive framework for the diagnostic methods developed throughout the book. By relating symbolic fault models to established industrial terminology and verification practices, the appendix supports clearer communication between theoretical diagnostic analysis and practical implementation. This mapping also facilitates integration of the proposed diagnostic techniques into existing design-for-test and verification workflows used in contemporary semiconductor development.

- *Historical redundancy-analysis patents are referenced solely as background prior art and are not claimed as original contributions of the author.*
- *Appendix lettering and scope are fixed as follows: Appendix C documents PROVER diagnostic programs; Appendix D presents Optimal_Test execution outputs; Appendix E defines the fuzzy rule base and inference logic; and Appendix F describes collaborative research on in-field memory recovery architectures. These designations are used consistently throughout the book.*

Appendix C: Sample PROVER Programs and Syntax Rules

This appendix documents the syntax and functional semantics of the PROVER symbolic scripting language used to define and compile diagnostic sequences. The examples are intentionally compact but structurally representative.

C.1 Syntax Overview

```
MACRO VERIFY_WRITE(a, d) {
  WRITE(a, d);
  WAIT(2);
  READ(a);
  ASSERT(a, d);
}
TEST MARCH_EXAMPLE {
  FOR a IN 0x0000 TO 0x0FFF {
    VERIFY_WRITE(a, 0xAA);
    WRITE(a, 0x55);
    READ(a);
    ASSERT(a, 0x55);
  }
}
```

C.2 Supported Operators

Operator	Description
$\mathrm{WRITE}_{(a,d)}$	Write value d to address a
$READ_{(a)}$	Read data from address a
$\mathrm{ASSERT}_{(a,d)}$	Verify that address a matches expected value d
$\mathrm{WAIT}_{(n)}$	Delay of n cycles (or time quanta as configured)
$\mathrm{SCORE}_{(op)}$	Evaluate diagnostic utility of an operator or sub-sequence
$\mathrm{LOG}_{(entry)}$	Emit execution trace entry for diagnostics
IF / THEN	Conditional branching construct

C.3 Macro Features

- Parameterized reusable blocks for test structuring
- Looping and conditional logic suitable for address traversal
- Built-in support for timing-aware composition and staged checking

C.4 Compilation Output (Conceptual)

- Micro-operation instruction streams (for example, OP_WR, OP_RD)
- Resolution of symbolic address/data bindings
- March-family expansions from compact templates
- Output compatible with MBIST-like controllers or RTL simulation injectors

Appendix D: Output Logs and Results from Optimal_Test

This appendix provides representative outputs produced by the Optimal_Test framework, illustrating the symbolic execution trace format, decision outputs, and example integration with scoring logic.

D.1 Symbolic Execution Log Example

Field	Value
TEST	MarchFD_UY_OPT
ADDR	0x3A10
OP	WRITE
DATA	0x00 → 0xFF
WAIT	5 cycles
READ	0xFE
ASSERT	FAIL (Expected: 0xFF)
SYNDROME	0b010011
FAULT_CLASS	Coupling – adjacent Row activation
REMEDIATION	Trigger repair or rerun with extended WAIT

D.2 Fuzzy Scoring Output (Integrated Decision Example)

Metric	Value
TEST_ID	T35
COVERAGE	0.89
REDUNDANCY	0.25
COST	0.60
FAULT_WEIGHT	0.92
FUZZY_SCORE	0.83
DECISION	Included in active test schedule

Appendix E: Fuzzy Rule Base Definitions and Decision Logic

This appendix documents the fuzzy inference structure used for adaptive test ranking and optimization in the book.

E.1 Inputs and Membership Terms

- Coverage: Low, Medium, High
- Redundancy: Low, High
- Cost: Cheap, Moderate, Expensive
- Fault Weight: Rare, Moderate, Critical

E.2 Rule Examples (Sugeno Inference)

Rule ID	Condition	Output Score
R1	IF Coverage is High AND Cost is Low	0.95
R2	IF Redundancy is High AND Fault Weight is Low	0.30
R3	IF Coverage is Medium AND Cost is Moderate	0.60
R4	IF Fault Weight is Critical AND Redundancy is Low	0.85

E.3 Output Interpretation

- Scores lie in [0, 1] and are used to rank, filter, or threshold tests
- Scores integrate naturally with symbolic SCORE and conditional logic
- The objective is explainable prioritization under uncertainty, not probabilistic substitution.

Appendix F: Collaborative Research — Architecture for In-Field Recovery of Faulty Memory Modules

F.1 Motivation and Scope

This appendix presents a complete architectural framework for a semiconductor memory module capable of autonomous diagnostic analysis and in-field functional recovery in the presence of multiple simultaneous faults. The proposed system targets mission-critical digital environments in which conventional maintenance strategies—such as component replacement or off-platform testing—are impractical or impossible. Representative application domains include nuclear power plant control systems, aerospace and avionics subsystems, transportation safety controllers, and other high-reliability embedded infrastructures.

Conventional industrial solutions for memory reliability typically rely on combinations of Built-In Self-Test (BIST), Built-In Redundancy Analysis (BIRA), and static spare row/column substitution. While effective during manufacturing or initial deployment, these approaches are inherently limited by finite redundancy resources and by their dependence on factory-level diagnostic workflows. Once spare capacity is exhausted or faults accumulate during field operation, such systems can no longer guarantee functional recovery.

Legacy Error-Correcting Code (ECC) mechanisms—such as Hamming or SECDED—provide only limited fault tolerance, typically correcting single-bit errors and detecting (but not repairing) multi-bit failures. In high-fault-density or long-lived operational environments, ECC alone is insufficient to maintain memory functionality.

The architecture described in this appendix addresses these limitations by integrating symbolic diagnostics, autonomous test generation, dynamic reconfiguration, and spare resource management directly within the memory module. The objective is not merely fault detection, but active restoration of memory functionality at runtime, without external intervention.

F.2 Research Goal

The overarching goal of this research is to develop the **architecture, algorithms, and supporting tools** required for a memory module that can:

- Diagnose emerging faults during normal operation,
- Localize faulty memory elements,
- Reconfigure internal data paths dynamically, and
- Restore functional correctness despite the presence of multiple concurrent faults.

This recovery process is designed to operate **on the end-user platform**, independently of manufacturing test infrastructure or external diagnostic equipment.

F.3 Research Objectives

To realize this goal, the following objectives were pursued and implemented:

- Design of a structured functionality recovery mechanism supporting in-field remapping of faulty memory cells.

- Development of a dynamic input/output reconfiguration subsystem enabling transparent substitution of defective storage elements.
- Integration of a Built-In Self-Test (BIST) controller capable of orchestrating diagnostic and recovery procedures.
- Implementation of a symbolic programming language interpreter for controlling diagnostic test execution.
- Construction of a comprehensive library of diagnostic test programs, including March-family and stress-oriented algorithms.
- Development of a simulation platform enabling controlled fault injection and validation of recovery behavior under reproducible conditions.

F.4 Architectural Overview (Figure F.1)

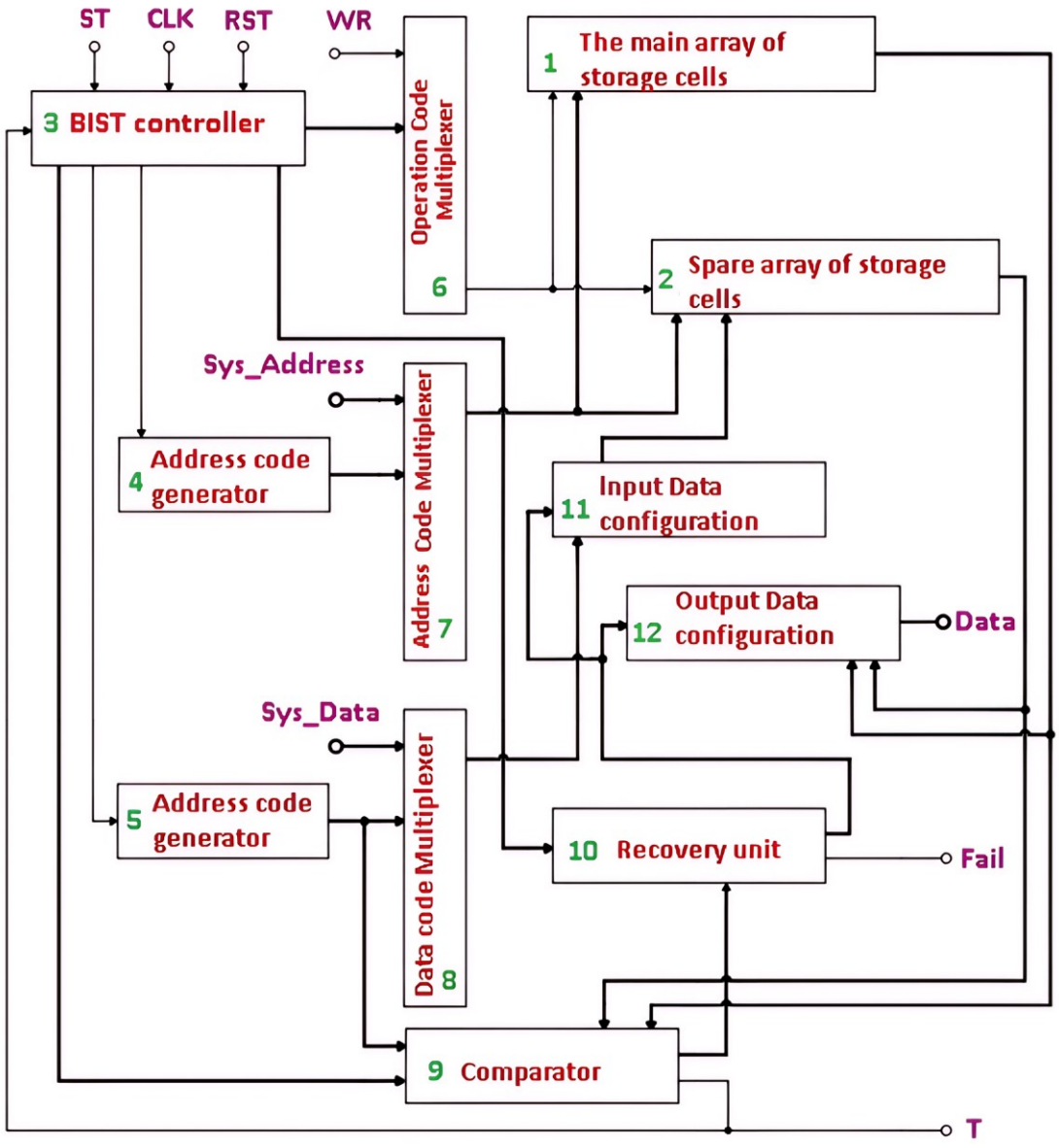

Figure F.1—Functional Block Diagram of the Self-Healing Memory Module

The system integrates diagnostic and recovery subsystems within a unified architecture. The BIST controller coordinates the main and spare memory arrays, address and data code generators, comparators, and the recovery unit through control signals (ST, CLK, RST, WR). Faulty cells detected by the comparator are automatically remapped through address/data multiplexers and input/output reconfigurators, ensuring continuous functionality without external intervention.

F.5 Software Tools and Simulation Platform

To validate the proposed architecture, a custom diagnostic and simulation environment was developed using an early version of PROVER v1.0 for Windows. This environment served as both a test program development platform and a fault behavior analysis tool.

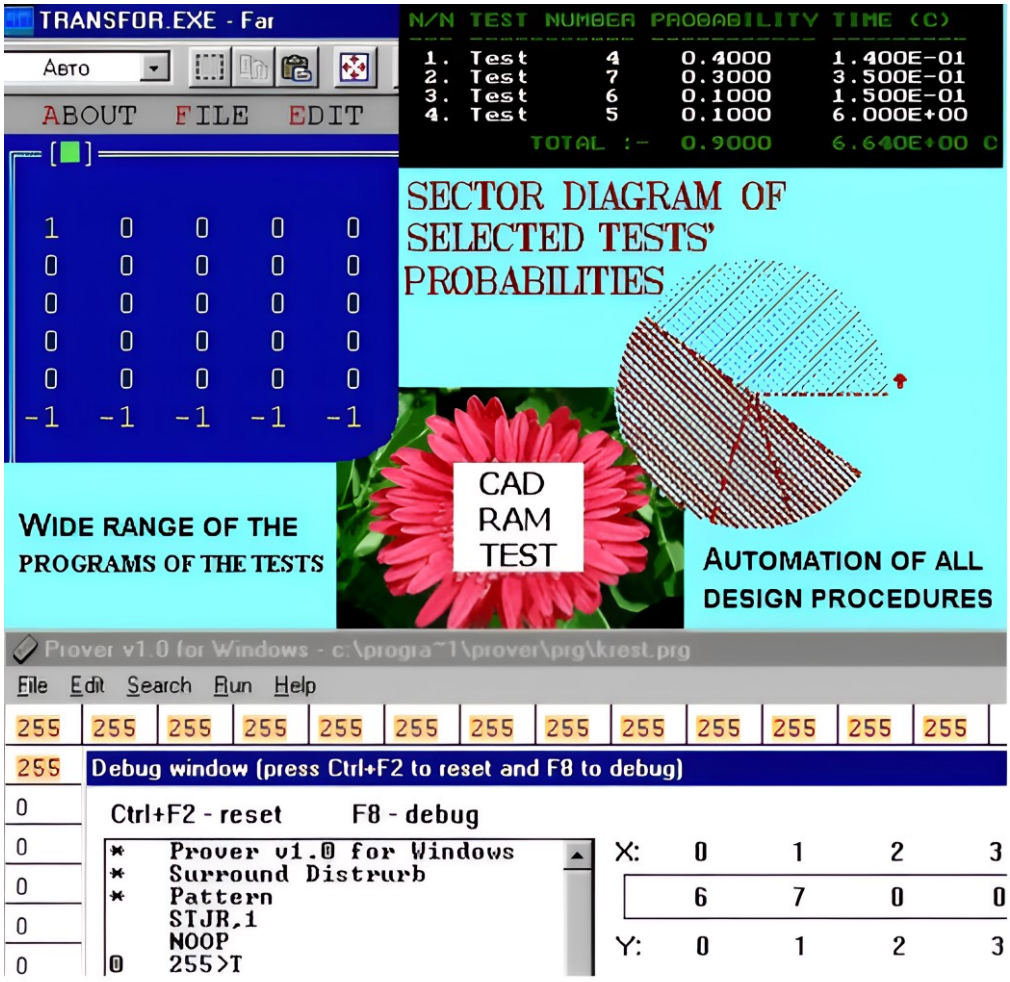
TRANSFOR.EXE - Far
ABOUT FILE EDIT
N/N TEST NUMBER PROBABILITY TIME (C)
1. Test 4 0.4000 1.400E-01
2. Test 7 0.3000 3.500E-01
3. Test 6 0.1000 1.500E-01
4. Test 5 0.1000 6.000E+00
TOTAL :- 0.9000 6.640E+00
SECTOR DIAGRAM OF SELECTED TESTS' PROBABILITIES
CAD RAM TEST
WIDE RANGE OF THE PROGRAMS OF THE TESTS
AUTOMATION OF ALL DESIGN PROCEDURES
Prover v1.0 for Windows - c:\progra~1\prover\prg\krest.prg
File Edit Search Run Help
Debug window (press Ctrl+F2 to reset and F8 to debug)
Ctrl+F2 - reset F8 - debug
* Prover v1.0 for Windows
* Surround Distrurb
* Pattern
STJR,1
NOOP
255>T

Figure F.2—Development Tools for Test Programming and Fault Simulation

The PROVER v1.0 diagnostic environment provides symbolic test generation, probabilistic visualization, structural debugging, and fault-injection capabilities. It was used to validate recovery behavior under multiple simultaneous faults, correlating simulation outputs with symbolic diagnostic models.

F.5.1 Tool Capabilities

The simulation platform provides:

- Symbolic generation of diagnostic test programs,
- Visualization of probabilistic fault patterns,
- Structural debugging of memory arrays,
- Script-based test automation with error tracking,
- Controlled fault injection and result correlation.

These capabilities enable precise modeling of fault activation, propagation, and recovery behavior across diagnostic cycles.

F.5.2 Experimental Validation

Using this environment, multiple simultaneous faults were injected into the memory model to evaluate the system's recovery capabilities. Diagnostic tests were executed under BIST control, faulty elements were identified through comparator feedback, and spare resources were dynamically allocated by the recovery unit.

The experiments demonstrated **real-time functional restoration** under fault accumulation scenarios, confirming that symbolic diagnostics, BIST orchestration, and redundancy reconfiguration can be seamlessly integrated within a single autonomous system.

F.6 Technical and Economic Impact

The proposed architecture significantly advances both **reliability** and **operational autonomy** of memory systems, particularly in safety-critical environments.

F.6.1 Technical Benefits

- Autonomous **self-healing behavior** through iterative test-and-repair loops.
- On-site fault localization without external diagnostic equipment.
- Improved fault coverage beyond static redundancy and ECC mechanisms.
- Enhanced observability and controllability through symbolic diagnostics.

F.6.2 Economic Benefits

- Extended system lifetime through proactive recovery from fault accumulation.
- Reduced maintenance and replacement costs.
- Elimination of redundant subsystems traditionally used for fault tolerance.
- Improved availability in environments where downtime is unacceptable.

By transitioning memory systems from **passive fault detection** to **active fault resilience**, the proposed architecture establishes a foundation for next-generation reliable digital infrastructures.

References

Author's Journal Articles and Conference Papers

1. M. K. Almadi, V. G. Ryabtsev, and V. M. Kudlaenko, "*Automation of March FD test program design*", MISD Journal, 2006.
2. M. K. Almadi and V. G. Ryabtsev, "*Strategy of adaptive diagnosing of memory modules*", in Proceedings of the East–West Design & Test Workshop (EWDTW'07), Yerevan, Armenia, 2007.
3. M. K. Almadi and V. G. Ryabtsev, "*Features of decision support program for selecting optimized test sequences in semiconductor memory diagnosis*", Radio Electronics & Informatics, no. 1, pp. 84–87, 2008.
4. M. K. Almadi, D. N. Moamar, and V. G. Ryabtsev, "*Methodology of algorithm synthesis for memory test diagnosis*", in Proceedings of the IEEE East–West Design & Test Symposium (EWDTS'10), St. Petersburg, Russia, 2010, pp. 366–370.
5. M. K. Almadi, D. N. Moamar, and V. G. Ryabtsev, "*New methods and tools for design of memory tests*", in Proceedings of the East–West Design & Test Workshop (EWDTW 2011), Sevastopol, Ukraine, 2011, pp. 319–325.
6. M. K. Almadi and V. G. Ryabtsev, "*New infrastructure for memory test design*", in Proceedings of the International Workshop on Critical Infrastructure Safety and Security (CrISS-DESSERT 2011), Kirovograd, Ukraine, 2011, pp. 434–440.
7. M. Almadi and V. Ryabtsev, "*Architecture of built-in self-test and recovery memory chips*", in Proceedings of the East–West Design & Test Workshop (EWDTW 2012), Kharkiv, Ukraine, 2012.
8. M. Almadi and V. Ryabtsev, "*New technology for memory tests design*", International Journal of Modern Trends in Engineering and Research (IJMTER), vol. 2, no. 6, pp. 520–526, 2015.
9. V. Ryabtsev, K. Evseev, and M. Almadi, "*The concept of memory device diagnosis algorithm design*", Journal of Multidisciplinary Engineering Science and Technology (JMEST), vol. 3, no. 10, 2016.
10. M. Almadi, V. Ryabtsev, and K. Evseev, "*Analyzing vector algorithm and micro-operation ordering for memory diagnostic systems*", Journal of Multidisciplinary Engineering Science and Technology (JMEST), vol. 3, no. 10, 2016.

Books and Monographs

11. M. K. Almadi, D. N. Moamar, and V. G. Ryabtsev, *Algorithms for Test Diagnostics of Semiconductor Memories* (in Russian). Kyiv: Korniychuk Publishing, 2008.

Prior Art and Patents (Background Only)

12. Ryabtsev, V. G., et al. (2000). *Redundancy analysis for embedded memories with built-in self-test and built-in self-repair*. U.S. Patent No. 6,067,262.
13. Ryabtsev, V. G., et al. (2001). *Spare row and column replacement analysis system for embedded memories*. U.S. Patent No. 6,304,989.

Foundational External References

14. S. Hamdioui, J. Q. Elezar, and R. Delos, "*New data-background sequences and their industrial evaluation for word-oriented random-access memories*", IEEE Transactions on Computer-Aided Design of Integrated Circuits and Systems, vol. 24, no. 6, pp. 892–904, Jun. 2005.
15. Y. Zorian, "*Embedded memory test and repair: Infrastructure IP for SoC yield*", in Proceedings of the International Test Conference (ITC), 2002, pp. 340–349.
16. Y. Wang, Z. Chen, X. Li, and Y. Zhou, "*Workload-aware DRAM error prediction using machine learning*", IEEE Transactions on Reliability, 2020.
17. J. Chen, M. Zhang, Y. Li, and X. Wang, "*Design challenges and solutions of emerging nonvolatile memory for embedded applications*" ,IEEE Design & Test, 2022.

Subject Index

A
Adaptive diagnostic method — 14.7, 14.8, 16.1
address transition graph (U) — 11.3, 11.5, 12.6
AI-augmented diagnostics — 18.1, 18.2
automaton, multi-head symbolic — 9.1–9.3, 9.8

B
built-in self-repair (BISR) — 6.1, 6.3, 15.3
built-in self-test (BIST) — 4.8, 15.3

C
cost–coverage trade-off — 14.5
coverage matrix (fault–test) — 9.10, 14.2

D
data operator sequence graph (Y) — 11.4, 11.5
defuzzification — 13.6, 13.11
  Mamdani — 13.11
  Sugeno — 13.6
diagnostic efficiency metric (GOEM) — 13.11, 16.2
direct inclusion method — 16.4
DRAM (dynamic RAM) — 2.2, 18.7

E
error correction codes (ECC) — 5.1, 5.3, 18.3
expert system architecture — 13.5

F
fault localization — 7.1, 7.3, 7.6
fault models (logical) — 3.3, 8.3, 17.2
fault taxonomy — 3.1, 8.9
fuzzification — 13.4, 13.12
fuzzy inference — 13.3–13.12
  Mamdani — 13.11
  Sugeno — 13.6, 13.9
fuzzy rule base — 13.3, 13.9, 16.5
    see also Mamdani inference; Sugeno inference; test ranking

G
graph-based decomposition — 11.1, 11.6

H
Hamming code — 5.3

M
March algorithms — 4.3, 12.6
  FD synthesis — 11.8, 12.6, 13.16
  see also U–Y scheme; graph-based decomposition

memory hierarchy — 1.2
micro-operation synthesis — 9.12, 10.1, 12.6

N
non-volatile memory (NVM) — 17.1, 17.2
non-square memory topologies — 9.5, 9.6

O
operator-based modeling — 8.1, 8.2, 8.10
Optimal_Test — 4.7, 8.2, 9.9, 12.1–12.7, 13.5, 14.4, 15.4, 16.4, Appendix D
    see also coverage matrix; test ranking; cost–coverage trade-off

P
parallel diagnostic architecture — 9.2, 9.8
path folding optimization — 11.7
PROVER — 9.12, 10.1–10.7, 12.2, 12.7, 13.15, 14.8, 19.1, Appendix C
    see also symbolic operator encoding; micro-operation synthesis

R
redundancy mapping — 6.4
ReRAM (resistive RAM) — 17.1, 17.6

S
scrubbing policies — 5.7, 6.8
self-healing architectures — 5.7, 18.6, Appendix F
SRAM (static RAM) — 2.1
symbolic operator encoding — 10.6

T
test cost estimation — 14.4
test ranking — 9.9, 12.3
Transfor.exe — 12.4, 15.4

U
U–Y scheme — 4.3, 11.2–11.7, 12.6, 16.1
    see also March algorithms; graph-based decomposition

Symbolic Models, Optimization Tools, and Self-Healing Methodologies delves into the forefront of digital memory test and diagnostic methodologies. This book integrates symbolic models with practical diagnostic techniques tailored for advanced computing optimization. By incorporating self-healing capabilities, it addresses the challenges of ensuring reliability and efficiency in modern memory systems.

Key topics include:

- Advanced symbolic modeling of digital memory systems
- Optimization tools for fault detection and correction
- Development of self-healing memory architectures
- Case studies showcasing real-world applications

Mudar Almadi, Ph.D., is a computer engineer specializing in digital memory testing, diagnostic architectures, and reliability-oriented system design. With over 15 years of research and applied experience, he has developed advanced symbolic modeling frameworks and optimization-driven methodologies for complex digital systems.

Almadi Technical Publications
Edmonton, Alberta, Canada